

**Molecular pharmacology
of histamine H₃ receptor ligands
and their implications in neurogenetic disorders**

Inaugural-Dissertation

zur Erlangung des Doktorgrades
der Mathematisch-Naturwissenschaftlichen Fakultät
der Heinrich-Heine-Universität Düsseldorf

vorgelegt von

David Reiner-Link
aus Frankfurt am Main

Düsseldorf, September 2020

aus dem Institut für Pharmazeutische und Medizinische Chemie
der Heinrich-Heine-Universität Düsseldorf

Gedruckt mit der Genehmigung der
Mathematisch-Naturwissenschaftlichen Fakultät der
Heinrich-Heine-Universität Düsseldorf

Berichterstatter:

1. Prof. Dr. Dr. h.c. Holger Stark

2. Prof. Dr. Holger Gohlke

Tag der mündlichen Prüfung: 22. Februar 2021

Dedicated to my brothers,

*Niclas
&
Maximilian*

*and to Steven,
without whom this journey would have ended too early.*

Table of Contents

Abstract	1
Zusammenfassung	2
1. Introduction	3
1.1. Physiological implications of the histamine H ₃ receptor	5
1.2. Molecular identity of the histamine H ₃ receptor	15
1.3. Medicinal chemistry of histamine H ₃ receptor ligands	23
1.4. Progress in molecular pharmacology of histamine H ₃ receptor ligands	33
1.5. Histamine H ₃ receptor ligands in neurogenetic disorders	39
1.6. Multitarget-directed histamine H ₃ receptor ligands in neurogenetic disorders	47
2. Objectives & scope of this research	55
3. Novel implications in molecular pharmacology of histamine H ₃ receptor ligands	59
3.1. Ligand binding kinetics at histamine H ₃ receptors by fluorescence polarization with real-time monitoring	61
3.2. Novel pyrrolidinone derivative lacks claimed histamine H ₃ receptor stimulation in receptor binding and functional studies	73
3.3. Design, synthesis, and biological evaluation of novel oxadiazole- and thiazole-based histamine H ₃ R ligands	83
4. Multitarget-directed histamine H ₃ receptor ligands in neurogenetic disorders	111
4.1. Profiling of LINS01 compounds at human dopamine D ₂ and D ₃ receptors	113
4.2. Dual target ligands with 4- <i>tert</i> -butylphenoxy scaffold as histamine H ₃ receptor antagonists and monoamine oxidase B inhibitors	123
4.3. Rasagiline derivatives combined with histamine H ₃ receptor properties	175
4.4. Histamine H ₃ receptor ligands by hybrid virtual screening, docking, molecular dynamics simulations, and investigation of their biological effects	185
4.5. In silico and in vitro studies of two non-imidazole multiple targeting agents at histamine H ₃ receptors and cholinesterase enzymes	207
4.6. The dual-active histamine H ₃ receptor antagonist and acetylcholine esterase inhibitor E100 ameliorates stereotyped repetitive behavior and neuroinflammation in sodium valproate-induced autism in mice	223
4.7. The dual-active histamine H ₃ receptor antagonist and acetylcholine esterase inhibitor E100 alleviates autistic-like behaviors and oxidative stress in valproic acid induced autism in mice	239
4.8. Epigenetics meets GPCR – Inhibition of histone H ₃ methyltransferase (G9a) and histamine H ₃ receptor for Prader-Willi syndrome	263
5. Summary & perspectives	275
6. References	289

7. List of abbreviations and synonyms	311
Appendix	317
Acknowledgements	319
Scientific CV	322
List of publications & presentations.....	324
Eidesstattliche Erklärung.....	327
Erklärungen zum Promotionsgesuch.....	327

Abstract

The histamine H₃ receptor (H₃R) regulates the release of histamine and various other central transmitters such as acetylcholine, norepinephrine, glutamate and γ -aminobutyric acid. Therefore, the receptor plays a part in numerous neurologic processes. Consequently, H₃R ligands have emerged as promising tools in neurogenetic disorders such as schizophrenia and Gilles de la Tourette syndrome (GTS), in the neurodegenerative conditions Alzheimer's disease (AD) and Parkinson's disease (PD), in autism-spectrum disorder (ASD) and the rare Prader–Willi syndrome (PWS). However, only two H₃R inverse agonists have been marketed to date of which only one emanated from dedicated drug development campaigns.

Firstly, this work aimed to identify novel strategies in the molecular pharmacological characterisation of H₃R ligands to elucidate their binding behaviour at the receptor. Secondly, novel H₃R ligands should be discovered, without or with strategical co-activity at relevant other targets to address neurogenetic disorders following the multitargeting ligand (MTDL) concept.

A novel homogeneous fluorescence polarisation approach revealed marked affinity differences between prominent receptor ligands, although, they are usually determined as highly-potent ligands by common reference methods. This study points towards differences in target binding modes of various receptor ligands and emphasises the importance of non-traditional methods and receptor-labelling tracers in molecular pharmacology of H₃R. Further studies revealed limits of the bioisosteric replacement according to the common pharmacophore blueprint for the medicinal chemistry of H₃R ligands and solutions for the design of potent H₃R drug candidates.

Furthermore, hit and lead compounds were discovered, but also drug candidates with co-activities at dopamine D₂/D₃ receptor (D₂R/D₃R) subtypes and enzymes involved in neurotransmitter degradation. Hit structures with combined H₃R/D₂R/D₃R activity showed novel drug design strategies for MTDLs against schizophrenia and GTS. New lead and drug candidates with combined activity at monoamine oxidase B and cholinesterases (ChE) emerged as potential tools against PD and AD. Furthermore, this study demonstrates the applicability of H₃R/ChE ligands in an *in vivo* model of ASD.

Finally, a novel MTDL approach to neurogenetic disorders was proposed, bridging to the recently identified involvement of the histone H3 methyltransferase G9a in AD, ASD and especially in PWS. Strategic manipulation of neurotransmitter levels, combined with the manipulation of cellular neuronal function, present multi-strategical perspectives to multifactorial disorders. Thus, combined H₃R antagonists/G9a inhibitors represent a single strategy against a plethora of neurogenetic disorders.

Zusammenfassung

Der Histamin-H₃-Rezeptor (H₃R) moduliert die Freisetzung von Histamin und weiteren zentralen Neurotransmittern, wie Acetylcholin, Noradrenalin, Glutamat und γ -Aminobuttersäure. Deshalb ist dieser Rezeptor in zahlreiche neurologische Prozesse involviert. Folglich haben sich H₃R Liganden als vielversprechender Ansatz in neurogenetischen Erkrankungen erwiesen, wie Schizophrenie, Gilles de la Tourette Syndrom (GTS), in den neurodegenerativen Erkrankungen wie dem Alzheimer und Parkinson Syndrom (AS und PS), in der Autismus-Spektrum-Störung (ASS) und dem seltenen Prader-Willi-Syndrom (PWS). Jedoch sind bis heute nur zwei inverse Agonisten des H₃R zugelassen, wovon nur einer aus gezielten Arzneistoffentwicklungsprogrammen stammt.

Als Erstes verfolgte diese Arbeit das Ziel, neue Strategien zur molekular-pharmakologischen Untersuchung des Rezeptorbindungsverhaltens von H₃R Liganden zu finden. Zweitens sollten neue H₃R Liganden entdeckt werden, um mit gezielter Koaktivität an relevanten weiteren Zielstrukturen im Rahmen des Multi-Targeting-Ligand (MTL) Konzeptes neurogenetische Erkrankungen zu adressieren.

Eine neue, kontinuierliche Fluoreszenzpolarisationsmethode zeigte deutliche Affinitätsunterschiede von Rezeptorliganden, die mittels Standardmethoden gewöhnlich als hoch potente Liganden charakterisiert werden. Diese Studie deutet auf Unterschiede im Rezeptorbindungsverhalten verschiedener Liganden hin und spricht für den Einsatz neuartiger Methoden in der Molekularpharmakologie des H₃R. Weitere Studien zeigten Grenzen des bioisosteren Ersatzes nach der Pharmakophor-Blaupause für die medizinische Chemie von H₃R Liganden auf und Lösungen für das Design potenter H₃R Arzneistoffkandidaten.

Ferner wurden Hit- und Leitstrukturen, aber auch Arzneistoffkandidaten mit Koaktivität an Dopamin D₂/D₃ Rezeptorsubtypen und Enzymen entdeckt, die für den Neurotransmitter-Abbau verantwortlich sind. Hitstrukturen mit kombinierter H₃R/D₂R/D₃R Aktivität zeigten neue Strategien für die Entwicklung von MTDLen gegen Schizophrenie und GTS auf. Neue Leitstrukturen und Arzneistoffkandidaten mit kombinierter Aktivität an Monoaminoxidase B und Cholinesterasen (ChE) traten als mögliche Ansätze gegen PS und AS hervor. Darüberhinaus konnte mittels *in vivo* Studien die Anwendbarkeit von H₃R/ChE-Liganden in der ASS aufgezeigt werden.

Abschließend wurde ein neuer MTDL Ansatz für neurogenetische Erkrankungen vorgestellt, als Brückenschlag zu den kürzlich identifizierten Verbindungen der Histon-H3-Methyltransferase G9a zu dem AS, der ASS und insbesondere, dem PWS. Die strategische Manipulation des Neurotransmitterhaushalts, kombiniert mit der Manipulation zellulärer, neuronaler Funktionen, eröffnet multistategische Perspektiven für multifaktorielle Erkrankungen. Deshalb stehen H₃R Antagonisten/G9a Inhibitoren für eine einzige Strategie gegen zahlreiche neurogenetische Erkrankungen.

1. Introduction

1.1. Physiological implications of the histamine H₃ receptor

Histamine (HA) was discovered by Sir Henry Dale, whose findings date back to the year 1907 (Riley, 1965). However, these credits must be taken with care. While he admitted that HA was already known from a synthesis project in the same year, he was initiating the isolation of the compound from the *Wernich's* preparation - a putrefied extract of ergot-alkaloids in which he assumed the presence of a compound with unprecedented pharmacological effects. In the same year of publishing this procedure, it was another researcher who identified HA in putrefied samples of L-histidine. However, it was Dale who correlated the pharmacological effects of specific fractions from the *Wernich's* preparation with known effects of an endogenously released compound that exerts anaphylaxis and with the then-recent identification of HA (Riley, 1965). Several decades had passed before HA was established as a neurotransmitter in the late 1970s, although several other neuronally released compounds have manifested well before (Tiligada et al., 2020). In contrast to other neurotransmitters such as norepinephrine (NE), HA is a hormone that exerts both, endocrine and neurohumoral, actions by the same chemical entity (Tiligada et al., 2020).

HA exerts its actions among receptor subtypes of the class-A of G protein-coupled receptors (GPCRs). Thereof, four histaminergic ones are known to date (H₁R, H₂R, H₃R and H₄R). They differ in tissue distribution within the mammalian organism as well as in their coupling to G proteins and other signalling pathways (Table 1). The subtypes H₁R, H₂R and H₃R shows relevant participation in the signalling of brain HA. The role of the H₄R, which shows high structural similarity to H₃R, is considered without functional expression in neurons; however, this is still a topic of discussion (Schneider et al., 2016).

Table 1. Coupling and tissue distribution of HA receptor subtypes.

	H ₁ R	H ₂ R	H ₃ R	H ₄ R
Main coupling partners^o	Gα _i /Gα ₁₁ β-arrestin2	Gα _s β-arrestin2	Gα _{i/o}	Gα _{i/o} β-arrestin2
Tissue distribution^o	Neuronal (CNS), lung, blood vessels	Neuronal (CNS), stomach, heart	Neuronal (CNS)	Bone marrow & haematopoietic cells

Abbreviations: CNS = central nervous system

References: (Panula et al., 2015; Southan et al., 2015; Bosma et al., 2016; Pandey-Szekeres et al., 2018)

As presynaptic receptors were found for other neurotransmitters before, the paradigm of an autoreceptor for HA has evolved concurrently with the discovery of neuronal HA. Therefore, the disclosure of H₃R and its characteristics was concluded from depolarisation-induced [³H]HA release from cortical slices

of the rat and in the human brain (Arrang et al., 1983; Arrang et al., 1988). In detail, Arrang and co-workers found that

- i. the release of [³H]HA from histaminergic neurons was inhibited in the presence of HA,
- ii. the effect was abolished by two competitive antagonists,
- iii. there was no evidence for product repression of L-histidine decarboxylase (HDC) by HA in vitro, and thus, the observed actions were unlikely to be linked to this enzyme,
- iv. the observed effects were saturable and thus, target mediated,
- v. the results were indistinguishably linked with an inhibitory process that was not in line with stimulation (Gα_s-mediated or Gα_q-mediated) that is elicited by H₁R or H₂R,
- vi. the potencies of a series of agonists differed significantly from such for H₁R and H₂R (Arrang et al., 1983).

Additionally, first hints for constitutive activity were revealed by the ability of the antagonists to increase the depletion of [³H]HA, though, this was not fully understood before the emerging of recombinant experimental systems in H₃R pharmacology (Arrang et al., 1983; Morisset et al., 2000).

In contrast to various other GPCRs, for which coupling to various isoforms of G proteins have been described, it was assumed that the H₃R transduced intracellular actions are exclusively mediated by Gα_{i/o} and the corresponding Gβγ-proteins (Inoue et al., 2019). After previous experiments, direct evidence was provided by Clark & Hill, who found pertussis-toxin sensitivity of agonist-mediated stimulation of ³⁵S-labelled analogue of guanosine 5'-O-[gamma-thio]triphosphate (GTPγ[³⁵S]) binding (Clark et al., 1996). Interestingly, Gα_{i/o} coupling is a shared feature of most auto- and heteroreceptors as they predominantly act via inhibition of neurotransmitter-release by a negative feedback mechanism (Hill, 1990).

After receptor activation, H₃R triggers various cell signalling pathways as depicted in **Figure 1**. The heterotrimeric G protein exchanges bound guanosine diphosphate (GDP) for guanosine triphosphate (GTP) and dissociates into subunits Gα_{i/o} and Gβγ (right panel, **Figure 1**). Gα_{i/o} reduces the activity of adenylyl cyclase and thereby cyclic adenosine monophosphate (cAMP)-elicited pathways. Both Gα_{i/o} and Gβγ seem to inhibit voltage-gated Ca²⁺ channels, which decrease Ca²⁺-influx and vesicular exocytosis (Nieto-Alamilla et al., 2016). Gβγ elicited pathways comprise of mitogen-activated protein kinase (MAPK) and PI3K/PKB/GSK3β (phosphoinositide 3 kinase/protein kinase B/ glycogen synthase kinase 3β), which are essential for antiapoptosis, neuronal development, and it is a mechanism that is supposed to be involved in H₃R-mediated neuroprotection (Bongers et al., 2007).

Moreover, H₃R triggers the release of lipid mediators such as arachidonic acid and may thereby elicit a direct role in neuroinflammatory processes (Bongers et al., 2007)

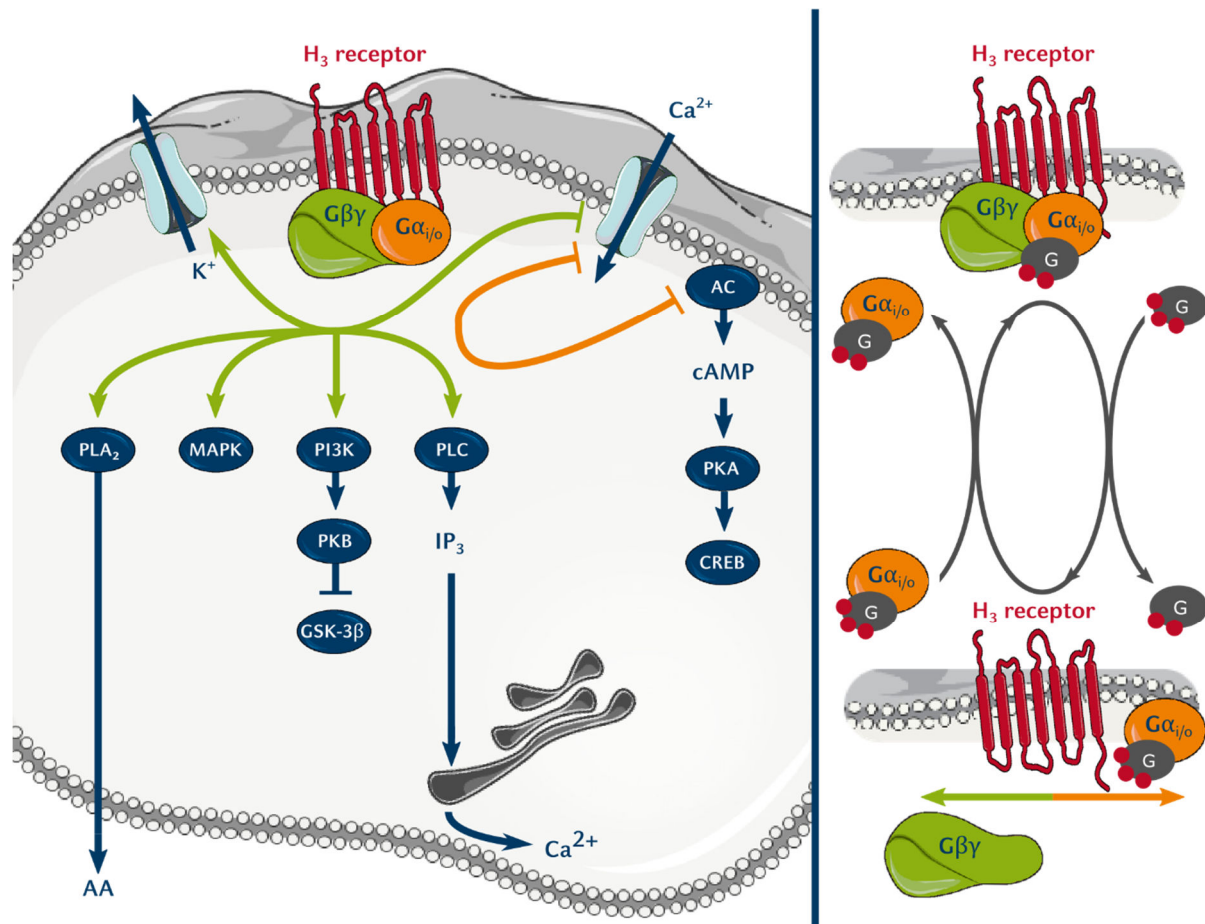


Figure 1. H₃R associated signalling pathways (left panel) and G protein activation (right panel), adapted from Bongers et al. (2007), Panula et al. (2015) and Nieto-Alamilla et al. (2016).

Left panel: green and orange arrows depict Gβγ and Gα-triggered pathways, respectively.

Abbreviations: PLA₂ = phospholipase A₂, AA = arachidonic acid, MAPK = mitogen-activated protein kinase, PI3K = phosphatidylinositol 3-kinase, PKB = protein kinase B, GSK-3β = glycogen synthase kinase 3β, PLC = phospholipase C, IP₃ = inositol-1,4,5-trisphosphate, AC = adenylyl cyclase, cAMP = cyclic adenosine monophosphate, PKA = protein kinase A, CREB = cAMP response element-binding protein.

Right panel: grey circles with two and three red dots depict GDP and GTP, respectively.

G protein-coupled inwardly rectifying potassium channels (GIRK) also belong to the Gβγ-associated pathway, mediate membrane hyperpolarisation and consequently, decrease in granular exocytosis (Hibino et al., 2010). Additionally, the typically Gα_{q/11} coupled phospholipase C/inositol-1,4,5-trisphosphate (PLC/IP₃)-pathway, which mediates Ca²⁺ influx, has been described within recombinant cell lines (Coge et al., 2001). While coupling of Gβγ to this pathway is known but usually less efficient than Gα_{q/11} coupling, the relevance for signalling *in vivo* remains to be clarified (Nieto-Alamilla et al., 2016).

Besides G proteins, arrestins have emerged as signalling modulators, which mediate receptor internalisation after prolonged activation. However, this signalling pathway could not be linked to the H₃R yet, while internalisation was shown in some previous studies (Lozeva et al., 2003; Bongers et al., 2007; Riddy et al., 2017).

Histaminergic neurons have been defined as HA producing, storing and releasing neurons which in mammalian brain exclusively emanate from the hypothalamic tuberomammillary nucleus (TMN) (Panula et al., 1984) but show extensive projections to the cerebral cortex, midbrain, cerebellum and stem brain (Haas et al., 2008). TMN neurons receive inputs from areas to which, conversely, histaminergic neurons themselves have projections (Brown et al., 2001), highlighting the regulatory functions of HA in the CNS. This supervisory role becomes even more perspicuous, considering the fine-tuning between the histaminergic and other neurotransmitter systems. As summarised in **Table 2**, the tone of histaminergic neurons is modulated through various neurotransmitter systems. In several cases, TMN neurons are not activated or inhibited directly but through neuronal circuits of non-histaminergic fibres. For example, norepinephrine shows both excitatory and inhibitory modulation of HA release. While the inhibition is performed by activation of α_2 heteroreceptors on terminals of histaminergic neurons, the excitation follows an indirect pathway among γ -amino butyric acid (GABA)ergic terminals in TMN (Gulati-Marnay et al., 1989a).

Table 2. Modulation of TMN-histaminergic neuronal activity.

Afferent origin ¹⁾	Neurotransmitter	Receptor ²⁾	Effect on histaminergic TMN neurons
DBB, VLPO, LHA	GABA	GABA _A R	postsyn. ↓ (direct)
		GABA _B R	presyn. ar. ↓ (indirect, via GABA)
VLPO	galanin (from GABAergic fibres)	GalR _x	presyn. hr. ↓ (indirect, via GABA)
LPO, LHA	glutamate	NMDAR	postsyn. ↑ (direct)
MPT	acetylcholine (ACh)	M ₁ R, M ₃ R	presyn. hr. ↓ (direct)
		nAChR	postsyn./ax. ↑ (direct)
NCA1/A2	norepinephrine (NE)	α_2 AR	presyn. hr. ↑ (indirect, via GABA)
PAG (?)	enkephalins	κ OR	postsyn. ↓ (direct)
ArcN (?)	nociceptin	ORL ₁	postsyn. ↓ (direct)
PFA (LHA)	orexin-A/-B (ORX-A/ORX-B)	ORX ₂ R	postsyn. ↑ (direct)
Raphe nuclei	serotonin (5-HT)	5-HT _{2c} R	postsyn. ↑ (direct)

¹⁾ **Abbreviations:** DBB = diagonal band of Broca; (V)LPO = (ventro)lateral preoptic area; LHA = lateral hypothalamic area; MPT = mesopontine tegmentum; NCA1/A2 = Noradrenergic cell group A1/A2 (formatio reticularis); PAG = periaqueductal grey;; ArcN = arcuate nucleus; PFA (LHA) = perifornical area (part of LHA).

²⁾ **Abbreviations:** postsyn. = postsynaptic, on histaminergic fibres; presyn. ar./hr. = presynaptic autoreceptor / heteroreceptor; ax. = axonal
Data were extracted from references (Ericson et al., 1989; Gulati-Marnay et al., 1989b; Gulati-Marnay et al., 1990; Arrang et al., 1991; Schönrock et al., 1991; Sherin et al., 1996; Uteshev et al., 1996; Yang et al., 1997; Stevens et al., 1999; Eriksson et al., 2000; Pillot et al., 2002; Yamanaka et al., 2002; Sergeeva et al., 2003; Stevens et al., 2004; Faucard et al., 2006)

The synthesis of HA starts from the naturally occurring semi-essential amino acid (aa) L-histidine, exclusively by HDC (Schwartz et al., 1970). This process is blocked upon H₃R activation (Arrang et al., 1987b). Ahead of cytosolic synthesis, L-amino acid-transporters mediate neuronal L-histidine resorption, and afterwards, the vesicular monoamine transporter 2 mediates the HA uptake into synaptic vesicles (Peter et al., 1994). Vesicular stored HA is released from depolarised histaminergic neurons in a [Ca²⁺]-dependent manner (Arrang et al., 1985). This release is slightly reduced in the presence of exogenously added HA, suggesting an influence of H₃R on Ca²⁺ influx. Additional studies in a perfused system allowed to diminish the contribution of endogenously released HA. There, the potency of exogenously added HA to inhibit HA release was shifted with increased frequency of electric stimulus that raised the assumption for an H₃R reserve within this physiological environment (van der Vliet et al., 1988).

A specific mechanism for a neuronal re-uptake of depleted HA has been doubted as there is a rather slow HA influx (Arrang et al., 1983), despite of an inflicting demonstration of an antagonisable HA enrichment in synaptosomes (Sakurai et al., 2006).

After release of HA into the synaptic cleft, the neurotransmitter is inactivated by the membrane linked HNMT to teMH whose turnover serves as a common surrogate for HA neuronal activity due to prolonged metabolic stability (Schayer et al., 1973; Barnes et al., 2002). The metabolite, but not HA itself, is subsequently further catabolised by diamine oxidase (DAO) or monoaminoxidase B (MAO B), DAO only occurring in the periphery (Burkard et al., 1963; Elsworth et al., 1980; Lin et al., 1991).

H₃R cloning facilitated the disclosure of the **receptor expression** pattern on messenger ribose nucleic acid (mRNA)-level, supplementing previous knowledge from receptor staining studies with radiotracers. In human, the H₃R encoding sequence is localised on chromosomal loci 20q13.32-13.33 and consists of three exons flanked by two introns. Based on indirect mRNA *in situ* hybridisation experiments and upon direct labelling with [³H]NAMH, high receptor densities were determined in the putamen of the corpus striatum with elevated levels in the human brain from Parkinson's disease (PD) (Anichtchik et al., 2001). Interestingly, the corresponding H₃R was not labelled there, but in substantia nigra (SN), pars reticulata (SNr) indicating either the histaminergic innervation of SN or striatonigral projections from presumably GABAergic neurons that co-express H₃R (Anichtchik et al., 2001).

Based on HA-induced GTPγ[³⁵S] binding, slightly lower activity was determined in SNr of PD patients compared to healthy brains (Anichtchik et al., 2001). Low H₃R expression was found in SN, pars compacta (SNc) of healthy humans which produce nigrostriatal dopaminergic output (Pillot et al., 2002). In rat brain, high receptor expression was found in thalamus, caudate nucleus, cerebral cortex, hippocampus, olfactory

tubercle (Lovenberg et al., 1999; Lovenberg et al., 2000). Within the hypothalamus, high receptor expression was found in the TMN as well as in neurons of the ventrolateral preoptic nucleus (VLPO), the suprachiasmatic nucleus (SCN), the lateral hypothalamic area (LHA) and the arcuate nucleus (ArcN) (Pillot et al., 2002). Interestingly, most of such regions are the origin of GABAergic (VLPO, LHA) and glutamatergic (LHA) projections, again emphasising the central regulatory role of HA in the mammalian brain. In the caudal area as well as in many (sub-)thalamic nuclei and the zona incerta, high H₃R mRNA expression can be found in Raphe nuclei, locus caeruleus (LC) and Purkinje layer of the cerebellar cortex. However, in these cases, binding sites were located elsewhere, supporting H₃R expression on serotonergic, noradrenergic, enkephalinergic and melanin-concentrating hormone (MCH) neurons (Pillot et al. 2002).

However, not all of them are linked with modulation of HA release. There are several ways how HA influences neuronal activation, as well, via **H₃ heteroreceptors** that inhibit the release of other neurotransmitters. This mechanism was demonstrated for NE and 5-HT, for striatonigral and striatopallidal GABAergic neurons, as well as in hypothalamic GABAergic neurons (Schlicker et al., 1988; Schlicker et al., 1989; Smits et al., 1991; Yamamoto et al., 1997; Zhou et al., 2006; González-Sepúlveda et al., 2013). Moreover, Schlicker et al. could evidence heteroreceptors on mouse striatal dopamine (DA) neurons, which failed in various previous research projects, presumably due to only mild modulation of striatal DA release in the presence of HA (Schlicker et al., 1993; Chiavegatto et al., 1998). This group assumed that this might be due to a negative interaction between H₃R and DA D₂ receptor (D₂R) that, indeed, could be evidenced 15 years later by the discovery of H₃R/D₂R **heteromers** (cf. page 19)(Ferrada et al., 2008). Conclusively, striatal DA levels are not influenced by H₃R inverse agonists, but they are elevated in the frontal cortex (Fox et al., 2005; Ligneau et al., 2007a). Functional heteroreceptors exist on corticostriatal glutamatergic neurons (Doreulee et al., 2001; Molina-Hernández et al., 2001), such as in the dentate gyrus and hippocampus that contain relevant circuits for facilitating the consolidation of memory (Brown et al., 1996). Finally, acetylcholine release is modulated by H₃R heteroreceptors on cholinergic neurons and is increased upon H₃R inhibition. However, H₃R activation is not sufficient for a complete abolishment of ACh release (Clapham et al., 1992; Prast et al., 1994).

Besides presynaptic expression of H₃R, evidence for **postsynaptic H₃R** has been made. For example, postsynaptic H₃R were found on MCH neurons (Parks et al., 2014) and are believed to dominate in histaminergic transmission within the caudate nucleus and putamen (Ellenbroek et al., 2014).

The most central function of the brain HA system is the control of arousal which is due to the involvement of the TMN in the **ascending (non-reticular) arousal system (AAS, Figure 2)**(Lin et al., 1990). A key indicator of arousal is pronounced activity of the layers 2/3 of cerebral pyramidal cells that influenced by

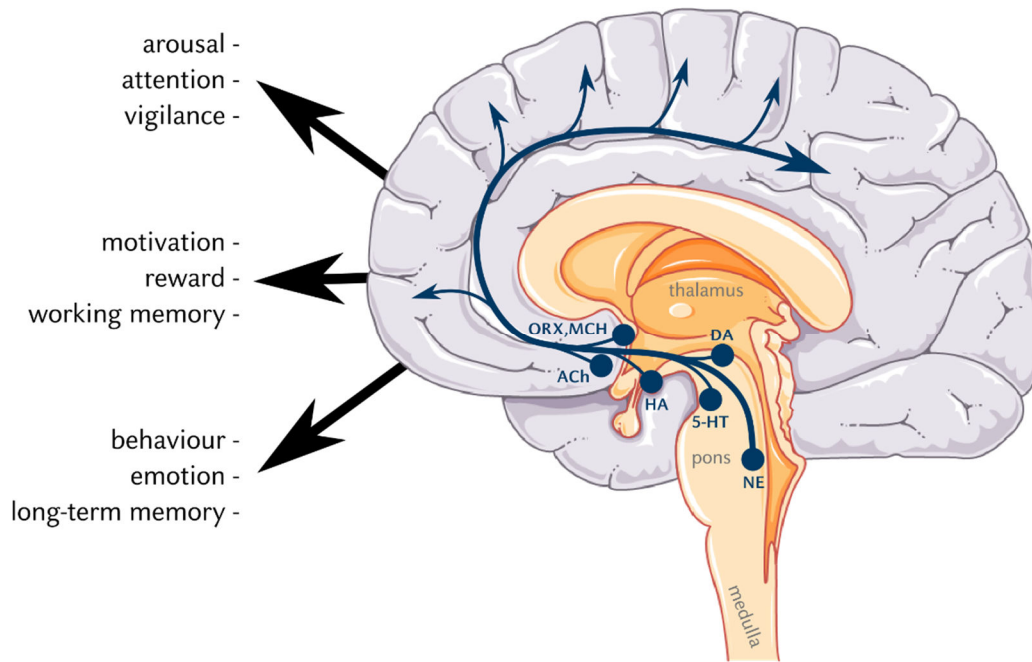


Figure 2. The brain HA system takes up an activator role in the ascending arousal system (AAS, blue arrows). Apart from histaminergic neurons, H₃R acts as a versatile regulator of the co-actors (ACh = acetylcholine, ORX = orexin, MCH = melanin-concentrating hormone, DA = dopamine, 5-HT = serotonin, NE = norepinephrine). Graphics was adopted and modified from (Saper et al., 2005; Wallis, 2019).

both the direct ascending reticular activation system and the bypassing AAS (Poulet et al., 2019). The latter makes use of cholinergic projections from pontine and tegmental nuclei to thalamocortical gatekeeper neurons (Saper et al. 2005, Haas et al. 2008). Within the AAS, the histaminergic neurons from TMN exert direct activation of lateral-, medial- and orbitofrontal cerebral cortex, in concerted action with excitatory input towards other neurotransmitter systems that ascend from the LHA (ORX), basal forebrain (ACh) and formation reticularis, in particular the PAG (DA), Raphe nuclei (5-HT) and LC (NE) (Saper et al., 2005). Apart from such activator circuits in AAS, this system is counteracted by inhibitory GABAergic inputs that emanate from the ventrolateral preoptic nucleus (VLPO) and MCH from LHA (Sherin et al., 1996; Jones et al., 2013). Conclusively, activation of AAS correlates with wakefulness, vigilance, memory, cognition, emotion and reward and motivation while deactivation contributes to wake-promotion (Saper et al., 2005; Sander et al., 2008; Edlow et al., 2012).

None of those neurotransmitters mentioned above contribute to the AAS in a simple, additive manner but rather in a comprehensive network of several fine-tuned circuitries. There, HA plays a central role as an activator for the AAS, as a mediator for the other neurotransmitter systems, but as well as a regulator for the feedback inhibition of neurotransmitter release. Consequently, reductions of HA levels, activity of tuberomammillary HA producing neurons and H₁R blockade are well known to alter arousal, vigilance, attention, cognition and wakefulness (Parmentier et al., 2016).

In more detail, the **orexinergic system** (hypocretin) which consists of two polypeptides (ORX-A/ORX-B) transmit their signals through two GPCRs, the orexin-1 and the orexin-2 receptor (ORX₁R and ORX₂R, respectively)(Gotter et al., 2012). Both receptors couple primarily, but not exclusively, to Gα_{q/11} proteins through which they exert excitatory input (Pandy-Szekeres et al., 2018). It has been demonstrated that orexin-A liberation in the TMN leads to HA release in the frontal cortex as well as ventrolateral preoptic area, which is followed by an ORX₂R-mediated and H₁R-dependent boost in arousal (Huang et al. 2001)(Nishino et al., 2001; Yamanaka et al., 2002). ORX^{-/-} mice have shown both reduced wakefulness and **narcolepsy**, and both can be reversed upon ORX administration (Chemelli et al. 1999). Additionally, overall brain HA levels are reduced under impaired ORX₂R signalling (Nishino et al., 2001). In contrast, it is noteworthy that H₁R knock-out mice show reductions in wakefulness but absence of narcoleptic attacks (Huang et al. 2001). In summary, histaminergic neurons in TMN serve as an interface for excitatory input from orexinergic neurons from the dorsal LHA (De Lecea et al., 1998).

H₃R inverse agonists can effectively increase histaminergic tone and thereby, bypass the missing activating input from orexinergic neurons and increase wakefulness under orexin-deficient conditions (De Lecea et al. 1998, Guo et al. 2009). Moreover, they have emerged to bypass orexin deficiency that commonly occurs in neurodegenerative diseases such as **Alzheimer's disease** (AD) and **PD** (section 1.5) where HA neurons have appeared unaffected from the main degradation process (Shan et al., 2015b).

Once activated, the TMN inhibits sleep-promoting MCH neurons to maintain wakefulness (Parks et al., 2014). HA release in or injection into TMN causes strong suppression of the activity of GABAergic VLPO neurons (Lin et al. 1994, Williams et al. 2014). Vice versa, GABAergic interneurons inhibit ascending histaminergic neurons via GABA_B receptors during sleep induction (Okakura-Mochizuki et al., 1996; Stevens et al., 1999).

The H₃R exercises its **role in cognition, learning & memory** as a modulator of other neurotransmitter levels acting as **heteroreceptors**. Among such neurotransmitters, ACh is of particular interest for its spacious cortical activation that leads to normalisation of impaired cognition as well as facilitated perception, association and attention (Sarter et al., 1997). The cholinergic and histaminergic activity is interdependent (Onodera et al., 1998). In particular, it has been shown that increased activity of histaminergic neurons can functionally antagonise memory deficits induced by the muscarinic cholinergic receptor antagonist scopolamine (Miyazaki et al., 1997; Onodera et al., 1998). Moreover, it has been demonstrated that histaminergic activity is a prerequisite for cholinergic signalling (Munari et al., 2013; Provensi et al., 2016b). As a consequence, H₃R inverse agonists have shown to facilitate cholinergic neurotransmission (Abdul Majeed et al., 2017).

Additionally, it seems likely that H₃R has a direct contribution to the establishment and the consolidation of memory. This assumption is based on their expression as heteroreceptors on glutamatergic neurons in the dentate gyrus that contains relevant neuronal circuits that have been associated with these processes (Brown et al., 1996; Hainmueller et al., 2020). The pro-cognitive effects of H₃R inverse agonists rendered them attractive for application in neurodegenerative disorders and, recently, this strategy was attested effectiveness in paediatric patients suffering from the **Prader–Willi syndrome** which represents a neurogenetic disorder with low prevalence (section 1.5).

From current knowledge, H₃R has only a minor part in the **modulation of striatal DA release** (cf. page 10). However, several studies have raised at least a modulatory participation of H₃R in **neurotransmission of basal ganglia** for a good reason, as more than 85% of striatal D₁R and D₂R-expressing neurons express H₃Rs (Hu et al., 2017). Regarding the **role in the regulation of motor activity**, it has been demonstrated that antagonising H₃R potentiates locomotion upon DA D₁ receptor (D₁R) activation that has been attributed to a shifted signal transduction (cf. page 19).

Moreover, *i.c.v.* injections of HA shows a dynamic and complex impact on motor activity that strongly depends on the administration route and involves an H₁R-mediated increase and an H₂R or (postsynaptic) H₃R mediated decrease in motor activity (Bristow et al. 1988, Chiavegatto et al. 1998). A transient phase of decreased locomotion is followed by a period of increased locomotion that may be explained by differential receptor affinity profiles of HA (section 1.3). Additionally, such effects disappear upon H₁R^{-/-}, H₂R^{-/-} or H₃R^{-/-} or their blockade, emphasising the central dependence of HA in these regulatory circuitries (Huang et al. 2006, Haas et al. 2008).

In some studies, the H₃R inverse agonist **thioperamide** (cf. page 28) showed a slight increase in locomotor activation whereas the compound and several other H₃R inverse agonists failed to do so in other related models (Clapham et al. 1994, Ligneau et al. 2007b). Interestingly, they were able for an effective abrogation of methamphetamine-induced hyperlocomotion (Clapham et al. 1994, Fox et al. 2005, Ligneau et al. 2007b). On a cellular level, it was evidenced that H₃R activation results in inhibited GABA release within SNr, in reduced glutamate release from **corticostriatal glutamatergic neurons**, but not from thalamostriatal ones that are involved in motor symptoms of PD (Molina-Hernández et al., 2001; González-Sepúlveda et al., 2013). Such findings provide several hints for a potential role of H₃R in fine-tuning the deregulated glutamatergic and GABAergic system in basal ganglia in PD.

Additional support has been provided by physiological studies, demonstrating an important role of HA in gating sensorimotor circuitries in the striatum. For example, lacking prepulse inhibition (PPI) was observed H₃R^{-/-} mice but not in H₁R and HDC-deficient mutants (Kononoff Vanhanen et al., 2016). PPI serves as an

in vivo surrogate for **schizophrenia** and has been validated in clinical tests (Braff et al. 1999). In this model, startle behaviour of a subject to two subsequent acoustic signals is measured with a first, soft signal (i.e., the "prepulse") followed by a louder one. In healthy subjects, startling response to the second signal is usually less than in, e.g., schizophrenia patients due to affected sensorimotor gating (Braff et al. 1999). Also, this model draws some evidence for impacted attention and perception associated with schizophrenia. To relate these differential observations, it seems likely that the H₃R mediated effects on locomotion do not rely on the modulation of the striatal dopaminergic system ("motor processor component") but the stimulation of the dopaminergic system in other brain areas such as the prefrontal cortex ("decision making/planning component"). While some roles of H₃R in basal ganglia and on the dopaminergic system in other brain areas have been revealed within the last years, the complete puzzle remains to be solved to evaluate the therapeutic role of H₃R ligands in PD and schizophrenia (section 1.5)(Ellenbroek et al., 2014; Hu et al., 2017).

1.2. Molecular identity of the histamine H₃ receptor

The H₃R belongs to the large class of GPCR, which represents a target class for about one-third of approved drugs (Hauser et al., 2018). Here, the receptor belongs to the subclass of class-A receptors (class-R, according to the GRAFS (glutamate, rhodopsin, adhesion, frizzled/Taste2 and secretin families) scheme (Fredriksson et al., 2003)), which represents the rhodopsin family and encompass olfactory, visual and taste receptors. Besides such receptors, 197 of them have a known ligand and play central roles in humoral function, immunomodulation and neurotransmission (Alexander et al., 2019a). As all GPCR reside as membrane proteins within phospholipid bilayer, elucidation of GPCR structure and signalling was obstructed for a long time and, after the extensive works by Brian Kobilka and Robert Lefkowitz, awarded with the 2012 Nobel prize in chemistry (Kobilka, 2013; Lefkowitz, 2013). Most recently, a receptor of the D₂R in a bio-membrane and interacting with a G protein heterotrimer was disclosed (Yin et al., 2020).

The H₃R receptor has been classified for detecting HA as endogenous transmitter based on findings from classical pharmacological experiments. Meanwhile, attempts to determine the receptor encoding sequence were unsuccessful for a long time. Upon intensive reverse transcriptase, polymerase chain reaction (rtPCR)-based screening with an expressed sequence tag (EST) of the previously known orphan receptor GPCR97 among a size-selected thalamic copy deoxyribose nucleic acid (cDNA) library, a nucleotide sequence encoding for a putative biogenic amine receptor was detected by Lovenberg and co-workers (1999; Bongers et al., 2007), showing low overall sequence similarity to other GPCRs for biogenic amines (20 – 27 %). This receptor sequence is localised on chromosome 20q13.33. Among them, low sequence similarity to H₃R is surprisingly shown by H₁R and H₂R sequences (22 % and 21.4 %, respectively), which was attributed as a reason of previous failure to identify the sequence (Lovenberg et al., 1999; Lovenberg et al., 2000).

Moreover, the low similarity was a reason that the H₃R sequence has been previously introduced as a novel muscarinergic receptor subtype within a patent application, due to higher sequence similarity to M₁R (Goodearl et al., 1999). Highest sequence similarity of 38 – 58 % is shared with H₄R (Sander et al., 2008). Subsequently, they could correlate their pharmacological findings with literature results for H₃R ligands, markedly, the ability of a novel HA receptor to couple Gα_i proteins instead of Gα_q or Gα_s like the H₁R or H₂R, respectively (Lovenberg et al., 1999).

About relevant **receptor isoforms** on early drug discovery stage, the human isoform shows 93.5 % sequence similarity with rH₃R (Ligneau et al., 2000), which rises to 97 % considering the transmembrane (TM) region only (Lovenberg et al., 2000). In turn, the TM region of rH₃R is homologue to the one of mH₃R

(Palczewski et al., 2000). Overall sequence similarity to other species has been determined as > 92 % (Hancock et al., 2003).

Several **splice variants** of the receptor have been identified so far. At least nine different **human H₃R isoforms** (hH₃R) emanating from combinatorial splicing are known, of which two have been characterised in more detail. The predominant isoform consists of 445 aa (hH₃R_{445aa}). In comparison, another functional one lacks 80 aa within the third intracellular loop (**ICL3**, hH₃R_{365aa}), has high brain expression levels (in particular in hippocampus and hypothalamus), shows decreased agonist affinity, but improved functional potency that might be due to a more efficient transducer coupling (Wellendorph et al., 2002). Interestingly, the two introns in H₃R encoding deoxyribose nucleic acid (DNA) sequences are located at positions corresponding to the expressed TMH2 and ICL2. The hH₃R_{365aa} variant with deletions in ICL3 is therefore not a product of exon splicing flanked by two introns but due to intra-exonic in-frame deletions on mRNA-level (Morisset et al. 2001). Recently, the H₃R_{365aa} isoform has been subjected to detailed investigation in recombinant cell lines on the consequences for the signalling behaviour (Riddy et al., 2017). Depending on the observed signalling pathway and in comparison to the hH₃R_{445aa}, it appeared that the hH₃R_{365aa} maintains or increases signalling performance among the G $\alpha_{i/o}$ pathway for agonists while signalling was abrogated among the G $\beta\gamma$ exerted pathway (Riddy et al., 2017). If not stated otherwise within this thesis, the hH₃R refers to the hH₃R_{445aa}.

The sequence of H₃R has enabled first efforts for drawing structural comparisons to resolved receptor structures such as the bovine rhodopsin model that was presented by Palczewski and co-workers in 2000 (Palczewski et al., 2000) and others that have been resolved within the last decade. Most recently, However, as no direct **structural information** is available for the H₃R to date, computational simulations have been widely applied to explain molecular features of the receptor (Schlegel et al., 2005; Axe et al., 2006; Dastmalchi et al., 2008; Roche et al., 2008; Ishikawa et al., 2010).

A spatial representation of the receptor structures is denoted in **Figure 3**. Conserved features within terminal regions of H₃R comprise of a glycosylation site at N11, as well as palmitoylation site at C428 that is believed to facilitate the spatial orientation of helix 8 parallel to the membrane (Qanbar et al., 2003)(Nieto-Alamilla et al. 2016). Additionally, it is supposed that C107 and C188 form a cystine bridge between the extracellular loop (ECL)1 and ECL2 (Tiligada et al., 2009). Structural features within the transmembrane segments have been drawn in analogy to conserved motifs from other GPCRs that is currently the only anchor point for the structural explanation of H₃R. In the rhodopsin receptor model, the conserved "DRY" motif (composed of D/E^{3.49}, R^{3.50}, F/Y^{3.51}) is responsible for keeping the receptor in the inactive state by an ionic interaction between the positively charged R^{3.50} residue and the negatively

charged E^{6.30} residue and is therefore referred to as the "ionic lock" (Rovati et al., 2007). In case of H₃R, this DRY motif consists of a DRF motif (Yao et al., 2003). Molecular dynamics simulations failed to reproduce this feature for H₃R, as the corresponding aa in TMH6 represents the shorter D353^{6.30} (Jończyk et al., 2017; Pandey-Szekeres et al., 2018). Thus, the homology model may give one rationale for the high **constitutive activity** observed for H₃R (Rovati et al., 2007). The "3-7 lock" is located within the upper receptor hemisphere and describes the congregation of TMH3 and TMH7 can be seen in the rhodopsin crystal structure as well (Palczewski et al., 2000). In the case of H₃R, it is represented by D114^{3.32} and W402^{7.42} and is abrogated upon agonist binding (Jończyk et al., 2017). The CWxP motif, which is responsible for the agonist-induced reorganisation of TMHs 3, 5 and 6 during receptor activation ("transmission switch"), is represented by C370^{6.47}, W371^{6.48}, A372^{6.49} and P373^{6.50} (Deupi et al., 2011; Jończyk et al., 2017). However, it is difficult to derive details of the dynamic changes within this region during receptor transition, as this process diverges considerably among different GPCRs (Trzaskowski et al., 2012). The NPVLY motif (N408^{7.49} - Y412^{7.53}, "Y-toggle switch") in TMH7 corresponds to the conserved NPxxY motif (Nieto-Alamilla et al., 2016) that plays a role in receptor interaction with intracellular signal transducers (Galés et al., 2000; Bouley et al., 2003).

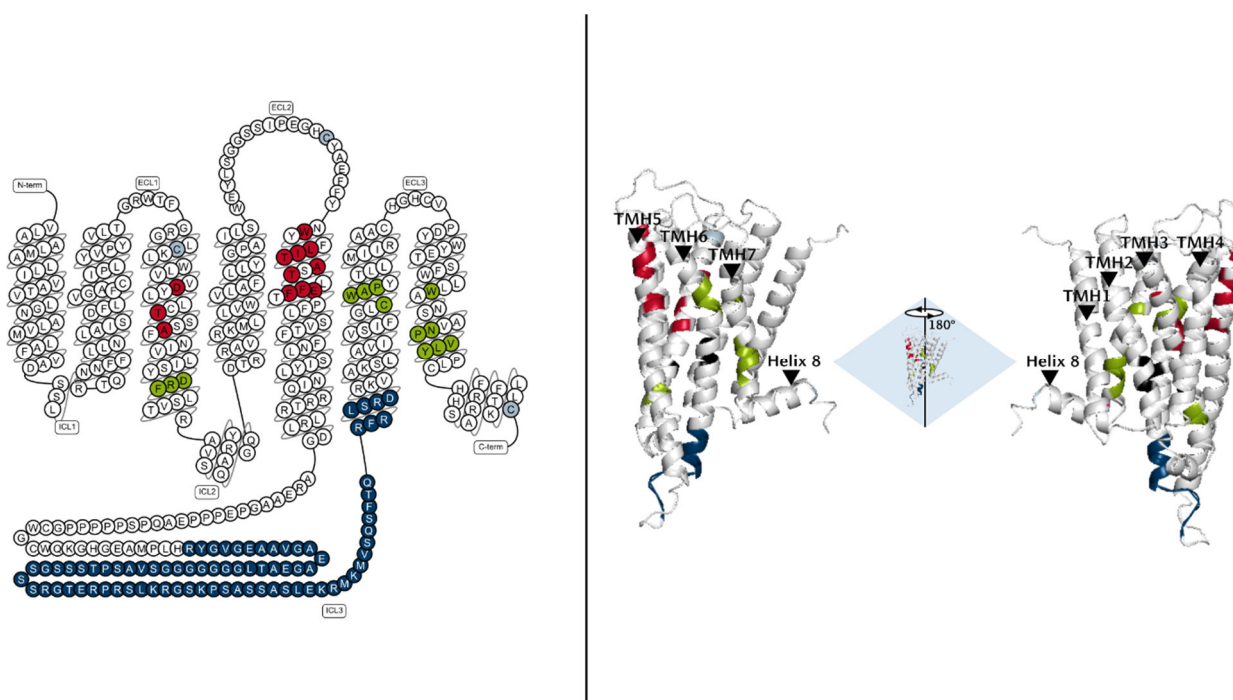


Figure 3. Receptor sequence given as snake-plot (left panel) and as a homology model with truncated ICL 3 (right panel). Light-blue and dark-blue residues denote post-translational modification sites (cystine bridge between TMH3 and ECL2, palmitoylation site in helix 8) and the lacking part in hH₃R_{365aa}, respectively. Residues in green depict conserved motifs which are important in receptor transition. Red highlighted residues are known to be involved in ligand binding, as determined from mutagenesis experiments. Snake-plot and H₃R homology model of the inactive receptor state have been taken from GPCRdb (<https://gpcrdb.org/>, (Pandey-Szekeres et al. 2018)). Data are taken from references, cited within the main text.

ICL3 often handled in its truncated form (i.e., the 413aa H₃R) in *in silico* models as structural homologies to other GPCRs are hard to draw for this region (Figure 3)(Schlegel et al., 2005; Rai et al., 2010). The truncated isoforms did not differ in binding affinities for the H₃R antagonists [¹²⁵I]iodophenpropit, clobenpropit and thioperamide. However, they showed slightly improved affinities for the agonists HA, [³H]NAMH and immpip at the rat receptor isoform (Drutel et al., 2001), whereas not at the human one (Nieto-Alamilla et al., 2018). Additionally, an A280V single-nucleotide polymorphism (SNP) within ICL3 was associated with reduced agonist-exhibited efficacy and reduced **constitutive activity** among the Gα_{i/o} pathway. However, no reduced potency and no overall changes were observed among the Gβγ exhibited one (cf. Figure 1)(Flores-Clemente et al., 2013). These findings imply that the ICL3 is not involved in ligand binding, but can change the transducer coupling and thereby, the potency of agonists. This property was recently supported by two studies demonstrating an agonist-induced conformational change between a YFP-substituted or HaloTag®-substituted ICL3 and C-terminal fused CFP or NanoLuc®, respectively (Liu et al., 2018; Schihada et al., 2020).

Various molecular biological experiments have assisted in elucidating the **binding pocket of H₃R** (Figure 4). Working with h_{1-144aa}/r_{145-445aa}H₃R chimaera have localised the first 144 to be involved in ligand binding (Yao et al., 2003). E206^{5,46} is supposed to interact with positively charged imidazole of HA as indicated by site-directed mutagenesis studies with E206^{5,46}A mutation (Uveges et al., 2002).

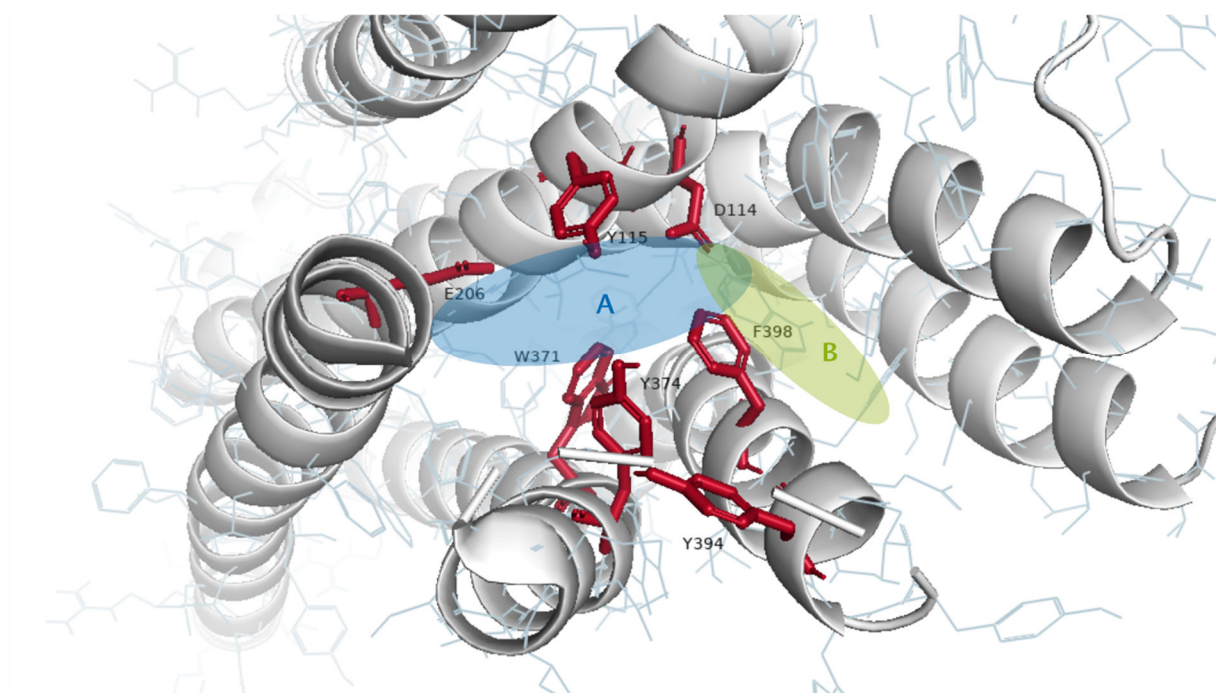


Figure 4. Binding pocket of H₃R with selected aa residues that are involved in ligand interaction (red), and highlighted 'A'-site of the binding pocket (blue) and 'B'-site (green). Modified from (Schaller et al., 2019). Homology model was taken from GPCRdb (<https://gpcrdb.org/>, (Pandy-Szekeres et al. 2018)).

D114^{3,32}, which is conserved among biogenic amine GPCRs, is assumed to interact with the positively charged amino-side chain of HA with resemblance to elucidated binding structures of other monoaminergic GPCRs. Interestingly, most agonists for H₃R possess imidazole as well as a basic side chain and thus, enabling interaction with both acidic amino residues (section 1.3). The H₃R binding pocket sub-divides into two hemispheres, stretching from D114^{3,32} (Levoine et al., 2008). The bulky 'A'-site of approx. 225 Å³ is formed between D114^{3,32} and E206^{5,46}, and a markedly smaller 'B'-site points out from D114^{3,32} towards the opposing side (Levoine et al., 2008). Interestingly, while previously generated models have predicted that agonists can interact with the receptor within both cavities, the same has not been demonstrated for antagonists which seem to always interact with E206^{5,46} within the 'A'-site (Levoine et al., 2008; Jończyk et al., 2017). Further residues within TMH5 involved in ligand binding have been identified by Uveges and co-workers (2002). W196^{5,36}A and T204^{5,44}A mutations have shown a 2 to 5-fold increase in potency of HA, the latter accompanied by an approximately 5-fold reduced affinity. In contrast, L199^{5,39}A and I200^{5,40}A reduced the affinity, with a depression of the maximum inhibitory effect in Gα_s signalling exhibited by HA, an observation that was aligned with the role of K191^{5,40} in H₁R in receptor activation (Uveges et al., 2002). The second-most pronounced affinity loss for the endogenous ligand was observed upon A202^{5,42}Q, causing 20-fold loss in potency due to a repulsive effect of the bulkier glutamine on E206^{5,46} (Uveges et al., 2002). The latter residue has shown the highest impact on HA affinity towards H₃R that almost diminishes upon E206^{5,46}A mutation (affinity loss > 2,000-fold). Conclusively, E206^{5,46} is an important residue for the detection of the endogenous ligand, while other ligands may not involve this residue and thus, not displace HA in a strictly competitive manner.

Additionally, sequence comparisons to **different species** have explicated binding residues for ligand recognition. Among them, the *Rattus norvegicus* isoform has been investigated most comprehensively. The residues A119^{3,37} and V122^{3,40} have been associated with discrepancies in affinity compared to the human isoform, which consists of T119^{3,37} and A122^{3,40} (Ligneau et al., 2000). Interestingly, such discrepancies have not been observed for H₃R agonists, including HA. In contrast, some inverse agonists showed either higher affinity (**ciproxifan**, **thioperamide**) or lower affinity (FUB349) at the rH₃R compared to the hH₃R (Ligneau et al., 2000; Lovenberg et al., 2000; Stark et al., 2001). Such observations enable for comparison with other species that share the same mutations, for which similar pharmacologic results are expectable. Similar to rH₃R, as well the *Mus musculus* isoform shows A119^{3,37} and V122^{3,40}, while the *Cavia porcellus* (guinea pig) isoform shows T119^{3,37} in analogy to the hH₃R.

Further evidence has been made that the H₃R may not mediate its actions as a monomolecular entity, but forming **heteromers with other receptors**, which has been investigated for D₁R, D₂R and A_{2A}R

(Ferrada et al., 2008; Ferrada et al., 2009; Márquez-Gómez et al., 2018). In each of such cases, the result of this interaction has been the inhibition of affinity towards the respective endogenous agonist (HA, DA or adenosine) and consequently, the inhibition of receptor function after activation of the other (Ferrada et al., 2008; Ferrada et al., 2009; Márquez-Gómez et al., 2018). Interestingly, each of such receptor dimers have been detected in striatal neurons, where predominantly postsynaptic expression of H₃R is assumed. Thus, such heteromers suggest a regulatory role and might be of importance to interpret the role of H₃R **in neurotransmission of basal ganglia** (cf. page 13). H₃R heteromers with D₁R have shown preferential coupling to Gα_{i/o} proteins, while D₁R primarily couple to Gα_s and sometimes to Gα_{q/11} (Inoue et al., 2019). Therefore, D₁R can shift the transduction pattern upon heteromerisation with activated H₃R and thereby, eliciting inhibitory instead of excitatory features (Ferrada et al., 2009). Such heteromers do not seem to have relevance *in vitro* only, as less ERK-1/2 phosphorylation in striatonigral GABAergic neurons is seen in D₁R^{-/-} mice (Moreno et al., 2011). Meanwhile, it is assumed that this mechanism requires as well σ₁R which modulate the functions of H₃R-D₁R complex (Moreno et al., 2014), which is an interesting finding as several H₃R ligands share the enigmatic σ₁R as co-target (Riddy et al., 2019).

H₃R shows a high degree of **constitutive activity**, a concept introduced in 1993 by Lefkowitz and co-workers (Lefkowitz et al., 1993; Morisset et al., 2000). This concept describes that a receptor spontaneously adopts active conformation(s) without priorly binding to an agonist. The discovery of this feature could not be observed before receptor cloning, as it is characteristic for overexpressed receptor systems that were introduced into molecular pharmacology after molecular biological techniques have emerged. This property is roughly detectable in native pharmacological systems (Morisset et al., 2000). The behaviour is extensively shown by H₃R along the Gα_{i/o} coupled pathway (**Figure 1**)(Morisset et al., 2000; Rouleau et al., 2002; Ellenbroek et al., 2014). Therefore, the receptor is not only a target for throttling HA release and the release of other neurotransmitters, but inverse agonists can even reverse this activity.

Such findings are in line with the assumption that GPCRs do not act as simple on-off-switches. Meanwhile, this concept has been expanded by the assumption that GPCRs can as well adopt **multiple receptor conformations** (Baker et al., 2007). The model of multiple intermediate states between ligand binding and receptor activation has to be extended by several further intermediates, as the aa framework represents a flexible interactome of partially rigid strands that are linked together. Therefore, a model of sequential replacements of such strands from a completely inactive to a completely active receptor conformation gives rise for multiple intermediates within the ternary complex model (Deupi et al., 2011; Latorraca et al., 2017). Also, this model gives rise to the assumption that potentially each receptor-ligand differentially

impacts the arrangement of this framework. Furthermore, if different ligand affinities would represent such constitutively occurring conformational states, as seen with NAMH coupling to two distinct receptor conformations with different affinity (Witte et al., 2006), it would lead to the hypothesis that differentially targetable fractions of the receptor population will exist.

1.3. Medicinal chemistry of histamine H₃ receptor ligands

From the very beginning of H₃R pharmacology, the characterisation of the receptor was inextricably linked with pharmacological tools as it was a pharmacologically defined target (Hill et al., 1997). Therefore, they not only have importance for therapeutic exploitation of this target due to its versatile central functions (section 1.1). Additionally, they served as tools for revealing essential characteristics of the receptor and its function in the brain.

In the same experiments that led to the discovery of H₃R, the very first **agonists** of the receptor have been detected that mimicked the actions of HA (Arrang et al., 1987a). Likewise to the discovery of many blockbusters, the search for potent H₃R ligands has started with the orientation on a biological sample at hand. This procedure led to detailed insights into structural variations in order to obtain potent and selective H₃R agonists.

Intriguingly, the endogenous ligand HA has a remarkably higher affinity to H₃R than to H₁R and H₂R (**Figure 5**). This observation can be rationalised by the interactions of HA within the receptor binding pocket (**Figure 4**). In contrast to H₁R and H₂R, where the ionisable E206^{5,46} is represented by asparagine or threonine, respectively, the H₃R binding pocket facilitates polar/ionic interactions with the imidazole moiety of HA (Ishikawa et al., 2010). This selectivity profile can be maintained in further methylated HA derivatives. Unfortunately, some H₃R agonists display comparable affinity at the H₄R as the E206^{5,46} residue is conserved between both receptors. Methylation at distinct key positions of HA leads to alterations in this selectivity profile: While methylation of the amino group or an α -methylene group leads to a slight increase in H₃R preference over H₄R, the selectivity profile reverses upon 5-methylation of the imidazole moiety (**Figure 5**). The receptor affinity diminishes upon extensive N^τ methylation that resembles the endogenous HA metabolite in the CNS and has a high affinity towards monoaminoxidase B (Elsworth et al. 1980, Rouleau et al. 1997, Labeeuw et al. 2016).

RAMH is one of the H₃R agonists that have been most extensively studied *in vivo*, representing a chiral, methylated HA derivative (**Table 3**). Azomethine analogues of **RAMH** were developed as prodrugs to overcome the susceptibility for extensive inactivation by HNMT and the subsequently low bioavailability in human species (e.g., **BP2.94**, **Table 3**)(Rouleau et al., 1997).

Extension of side chain has been investigated regarding the influence on H₃R affinity. **Imetit**, **imbutamine**, **immepip** and **methimmepip** maintain a basic moiety, which is shifted by two methylene units from the imidazole moiety compared to HA (**Table 3**). In contrast to **RAMH** and HA, imetit does not serve as a substrate for HNMT (Garbarg et al., 1992). Various structural variations have been undertaken to derive potent and selective agonists. Direct derivatives of HA with increased alkyl linker between the imidazole

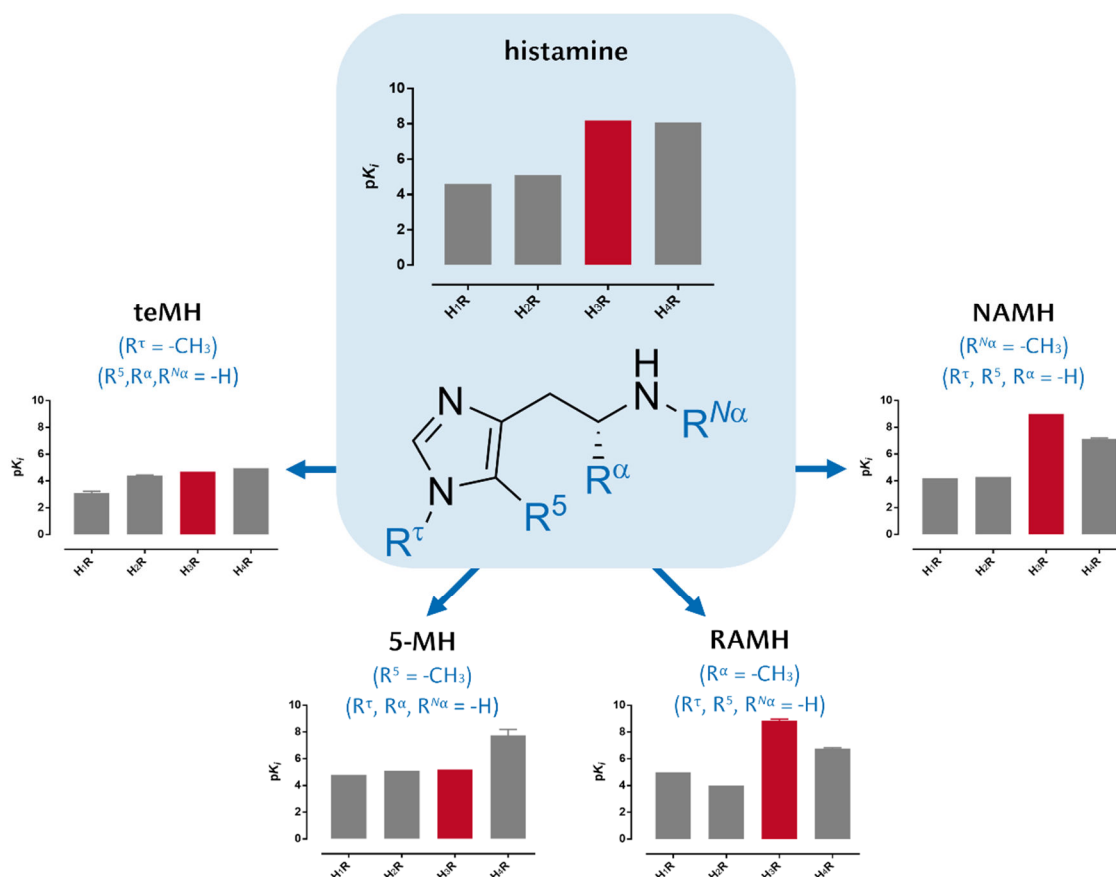


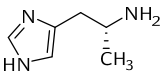
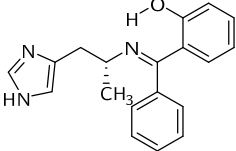
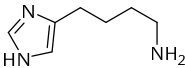
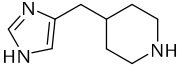
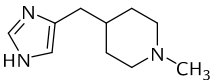
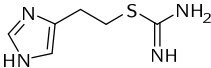
Figure 5. Differential methylation of HA and corresponding affinity profiles at HA receptor subtypes. Data were taken from Panula et al. (2015), Gaulton et al. (2016) and Chazot et al. (2019), except for teMH, which were taken from elsewhere (Driver et al., 1987; Baker, 2009; Labeeuw et al., 2016). Data were stated as means and s.e.m.

Abbreviations: teMH = *N*^τ-methylhistamine, 5-MH = 5-methylhistamine, RAMH = (*R*)- α -methylhistamine, NAMH = *N* ^{α} -methylhistamine.

and primary amine encompass VUF-8326 (n=3), **imbutamine** (n=4), impentamine (n=5) and VUF4732 (n=6, with n depicting the number of methylene units between the imidazole and primary amine).

The propylene and ethylene (i.e., HA) analogues do not distinguish between H₃R and H₄R, both having affinities in low nanomolar concentration ranges (Kitbunnadaj et al., 2003). Upon side chain extension, however, selectivity increases progressively, but accompanied by a loss in their intrinsic efficacy as determined in CRE-driven β -galactosidase reporter gene assays in recombinant H₃R-SK-N-MC cells (Kitbunnadaj et al., 2003). Thus, one could conclude, that the efficiency for stabilisation of the active receptor conformation inversely correlates with the spacer length between the amino moieties interacting with E206^{5,46} and D114^{3,32}. **Immepip** resembles a structurally constrained rotamer of imbutamine that has an 8-fold increased H₃R affinity (Table 3). After the discovery of H₄R, imetit and immepip were re-characterised as potent agonists thereof which revitalised efforts for design of selective H₃R agonists. The latter resulted in **methimmepip** that has a > 2,000-fold selectivity for H₃R over H₄R.

Table 3. H₃R agonists with side chain variations.

	RAMH ➤ hH ₃ R: $K_i = 2.5 \text{ nM}$ ➤ <u>off-targets</u> : hH ₄ R: $K_i = 160 \text{ nM}$ HNMT: $K_M = 3,000 \text{ nM}$
	BP2.94 ➤ hH ₃ R: $EC_{50} = 10 \text{ nM}$
	imbutamine ➤ hH ₃ R: $K_i = 4.1 \text{ nM}$ ➤ <u>off-targets</u> : hH ₄ R: $K_i = 15 \text{ nM}$
	immepip ➤ hH ₃ R: $K_i = 0.5 \text{ nM}$ ➤ <u>off-targets</u> : hH ₄ R: $K_i = 22 \text{ nM}$ hH _{1/2} R: $K_i > 16,000 \text{ nM}$
	methimmemip ➤ hH ₃ R: $K_i = 1.0 \text{ nM}$ ➤ <u>off-targets</u> : hH ₄ R: $K_i = 2,000 \text{ nM}$ hH _{1/2} R: $K_i > 10,000 \text{ nM}$
	imetit ➤ hH ₃ R: $K_i = 0.5 \text{ nM}$ ➤ <u>off-targets</u> : hH ₄ R: $K_i = 3.3 \text{ nM}$ hH _{1/2} R: $K_i > 7,900 \text{ nM}$

References: (Vollinga et al., 1994; Rouleau et al., 1997; Kitbunnadaj et al., 2003; Kitbunnadaj et al., 2005; Panula et al., 2015; Chazot et al., 2019)

Side-directed mutagenesis experiments of H₃R suggest that RAMH, imetit and impentamine show similar receptor interactions like HA. However, these agonists differ in their susceptibility for alterations in receptor binding and activation upon mutation in distinct key positions as studied by Uveges et al. (2002).

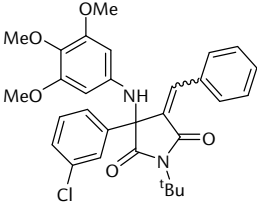
Here, the long-chain analogue impentamine shows only a slight loss in potency and no alterations in G protein coupling upon E206^{5.46}A mutation. On the contrary, this agonist is more sensitive to mutations of F208A and completely diminishes receptor binding upon L199^{5.40}A shift, where the others still excite the receptor in a nanomolar concentration range.

In 2018, putative H₃R agonists with almost no structural resemblance to canonical structures for H₃R ligands were reported, which consisted of either β -lactams or pyrrolidine-2,5-diones and were presented to the scientific community as potent H₃R agonists with selectivity over HA

receptor subtypes and 5-HT_{2c}R (Ghoshal et al., 2018a; b). Compound **6-k** as the lead structure of this project will be subjected for profound pharmacological characterisation within this work as it exerted its action in subnanomolar concentration range and showed promising *in vivo* effects concerning food intake in obese mice. The latter might be beneficial as the previous question whether agonists or inverse agonists of the H₃R are more beneficial in controlling food intake remains a highly debated topic.

VUF16839 was presented as another potent non-imidazole-based agonist. It has potency in subnanomolar concentration range and showed an amnesic effect after i.p. application *in vivo*. However, usage as a pharmacological tool to investigate H₃R function may be limited by two factors (Wágner et al., 2019).

Table 4. Novel non-imidazole agonists.

	6-k ➤ hH ₃ R: $EC_{50} = 0.1 \text{ nM}$
	VUF16839 ➤ hH ₃ R: $K_i = 3.2 \text{ nM}$ ➤ <u>off-targets</u> : hH ₄ R: $K_i = 7.9 \text{ nM}$

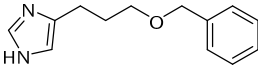
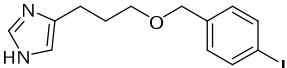
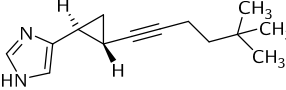
References: (Ghoshal et al., 2018b; a; Wágner et al., 2019)

Due to the aminopyrimidine moiety, the compound shows substantial activity at H₄R as well, and data for blood-brain barrier permeability have not been disclosed yet despite a highly polar structure.

After cloning of H₃R and concomitant expression in recombinant cell lines with different receptor-effector coupling efficiency (i.e., an introduced "system

bias"), systematic re-investigation of previously developed ligands was enabled due to novel opportunities in *in vitro* screening (Gbahou et al., 2003; Krueger et al., 2005; Kenakin et al., 2013). Occasionally, agonist properties have been measured for numerous ligands though they were initially identified as inverse agonists at the same receptor isoform (Krueger et al., 2005). This phenomenon, which was poorly understood in the early 2000s, has been termed '**protean**' (Kenakin, 2001). Meanwhile, the most common terminology for such phenomena encompass the terms "biased agonism/signalling" or "functional selectivity" (Kenakin et al., 2013).

Table 5. H₃R ligands with protean agonist behaviour.

		
proxyfan	iodoproxyfan	cipralisant
hH ₃ R: $K_i = 5.0 \text{ nM}$	hH ₃ R: $K_i = 0.10 \text{ nM}$	hH ₃ R: $K_i = 2.4 \text{ nM}$

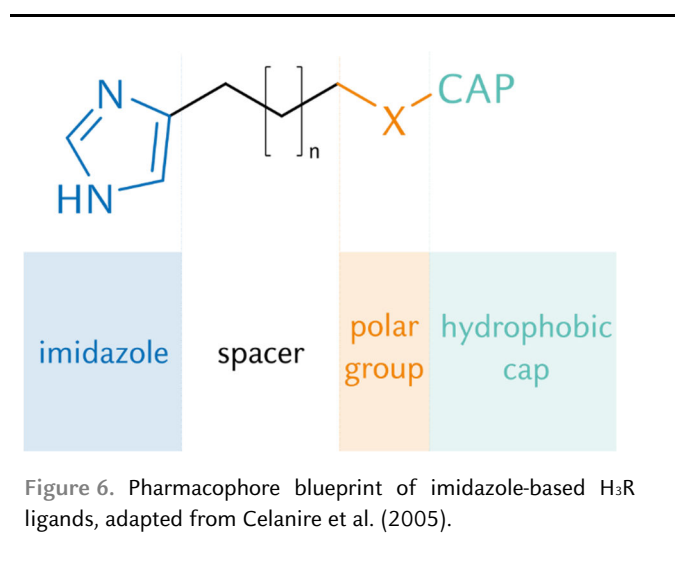
Affinity data were taken from Wulff et al. (2002)

For H₃R and in contrast to other GPCRs, biased signalling could not be subdivided into a G protein-dependent and an independent (e.g., arrestin-mediated) component. So far, all observations for functional selectivity at H₃R have been linked with Gα_i proteins and the corresponding Gβγ subunits (Riddy et al., 2017) and therefore, emphasising **multiple receptor conformations** with different active GPCR conformations (Kenakin, 2001; Krueger et al., 2005). The latter is supported by [¹²⁵I]iodoproxyfan binding

studies to E206^{5,46}A receptor mutants, in which HA completely loses competitiveness, while the receptor affinity of iodoproxyfan remains unaltered (Uveges et al., 2002).

This protean behaviour has been extensively investigated for **proxyfan**, **iodoproxyfan** and **cipralisant** (Table 5), which exert submaximal G $\alpha_{i/o}$ -protein activation in recombinant cell systems but not in rat cerebral cortex membranes. In contrast, a pronounced bias towards G $\beta\gamma$ coupled pathways (GSK-3 β , MAPK, PLA₂) was found for proxyfan and its iodinated analogue, in comparison to G $\alpha_{i/o}$ mediated cAMP-accumulation and to RAMH-induced signalling (Riddy et al., 2017). Moreover, this study evidenced that this behaviour is abolished in the shorter hH₃R_{365aa} isoforms with truncation in **ICL3** (Riddy et al., 2017).

H₃R inverse agonists have been developed as agents to increase the activity of histaminergic neurotransmission by enhanced release of HA and as well to influence the signalling of other neurotransmitters upon enhanced release thereof, mediated by **heteroreceptors** (cf. page 10).

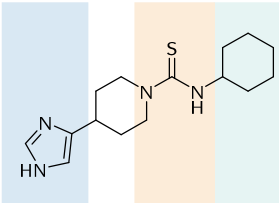
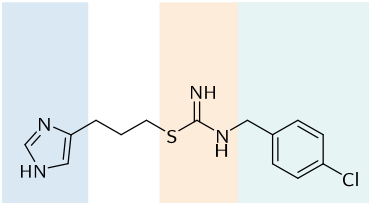
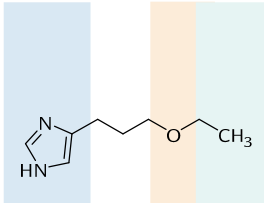


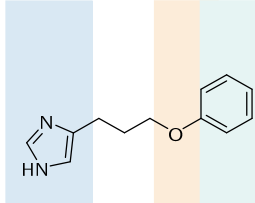
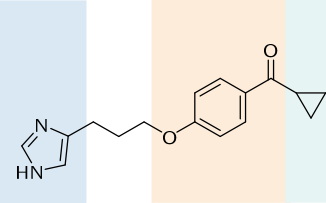
With orientation on the structure of HA, first rationally designed H₃R inverse agonists included an imidazole moiety for which this first-generation is referred to as the class of **imidazole-based ligands** (Figure 6)(Celanire et al., 2005). **Thioperamide** (Table 6) was one of the very first potent H₃R antagonists/inverse agonists and has contributed as a pharmacological tool to many insights into H₃R pharmacology. Clinical

development was, however, hindered due to a marked hepatotoxicity of the compound that has been attributed to the incorporated thiourea moiety, and also poor pharmacokinetic properties such as relevant cytochrome P450 (CYP) inhibition and slow blood-brain barrier (BBB) permeability, associated with the imidazole moiety (Ganellin et al., 1996; Schwartz, 2011). Another standard H₃R ligand with the antagonist or inverse agonist efficacy is given with **clobenpropit**. The development of this ligand had the agonist **imetit** as a starting point for which it serves as a chlorobenzyl-substituted congener. This design strategy led to the working hypothesis that the introduction of a large hydrophobic cap like an aromatic moiety inverses efficacy of H₃R agonists (Celanire et al., 2005). While clobenpropit and thioperamide appeared selective before the early 2000s, both tool compounds must have been re-classified being potent inverse agonists at the H₄R as well, after this receptor was discovered (Table 6).

In analogy to the design strategy of clobenpropit to modify the side chain upon introduction of a

Table 6. Imidazole-based H₃R ligands with antagonist or inverse agonist efficacy.

		
thioperamide	clobenpropit	FUB 465
➤ hH ₃ R: $K_i = 6.5 - 600$ nM	➤ hH ₃ R: $K_i = 0.34 - 3.2$ nM	➤ hH ₃ R: $K_i = 190$ nM
➤ <u>off-targets</u> :	➤ <u>off-targets</u> :	➤ <u>off-targets</u> :
hH ₄ R: $K_i = 9.1$ nM	hH ₄ R: $K_i = 10.5$ nM	hH ₄ R: $K_i = 700$ nM
α_{2A} AR: $K_i = 130$ nM	hH _{1/2} R: $K_i > 3,400$ nM	
α_{2C} AR: $K_i = 320$ nM	$\alpha_{2A/2C}$ AR: $K_i = 160$ nM	
5-HT ₃ R: $K_i = 2,500$ nM	5-HT ₃ R: $K_i = 7.9$ nM	

	
4-(3-(phenoxy)propyl)-1H-imidazole	ciproxifan
➤ hH ₃ R: $K_i = 27$ nM	➤ hH ₃ R: $K_i = 50 - 280$ nM
	➤ <u>off-targets</u> :
	α_{2A} AR: $K_i = 40$ nM
	α_{2C} AR: $K_i = 63$ nM
	5-HT ₃ R: $K_i = 320$ nM
	hH ₄ R: $K_i = 1,900$ nM

References: (Ligneau et al., 2000; Meier et al., 2001; Morisset et al., 2001; Stark et al., 2001; Meier et al., 2002; Esbenshade et al., 2003; Liedtke et al., 2003; Lippert et al., 2004; Mikó et al., 2004; Gbahou et al., 2006; Kottke et al., 2011; Panula et al., 2015; Hagenow et al., 2017; Affini et al., 2018; Chazot et al., 2019)

hydrophobic cap (Figure 6), but now with HA as starting point instead of imetit, pointed out prospects for the development of further antagonists that are devoid of (iso)thiourea moieties (Ganellin et al., 1995).

Consequently, the introduction of a second aryl moiety resulted in numerous potent antagonists/inverse agonists that avoid (iso)thiourea scaffolds and of which some have been exemplified in Table 6.

Introduction of electron-withdrawing groups at the aryl moiety increases the potency (Ganellin et al., 1996; Krause et al., 1998). This strategy has paved the path towards enlargement of the class of potent first-generation H₃R antagonists. Retrospectively, the exact spatial position of the aryl moiety apparently seems to play a role for the susceptibility for protean agonist behaviour (cf. page 26), which was observed for proxyfan and its iodinated analogue but not for others, e.g., ciproxifan or clobenpropit (Krueger et al., 2005).

Unfortunately, clinical investigation of H₃R ligands within the first two decades after H₃R discovery was without successful results, that has been retrospectively attributed to two reasons: First, the

pharmacological characterisation initially relied on models employing H₃R isoforms other than the human one (cf. page 19)(Sander et al., 2008). This issue was resolved after cloning of the hH₃R and facilitated the introduction of hH₃R already in *in vitro* studies. Secondly, the first representatives of H₃R inverse agonists relied on incorporated imidazoles (Table 6). Such scaffolds have higher liability to detrimental pharmacokinetic properties, as imidazoles tend to bind and inhibit isoforms of cytochrome-P450 upon coordination to the hem-iron of such enzymes (Alves-Rodrigues et al., 1996; Davenas et al., 2008). As exemplified above, such imidazole-based ligands often represent substrates of HNMT as degrading enzyme (Rouleau et al., 1997) Furthermore, tolerance to *in vivo* effects after repeated dosage was more often correlated with imidazole-based H₃R ligands than with non-imidazole ones (Guo et al., 2009). Probing for a potential bioisosteric replacement of imidazole by basic alicyclic amines in the late 90's led to a paradigmatic change in the design of H₃R antagonists and inverse agonist (Ganellin et al., 1991; Ganellin et al., 1998; Meier et al., 2001).

Thereby, a new, **second-generation of H₃R ligands** was proclaimed. However, not only disadvantages were associated with the inherent imidazole-motif. The beneficial potency that is attributed to them is

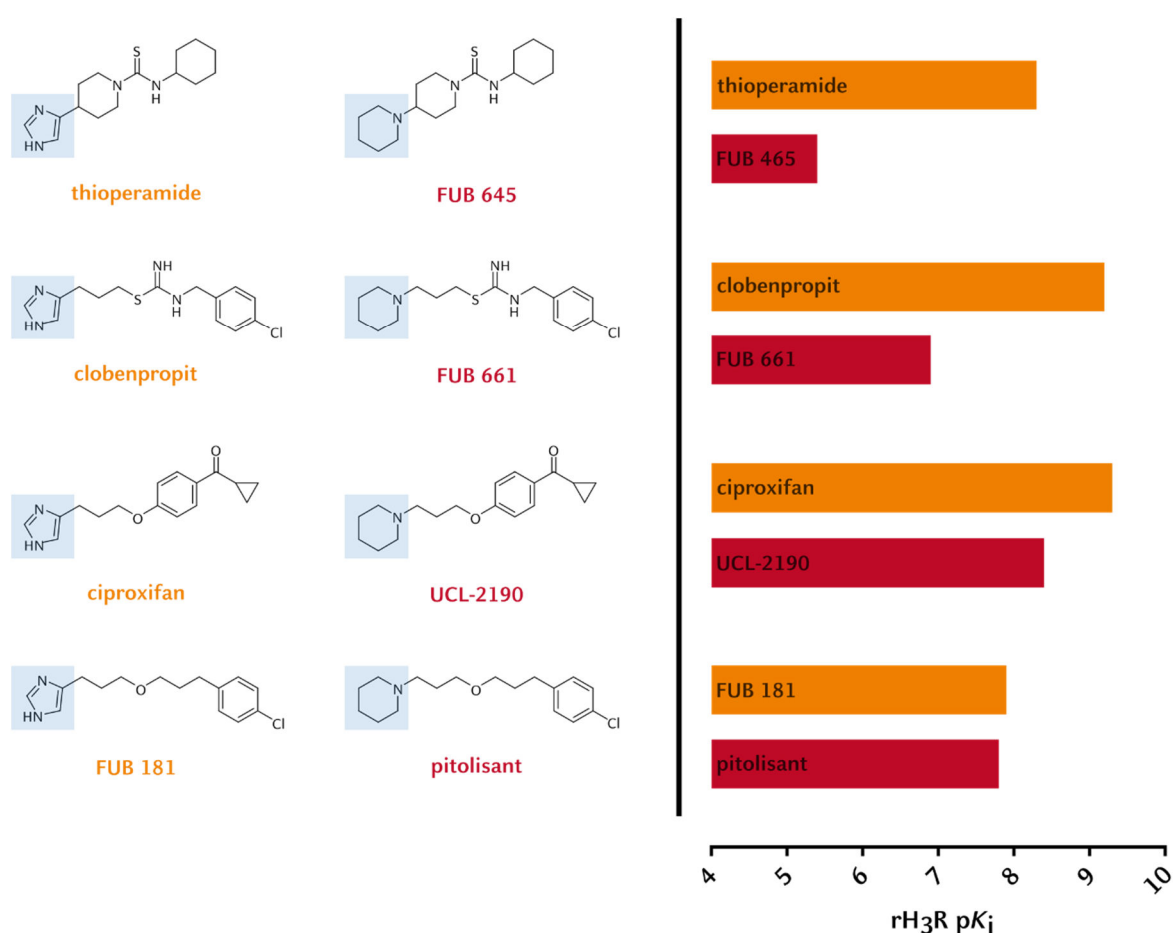


Figure 7. Bioisosteric replacement approach towards non-imidazole H₃R inverse agonists with affinity scales at rH₃R. Data were taken from (Meier et al., 2001; Liedtke et al., 2003).

accompanied by selectivity towards H₁ and H₂ receptor subtypes (Gemkow et al., 2009). Therefore, the imidazole replacement came with new obstacles, as it was accompanied by a significant drop in receptor affinity, which might impact their selectivity profile. This behaviour was shown for **thiopramide** and **clobenpropit** of which the piperidine congeners (FUB 645 and FUB 661, respectively) showed reduced potencies in models of rH₃R in rat cerebral cortex (Figure 7)(Meier et al., 2001; Liedtke et al., 2003).

In the same models, it was demonstrated that the potency of **pitolisant** was considerably less affected compared to its imidazole congener FUB 181 (Figure 7). This observation may be a reason for a good correlation of its preclinical effects *in vivo* and the clinical performance of pitolisant, which was granted with marked approval in the EU and the U.S.A for the treatment of excessive daytime sleepiness in narcoleptic patients with or without cataplexy (Syed, 2016; Kumar et al., 2019). Preclinical characterisation demonstrated lack of off-target interaction among approx. 100 known human targets (Ligneau et al., 2007b). In contrast, pitolisant showed potent inhibition of [¹²⁵I]iodoproxyfan and [³⁵S]GTPγS binding to recombinantly and natively expressed hH₃R, synaptosomal release of [³H]HA mediated by rH₃R, and inhibition of histamine-elicited twitches of isolated guinea pig ileum (Ligneau et al., 2007b). Despite previous reports of hERG binding liability associated with the non-imidazole strategy, this issue was not observed for pitolisant (Levoine et al., 2011; Shah et al., 2016). Consistent with previous results of H₃R inverse agonists, the pharmacological tool showed increased teMH levels in the cerebral cortex as well as in striatum and hypothalamus (Ligneau et al., 2007a). The observed elevated DA turnover in the prefrontal cortex, but unaffected one in striatum, raised the hope for pitolisant and other H₃R agonists as drug candidates against negative symptoms in **schizophrenia** for which effective compounds have been overdue until today (Ligneau et al., 2007a). Previous clinical studies have demonstrated the effectiveness and tolerability of pitolisant in **narcolepsy** compared to placebo, and a non-inferiority to the well-established modafinil (Dauvilliers et al., 2013; Kumar et al., 2019).

Another compound derived from bioisosteric replacement efforts has been **UCL-2190** (Figure 7). Although

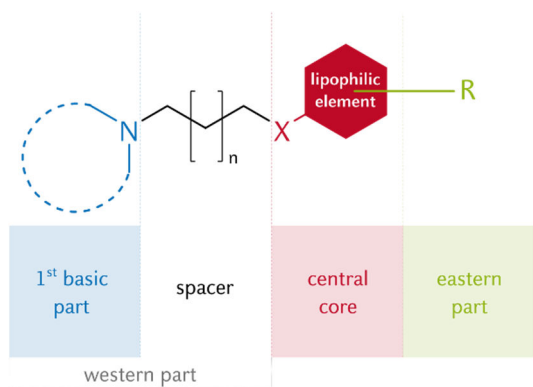
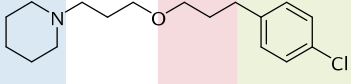
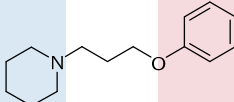
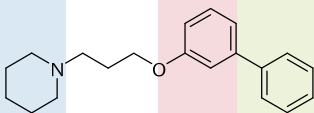
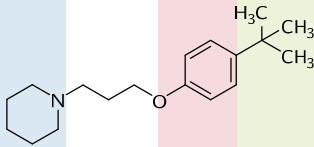
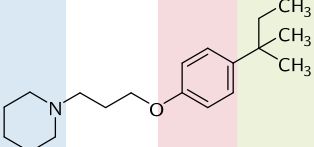


Figure 8. Pharmacophore blueprint of second-generation / non-imidazole H₃R antagonists, modified from (Celanire et al., 2005; Walter et al., 2010).

this compound displayed a slightly decreased affinity at rH₃R compared to **ciproxifan**, this behaviour reverses at the human isoform, where it shows an even increased affinity compared to the imidazole congener **ciproxifan** (Figure 7)(Mikó et al., 2004). However, ciproxifan is still highly rated as a

Table 7. Selected non-imidazole-based ligands, derived from the pharmacophore blueprint (Figure 8).

	pitolisant ➤ hH ₃ R: K_i = 8.7 nM ➤ <u>off-targets</u> : σ ₁ R: K_i = 10 nM hH ₁ R: K_i = 1,700 nM CYP: IC_{50} = 2,600 nM
	1-(3-phenoxypropyl)piperidine ➤ hH ₃ R: K_i = 310 nM
	1-(3-([1,1'-biphenyl]-3-yloxy)propyl)piperidine ➤ hH ₃ R: K_i = 76 nM
	DL76 ➤ hH ₃ R: K_i = 22 nM
	DL77 ➤ hH ₃ R: K_i = 8.4-37 nM ➤ <u>off-targets</u> : hMAO B: K_i = 19 nM

References: (Lazewska et al., 2006; Sander et al., 2010; Panula et al., 2015; Calik, 2017; Łazewska et al., 2017; Lazewska et al., 2018; Riddy et al., 2019)

pharmacological tool for *in vivo* investigations (Hagenow et al., 2017).

Today, most second-generation inverse agonists follow the pharmacophore blueprint depicted in Figure 8 (Celanire et al., 2005; Walter et al., 2010). This guide has led to a plethora of H₃R inverse agonists that have been developed to the present. The most prototypical second-generation ligand is represented by 1-(3-phenoxypropyl)piperidine which consists of a benzene ring as an aromatic core scaffold and shows a more than tenfold reduced receptor affinity compared to its first-generation analogue. As hinted in Table 7, the receptor affinity can be modulated upon modifications within the eastern part of the

molecule, where not only lipophilic residues can be placed as a strategy to a probably entropy-driven affinity increase.

This strategy is inherent in the tert-butyl and tert-pentyl substituted analogues DL76 and DL77, as well as in the biphenyl-derivative 1-(3-([1,1'-biphenyl]-3-yloxy)propyl)piperidine. Besides, polar groups, basic moieties and acidic moieties are tolerated within this region as will be shown in several studies throughout this work (Celanire et al., 2005; Sander et al., 2008; Walter et al., 2010; Ghamari et al., 2019a).

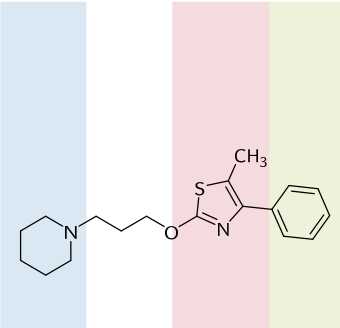
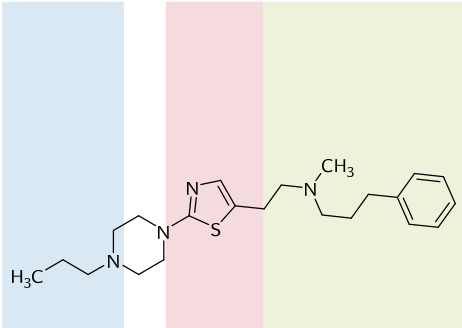
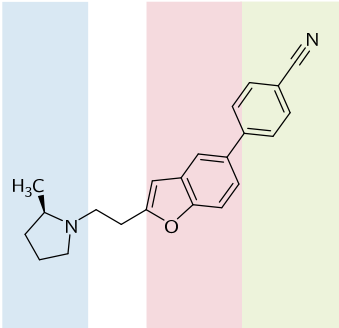
DL76 and DL77 have both already been profiled on preclinical investigation stage. As DL76 belongs to the first H₃R inverse agonists from the second-generation and was presented almost 15 years ago (Lazewska et al., 2006), pharmacokinetic parameters have already been determined (Szymura-Oleksiak et al., 2012; Szafarz et al., 2015). Therefore, this drug candidate has already been applied in *in vivo* model of non-neurogenetic disorders such as vascular dementia and, recently, glaucoma (Stasiak et al., 2011; Lanzi et al.,

2019). Besides, the more recent *tert*-pentyl analogue has shown anticonvulsant and pro-cognitive effects in rats, reduced ethanol intake in conditioned mice and alleviation of deficits associated with a mouse model of **autism-spectrum disorder** (Bahi et al., 2015; Sadek et al., 2016a; Eissa et al., 2018).

In contrast, the prototypic ligand **1-(3-phenoxypropyl)piperidine** and its biphenyl congener have so far only got importance as *in vitro* tool compounds and can be ruled out as promising drug candidates due to their unsubstituted phenyl residues which are prone to extensive metabolism (Sharma et al., 2009).

As the H₃R pharmacophore shows as well tolerability for modifications at the central moiety, one approach towards increased drug-likeness has been the application of heterocyclic cores. This idea is based on the assumption that containing heteroatoms enable specific interactions within binding pockets of targets, and heterocyclic cores show increased metabolic stability and pharmacokinetic properties (Gomtsyan 2012). Another rationale is that a decreased lipophilicity may lead to decreased entropy-driven, unspecific interactions with off-targets and therefore, a reduced risk of toxicity and side-effects (Raymer et al., 2018). Several of H₃R inverse agonists that were designed upon this assumption have been investigated *in vivo* (**ADS-531**) or have already reached out for clinics, such as **ABT-239** (Sadek et al., 2016b; Ghamari et al., 2019a). **ADS-531** represents a 1,3-thiazole-based congener which shows high affinity towards H₃R and selectivity over H₁R. In a recent study, this tool compound was characterised as multitarget-directed agent with combined activity at cholinesterases and revealed pro-cognitive effects in *in vivo* studies (Jończyk et al., 2019). From docking studies, it was elucidated that the thiazole ring facilitates specific interactions with the cholinesterases and therefore, supporting the general hypothesis for employing heterocycles within drug development campaigns.

Table 8. Non-imidazole H₃R inverse agonists with heterocycles as central cores.

		
ST-979	ADS-531	ABT-239
➤ hH ₃ R: $K_i = 41 \text{ nM}$	➤ hH ₃ R: $K_i = 3.2 \text{ nM}$	➤ hH ₃ R: $K_i = 0.45 \text{ nM}$
	➤ <u>off-targets</u> :	➤ <u>off-targets</u> :
	eeAChE: $IC_{50} = 14,000 \text{ nM}$	σ_1 R: $K_i = 6.3 \text{ nM}$
	eqBuChE: $IC_{50} = 15,000 \text{ nM}$	α_{2C} R: $K_i = 63 \text{ nM}$
		α_{2A} R: $K_i = 250 \text{ nM}$
		hH _{1/2/4} R: $K_i > 1,000 \text{ nM}$

References: (Cowart et al., 2004; Frymarkiewicz et al., 2009; Walter et al., 2010; Riddy et al., 2019)

1.4. Progress in molecular pharmacology of histamine H₃ receptor ligands

Given the various implications of H₃R, several pharmacological concepts have emerged and are of current interest to reveal pharmacological secrets of H₃R and to screen and characterise potent H₃R ligands with improved clinical profile.

More than one decade ago, it was suggested that **receptor binding kinetics** might be more relevant in future screening campaigns. The parameter “drug-target residence time” (τ) was postulated as an improved predictor for clinical effectiveness in screening campaigns than affinity measures (only) (Copeland et al., 2006). As introduced by Robert Copeland (2006), this parameter has been defined as

$$\tau = \frac{1}{k_{\text{off}}}, \quad (1)$$

that is proportional to the dissociation half-life, and with k_{off} being the dissociation rate constant for the given drug-target interaction:



where R is the receptor and L ligand that together form the receptor-ligand complex RL . For the dissociation of L from LR under sink conditions, the empiric rate law is defined as

$$-\frac{d[RL]}{dt} = k_{\text{off}} * [RL], \quad (3)$$

that leads to the solution for $[RL]_t$:

$$[RL]_t = [RL]_0 * e^{-k_{\text{off}} * t}. \quad (4)$$

The relationship between affinity and kinetic rate constants is given by

$$K_D = \frac{[L] * [R]}{[LR]} = \frac{k_{\text{off}}}{k_{\text{on}}}, \quad (5)$$

for the equilibration of L with R ,



In equation (5), k_{on} depicts the association rate constant of a ligand according to equation (6). For the latter, the rate for the equilibrium reaction is defined by the reversible, second-order rate equation

$$\frac{d[RL]}{dt} = k_{\text{on}} * [R] * [L] - k_{\text{off}} * [RL]. \quad (7)$$

Substituting experimental conditions $[L] \gg [R]$, so that $[L] \approx [L]_{t=0}$, and $[R]_{t=0} = [R] + [RL]$ into (7), integration and solving for $[RL]_t$ leads to the expression for

$$[RL]_t = [RL]_{t \rightarrow \infty} * (1 - e^{-(k_{\text{on}} * [L]_{t=0} + k_{\text{off}}) * t}). \quad (8)$$

The idea to focus on ligands with slow receptor dissociation rate has been derived from the pharmacological concept of insurmountability, which describes the inability of a ligand to displace from the receptor in an appropriate time and which, in turn, has similar effects as pseudo-irreversibility. It was alleged, τ being a better predictor for drug-effectiveness as it leads to a longer duration of target-occupancy and therefore, to sustained action in the organism (Copeland et al., 2006). This was justified referring to the organism as an open system, where equilibrium conditions do not apply, and therefore, kinetic descriptions may be more suitable to approximate the situation in organisms. Simultaneously, it was justified as a strategy to achieve kinetic selectivity and, conclusively, reducing off-target associated side-effects (Copeland, 2010). However, this claim is far from conclusions and needs more profound investigation, not only at the H₃R (Schuetz et al., 2017). In particular, this idea has been limited for the following reasons:

- Despite the aim of approximating the open system situation *in vivo*, most of the applied models utilise derivations from steady-state kinetics such as the derivations of Colquhoun (1968) and Motulsky & Mahan (1984) for competitive binding kinetics.
- Comparisons between τ and *in vivo* effectiveness are not always feasible as shown for tiotropium that shows a long residence time towards M₃R as well as kinetic selectivity over M₂R (Sykes et al., 2012). On the other hand, it is often not rationalisable, which *in vivo* parameters to correlate with (Folmer, 2018).
- If $t_{1/2, \text{dissociation}} < t_{1/2, \text{elimination}}$, then estimation of τ would be useless, meaning the drug would enable re-association as long as it is not cleared from the organism (Dahl et al., 2013). In this case, persisting drug action would emanate from its pharmacokinetic, not from pharmacodynamic, properties (Sykes et al., 2012). Additionally, $t_{1/2, \text{elimination}}$ is a mostly unknown parameter on the screening stage of drug discovery.
- Ranking based on dissociation kinetics only may be misleading for ligands with similar association rate constants as k_{off} then correlates with K_D , both becoming interchangeable parameters for drug screening (Copeland, 2016; de Witte et al., 2018; Folmer, 2018).

Taking account of the limitations mentioned above, the drug-target residence time concept was expanded by prompting investigation of association kinetics and reflecting τ together with the temporal receptor occupancy (de Witte et al., 2016; 2018). For example, if K_D is similar for two compounds, but they would differ in k_{off} , k_{on} will change consequently. In turn, this will affect receptor occupancy.

Albeit the unsolved question for medicinal chemistry, whether τ serves as a better surrogate for clinical effectiveness of leads, receptor binding kinetics are of general interest in molecular pharmacology. Given

limited approaches for systematic manipulation for k_{on} so far, this parameter plays a subordinate role for a medicinal chemist in lead optimisation (Copeland et al., 2006), while providing hints for the binding mechanism (Sykes et al., 2019). This rate constant consists of several micro-constants, characterising the ‘journey’ of a drug towards its target, such as diffusion towards the target, isomerisation processes, concentration next to and subsequent diffusion into the binding pocket and, maybe, conformational changes that reduce the probability of unbinding (i.e., induced fit). Considering a simple one-step binding mechanism, k_{on} is often limited by the diffusion rate, which is around 10^8 to $10^9 \text{ M}^{-1} \text{ min}^{-1}$ (Copeland et al., 2006).

Radioligand-based **methods** to investigate target binding kinetics have so far been of choice if target manipulation is not desired (Schuetz et al., 2017), with the accompanying disadvantage of low-throughput. The requirement of a labelled ligands puts further limits so far as direct monitoring is desired. Therefore, indirect models have been developed, such as the model of Motulsky & Mahan (1984). This model serves as a mathematical solution for the kinetics of an unlabelled ligand in competition with a labelled ligand, of which the association and dissociation rates are known. As it is derived from the law of mass action and the corresponding rate laws, this model can be described as a temporal resolution of a traditional displacement curve of a three parametric logistic fit (**Figure 9**). Previous efforts towards H₃R binding kinetics have relied on determining ligand binding by NanoBRET sensors attached to the receptor (Mocking et al., 2018), or functional $[\text{Ca}^{2+}]$ -mobilisation assays under hemi-equilibrium conditions (Riddy et al., 2019).

For labelling the receptor, some H₃R agonists and inverse agonists have been designed as radio- and fluorescence-labelled tracers. Working with commonly used and commercially available tracers in binding studies establishes comparability of data within the scientific community. However, working with radiolabelled ligands always puts constraints on the observable space of the targeted receptor and may,

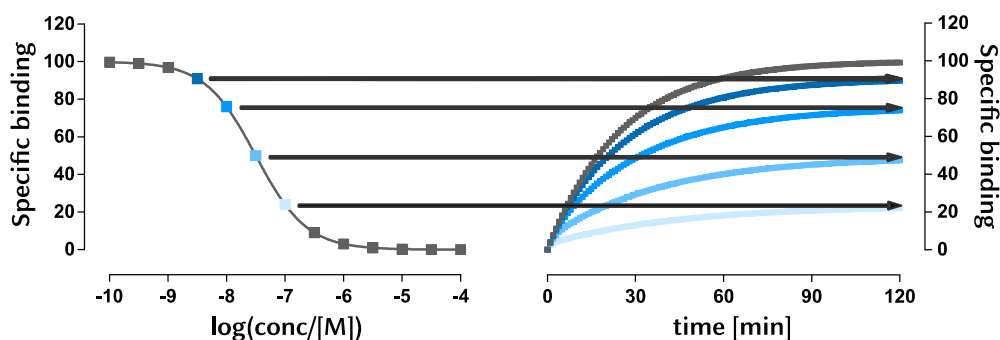
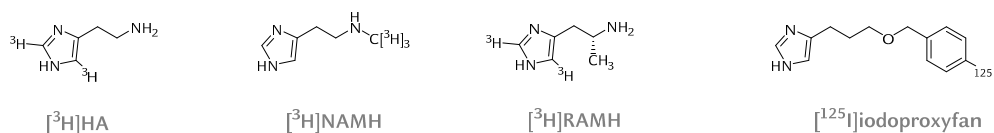


Figure 9. Relation of equilibrium and kinetics of competitive binding, simulated according to the model of Motulsky & Mahan (1984). Simulations were made with data for a labelled ligand ($k_{\text{on}} = 1 \cdot 10^7 \text{ M}^{-1} \text{ min}^{-1}$, $k_{\text{off}} = 0.02 \text{ min}^{-1}$, $K_D = 2 \text{ nM}$ [L] = 2 nM) and unlabelled ligand ($k_{\text{on}} = 1 \cdot 10^7 \text{ M}^{-1} \text{ min}^{-1}$, $k_{\text{off}} = 0.2 \text{ min}^{-1}$).

therefore, hide its essential characteristics (Kenakin, 2010). Radiolabelled tracers with widespread use in H₃R pharmacology are depicted in **Figure 10**. To date, only the presented agonist probes are commercially available for screening purposes even though interesting molecular pharmacological findings have been reported for the antagonist ones. For example, binding to a larger fraction of the receptor population was shown for both [³H]A-349821 and [³H]-thioperamide compared to agonists such as [³H]NAMH or RAMH, as well as they were able to label multiple receptor conformations with distinct affinities (Alves-Rodrigues et al., 1996; Witte et al., 2006). As introduced previously, [¹²⁵I]iodoproxyfan, which has been widely used to characterise H₃R antagonists earlier (Panula et al., 2015), despite its protean agonist behaviour and apparent insensitivity to E206^{5,46} mutation that both indicate different binding modes of this chemical probe (cf. page 18).

Careful choice of a tracer for such heterologous experiments has been suggested as crucial for accurate resolution of receptor kinetics (van der Velden et al., 2020). In particular, selection of agonists may compromise the performance of kinetic experiments due to their marked biphasic binding kinetics (West et al., 1990).

full / protean agonists:



inverse agonists / antagonists:

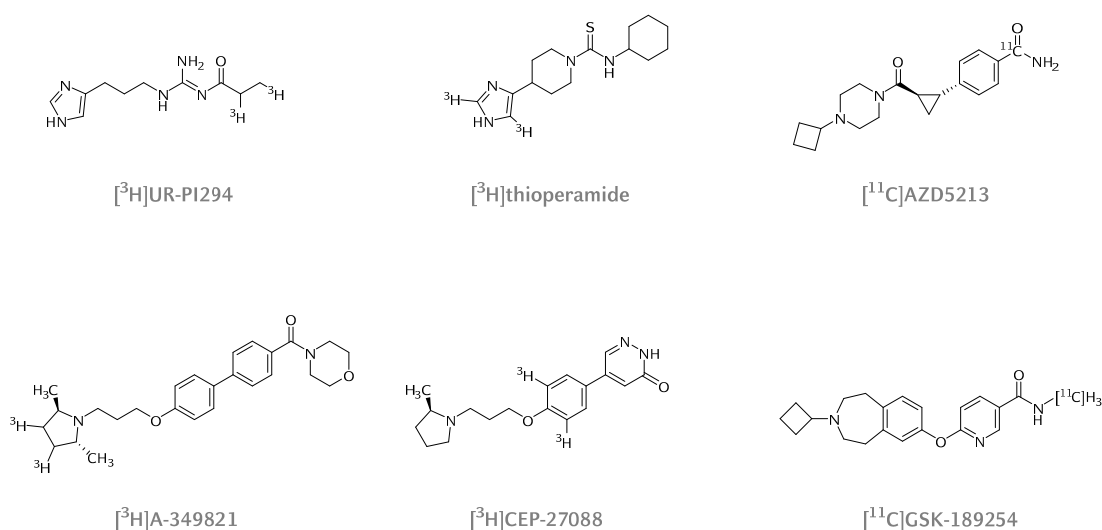
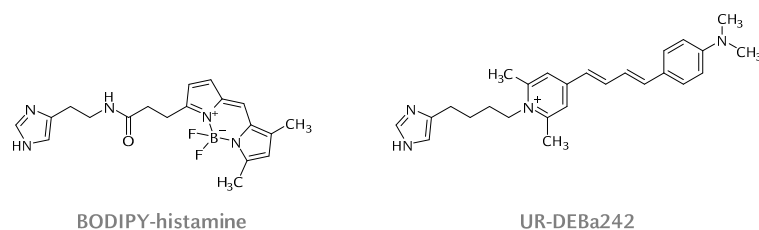


Figure 10. Selected radiolabelled tracers for pharmacological characterisation of H₃R taken from (Arrang et al., 1987a; Alves-Rodrigues et al., 1996; Stark et al., 1996; Hamill et al., 2009; Igel et al., 2009; Andrews et al., 2012; Panula et al., 2015; Dahl et al., 2018).

Fluorescently labelled tracers are of high interest in modern molecular pharmacology due to their wide applicability in fluorescence-imaging and (fluorescence/bioluminescence) resonance energy transfer ((F/B)RET) techniques (Stoddart et al., 2016). Compared to radiolabelled ligands, they reduce the regulatory efforts and safety concerns (Sridharan et al., 2014). However, only a few attempts have been made in the application of fluorescently labelled ligands to elucidate further features of H₃R pharmacology, despite of commercial availability of several potent and selective tools such as mirisant-405 and bodilisant that are depicted in **Figure 11**. In addition to them, a BODIPY-labelled analogue of clobenpropit is commercially available, without disclosed structure but probably belonging to the imidazole-based type (Mocking et al., 2018). Additionally, a BODIPY-labelled histamine analogue shows mediocre binding at H₃R (Mocking et al., 2018). UR-DEBa242 represents the most recently published fluorescent tracer for H₃R (Bartole et al., 2020). However, as BODIPY-histamine and BODIPY-clobenpropit, the novel probe is not selective over other histamine receptor subtypes (Mirzahosseini et al., 2015; Mocking et al., 2018; Bartole et al., 2020). In contrast to the imidazole-based analogues, bodilisant resembles a selective H₃R ligand which is suitable for *ex vivo* receptor staining in tissues (Tomasch et al., 2013). Conclusively, this chemical probe permits novel approaches to H₃R binding behaviour with satisfactory properties for replacing radiolabelled tracers in the molecular pharmacology of the receptor.

imidazole-based fluorescence tracers



non-imidazole-based fluorescence tracers

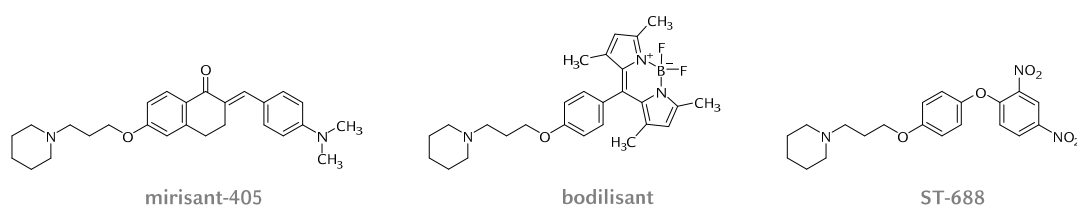


Figure 11. Fluorescence tracers for H₃R, taken from (Amon et al., 2006; Tomasch et al., 2012; Tomasch et al., 2013; Mirzahosseini et al., 2015; Bartole et al., 2020).

1.5. Histamine H₃ receptor ligands in neurogenetic disorders

Many diseases for which H₃R ligands may provide beneficial effects accompany disorders that are linked with alterations on gene expression level. Such diseases termed neurogenetic disorders have been defined as clinical diseases that are based on genetical defects with alterations in “differentiation and function of the neuroectoderm and its derivatives” (Müller et al., 1994). This large group of disorders can be subdivided into four major classes according to their genetic aetiology (Bird, 2009):

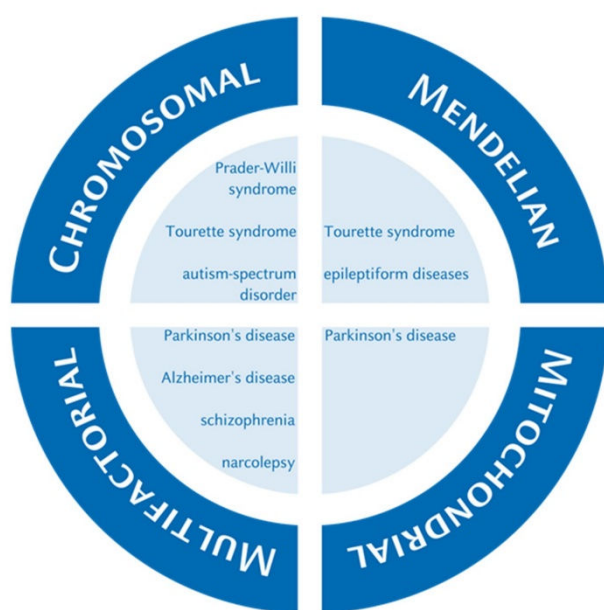


Figure 12. Classification of neurogenetic disorders with selected indications for H₃R ligands, according to literature (Bird, 2009; Ghamari et al., 2019a).

Chromosomal disorders are characterised by chromosomal deletions, inversions, translations and multiplications as well as *de novo* genetic mutations with strong selective pressure. **Mendelian disorders** consist of an inheritable component due to genetic mutations or copy-number variations. **Mitochondrially** denoted neurogenetic diseases show deficits in electron transport chain components and are as well inheritable, either maternally from mitochondrial DNA or autosomal from nuclear DNA. A fourth group encompass diseases which combine genetic disposition (polygenic) with environmental factors (**multifactorial**) and, thus, represent diseases of heterogenous aetiology, which

usually manifests after infancy (Müller et al., 1994; Bird, 2009). Various neurogenetic diseases where histamine H₃ receptor ligands have been under clinical evaluation are depicted within this classification in **Figure 12**. Of such, relevant conditions for this work are elaborated below in more detail.

Neurogenetic disorders often share **co-morbidities** of other mental diseases. Vice versa, candidate genes for several disorders often overlap with such for others, as seen from recent genome-wide association studies (GWAS). Such shared co-morbidities encompass

- intellectual disability,
- behavioural conspicuousness,
- impacted attention and perception (Ornitz, 1969),
- sleep disorders (Dosier et al., 2017),

- schizophrenia, 1 in 100-200 individuals with schizophrenia are linked with 22q11.2 deletion syndrome (Gur et al., 2017),
- autism-spectrum disorders (American Psychiatric Association, 2013a) and
- compulsive-obsessive disorders (Grove et al., 2019).

Additionally, many syndromes belonging to mental disorders show remarkable inheritability, although the molecular genetic nature is in most cases as elusive as the neuropathology. However, major advances have been made within the last two decades upon increasing cohorts of GWAS that allow for correlation with rare genetic variants (Hirschhorn et al., 2005). In all neurogenetic diseases, alterations on genomic level lead to alterations in distinct neuron populations and therefore, in different neurotransmitter systems. Two central theories have evolved to explain how ubiquitous genetic alterations can impact the function and even degeneration of specific cell-types: The theory of **selective vulnerability** rationalises that variances in a broadly/ubiquitously expressed gene makes one specific cell-type vulnerable (Fu et al., 2018). In contrast, that of **selective expression** describes a defect cell-type as consequence of perturbed gene expression that is usually expressed from this one cell-type only.

The sleep disorder **narcolepsy** is characterised by severe daytime sleepiness during phases where vigilance is required, and REM sleep during the wake period, despite adequate sleep during the night (Scammell, 2015). The disorder can be accompanied by cataplectic attacks which are characterised by sudden loss of muscular tone. According to the aetiology, narcolepsy is classified as type 1 that is characterised by loss of ORX-A or ORX-B and as an idiopathic type 2 (Scammell, 2015). It has been hypothesised that the loss of orexin producing neurons is linked to an autoimmune mechanism as a specific human leukocyte antigene (HLA) expression pattern has been associated with 95 % of the cases (HLA class II allele: HLA-DQB1*0602) (Mignot et al., 1997). However, previous descriptions of an infantile case of narcolepsy has been attributed to a *de novo* non-functional L16A mutation in the signal domain of the ORX precursor prepro-orexin (Peyron et al., 2000; Kornum et al., 2017). Given the multifactorial explanation of pathogenesis, the disorder is classified as a disorder of multifactorial genesis (**Figure 12**)(Yamasaki et al., 2016). The neuronal circuits of orexigenic neurons are directly linked to the pharmacotherapeutic strategy for H₃R ligands. Their application aim to compensate the missing orexinergic excitatory input to TMN histaminergic neurons by H₃ auto- and **heteroreceptors**. Thus, **pitolisant** has been granted market authorisation by the U.S. Food and Drug Administration (FDA, 2016) and the European Medicines Agency (EMA, 2019) while some other H₃R inverse agonists are on clinical development state (Syed, 2016; Ghamari et al., 2019a; Kumar et al., 2019).

Schizophrenia is a psychiatric syndrome characterised by episodic (> 1 months) hallucinations, delusions or disorganised speech, while each of such symptoms presents in complex forms and can appear in combination with each other (American Psychiatric Association, 2013d). During and in between of such episodes, patients appear as well with negative symptoms such as social withdrawal, cognitive impairments, lacking motivation as well as deficits in executive function and memory (McCutcheon et al., 2020). The still supported molecular pathological theory focussing on imbalanced dopaminergic, and subsequent glutamatergic and GABAergic neurotransmission, relies on the consistency with clinical effects of applied D₂R/D₃R antagonists (Lau et al., 2013). However, only the hypothesis of GABAergic hypofunction remains irrefutable up to post-mortem analysis (Birnbaum et al., 2017). The difficulties in the alignment of results from *in vivo* and post-mortem studies is mostly due to that examined tissues have persisted in pathological environment for up to several decades and may have undergone compensatory mechanisms (Birnbaum et al., 2017). Typically, the disease manifests in early maturity and has a long-since known inheritable component (Kallmann, 1938), which is estimated to be about 80 % (Cardno et al., 2000). Theories for attributing positive and negative symptoms to specific alterations in specific neuronal circuits dominate current discussion as well for the molecular genetic trigger. Despite remarkable inheritability and several identified candidate genes from genome-wide association studies (GWASs) (Hirschhorn et al., 2005), unambiguous ramifications with the aetiology of schizophrenia remains impossible as long as comprehensive pathophysiological explanations are overdue (Birnbaum et al., 2017). Thus, and due to non-excludable environmental factors contributing to schizophrenia, the disorder is best classified as of multi-factorial and polygenic origin, as done in **Figure 12**. Relying on the dopaminergic hypothesis, which is based in dopaminergic hyperactivity in the mesolimbic system but as well in caudate nucleus, H₃R inverse agonists have emerged as potential treatment of schizophrenia. Even if an effect of H₃R inverse agonists on psychosis is without evidence, they emerged due to their pro-cognitive properties and their ability to ameliorate glutamatergic hypoactivity seen in basal ganglia of many patients. The latter is a feature of H₃R inverse agonists that D₂R antagonists do not exert (Faucard et al., 2006; Moghaddam et al., 2012; Ellenbroek et al., 2014).

Gilles de la Tourette syndrome (GTS) is a disease belonging to tic disorders with involuntary, stereotyped motoric and vocal movements. It has an unknown genetic cause but a strong heritable component (Albin et al., 2006). However, some accordance with chromosomal translocations and genetic polymorphisms with impacts on neuronal growth and dopaminergic neurotransmission was found (O'Rourke et al., 2009). So far, mainly D₂R and D₃R antagonists have been used in the pharmacotherapy of GTS (Thomas et al., 2013). The linkage to H₃R in the disease is attributed to its role in basal ganglia,

where increased inhibitory striatonigral and striatopallidal input leads to insufficient curbing of motoric events (Albin et al., 2006; Rapanelli et al., 2016). From a genetic perspective, interestingly, an association to histaminergic neurotransmission seems likely for frequently observed SNP on the *hdc* gene on chromosome 15q21.2 (Karagiannidis et al., 2013; Udvardi et al., 2013). Interestingly, upregulated H₃R expression in striatum was reported for HDC^{-/-} mice (Pittenger, 2020) as well as affected gene expression in H₁R and H₂R signalling pathways (Fernandez et al., 2012). Finally, promising effects from a phase II clinical trial in GTS patients have been reported for the H₃R inverse agonist AZD5213 (Rizzo et al., 2019). However, no follow-up has been communicated so far. Common co-morbidities with GTS are attention-deficit disorders, for which H₃R inverse agonists have been investigated clinically (Ghamari et al., 2019a), as well as compulsive-obsessive disorders which are shown by 52-75 % of GTS patients (McDougle et al., 1993).

Alzheimer's disease (AD) belongs to the neurodegenerative disorders and represents a dementia syndrome, characterised by a loss of acetylcholine producing neurons. It is either diagnosed upon a decline in memory and learning, with a steadily progressive decline in cognitive functions, which is without transient stagnation and other cause (e.g., cerebrovascular events), or upon familial history associated with causative genetic basis (American Psychiatric Association, 2013b). In 2016, this disease affected around 43 Mio people globally, which was more than twice as much as in 1990, and this number is expected to double within another 15 years (Nichols et al., 2019). With about 2.4 Mio deaths within that year, AD became the fifth leading death cause in 2016 (Nichols et al., 2019). Slightly more women (1.17-fold, after standardisation for generally longer lifetime of women) suffered from the disease compared to men (Nichols et al., 2019). While most of the AD patients become symptomatic above the age of 65, it does not preclude events of earlier onset (Tellechea et al., 2018). Overall, a disease heritability of 80 % have been estimated while environmental factors contribute to the aetiology. Thus, AD also belongs to polygenic/multifactorial neurogenetic disorders (**Figure 12**)(Bettens et al., 2013; Van Cauwenberghe et al., 2016).

Progress has been made in delineating genetic predisposition of AD, which has found to attribute to 5-10 % of early-onset AD cases and show high degrees of inheritability (Van Cauwenberghe et al., 2016). Such approaches have focussed on neurotoxic β -amyloid plaques presented in the pathophysiology. First, autosomal-dominant mutations in genes encoding for amyloid precursor protein (APP, gene-locus 21q21.3) were ascribed responsible for driving the formation of the fibril precursor β -amyloid fragment, aa sequence 1-42 ($A\beta_{1-42}$)(Van Cauwenberghe et al., 2016). Secondly, mutations in components of the γ -secretase complex, which is responsible for $A\beta_{1-42}$ cleavage (presenilin 1 and 2, loci 14q24.2 and 1q42.13,

respectively), were correlated with several cases (Van Cauwenberghe et al., 2016). Thirdly, the high-density lipoprotein component apolipoprotein-E (ApoE), which has been found present in amyloid plaques, appears in different isoforms from allelic variants (ϵ 2, ϵ 3, ϵ 4) on locus 19q13.32, of which ϵ 3 is most common (Weisgraber et al., 1996). However, ϵ 4 has been associated with increased susceptibility for AD with a positive correlation to ϵ 4-concentration (Corder et al., 1993). At the age of 85, the ϵ 4-allele accounts for an increased lifetime risk (LTR) for AD in heterozygous carriers of the ϵ 4-allele (female: LTR = 30 %, male: LTR = 23 %) which duplicates again for homozygous ones (female: LTR = 60 %, male: LTR = 51 %), compared to people with homozygous ϵ 3-allele (female: LTR = 14 %, male: LTR = 11 %). By contrast, a protective value was attributed to the second isoform (ϵ 2) (Corder et al., 1994). A large GWAS among approx. 74,000 individuals was conducted and resulted in several loci, of which SNPs could be correlated with late-onset of AD (Lambert et al., 2013). Further GWASs revealed further genetic polymorphisms in the context of AD, and raised implications for intracellular deposited hyperphosphorylated tau protein-aggregates which represents another neurotoxic process in AD (Van Cauwenberghe et al., 2016).

AD has been associated with decreased activities of HA and ACh synthesising enzymes (HDC and choline acetyltransferase, respectively) that contributes to the overall cholinergic deficits in patients (Schneider et al., 1997). In addition to reductions in norepinephrine, 5-HT and DA brain levels as a result of a progredient global neurodegeneration, the orexinergic system has evolved as putative co-actor as it triggers generation of amyloid plaques in AD (Wang et al., 2018). H₃R ligands are clinically examined for their symptomatic approach to AD due to their **role in cognition, learning & memory**, such as GSK-239512 and AZD5213 (cf. **Figure 13**)(Nathan et al., 2013; Ghamari et al., 2019a).

After AD, **Parkinson's disease (PD)** represents the second-most prevalent neurodegenerative disorder with 6.1 Mio persons affected in 2016. Similar to AD, this number has doubled from 1990 and is assumed to double once again until 2040 as a result of higher life expectancy (Dorsey et al., 2018; Rocca, 2018). Also, this disease has an onset after the 50th year of age, but, in contrast to AD, affects 1.4 times more males than females. PD is a clinical diagnosis made upon loss of motoric movement (bradykinesia) with rest tremor, lead-pipe rigidity and assessment of selective or supportive criteria (such as response to levodopa or olfactory loss) (Kalia et al., 2016). Patients suffering from PD can show neurocognitive decline, anxiety, depressive and sleep-wake disorders during the progression of the disease (American Psychiatric Association, 2013c). Hence, **pitolisant** as well as **bavisant** (cf. **Figure 13**) were examined in phase 3 and phase 2 clinical trials concerning excessive daytime sleepiness (EDS) in PD (clinicaltrials.gov identifiers: NCT01066442, NCT01036139 and NCT03194217)(Ghamari et al., 2019a). Based on a case series, marked changes in the Epworth sleepiness scale-score were reported for which the community waits for

the pending results from the interventional study (Liguori et al., 2020). From the neuropathologic point of view, PD is based on the degeneration of dopaminergic neurons in SN well before the onset of symptoms, which has decoupling of motoric regulation between frontal motor-cortex, subthalamus and basal ganglia as common consequence (Poewe et al., 2017). On a molecular level, the detection of intraneuronal oligomeric aggregates consisting of α -synuclein (SNCA), ubiquitin and other protein filaments (termed “Lewy bodies”) have been found as neurotoxic agent (Poewe et al., 2017). Recent progress on a molecular level has pointed towards a prion-like behaviour due to an apparent transferability of SNCA aggregates between different neurons, the ability of such aggregates to recruit additional SNCA in unaffected cells, and the potential of SNCA aggregates to cross the BBB (Kalia et al., 2015). However, the point of origin of the aggregation process is elusive in most of the PD cases, despite some cases of genetically determined forms (Blauwendraat et al., 2020). Furthermore, a potentially environmental intake of SNCA aggregates which trigger the pathophysiological process is under current discussion (Scialò et al., 2020).

More than 20 rare variants are known to predispose PD, and despite the increasing assumption of a genetic background for most cases, not all of the rare variants are unambiguously associated with the disease; still, larger cohorts with more rare or very rare variants in GWAS are needed to complete evidence (Blauwendraat et al., 2020). Prominent examples with reasonable relation to PD include autosomal-recessively inherited parkin (PRKN/PARK2, gene-locus: 6q26), PTEN-induced kinase (PINK/PARK6, gene-locus: 1p36) and DJ-1 (PARK7, locus: 1p36.23), all of which being essential for adequate mitochondrial function, for which genetic alterations can cause early-onset PD (Canet-Avilés et al., 2004; Valente, 2004). Besides such mitochondrial diseases, prominent monogenic variants are found for the lysosomal leucine-rich repeat kinase 2 (LRRK2/PARK8, locus: 12p11.2-q13.1) and SNCA encoding genes with autosomal-dominant inheritance and with either late- or early-onset characteristics, respectively (Deng et al., 2018).

Autism-spectrum disorder (ASD) is defined by deficits in social interaction, in communication to a verbal and non-verbal extent, and includes restriction or repetition in behaviour and motoric movements, all with typical onset in infancy (American Psychiatric Association, 2013a). It is a heterogeneous disease spectrum, based on the clinical appearance between several patients but as well on intra-individual differences in autistic behaviour throughout development, and it frequently occurs with a cognitive component (Lord et al., 2000). While a genetic cause of ASD seems confirmed based on correlations between twin pairs suffering from the disorder (Lichtenstein et al., 2010; Hallmayer, 2011), no pertinent link to one specific genetic aberration could be drawn yet. For example, ASD has been associated with partial tetrasomy on chromosome 15q11-13, together with various other chromosomal aberrations in some individuals (Gillberg, 1998). Conversely, *de novo* events have been put as a cause in the last years based

on the observation that ASD is often accompanied by fertility and, thus, genetic marks being mostly noninheritable (Castellani et al., 2020). Such missense and nonsense variants are found approximately in half (46.3 %) of the patients (Neale et al., 2012). Recently, some correlations between missense variants and ASD could be made in a whole-exome association study among approx. 12,000 patients, in which gain-of-function mutations were described, e.g., in the *kcnq3* gene for K_v7.3 channel or *scn1a* gene for Na_v1.1. The first finding is an intriguing one as HA, through H₁Rs, can decrease the activity of K_v7-type channels (Obara et al., 2020). Besides possibly direct links between ASD and the brain HA system, recent findings point towards decreased acetylcholine levels in mouse models with autism-like characteristics (Karvat et al., 2014). Therefore, this may be a hint for the molecular action of the H₃R inverse agonist **DL77** that provided promising effects in previous *in vivo* studies with ASD mice (Eissa et al., 2018). A direct effect of DL77 on H₁R cannot be precluded as the compound appeared selective towards H₃R but still with remarkable activity at H₁R in submicromolar concentration range (Eissa et al., 2018). Nevertheless, application of H₃R inverse agonists for the treatment of ASD represents an indication on preclinical investigation stage (Ghamari et al., 2019a).

Compared to other genetic disorders introduced above, **Prader–Willi syndrome (PWS)** represents a neurogenetic disorder with well-characterised genetic determinism which is long-since known and, thus, forms part of diagnosis (Buiting, 2010; Beygo et al., 2019). In more detail, PWS is an imprinting disorder that is caused by a loss of genes from paternal chromosome 15q11.2-13 by either *de novo* deletion, uniparental disomy, microdeletions or imprinting defects. Additionally, the corresponding genes on the maternal chromosome are epigenetically silenced under physiological conditions (Beygo et al., 2019). Within this imprinted domain, several genes encoding for proteins and small nucleolar RNA (snoRNA) clusters (SNORD) are located, the latter being involved in RNA editing processes (Mehler, 2008; Beygo et al., 2019). While the unique lack of several proteins (MKRN3, MAGEL2, NDN) have demonstrated not to induce PWS in full extent (Kanber et al., 2008), lacking the protein SNURF-SNRPN and SNORD116 cluster is strongly correlated with the full phenotype. However, no functional role thereof is known to date (Bieth et al., 2015; Beygo et al., 2019).

Langdon Down made the earliest known documentation of a PWS patient in 1864, but Andrea Prader, Alexis Labhart and Heinrich Willi provided a detailed clinical description about 90 years later (Prader et al., 1956; Ward, 1997). The disorder is in its initial prenatal and infantile stage characterised by markedly reduced muscular tone, leading to reduced foetal movements. After birth, complications in feeding and metabolism leads to a predisposition for increased mortality due to decreased energy intake and aspiration risk (Holm et al., 1993). Following normalisation of this hypotonia, which has an onset between the second

and mandatorily, before the sixth year of age, the situation reverses with weight gain and hyperphagia accompanied by delayed development, which leads to a reduced foetal movement (Cassidy, 1997; Cassidy et al., 2009). Mortality during adulthood is increased due to the occurrence of metabolic disorders, without accounting for an additional risk component due to mild intellectual disability (Einfeld et al., 2006). Besides, additional behavioural characteristics of PWS patients can be compulsivity, obsessiveness, manipulative and argumentative behaviour and problems with changes in daily routine (Cassidy et al., 2012).

Similar to other neurogenetic disorders, PWS shares many facultative co-morbidities such as sleep disorders/EDS, cognitive deficits, autism, attention-deficit/hyperactivity disorder and psychosis (Cassidy et al., 2012) for which H₃R inverse agonists have emerged as pharmacotherapeutic option. Interestingly, the long-since known betahistidine emerged as a potential drug for PWS with market-approval for more than 50 years (cf. Figure 13). While it has been tried to exploit its H₃R antagonist and H₁R (partial) agonist mode of actions on improved vestibulocochlear blood flow in preclinical studies, these effects have not been sufficiently evidenced in clinics yet as elaborated by the Cochrane collaboration (Murdin et al., 2016). These drawbacks and the low interest in betahistidine as combined H₁R (partial) agonist / H₃R antagonist are for one thing attributed to its low potency at H₁R but, maybe more relevant, to its poor bioavailability and BBB permeability. To overcome these obstacles, an intranasal formulation of this drug was developed and subjected to clinical trials. Recently, it was granted an orphan drug status by the FDA for the therapy of obesity that is associated with PWS (Provinsi et al., 2016a; Timmins, 2019). Furthermore, **pitolisant** has emerged as a potential drug in the treatment of PWS as improvements in cognitive performance and mental clarity, decreased sleepiness, as well as moderate amelioration in behavioural problems, have been reported on case series (Pullen et al., 2019a; Pullen et al., 2019b; c).

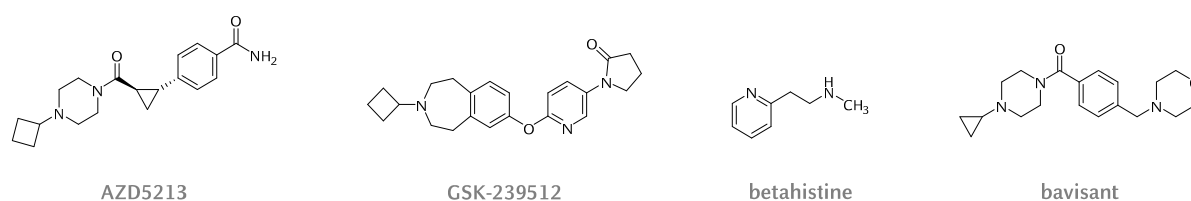


Figure 13. Selected H₃R antagonists as current clinical candidates against neurogenetic disorders.

1.6. Multitarget-directed histamine H₃ receptor ligands in neurogenetic disorders

The variety of H₃R in neurological processes as outlined in section 1.1 in addition to the traditional role of H₃R in neurogenetic diseases (section 1.5) prompt for novel strategies to improve the effectiveness of H₃R ligands on clinical investigation stage. Studiously designed ligands that combine several activities among relevant neurological circuits have emerged, promising to achieve additive effects, while reducing side-effects due to off-targets (Proschak et al., 2018). In contrast to dirty drugs, a perfect multitarget-directed ligand (MTDL) would elicit its actions only on the desired targets while maintaining selectivity over off-targets (Dessalew et al., 2008). Besides, the application of such agents can reduce the number of administered drugs and thereby, reduce the metabolic work-load (Proschak et al., 2018).

The principle of H₃R-MTDLs is as old as the discovery of H₃R, with the early finding of potent H₃R antagonism exerted by a previously known H₁R partial agonist (betahistine, **Figure 13**). Thereby, this drug became the first marketed H₃R antagonist and first MTDL with H₃R potency. While clinical effectiveness in Menière's disease is questioned based on a recent Cochrane review (Murdin et al., 2016), it has been subjected for clinical investigation proving for its effectiveness in CNS-mediated diseases such as primary and secondary obesity, associated with administration of antipsychotics and in the **PWS** (Nelson et al., 2012; Kang et al., 2018; Ghamari et al., 2019a).

From a drug design perspective, MTDL approaches can be subdivided in linking, fusing or merging pharmacophores and pharmacophore fragments (Morphy et al., 2005). Of such, the latter one is preferred due to the avoidance of decreased drug-likeness as a consequence of increased molecular size (Proschak et al., 2018).

MTDL approaches involving the H₃R can be subdivided among several co-targets, such as other (GPC)Rs, enzymes, transporters or releasing mediators for signalling (Khanfar et al., 2016). Various have been subject matter of successful drug design campaigns, but the only evidence for almost all of such drug candidates is of preclinical nature (Ghamari et al., 2019a). In most of such examples, strategic coactivity not only follows the purpose to address several neurotransmitter systems involved in a given disease, e.g., by addressing their receptors or inhibiting their degradation. Due to the widespread involvement of **heteroreceptors**, the major driver of MTDL approaches has been the purpose of achieving synergistic effects in specific neurotransmitter systems upon activation of their release, combined with inhibiting their catabolism (Bautista-Aguilera et al., 2018). Furthermore, several neurogenetic disorders share psychiatric **co-morbidities**, such as attention deficit ADHD, schizophrenia, sleep-wake disorders. Thus, these disorders may be best addressed in a multi-strategical approach.

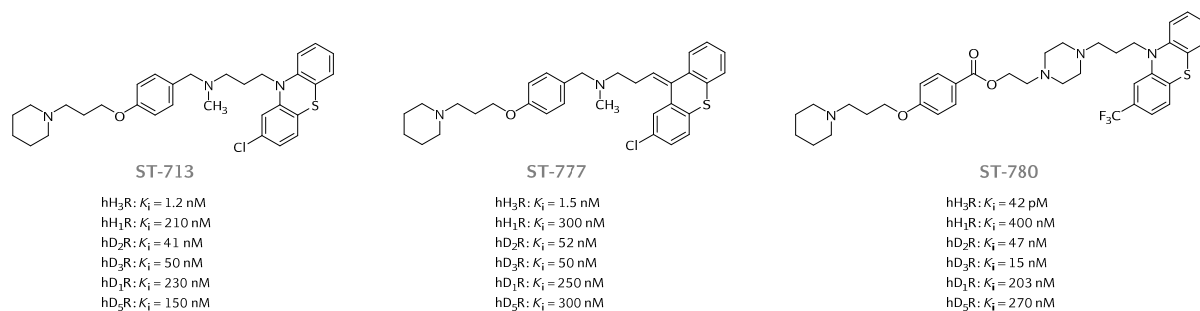


Figure 14. H₃R-MTDLs with co-target activity at DA receptor subtypes, taken from von Coburg et al. (2009).

Besides the previously outlined example of the combined H₁R/H₃R activity exerted by **betahistidine** (cf. page 46), DA and 5-HT receptors have emerged as reasonable co-targets among neurological GPCRs (Butini et al., 2016). Among them, **dopamine receptor subtypes** are potential co-targets to H₃R for antagonists applied in **schizophrenia**. However, they may have their implications for **GTS** and **ASD** as well, where antipsychotics have shown symptomatic amelioration (Posey et al., 2008; Roessner et al., 2011). Albeit the strategy to address striatal glutamatergic activity in patients suffering from schizophrenia and GTS, selective H₃R antagonists have appeared without consistent effectivity in models for schizophrenia (Ligneau et al., 2007a; Ellenbroek et al., 2014), for which H₃R/D₂R/D₃R antagonists/inverse agonists may be useful. Their implications in GTS is linked to the reduced HA synthesis, but as well to elevated striatal DA levels that have been found upon impairment of HDC function (Rapanelli et al., 2014). **Figure 14** exemplifies several ligands with combined affinity at H₃R and dopaminergic receptor subtypes. Such were derived by fusing the H₃R pharmacophore with chlorpromazine (ST-713), chlorprothixene (ST-777) or fluphenazine (ST-780), a strategy making them appear with relatively large molecular size (M_r = 530 to 680 Da) (von Coburg et al., 2009). Hence, pharmacophores with decreased molecular size are of current interest.

Acetyl- and butyrylcholinesterase (AChE/BuChE) are enzymes, which belong to serin hydrolases and are responsible for the degradation of ACh in order to abrogate cholinergic neurotransmission (Alexander et al., 2019b). In turn, ACh is a crucial neurotransmitter in the parasympathetic nervous system, where it mediates vegetative functions among nicotinic and muscarinergic receptor subtypes, but as well in neuromuscular excitation upon activation of nicotinic receptors. In the central nervous system, where ACh elicits actions among both receptor types, this neurotransmitter is responsible for (re)cognition processes and consolidation of memory (Hasselmo, 2006). Thus, ACh catabolic enzymes are targets for the treatment of **AD** (cf. page 42). However, among several approved AChE/BuChE inhibitors, only one selective ligand with sufficient blood-brain-barrier permeability has been marketed so far (donepezil, **Figure 15**). While a recent review by the Cochrane collaboration ascribes some benefits in cognition, learning and memory for

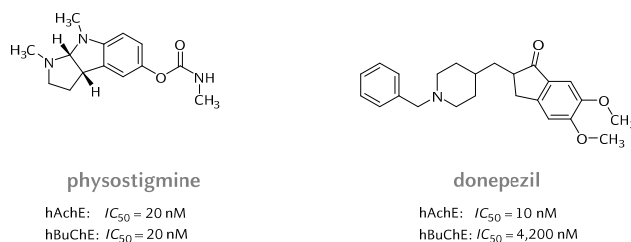


Figure 15. Structures of approved non-selective and selective AChE/BuChE inhibitors with activities (Luo et al., 2006; Alexander et al., 2019b).

donepezil, it did not markedly change the quality of life for patients suffering from AD (Birks et al., 2018). The engagement of H₃R in cholinergic transmission and its role in cognition, learning and memory conveyed its targetability in diseases such as Alzheimer's (Esbenshade et al., 2008; Reitz et al., 2011; Shan et al., 2015a; Zlomuzica et al., 2016).

Even if H₃R antagonists still do not provide a causal cure to the disease, they have emerged as promising candidates being on clinical investigation stage, however, without relevant results (Ghamari et al., 2019a). Various demonstrations of increased acetylcholine levels in hippocampus and prefrontal cortex upon administration of H₃R inverse agonists (Panayi et al., 2017), together with retardation of acetylcholine degradation leads to additive synergism (Schwartz et al., 2016). Therefore, MTDLs involving H₃R, AChE and BuChE have been the subject matter of several research campaigns for exerting direct and indirect stimulation of cholinergic neurotransmission and thereby, increased cognitive performance.

Facilitating cholinergic signalling is not only valuable in AD. Moreover, it has recently found relevance for ASD (cf. page 44) as cholinergic deficits were observed in the BTBR T⁺tf/J mouse strain, which fulfils all behavioural symptoms of autism (McFarlane et al., 2008; Karvat et al., 2014). However, studies with rivastigmine and donepezil have shown inconsistent effectiveness towards behavioural and articulatory features of ASD (Handen et al., 2011; Lee et al., 2014). Besides, amelioration in glutamatergic signalling showed to improve sociability deficits in BTBR T⁺tf/J mice (Silverman et al., 2010; Meyza et al., 2013). Finally, cognitive improvements upon administration of AChE inhibitors have been suggested to treat Lewy body dementia in PD (Hutchinson et al., 1996).

Ladostigil represents an MTDL drug candidate on clinical investigation stage for the treatment of AD and Lewy body dementia (Figure 16). From a structural point of view, it consists of a rasagiline fragment,

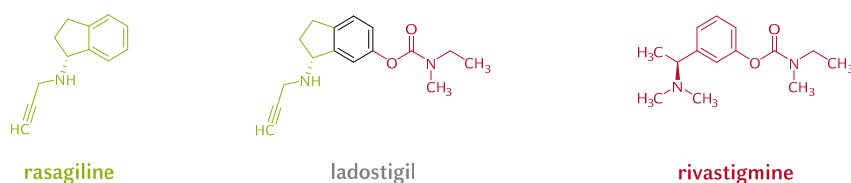


Figure 16. Rational design of ladostigil as merged rasagiline and rivastigmine pharmacophore fragments and with combined MAO & cholinesterase affinity (Weinreb et al., 2012).

merged with the pharmacophore of rivastigmine to combine inhibition of ChE with MAO (Weinstock et al., 2000; Weinstock et al., 2003; Weinreb et al., 2012). However, and following rasagiline, ladostigil exerts inhibition of **MAO B** as 6-hydroxyrasagiline, which is formed as metabolite after carbamate cleavage (Sterling et al., 2002). The latter enzyme exists in two therapeutically exploited isoforms for which reversible and irreversible, and as well some subtype-selective inhibitors have been granted market authorisation for the treatment of **PD** (cf. page 43) and depression (Youdim et al., 2006).

The underlying pharmacodynamics is a diminished degradation of neurotransmitters DA, 5-HT and norepinephrine that results in increased availability of such within the synaptic cleft. For ladostigil, however, introduction of a propargylamine in order to irreversibly inhibit MAO was neither rationalised on increasing neurotransmitter levels nor as MAO being an established target of classic antidementives. The strategy for the design of ladostigil was based on neuroprotective effects associated with propargylamine. Such effects are a consequence of specific mechanisms in APP secretion (Weinreb et al., 2012). First, rasagiline triggered the secretion of soluble non-amyloidogenic APP via α -secretase and PKC/MAPK-dependent mechanisms. The same was shown by ladostigil, the distomer of rasagiline and even propargylamine alone (Yogev-Falach et al., 2002; Yogev-Falach et al., 2003). Secondly, all of such compounds showed a neuroprotective effect against A β ₁₋₄₂ due to antiapoptotic effects (Yogev-Falach et al., 2003; Yogev-Falach et al., 2006). Unfortunately, the expectations of almost 20 years research about ladostigil failed the primary endpoint in phase 2 clinical trial, which was the delay of progression from mild cognitive impairment to AD (Schneider et al., 2019).

Combined H₃R antagonist/ChE inhibitors have been proposed and designed for more than ten years and emerged as potential lead compounds for cognitive impairment in dementia and AD. Such ligands consisted of a fused tacrine pharmacophore or donepezil fragment (Apelt et al., 2002; Petroianu et al., 2006; Morini et al., 2008), but still bearing a molecular weight below 480 Da (**Figure 17**). Recent developments in H₃R MTDLs have been the discovery of inherent reversible MAO-inhibiting properties of prominent H₃R ligands such as **ciproxifan** and **UCL-2190** (cf. page 28 and 30), and the subsequent design of reversible **H₃R ligands/MAO B inhibitors** with the purpose to obtain leads for preclinical investigation in models of PD (Hagenow et al., 2017; Affini et al., 2018). Similar inhibition of MAO B elicited by ciproxifan, and its non-imidazole congener UCL-2190 raised the assumption that the pharmacophore for MAO B consist of the cyclopropylcarbonyl substituent (Bautista-Aguilera et al., 2017). As a combination of both strategies, such efforts were applied to the systematic design of ASS234 and contilisant that represent small-molecule H₃R inverse agonists (Bautista-Aguilera et al., 2017). Whereas ASS234 consists of a merged H₃R/ChE motif fused with a donepezil fragment, contilisant represents an MTDL with

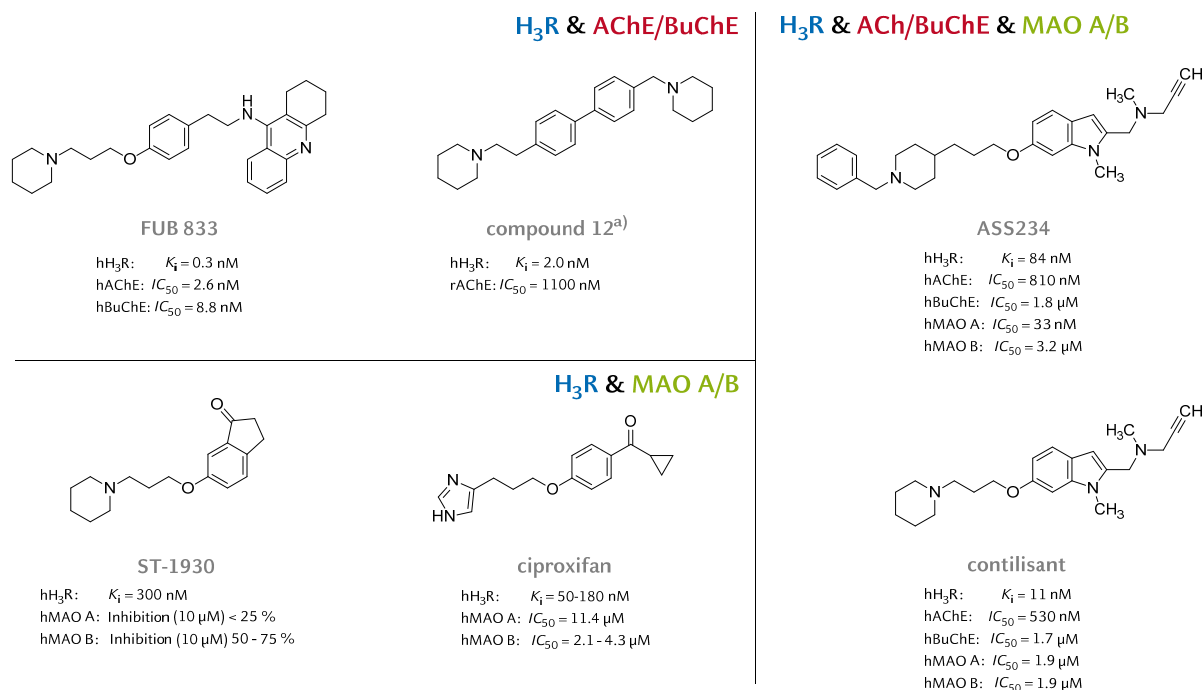


Figure 17. H₃R with inhibitory activity at either ChEs (upper left) or MAOs (lower left), or both (right panel) with pharmacological data taken from (Petroianu et al., 2006; Bautista-Aguilera et al., 2017; Hagenow et al., 2017). ^{a)}Ref. (Morini et al., 2008)

completely merged pharmacophores and tetra-target activity among the former targets and towards σ_1 Rs (Bautista-Aguilera et al., 2018). Finally, contilisant has appeared with neuroprotective properties that, together with previous results, have elicited promising *in vivo* effects in models of impaired cognition elicited by lipopolysaccharides and A β_{1-42} (Bautista-Aguilera et al., 2017; Bautista-Aguilera et al., 2018).

Apart from the strategies mentioned above to facilitate neurotransmission, strategies focussing on the genetic aetiology are emerging in neurogenetic disorders. The most straightforward methods rely on genetic intervention such as vectorial substitution of missing or defective genes, which have already progressed into clinics for the treatment of AD or PD (Eberling et al., 2008; Malkki, 2015). However, the associated costs (5 to 6-digit U.S.\$) will put an inconceivable financial burden on patients and will be intolerable by any health insurance system working in an intact ethical culture (Johnson et al., 2015). Thus, the development of small molecules to intervene on a genetic level by modulating physiological mechanisms that are involved in gene organisation (epigenetics), has resulted in remarkable progress within last years and will dominate future pharmacotherapeutic interventions. In neurogenetic disorders, epigenetic marks and the corresponding editing enzymes seem a promising mechanism of intervention.

Several of genes that are correlated with previously described pathologies are under the control of **epigenetic** regulatory mechanisms. Together, all distinct mechanisms interplay in a non-isolated, orchestrated manner in order to regulate cell cycle regulation, chromatin organisation, gene transcription,

post-translational modifications, translation of mRNA and DNA repair (Mehler, 2008). Such complex mechanisms can be subdivided upon their molecular nature (Mehler, 2008), into

- **histone modifications** acting by introduction and removal of acetylation and methylation marks by a plethora of residue-specific modifying enzymes,
- **DNA methylation**,
- regulation of **non-coding RNAs** (such as micro RNAs, spliceosomal RNAs and snoRNAs), and
- enzymes that are responsible for **RNA editing**.

Finally, such mechanisms provide a broad range of chances for pharmacological intervention. Therefore, several drugs or drug candidates have been investigated on preclinical or clinical investigation stage, or have already been granted market authorisation (Teijido et al., 2018; Peedicayil, 2019):

- inhibitors of histone acetylation (nicotinamide, vorinostat, panobinostat; all approved) or methylation (A-366, UNC-0642; on preclinical investigation stage),
- nucleoside analogues to be incorporated as demethylated DNA (decitabine; approved),
- non-nucleoside DNA methyltransferase inhibitors of which several have been discovered among approved drugs and natural compounds (procain, epigallocatechingallate; both approved), and
- non-nucleoside analogues acting as methyl donors (L-methyl folate, S-adenosylmethionine).

While most of the interventions mentioned above were aiming for the treatment of cancer, some preclinical progress in treatment of neurogenetic disorders have been made within recent years.

Among previously mentioned drugs and candidate drugs, inhibitors of the **histone H3 methyltransferase G9a** have emerged as potential tools to intervene at the basis of neurogenetic disorders, and several of them have been linked with this target. Interestingly, recent reports indicated the restoration of SNURF-SNRPN, SNORD116 and other candidate genes from the maternal copy by inhibition of the histone H3 methyltransferase G9a (syn. EHMT2/SU(VAR)3-9) and associated the findings with improved survival in a mouse PWS-model (Kim et al., 2017; Kim et al., 2019). Additionally, G9a inhibitors have shown to ameliorate autism-like social deficits in Shank3-deficient mice (Kim et al., 2017; Kim et al., 2019; Wang et al., 2019). Moreover, G9a inhibition recently showed ameliorated cognitive performance and reduced molecular risk-factors such as beta-amyloid plaques and consecutive neuroinflammation in mouse models of early-onset AD (Griñán-Ferré et al., 2019). Without pharmacological effects, G9a was associated in transcriptional repression of a factor involved in DA neuron maintenance and involvement in PD (Habibi et al., 2011).

Interestingly, it is especially this target that shows multiple implications in multifactorial diseases, while meanwhile, as well the H₃R has emerged as a therapeutic approach. Thus, from a MTDL perspective, G9a appears as an attractive co-target for H₃R ligands. However, studies focussing on MTDLs with binding towards H₃R and the histone H3 methyltransferase have not been conducted yet. Ultimately, the genetic and epigenetic basis of neurogenetic disorders is now progressively elucidated and thereby, accompanied by novel pharmacotherapeutic approaches.

Together with the multi-faceted neurological roles of H₃R that were outlined within this introduction, both approaches will be alongside one another for combined symptomatic and causal treatments.

2. Objectives & scope of this research

Preclinical insights that pinned hopes on H₃R inverse agonists have often been counteracted within clinical campaigns, leading to high attrition risk in development campaigns of H₃R ligands, and despite almost 40 years of H₃R research, only one progressed into the market (Schwartz et al., 2016; Ghamari et al., 2019a). Given the various physiological implications of H₃R that were outlined previously (section 1.1), the high failure rate of potent H₃R ligands in clinics puts several questions to molecular pharmacology as the proximal part of the drug discovery process.

Dedication of my work will be given to the development and application of molecular pharmacological methods to H₃R ligands, for profiling novel hit and lead compounds with improved pharmacological profile for investigation within *in vivo* models.

The section 3 starts with the development of a novel fluorescence polarisation (FP)-based method for the objective, to assess novel tracers in binding studies, to shift equilibrium read-outs towards a kinetic, and to increase the throughput upon working in a homogeneous environment. Thereby, this method will be tested among imidazole-based and non-imidazole-based inverse agonists, but also agonists. The desired increase in throughput will be required for the further purposes of my studies. There, the applicability of the pharmacophore blueprint of non-imidazole-based H₃R inverse agonists will be analysed within a bioisosteric replacement approach towards heterocyclic receptor ligands with improved drug-likeness.

Within the projects in section 4, I aim for the discovery of novel H₃R ligands with or without activities at promising co-targets, as a strategy to improve existing pharmacological approaches to neurogenetic disorders such as schizophrenia and GTS, the highly prevalent neurodegenerative diseases PD and AD, and the less prevalent ASD and PWS. This search will be conducted among novel hit and lead structures from medicinal chemistry or *in silico* screening efforts, but will as well encompass well-characterised drug candidates. As potential co-targets, dopaminergic GPCRs, MAO B, AChE and BuChE enzymes appear as the most attractive ones from current knowledge. Some of such MTDLs will be explored in *in vivo* models of PD and ASD, for which detailed knowledge of their molecular pharmacological profile is essential. Final queries will be made to expand the concept of H₃R-MTDLs on novel candidate structures which combine H₃R antagonism with epigenetic modulatory function. Such novel MTDLs could be promising tools against neurogenetic disorders, which often are multifactorial and that often share co-morbidities. Therefore the pharmacological manipulation of neurotransmitter levels, as well as re-programming cellular function, may open novel perspectives towards this class of neurological conditions.

3. Novel implications in molecular pharmacology of histamine H₃ receptor ligands

3.1. Ligand binding kinetics at histamine H₃ receptors by fluorescence polarization with real-time monitoring

David Reiner¹⁾ and Holger Stark²⁾

1) Institute of Pharmaceutical and Medicinal Chemistry, Heinrich Heine University Düsseldorf, Universitätsstr. 1, 40225 Duesseldorf, Germany

Published in: *European Journal of Pharmacology*, 2019, 848:112-120.
DOI: 10.1016/j.ejphar.2019.01.041

Contribution to research: DR developed the novel assay system, designed, planned, prepared and conducted the pre- and main-experiments. He analysed the data, wrote the manuscript and processed the revision.

Abstract:

Growing evidence recommends incorporating the concept of drug-target residence times within drug development and screening programmes. For many targets, systematic research for binding kinetics is emerging and reported, as in case of the histamine H₃ receptor. Alternatively, fluorescent methods based on Foerster resonance energy transfer have been reported recently but application of fluorescence polarization to kinetics of unlabeled ligands is not known to us. Thus, we established a radiolabel-free, real-time resolving method that is compatible to high-throughput-screening programmes with the objective to explore the underlying binding kinetics. This method takes benefit of bodilisant as H₃ receptor ligand. Thereby, we detected short residence times around 5 min for the H₃ receptor ligands ciproxifan, clobenpropit, thioperamide as well as pitolisant. Monitoring association rates, remarkably slower association rate constants were examined for ciproxifan and thioperamide when compared to those of pitolisant or clobenpropit. The affinities for the ligands derived by the kinetic approach differ from affinity estimates in literature using radiolabeled agonists in displacement assays. Further investigation raised exceptional pharmacological properties, consistent with occurrence of secondary binding sites at the H₃ receptor. Validation of resulting affinity constants was successfully performed by displacement assays based on fluorescence polarization with bodilisant.

Reproduced from Reiner D and Stark H, Ligand binding kinetics at histamine H₃ receptors by fluorescence polarization with real-time monitoring, *Eur. J. Pharmacol.*, 2019, 848:112-120, with permission for personal use from Elsevier.

Copyright 2019 Elsevier B.V.



Molecular and cellular pharmacology

Ligand binding kinetics at histamine H₃ receptors by fluorescence-polarization with real-time monitoring

David Reiner, Holger Stark*

Heinrich Heine University Düsseldorf, Institute of Pharmaceutical and Medicinal Chemistry, Universitätsstr. 1, 40225 Düsseldorf, Germany



ARTICLE INFO

Keywords:

Histamine
H₃ receptor
Drug-target residence time
Receptor kinetics
Fluorescence polarization

ABSTRACT

Growing evidence recommends incorporating the concept of drug-target residence times within drug development and screening programs. For many targets, systematic research for binding kinetics is emerging and reported, as in case of the histamine H₃ receptor. Alternatively, fluorescent methods based on Förster resonance energy transfer have been reported recently but application of fluorescence polarization to kinetics of unlabeled ligands is not known to us. Thus, we established a radiolabel-free, real-time resolving method that is compatible to high-throughput-screening programs with the objective to explore the underlying binding kinetics. This method takes benefit of bodilisant as H₃ receptor ligand. Thereby, we detected short residence times around 5 min for the H₃ receptor ligands ciproxifan, clobenpropit, thioperamide as well as pitolisant. Monitoring association rates, remarkably slower association rate constants were examined for ciproxifan and thioperamide when compared to those of pitolisant or clobenpropit. The affinities for the ligands derived by the kinetic approach differ from affinity estimates in literature using radiolabeled agonists in displacement assays. Further investigation raised exceptional pharmacological properties, consistent with occurrence of secondary binding sites at the H₃ receptor. Validation of resulting affinity constants was successfully performed by displacement assays based on fluorescence polarization with bodilisant.

1. Introduction

In vitro screening of compounds for affinities and selectivity to a respective target has been the basis in pharmacological research over decades. Those methods investigate the attainment to Ehrlich's prerequisite for any drug to take effect in vivo even if it is not a sufficient condition to prove effectiveness of drugs. Copeland et al. (2006) presented the drug-target residence time concept (hereinafter also termed 'residence time', τ , Eq. (1)) about 10 years ago to take further assumptions into account, namely (i) to regard the dynamic situation beyond target binding that is rather an estimate to describe the open-system physiological conditions, (ii) to correlate the duration of an effect to the time a drug resides at the receptor, (iii) to use this information to systematically improve in vivo effectiveness and (iv) finally, to reduce attrition risk on late-stage drug development (Lu and Tonge, 2010; Guo et al., 2014; Hoffmann et al., 2015; Copeland, 2016; Schuetz et al., 2017).

$$\tau = 1/k_{off} \quad (1)$$

Despite drug-target residence time emerges as new concept, the theoretical background for experimental procedures has already been

set up for enzymes by Colquhoun in 1968 and refined by Motulsky and Mahan (1984) who delivered an analytical solution of the differential equations of a radioligand competing with an unlabeled ligand for one receptor site simultaneously. Applicability to radiolabel-free approaches as Förster/bioluminescence resonance energy transfer (FRET/BRET) has been demonstrated at the histamine H₁, H₃ and H₄ receptor (Bosma et al., 2016; Liu et al., 2018; Stoddart et al., 2018; Mocking et al., 2018; Riddy et al., 2019).

One major disadvantage of the latter methods is the requirement of labeling two components attributing to the binding reaction, likewise the target itself that pharmacologically manipulates the target of investigation. Thus, we decided to use a method based on fluorescence polarization as it requires only one partner to be labeled (Banks et al., 2000), works with native receptors and as it was proposed by Copeland et al. (2006) that it might be applicable in examining residence times. This technique is based on the polarization of emitted light by a molecule excited with linearly polarized light (Perrin, 1926). When regarding those molecules as spinning dipoles that radiate with a different intensity at each angle of observation, high polarization will be seen at relatively slow rotation as caused by binding of this compound to a target (Lea and Simconov, 2011; Rossi and Taylor, 2011).

* Corresponding author.

E-mail address: stark@hhu.de (H. Stark).<https://doi.org/10.1016/j.ejphar.2019.01.041>

Received 3 August 2018; Received in revised form 24 January 2019; Accepted 24 January 2019

Available online 28 January 2019

0014-2999/ © 2019 Elsevier B.V. All rights reserved.

The considerations above motivated us to set up a new method to investigate drug-target kinetics at the H₃ receptor (for review, see Panula et al. (2015)). The choice of a measurement technique based on fluorescence polarization is driven by its time resolving competence, its compatibility for high-throughput screening, the reduced hands-on work required compared to radioligand binding and functional studies, the yet successful application to classical competition studies at G-protein coupled receptors and finally, to extend this simple approach to kinetic investigations (Gagne et al., 2002; Kecskes et al., 2010; Stoddart et al., 2016).

2. Materials and methods

2.1. Materials and chemicals

HEK-293 cells stably expressing the 445-amino acid encoding gene of the human H₃ receptor were kindly gifted by Prof. Dr. Jean-Charles Schwartz (Bioprojet, France). 25 cm² cell-culture flasks (CELLSTAR[®] Tissue culture flasks) and 96-well, black microtiterplates (polystyrene, half-area, medium binding) were from Greiner bio-one (Frickenhausen, Germany). 75 cm² and 175 cm² cell-culture flasks (NUNC[®] EasyFlask), Dulbecco's Modified Eagle Medium, Penicillin (10,000 U)/Streptomycin (10 mg/ml) solution, L-Glutamine-solution (200 mM), HEPES solution (1 M, pH: 7.0–7.6), Pluronic[®] F-127 as well as thioperamide maleate were purchased from Sigma-Aldrich (Taufkirchen, Germany). Fetal bovine serum albumin (FBS Good-Forte[®]) and Dulbecco's phosphate buffered saline (hereinafter termed 'phosphate buffer') were gained from PAN-Biotech (Aidenbach, Germany). Clobenpropit hydrobromide was purchased from Biotrend (Zurich, Switzerland), TRIS, sodium chloride and magnesium chloride were from Carl Roth (Karlsruhe, Germany). Bodilisant was obtained from our own synthesis as described by Tomasch et al. (2013), as well as ciproxifan, pitolisant oxalate and N^α-methylhistamine dihydrochloride (Stark, 2000; Meier et al., 2001; Grassmann et al., 2003).

2.2. Cell culture and membrane preparation

The above-mentioned cells were cultured in Dulbecco's Modified Eagle Medium supplemented with 10% fetal serum albumin (FBS), 2 mM L-Glutamine, 10 mM HEPES, 100 units benzylpenicillin and 0.1 mg/ml streptomycin. Flasks were stored in an incubator (Binder, Tuttlingen, Germany) at 37 °C with 5.0% CO₂ saturation. Upon confluence, the medium was discarded, and cells were detached mechanically through aspiration in phosphate buffer. After centrifugation (Hettich, Tuttlingen, Germany) at approx. 1400 × g, 4 °C for 10 min, the pellet was resuspended in phosphate buffer and centrifugated repeatedly. The resulting pellet was taken into membrane buffer (75 mM Tris, 100 mM NaCl, 10 mM MgCl₂; pH = 7.4) and homogenized using an UltraTurrax[®] T 25 (IKA[®]-Werke, Staufen, Germany) at 10,000 rpm. Two further centrifugation steps followed at approx. 50,000 × g for 20 min each with a wash step using membrane buffer in between. The resultant pellet was resuspended in membrane buffer and aliquots were prepared for storage at –80 °C until further use. Protein content was quantified by the method of Bradford (1976). Ahead of all experiments, membrane preparations were thawed, diluted with membrane suspension and sonicated 3 times keeping the preparation on ice. Subsequently, the mixture was tempered on a water bath to 28 °C.

2.3. [³H]-N^α-methylhistamine in saturation binding and radioligand displacement assays

H₃ receptor expression was determined by saturation binding experiments using duplicates of eight concentrations of [³H]-N^α-methylhistamine titrated against 20 µg/well of receptor containing membrane preparations (volume = 200 µl), including samples with 10 µM of pitolisant for quantification of non-specific binding (same buffer as

described above, supplemented with 0.01% Pluronic[®] F-127). To determine the competitiveness of bodilisant interacting with H₃ receptor, similar samples were prepared in presence of different concentrations of bodilisant (0.1, 1, 10 and 100 nM) to yield apparent K_D values of [³H]-N^α-methylhistamine. Displacement assays were carried out as described by Kottke et al. (2011) to determine affinities of test-ligands under experimental conditions close to those of the following procedures, using a titration pattern of seven competitor concentrations against [³H]-N^α-methylhistamine (2 nM, final concentration) and the same receptor concentration as above. For all radioligand experiments, the incubation was terminated after 90 min using the standard procedure for vacuum-filtration, filter mat-preparation and scintillation counting as described previously (Khanfar et al., 2018).

2.4. Optimization of assay conditions

All samples were prepared on microtiterplates and prewarmed to 28 °C in a TECAN[®] Infinite 1000 Pro multi-use-reader for 15 min, before starting the binding reaction. Measurements were carried out using the fluorescence polarization mode (excitation wavelength: 470 ± 5 nm, emission wavelength: 520 ± 20 nm, gain: 60, flashes: 50 s^{–1}, Z-level: 26,008 µm and 24,467 µm for 150 µl and 75 µl samples, respectively). All experiments were carried out at least in duplicates and contained buffer blanks solely consisting of buffer, protein blanks with H₃ receptor carrying membrane suspension, and samples for determination of anisotropy of free ligand. For determination of non-specific binding, one sample was prepared with 10 µM of pitolisant as competitor solution. The first step of optimization for all measurements within this assay was the selection of suitable concentrations of protein and fluorescence ligand within the standard pattern described above. First, different concentrations of bodilisant corresponding to 1, 2, 4, 8 and 10 times of its K_i value, determined by radioligand displacement assays (Tomasch et al., 2013) were titrated against a fixed amount of membrane preparation (120 µg/well) in membrane buffer (without detergents). Measurements were performed repeatedly after 45, 60 and 75 min. Secondly, as 12 nM provided a sufficient signal to noise-ratio based on Z'-level, this concentration was investigated against various concentrations of membrane preparation. Thirdly, the membrane buffer used for membrane preparation was modified subsequently by serial dilution of a solution (10%, m/m) of Pluronic[®] F-127 with membrane buffer. For determination of signal stability over time, the binding reaction was monitored every 10 min up to 12 h. For all further experiments in the sections below, 0.01% Pluronic[®] F-127 was added to the membrane buffer (hereinafter termed as "assay buffer").

2.5. Fluorescence polarization-based estimation of kinetics of bodilisant

Kinetics of bodilisant binding to the H₃ receptor was examined by measuring association and dissociation. For starting the association reaction, 50 µl of protein were pipetted to 100 µl of prewarmed bodilisant (12 nM, final) and polarization was measured every min for at least 60 min. Dissociation was initiated by addition of 5 µl of pitolisant (10 µM, final) to the same samples using an injector system integrated into the reader, shaking for 10 s and another read-out period of at least 75 min (minimum 5-fold k_{off}) pursued.

2.6. Fluorescence polarization-based kinetics of unlabeled ligands

To determine the kinetics of unlabeled ligands, 50 µl of bodilisant (12 nM, final conc.) and 50 µl of competitors at various concentrations were prewarmed inside the multi-use reader (10 min, 28 °C). Simultaneous incubation of competitor and labeled ligand was initiated through addition of 50 µl protein solution (100 µg/well) by means of automated pipetting. Plate transfer was carried out exclusively automated to maintain a reproducible lag-time between pipetting and the first measurement point t₁. Competitors used in the presented

investigations were the H₃ receptor inverse agonists pitolisant, ciproxifan, thioperamide clobenpropit and the agonist N^α-methylhistamine.

2.7. Fluorescence polarization-based displacement assay

For displacement assays the procedure above was modified to yield dose-inhibition curves. Serial dilution of 10 μM stock solutions by assay buffer were performed either manually or by using an automated pipetting robot Freedom Evo (Tecan, Maennedorf, Switzerland) connected to the previously mentioned reader. 25 μl of membrane preparations (50 μg/well) were added to 50 μl solutions of competitors and bodilisant (12 nM, final concentration). Maximum anisotropy of bound ligand (r_{max}) was determined by including a sample containing an excess of protein (150 μg/well). Reading was performed after an incubation period of 90 min at 28 °C as indicated above. Experiments were carried out using ten different concentrations per competitor in duplicates.

2.8. Data handling, calculations and curve fitting procedures

Fluorescence polarization was measured as parallel and perpendicular fluorescence intensity (I_{\parallel} and I_{\perp} , respectively) and transformed into anisotropy (r) according to Eq. (2). The included G-factor (G) is a system property accounting for differences in sensitivity of emission filters to parallel and perpendicular polarized light, respectively (Note that G is most commonly the multiplicative of perpendicular intensity (I_{\perp}) but may be shifted, being the multiplicative of parallel intensity (I_{\parallel}), according to the manufacturers' instructions of the reader in use). G-factor ($G = 1.187$) of the reader was determined according to the instructions of the manufacturer.

$$r = (G \times I_{\parallel} - I_{\perp}) / (G \times I_{\parallel} + 2 \times I_{\perp}) \quad (2)$$

The measured anisotropy (r_M) is a ratiometric value that consists of the weighted sum of the anisotropy of free and bound ligand. The procedure to convert the r_M values of each sample into the fraction of labeled ligand specifically bound to the receptor (F_{SB}) was adopted from Roehrl et al. (2004) (Eqs. (3)–(6)). First, the fraction of labeled ligand bound to the receptor (F_B) of each sample was calculated by Eq. (3) (r_D denotes the anisotropy of free ligand, r_{max} the anisotropy of maximally bound ligand):

$$F_B = (r_M - r_D) / (r_{\text{max}} - r_D) \quad (3)$$

The bound fraction within the probe to determine non-specific binding F_B^{NSB} and the estimate of non-specific binding N_B were derived by Eqs. (4) and (5), respectively, with r_i denoting anisotropy measured at large excess of unlabeled competitor:

$$F_B^{\text{NSB}} = (r_i - r_D) / (r_{\text{max}} - r_D) \quad (4)$$

$$N_B = F_B^{\text{NSB}} / (1 - F_B^{\text{NSB}}) \quad (5)$$

Finally, F_{SB} (in % of total binding) of each sample was derived by:

$$F_{\text{SB}} = [(1 + N_B) \times F_B - N_B] \times 100\% \quad (6)$$

The resultant F_{SB} were analyzed by non-linear least-squares fit using the software GraphPad Prism™ (2012, vers. 6.01, La Jolla, CA, USA).

For determination of dissociation rate constants k_{off} , data of dissociation reactions were fitted to the following expression accounting for monophasic dissociation (Eq. (7), $F_{\text{SB},t=0}$ depicts the Fraction of receptor bound labeled species before initiating the dissociation):

$$F_{\text{SB}} = F_{\text{SB},t=0} \times \exp(-k_{\text{off}} \times t) \quad (7)$$

k_{off} values were used to determine k_{on} values from Eq. (8) ($F_{\text{SB},\text{max}}$ and $[L]$ accounts for bound fraction after equilibration and concentration of labeled species, respectively):

$$F_{\text{SB}} = F_{\text{SB},\text{max}} \times (1 - \exp^{-(k_{\text{on}} \times [L] + k_{\text{off}}) \times t}) \quad (8)$$

Knowing these parameters, substitution into the following expressions can be used for determination of $[C]$, $k_{\text{on},C}$ and $k_{\text{off},C}$ being the concentration, the association and dissociation rate constants of the unlabeled species, respectively (Eq. (9a)–(9f), (Motulsky and Mahan, 1984)):

$$k_A = k_{\text{on}} \times [L] + k_{\text{off}} \quad (9a)$$

$$k_B = k_{\text{on},C} \times [C] + k_{\text{off},C} \quad (9b)$$

$$S = \sqrt{(K_A - K_B)^2 + 4 \times k_{\text{on}} \times k_{\text{on},C} \times [L] \times [C]} \quad (9c)$$

$$K_F = 0.5 \times (K_A + K_B + S) \quad (9d)$$

$$K_S = 0.5 \times (K_A + K_B - S) \quad (9e)$$

$$F_{\text{SB}} = (B_{\text{max}} \times k_{\text{on}} \times [L]) / (K_F - K_S) \times [(k_{\text{off},C} \times (K_F - K_S)) / (K_F \times K_S) + (k_{\text{off},C} - K_F) / K_F \times \exp(-K_F \times t) - (k_{\text{off},C} - K_S) / K_S \times \exp(-K_S \times t)] \quad (9f)$$

Competitive binding data were fit to Eq. (10) to yield IC_{50} values.

$$F_{\text{SB}} = F_{\text{SB},\text{max}} / (1 + 10^{((C) - \log(IC_{50}))}) \quad (10)$$

Since concentrations of free ligand, free receptor and ligand-receptor-complex do not change at equilibrium and the total association rate approaches zero, there is a direct link between receptor kinetics enabling the calculation of K_D by association (k_{on}) and dissociation rate constant (k_{off} , Eq. (11)).

$$K_D = [L] \times [R] / [RL] = k_{\text{off}} / k_{\text{on}} \quad (11)$$

K_i values were calculated via the correction derived by Cheng and Prusoff (1973) as stated in Eq. (12), where K_D represents the dissociation constant of the labeled ligand as obtained by Eq. (11). Munson and Rodbard (1988) derived an exact solution to Eq. (12) that accounts for errors due to ligand depletion. $K_{i,\text{ex}}$ values derived by the exact correction (Eq. (13)) were compared to K_i values of the first solution.

$$K_i = IC_{50} / (1 + [L] / K_D) \quad (12)$$

$$K_{i,\text{ex}} = IC_{50} / (1 + y_0 + [L] \times (y_0 + 2) / (2 \times K_D \times (y_0 + 1))) + K_D \times y_0 / (y_0 + 2) \quad (13)$$

Z' factors were calculated as 1 minus the third ratio between the sum of the standard deviations σ_m , σ_{NSB} and the difference of the corresponding means of measured anisotropy r_m and r_i , used as a commonly used signal-to-noise substitute in fluorescence polarization (Eq. (14)) (Banks and Harvey, 2002).

$$Z' = 1 - 3 \times (\sigma_m + \sigma_{\text{NSB}}) / (\hat{r}_M - \hat{r}_i) \quad (14)$$

For saturation binding experiments using [³H]-N^α-methylhistamine, specific binding was fit to Eq. (15), where $[L_R]$ and B_{max} stand for concentration of radioligand and maximum number of binding sites, respectively, and Y depicts specific binding to the receptor [c.p.m.].

$$Y = B_{\text{max}} \times [L_R] / ([L_R] + K_D) \quad (15)$$

Same fitting was conducted for saturation binding experiments in presence of bodilisant, yielding apparent dissociation constants ($K_{D,\text{app}}$). The latter were converted to $\log(K_{D,\text{app}} / K_D - 1)$, plotted against logarithmic bodilisant concentration and inspected as Schild-type plots for competitiveness by linear regression (Ehlert, 1988; Christopoulos and Kenakin, 2002).

Where applicable, Kolmogorov-Smirnov test was conducted to assess significance while considering a limit of $p < 0.05$ and correlations are presented as Pearson correlation coefficient r_s .

D. Reiner, H. Stark

European Journal of Pharmacology 848 (2019) 112–120

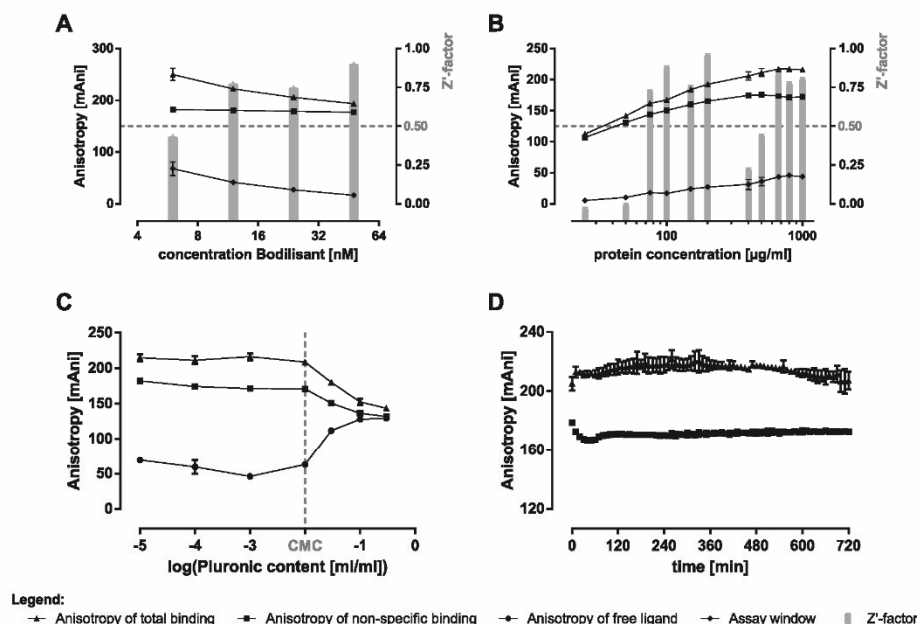


Fig. 1. Optimization of anisotropy measurements of bodilisant at H₃ receptor with (■ = signal of non-specific binding) and without (▲ = signal of total binding) large excess of pitolisant (10 μM), plotted against left ordinate. The values represent means ± S.D. from a representative of three independent experiments performed in duplicate each. (A) Four concentrations of bodilisant (6 nM, 12 nM, 24 nM and 48 nM; abscissa) were incubated with 800 μg/ml of protein for 60 min. Grey bars plotted against the right ordinate indicate the calculated Z'-factor with Z' > 0.5 (dashed line) indicating high-throughput screening compatibility. (B) Various protein concentrations were titrated against 12 nM of bodilisant and incubated for 60 min ♦ indicate the difference between anisotropy of total and non-specific binding whereas grey bars indicate the calculated Z'-factors plotted against the right scale. (C) Effect of supplementation of buffer with a detergent. Various concentrations of a Pluronic®-F127 solution (10%) were added to the buffer. The dashed line indicates the critical micellar concentration of detergent (approx. 1000 ppm) and • denotes the anisotropy of free ligand. (D) Signal stability of total and non-specific binding of bodilisant up to 12 h. Concentrations of fluorescent ligand and membrane protein were 12 nM and 100 μg/well, respectively in buffer supplemented with Pluronic®-F127 (0.01%).

3. Results

3.1. Optimization of measurements

Selection of suitable concentrations of the reaction partners, bodilisant as fluorescently labeled ligand and the H₃ receptor, was the first crucial step for obtaining a signal in fluorescence polarization. A sufficient concentration of bodilisant at a fixed concentration of receptor was found to be 12 nM (approx. 2 times K_D derived by radioligand displacement curves), providing satisfactory signal to noise ratio and assay-window (Fig. 1A and Fig. S1.1A, Supplementary material). Higher concentrations lowered r_M due to the contribution of signal of unbound ligand, whereas lower concentrations did not provide sufficient fluorescence intensity signal compared to background, resulting in imprecision of measurement and Z'-factor below 0.5. Subsequently, different concentrations of receptor were titrated against bodilisant (12 nM), whereas the receptor content corresponded to 0.73 pmol/mg protein as determined by saturation binding curves ($pK_D = 8.44 \pm 0.08$ nM). As higher protein concentration causes elevated binding of labeled ligand, assay windows have correlated with increasing protein content in contrast to Z'-factors. That might be rationalized as Z'-factors are influenced by both, assay window and precision of measurement, the latter being higher at decreasing background fluorescence. However, 100 μg/well (corresponding to approx. 666 μg/ml) provided a sufficient assay window at lowest receptor concentration and Z'-factor exceeding 0.5 (Fig. 1, panel B and Fig. S1.1, panel B, Supplementary material), indicating excellent assay conditions for

high-throughput screening assays (Zhang et al., 1999). As tentative addition of Pluronic® F-127 to the binding buffer resulted in less fluctuation of the anisotropy signals over time, we figured out the optimal concentration being 0.01%. At concentrations above the critical micellar concentration ($c > 0.1\%$ as stated in the analytical supplements of the manufacturer), anisotropy values of bound ligand decreased and increased for free ligand (Fig. 1, panel C). Given this standard set-up, signal stability was tracked up to twelve h showing no significant changes (Fig. 1, panel D).

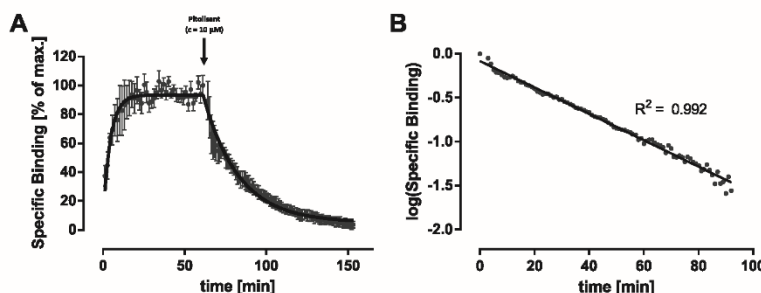
3.2. Kinetic characterization of bodilisant

The kinetic parameters of the labeled probe were determined as they are prerequisite in mathematical models for determination of the kinetics of unlabeled ligands and to examine the corresponding affinity to the receptor. In contrast to radioligand binding experiments where the binding reaction is terminated upon filtration to separate bound from unbound ligands, fluorescence polarization experiments allow homogeneous, multiple measurements in real-time resolution and reuse of the reaction mixture for further examinations. Therefore, we monitored the association reaction after assembling bodilisant (12 nM) with membrane preparations carrying the H₃ receptor (100 μg/well) and using the same samples to examine the dissociation after addition of a large excess of the inverse agonist pitolisant (10 μM). After conversion of the measured anisotropy values to F_{SB} association/dissociation curves were plotted and fitted as shown in Fig. 2. This procedure delivers $k_{on} = 22.5 \pm 8.7 \cdot 10^6 \text{ M}^{-1} \text{ min}^{-1}$ and k_{off}

3.1 Ligand binding kinetics at histamine H₃ receptors by fluorescence polarization with real-time monitoring

D. Reiner, H. Stark

European Journal of Pharmacology 848 (2019) 112–120



$= 22 \pm 9 \cdot 10^6 \text{ M}^{-1} \text{ min}^{-1}$ and $k_{\text{off}} = 0.034 \pm 0.010 \text{ min}^{-1}$ were calculated from 7 independent experiments (mean \pm S.E.M.). Non-linear least-squares regression yielded association and dissociation rate constants (mean \pm S.E.M.). (B) Semilogarithmic transformation of dissociation data from panel A (dissociation start was set as $t = 0$) and linear regression of the corresponding means obtains a straight line ($R^2 = 0.992$), indicating that bodilisant binds to a single class of binding site.

$= 0.034 \pm 0.010 \text{ min}^{-1}$. Furthermore, we calculated $\text{p}K_D = 8.72 \pm 0.19$ as affinity measures not differing from the $\text{p}K_i$ obtained by radioligand displacement assays that were performed and published earlier by our research group ($\text{p}K_i = 8.37 \pm 0.16$; $p = 0.07$; Tomasch et al., 2013). A useful method to check for numbers and interactions of different binding sites is the semilogarithmic conversion of dissociation-time curve that returned a straight line ($R^2 = 0.992$) indicating a single class of binding sites (Fig. 2, panel B).

3.3. Kinetic characterization of unlabeled ligands

Through investigation of the changes in the kinetic behavior of a labeled ligand in presence of an unlabeled ligand, the kinetics of the latter can be determined through the aforementioned mathematical framework of Motulsky and Mahan (1984) and Colquhoun (1968). Different concentrations of unlabeled competitor in presence of bodilisant were incubated with H₃ receptor simultaneously and the binding reaction was followed for about 90 min (Fig. 3). The kinetics of some

Table 1
Kinetic parameters of prominent histamine H₃ receptor ligands, obtained by a fluorescence polarization method.^a

	$k_{\text{on}} [10^6 \text{ M}^{-1} \text{ min}^{-1}]$	$k_{\text{off}} [\text{min}^{-1}]$	$\tau [\text{min}]$	n
Pitolisant	19 ± 6	0.22 ± 0.05	4.6 ± 1.0	6
Ciproxifan	0.072 ± 0.011	0.21 ± 0.04	4.7 ± 0.9	5
Thioperamide	0.10 ± 0.04	0.16 ± 0.02	6.3 ± 0.6	6
Clobenpropit	0.42 ± 0.02	0.19 ± 0.05	5.3 ± 1.5	4

^a Fluorescence polarization was monitored over time after addition of membrane-preparations of H₃ receptor expressing HEK-293 cells to the fluorescent ligand bodilisant (12 nM) and different concentrations of competitor. Data were converted to fraction of bodilisant bound specifically to the receptor (F_{SB}) and fit to the model of Motulsky and Mahan (1984) to derive association rate constants (k_{on}) and dissociation rate constants (k_{off}). Drug-target residence times (τ) were calculated as reciprocal of means of k_{off} . All data represent means \pm S.E.M. from the indicated number of experiments (n) performed in triplicate.

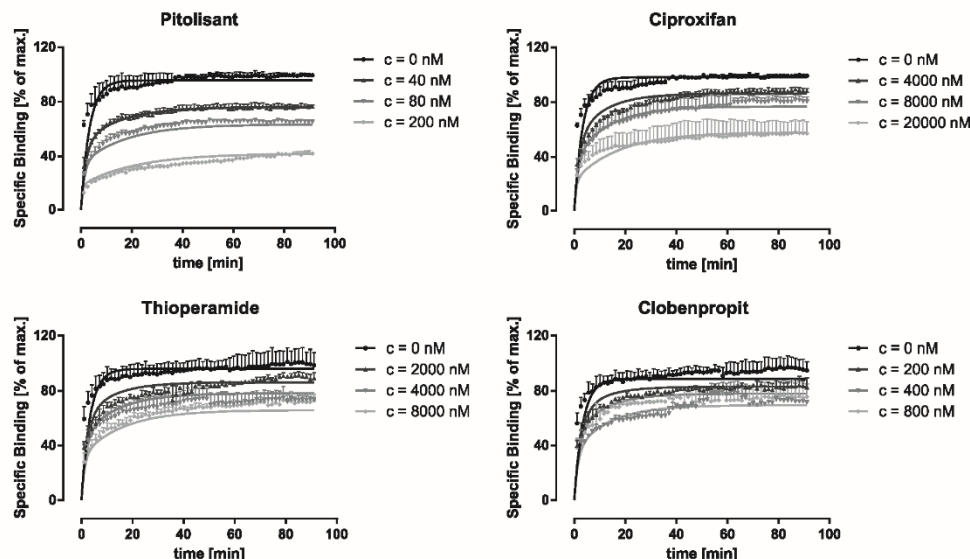


Fig. 3. Binding kinetics of representative ligands at the H₃ receptor. Three different concentrations of competitor were incubated simultaneously with bodilisant (12 nM) and receptor containing membrane preparations. Anisotropy values were converted to fraction of ligand specifically bound to the receptor (normalized as % of maximum) and plotted against a time-scaled abscissa.

Table 2
Affinities of histamine H₃ receptor ligands, obtained by fluorescence polarization method using bodilisant.^a

	Kinetic estimation ^b		Competitive displacement assay ^c			[³ H]-N ^α -methylhistamine displacement assays ^d	
	pK _D	n	pK _i	n	pK _{i,ex}	pK _i	n
Pitolisant	7.89 ± 0.14	6	7.68 ± 0.08	3	7.67 ± 0.06	7.92 ± 0.04	5
Ciproxifan	5.54 ± 0.06	5	5.30 ± 0.12	3	5.35 ± 0.11	6.49 ± 0.12	3
Thioperamide	5.70 ± 0.11	6	5.32 ± 0.09	4	5.33 ± 0.10	7.15 ± 0.04	3
Clobenpropit	6.40 ± 0.13	4	5.87 ± 0.18	3	5.89 ± 0.19	8.73 ± 0.08	3

^a Data represent means ± S.E.M. from the indicated number of experiments (n).
^b pK_D values were calculated from association and dissociation rate constants of each independent experiment (n) and expressed as means ± S.E.M.
^c Competitive displacement assays were carried out by titration of ten different concentrations of competitors in duplicates against bodilisant at H₃ receptor. Fluorescence polarization was measured after 90 min pK_i values were calculated from IC₅₀ values via the correction by Cheng and Prusoff (1973) and compared to pK_{i,ex} values representing the affinities calculated from the exact correction by Munson and Rodbard (1988), using pK_D of bodilisant obtained by kinetic estimation (Eq. (11) and Fig. 2).
^d Competitive displacement assays using [³H]-N^α-methylhistamine as radiolabeled ligand as described by Kottke et al. (2011).

prominent ligands were determined as representatives (Table 1). Whereas comparable dissociation rate constants were observed among them, showing a tenfold faster dissociation rate than the fluorescently labeled ligand bodilisant, drastic differences were observed between the association rate constants: pitolisant displayed the highest association rate constant comparable with bodilisant, followed by the imidazole-based ligand clobenpropit. Ciproxifan and thioperamide showed a k_{on} being about one twentieth of clobenpropit. The corresponding K_D values were calculated according to Eq. (2), transformed into pK_D and reported in Table 2. Pitolisant showed the highest affinity whereas a tenfold lower affinity was observed for clobenpropit. Thioperamide and ciproxifan appeared even less active, showing only micromolar K_D values. Comparison with data obtained by a recently published method show significantly slower dissociation rate constants for thioperamide and clobenpropit with k_{off} $0.026 \pm 0.01 \text{ min}^{-1}$ for both compounds ($p < 0.05$). Significance was not assessed for pitolisant as two different dissociation rate constants were observed in recently published literature, one being lower ($k_{off} = 0.086 \pm 0.07 \text{ min}^{-1}$), whereas another revealing a faster dissociation ($k_{off} = 1.53 \pm 0.94 \text{ min}^{-1}$) (Mocking et al., 2018; Riddey et al., 2019).

3.4. Fluorescence polarization-based displacement assay

As no kinetic rate constants for the chosen competitors were available during the assay development, competitive displacement assays based on fluorescence polarization were conducted to validate the pK_D values derived by the kinetic approach (Fig. 4A). Thereby, pK_i values validated the pK_D values obtained above (p – values being 0.68, 0.12,

0.18, 0.23 for pitolisant, ciproxifan, thioperamide and clobenpropit, respectively), showing a good correlation ($r = 0.992$, $P = 0.008$, Fig. 4B). Pitolisant appeared with affinities in nanomolar concentration range, whereas ciproxifan, thioperamide and clobenpropit showed only micromolar K_i values, thereby deviating from values obtained by [³H]-N^α-methylhistamine displacement assays (Table 2). F_{SR} in competition binding assays showed maximum binding below saturation that is important as erroneous K_i values may occur if an exceedingly high amount of labeled ligand is bound. To assess the influence of this termed ‘ligand depletion’ as possible reason for the observed discrepancies, the exact correction to Cheng and Prusoffs translation of IC₅₀ values into K_i values was applied (Munson and Rodbard, 1988), not showing significant differences (Table 2). Thus, errors were not due to large contents of H₃ receptor preparation.

3.5. Characterization of concerted N^α-methylhistamine and bodilisant binding to H₃R

The results obtained above prompted us to investigate the binding behavior of N^α-methylhistamine and bodilisant. Competitiveness of bodilisant and N^α-methylhistamine at H₃ receptors was assessed by saturation binding curves of tritiated ligand in presence of different bodilisant concentrations that should cause a linear shift in affinity (Fig. 5A) (Christopoulos, 2002). Indeed, such a correlation ($R^2 = 0.94$) could be found if examining the data in a Schild-type plot using specific binding instead of functional data (Fig. 5B). However, the slope being 0.58 ± 0.06 showed a large deviation from unity.

Taking advantage of the newly developed method above, we also

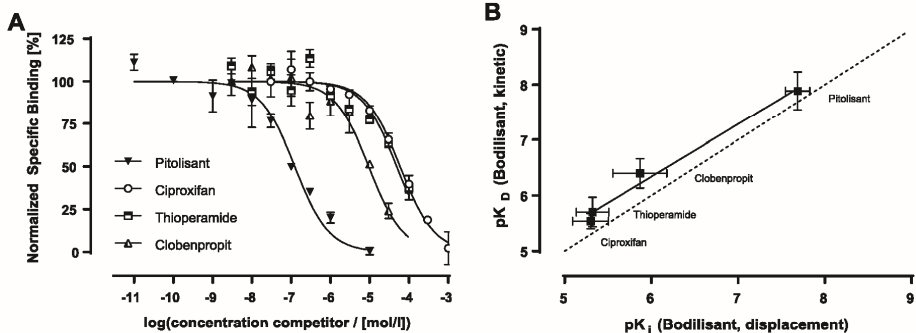


Fig. 4. Fluorescence polarization-based bodilisant displacement assays. (A) Different competitors were titrated against 12 nM bodilisant. Anisotropy data were transformed to specific binding (F_{SB}) and normalized to fitted maximum for presentation ($\%F_{SB} \pm S.D.$). (B) Pearson correlation of kinetically derived affinity measure (pK_D) with that derived by fluorescence polarization-based displacement assay (pK_i) adopted from Table 2, resulting in a correlation of $r = 0.992$ ($P = 0.008$). The dashed line indicates a line with unity slope.

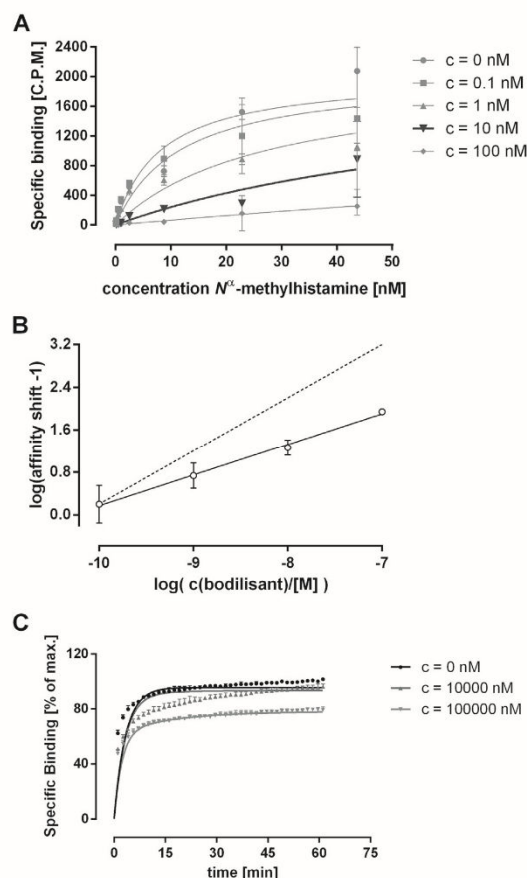


Fig. 5. Characterization of binding properties of *N*^α-methylhistamine and bodilisant. (A) Saturation experiments included eight different concentrations of [³H]-*N*^α-methylhistamine against 0.1, 1, 10 and 100 nM bodilisant and membrane preparations containing histamine H₃ receptor (20 μg/well) within binding buffer (75 mM Tris, 100 mM NaCl, 10 mM MgCl₂, 0.01% Pluronic® F-127 pH = 7.4). Incubation was terminated after 90 min according to the procedure described by Khanfar et al. (2018). Data display one representative of two independent experiments performed in duplicate while highlighting the approximate conditions for *N*^α-methylhistamine within a fluorescence polarization-based kinetic assay in black. (B) Apparent *K*_D values from both independent experiments were converted to logarithmic affinity shifts - 1 (concentration ratio) and plotted against bodilisant concentration in a Schild-type regression. Linear regression yielded a straight line (*R*² = 0.94) with a slope = 0.58 ± 0.06 (mean ± S.D.). The dashed line indicates a straight line with unity slope. (C) Fluorescence polarization-based kinetics of *N*^α-methylhistamine as described previously, revealing high concentrations of competitor needed to inhibit binding of bodilisant. The panel shows data of a representative of three independent experiments as means ± S.D. of triplicates.

determined binding kinetics of unlabeled *N*^α-methylhistamine and the corresponding affinity (Fig. 5C). With *k*_{off} = 0.045 ± 0.015 min⁻¹ a residence time of 22 ± 8 min was demonstrated. A remarkably slow association rate (with *k*_{on} = 0.86 ± 0.32 mM⁻¹ min⁻¹) emanate from unusually high concentrations of *N*^α-methylhistamine (> 10 μM) demanding to cause inhibition of bodilisant (*c* = 12 nM) within the time-course, consequently resulting in affinity of high micromolar concentration range (*pK*_D = 4.25 ± 0.06). In contrast, the highlighted

dataset of Fig. 5A shows the radiolabeled congener still binding to the receptor despite remarkably lower concentrations.

4. Discussion

The newly established method permits measurements of binding kinetics at the H₃ receptor and thereby allows determination of *τ*. Taking the considerations of setting up assays using fluorescence polarization into account, the protocol consists of typical elements of competition assays based on this technique and subsequently, it was expanded to established frameworks for studying receptor binding kinetics. Once this pair was found, signal stability was determined as the method should be capable of monitoring long residence times without conflicting with receptor degradation processes. The receptor concentration appeared relatively high when compared to classical radioligand binding experiments due to the need of binding a significant amount of fluorescence ligand for detecting a signal. Occurrence of ligand depletion might cause alterations of basic terms in mathematical derivations used for affinity estimates as the *K*_i value derived by Cheng and Prusoff (1973) or the previously mentioned mathematical model by Motulsky and Mahan. In this case, measured affinity estimates as *K*_D and *K*_i would appear erroneous and may be a reason for the estimates derived by our method. However, *K*_{i,ex} derived by an exact solution accounting for ligand depletion did not show significantly different values compared to *K*_i estimations by the first method. *K*_D values were validated with consistent *K*_i values observed within the displacement assay using bodilisant as labeled ligand.

We detected medium *τ* for the fluorescently labeled ligand bodilisant. *k*_{off} values did not differ among the representative H₃ inverse agonists ciproxifan, pitolisant as well as for thioperamide and clobenpropit, that show slower dissociation rate constants in literature (Mocking et al., 2018). We attribute these findings to an apparent high dependency of kinetic off-rates on the respective assay conditions as in recent literature higher *k*_{off} values can be found for pitolisant as well (Riddy et al., 2019). The association rate constants were distinct, ranging about three orders of magnitude from bodilisant (fastest association) to thioperamide and ciproxifan (slowest association). For interpretation of the results we take the initial considerations of the drug-target residence time concept by Copeland into account, namely *k*_{off} being an indicator accounting for interactions between ligand and receptor that control the dissociation, whereas *k*_{on} being influenced by many further processes such as diffusion, desolvation and conformational changes of the ligand as well as of the receptor (Copeland et al., 2006; Schuetz et al., 2017). This would indicate that the observed inverse agonists display comparable interaction modes and the binding event of ciproxifan and thioperamide appear more complex as of clobenpropit or pitolisant.

Due to low association rate constants, the method seems to lack observing affinities within the range of those typically found for the assessed ligands in literature and by radioligand displacement experiments, while no difference was found for pitolisant and bodilisant. From a structural point of view, this observation might be rationalized as with bodilisant, our assay makes use of a non-imidazole H₃ receptor ligand, whereas most radioligand binding experiments at H₃ receptor are performed using [³H]-*N*^α-methylhistamine, [³H]-histamine or [¹²⁵I]-iodoproxyfan. Various research projects revealed the existence of further receptor states for G-protein coupled receptors beyond the active and inactive state (Baker and Hill, 2007). Taking this and the structural differences of pitolisant and bodilisant compared to the imidazole-based H₃ receptor ligands into account, we postulate that bodilisant addresses another affinity state if not another binding site at the histamine H₃ receptor. The second hypothesis may be supported by the evidence of further binding sites at many other G-protein coupled receptors beyond those for endogenous ligand and G-proteins that is increasingly presumed to exist at many more receptors (Christopoulos, 2002; Wootton et al., 2013; Chan et al., 2018; Goulding et al., 2018).

D. Reiner, H. Stark

European Journal of Pharmacology 848 (2019) 112–120

Despite such evidence being best provided by resolving the structure of the target in question, the results of the present study do not minimize this probability but contribute with indicators thereof as a Schild-type plot using tritiated *N*^α-methylhistamine and bodilisant (Christopoulos and Kenakin, 2002). This approach revealed a straight line, an indicator for potential competitive behavior within the examined concentration range but a slope smaller than unity, describing a disproportional increase of competitor action at the receptor with increasing concentrations. The latter finding may be attributable to experimental factors such as inactivation or uptake processes of labeled species within the receptor compartment but seems unlikely while working with membrane preparations and the well-established use of *N*^α-methylhistamine as radiolabeled ligand (Alexander et al., 2015). Alternatively, competition of the investigated ligands for two binding sites may emerge to such extend (Neubig et al., 2003). We could additionally demonstrate binding of [³H]-*N*^α-methylhistamine while not displacing bodilisant at even higher concentration of untritiated analogue. Despite this unusual approach, it expands our hypothesis of bodilisant binding to a second binding site with higher receptor occupancy but similar affinity that is consistent with bodilisant kinetics indicating a single class of binding sites (Fig. 2B). *N*^α-methylhistamine would then exhibit different affinities for both sites.

Reflection of the kinetic results in this context deduce the observed differences in affinity of competing ligands from molecular perspective: Measurable dissociation rate constants show a degree of drug-receptor interaction that would have been concealed by simple displacement assays. Slow association rates among the presented imidazole-containing H₃ receptor ligands describe the complexity of the binding event, hindering the association and leading to weaker binding affinities to this binding site. In addition, this method does not preclude different rate constants and affinity to other binding sites. Qualitatively, the results exemplify the possible high probe-dependency of competitive displacement assays that are never direct affinity measurements, but estimations depending on assay conditions as well as of the properties of the labeled ligand in use.

5. Conclusion

Growing demand for hit-to-lead optimization oriented on drug-target residence time prompted us to set up a method to assess receptor binding kinetics. Application of fluorescence polarization instead of binding experiments using radiolabeled ligands appeared as a modern and useful approach as it enables multiparameter analysis through real-time resolution and to further extend the recently burgeoning portfolio of methods to investigate drug-target residence times at the H₃ receptor. Upon this, embedded into an automated pipetting surrounding, this method can be further applied to high throughput screening programs. Residence times of clobenpropit, thioperamide, ciproxifan and pitolisant adjoined around five min. Large differences for association rate constants were observed resulting in a reduced affinity of ciproxifan, thioperamide, clobenpropit and *N*^α-methylhistamine compared to that observed in radioligand displacement assays. Validation of the kinetically derived affinity estimates was successfully performed using bodilisant as labeled analogue within displacement assays based on fluorescence polarization. However, the results suggest the presumptive existence of a second binding site needing further pharmacological elucidation. Thus, this method would not serve as substitute for radioligand binding experiments, but provides useful kinetic information about a binding event even in case of low-affinity ligands. Moreover, the given protocol provides a roadmap for expanding fluorescence-polarization based investigations using other fluorescently labeled ligands at histamine H₃ receptors.

Acknowledgements

We thank Prof. Dr. Jean-Charles Schwartz (Bioprojet, France), the

German Research Society (DFG INST 208/664-1 FUGG) and the EU COST Actions CA18133 and CA15135 for support. We further acknowledge the technical support of Dr. Miriam Tomasch, Dr. Tim Kottke, Mr. Johann Stephan Schwed and Ms. Kathrin Grau.

Declarations of interest

None.

Author contributions

DR planned, conducted the experiments, analyzed the data, wrote and approved the manuscript. HS initiated and supervised the project, provided reagents, read and approved the manuscript.

Appendix A. Supporting information

Supplementary data associated with this article can be found in the online version at doi:10.1016/j.ejphar.2019.01.041.

References

- Alexander, S.P.H., Davenport, A.P., Kelly, E., Marrion, N., Peters, J.A., Benson, H.E., Faccenda, E., Pawson, A.J., Sharman, J.L., Southan, C., Davies, J.A., Collaborators, C., 2015. The concise guide to PHARMACOLOGY 2015/16: G protein-coupled receptors. *Br. J. Pharmacol.* 172, 5744–5869. <https://doi.org/10.1111/bph.13348>.
- Baker, J.G., Hill, S.J., 2007. Multiple GPCR conformations and signalling pathways: implications for antagonist affinity estimates. *Trends Pharmacol. Sci.* 28, 374–381. <https://doi.org/10.1016/j.tips.2007.06.011>.
- Banks, P., Gosselin, M., Prystay, L., 2000. Fluorescence polarization assays for high throughput screening of G protein-coupled receptors. *J. Biomol. Screen.* 5, 159–167. <https://doi.org/10.1177/108705710000500308>.
- Banks, P., Harvey, M., 2002. Considerations for using fluorescence polarization in the screening of G protein-coupled receptors. *J. Biomol. Screen.* 7, 111–117. <https://doi.org/10.1177/108705710200700203>.
- Bosma, R., Moritani, R., Leurs, R., Vischer, H.F., 2016. BRET-based beta-arrestin2 recruitment to the histamine H1 receptor for investigating antihistamine binding kinetics. *Pharmacol. Res.* 111, 679–687. <https://doi.org/10.1016/j.phrs.2016.07.034>.
- Bradford, M.M., 1976. A rapid and sensitive method for the quantitation of microgram quantities of protein utilizing the principle of protein-dye binding. *Anal. Biochem.* 72, 248–254. [https://doi.org/10.1016/0003-2697\(76\)90527-3](https://doi.org/10.1016/0003-2697(76)90527-3).
- Chan, H.C.S., Wang, J., Palczewski, K., Filipek, S., Vogel, H., Liu, Z.-J., Yuan, S., 2018. Exploring a new ligand binding site of G protein-coupled receptors. *Chem. Sci.* 9, 6480–6489. <https://doi.org/10.1039/C8SC01680A>.
- Cheng, Y.C., Prusoff, W., 1973. Relationship between the inhibition constant (K_i) and the concentration of inhibitor which causes 50 per cent inhibition (I₅₀) of an enzymatic reaction. *Biochem. Pharmacol.* 22, 3099–3108. [https://doi.org/10.1016/0006-2952\(73\)90196-2](https://doi.org/10.1016/0006-2952(73)90196-2).
- Christopoulos, A., 2002. Allosteric binding sites on cell-surface receptors: novel targets for drug discovery. *Nat. Rev. Drug Discov.* 1, 198. <https://doi.org/10.1038/nrd746>.
- Christopoulos, A., Kenakin, T., 2002. G protein-coupled receptor allostery and complexing. *Pharmacol. Rev.* 54, 323–374.
- Colquhoun, D., 1968. The rate of equilibration in a competitive drug system and the auto-inhibitory equations of enzyme kinetics: some properties of simple models for passive sensitization. *Proc. Roy. Soc. B* 170, 135–154. <https://doi.org/10.1098/rspb.1968.0030>.
- Copeland, R.A., 2016. The drug-target residence time model: a 10-year retrospective. *Nat. Rev. Drug Discov.* 15, 87–95. <https://doi.org/10.1038/nrd.2015.18>.
- Copeland, R.A., Pompliano, D.L., Meek, T.D., 2006. Drug-target residence time and its implications for lead optimization. *Nat. Rev. Drug Discov.* 5, 730–739. <https://doi.org/10.1038/nrd2082>.
- Ehlert, F.J., 1988. Estimation of the affinities of allosteric ligands using radioligand binding and pharmacological null methods. *Mol. Pharmacol.* 33, 187–194.
- Gagne, A., Banks, P., Hurt, S.D., 2002. Use of fluorescence polarization detection for the measurement of fluopeptidom binding to G protein-coupled receptors. *J. Recept. Signal Transduct. Res.* 22, 333–343. <https://doi.org/10.1081/RRS-120014605>.
- Goulding, J., May, L.T., Hill, S.J., 2018. Characterisation of endogenous A2A and A2B receptor-mediated cyclic AMP responses in HEK 293 cells using the GloSensor™ biosensor: evidence for an allosteric mechanism of action for the A2B-selective antagonist PSB 603. *Biochem. Pharmacol.* 147, 55–66. <https://doi.org/10.1016/j.bcp.2017.10.013>.
- Grassmann, S., Apelt, J., Sippl, W., Ligneau, X., Pertz, H.H., Zhao, Y.H., Arrang, J.M., Ganellin, C.R., Schwartz, J.C., Schunack, W., Stark, H., 2003. Imidazole derivatives as a novel class of hybrid compounds with inhibitory histamine N-methyltransferase potencies and histamine H₃ receptor affinities. *Bioorg. Med. Chem.* 11, 2163–2174. [https://doi.org/10.1016/S0968-0896\(03\)00120-2](https://doi.org/10.1016/S0968-0896(03)00120-2).
- Guo, D., Hillger, J.M., AP, I.J., Heitman, L.H., 2014. Drug-target residence time—a case for G protein-coupled receptors. *Med. Res. Rev.* 34, 856–892. <https://doi.org/10.1002/med.21307>.

3.1 Ligand binding kinetics at histamine H3 receptors by fluorescence polarization with real-time monitoring

D. Reiner, H. Stark

European Journal of Pharmacology 848 (2019) 112–120

- Hoffmann, C., Castro, M., Rinken, A., Leurs, R., Hill, S.J., Vischer, H.F., 2015. Ligand residence time at G-protein-coupled receptors-why we should take our time to study it. *Mol. Pharmacol.* 88, 552–560. <https://doi.org/10.1124/mol.115.099671>.
- Kecskes, M., Kumar, T.S., Yoo, L., Gao, Z.G., Jacobson, K.A., 2010. Novel Alexa Fluor-488 labeled antagonist of the A(2A) adenosine receptor: application to a fluorescence polarization-based receptor binding assay. *Biochem. Pharmacol.* 80, 506–511. <https://doi.org/10.1016/j.bcp.2010.04.027>.
- Khanfar, M.A., Reiner, D., Hagenow, S., Stark, H., 2018. Design, synthesis, and biological evaluation of novel oxadiazole- and thiazole-based histamine H3R ligands. *Bioorg. Med. Chem.* 26, 4034–4046. <https://doi.org/10.1016/j.bmc.2018.06.028>.
- Kottke, T., Sander, K., Weizel, L., Schneider, E.H., Seifert, R., Stark, H., 2011. Receptor-specific functional efficacies of alkyl imidazoles as dual histamine H3/H4 receptor ligands. *Eur. J. Pharmacol.* 654, 200–208. <https://doi.org/10.1016/j.ejphar.2010.12.033>.
- Lea, W.A., Simeonov, A., 2011. Fluorescence polarization assays in small molecule screening. *Expert Opin. Drug Discov.* 6, 17–32. <https://doi.org/10.1517/17460441.2011.537322>.
- Liu, Y., Zeng, H., Pediani, J.D., Ward, R.J., Chen, L.Y., Wu, N., Ma, L., Tang, M., Yang, Y., An, S., Guo, X.X., Iiao, Q., Xu, T.R., 2018. Visualization of the activation of the histamine H3 receptor (H3R) using novel fluorescence resonance energy transfer biosensors and their potential application to the study of H3R pharmacology. *FEBS J.* 285, 2319–2336. <https://doi.org/10.1111/febs.14484>.
- Lu, H., Tonge, P.J., 2010. Drug-target residence time: critical information for lead optimization. *Curr. Opin. Chem. Biol.* 14, 467–474. <https://doi.org/10.1016/j.cbpa.2010.06.176>.
- Meier, G., Apelt, J., Reichert, U., Grassmann, S., Ligneau, X., Elz, S., Leurquin, F., Ganellin, C.R., Schwartz, J.C., Schunack, W., Stark, H., 2001. Influence of imidazole replacement in different structural classes of histamine H(3)-receptor antagonists. *Eur. J. Pharm. Sci.* 13, 249–259. [https://doi.org/10.1016/S0928-0987\(01\)00106-3](https://doi.org/10.1016/S0928-0987(01)00106-3).
- Mocking, T.A.M., Verweij, E.W.E., Vischer, H.F., Leurs, R., 2018. Homogeneous, real-time NanoBRET binding assays for the histamine H3 and H4 receptors on living cells. *Mol. Pharmacol.* 94, 1371–1381. <https://doi.org/10.1124/mol.118.113373>.
- Motulsky, H.J., Mahan, L.C., 1984. The kinetics of competitive radioligand binding predicted by the law of mass action. *Mol. Pharmacol.* 25, 1–9.
- Munson, P., Rodbard, D., 1988. An exact correction to the “Cheng-Prusoff” correction. *J. Recept. Res.* 8, 533–546. <https://doi.org/10.3109/10799898809049010>.
- Neubig, R.R., Spedding, M., Kenakin, T., Christopoulos, A., 2003. International union of pharmacology committee on receptor nomenclature and drug classification. XXXVIII. Update on terms and symbols in quantitative pharmacology. *Pharmacol. Rev.* 55, 597–606. <https://doi.org/10.1124/pr.55.4.4>.
- Panula, P., Chazot, P.L., Cowart, M., Gutzmer, R., Leurs, R., Liu, W.L., Stark, H., Thurmond, R.L., Haas, H.L., 2015. International union of basic and clinical pharmacology. XCVIII. Histamine receptors. *Pharmacol. Rev.* 67, 601–655. <https://doi.org/10.1124/pr.114.010249>.
- Perrin, F., 1926. Polarisation de la lumière de fluorescence. Vie moyenne des molécules dans l'état excité. *J. Phys. Radium* 7, 390–401. <https://doi.org/10.1051/jphysrad:01926007012039000>.
- Riddy, D.M., Cook, A.E., Shackelford, D.M., Pierce, T.L., Mocaer, E., Mannoury la Cour, C., Sors, A., Charman, W.N., Summers, R.J., Sexton, P.M., Christopoulos, A., Langmead, C.J., 2019. Drug-receptor kinetics and sigma-1 receptor affinity differentiate clinically evaluated histamine H3 receptor antagonists. *Neuropharmacology* 144, 244–255. <https://doi.org/10.1016/j.neuropharm.2018.10.028>.
- Roehrl, M.H.A., Wang, J.Y., Wagner, G., 2004. A general framework for development and data analysis of competitive high-throughput screens for small-molecule inhibitors of protein-protein interactions by fluorescence polarization. *Biochemistry* 43, 16056–16066. <https://doi.org/10.1021/bi048233g>.
- Rossi, A.M., Taylor, C.W., 2011. Analysis of protein-ligand interactions by fluorescence polarization. *Nat. Protoc.* 6, 365–387. <https://doi.org/10.1038/nprot.2011.305>.
- Schuetz, D.A., de Witte, W.E.A., Wong, Y.C., Knasmueller, B., Richter, L., Kokh, D.B., Sadiq, S.K., Bosma, R., Nederpelt, L., Heitman, L.H., Segala, E., Amaral, M., Guo, D., Andres, D., Georgi, V., Stoddart, L.A., Hill, S., Cooke, R.M., De Graaf, C., Leurs, R., Frech, M., Wade, R.C., de Lange, E.C.M., Ijzerman, A.P., Müller-Fahrnow, A., Ecker, G.F., 2017. Kinetics for Drug Discovery: an industry-driven effort to target drug residence time. *Drug Discov. Today* 22, 896–911. <https://doi.org/10.1016/j.drudis.2017.02.002>.
- Stark, H., 2000. Convenient procedures for synthesis of ciproxifan, a histamine H3-receptor antagonist. *Arch. Pharm.* 333, 315–316. [https://doi.org/10.1002/1521-4184\(200009\)333:9<315::AID-ARDP315>3.0.CO;2-M](https://doi.org/10.1002/1521-4184(200009)333:9<315::AID-ARDP315>3.0.CO;2-M).
- Stoddart, L.A., Vernall, A.J., Bouzo-Lorenzo, M., Bosma, R., Kooistra, A.J., de Graaf, C., Vischer, H.F., Leurs, R., Bridson, S.J., Kellam, B., Hill, S.J., 2018. Development of novel fluorescent histamine H1-receptor antagonists to study ligand-binding kinetics in living cells. *Sci. Rep.* 8, 1572. <https://doi.org/10.1038/s41598-018-19714-2>.
- Stoddart, L.A., White, C.W., Nguyen, K., Hill, S.J., Pfeleger, K.D.G., 2016. Fluorescence- and bioluminescence-based approaches to study GPCR ligand binding. *Br. J. Pharmacol.* 173, 3028–3037. <https://doi.org/10.1111/bph.13316>.
- Tomasch, M., Schwed, J.S., Paulke, A., Stark, H., 2013. Bodilissant a novel fluorescent, highly affine histamine h3 receptor ligand. *ACS Med. Chem. Lett.* 4, 269–273. <https://doi.org/10.1021/ml300383n>.
- Wootten, D., Christopoulos, A., Sexton, P.M., 2013. Emerging paradigms in GPCR allostery: implications for drug discovery. *Nat. Rev. Drug Discov.* 12, 630. <https://doi.org/10.1038/nrd4052>.
- Zhang, J.-H., Chung, T.D.Y., Oldenburg, K.R., 1999. A simple statistical parameter for use in evaluation and validation of high throughput screening assays. *J. Biomol. Screen.* 4, 67–73. <https://doi.org/10.1177/108705719900400206>.

Supplementary Material

Ligand binding kinetics
at histamine H₃ receptors by fluorescence-polarization
with real-time monitoring

David Reiner¹, Holger Stark^{1,*}

¹Heinrich Heine University Düsseldorf, Institute of Pharmaceutical and Medicinal Chemistry,
Universitätsstr. 1, 40225 Düsseldorf, Germany

*Corresponding author: Prof. Holger Stark, Tel.: +49 211 81-10478, Fax: +49 211 81-13359,
email: stark@hhu.de

S1. Optimization of Assay conditions

S1.1 Z'-values

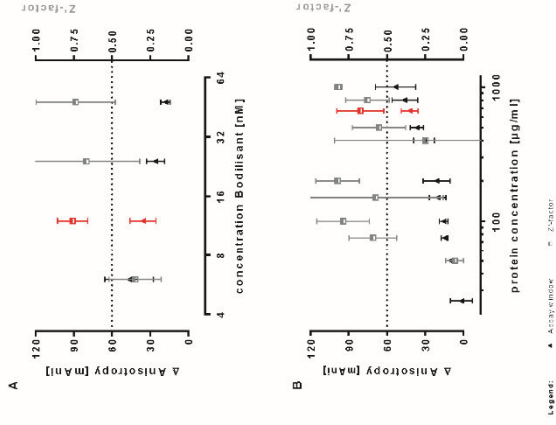


Fig. 1 Optimisation of anisotropy measurements of bodilisant at H₃ receptor. The panels show assay windows (left ordinate: difference of anisotropy signals of samples with and without 10 nM of pitolisant) and Z'-factors (right ordinate) calculated as means ± S.D. from three independent experiments performed in duplicate. The dashed line indicates Z' > 0.5, a factor signifying high-throughput screening compatibility. Red highlighted data pairs indicate the chosen assay conditions for later experiments. (A) Four concentrations of bodilisant (6 nM, 12 nM, 24 nM and 48 nM; abscissa) were incubated with 800 µg/ml of protein for 60 min. (B) Various protein concentrations were titrated against 12 nM of bodilisant and incubated for 60 min.

3.2. Novel pyrrolidinone derivative lacks claimed histamine H₃ receptor stimulation in receptor binding and functional studies

David Reiner¹⁾, Aleksandra Zivkovic¹⁾, Olivier Labeeuw²⁾, Stéphane Krief²⁾, Marc Capet²⁾ and Holger Stark¹⁾

1) Institute of Pharmaceutical and Medicinal Chemistry, Heinrich Heine University Düsseldorf, Universitätsstr. 1, 40225 Düsseldorf, Germany

2) Bioprojet Biotech, 4 Rue du Chesnay Beauregard, 35760, Saint-Grégoire, France

Published in: *European Journal of Medicinal Chemistry*, 2020, 191:112150

DOI: 10.1016/j.ejmech.2020.112150

Contribution to research: DR designed, prepared and conducted radioligand displacement experiments and fluorescence polarisation-based binding studies and was involved in planning and interpretation of LC-MS based purity analysis. He analysed and interpreted the data from binding and functional assays, wrote the manuscript and processed the revision.

Abstract:

Since the discovery and early characterization of the histamine H₃ receptor (H₃R) in the 1980's, predominantly imidazole-based agonists were presented to the scientific community such as N-methylhistamine (N^α-MeHA) or (R)-α-methylhistamine ((R)α-MeHA). Whereas therapeutic applications have been prompted for H₃R agonists such as treatment of pain, asthma and obesity, several drawbacks associated with imidazole-containing ligands makes the search for new agonists for this receptor demanding. Accordingly, high interest arose after publication of several pyrrolidindione-based, highly affine H₃R agonists within this journal that avoid the imidazole moiety and thus, presenting a novel type of potential pharmacophores (Ghoshal, Anirban et al., 2018). In our present study performed in two independent laboratories, we further evaluated the exposed lead-compound (*EC*₅₀ = 0.1 nM) of the previous research project with regards to pharmacological behavior at H₃R. Thereby, no binding affinity was observed in neither [³H]N^α-MeHA nor bodilisant displacement assays that contradicts the previously published activity. Additional functional exploration employing GTPγ[³⁵S], cAMP-accumulation assay and cAMP response element (CRE)-driven reporter gene assays exhibited slight partial agonist properties of such pyrrolidindiones but acting apart from the reported concentration range. We conclude, that the previously reported actions of such pyrrolidindiones result from an overestimation based on the method of measurement and thus, we cast doubt on the new pharmacophores with H₃R agonist activity.

Reproduced from Reiner D, Zivkovic A, Labeeuw O, Krief S, Capet M and Stark H, Novel pyrrolidinone derivative lacks claimed histamine H₃ receptor stimulation in receptor binding and functional studies, *Eur. J. Med. Chem.*, 2020, 191:112150, with permission for personal use from Elsevier.

Copyright 2019 Elsevier Masson SAS.



Contents lists available at ScienceDirect

European Journal of Medicinal Chemistry

journal homepage: <http://www.elsevier.com/locate/ejmech>



Research paper

Novel pyrrolidinone derivative lacks claimed histamine H₃ receptor stimulation in receptor binding and functional studies



David Reiner^a, Aleksandra Zivkovic^a, Olivier Labeeuw^b, Stéphane Krief^b, Marc Capet^b, Holger Stark^{a,*}

^a Heinrich Heine University Düsseldorf, Institute of Pharmaceutical and Medicinal Chemistry, Universitätsstr. 1, 40225, Düsseldorf, Germany

^b Binprojet Biotech, 4 Rue du Chesnay Beauregard, 35760, Saint-Grégoire, France

ARTICLE INFO

Article history:

Received 10 December 2019

Received in revised form

31 January 2020

Accepted 13 February 2020

Available online 14 February 2020

Keywords:

GPCR

Histamine

Histamine H₃ receptor

Agonist

Reporter assay

ABSTRACT

Since the discovery and early characterization of the histamine H₃ receptor (H₃R) in the 1980's, predominantly imidazole-based agonists were presented to the scientific community such as N²-methylhistamine (N²-MeHA) or (R)-α-methylhistamine ((R)-α-MeHA). Whereas therapeutic applications have been prompted for H₃R agonists such as treatment of pain, asthma and obesity, several drawbacks associated with imidazole-containing ligands makes the search for new agonists for this receptor demanding. Accordingly, high interest arose after publication of several pyrrolidinone-based, highly affine H₃R agonists within this journal that avoid the imidazole moiety and thus, presenting a novel type of potential pharmacophores (Ghoshal, Anirban et al., 2018). In our present study performed in two independent laboratories, we further evaluated the exposed lead-compound (EC₅₀ = 0.1 nM) of the previous research project with regards to pharmacological behavior at H₃R. Thereby, no binding affinity was observed in neither [³H]N²-MeHA nor bodilysant displacement assays that contradicts the previously published activity. Additional functional exploration employing GTPγ[³⁵S], cAMP-accumulation assay and cAMP response element (CRE)-driven reporter gene assays exhibited slight partial agonist properties of such pyrrolidinones but acting apart from the reported concentration range. We conclude, that the previously reported actions of such pyrrolidinones result from an overestimation based on the method of measurement and thus, we cast doubt on the new pharmacophores with H₃R agonist activity.

© 2020 Elsevier Masson SAS. All rights reserved.

1. Introduction

The discovery of the histamine H₃ receptor (H₃R) back in 1983 consolidated the role of histamine as a neurotransmitter [1–3]. Histamine was former known as tissue hormone to be involved in the etiology of allergies and gastritis that led to the development of successful drugs. After this successful period that relied on therapeutically influencing histamine H₁ and H₂ receptor mediated effects, new hope to resume this blockbuster period was raised by targeting brain-histamine function through the newly recognized

histamine receptor family member [4,5]. In parallel, the physiological characterization revealed constitutive activity and the responsibility of H₃Rs for modulating neuronal histamine release as autoreceptors [6–8] and as heteroreceptors being responsible for the release of further neurotransmitters such as acetylcholine, noradrenaline and dopamine [9–13].

Owing to the pivotal role of histamine as neurotransmitter and the corresponding involvement in pathophysiological processes, numerous H₃R ligands entered the clinical research stage, proving the therapeutic potential in disorders as Alzheimer's disease, Parkinson's disease, schizophrenia, epilepsy, attention-deficit and hyperactivity disorder (ADHD) and sleep-disorders [7,9,14,15]. Finally, the intense work was rewarded with a market authorization of pitolisant for the treatment of narcolepsy [16]. Whereas most preclinical and clinical research projects employ H₃R antagonists/inverse agonists, the development of H₃R agonists has been focused marginally. Potential applications were prompted for conditions of cardiac dysfunction, asthma, pain and migraine [17] as well as for

Abbreviations: ADHD, attention-deficit hyperactivity disorder; cAMP, 3'-5'-cyclic adenosine monophosphate; CRE, cAMP response element; CREB, cAMP response element binding protein; H₃R, histamine H₃ receptor; HMT, histamine N-methyltransferase; (R)-α-MeHA, (R)-α-methylhistamine; N²-MeHA, N²-methylhistamine; MRE, multiple response element.

* Corresponding author.

E-mail address: stark@hhu.de (H. Stark).

<https://doi.org/10.1016/j.ejmech.2020.112150>

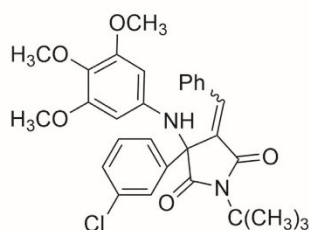
0223-5234/© 2020 Elsevier Masson SAS. All rights reserved.

obesity [18,19]. Structural features of well investigated H₃R agonists encompass an obligate 4- or 5-monosubstituted imidazole core, whereas the side chain tolerates some structural modifications. (*R*)- α -Methylhistamine ((*R*)- α -MeHA) as one of the first H₃R agonists used for pharmacological characterization of H₃R showed lacking applicability due to its high metabolism by histamine *N*-methyltransferase (HMT) that inactivates the agonist by *N*⁺-methylation, leading to the development of several prodrugs with low HMT affinity [20]. Additionally, their liability to interactions with the cytochrome P-450 enzyme system make 4-substituted imidazoles less attractive for optimization towards promising lead compounds [21].

Concluding such open questions in therapeutic application of H₃R agonists, some efforts for developing non-imidazole-based H₃R agonists have been currently presented to the scientific community [22]. In addition, we have been attracted by a recent publication that claims the identification of H₃R agonists comprising of pyrrolidindione cores as option to avoid the imidazole moiety (Fig. 1, compound **6k**) [23]. In remarkable contrast to all previously presented H₃R ligands, the compounds are devoid of basic amine with the property to be protonated at physiological pH values. The comprehensively investigated lead compound was identified in a screening program among 94 compounds employing cAMP accumulation in transiently H₃R-transfected HEK-293T cells based on the GloSensor™ technique [24]. Thereby, it displayed inhibition of cAMP-accumulation corresponding to an agonist in the low nanomolar concentration range as well as selectivity over histamine H₁, H₂ and H₄ receptors [23]. Specificity of H₃R mediated effects was investigated by monitoring the cAMP-response using such biosensors in HEK-293T cells without H₃R transfection, reversal of agonism by a H₃R-selective agonist (GSK334429) at 1 μ M of compound and by *in silico* screening excluding the compound belonging to pan assay interference compounds (PAINS) [23,25].

2. Results & discussion

The promising results from pyrrolidindiones as new chemical entity for H₃R pharmacophores prompted us for further elucidation but starting with the pharmacological investigation of binding properties at membrane preparations of HEK-293T cells stably transfected with the human 445-amino acid isoform encoding cDNA of H₃R. Therefore, compound **6k** was synthesized as described by Ghoshal et al. [23,25] (see materials & methods) as a yellow solid.



6k

H₃R: EC₅₀ = 0.1 nM^[23]

Fig. 1. Structure of **6k** that was claimed as H₃R selective agonist by Ghoshal et al. [23]. The EC₅₀ was derived from HEK-293T cells transiently expressing the human H₃R isoform and biosensors for monitoring cAMP accumulation (GloSensor™, Promega).

Interestingly, the compound did not show entire displacement of the highly affine H₃R agonist [³H]*N*²-methylhistamine (*N*²-MeHA, *c* = 2.0 nM, *K*_D = 3.1 nM) in radioligand displacement assays that were performed as described elsewhere [26]. Due to insolubility of the substance in assay buffer at 100 μ M (75 mM TRIS, pH = 7.4, 100 mM NaCl, 10 mM MgCl₂), only concentrations up to 10 μ M could be monitored, while full inhibition following a hill coefficient equal to unity was not observed (Fig. 2(A)). This effect may be attributable to different affinity states of receptor that two agonists are able to differentiate [27]. We are aware that the same effect may occur from impurities that were detected in the purchased compounds, however significant inhibition in low nanomolar concentration range corresponding to the reported EC₅₀ was lacking in our studies. We therefore subjected **6k** for further binding studies based on fluorescence polarization in an orthogonal screening system that makes use of bodilisant, a fluorescently labelled second generation H₃R ligand with binding characteristics directed towards secondary binding sites [28]. Through monitoring the time course of competition between **6k** and bodilisant (bodilisant: *c* = 12 nM, *K*_D = 1.9 nM) binding to H₃R, no inhibition was observed at concentrations of 1 μ M or 10 μ M (Fig. 2(B)), prohibiting the determination of kinetic rate constants. In contrast, pitolisant as reference antagonist markedly displaced bodilisant, leading to an affinity consistent with literature determinations (*K*_D = 8.6 nM, *k*_{on} = 1.5 · 10⁷ mol⁻¹ min⁻¹; *k*_{off} = 0.13 min⁻¹). Therefore, we conclude that binding of **6k** at H₃R is not the trigger of the effects reported by Ghoshal et al. [23].

We further applied three complementary functional systems, being GTP γ [³⁵S], cAMP-accumulation assay and a cAMP or multiple response element (CRE/MRE)-driven reporter-gene assay, as described below. With regards to effects most proximal within the signal cascade of H₃R mediated signal-transduction, the results of GTP γ [³⁵S] assay using human-isoform H₃R expressing HEK-293 cells failed to demonstrate G-protein activation by **6k**, though that should occur upon receptor activation by an agonist such as (*R*)

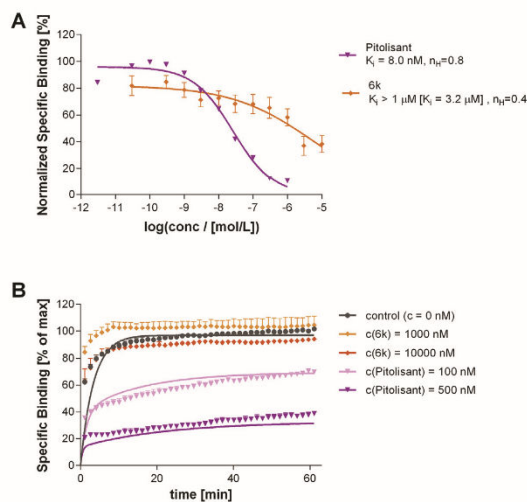


Fig. 2. Displacement curves of compound **6k** employing [³H]*N*²-methylhistamine (A) or bodilisant (B). (A): [³H]*N*²-methylhistamine displacement by pitolisant (*K*_i = 15.9 [10.1; 24.9] nM) and **6k** (*K*_i > 1 μ M). Values were derived from global fitting normalized specific binding of four independent experiments performed in duplicate as described by Khanfar et al. [26]. (B): The time course of bodilisant being displaced by pitolisant and **6k**, determined by fluorescence-polarization as described previously [28].

α -MeHA ($EC_{50} = 40$ nM; Fig. 3 (A)) [29]. To test for presumable antagonist efficacy, reversion of (*R*)- α -MeHA by **6k** was investigated. In contrast to pitolisant ($K_B = 3.7$ nM), compound **6k** exerted a slight inhibition in micromolar concentration range and thereby, was in consistence with the observations of the binding studies outlined above. The next distal step in the transduction pathway was examined, being the mitigation of cAMP accumulation upon inhibition of adenylyl cyclase by interaction with $G\alpha_i$ -proteins. This effect was illustrated for agonism by histamine ($EC_{50} = 30$ nM) within our studies using CHO cells with stably transfected H₃R,

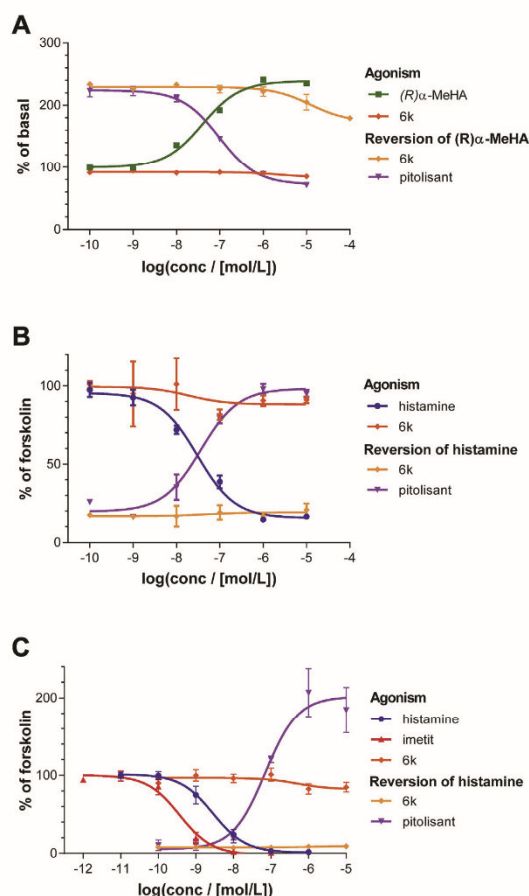


Fig. 3. Efficacy of compound **6k** investigated in three orthogonal assays. (A): GTPγ [³⁵S]-binding in membrane preparations of H₃R-expressing HEK-293 cells, showing changes of H₃R activity relative to basal receptor activity that was exerted by agonist (*R*)- α -MeHA and compound **6k**. Additionally, reversion of (*R*)- α -MeHA agonist (1 μ M) response according to antagonist by pitolisant and **6k** is displayed. (B): cAMP accumulation as assayed with a HitHunter® cAMP assay for small molecules (DiscoverX) within CHO-DUKX cells stably expressing H₃R and a CRE/MRE-luciferase reporter gene [36]. The curves illustrate the extend of inhibition of adenylyl cyclase mediated by **6k** and histamine as reference agonist, as well as reversion of histamine (1 μ M) activity by **6k** and pitolisant as reference inverse agonist. (C): CRE/MRE-luciferase reporter gene assays conducted in the same cells as described in Panel (B). Data correspond to luciferase expression resulting from changes in cAMP accumulation due to agonism by histamine, imetit or **6k** or reversal of histamine (100 nM) by pitolisant and **6k**.

whereas weak partial agonist properties with a low intrinsic activity of 0.14 (relative to histamine) could be observed for the compound in question (Fig. 3(B)). However, the corresponding partial antagonist properties could not be confirmed in presence of histamine, again in contrast to the well characterized H₃R inverse agonist/antagonist pitolisant ($K_B = 1.0$ nM). A similar effect could be observed in more distal CRE/MRE-luciferase reporter gene assays relying on the expression of luciferase upon binding of the cAMP response element binding protein (CREB) to the corresponding promoter-region within DNA (Fig. 3(C)). As well, a response corresponding to full agonism was observed for both H₃R agonists, imetit and histamine ($EC_{50} = 2.9$ and 0.4 nM, respectively), but not for **6k**. Additionally, the latter was not able to reverse the effects of histamine while antagonization of agonist-mediated inhibition of cAMP accumulation with pitolisant resulted in $K_B = 2.0$ nM. Control measurements using paternal CHO-cells deprived of H₃R but being transfected with CRE/MRE-luciferase reporter gene construct suggest that the observed effects are H₃R mediated (cf. Supporting Information, Fig. S2.1).

The herein presented studies from our characterization being performed in two independent laboratories show contrary results to those obtained by the originators of **6k**. The initial investigation by Ghoshal et al. was comprehensively performed based on cAMP accumulation [23]. Whereas cAMP can evolve from various cellular sources [30], the group did not observe same effects in HEK-293T cells that were not transfected with H₃R being indicative of H₃R mediated effects. Nonetheless, herein described results from [³H]N²-MeHA and bodilisan displacement studies raise strong concerns about the presented specificity of those effects. Secondly, the group reported reversal of agonism exerted by **6k** (see Ref. [23]) by GSK334429 as H₃R selective inverse agonist [31]. However, thorough inspection of the data shows that **6k** shows only slight abrogation of forskolin induced response. The GloSensor™ application relies on complementation of functional Firefly luciferase enzyme in presence of cAMP [24]. Due to the affiliation of this technique to competition following the law of mass-action, the signal is not linear to the accumulated second messenger [24]. As extensively reviewed by Hill et al. (2010), this provokes false positive results if the dynamic range of the assay is exceeded and/or results being interpreted on luminescence data instead of transforming such to cAMP-levels before further analysis [32]. This, in combination with the slight inhibition of forskolin-induced response displayed in the Supplementary Information to the research paper and seen in our investigation to some extent, is one potential explanation for the observations by Ghoshal et al. (2018) [23].

3. Conclusion

The cAMP accumulation displayed in the presented study by Ghoshal et al. (2018) may originate from unspecific effects or misinterpretation of the measurement data, but we do not support the hypothesis of them being ligands at the H₃R. We conclusively cast doubt on the presented pyrrolidinediones being representatives for a new pharmacophoric entity with affinity and agonist efficacy at H₃R, though such new pharmacophores would be of high interest for the H₃R research community.

4. Materials & methods

4.1. Synthesis & analytics of compound **6k** [(*E/Z*)-4-benzylidene-1-(*tert*-butyl)-3-((3,4,5-trimethoxyphenyl)amino)-3-(3-chlorophenyl)pyrrolidine-2,5-dione]

Compound **6k** [(*E/Z*)-4-benzylidene-1-(*tert*-butyl)-3-((3,4,5-trimethoxyphenyl)amino)-3-(3-chlorophenyl)pyrrolidine-2,5-

dione] was resynthesized as a yellow solid according to the procedure described by Ghoshal et al. (2018) [23].

Briefly, a solution of phenylpropionic acid (500 mg, 3.42 mmol), 3,4,5-trimethoxyaniline (627 mg, 1 eq.), *m*-chlorobenzaldehyde (388 μ L, 1 eq.) and *tert*-butyl isocyanate (387 μ L, 1 eq.) in methanol (5 mL) was stirred for 12 h at room temperature. Solid potassium carbonate (1.42 g, 3 eq.) was then added and the mixture refluxed for 5 h. After cooling to room temperature, the mixture was filtered on a pad of Celite, rinsed with methanol and the filtrate concentrated under reduced pressure. Two consecutive flash chromatographic separations on silica (40 g/50 μ m and 25 g/20 μ m, elution with ethyl acetate/*n*-heptane from 4/1 to 2/1) were necessary to afford the sample (120 mg, yellow solid, m.p. = 79 °C).

¹H and ¹³C NMR spectra were recorded on a Varian 400 MHz instrument and matched the reference ones. ¹H NMR (400 MHz, CDCl₃): δ 7.90 (s, 1H, Ph-CH=C-), 7.69 (s, 1H, ArH), 7.46 (d, *J* = 7.2 Hz, 1H, ArH), 7.37–7.22 (m, 7H, ArH), 5.58 (s, 2H, ArH), 4.26 (s, 1H, NH), 3.68 (s, 3H, OCH₃), 3.58 (s, 6H, -(OCH₃)₂), 1.54 (s, 9H, -(CH₃)₃); ¹³C NMR (125 MHz, CDCl₃): δ 176.25 (-C=C-CO), 170.30 (CO), 153.15, 140.37, 140.06, 138.52, 135.28, 133.05, 132.80, 131.04, 130.34, 130.12, 129.29, 128.61, 128.32, 126.64, 124.39, 96.05, 67.61 (C-quaternary), 60.91 (C-(CH₃)₃), 59.17 (OCH₃), 55.72 (OCH₃)₂, 28.34 (-(CH₃)₃) (Full spectra are depicted in supp. inf., Fig. S1.1 and Fig. S1.2.).

UV purity was found to be over 94% by HPLC (Sunfire C18 5 μ m 4.6 \times 150mm column, eluents: water/0.1% formic acid (A) and acetonitrile/0.1% formic acid (B), linear gradient from 5% (B) to 95% (B) in 10 min) (supp. inf., Fig. S1.3), comparable to the method used by the inventors of the compound [23]. Additional LC-MS analysis was performed using an Intensity Solo 2C18 2.1 \times 100mm column (temperature = 50 °C, flow rate = 0.2 ml/min, eluents: water/0.1% formic acid (A) and acetonitrile (B), linear gradient from 5% (B) to 95% (B) in 10 min), revealing a hidden impurity (*m/z* = 509.1) eluting with the main analyte. Isolation and quantification of the containing impurity (14.9%) could be performed using different eluent composition and thereby, resulted in purity of the main-analyte to be 82% (eluents: water/0.1% formic acid (A) and acetonitrile (B). Isocratic elution: 55% (B) within the first 10 min. A linear gradient (10–12 min) from 55% (B) to 60% (B), followed by isocratic elution with 60% (B) for 2 min) than used within the UV purity method (see supporting information, section S1.2).

4.2. [³H]N^α-methylhistamine displacement assays

Membrane preparations and cell culture of HEK-293T cells that were stably transfected with the human H₃ receptor encoding cDNA, as well as radioligand ([³H]N^α-methylhistamine) displacement studies were conducted as described previously [26]. Reference compound pitolisant was synthesized as oxalate-salt according to the procedure described by Meier et al. [33].

4.3. Fluorescence polarization-based bodilisant displacement assays

The same membrane preparations as used for radioligand displacement assays (section 4.2) were used for fluorescence polarization-based displacement studies using bodilisant that originated from the laboratory stocks of Tomasch et al. [34]. Assay conditions and data evaluation were as described previously [28].

4.4. GTP γ [³⁵S] assay

HEK-293 cells stably expressing human H₃ receptor were grown until confluence and centrifuged at 300 \times g for 15 min at 4 °C. Pellets were resuspended in buffer I (Tris-HCl 50 mM, MgCl₂ 10 mM, NaCl 140 mM, pH = 7.4 supplemented by Phenyl Methyl Sulphonyl

Fluoride (PMSF) 1 mM). The obtained suspension was stirred gently and submitted to a 25–26 \times g mechanic pressure exerted through a syringe. The cell lysate was then centrifuged at 300 \times g for 5 min at 4 °C in order to eliminate nucleus and cell scraps. The obtained supernatant was then centrifuged at 48,000 g for 30 min at 4 °C. The final pellet was resuspended in buffer I. Aliquots were frozen in liquid nitrogen and stored until use at –80 °C. Protein content was measured by the Bradford method [35].

For conducting GTP γ [³⁵S] binding assays, defreezed membranes were diluted at a final concentration of 2.5 μ g/180 μ L/well and incubated at room temperature with compounds for 30 min in a binding buffer containing Tris-HCl 50 mM, MgCl₂ 10 mM, NaCl 140 mM, GDP 10 μ M, pH = 7.4 and distributed in 96-well polystyrene microplate. GTP γ [³⁵S] labelled ligand (0.2–0.3 nM) was added for additional 30 min. After transfer in a Millipore GF/C HTS® microplate, the filtration of the reactional mix followed by a three time 250 μ L wash was used to terminate the reaction. The filter-bound radioactivity was measured in a liquid scintillation counter Microbeta TRILUX® with 50 μ L of scintillation fluid. GTP γ [³⁵S] dependent binding activity was determined in vitro for histamine, imetit, (*R*)- α -methylhistamine and the compound of interest.

4.5. cAMP-accumulation assay

Chinese hamster ovary cells (CHO-DUKX, ATCC No. CRL-9010) expressing stable human histamine H₃ receptor cDNA (GenBank accession No. NM_007232) and stable multiple-responsive element/cAMP-responsive-element driving luciferase gene reporter were used [36].

The assay was performed with non-adherent cells in a 96 wells format using 20,000 cells per well in alphaMEM without serum in the presence of IBMX (500 μ M). cAMP was measured in whole cells in the presence of forskolin (10 μ M) using the HitHunter® cAMP Assay for Small Molecules kit (Art. No. 90-0075SM2, DiscoverX) according to the manufacturer's recommendations. Bioluminescence was measured using a FDSS/ μ cell apparatus (Hamamatsu). Results were expressed as percentage of forskolin-stimulated bioluminescence.

4.6. CRE/MRE luciferase reporter-gene assay

Employed CHO cells were the same as for the cAMP accumulation assay. Cells were seeded overnight at a density of 25,000 cells per well in a 96 well microplate with black wall and clear flat bottom (Art. No. 3904, Costar). Cells were washed twice with alphaMEM (Art. No. BE02-002F, Lonza) without serum, then treated with forskolin (Art. No. F6686, Sigma) at 0.3 μ M or 1 μ M final concentration, in the agonist or the antagonist mode, respectively, and with the compounds of interest.

After 4 h placed in a cell incubator (37 °C), the medium was removed and replaced with 50 μ L of luciferase reporter gene assay kit reagent (Steady-Glo, Promega) (50/50 Steady-Glo reagent/alphaMEM). The bioluminescence was measured 10–20 min later using a FDSS/ μ cell apparatus (Hamamatsu). Results have been expressed as percentage of forskolin-stimulated bioluminescence.

Declaration of competing interest

OL, SK and MC are employees of Bioprojet Biotech. HS is an inventor of pitolisant.

Acknowledgements

The authors thank Isabelle Nagmar and Kathrin Grau for their expert technical assistance.

3.2 Novel pyrrolidinone derivative lacks claimed histamine H₃ receptor stimulation in receptor binding and functional studies

D. Reiner et al. / European Journal of Medicinal Chemistry 191 (2020) 112150

5

Appendix A. Supplementary data

Supplementary data to this article can be found online at <https://doi.org/10.1016/j.ejmech.2020.112150>.

References

- [1] J.-M. Arrang, M. Garbarg, J.-C. Schwartz, Auto-inhibition of brain histamine release mediated by a novel class (H₃) of histamine receptor, *Nature* 302 (1983) 832, <https://doi.org/10.1038/302832a0>.
- [2] J.C. Schwartz, Histaminergic transmission in the mammalian brain, *Physiol. Rev.* 71 (1991) 1, <https://doi.org/10.1152/physrev.1991.71.1.1>.
- [3] J.C. Schwartz, J.M. Arrang, M. Garbarg, H. Pollard, A third histamine receptor subtype: characterisation, localisation and functions of the H₃-receptor, *Agents Actions* 30 (1990) 13–23, <https://doi.org/10.1007/bf01968988>.
- [4] H.L. Haas, P. Panula, Histamine receptors, *Neuropharmacology* 106 (2016) 1–2, <https://doi.org/10.1016/j.neuropharm.2016.04.007>.
- [5] M.J. Gemkow, A.J. Davenport, S. Harich, B.A. Ellenbroek, A. Cesura, D. Hallett, The histamine H₃ receptor as a therapeutic drug target for CNS disorders, *Drug Discov. Today* 14 (2009) 509–515, <https://doi.org/10.1016/j.drudis.2009.02.011>.
- [6] R.E. Brown, D.R. Stevens, H.L. Haas, The physiology of brain histamine, *Prog. Neurobiol.* 63 (2001) 637–672, [https://doi.org/10.1016/S0304-0082\(00\)00039-3](https://doi.org/10.1016/S0304-0082(00)00039-3).
- [7] P. Panula, P.L. Chazot, M. Cowart, R. Gutzmer, R. Leurs, W.L. Liu, H. Stark, R.L. Thurmond, H.L. Haas, International union of basic and clinical pharmacology. XCVIII. Histamine receptors, *Pharmacol. Rev.* 67 (2015) 601–655, <https://doi.org/10.1124/pr.114.010249>.
- [8] S. Morisset, A. Rouleau, X. Ligneau, F. Gbahou, J. Tardivel-Lacombe, H. Stark, W. Schunack, C.R. Ganellin, J.-M. Arrang, High constitutive activity of native H₃ receptors regulates histamine neurons in brain, *Nature* 408 (2000) 860–864, <https://doi.org/10.1038/35048583>.
- [9] G. Nieto-Alamillo, R. Márquez-Gómez, A.-M. García-Gálvez, G.-E. Morales-Figueroa, J.-A. Arias-Montaña, The histamine H₃ receptor: structure, pharmacology, and function, *Mol. Pharmacol.* 90 (2016) 649–673, <https://doi.org/10.1124/mol.116.104752>.
- [10] J. Clapham, G. Kilpatrick, Histamine H₃ receptors modulate the release of [3H]-acetylcholine from slices of rat entorhinal cortex: evidence for the possible existence of H₃ receptor subtypes, *Br. J. Pharmacol.* 107 (1992) 919–923, <https://doi.org/10.1111/j.1476-5381.1992.tb13386.x>.
- [11] P. Blandina, M. Giorgetti, L. Bartolini, M. Cecchi, H. Timmerman, R. Leurs, G. Pepeu, M.G. Giovannini, Inhibition of cortical acetylcholine release and cognitive performance by histamine H₃ receptor activation in rats, *Br. J. Pharmacol.* 119 (1996) 1656–1664, <https://doi.org/10.1111/j.1476-5381.1996.tb16086.x>.
- [12] E. Schlicker, S. Werthwein, J. Zentner, Histamine H₃ receptor-mediated inhibition of noradrenaline release in the human brain, *Fundam. Clin. Pharmacol.* 13 (1999) 120–122, <https://doi.org/10.1111/j.1472-8206.1999.tb00330.x>.
- [13] E. Schlicker, K. Fink, M. Detsner, M. Göthert, Histamine inhibits dopamine release in the mouse striatum via presynaptic H₃ receptors, *J. Neural Transm. Gen. Sect.* 93 (1993) 1–10, <https://doi.org/10.1007/bf01244933>.
- [14] B. Sadek, H. Stark, Cherry-picked ligands at histamine receptor subtypes, *Neuropharmacology* 106 (2016) 56–73, <https://doi.org/10.1016/j.neuropharm.2015.11.005>.
- [15] N. Ghamari, O. Zarei, J.-A. Arias-Montaña, D. Reiner, S. Dastmalchi, H. Stark, M. Hamzeh-Mivehroud, Histamine H₃ receptor antagonists/inverse agonists: where do they go? *Pharmacol. Ther.* 200 (2019) 69–84, <https://doi.org/10.1016/j.pharmthera.2019.04.007>.
- [16] Y.Y. Syed, Pitolisant: first global approval, *Drugs* 76 (2016) 1313–1318, <https://doi.org/10.1007/s40265-016-0620-1>.
- [17] R. Leurs, P. Blandina, C. Tedford, H. Timmerman, Therapeutic potential of histamine H₃ receptor agonists and antagonists, *Trends Pharmacol. Sci.* 19 (1998) 177–183, [https://doi.org/10.1016/S0165-6147\(98\)01201-2](https://doi.org/10.1016/S0165-6147(98)01201-2).
- [18] R. Yoshimoto, Y. Miyamoto, K. Shimamura, A. Ishihara, K. Takahashi, H. Kotani, A.S. Chen, H.Y. Chen, D.J. Macneil, A. Kanatani, S. Tokita, Therapeutic potential of histamine H₃ receptor agonist for the treatment of obesity and diabetes mellitus, *Proc. Natl. Acad. Sci. U. S. A.* 103 (2006) 13866–13871, <https://doi.org/10.1073/pnas.0506104103>.
- [19] P.H. Jethwa, P. Barrett, Y. Turnbull, R.A. Enright, A. Warner, M. Murphy, F.J. Ebling, The role of histamine 3 receptors in the control of food intake in a seasonal model of obesity: the Siberian hamster, *Behav. Pharmacol.* 20 (2009) 155–165, <https://doi.org/10.1097/fbp.0b013e328328a809>.
- [20] A. Rouleau, M. Garbarg, X. Ligneau, C. Mantion, P. Lavie, C. Advenier, J.M. Lecomte, M. Krause, H. Stark, W. Schunack, J.C. Schwartz, Bioavailability, antinociceptive and antiinflammatory properties of BP 2-94, a histamine H₃ receptor agonist prodrug, *J. Pharmacol. Exp. Ther.* 281 (1997) 1085–1094.
- [21] M. Berlin, P.C. Ting, W.D. Vaccaro, R. Aslanian, K.D. McCormick, J.F. Lee, M.M. Albanese, M.W. Mutaht, J.J. Piwinski, N.-Y. Shih, L. Duguma, D.M. Solomon, W. Zhou, R. Sher, L. Favreau, M. Bryant, W.A. Korfmacher, C. Nardo, R.E. West, J.C. Anthes, S.M. Williams, R.-L. Wu, H. Susan She, M.A. Rivelli, M.R. Corboz, J.A. Hey, Reduction of CYP450 inhibition in the 4-[(1H-imidazole-4-yl)methyl]piperidine series of histamine H₃ receptor antagonists, *Bioorg. Med. Chem. Lett.* 16 (2006) 989–994, <https://doi.org/10.1016/j.bmcl.2005.10.087>.
- [22] G. Wäger, T. Mocking, M. Arimont, G. Provensi, B. Rani, B. Silva-Marques, G. Latacz, D. Da Costa Pereira, C. Karatzidou, H.F. Vischer, M. Wijnmans, K. Kiec-Kononowicz, I.J.P. De Esch, R. Leurs, 4-(3-Aminoazetidin-1-yl)pyrimidin-2-amine as high-affinity non-imidazole histamine H₃ receptor agonists with in vivo central nervous system activity, *J. Med. Chem.* 62 (2019) 10848–10866, <https://doi.org/10.1021/acs.jmedchem.9b01462>.
- [23] A. Ghoshal, A. Kumar, D. Yugandhar, C. Sona, S. Kurikose, K. Nagesh, M. Rashid, S.K. Singh, M. Wahajuddin, P.N. Yadav, A.K. Srivastava, Identification of novel β -lactams and pyrrolidinone derivatives as selective Histamine-3 receptor (H3R) modulators as possible anti-obesity agents, *Eur. J. Med. Chem.* 152 (2018) 148–159, <https://doi.org/10.1016/j.ejmech.2018.04.020>.
- [24] F. Fan, B.F. Binkowski, B.L. Butler, P.F. Stecha, M.K. Lewis, K.V. Wood, Novel genetically encoded biosensors using firefly luciferase, *ACS Chem. Biol.* 3 (2008) 346–351, <https://doi.org/10.1021/cb8000414>.
- [25] J.B. Baell, G.A. Holloway, New substructure filters for removal of Pan assay interference compounds (PAINS) from screening libraries and for their exclusion in bioassays, *J. Med. Chem.* 53 (2010) 2719–2740, <https://doi.org/10.1021/jm901137j>.
- [26] M.A. Khanfar, D. Reiner, S. Hagenow, H. Stark, Design, synthesis, and biological evaluation of novel oxadiazole- and thiazole-based histamine H₃R ligands, *Bioorg. Med. Chem.* 26 (2018) 4034–4046, <https://doi.org/10.1016/j.bmc.2018.06.028>.
- [27] T.P. Kenakin, *Pharmacologic Analysis of Drug-Receptor Interaction*, third ed., Lippincott-Raven Publishers, Philadelphia (PA), 1997.
- [28] D. Reiner, H. Stark, Ligand binding kinetics at histamine H₃ receptors by fluorescence-polarization with real-time monitoring, *Eur. J. Pharmacol.* 848 (2019) 112–120, <https://doi.org/10.1016/j.ejphar.2019.01.041>.
- [29] C. Liu, X.-J. Ma, X. Jiang, S.J. Wilson, C.L. Hofstra, J. Blevitt, J. Pyati, X. Li, W. Chai, N. Carruthers, T.W. Lovenberg, Cloning and pharmacological characterization of a fourth histamine receptor (H₄) expressed in bone marrow, *Mol. Pharmacol.* 59 (2001) 420–426, <https://doi.org/10.1124/mol.59.3.420>.
- [30] S.E. George, P.J. Bungay, L.H. Naylor, Evaluation of a CRE-directed luciferase reporter gene assay as an alternative to measuring cAMP accumulation, *J. Biomol. Screen* 2 (1997) 235–240, <https://doi.org/10.1177/108705719700200408>.
- [31] A.D. Medhurst, M.A. Briggs, G. Bruton, A.R. Calver, I. Chessell, B. Crook, J.B. Davis, R.P. Davis, A.G. Foley, T. Heslop, W.D. Hirst, S.J. Medhurst, S. Ociepa, A. Ray, C.M. Regan, B. Sargent, J. Schogger, T.O. Stean, B.K. Trail, N. Upton, T. White, B. Orlek, D.M. Wilson, Structurally novel histamine H₃ receptor antagonists GSK207040 and GSK334429 improve scopolamine-induced memory impairment and capsaicin-induced secondary allodynia in rats, *Biochem. Pharmacol.* 73 (2007) 1182–1194, <https://doi.org/10.1016/j.bcp.2007.01.007>.
- [32] S.J. Hill, C. Williams, L.T. May, Insights into GPCR pharmacology from the measurement of changes in intracellular cyclic AMP: advantages and pitfalls of differing methodologies, *Br. J. Pharmacol.* 161 (2010) 1266–1275, <https://doi.org/10.1111/j.1476-5381.2010.00779.x>.
- [33] G. Meier, J. Apelt, U. Reichert, S. Grassmann, X. Ligneau, S. Elz, F. Leurquin, C.R. Ganellin, J.C. Schwartz, W. Schunack, H. Stark, Influence of imidazole replacement in different structural classes of histamine H₃-receptor antagonists, *Eur. J. Pharm. Sci.* 13 (2001) 249–259, [https://doi.org/10.1016/S0928-0987\(01\)00106-3](https://doi.org/10.1016/S0928-0987(01)00106-3).
- [34] M. Tomasch, J.S. Schwed, A. Paulke, H. Stark, Bodilisant-a novel fluorescent, highly affine histamine h₃ receptor ligand, *ACS Med. Chem. Lett.* 4 (2013) 269–273, <https://doi.org/10.1021/ml300383n>.
- [35] M.M. Bradford, A rapid and sensitive method for the quantitation of micro gram quantities of protein utilizing the principle of protein-dye binding, *Anal. Biochem.* 72 (1976) 248–254, [https://doi.org/10.1016/0003-2697\(76\)90527-3](https://doi.org/10.1016/0003-2697(76)90527-3).
- [36] L.R. Fitzgerald, I.J. Mannan, G.M. Dytko, H.L. Wu, P. Nambi, Measurement of responses from Gi-, Gs-, or Gq-coupled receptors by a multiple response element/cAMP response element-directed reporter assay, *Anal. Biochem.* 275 (1999) 54–61, <https://doi.org/10.1006/abio.1999.4295>.

SL Analytics of compound **6k**

S1.1. NMR-Spectrometry (H/¹³C)

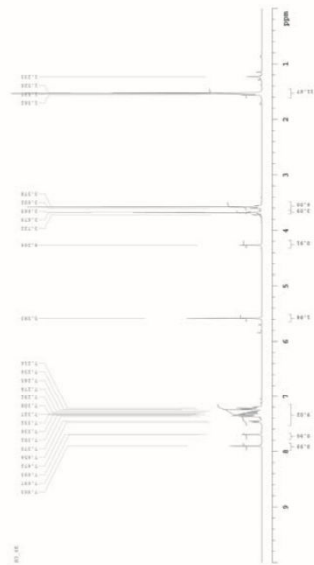


Fig. S1.1. ¹H NMR spectrum of compound **6k**

S2 *In vitro* Pharmacology

S2.1 CRE/MRE luciferase reporter gene assays

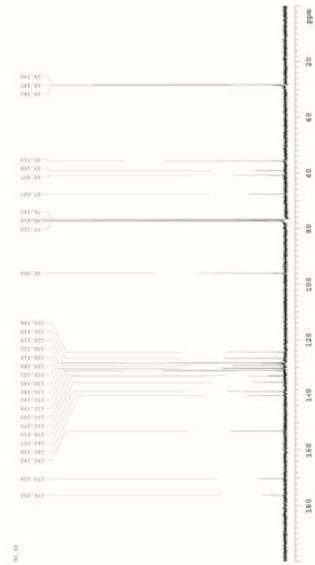


Fig. S1.2. ¹³C NMR spectrum of compound **6k**

Supporting Information

Novel pyrrolidinone derivative lacks claimed histamine H₃ receptor stimulation in receptor binding and functional studies

David Reimer¹, Aleksandra Zivkovic¹, Olivier Labeeuw², Stéphanie Krief², Marc Capet², Holger Stark^{1,*}

¹ Heinrich Heine University Düsseldorf, Institute of Pharmaceutical and Medicinal Chemistry, Universitätsstr. 1, 40225 Düsseldorf, Germany;
² Bioprojet Biotech, 4 Rue du Chesnay Beauregard, 33760 Saint-Grégoire, France.

*Corresponding author: Holger Stark, Tel.: +49 211 81-10478, Fax: +49 211 81-13359, email: stark@ihhu.de

Contents:

SL	Analytics of compound 6k	
S1.1.	NMR-Spectrometry (H/ ¹³ C)	p. 2
S1.2.	Purity determination (HPLC / LC-MS)	p. 3–6
S2	<i>In vitro</i> Pharmacology	
S2.1	CRE/MRE luciferase reporter gene assays	p. 6

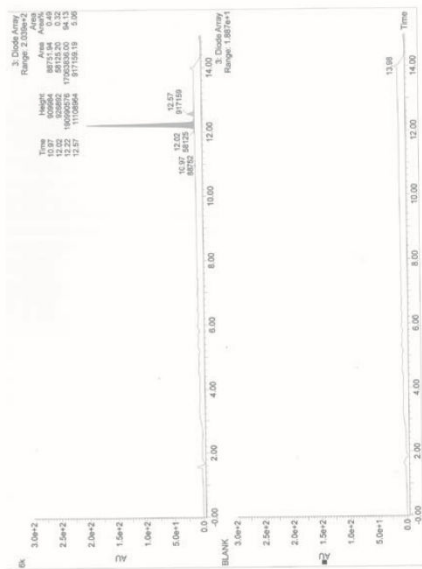


Fig. S1.3. HPLC chromatogram (UV detection).

S1.2. Purity determination (HPLC / LC-MS)

1 HPLC-UV-determined purity was found to be over 94% (instrument data: Sunfire C18 5µm 4.6x150mm column, eluents: water(0.1% formic acid (A) and acetonitrile(0.1% formic acid (B), linear gradient from 5% (B) to 95% (B) in 10 min) (Fig. S1.3). LC-MS analysis was performed using an Intensity Solo 2 C18 2.1x100mm column (temperature = 50 °C, flow rate = 0.2 ml/min). Eluents: water(0.1% formic acid (A) and acetonitrile (B) with a linear gradient from 5% (B) to 95% (B) in 10 min, followed by isocratic elution with 95% (B) for 4 min). The LC-MS based method revealed a hidden impurity eluting with the main-peak (Fig. S1.4). By modification of the method using initially higher elution strength (Eluents: water(0.1% formic acid (A) and acetonitrile (B), isocratic elution: 55% (B) within the first 10 min, A linear gradient (10-12 min) from 55% (B) to 60% (B), followed by isocratic elution with 60% (B) for 2 min), a faster elution of the main peak could be achieved, whereas full isolation of the impurity and final quantification of compound 6k could be achieved (Fig. S1.5) at lower elution strength during the elution of main analyte (60% (B) instead of 95% (B)).

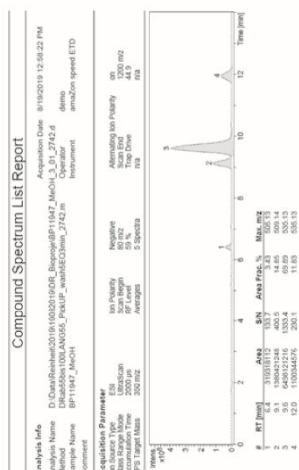


Fig. S1.5. LC-MS chromatogram with isolated impurity ($m/z = 509.1$) and main-analyte ($m/z = 535.1$) eluting at 9.1 min.

82. *In vitro* Pharmacology

S2.1 CRE/MRE luciferase reporter gene assays

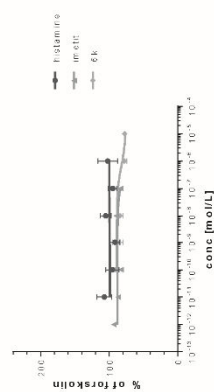


Fig. S2.1. Control measurement of luciferase expression within CHO-DUKX cells, stably transfected with pCMV-MRE-luciferase reporter gene but without H3R cDNA. Neither histamine, imetit, nor compound **6k** exerted remarkable activity.

5

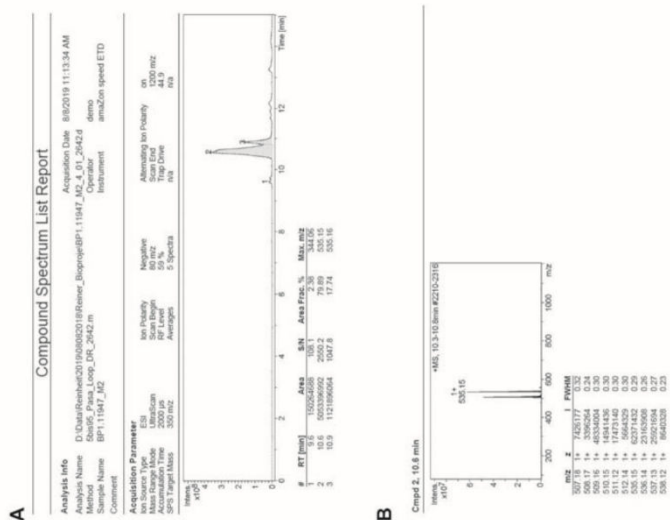


Fig. S1.4. LC-MS chromatogram (A) and mass-spectrum corresponding to second peak (B), revealing the hidden impurity ($m/z = 509.1$) eluting with main analyte ($m/z = 535.2$) at 18.9 min.

5

3.3. Design, synthesis, and biological evaluation of novel oxadiazole- and thiazole-based histamine H₃R ligands

Mohammad A. Khanfar^{1),2),3)}, David Reiner¹⁾, Stefanie Hagenow¹⁾, Holger Stark¹⁾

1) Heinrich Heine University Düsseldorf, Institute of Pharmaceutical and Medicinal Chemistry, Universitätsstr. 1, 40225 Düsseldorf, Germany

2) Faculty of Pharmacy, University of Jordan, P.O Box 13140, Amman 11942, Jordan

3) College of Pharmacy, Alfaisal University, Al Takhassusi Rd, Riyadh 11533, Saudi Arabia

Published in: *Bioorganic & Medicinal Chemistry*, 2018, 26:4034–4046.

DOI: 10.1016/j.bmc.2018.06.028.

Contribution to research: DR was in major parts involved in preparation, planning and conduction of radioligand displacement experiments, in maintenance of the corresponding cell-culture and evaluated corresponding data to determine H₃R affinity. DR drafted the supplementary material, wrote the pharmacological parts of the manuscript, and processed the revision.

Abstract:

Histamine H₃ receptor (H₃R) is largely expressed in the CNS and modulation of the H₃R function can affect histamine synthesis and liberation, and modulate the release of many other neurotransmitters. Targeting H₃R with antagonists/inverse agonists may have therapeutic applications in neurodegenerative disorders, gastrointestinal and inflammatory diseases. This prompted us to design and synthesize azole-based H₃R ligands, i.e. having oxadiazole- or thiazole-based core structures. While ligands of oxadiazole scaffold were almost inactive, thiazole-based ligands were very potent and several exhibited binding affinities in a nanomolar concentration range. Ligands combining 4-cyanophenyl moiety as arbitrary region, *para*-xylene or piperidine carbamoyl linkers, and/or pyrrolidine or piperidine basic heads were found to be the most active within this series of thiazole based H₃R ligands. The most active ligands were in silico screened for ADMET properties and drug-likeness. They fulfilled Lipinski's and Veber's rules and exhibited potential activities for oral administration, blood-brain barrier penetration, low hepatotoxicity, combined with an overall good toxicity profile.

Reprinted from Khanfar MA, Reiner D, Hagenow S, Stark H, Design, synthesis, and biological evaluation of novel oxadiazole- and thiazole-based histamine H₃R ligands, *Bioorg. Med. Chem.*, 2018, 26:4034–4046, with permission for personal use from Elsevier.

Copyright 2018 Elsevier Ltd.



Design, synthesis, and biological evaluation of novel oxadiazole- and thiazole-based histamine H₃R ligands

Mohammad A. Khanfar^{a,b,c}, David Reiner^a, Stefanie Hagenow^a, Holger Stark^{a,*}

^a Heinrich Heine University Düsseldorf, Institute of Pharmaceutical and Medicinal Chemistry, Universitätsstr. 1, 40225 Düsseldorf, Germany

^b Faculty of Pharmacy, University of Jordan, P.O. Box 13140, Amman 11942, Jordan

^c College of Pharmacy, Alfaisal University, Al Takhassusi Rd, Riyadh 11533, Saudi Arabia

ARTICLE INFO

Keywords:

Histamine
H₃ receptor
Ligands
ADMET
Thiazole
Oxadiazole

ABSTRACT

Histamine H₃ receptor (H₃R) is largely expressed in the CNS and modulation of the H₃R function can affect histamine synthesis and liberation, and modulate the release of many other neurotransmitters. Targeting H₃R with antagonists/inverse agonists may have therapeutic applications in neurodegenerative disorders, gastrointestinal and inflammatory diseases. This prompted us to design and synthesize azole-based H₃R ligands, i.e. having oxadiazole- or thiazole-based core structures. While ligands of oxadiazole scaffold were almost inactive, thiazole-based ligands were very potent and several exhibited binding affinities in a nanomolar concentration range. Ligands combining 4-cyanophenyl moiety as arbitrary region, *para*-xylene or piperidine carbamoyl linkers, and/or pyrrolidine or piperidine basic heads were found to be the most active within this series of thiazole-based H₃R ligands. The most active ligands were *in silico* screened for ADMET properties and drug-likeness. They fulfilled Lipinski's and Veber's rules and exhibited potential activities for oral administration, blood–brain barrier penetration, low hepatotoxicity, combined with an overall good toxicity profile.

1. Introduction

Histamine belongs to biogenic amines, which influence several intracellular pathways, including its neurotransmission activities.^{1–4} Histamine's regulatory character in cellular activities is attributed to its binding to four subtypes of G-protein-coupled receptors (GPCRs); H₁, H₂, H₃, and H₄ that are differentially expressed in several cell types.^{5,6}

Histamine H₃ receptor (H₃R) is a member of transmembrane class A of GPCR family.^{7,8} H₃R is largely expressed on the histaminergic neurons of the CNS, located pre- and postsynaptically.⁹ It plays an essential role in the biosynthesis and release of histamine as well as in the modulation of the release of different neurotransmitters (e.g., dopamine, serotonin, acetylcholine, noradrenaline, GABA, and glutamate).^{10,11} Peripherally, H₃R is marginally distributed in the peripheral nervous system and regulates the sympathetic effector systems and pain sensation.¹² Consequently, modulation of the H₃R function can potentially affect histaminergic neurotransmission. Therefore, targeting H₃R with antagonists/inverse agonists may have therapeutic applications in neurodegenerative disorders, such as Parkinson's disease, Alzheimer's disease, as well as in depression, epilepsy, schizophrenia and in sleep disorders.^{13–19}

Recently, a number of H₃R antagonists/inverse agonists have entered late clinical trials for the treatment of several CNS

disorders.^{15,20,21} In March 2016, the European Medicines Agency authorized marketing of pitolisant (Wakix®) as the first H₃R inverse agonist for the treatment of narcolepsy, designated as an orphan drug since narcolepsy belongs to the rare diseases.^{22–24} Pitolisant is also currently in phase III clinical trials for the treatment of hypersomnia.²⁵

First H₃R antagonists/inverse agonists reported in literature were imidazole-based compounds followed by non-imidazoles in the next generation. They share a general pharmacophore generated from numerous chemical scaffolds (Fig. 1).^{15,26,27} Prototype H₃R antagonists/inverse agonists pharmacophore consist of basic moiety (mainly tertiary amine electrostatically interacting with Asp114 within H₃R binding site) separated by a spacer to a central core (mainly electron-rich moiety).²⁸ The distance between the basic head and the electron rich moiety is approximately 4–5 Å, equivalent to 4 bonds in linear arrangement. The central core is usually connected to an arbitrary region, mainly lipophilic, but polar or basic and even acidic moieties are also tolerable.²⁹ This arbitrary region modulates potency and pharmacokinetic properties of H₃R antagonists/inverse agonists.^{27,30}

Oxadiazole and thiazole nuclei have attracted a wide attention in the search for new therapeutic molecules. They are widely exploited in various applications because of their versatile applicability in multiple therapeutic agents and their blood–brain barrier (BBB)

* Corresponding author.

E-mail address: stark@hhu.de (H. Stark).

<https://doi.org/10.1016/j.bmc.2018.06.028>

Received 20 April 2018; Received in revised form 8 June 2018; Accepted 20 June 2018

Available online 21 June 2018

0968-0896/ © 2018 Elsevier Ltd. All rights reserved.

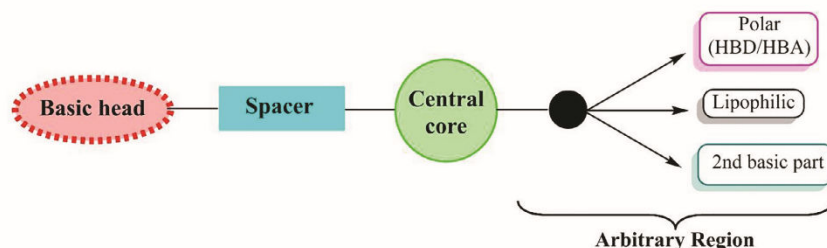


Fig. 1. Schematic presentation of the pharmacophore model of H₃R antagonists/inverse agonists.

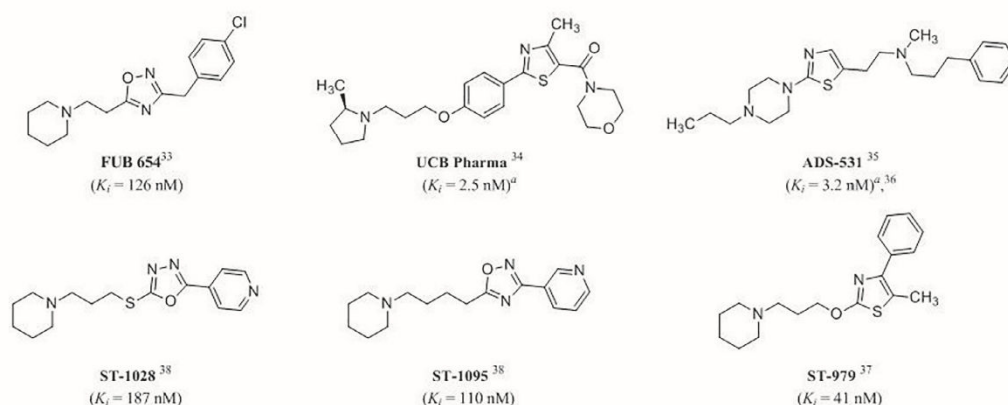


Fig. 2. Selected oxadiazole- and thiazole-based H₃ receptor ligands serving as a basis for design of new H₃R ligands. ^a K_i values calculated from published p*K_i* values.

permeability.^{31,32} Five-membered heterocycles as core motifs in non-imidazole H₃R ligands with structural resemblance to the presented structures were explored in earlier research projects resulting in affine compounds (Fig. 2).^{33,34} Among them ADS-531 that recently underwent *in vivo* examination upon effects on food-intake and neurotransmitter systems.^{35,36} The former progress in the design of potent oxadiazole- and thiazole-based H₃R ligands prompted our research group to explore 2-arylthiazole-4-ylethers as analogues to ST-979 but differing in the arrangement of the substituents.³⁷ Furthermore, *N*-aryl-1,3,4-oxadiazole-2-amines and 3-phenyl-1,2,4-oxadiazole-5-carboxamides (cf. GSK247246 and ST-1095) were designed to increase structural and linkage diversity in the H₃R central core motif, basically linked to our previous work on variations of polar azole core motifs in H₃R ligands (Fig. 2).^{37–40} Our synthetic effort combines various aliphatic and aromatic spacers of variable length, and arbitrary region of electronically and sterically variable substituents. Several H₃R analogues with binding affinities in low nanomolar concentrations were obtained within this project.

2. Results and discussions

2.1. Hit-identification and hit-to-lead-optimization

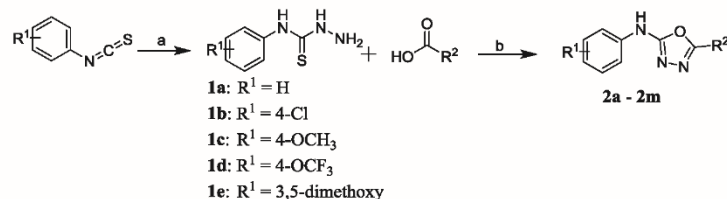
Synthetic design strategy was driven by an initial structural hypothesis for various azole-based H₃R ligands fitting the H₃R-pharmacophoric map (Fig. 1).^{37–39} The following structural modification strategies were applied to design potent H₃R ligands: (1) employing oxadiazole (1,2,4 and 1,3,4) or thiazole rings as a polar, electron-rich central core; (2) several cyclic and noncyclic amines were examined as a basic head of the designed H₃R ligands including: pyrrolidine,

piperidine, piperazine and noncyclic aliphatic tertiary amines; (3) variable spacers of different chain length connecting the central core and the basic head were examined using aliphatic and aromatic linkers. Linkers of 2 to 5 elements of cyclic or noncyclic structure were tested for optimal length; (4) substituted and unsubstituted aromatic and heteroaromatic rings of variable size and electronic properties were placed on the arbitrary region. Substantial modifications can be conducted on the arbitrary region to modulate potency, solubility and pharmacokinetic properties. Initially, only a few ligands of each compound series without changes in the arbitrary region were synthesized and evaluated for hit identification. Hit-to-lead optimization was conducted for those structures with promising results.

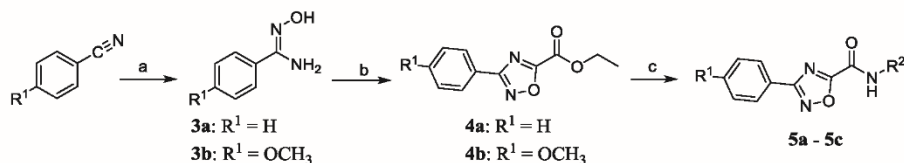
2.2. Chemistry

An efficient one-pot synthesis of substituted 2-anilino-1,3,4-oxadiazoles was applied. A carboxylic acid (1.0 eq.) and 4-phenyl-3-thiosemicarbazide (1.0 eq.) were mixed in DCM at room temperature with three equivalents of *N*-(3-dimethylaminopropyl)-*N*¹-ethylcarbodiimide (EDCI) as coupling reagent, producing the corresponding 2-anilino-1,3,4-oxadiazoles (**2a–m**) (Scheme 1). The thiosemicarbazides **1a–e** were readily prepared by reacting the corresponding isothiocyanate with hydrazine under reflux in MeOH.

The synthesis of 1,2,4-oxadiazole derivatives started from commercially available nitriles that were reacted with hydroxylamine in EtOH/H₂O in the presence of NaHCO₃ to give the corresponding phenylamidoximes **3a–b** in good yields. The latter were suspended in DCM and then refluxed for 5 h in pyridine with ethyl chlorooxalate to provide 3-aryl-1,2,4-oxadiazole-5-carboxylates **4a–b**. Then, the obtained esters were easily converted into the desired compounds **5a–c** by reaction



Scheme 1. Synthesis of 2-Anilino-1,3,4-oxadiazoles. Reagents and Conditions: (a) (1) N₂H₄, MeOH, rt, 1 h. (2) 65–80 °C, 20 min (88–96%); (b) EDCI (3 eq), CH₂Cl₂, rt, 12 h (50–84%). Structure of compounds **2a–2m** are listed in Table 1.



Scheme 2. Synthesis of 3-phenyl-1,2,4-oxadiazole derivatives. Reagents and Conditions: (a) NH₂OH, EtOH, NaHCO₃, reflux, 3 h (67–77%); (b) ClCH₂COOEt, ethyl chloroacetate, rt for 30 min, then refluxed for 5 h (79–82%); (c) EtOH, alkyl amine, reflux for 8 h (73–87%). Structure of compounds **5a–5c** are listed in Table 1.

with 3-substituted amine-1-yl propan-1-amine (Scheme 2).

The synthesis of 5-methyl thiazole analogues (**7–36**) was based on literature procedure where the aryl/heteroaryl nitrile, α -mercapto-carboxylic acid, and pyridine were reacted to form the corresponding hydroxymethylthiazole (**6**).⁴¹ Subsequently, the hydroxymethylthiazole was O-alkylated following a Williamson-type etherification with K₂CO₃ as the base to afford the final compounds (**7–36**) (Scheme 3). Analogues **39–42** were synthesized by first refluxing 4-hydroxythiazole with 4 equivalents of α,α' -dibromo-*p*-xylene in acetone and K₂CO₃. After column chromatography, the monoether products (**38a–b**) were reacted with either piperidine or pyrrolidine to furnish the corresponding final compounds (**39–42**) (Scheme 4). The 5-ethyl thiazole analogues (**44–46**) were synthesized by first mixing the corresponding phenylthioamide, ethyl 2-bromobutanoate and pyridine under argon and slowly heating up to 100–110 °C for 2 h to form hydroxyethylthiazole (**43**), which was O-alkylated to afford the final compounds (**44–46**) (Scheme 5).⁴²

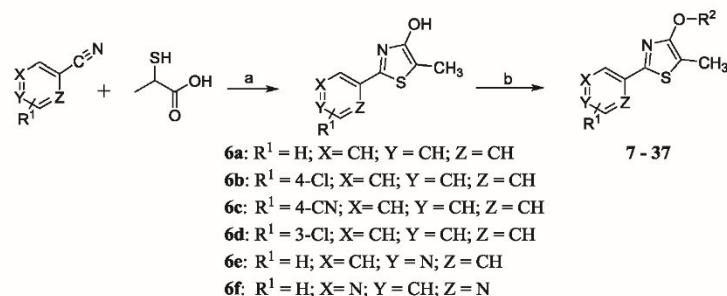
2.3. Biological evaluation

All final synthesized compounds were tested for their *in vitro* H₃R binding affinity in a binding assay by competitive displacement of [³H]-N^a-methylhistamine as radioligand. Their corresponding K_i values with 95% confidence intervals are listed in Tables 1 and 2.

2.3.1. Oxadiazole-based ligands

As it was previously demonstrated that oxadiazoles, e.g. linked either via oxy-/thioethers or carboxamides to the basic amine moiety, are accepted as central core in H₃R ligands, a small series of 1,2,4- and 1,3,4-oxadiazole derivatives were designed.^{38,43}

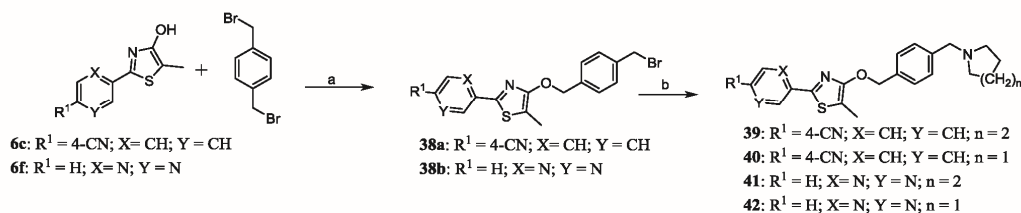
Analogues of 1,3,4-oxadiazole scaffold showed low binding affinities at H₃R (K_i > 1000 nM), thus, permitting only limited conclusions for structural variations to improve H₃R affinity. The prototypes (**2a–2d**) without modifications at the anilino substructure resulted in ligand **2d** showing weak affinity. Only a few variations of these ligands were constructed to examine possibilities for improving this binding behavior, resulting in **2e–2m**. Ligands with alicyclic basic head and 2–3 carbon linkers showed comparable activity with **2d** exhibiting low micromolar K_i values (**2c**, **2g**, **2j**, **2k**, and **2m**). However, analogues with the same linker length but rigid linker and basic head have negligible binding affinity (**2b**, **2f**, **2i**). This behavior implies the necessity of flexibility to position the basic head in favorable orientation for salt bridge formation with Asp114, described as crucial for H₃R antagonists/inverse agonists binding.⁴⁴ Moreover, ligands with noncyclic basic head and/or shorter linker (**2a**, **2h**, **2l**) appeared inactive, except the 4-chlorine derivative showing micromolar affinity (**2e**). These data suggest the need of a defined distance between the central core and the cyclic basic head for these compounds. Nevertheless, the modifications performed here were not able to improve affinity substantially, limiting any SAR interpretations in this series.



Scheme 3. Synthesis of 5-methyl thiazole derivatives. Reagents and Conditions: (a) pyridine, 100 °C for 2 h (69–96%); (b) DMF (or acetone), Cs₂CO₃ (or K₂CO₃) (3.0 eq.), KI (1.0 eq.), alkyl halide (0.9 eq.) (57–95%). Structure of compounds **7–37** are listed in Table 2.

M.A. Khanfar et al.

Bioorganic & Medicinal Chemistry 26 (2018) 4034–4046



Scheme 4. Synthesis of xylene linker thiazole derivatives. Reagents and conditions: (a) K₂CO₃, acetone, reflux, 12 h (74–86%); (b) alicyclic amine, K₂CO₃, DMF, 60 °C, 12 h (84–90%).

The smaller series of 1,2,4-oxadiazole-5-carboxamides analogues structurally related to previously described compounds FUB 654, ST-1095 or GSK247246 were inactive (**5a**, **5b** and **5c**, Table 1).^{33,38,39} Therefore, they are considered as unsuitable fundamental structure for further synthetic efforts, compared to 1,2,4-oxadiazole FUB 654 (Fig. 2), a non-imidazole analogue of the highly affine Glaxo Wellcome compound GR175737 ($K_i = 2.5$ nM).^{33,45} Compared to previously published more potent alkyl-/thioether-linked oxadiazole derivatives (Fig. 2),³⁸ *N*-phenyl-1,3,4-oxadiazole-2-amines and 1,2,4-oxadiazole-5-carboxamides seem to bear a less promising or more restricted core motif on substitution and linkage, respectively. Subsequently, the more promising thiazole class has been followed in more detail.

2.3.2. Thiazole-based ligands

The synthetic approach for thiazole-based ligands was supported by the previously published structure ST-979 (Fig. 1).³⁷ They can be considered as analogues where the substituents were shifted by one carbon atom yielding **11** as initial structure with moderate affinity. The resulting analogues exhibited superior binding affinities with K_i values ranging from low micromolar to nanomolar concentrations. Similar to 1,3,4-oxadiazole analogues, optimum binding activities are achieved with pyrrolidine or piperidine basic heads. For example, compound **21** with pyrrolidine basic head and three-carbon chain linker demonstrated a K_i value of 4 nM. Yet, analogues with *para*-xylene (e.g., **41** and **42** with K_i values 7.0 nM and 72 nM, respectively) or piperidine carbamoyl (e.g., **14**, **20**, **23** with K_i values 5.4 nM, 54 nM and 42 nM, respectively) linkers showed high binding affinities. Interestingly, the methylpiperazine carbamoyl substituted thiazole **13** showed only weak affinity ($K_i = 5800$ nM) compared to the piperidine carbamoyl linked analogue **14** being more active by more than three orders of magnitude. Different affinities of 2- and 3-carbon linked pyrrolidine or piperidine-analogues were detected between the corresponding structures of (pyrrolidine-1-yl)alkoxy linked 2-phenylthiazoles with K_i of 47 nM and 520 nM for dimethylen **8** and trimethylen analogue **10**, respectively. Comparable binding behavior was detected between the corresponding 4-chlorophenylthiazole analogues **16** and **18** as well as between **17** and **19**, both carrying a (piperidin-1-yl)alkoxy linker instead (Table 2). The arbitrary region (i.e. the phenyl moiety) showed wide electronic and steric tolerability. Replacing the phenyl ring with pyridine was tolerable (or slightly less active) but not with pyrimidine (except when it is coupled with *para*-xylene linker in **41** and **42**). A cyano group in *para*-position generated the most active analogues (e.g., **21**, **22**), which may indicate the favorable positioning of hydrogen bond acceptor at this site presumably interacting with the Threonine residue identified by Roche

et al.²⁷ Replacing the 5-methyl by an 5-ethyl substituent showed inconsistent pattern; it improves the binding affinity as with **46** ($K_i = 200$ nM), which is about five fold more active than its methyl counterpart (**19**, $K_i = 930$ nM), but not with **44** and **45**.

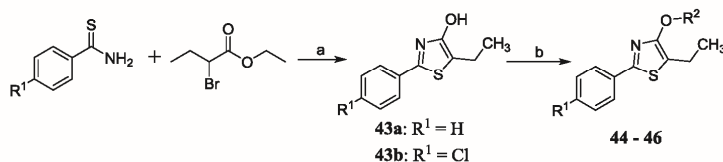
Accordingly, analogues combining optimum moieties, i.e. 4-cyano-phenyl moiety as arbitrary region, *para*-xylene or piperidine carbamoyl linkers, and/or pyrrolidine or piperidine basic heads were found to be the most active within this series of thiazole-based H₃R ligands.

2.4. In silico molecular and ADMET properties of designed thiazole ligands

Prediction of how much a ligand would have proper pharmacokinetic (ADME) and pharmacodynamic (e.g., toxicological) properties (drug-likeness) is of great importance during pre-clinical evaluation to assist drug discovery/development process, to guide the optimization from a lead compound to a successful drug candidate, and to reduce attrition rates during clinical trials, hence increasing the chance of reaching the market.⁴⁶

Some important chemical descriptors correlate well with ADMET properties such as polar surface area (PSA) and low molecular weight (MW) for high oral absorption.⁴⁷ Likewise, rapid renal clearance is correlated with hydrophilic and small compounds. The hepatic metabolism of most drugs is associated with large and hydrophobic compounds. Higher lipophilicity of compounds leads to increased metabolism and poor absorption, along with an increased probability of binding to undesired hydrophobic macromolecules, thereby increasing the potential for toxicity.⁴⁸

Lipinski's⁴⁸ and Veber's⁴⁹ rules are one of the most important measures to evaluate the drug-likeness and to predict if a compound of certain chemical properties would be orally bioavailable. In spite of some observed exceptions to Lipinski's and Veber's rules, the vast majority (90%) of the orally bioavailable compounds are within their cut-off limits. Lipinski's rule of five states that, generally, an orally bioavailable compound should not violate the following criteria: ≤ 5 hydrogen bond donors (HBD); ≤ 10 hydrogen bond acceptors (HBA); MW < 500; and logP value of < 5. Alternatively, Veber's findings described the role of PSA and number of rotatable bonds as criteria to estimate the oral bioavailability. Veber's rule stated that for a compound to be orally bioavailable it should have either: a PSA ≤ 140 Å² and ≤ 10 rotatable bonds, or ≤ 12 HBD and HBA in total and ≤ 10 rotatable bonds. Clearly from Table 3, the most potent ligands (those with $K_i < 100$ nM) followed all Lipinski's and Veber's rules without any exception, which highlight their drug-likeness properties and their potential to pass the drug development process.



Scheme 5. Synthesis of 5-ethyl thiazole derivatives. Reagents and Conditions: (a) pyridine (1.0 eq.), 100–110 °C, 3 h (76–98%); (b) DMF, K₂CO₃ (3.0 eq.), KI (1.0 eq.), alkyl halide (0.9 eq.) (62–94%). Ligand structures of **44–46** are listed in Table 2.

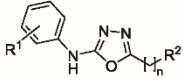
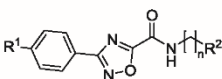
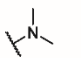
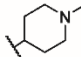
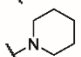
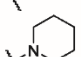
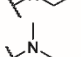
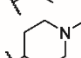
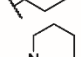
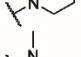
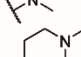
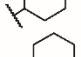
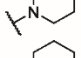
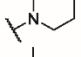
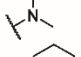
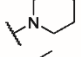
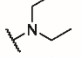
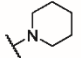
4037

3.3 Design, synthesis, and biological evaluation of novel oxadiazole- and thiazole-based histamine H₃R ligands

M.A. Khanfar et al.

Bioorganic & Medicinal Chemistry 26 (2018) 4034–4046

Table 1
Oxadiazole-based ligands along with H₃R binding affinities.

					
		I	II		
Compd No.	Scaffold	R ¹	n	R ²	H ₃ R K _i [nM] [95% CI] ^a ; (n) ^b
2a	I	H	3		> 5000; (3)
2b	I	H	0		> 5000; (2)
2c	I	H	2		2000 [100; 72,200]; (2)
2d	I	H	3		1300 [700; 2500]; (2)
2e	I	4-Cl	3		5700 [300; 112,800]; (3)
2f	I	4-Cl	0		> 5000; (2)
2g	I	4-Cl	2		1600 [100; 55,200]; (2)
2h	I	4-OCH ₃	1		> 5000; (2)
2i	I	4-OCH ₃	0		> 5000; (2)
2j	I	4-OCH ₃	2		1600 [700; 3800]; (2)
2k	I	4-OCF ₃	2		1300 [100; 34,800]; (2)
2l	I	3,5-dimethoxy	1		> 5000 (2)
2m	I	3,5-dimethoxy	2		1100 [1000; 1200]; (2)
5a	II	H	3		> 5000 (2)
5b	II	H	3		> 5000 (4)
5c	II	OCH ₃	3		> 5000; (2)

^a Binding affinity values (K_i) are expressed as mean with 95% confidence intervals.

^b Number of experiments.

The most active ligands were *in silico* screened for predicted pharmacokinetic properties (BBB penetration, absorption, solubility (Sw), hepatotoxicity, inhibition of CYP2D6, and plasma protein binding (PPB)) being summarized in Table 4. The intestinal absorption and BBB penetration were predicted by developing an ADME model using descriptors 2D PSA and AlogP98 that include 95% and 99% confidence

ellipses. These ellipses define regions where well-absorbed compounds are expected to be found. All active ligands showed medium (brain-blood ratio between 0.3:1 and 1:1) to high (brain-blood ratio between 1:1 and 5:1) penetration of BBB and good intestinal absorption (at least 90% absorbed into bloodstream) within 95% confidence ellipses (Table 4 and Fig. 3). These results are therapeutically crucial for H₃R

$$\text{R}^1-\text{C}_6\text{H}_3(\text{X})(\text{Y})-\text{C}_4\text{H}_2\text{N}_2\text{S}-\text{O}-\text{C}_n\text{H}_{2n}-\text{R}^2$$

(continued on next page)

3.3 Design, synthesis, and biological evaluation of novel oxadiazole- and thiazole-based histamine H₃R ligands

M.A. Khanfar et al.

Bioorganic & Medicinal Chemistry 26 (2018) 4034–4046

Table 2 (continued)

Compd No.	X	Y	Z	R ¹	n	R ²	R ³	H ₃ R K _i [nM] [95% CI] ^a , (n) ^b
26	CH	CH	CH	3-Cl	3		CH ₃	300 [130; 700]; (4)
27	CH	CH	CH	3-Cl	0		CH ₃	98 [56; 170]; (6)
28	CH	N	CH	H	3		CH ₃	110 [40; 300]; (4)
29	CH	N	CH	H	2		CH ₃	100 [30; 380]; (4)
30	CH	N	CH	H	2		CH ₃	57 [42; 78]; (3)
31	CH	N	CH	H	3		CH ₃	410 [170; 1010]; (4)
32	CH	N	CH	H	3		CH ₃	130 [20; 820]; (3)
33	N	CH	N	H	3		CH ₃	5900 [2800; 12,600]; (4)
34	N	CH	N	H	2		CH ₃	2100 [800; 6100]; (4)
35	N	CH	N	H	3		CH ₃	1100 [500; 2400]; (6)
36	N	CH	N	H	0		CH ₃	> 10,000
37	CH	CH	CH		3		CH ₃	87 [16; 462]; (5)
39	CH	CH	CH	4-CN	1		CH ₃	450 [190; 1100]; (4)
40	CH	CH	CH	4-CN	1		CH ₃	190 [130; 280]; (3)
41	N	CH	N	H	1		CH ₃	7.0 [2.6; 18.4]; (4)
42	N	CH	N	H	1		CH ₃	72 [11; 492]; (4)
44	CH	CH	CH	H	3		CH ₂ CH ₃	380 [180; 810]; (3)
45	CH	CH	CH	4-Cl	3		CH ₂ CH ₃	170 [30; 870]; (4)
46	CH	CH	CH	4-Cl	3		CH ₂ CH ₃	200 [100; 370]; (4)

^a Binding affinity values (K_i) are expressed as average along with 95% confidence intervals.

^b Number of experiments.

Table 3

Compliance of the most active ligands to Lipinski's and Veber's rules.

Compound	AlogP (< 5)	MW (< 500)	No. HBA ^a (≤ 10)	No. HBD ^b (≤ 5)	No. rotatable bonds (≤ 10)	Molecular PSA ^c (< 140 Å)
14	2.33	386.5	5	1	4	75
20	3.00	421.0	5	1	4	75
21	1.80	314.4	4	1	5	79
23	2.21	411.5	6	1	4	99
27	3.00	421.0	5	1	4	75
41	1.56	367.5	5	1	6	81

^a Number of Hydrogen-bond acceptors (HBA).^b Number of Hydrogen-bond donors (HBD).^c Polar Surface Area (PSA).

Table 4

Predicted ADME profiles of the most active ligands.

Compound	BBB ^a	Absorption ^b	Solubility ^c	Hepatotoxicity ^d	CYP2D6 ^e	PPB ^f
14	2	0	3	Nontoxic	Inhibitor	2 (> 95%)
20	1	0	2	Nontoxic	Non-inhibitor	0 (90%)
21	2	0	3	Nontoxic	Non-inhibitor	1 (> 90%)
23	2	0	3	Nontoxic	Non-inhibitor	0 (< 90%)
27	1	0	2	Nontoxic	Non-inhibitor	0 (< 90%)
41	2	0	3	Nontoxic	Non-inhibitor	2 (> 95%)

^a Predicts ability of the compound to penetrate the blood-brain barrier (BBB). Levels 0, 1, 2, 3, or 4 correspond to very high, high, medium, low, or undefined penetration, respectively.^b Predicts human intestinal absorption after oral administration. Levels 0, 1, 2, or 3 correspond to good, moderate, poor, or very poor absorption, respectively.^c Predicts the solubility of each compound in water at 25 °C. Levels 0, 1, 2, 3, 4, 5, or 6 correspond to extremely low, very low, low, good, optimal, too soluble, or unknown solubility, respectively.^d Predicts the occurrence of dose-dependent human hepatotoxicity.^e Predicts cytochrome P450 2D6 inhibition.^f Predicts the likelihood that a compound will be highly bound to carrier proteins on the blood (PPB, plasma protein binding).

ligands to be effective for targeting neurodegenerative diseases and their potential for oral administration. Moreover, these ligands showed low ($-6.0 < \log Sw < -4.0$) to good ($-4.0 < \log Sw < -2.0$) solubility, non-hepatotoxicity, and variable properties for inhibition of CYP2D6 and PPB (Table 4). However, the compounds with highest affinity in the series (14, 21 and 41) provide some deficiencies regarding BBB permeability and display high PPB (PPB > 95% as with 14 and 41).

As ligand efficiency measures emerge as increasingly important parameters in hit-to-lead optimization, we calculated ligand efficiency

(LE) and lipophilic ligand efficiency (LLE) according to literature, based on *in silico* AlogP-values and *in vitro* binding affinities.⁵⁰ LE values were within the commonly accepted limits with $LE > 0.3$ kcal per mole per non-H-atoms (nHA) (0.42, 0.50 and 0.41 kcal/mole/nHA for compounds 14, 21 and 41 respectively).⁵¹ LLE values conform to the acceptance criteria of $LLE > 5$, being 5.9, 6.6 and 6.6 for 14, 21 and 41, respectively.⁵²

The United States Food and Drug Administration (US FDA) standard toxicity risk predictor software TOPKAT (Discovery Studio, Accelrys, USA) locates fragments within the compound that indicate a potential

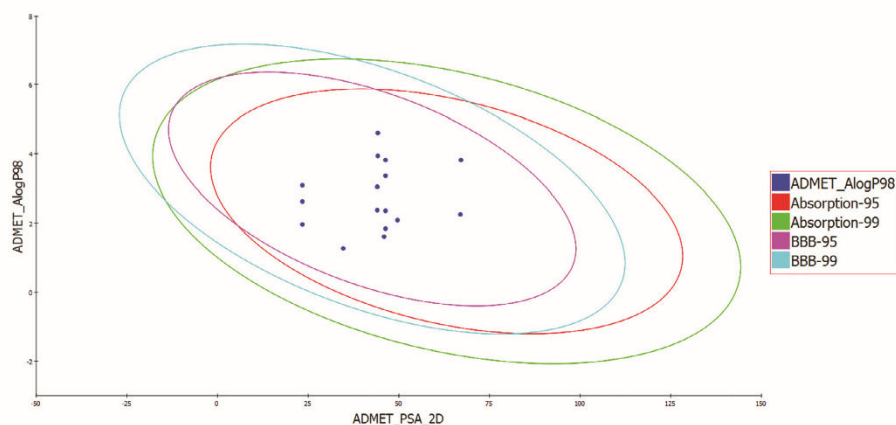


Fig. 3. Plot of PSA vs AlogP (calculated via "Calculate Molecular Properties" module of Discovery Studio 2.5.5) for the most active ligands showing 95% and 99% confidence limit ellipses corresponding to penetration of BBB and intestinal absorption.

Table 5

Toxicity profile of the most active ligands using toxicity prediction, extensible protocol of Accelrys Discovery studio 2.5.5.

Compound	Aerobic BioDegradability ^a	AMES Mutagenicity ^b	Ocular Irritancy ^c	Skin Irritancy ^c	Skin Sensitizer ^c	Carcinogenicity_USFDA ^d			
						Female Mouse	Male Mouse	Female rat	Male Rat
14	–	–	+	–	–	–	+	+	–
20	–	–	+	–	–	–	–	–	–
21	–	–	+	–	++	–	+	++	++
23	–	–	+	–	–	–	+	++	++
27	–	–	+	–	–	–	–	–	–
41	–	–	+	+	++	+	+	+	++

^a Prediction of oxidative degradability-properties of compounds. Indicators –, or + correspond to non-biodegradability, or degradability by bioorganisms, respectively.

^b Predicted mutagenicity in AMES mutagenicity test. Indicators –, or + correspond to non-mutagenicity, or mutagenicity, respectively.

^c Prediction of organic toxicity. Indicators –, +, or ++ correspond to none, mild, or severe/strong toxic properties, respectively.

^d Prediction of carcinogenic properties. Indicators –, +, or ++ correspond to classification as Non-Carcinogen, Single-Carcinogen, or Multi-Carcinogen, respectively.

toxicity risk. TOPKAT (TOxicity Prediction by Komputer Assisted Technology) employs robust and cross-validated Quantitative Structure Toxicity Relationship (QSTR) models for assessing various measures of toxicity and utilizing the patented Optimal Predictive Space validation method to assist in interpreting the results. Toxicity screening results of TOPKAT for the most active H₃R ligands showed no risk of AMES mutagenicity, and tolerable ocular and skin irritation (Table 5); however, they possess potential US FDA rodent carcinogenicity, except against female mouse. Compound **14** is the only non-skin sensitizing agent among the three most active compounds and appears as single-carcinogen in male mouse and female rat, whereas the cyano-containing ligands **21** and **41** differentiate as skin sensitizing and multi-carcinogenic agents. Moreover, particular attention was paid to the risk of aerobic biodegradability as 2-phenylthiazoles are known to produce hepatotoxic and/or nephrotoxic thioamides and 1,2-dicarbonyl-species upon oxidative metabolism.^{53,54} Thus, exclusively in 5-position alkylated thiazole derivatives were synthesized to achieve reduced oxidative ring-scission and biodegradable probability, confirmed by the TOPKAT screening results.⁵⁵

Besides the biological evaluation, this *in silico* screening provided additional information that could be useful for further lead optimization of the presented compounds (cf. additional *in silico* ADMET and toxicity information on compounds **8**, **16**, **17**, **22**, **30**, **37**, and **42** is provided in Supplementary Material).

3. Conclusions

A novel series of oxadiazole and thiazole derivatives as H₃R ligands are explored in the present study. Oxadiazole ligands showed mediocre affinities unlike the thiazole, which showed potent H₃R affinities in low nanomolar concentration range. The highest affinities are observed with ligands of pyrrolidine or piperidine basic heads and 2–3 carbon linkers. However, thiazole ligands of *para*-xylene or piperidine carbonyl linkers showed high binding affinities, too. The examined compounds show excellent drug-like properties in compliance with Lipinski's and Veber's rules and satisfactory *in silico* ADMET properties. The results from this study will be helpful for further improvements of potent H₃R ligands.

4. Experimental

4.1. Chemistry

Reagents and solvents for synthesis were purchased from Sigma-Aldrich, VWR Chemicals, Fisher Scientific, Alfa Aesar and Chemsolute and were used without further purifications. ¹H NMR and ¹³C NMR were recorded on a Bruker AMX spectrometer (Bruker, Germany) at

300 and 75 MHz respectively, where CDCl₃ or DMSO-*d*₆ was used as a solvent. Tetramethylsilane was used as standard and chemical shifts are reported in parts per million (ppm). Spin multiplicities are given as s (singlet), d (doublet), dd (doublet of doublets), t (triplet), q (quintet) or m (multiplet). Approximate coupling constants (J) are given in Hertz (Hz). Number and assignment of protons (ax, axial; eq, equatorial; ph, phenyl; pip, piperidine; pyra, pyrazine; pyr, pyridine; pyrr, pyrrolidine). Elementary analyses (C, H, N) were measured on a CHN-Rapid (Heraeus, Germany) and all final compounds were within 0.4% of the theoretical values. Electrospray ionization mass spectrometry (ESI-MS) was performed on an amaZon speed (Bruker, Germany) in positive polarity. Data are listed as mass number ([M+H]⁺). High-resolution mass spectra (HRMS) were run in electrospray ionization (ESI) mode. Melting points (m.p., uncorrected) were determined on a M-564 Büchi melting point apparatus (Büchi, Germany). Preparative column chromatography was performed on silica gel 60 M, 0.04–0.063 mm (Macherey-Nagel, Germany) and thin-layer chromatography (TLC) was carried out using pre-coated silica gel 60 with fluorescence indicator at UV 254 nm (Macherey-Nagel, Germany).

4.1.1. General reaction procedures

4.1.2.1. General procedure (A). Preparation of 4-Phenyl-3-thiosemicarbazide. The phenylisothiocyanate (30 mmol) was added, dropwise, over a period of 1 h to a stirred solution of hydrazine (30 mmol) in methanol (8 mL) at 65–80 °C. The reaction mixture was stirred for 20 min more at the same temperature. The solvent was removed by evaporation *in vacuo* and the precipitate was collected by filtration and washed with petroleum ether. The compound was used without further purification.

4.1.2.2. General procedure (B). Preparation of 2-Anilino-5-alkyl-1,3,4-oxadiazole. A carboxylic acid (0.33 mmol), a 4-phenyl-3-thiosemicarbazide (0.33 mmol), and EDCI (182 mg, 1.0 mmol) were mixed in CH₂Cl₂ (15 mL), and the reaction mixture was stirred at room temperature for 12 h. The organic layer was washed three times with saturated NaHCO₃, dried over MgSO₄, filtered, and concentrated. Chromatography (5:95 MeOH/DCM, silica gel) of the residue afforded the title compound.

4.1.2.3. General procedure (C). Preparation of Phenyl amidoximes. To a stirred solution of phenyl nitrile (0.1 mol) in ethanol (100 mL), a solution of hydroxylamine (0.6 mol) in H₂O (150 mL) was slowly added followed by NaHCO₃ (0.3 mol). The resulting mixture was refluxed for 3 h. The solvent was evaporated *in vacuo* and the resulting residue was poured into cold water. The formed precipitate was filtered off, washed with water and dried *in vacuo*. The obtained product was recrystallized from methanol.

4.1.2.4. General procedure (D). Preparation of 1,2,4-Oxadiazole-5-carboxylates. Pyridine (0.015 mol) was added to a solution of phenyl amidoxime (0.01 mol) dissolved in dry CHCl₃ (100 mL). Ethyl chloroxalate (0.025 mol) was then added to the solution under vigorous stirring. The mixture was stirred at room temperature for 30 min, then refluxed for 5 h, cooled to rt, washed with water and HCl (5%). Organic layer was dried under MgSO₄, concentrated *in vacuo* and the formed residue was purified by flash-chromatography on silica gel.

4.1.2.5. General procedure (E). Preparation of 1,2,4-Oxadiazole-5-carboxamides. A primary amine (0.5 mmol) was added to the carboxylate (0.5 mmol) dissolved in dry ethanol (5 mL). The reaction mixture was refluxed for 12 h, and then cooled to rt. The organic solvent was dried *in vacuo* and the crude product was purified by flash-chromatography on silica gel to give the target compounds.

4.1.2.6. General procedure (F). Preparation of 4-Hydroxy-5-methylthiazole. Pyridine (0.005 mol) was added to a mixture of thiolactic acid (0.02 mol) and nitrile (0.02 mol) at 23 °C under argon. The reaction mixture was then heated at 100 °C for 2 h. After cooling, the precipitate was collected, washed with absolute ethanol, and recrystallized from methanol to afford the product.

4.1.2.7. General procedure (G). O-Alkylations of Hydroxy thiazoles. To a solution of thiazole (1.0 eq.) dissolved in DMF (4 mL), K₂CO₃ (3.0 eq.) was added, and the reaction mixture was left for 30 min at 60 °C. Then, KI (1.0 eq.) and the alkyl halide (0.9 eq.) was added and the reaction was left for an additional 8 h. The reaction mixture was taken up in DCM, washed with Na₂CO₃ (3x) and dried over MgSO₄ and concentrated *in vacuo*. The concentrate was purified by flash chromatography yielding the desired compound.

4.1.2.8. General procedure (II). Preparation of 2-Phenyl-4-hydroxy-5-ethylthiazole. Pyridine (5.83 mmol) was added to a mixture of ethyl 2-bromobutanoate (6.41 mmol) and thiobenzamide (5.83 mmol) at 23 °C under argon. The reaction mixture was then heated at 100 °C for 2 h. After cooling, the precipitate was collected and washed with absolute ethanol, and the recrystallized from methanol to afford the desired product.

4.1.2.9. General procedure (I). Preparation of Bromoethyl benzyl thiazole. 1,4-Bis(bromomethyl)benzen (4.0 mmol), 4-hydroxythiazole (1.0 mmol) and K₂CO₃ (2.0 mmol) dissolved in 50 mL acetone was refluxed for 12 h. After cooling, acetone was evaporated and the crude product was constituted in DCM. The organic layer was washed with NaHCO₃ solution (3x) and dried over Na₂SO₃. The final compound was purified with flash chromatography.

4.1.2.10. General procedure (J). Nucleophilic Substitution of Bromoethyl benzyl thiazole. The bromoethyl benzyl thiazole (1.0 eq.) was dissolved in DMF (4 mL) and K₂CO₃ (3.0 eq.) was added. The reaction mixture was left for 30 min at 60 °C, then the piperidine or pyrrolidine (0.9 eq.) was added and the reaction was left for an additional 8 h. The reaction mixture was taken up in DCM, washed with Na₂CO₃ (3x) and dried over MgSO₄ and concentrated *in vacuo*. The concentrate was purified by flash chromatography yielding the desired compound.

4.1.2.11. 5-Methyl-2-phenyl-4-(2-(pyrrolidin-1-yl)ethoxy)thiazole (8). Compound **8** was prepared according to procedure G from 5-methyl-2-phenylthiazol-4-ol and 1-(2-chloroethyl)pyrrolidine to afford 62 mg of yellow solid (70%). ¹H NMR (CDCl₃, 300 MHz) δ 7.77 (dd, *J* = 8.1, 1.8 Hz, 2H, ph-2,6H), 7.38–7.23 (m, 3H, ph-3,4,5H), 4.45 (t, *J* = 6.0 Hz, 2H, OCH₂), 2.87 (t, *J* = 6.0 Hz, 2H, OCH₂CH₂N), 2.73–2.50 (m, 4H, pyr-2,5H₂), 2.22 (s, 3H, CH₃), 1.77 (p, *J* = 1.8 Hz, 4H, pyr-3,4H₂). ¹³C NMR (151 MHz, CDCl₃) δ 9.40, 23.53, 54.67, 55.32, 69.26, 107.09, 125.34, 128.78, 129.29, 134.00, 159.47, 159.53. HRMS *m/z*

289.1384 [M + H⁺] (calcd for C₁₆H₂₁N₂O₂S, 289.1375). Anal. Calcd for C₁₆H₂₀N₂O₂S: C 66.63, H 6.99, N 9.51, S 11.12. Found: C 66.82, H 7.24, N 9.18, S 11.51.

4.1.2.12. 5-Methyl-2-phenylthiazol-4-yl [1,4'-bipiperidine]-1'-carboxylate (14). Compound **14** was prepared according to procedure G from 5-methyl-2-phenylthiazol-4-ol and [1,4'-bipiperidine]-1'-carbonyl chloride to afford 74 mg of yellow solid (80%). ¹H NMR (CDCl₃, 300 MHz) δ 7.79–7.74 (dd, *J* = 2.1, 1.8 Hz, 2H, ph-2,6H), 7.31 (d, *J* = 1.8 Hz, 1H, ph-4H), 7.29 (d, *J* = 2.1 Hz, 2H, ph-3,5H), 4.27 (dd, *J* = 30.2, 12.8 Hz, 2H, pip¹-2,6H_{eq}), 2.85 (m, 2H, pip¹-2,6H_{ax}), 2.55–2.32 (m, 5H, pip²-4H, pip²-2,6H_{2ax/eq}), 2.22 (s, 3H, CH₃), 1.94–1.72 (m, 2H, pip¹-3,5H_{eq}), 1.67–1.42 (m, 6H, pip¹-3,5H_{ax}, pip²-3,5H_{2ax/eq}), 1.42–1.27 (m, 2H, pip²-4H_{2ax/eq}). ¹³C NMR (75 MHz, CDCl₃) δ 10.03, 24.63, 26.21, 28.10, 44.40, 50.20, 62.36, 117.88, 125.72, 128.76, 129.81, 133.37, 151.79, 152.31, 161.20. HRMS *m/z* 386.1910 [M + H⁺] (calcd for C₂₁H₂₈N₃O₂S, 386.1902). Anal. Calcd for C₂₁H₂₇N₃O₂S: C 65.43, H 7.06, N 10.90, S 8.32. Found: C 66.18, H 7.12, N 10.84, S 8.38.

4.1.2.13. 2-(4-Chlorophenyl)-5-methyl-4-(2-(pyrrolidin-1-yl)ethoxy)thiazole (16). Compound **16** was prepared according to procedure G from 2-(4-chlorophenyl)-5-methylthiazol-4-ol and 1-(2-chloroethyl)pyrrolidine to afford 79 mg of yellow solid (91%). ¹H NMR (CDCl₃, 300 MHz) δ 7.66 (d, *J* = 8.6 Hz, 2H, ph-2,6H), 7.24 (d, *J* = 8.6 Hz, 2H, ph-3,5H), 4.40 (t, *J* = 6.0 Hz, 2H, OCH₂), 2.81 (t, *J* = 6.0 Hz, 2H, OCH₂CH₂N), 2.63–2.47 (m, 4H, pyr-2,5H₂), 2.19 (s, 3H, CH₃), 1.72 (p, *J* = 3.0 Hz, 4H, pyr-3,4H₂). ¹³C NMR (75 MHz, DMSO) δ 9.28, 23.42, 54.59, 55.26, 69.42, 107.31, 126.37, 128.82, 132.38, 134.89, 157.85, 159.64. HRMS *m/z* 323.0991 [M + H⁺] (calcd for C₁₆H₁₉ClN₂O₂S, 323.0985). Anal. Calcd for C₁₆H₂₀ClN₂O₂S: C 59.52, H 5.93, N 8.68, S 9.93. Found: C 59.88, H 6.07, N 8.41, S 10.37.

4.1.2.14. 2-(4-Chlorophenyl)-5-methyl-4-(2-(piperidin-1-yl)ethoxy)thiazole (17). Compound **17** was prepared according to procedure G from 2-(4-chlorophenyl)-5-methylthiazol-4-ol and 1-(3-chloroethyl)piperidine to afford 43 mg of yellow solid (57%). ¹H NMR (CDCl₃, 300 MHz) δ 7.69 (d, *J* = 8.5 Hz, 2H, ph-2,6H), 7.28 (d, *J* = 8.5 Hz, 2H, ph-3,5H), 4.44 (t, *J* = 6.0 Hz, 3H, OCH₂), 2.76 (t, *J* = 6.0 Hz, 3H, OCH₂CH₂N), 2.62–2.47 (m, 4H, pip-2,6H_{2ax/eq}), 2.21 (s, 3H, CH₃), 1.72–1.52 (m, 4H, pip-3,5H_{2ax/eq}), 1.45–1.32 (m, 2H, pip-4H_{2ax/eq}). ¹³C NMR (75 MHz, CDCl₃) δ 9.73, 24.63, 26.34, 55.33, 58.66, 68.65, 107.37, 126.48, 128.93, 132.48, 134.99, 158.01, 159.78. HRMS *m/z* 337.1148 [M + H⁺] (calcd for C₁₇H₂₂ClN₂O₂S, 337.1141). Anal. Calcd for C₁₇H₂₁ClN₂O₂S: C 60.61, H 6.28, N 8.32, S 9.52. Found: C 61.08, H 6.51, N 8.41, S 9.85.

4.1.2.15. 2-(4-Chlorophenyl)-5-methylthiazol-4-yl [1,4'-bipiperidine]-1'-carboxylate (20). Compound **20** was prepared according to procedure G from 2-(3-chlorophenyl)-5-methylthiazol-4-ol and [1,4'-bipiperidine]-1'-carbonyl chloride to afford 84 mg of yellow solid (89%). ¹H NMR (CDCl₃, 300 MHz) δ 7.69 (d, *J* = 8.6 Hz, 2H, ph-2,6H), 7.27 (d, *J* = 8.6 Hz, 2H, ph-3,5H), 4.27 (dd, *J* = 28.1, 13.3 Hz, 2H, pip¹-2,6H_{eq}), 2.86 (m, 2H, pip²-2,6H_{eq}), 2.62–2.34 (m, 5H, pip¹-4H, pip²-2,6H_{2ax/eq}), 2.22 (s, 3H, CH₃), 1.96–1.74 (m, 2H, pip¹-3,5H_{eq}), 1.68–1.45 (m, 6H, pip¹-3,5H_{ax}, pip²-3,5H_{2ax/eq}), 1.44–1.29 (m, 2H, pip²-4H₂). ¹³C NMR (75 MHz, CDCl₃) δ 10.02, 24.46, 25.96, 27.40, 27.97, 44.04, 44.33, 50.16, 62.39, 118.40, 126.90, 128.99, 131.86, 135.69, 151.88, 152.22, 159.79. HRMS *m/z* 420.1514 [M + H⁺] (calcd for C₂₁H₂₆ClN₃O₂S, 420.1513). Anal. Calcd for C₂₁H₂₇ClN₃O₂S: C 60.06, H 6.24, N 10.01, S 7.63. Found: C 60.12, H 6.20, N 10.18, S 7.66.

4.1.2.16. 4-(5-Methyl-4-(2-(pyrrolidin-1-yl)ethoxy)thiazol-2-yl)benzonitrile (21). Compound **21** was prepared according to procedure G from 2-(3-cyanophenyl)-5-methylthiazol-4-ol and 1-(2-chloroethyl)pyrrolidine to afford 67 mg of yellow solid (80%). ¹H NMR (CDCl₃,

300 MHz) δ 7.74 (d, J = 8.7 Hz, 2H, ph-2,6H), 7.49 (d, J = 8.7 Hz, 2H, ph-3,5H), 4.38 (t, J = 5.4 Hz, 2H, OCH₂), 2.84 (t, J = 5.5 Hz, 2H, OCH₂CH₂N), 2.66–2.55 (m, 4H, pyr-2,5H₂), 2.16 (s, 3H, CH₃), 1.80–1.64 (m, 4H, pyr-3,4H₂). ¹³C NMR (75 MHz, CDCl₃) δ 9.36, 31.25, 36.37, 54.98, 68.92, 109.48, 111.85, 118.48, 125.35, 132.44, 137.43, 156.31, 160.10. HRMS m/z 314.1332 [M+H⁺] (calcd for C₁₇H₂₀N₃OS, 314.1327). Anal. Calcd for C₁₇H₂₀N₃OS: C 66.03, H 6.46, N 12.83, S 9.79. Found: C 66.18, H 6.51, N 12.79, S 9.72.

4.1.2.17. 4-(5-Methyl-4-(3-(piperidin-1-yl)propoxy)thiazol-2-yl)benzonitrile (22). Compound **22** was prepared according to procedure G from 2-(3-cyanophenyl)-5-methylthiazol-4-ol and 1-(3-chloropropyl)piperidine to afford 75 mg of yellow solid (83%). ¹H NMR (CDCl₃, 300 MHz) δ 7.81 (d, J = 8.7 Hz, 2H, ph-2,6H), 7.55 (d, J = 8.7 Hz, 2H, ph-3,5H), 4.29 (t, J = 6.4 Hz, 2H, OCH₂), 2.45–2.40 (m, 2H, OCH₂CH₂), 2.39–2.31 (m, 4H, pip-2,6H_{2ax/eq}), 2.21 (s, 3H, CH₃), 2.03–1.82 (m, 2H, OCH₂CH₂CH₂N), 1.68–1.48 (m, 4H, pip-3,5H_{2ax/eq}), 1.45–1.27 (m, 2H, pip-4H_{2ax/eq}). ¹³C NMR (75 MHz, CDCl₃) δ 9.40, 24.31, 25.80, 26.97, 54.54, 55.91, 69.11, 109.34, 112.00, 118.62, 125.45, 132.53, 137.66, 156.33, 160.53. HRMS m/z 342.1645 [M+H⁺] (calcd for C₁₉H₂₄N₃OS, 342.1640). Anal. Calcd for C₁₉H₂₄N₃OS: C 66.83, H 6.79, N 12.31, S 9.39. Found: C 66.79, H 6.80, N 12.31, S 9.44.

4.1.2.18. 2-(4-Cyanophenyl)-5-methylthiazol-4-yl [1,4'-bipiperidine]-1'-carboxylate (23). Compound **23** was prepared according to procedure G from 4-(4-hydroxy-5-methylthiazol-2-yl)benzonitrile and [1,4'-bipiperidine]-1'-carbonyl chloride to afford 91 mg of yellow solid (91%). ¹H NMR (CDCl₃, 300 MHz) δ 7.85 (d, J = 8.7 Hz, 2H, ph-2,6H), 7.59 (d, J = 8.2 Hz, 2H, ph-3,5H), 4.26 (dd, J = 31.1, 13.0 Hz, 2H, pip¹-2,6H_{eq}), 2.84 (m, 2H, pip²-2,6H_{eq}), 2.56–2.44 (m, 5H, pip¹-4H, pip²-2,6H_{2ax/eq}), 2.26 (s, 3H, CH₃), 2.01–1.76 (m, 2H, pip¹-3,5H_{eq}), 1.66–1.47 (m, 6H, pip¹-3,5H_{ax}, pip²-3,5H_{2ax/eq}), 1.45–1.30 (m, 2H, pip²-4H₂). ¹³C NMR (75 MHz, CDCl₃) δ 10.08, 24.41, 25.93, 27.41, 27.96, 44.03, 44.31, 50.13, 62.24, 112.75, 118.37, 120.43, 125.93, 132.55, 137.00, 152.02, 152.55, 158.24. HRMS m/z 411.1862 [M+H⁺] (calcd for C₂₂H₂₇N₄O₂S, 411.1855). Anal. Calcd for C₂₂H₂₆N₄O₂S: C 64.37, H 6.38, N 13.65, S 7.81. Found: C 64.44, H 6.51, N 13.51, S 7.70.

4.1.2.19. 2-(3-Chlorophenyl)-5-methylthiazol-4-yl [1,4'-bipiperidine]-1'-carboxylate (27). Compound **27** was prepared according to procedure G from 2-(3-chlorophenyl)-5-methylthiazol-4-ol and [1,4'-bipiperidine]-1'-carbonyl chloride to afford 85 mg of yellow solid (89%). ¹H NMR (CDCl₃, 300 MHz) δ 7.81–7.78 (m, 1H, ph-2H), 7.64–7.58 (m, 1H, ph-5H), 7.35–7.19 (m, 2H, ph-3,4H), 4.27 (dd, J = 29.0, 13.3 Hz, 2H, pip¹-2,6H_{eq}), 2.86 (m, 2H, pip¹-2,6H_{ax}), 2.54–2.34 (m, 5H, pip¹-4H, pip²-2,6H_{2ax/eq}), 2.23 (s, 3H, CH₃), 1.72–1.94 (m, 2H, pip¹-3,5H_{eq}), 1.67–1.46 (m, 6H, pip¹-3,5H_{ax}, pip²-3,5H_{2ax/eq}), 1.44–1.33 (m, 2H, pip²-4H₂). ¹³C NMR (75 MHz, CDCl₃) δ 10.05, 24.54, 26.08, 27.47, 28.03, 44.09, 44.38, 50.19, 62.36, 118.83, 123.79, 125.64, 129.70, 130.04, 134.90, 134.95, 151.99, 152.21, 159.37. HRMS m/z 420.1504 [M+H⁺] (calcd for C₂₁H₂₇ClN₃O₂S, 420.1513). Anal. Calcd for C₂₁H₂₆ClN₃O₂S: C 60.06, H 6.24, N 10.01, S 7.63. Found: C 60.10, H 6.29, N 10.10, S 7.58.

4.1.2.20. 5-Methyl-4-(2-(piperidin-1-yl)ethoxy)-2-(pyridin-4-yl)thiazole (30). Compound **30** was prepared according to procedure G from 5-methyl-2-(pyridin-4-yl)thiazol-4-ol and 1-(3-chloroethyl)piperidine to afford 78 mg of yellow solid (82%). ¹H NMR (CDCl₃, 300 MHz) δ 8.55 (dd, J = 4.6, 1.7 Hz, 2H, pyr-3,5H), 7.61 (dd, J = 4.6, 1.7 Hz, 2H, pyr-2,6H), 4.46 (t, J = 6.0 Hz, 2H, OCH₂), 2.75 (t, J = 6.0 Hz, 2H, OCH₂CH₂N), 2.58–2.44 (m, 4H, pip-2,6H_{2ax/eq}), 2.25 (s, 3H, CH₃), 1.69–1.52 (m, 4H, pip-3,5H_{2ax/eq}), 1.46–1.32 (m, 2H, pip-4H_{2ax/eq}). ¹³C NMR (75 MHz, CDCl₃) δ 9.51, 24.01, 25.68, 54.87, 58.04, 68.07, 109.80, 119.04, 140.55, 150.42, 155.92, 160.37. HRMS m/z

304.1482 [M+H⁺] (calcd for C₁₆H₂₂N₃OS, 304.1484). Anal. Calcd for C₁₆H₂₁N₃OS: C 63.33, H 6.98, N 13.85, S 10.57. Found: C 63.67, H 7.22, N 13.92, S 10.67.

4.1.2.21. 5-(5-Methyl-4-(3-(piperidin-1-yl)propoxy)thiazol-2-yl)isobenzofuran-1(3H)-one (37). Compound **37** was prepared according to procedure G from 5-(4-hydroxy-5-methylthiazol-2-yl)isobenzofuran-1(3H)-one and 1-(3-chloropropyl)piperidine to afford 72 mg of yellow solid (84%). ¹H NMR (CDCl₃, 300 MHz) δ 7.92–7.85 (m, 2H, isobenzofuran-4,7H), 7.82 (dd, J = 8.1, 0.8 Hz, 1H, isobenzofuran-6H), 5.27 (s, 2H, isobenzofuran-3H₂), 4.33 (t, J = 6.3 Hz, 2H, OCH₂), 2.68–2.39 (m, 6H, OCH₂CH₂CH₂N, pip-2,6H_{2ax/eq}), 2.24 (s, 3H, CH₃), 2.09–1.89 (m, 2H, OCH₂CH₂), 1.70–1.52 (m, 4H, pip-3,5H_{2ax/eq}), 1.50–1.33 (m, 2H, pip-4H_{2ax/eq}). ¹³C NMR (75 MHz, CDCl₃) δ 9.45, 23.98, 25.33, 26.59, 54.41, 55.84, 68.92, 69.55, 109.43, 118.37, 125.74, 126.15, 126.19, 139.17, 147.32, 156.86, 160.40, 170.53. HRMS m/z 373.1593 [M+H⁺] (calcd for C₂₀H₂₅N₂O₃S, 373.1586). Anal. Calcd for C₂₀H₂₄N₂O₃S: C 64.49, H 6.49, N 7.52, O 12.89, S 8.61. Found: C 64.57, H 6.35, N 7.62, S 8.67.

4.1.2.22. 5-Methyl-4-((4-(piperidin-1-ylmethyl)benzyl)oxy)-2-(pyrazin-2-yl)thiazole (41). Compound **41** was prepared according to procedure J from 4-((4-(bromomethyl)benzyl)oxy)-5-methyl-2-(pyrazin-2-yl)thiazole and piperidine to afford 91 mg of yellow solid (89%). ¹H NMR (CDCl₃, 300 MHz) δ 9.22 (d, J = 1.5 Hz, 1H, pyra-6H), 8.60–8.12 (m, 2H, pyra-3,4H), 7.34 (d, J = 8.1 Hz, 2H, ph-2,6H), 7.25 (d, J = 8.1 Hz, 2H, ph-3,5H), 5.33 (s, 2H, phCH₂O), 3.42 (s, 2H, phCH₂N), 2.36–2.27 (m, 4H, pip-2,6H_{2ax/eq}), 2.23 (s, 3H, CH₃), 1.56–1.42 (m, 4H, pip-3,5H_{2ax/eq}), 1.40–1.26 (m, 2H, pip-4H_{2ax/eq}). ¹³C NMR (75 MHz, CDCl₃) δ 9.63, 24.23, 25.76, 54.37, 63.39, 72.04, 112.07, 127.90, 129.40, 136.17, 137.86, 140.81, 143.68, 144.16, 146.96, 156.57, 160.42. HRMS m/z 381.1758 [M+H⁺] (calcd for C₂₁H₂₅N₄O₂S, 381.1749). Anal. Calcd for C₂₁H₂₄N₄O₂S: C 66.29, H 6.36, N 14.72, S 8.43. Found: C 66.37, H 6.35, N 14.62, S 8.67.

4.1.2.23. 5-Methyl-2-(pyrazin-2-yl)-4-((4-(pyrrolidin-1-ylmethyl)benzyl)oxy)thiazole (42). Compound **42** was prepared according to procedure J from 4-((4-(bromomethyl)benzyl)oxy)-5-methyl-2-(pyrazin-2-yl)thiazole and pyrrolidine to afford 87 mg of yellow solid (84%). ¹H NMR (CDCl₃, 300 MHz) δ 9.21 (d, J = 1.5 Hz, 1H, pyra-4H), 8.42 (d, J = 2.6 Hz, 1H, pyra-6H), 8.38 (dd, J = 2.6, 1.5 Hz, 1H, pyra-3H), 7.37 (d, J = 8.4 Hz, 2H, ph-2,6H), 7.32 (d, J = 8.4 Hz, 2H, ph-3,5H), 5.33 (s, 2H, phCH₂O), 3.66 (s, 2H, phCH₂N), 2.68–2.47 (m, 4H, pyr-2,5H), 2.24 (s, 3H, CH₃), 1.85–1.58 (m, 4H, pyr-3,4H). ¹³C NMR (75 MHz, CDCl₃) δ 9.62, 23.36, 53.88, 59.88, 71.87, 112.08, 128.10, 129.33, 136.77, 137.02, 140.78, 143.68, 144.18, 146.92, 156.60, 160.32. HRMS m/z 367.1587 [M+H⁺] (calcd for C₂₀H₂₃N₄O₂S, 367.1593). Anal. Calcd for C₂₀H₂₂N₄O₂S: C 65.55, H 6.05, N 15.29, S 8.75. Found: C 65.67, H 6.11, N 15.32, S 8.67.

4.2. Pharmacology

4.2.1. [³H]-N^α-Methylhistamine hH₃ receptor displacement assay

The procedure was performed as described previously⁵⁶ with slight modification: In brief, membrane preparations (20 µg/well) of HEK-293 cells stably expressing the human H₃ receptor (hH3R) were incubated in a mixture of [³H]-N^α-methylhistamine (2 nM; K_D = 3.08 nM as determined by saturation binding experiments) and appropriate concentrations of the present competitors (seven to eleven concentrations between 0.01 nM and 10 µM) in 96-well microtiter plates with a final assay volume of 200 µl per well. Preparation of competitor-concentrations was carried out by serial dilution of 10 mM and 3 mM stocks using a Freedom EVO pipetting instrument (TECAN®, Männedorf, Switzerland). For sample filtration ice-cold demineralized water was used. Specific binding was analyzed by non-linear squares fit via GraphPad-Prism™ (2012, vers. 6.01, La Jolla, CA, USA). Affinities (K_i) were

M.A. Khanfar et al.

Bioorganic & Medicinal Chemistry 26 (2018) 4034–4046

calculated from IC₅₀-values using the Cheng-Prusoff equation and expressed as means from at least two independent experiments in triplicates within 95% confidence intervals.⁵⁷

4.3. Molecular descriptor analysis

Molecular properties of most active ligands (those with $K_i < 100$ nM) were calculated using “Calculate Molecular Properties” module of Discovery Studio 2.5.5 client package (Accelrys, San Diego, USA). These descriptors include MW, number HBD and HBA, an octanol/water partition coefficient (log *P*), number of rotatable bonds, and molecular PSA.

4.4. ADME and toxicity studies

In silico ADME profiling for the most active ligands were measured using “ADMET Descriptors” module of Accelrys Discovery studio 2.5.5. The calculated ADME descriptors include BBB, intestinal absorption, solubility, hepatotoxicity, inhibition of CYP2D6, and plasma protein binding.

Toxicity profiling of the active ligands were conducted using TOPKAT toxicity estimation of Discovery Studio 2.5.5. TOPKAT computes a probable value of toxicity for a submitted chemical structure from a quantitative structure–toxicity relationship (QSTR) equation. The product of a structure descriptors and its corresponding coefficient is the descriptors contribution to the probable toxicity. Toxicity profile involves screening for aerobic biodegradability, AMES (activity in the salmonella/mammalian microsome mutagenicity) mutagenicity, ocular and skin irritancy, skin sensitizer, and carcinogenicity.

Acknowledgements

This work was facilitated by the George Forster Research Fellowship, granted by the Alexander von Humboldt-Foundation (MAK). We thank Gina Alpert for the initial pharmacological screening of the present compounds. HEK-293 cells stably expressing the H₃R were a kind gift of Prof. Dr. Jean-Charles Schwartz (Bioprojet, France). Further parts of this work were supported by funding of the German Research Society (DFG INST 208/664-1 FUGG) and the EU COST action CA15135.

A. Supplementary data

Supplementary data associated with this article can be found, in the online version, at <http://dx.doi.org/10.1016/j.bmc.2018.06.028>.

References

- Hu W, Chen Z. The roles of histamine and its receptor ligands in central nervous system disorders: An update. *Pharmacol Ther.* 2017;175:116–132.
- Nieto-Alamillos G, Márquez-Gómez R, García-Gálvez A-M, et al. The Histamine H₃ Receptor: Structure, Pharmacology, and Function. *Mol Pharmacol.* 2016;90:649–673.
- Panula P, Nuutinen S. The histaminergic network in the brain: basic organization and role in disease. *Nat Rev Neurosci.* 2013;14:472.
- Tiligada E, Kyriakidis K, Chazot PL, et al. Histamine pharmacology and new CNS drug targets. *CNS Neurosci Ther.* 2011;17:620–628.
- Parsons ME, Ganellin CR. Histamine and its receptors. *Br J Pharmacol.* 2006;147:S127–135.
- Panula P, Chazot PL, Cowart M, et al. International union of basic and clinical pharmacology XCIII. Histamine receptors. *Pharmacol Rev.* 2015;67:601–655.
- Arrang JM, Garbarg M, Schwartz JC. Auto-inhibition of brain histamine release mediated by a novel class (H₃) of histamine receptor. *Nature.* 1983;302:832–837.
- Schwartz JC, Arrang JM, Garbarg M, et al. Histaminergic transmission in the mammalian brain. *Physiol Rev.* 1991;71:1–51.
- Singh M, Jadhav HR. Histamine H₃ receptor function and ligands: recent developments. *Mini Rev Med Chem.* 2013;13:47–57.
- Schlicker E, Fink K, Göthert M, et al. The pharmacological properties of the presynaptic serotonin autoreceptor in the pig brain cortex conform to the 5-HT_{1D} receptor subtype. *Naunyn-Schmiedeberg Arch Pharmacol.* 1989;340:45–51.
- Schlicker E, Schunack W, Göthert M. Histamine H₃ receptor-mediated inhibition of noradrenaline release in pig retina discs. *Naunyn-Schmiedeberg Arch Pharmacol.* 1990;342:497–501.

- Heron A, Rouleau A, Cochois V, et al. Expression analysis of the histamine H₃ receptor in developing rat tissues. *Mech Dev.* 2001;105:167–173.
- Krementsov DN, Wall EH, Martin RA, et al. Histamine H₃ receptor integrates peripheral inflammatory signals in the neurogenic control of immune responses and autoimmune disease susceptibility. *PLoS One.* 2013;8:e62743.
- Sharma HS, Skaper SD, Sharma A. Commentary: Histaminergic Drugs Could be Novel Targets for Neuroprotection in CNS Disorders. *CNS Neurol Disord Drug Targets.* 2016;15:642–643.
- Khanfar MA, Affini A, Lutsenko K, et al. Multiple targeting approaches on histamine H₃ receptor antagonists. *Front Neurosci.* 2016;10:201.
- Lin JS, Sergeeva OA, Haas HL. Histamine H₃ receptors and sleep-wake regulation. *J Pharmacol Exp Ther.* 2011;336:17–23.
- Raddatz R, Tao M, Hudkins RL. Histamine H₃ antagonists for treatment of cognitive deficits in CNS diseases. *Curr Top Med Chem.* 2010;10:153–169.
- Gemkow MJ, Davenport AJ, Harich S, et al. The histamine H₃ receptor as a therapeutic drug target for CNS disorders. *Drug Discov Today.* 2009;14:509–515.
- Esenshade TA, Brownman KE, Bitner RS, et al. The histamine H₃ receptor: an attractive target for the treatment of cognitive disorders. *Br J Pharmacol.* 2008;154:1166–1181.
- Łażewska D, Kieć-Kononowicz K. Progress in the development of histamine H₃ receptor antagonists/inverse agonists: a patent review (2013–2017). *Expert Opin Ther Pat.* 2018;28:175–196.
- Sander K, Kottke T, Stark H. Histamine H₃ receptor antagonists go to clinics. *Biol Pharm Bull.* 2008;31:2163–2181.
- Syed YY. Pitolisant: first global approval. *Drugs.* 2016;76:1313–1318.
- Schwartz JC. The histamine H₃ receptor: from discovery to clinical trials with pitolisant. *Br J Pharmacol.* 2011;163:713–721.
- Longstreth Jr WT, Koepsell TD, Ton TG, et al. The epidemiology of narcolepsy. *Sleep.* 2007;30:13–26.
- Abad VC, Guilleminault C. New developments in the management of narcolepsy. *Nat Sci Sleep.* 2017;9:39–57.
- Berlin M, Boyce CW, Ruiz Mde L. Histamine H₃ receptor as a drug discovery target. *J Med Chem.* 2011;54:26–53.
- Roche O, Nettekoven M, Vifian W, et al. Refinement of histamine H₃ ligands pharmacophore model leads to a new class of potent and selective naphthalene inverse agonists. *Bioorg Med Chem Lett.* 2008;18:4377–4379.
- Axe FU, Bembek SD, Szalma S. Three-dimensional models of histamine H₃ receptor antagonist complexes and their pharmacophore. *J Mol Graph Model.* 2006;24:456–464.
- Wingen K, Stark H. Scaffold variations in amine warhead of histamine H₃ receptor antagonists. *Drug Discov Today Technol.* 2013;10:e483–489.
- Schlegel B, Laggner C, Meier R, et al. Generation of a homology model of the human histamine H₃ receptor for ligand docking and pharmacophore-based screening. *J Comput Aided Mol Des.* 2007;21:437–453.
- Saha R, Tanwar O, Marella A, et al. Recent updates on biological activities of oxadiazoles. *Mini Rev Med Chem.* 2013;13:1027–1046.
- Chhabria MT, Patel S, Modi P, et al. Thiazole: A Review on Chemistry, Synthesis and Therapeutic Importance of its Derivatives. *Curr Top Med Chem.* 2016;16:2841–2862.
- Meier G, Apelt J, Reichert U, et al. Influence of imidazole replacement in different structural classes of histamine H₃-receptor antagonists. *Eur J Pharm Sci.* 2001;13:249–259.
- Denonne F, Atienzar F, Celanire S, et al. Phenyl-oxazoles, a new family of inverse agonists at the H₃ histamine receptor. *ChemMedChem.* 2010;5:206–212.
- Frymarkiewicz A, Walczynski K. Non-imidazole histamine H₃ ligands, part IV: SAR of 1-[2-thiazol-5-yl-(2-aminoethyl)]-4-*n*-propylpiperazine derivatives. *Eur J Med Chem.* 2009;44:1674–1681.
- Guryn R, Staszewski M, Stasiak A, et al. Non-Imidazole Histamine H₃ Ligands. Part VII. Synthesis, In Vitro and In Vivo Characterization of 5-Substituted-2-thiazol-4-*n*-propylpiperazines. *Molecules.* 2018; 23.
- Walter M, von Coburg Y, Isensee K, et al. Azole derivatives as histamine H₃ receptor antagonists, Part I: Thiazol-2-yl ethers. *Bioorg Med Chem Lett.* 2010;20:5879–5882.
- Walter M, Isensee K, Kottke T, et al. Azole derivatives as histamine H₃ receptor antagonists, Part 2: C-C and C-S coupled heterocycles. *Bioorg Med Chem Lett.* 2010;20:5883–5886.
- Wang R, Lu H, inventor; GlaxoSmithKline Intellectual Property Development Limited, assignee. Therapeutic uses. Patent WO2013107336. July 25, 2013.
- Chen Y, Zhen W, Guo T, et al. Histamine Receptor 3 negatively regulates oligodendrocyte differentiation and remyelination. *PLoS One.* 2017;12:e0189380.
- Kerdesky FA, Holms JH, Moore JL, et al. 4-Hydroxythiazole inhibitors of 5-lipoxygenase. *J Med Chem.* 1991;34:2158–2165.
- Badiali E, Fiser B, Gomez-Bengoa E, et al. Enantioselective construction of tetra-substituted stereogenic carbons through Bronsted base catalyzed Michael reactions: alpha-hydroxy enones as key enolate equivalent. *J Am Chem Soc.* 2014;136:17,869–17,881.
- Polmer J, Hunt SF, Hamley P, et al. Novel piperidine derivative for the treatment of depression, Google Patents; 2006.
- Kuder KJ, Łażewska D, Kaleta M, et al. Synthesis and biological activity of novel tert-amylphenoxyalkyl (homo)piperidine derivatives as histamine H₃R ligands. *Bioorg Med Chem.* 2017;25:2701–2712.
- Clitherow JW, Beswick P, Irving WJ, et al. Novel 1, 2, 4-oxadiazoles as potent and selective histamine H₃ receptor antagonists. *Bioorg Med Chem Lett.* 1996;6:833–838.
- Meanwell NA. Improving drug candidates by design: a focus on physicochemical properties as a means of improving compound disposition and safety. *Chem Res Toxicol.* 2011;24:1420–1456.
- Wessel MD, Jurs PC, Tolan JW, et al. Prediction of human intestinal absorption of

3.3 Design, synthesis, and biological evaluation of novel oxadiazole- and thiazole-based histamine H₃R ligands

M.A. Khanfar et al.

Bioorganic & Medicinal Chemistry 26 (2018) 4034–4046

- drug compounds from molecular structure. *J Chem Inf Comput Sci*. 1998;38:726–735.
48. Lipinski CA, Lombardo F, Dominy BW, et al. Experimental and computational approaches to estimate solubility and permeability in drug discovery and development settings. *Adv Drug Deliv Rev*. 2001;46:3–26.
49. Veber DF, Johnson SR, Cheng HY, et al. Molecular properties that influence the oral bioavailability of drug candidates. *J Med Chem*. 2002;45:2615–2623.
50. Hopkins AI, Keseru GM, Leeson PD, et al. The role of ligand efficiency metrics in drug discovery. *Nat Rev Drug Discov*. 2014;13:105–121.
51. Hopkins AI, Groom CR, Alex A. Ligand efficiency: a useful metric for lead selection. *Drug Discov Today*. 2004;9:430–431.
52. Leeson PD, Springthorpe B. The influence of drug-like concepts on decision-making in medicinal chemistry. *Nat Rev Drug Discov*. 2007;6:881–890.
53. Mizutani T, Suzuki K. Relative hepatotoxicity of 2-(substituted phenyl)thiazoles and substituted thiobenzamides in mice: evidence for the involvement of thiobenzamides as ring cleavage metabolites in the hepatotoxicity of 2-phenylthiazoles. *Toxicol Lett*. 1996;85:101–105.
54. Mizutani T, Yoshida K, Kawazoe S. Possible role of thioformamide as a proximate toxicant in the nephrotoxicity of thiabendazole and related thiazoles in glutathione-depleted mice: structure-toxicity and metabolic studies. *Chem Res Toxicol*. 1993;6:174–179.
55. Kalgutkar AS, Gardner I, Obach RS, et al. A comprehensive listing of bioactivation pathways of organic functional groups. *Curr Drug Metab*. 2005;6:161–225.
56. Kottke T, Sander K, Weizel L, et al. Receptor-specific functional efficacies of alkyl imidazoles as dual histamine H₃/H₄ receptor ligands. *Eur J Pharmacol*. 2011;654:200–208.
57. Cheng Y, Prusoff WH. Relationship between the inhibition constant (K_i) and the concentration of inhibitor which causes 50 per cent inhibition (I₅₀) of an enzymatic reaction. *Biochem Pharmacol*. 1973;22:3099–3108.

Supplementary Material

Design, Synthesis, and Biological Evaluation of Novel Oxadiazole- and Thiazole-Based Histamine H₃R Ligands

Mohammad A. Khanfar^{1,2,3}, David Reiner¹, Stefanie Hagenow¹, Holger Stark^{1*}
¹Henrich Heine University Düsseldorf, Institute of Pharmaceutical and Medicinal Chemistry, Universitätsstr. 1, 40225 Düsseldorf, Germany
²Faculty of Pharmacy, University of Jordan, P.O Box 13140, Amman 11942, Jordan.
³College of Pharmacy, Alfaisal University, AlTakhassusi Rd. Riyadh, 11533, Saudi Arabia

*Corresponding author: Prof. Holger Stark, Tel.: +49 211 81-10478; Fax: +49 211 81-13359; email: stark@ihh.uni.de

Table of Contents

	Page
S.1 Analytical Data	2
S.2 Predicted ADME profiles of further active ligands.	23
S.3 Predicted ADME profiles of further active ligands.	23
S.4 Toxicity profile of further active ligands using toxicity prediction	24

S.1) Analytical Data

N-(4-Chlorophenyl)hydrazinecarbothioamide (**1b**). **1b** was prepared according to procedure A from 1-chloro-4-isothiocyanatobenzene to afford 4.87 g of yellow solid (96%). ¹H NMR (300 MHz, DMSO-*d*₆) δ 9.23 (s, 1H), 7.70 (d, *J* = 7.9 Hz, 2H), 7.34 (d, *J* = 8.8 Hz, 2H), 4.85 (bs, 2H), 3.34 (s, 1H).

N-(4-Methoxyphenyl)hydrazinecarbothioamide (**1c**). **1c** was prepared according to procedure A from 1-methoxy-4-isothiocyanatobenzene to afford 5.2 g of yellow solid (88%). ¹H NMR (300 MHz, DMSO-*d*₆) δ 9.23 (s, 1H), 7.32 (d, *J* = 9.0, 2H), 6.79 (d, *J* = 9.0, 2H), 4.85 (bs, 2H), 3.70 (s, 3H), 3.34 (s, 1H).

N-(4-(Trifluoromethoxy)phenyl)hydrazinecarbothioamide (**1d**). **1d** was prepared according to procedure A from 1-isothiocyanato-4-(trifluoromethoxy)benzene to afford 6.78 g of yellow solid (90%). ¹H NMR (300 MHz, DMSO-*d*₆) δ 9.25 (s, 1H), 7.72 (d, *J* = 7.9 Hz, 2H), 7.33 (d, *J* = 8.8 Hz, 2H), 4.89 (bs, 2H), 3.34 (s, 1H).

N-(3,5-Dimethoxyphenyl)hydrazinecarbothioamide (**1e**). **1e** was prepared according to procedure A from 1-isothiocyanato-3,5-dimethoxybenzene to afford 6.13 g of yellow solid (91%). δ 9.25 (s, 1H), 7.15 (d, *J* = 2.6 Hz, 1H), 6.88 (dd, *J* = 8.6, 2.6 Hz, 1H), 6.74 (d, *J* = 8.6 Hz, 1H), 4.89 (bs, 2H), 3.81 (s, 3H), 3.77 (s, 3H), 3.33 (s, 1H).

5-(3-(Dimethylamino)propyl)-*N*-phenyl-1,3,4-oxadiazol-2-amine (2a). Compound **2a** was prepared according to procedure B from *N*-phenylhydrazinecarbothioamide and 4-(dimethylamino)butanoic acid to afford 50 mg of white powder (61%). ¹H NMR (CDCl₃, 300 MHz) δ 9.17 (bs, 1H, NH), 7.42 (dd, *J* = 8.7, 1.2 Hz, 2H, ph-2,6H), 7.26 (d, *J* = 8.7 Hz, 2H, ph-3,5H), 6.99 – 6.88 (m, 1H, ph-4H), 2.74 (t, *J* = 7.5 Hz, 2H, 1CH₂), 2.36 (t, *J* = 8.4 Hz, 2H, 3CH₂), 2.21 (s, 6H, 2 x CH₃), 1.88 (m, 2H, 2CH₂). ¹³C NMR (75 MHz, CDCl₃)

N-Phenyl-5-(3-(piperidin-1-yl)propyl)-1,3,4-oxadiazol-2-amine (2d). Compound **2d** was prepared according to procedure B from *N*-phenylhydrazinecarbothioamide and 4-(piperidin-1-yl)butanoic acid to afford 50 mg of white powder (53%). ¹H NMR (CDCl₃, 300 MHz) δ 9.28 (bs, 1H, NH), 7.39 (dd, *J* = 8.7, 1.2 Hz, 2H, ph-2,6H), 7.24 (dd, *J* = 8.7, 7.2 Hz, 2H, ph-3,5H), 6.94 (dd, *J* = 7.2, 1.2 Hz, 1H, ph-4H), 2.72 (t, *J* = 7.4 Hz, 2H, 1CH₂), 2.45 – 2.26 (m, 6H, 3CH₂, pip-2,6H₂), 1.99 – 1.82 (m, 2H, 2CH₂), 1.51 (dt, *J* = 11.0, 5.2 Hz, 4H, pip-3,5H₂), 1.40 – 1.28 (m, 2H, pip-4H₂). ¹³C NMR (75 MHz, CDCl₃) δ 23.14, 24.19, 44.69, 45.20, 58.34, 117.57, 122.58, 129.22, 138.33, 160.40, 160.53. HRMS *m/z* 287.1869 [M+H]⁺ (calcd 287.1872). Anal. Calcd for C₁₆H₂₀N₄O: C 67.11, H 7.74, N 19.56. Found: C 67.43, H 7.81, N 18.89.

N-(4-Chlorophenyl)-5-(3-(dimethylamino)propyl)-1,3,4-oxadiazol-2-amine (2e). Compound **2e** was prepared according to procedure B from *N*-(4-chlorophenyl)hydrazinecarbothioamide and 4-(dimethylamino)butanoic acid to afford 45 mg of white powder (49%). ¹H NMR (CDCl₃, 300 MHz) δ 7.38 (d, *J* = 9.0 Hz, 2H, ph-2,6H), 7.19 (d, *J* = 9.0 Hz, 2H, ph-3,5H), 2.74 (t, *J* = 7.5 Hz, 2H, 1CH₂), 2.39 – 2.33 (m, 2H, 3CH₂), 1.99 – 1.79 (m, 2H, 2CH₂), 2.20 (s, 6H, 2 x CH₃). ¹³C NMR (75 MHz, CDCl₃) δ 23.10, 44.75, 45.21, 58.30, 118.80, 127.47, 129.14, 136.95, 160.18, 160.57. ESI-MS *m/z* 281.1 [M+H]⁺ (calcd 281.1). Anal. Calcd for C₁₈H₂₂ClN₄O: C 55.62, H 6.10, N 12.63. Found: C 55.81, H 6.28, N 12.61.

N-(4-Chlorophenyl)-5-(1-methylpiperidin-4-yl)-1,3,4-oxadiazol-2-amine (2f). Compound **2f** was prepared according to procedure B from *N*-(4-chlorophenyl)hydrazinecarbothioamide and 1-methylpiperidine-4-carboxylic acid to

δ 23.14, 24.19, 45.20, 58.34, 117.57, 122.58, 129.22, 138.33, 160.40, 160.53. HRMS *m/z* 247.1556 [M+H]⁺ (calcd 247.1559). Anal. Calcd for C₁₄H₁₈N₄O: C 63.39, H 7.37, N 22.75. Found: C 63.77, H 7.54, N 23.04.

5-(1-Methylpiperidin-4-yl)-N-phenyl-1,3,4-oxadiazol-2-amine (2b). Compound **2b** was prepared according to procedure B from *N*-phenylhydrazinecarbothioamide and 1-methylpiperidine-4-carboxylic acid to afford 69 mg of white powder (81%). ¹H NMR (CDCl₃, 300 MHz) δ 8.46 (bs, 1H, NH), 7.38 (d, *J* = 7.8 Hz, 2H, ph-2,6H), 7.26 (dd, *J* = 7.8, 7.2 Hz, 2H, ph-3,5H), 6.97 (dd, *J* = 7.2, 1.2 Hz, 1H, ph-4H), 3.03 – 2.75 (m, 3H, pip-2,6H₂, pip-4H), 2.34 (s, 3H, CH₃), 2.26 – 1.82 (m, 6H, pip-2,6H₂, pip-3,5H₂). ¹³C NMR (75 MHz, CDCl₃) δ 14.26, 29.19, 32.67, 44.70, 46.28, 54.71, 117.50, 122.75, 129.29, 138.09, 160.27, 162.81. ESI-MS *m/z* 259.2 [M+H]⁺ (calcd 259.2). Anal. Calcd for C₁₄H₁₈N₄O: C 65.09, H 7.02, N 21.09. Found: C 64.49, H 7.17, N 21.01.

N-Phenyl-5-(2-(piperidin-1-yl)ethyl)-1,3,4-oxadiazol-2-amine (2c). Compound **2c** was prepared according to procedure B from *N*-phenylhydrazinecarbothioamide and 3-(piperidin-1-yl)propanoic acid to afford 55 mg of white powder (61%). ¹H NMR (CDCl₃, 300 MHz) δ 8.45 (bs, 1H, NH), 7.41 (d, *J* = 7.8 Hz, 2H, ph-2,6H), 7.26 (dd, *J* = 7.8, 7.2 Hz, 2H, ph-3,5H), 6.98 (dd, *J* = 7.2, 1.2 Hz, 1H, ph-4H), 3.00 (t, *J* = 6.8 Hz, 2H, 1CH₂), 2.94 – 2.74 (m, 2H, 2CH₂), 2.66 – 2.39 (m, 4H, pip-2,6H₂), 1.59 (dt, *J* = 10.0, 5.4 Hz, 4H, pip-3,5H₂), 1.41 (t, *J* = 5.8 Hz, 2H, pip-4H₂). ¹³C NMR (75 MHz, CDCl₃) δ 23.05, 23.82, 25.34, 54.14, 55.08, 117.55, 122.79, 129.30, 138.03, 159.14, 160.43. HRMS *m/z* 273.1719 [M+H]⁺ (calcd 273.1715). Anal. Calcd for C₁₅H₁₈N₄O: C 66.15, H 7.40, N 19.96. Found: C 65.69, H 7.37, N 19.96.

- afford 77 mg of white powder (80%). ¹H NMR (MeOD, 300 MHz) δ 7.35 (d, J = 9.0 Hz, 2H, ph-2,6/ f), 7.21 (d, J = 9.0 Hz, 2H, ph-3,5/ f), 3.03 – 2.75 (m, 3H, pip-2,6/ f), 2.34 (s, 3H, CH₃), 2.26 – 1.82 (m, 6H, pip-2,6/ f), 1.30 (s, 3H, CH₃). ¹³C NMR (75 MHz, MeOD) δ 28.01, 31.60, 44.00, 54.59, 120.13, 128.61, 130.12, 138.53, 161.73, 162.53. ESI-MS m/z 293.1 [M+H]⁺ (calcd for C₁₄H₁₈ClN₄O [M+H]⁺, 293.1).
- N-(4-Chlorophenyl)-5-(2-(piperidin-1-yl)ethyl)-1,3,4-oxadiazol-2-amine (2g).** Compound **2g** was prepared according to procedure B from *N*-(4-chlorophenyl)hydrazinecarbothioamide and 3-(piperidin-1-yl)propanoic acid to afford 85 mg of white powder (84%). ¹H NMR (CDCl₃, 300 MHz) δ 7.35 (d, J = 9.0 Hz, 2H, ph-2,6/ f), 7.21 (d, J = 9.0 Hz, 2H, ph-3,5/ f), 2.94 (t, J = 7.5 Hz, 2H, 1CH₂), 2.77 (t, J = 7.5 Hz, 2H, 2CH₂), 2.58 – 2.36 (m, 4H, pip-2,6/ f), 1.58 (dt, J = 10.8, 5.1 Hz, 4H, pip-3,5/ f), 1.42 (t, J = 5.8 Hz, 2H, pip-4/ f), 1.27 (s, 3H, CH₃). ¹³C NMR (75 MHz, CDCl₃) δ 22.63, 23.64, 25.12, 54.01, 54.90, 118.61, 127.29, 129.03, 136.88, 158.93, 160.23. ESI-MS m/z 307.1 [M+H]⁺ (calcd for C₁₄H₁₆ClN₄O [M+H]⁺, 307.1).
- 5-(Dimethylamino)methyl)-N-(4-methoxyphenyl)-1,3,4-oxadiazol-2-amine (2h).** Compound **2h** was prepared according to procedure B from *N*-(4-methoxyphenyl)hydrazinecarbothioamide and dimethylglycine to afford 49 mg of white powder (60%). ¹H NMR (CDCl₃, 300 MHz) δ 8.69 (bs, 1H, NH), 7.32 (d, J = 9.0 Hz, 2H, ph-2,6/ f), 6.79 (d, J = 9.0 Hz, 2H, ph-3,5/ f), 3.70 (s, 3H, OCH₃), 3.62 (s, 2H, CH₂), 2.30 (s, 6H, 2 x CH₃). ¹³C NMR (75 MHz, CDCl₃) δ 44.91, 52.82, 55.53, 114.52, 119.85, 131.15, 155.68, 157.03, 161.44. ESI-MS m/z 249.1 [M+H]⁺ (calcd 249.1). Anal. Calcd for C₁₂H₁₆N₄O₂: C 58.05, H 6.50, N 22.57. Found: C 58.41, H 6.84, N 22.77.
- N-(4-Methoxyphenyl)-5-(1-methylpiperidin-4-yl)-1,3,4-oxadiazol-2-amine (2i).** Compound **2i** was prepared according to procedure B from *N*-(4-methoxyphenyl)hydrazinecarbothioamide and 1-methylpiperidine-4-carboxylic acid to afford 52 mg of white powder (54%). ¹H NMR (CDCl₃, 300 MHz) δ 8.77 (bs, 1H, NH), 7.37 (d, J = 9.0 Hz, 2H, ph-2,6/ f), 6.87 (d, J = 9 Hz, 2H, ph-3,5/ f), 3.03 – 2.75 (m, 3H, pip-2,6/ f), 2.34 (s, 3H, CH₃), 2.26 – 1.82 (m, 6H, pip-2,6/ f), 1.30 (s, 3H, CH₃). ¹³C NMR (75 MHz, CDCl₃) δ 29.01, 32.51, 46.15, 54.59, 55.54, 114.53, 119.58, 131.45, 155.50, 160.87, 162.40. ESI-MS m/z 289.2 [M+H]⁺ (calcd 289.2). Anal. Calcd for C₁₄H₂₀N₄O₂: C 62.48, H 7.69, N 19.43. Found: C 62.48, H 7.68, N 18.81.
- N-(4-Methoxyphenyl)-5-(2-(piperidin-1-yl)ethyl)-1,3,4-oxadiazol-2-amine (2j).** Compound **2j** was prepared according to procedure B from *N*-(4-methoxyphenyl)hydrazinecarbothioamide and 3-(piperidin-1-yl)propanoic acid to afford 72 mg of white powder (72%). ¹H NMR (CDCl₃, 300 MHz) δ 8.45 (bs, 1H, NH), 7.32 (d, J = 9.0 Hz, 2H, ph-2,6/ f), 6.79 (d, J = 9.0 Hz, 2H, ph-3,5/ f), 3.72 (s, 3H, CH₃), 2.96–3.01 (m, 2H, 1CH₂), 2.80–2.85 (m, 2H, 2CH₂), 2.50–2.54 (m, 4H, pip-2,6/ f), 1.55–1.63 (m, 4H, pip-3,5/ f), 1.36–1.44 (m, 2H, pip-4/ f). ¹³C NMR (75 MHz, CDCl₃) δ 22.91, 23.72, 25.19, 54.09, 54.58, 55.55, 114.49, 119.68, 131.34, 155.55, 158.72, 160.92. HRMS m/z 303.1827 [M+H]⁺ (calcd 303.1816). Anal. Calcd for C₁₄H₂₀N₄O₂: C 63.55, H 7.33, N 18.53. Found: C 63.49, H 7.17, N 18.60.
- 5-(2-(Piperidin-1-yl)ethyl)-N-(4-(trifluoromethoxy)phenyl)-1,3,4-oxadiazol-2-amine (2k).** Compound **2k** was prepared according to procedure B from *N*-(4-(trifluoromethoxy)phenyl)hydrazinecarbothioamide and 3-(piperidin-1-yl)propanoic acid to

6

5

afford 75 mg of white powder (64%). ¹H NMR (CDCl₃, 300 MHz) δ 7.43 (d, *J* = 8.25, 2H, ph-2,6*H*), 7.10 (d, *J* = 8.25, 2H, ph-3,5*H*), 2.91 (t, *J* = 8.6 Hz, 2H, 1*C*/i2), 2.73 (t, *J* = 8.6 Hz, 2H, 2*C*/i2), 2.42 (t, *J* = 5.4 Hz, 4H, pip-2,6*H*), 1.51 (m, 4H, pip-3,5*H*), 1.37 (m, 2H, 2H, 2*C*/i2), 2.42 (t, *J* = 5.4 Hz, 4H, pip-2,6*H*), 1.51 (m, 4H, pip-3,5*H*), 1.37 (m, 2H, 2H, 2*C*/i2). ¹³C NMR (75 MHz, CDCl₃) δ 22.70, 23.64, 25.10, 48.47, 49.04, 49.33, 49.61, 49.90, 50.18, 54.06, 54.90, 118.37, 122.02, 137.01, 143.98, 158.97, 160.25. ESI-MS *m/z* 357.2 [M+H]⁺ (calcd 357.2). Anal. Calcd for C₁₈H₁₉F₃N₅O₂: C 53.93, H 5.57, N 15.72. Found: C 53.72, H 5.31, N 15.57.

***N*-(3,5-Dimethoxyphenyl)-5-((dimethylamino)methyl)-1,3,4-oxadiazol-2-amine (2l).** Compound **2l** was prepared according to procedure B from *N*-(3,5-dimethoxyphenyl)hydrazinecarbothioamide and dimethylglycine to afford 51 mg of white powder (55%). ¹H NMR (CDCl₃, 300 MHz) δ 7.15 (d, *J* = 2.6 Hz, 1H, ph-4*H*), 6.88 (dd, *J* = 8.6, 2.6 Hz, 1H, ph-2*H*), 6.74 (d, *J* = 8.6 Hz, 1H, ph-6*H*), 3.81 (s, 3H, CH₃), 3.77 (s, 3H, CH₃), 3.63 (s, 2H, C/i2), 2.31 (s, 6H, 2 x C/i3). ¹³C NMR (75 MHz, CDCl₃) δ 44.87, 52.78, 56.20, 103.29, 109.87, 111.83, 131.57, 145.06, 149.44, 157.01, 161.18. ESI-MS *m/z* 279.1 [M+H]⁺ (calcd 279.1). Anal. Calcd for C₁₃H₁₈N₄O₂: C 56.10, H 6.52, N 20.13. Found: C 56.28, H 6.55, N 20.49.

***N*-(3,5-Dimethoxyphenyl)-5-(2-(piperidin-1-yl)ethyl)-1,3,4-oxadiazol-2-amine (2m).** Compound **2m** was prepared according to procedure B from *N*-(3,5-dimethoxyphenyl)hydrazinecarbothioamide and 3-(piperidin-1-yl)propanoic to afford 57 mg of white powder (52%). ¹H NMR (CDCl₃, 300 MHz) δ 8.74 (s, 1H, NH), 7.10 (d, *J* = 2.5 Hz, 1H, ph-4*H*), 6.86 (d, *J* = 2.5 Hz, 1H, ph-2*H*), 6.72 (d, *J* = 2.5 Hz, 1H, ph-6*H*), 3.80 (s, 3H, CH₃), 3.77 (s, 3H, CH₃), 2.91 (t, *J* = 8.6 Hz, 2H, 1*C*/i2), 2.73 (t, *J* = 8.6 Hz, 2H, 2*C*/i2).

2*CH*₃), 2.42 (t, *J* = 5.4 Hz, 4H, pip-2,6*H*), 1.51 (m, 4H, pip-3,5*H*), 1.37 (m, 2H, pip-4*H*), ¹³C NMR (75 MHz, CDCl₃) δ 25.24, 24.02, 25.60, 54.18, 55.32, 55.92, 56.20, 103.26, 109.71, 111.83, 131.88, 144.87, 149.41, 159.08, 160.79. HRMS *m/z* 333.1918 [M+H]⁺ (calcd 333.1927). Anal. Calcd for C₁₇H₂₁N₅O₂: C 61.43, H 7.28, N 16.86. Found: C 61.80, H 7.37, N 16.17.

(*E*)-*N*-Hydroxybenzimidamide (3a). **3a** was prepared according to procedure C from benzonitrile to afford 7.93 g of white solid (77%). ¹H NMR (300 MHz, DMSO-*d*₆) δ 9.66 (s, 1H), 7.77 – 7.62 (m, 2H), 7.46 – 7.30 (m, 3H), 5.81 (s, 2H).

(*E*)-*N*'-Hydroxy-4-methoxybenzimidamide (3b). **3b** was prepared according to procedure C from 4-methoxybenzonitrile to afford 8.91 g of white solid (67%). ¹H NMR (300 MHz, DMSO-*d*₆) δ 9.46 (s, 1H), 7.61 (d, *J* = 8.9 Hz, 2H), 6.92 (d, *J* = 8.9 Hz, 2H), 5.72 (s, 2H), 3.77 (s, 3H).

Ethyl 3-phenyl-1,2,4-oxadiazole-5-carboxylate (4a). **4a** was prepared according to procedure D from MAK-A to afford 1.07 g of white solid (79%). ¹H NMR (300 MHz, Chloroform-*d*) δ 8.08 (dd, *J* = 8.0, 1.7 Hz, 2H), 7.54 – 7.36 (m, 3H), 4.50 (q, *J* = 7.1 Hz, 2H), 1.41 (t, *J* = 7.1 Hz, 3H).

Ethyl 3-(4-methoxyphenyl)-1,2,4-oxadiazole-5-carboxylate (4b). **4b** was prepared according to procedure D from MAK-C to afford 1.36 g of white solid (82%). ¹H NMR (300 MHz, Chloroform-*d*) δ 8.01 (d, *J* = 9.0 Hz, 2H), 6.92 (d, *J* = 9.0 Hz, 2H), 4.49 (q, *J* = 7.1 Hz, 2H), 3.79 (s, 3H), 1.41 (t, *J* = 7.1 Hz, 3H).

***N*-(3-(Diethylamino)propyl)-3-phenyl-1,2,4-oxadiazole-5-carboxamide (5a).** Compound **5a** was prepared according to procedure E from ethyl 3-phenyl-1,2,4-

oxadiazole-5-carboxylate and *N,N'*-diethylpropane-1,3-diamine to afford 124 mg of yellow oil (82%). ¹H NMR (CDCl₃, 300 MHz) δ 10.08 (s, 1H, NH), 8.49–7.64 (m, 3H, ph-2,4,6/H), 7.52–6.89 (m, 2H, ph-3,5/H), 3.90–3.06 (m, 2H, CONHCH₂/I₂), 2.69–2.27 (m, 6H, CONHCH₂CH₂/I₂, N(CH₂CH₃)₂), 1.67 (m, 2H, CONHCH₂CH₂/I₂), 1.01 (t, *J* = 7.1 Hz, 6H, N(CH₂CH₃)₂). ¹³C NMR (75 MHz, CDCl₃) δ 11.49, 24.11, 41.22, 46.73, 53.29, 126.04, 127.34, 128.88, 131.53, 152.80, 168.65, 169.29. ESI-MS *m/z* 303.2 [M+H]⁺ (calcd 303.2). Anal. Calcd for C₁₆H₂₂N₄O₂: C 63.55, H 7.33, N 18.53. Found: C 64.12, H 7.58, N 18.57.

3-Phenyl-N-(3-(piperidin-1-yl)propyl)-1,2,4-oxadiazole-5-carboxamide (5b). Compound **5b** was prepared according to procedure E from ethyl 3-phenyl-1,2,4-oxadiazole-5-carboxylate and 3-(piperidin-1-yl)propan-1-amine to afford 115 mg of yellow oil (73%). ¹H NMR (CDCl₃, 300 MHz) δ 9.99 (s, 1H, NH), 8.00–7.99 (m, 2H, ph-2,6/H), 7.64–7.28 (m, 3H, ph-3,4,5/H), 3.52 (t, *J* = 3.9 Hz, 2H, CONHCH₂/I₂), 2.47 (t, *J* = 2.7 Hz, 2H, CONHCH₂CH₂/I₂), 2.44–2.32 (m, 4H, pip-2,6/*I*₂aeq), 1.76–1.59 (m, 6H, pip-3,5/*I*₂aeq, pip-*I*₂aeq). 1.43 (m, 2H, CONHCH₂CH₂/I₂CH₂). ¹³C NMR (151 MHz, CDCl₃) δ 23.42, 24.40, 25.67, 41.45, 54.80, 59.22, 126.12, 127.41, 128.88, 131.56, 152.95, 168.73, 169.26. HRMS *m/z* 315.1833 [M+H]⁺ (calcd for C₁₇H₂₂N₄O₂, 315.1821).

***N*-(3-(Diethylamino)propyl)-3-(4-methoxyphenyl)-1,2,4-oxadiazole-5-carboxamide (5c).** Compound **5c** was prepared according to procedure E from ethyl 3-(4-methoxyphenyl)-1,2,4-oxadiazole-5-carboxylate and *N,N'*-diethylpropane-1,3-diamine to afford 145 mg of yellow oil (87%). ¹H NMR (CDCl₃, 300 MHz) δ 9.95 (s, 1H, NH), 7.91 (d, *J* = 8.8 Hz, 2H, ph-2,6/H), 6.88 (d, *J* = 8.8 Hz, 2H, ph-3,5/H), 3.75 (s, 3H, C/I₂), 3.63–

3.38 (m, 2H, CONHCH₂/I₂), 2.93–2.32 (m, 6H, CONHCH₂CH₂, N(CH₂CH₃)₂), 1.71 (m, 2H, CONHCH₂CH₂/I₂CH₂), 1.04 (t, *J* = 7.1 Hz, 6H, N(CH₂CH₃)₂). ¹³C NMR (75 MHz, CDCl₃) δ 11.29, 24.10, 40.92, 46.70, 53.03, 55.34, 114.28, 118.38, 129.00, 152.97, 162.16, 168.38, 168.94. ESI-MS *m/z* 333.2 [M+H]⁺ (calcd for C₁₇H₂₄N₄O₂, 333.2).

5-Methyl-2-phenylthiazol-4-ol (6a). **6a** was prepared according to procedure F to afford 1.55 g of yellow solid (75%). ¹H NMR (300 MHz, DMSO-*d*₆) δ 10.31 (s, 1H), 7.79 (dd, *J* = 8.1, 1.6 Hz, 2H), 7.50–7.39 (m, 3H), 2.22 (s, 3H).

2-(4-Chlorophenyl)-5-methylthiazol-4-ol (6b). **6b** was prepared according to procedure F to afford 2.27 g of yellow solid (83%). ¹H NMR (300 MHz, DMSO-*d*₆) δ 10.36 (s, 1H), 7.77 (d, *J* = 8.7 Hz, 2H), 7.48 (d, *J* = 8.8 Hz, 2H), 2.21 (s, 3H), ¹³C NMR (75 MHz, DMSO) δ 9.10, 103.27, 126.37, 129.10, 132.15, 133.83, 156.78, 158.91.

4-(4-Hydroxy-5-methylthiazol-2-yl)benzonitrile (6c). **6c** was prepared according to procedure F to afford 2.05 g of yellow solid (80%). ¹H NMR (300 MHz, DMSO-*d*₆) δ 10.55 (s, 1H), 7.97–7.87 (m, 4H), 2.25 (s, 3H).

2-(3-Chlorophenyl)-5-methylthiazol-4-ol (6d). **6d** was prepared according to procedure F to afford 1.89 g of yellow solid (69%). ¹H NMR (300 MHz, DMSO-*d*₆) δ 10.40 (s, 1H), 7.78 (dt, *J* = 2.5, 1.0 Hz, 1H), 7.74–7.68 (m, 1H), 7.50–7.45 (m, 2H), 2.23 (s, 3H).

5-Methyl-2-(pyridin-4-yl)thiazol-4-ol (6e). **6e** was prepared according to procedure F to afford 1.93 g of yellow solid (93%). ¹H NMR (300 MHz, DMSO-*d*₆) δ 10.61 (s, 1H), 8.81–8.50 (dd, *J* = 1.65, 4.47, 2H), 7.81–7.58 (dd, *J* = 1.65, 4.47, 2H), 2.25 (s, 3H), ¹³C NMR (75 MHz, DMSO) δ 9.23, 105.86, 118.62, 139.77, 150.49, 155.04, 159.63.

10

9

5-Methyl-2-phenyl-4-(3-(pyrrolidin-1-yl)propoxy)thiazole (10). Compound **10** was prepared according to procedure G from 5-methyl-2-phenylthiazol-4-ol and 1-(3-chloropropyl)pyrrolidine to afford 78 mg of yellow solid (85%). ¹H NMR (CDCl₃, 300 MHz) δ 7.74 (dd, *J* = 8.6, 1.6 Hz, 2H, ph-2,6*H*), 7.31 – 7.19 (m, 3H, ph-3,4,5*H*), 4.30 (t, *J* = 6.4 Hz, 2H, OCH₂), 2.61 – 2.53 (m, 2H, OCH₂CH₂CH₂), 2.50 – 2.41 (m, 4H, pyr-2,5*H*), 2.18 (s, 3H, CH₃), 2.01 – 1.83 (m, 2H, OCH₂CH₂), 1.78 – 1.64 (m, 4H, pyr-3,4*H*). ¹³C NMR (75 MHz, CDCl₃) δ 9.32, 23.46, 29.14, 53.20, 54.23, 68.96, 106.82, 125.30, 128.73, 129.21, 134.01, 159.37. ESI-MS *m/z* 303.1 [M+H]⁺ (calcd 303.1). Anal. Calcd for C₁₅H₂₀N₂O₃: C 67.51, H 7.33, N 9.26, S 10.60. Found: C 67.55, H 7.20, N 9.28, S 10.63.

5-Methyl-2-phenyl-4-(3-(piperidin-1-yl)propoxy)thiazole (11). Compound **11** was prepared according to procedure G from 5-methyl-2-phenylthiazol-4-ol and 1-(3-chloropropyl)piperidine to afford 64 mg of yellow solid (68%). ¹H NMR (CDCl₃, 300 MHz) δ 7.76 (dd, *J* = 8.1, 1.8 Hz, 2H, ph-2,6*H*), 7.34 – 7.24 (m, 3H, ph-3,4,5*H*), 4.30 (t, *J* = 6.4 Hz, 2H, OCH₂), 2.48 – 2.41 (m, 2H, OCH₂CH₂), 2.40 – 2.33 (m, 4H, pip-2,6*H*), 2.20 (s, 3H, CH₃), 1.99 – 1.83 (m, 2H, OCH₂CH₂CH₂), 1.61 – 1.46 (m, 4H, pip-3,5*H*), 1.43 – 1.29 (m, 2H, pip-4*H*). ¹³C NMR (75 MHz, CDCl₃) δ 9.34, 24.35, 25.81, 27.04, 54.57, 56.05, 69.14, 106.98, 125.33, 128.75, 129.23, 134.02, 159.43, 159.71. HRMS *m/z* 317.1672 [M+H]⁺ (calcd 317.1688). Anal. Calcd for C₁₆H₂₂N₂O₃: C 68.40, H 7.69, N 8.57, S 10.51. Found: C 68.40, H 7.69, N 8.57, S 10.51.

5-Methyl-4-((1-methylpiperidin-4-yl)methoxy)-2-phenylthiazole (12). Compound **12** was prepared according to procedure G from 5-methyl-2-phenylthiazol-4-ol and 4-(chloromethyl)-1-methylpiperidine to afford 67 mg of yellow solid (77%). ¹H NMR

5-Methyl-2-(pyrazin-2-yl)thiazol-4-ol (6f). **6f** was prepared according to procedure F to afford 2.02 g of yellow solid (96%). ¹H NMR (300 MHz, DMSO-*d*₆) δ 10.38 (s, 1H, 9.18 (d, *J* = 1.5 Hz, 1H), 8.40 (d, *J* = 2.6 Hz, 1H), 8.36 (dd, *J* = 2.6, 1.5 Hz, 1H), 2.23 (s, 3H), (d, *J* = 1.5 Hz, 1H).

N,N-Dimethyl-3-((5-methyl-2-phenylthiazol-4-yl)oxy)propan-1-amine (7). Compound **7** was prepared according to procedure G from 5-methyl-2-phenylthiazol-4-ol and 3-chloro-N,N-dimethylpropan-1-amine to afford 51 mg of yellow solid (73%). ¹H NMR (CDCl₃, 300 MHz) δ 7.76 (dd, *J* = 8.1, 1.8 Hz, 2H, ph-2,6*H*), 7.35 – 7.24 (m, 3H, ph-3,4,5*H*), 4.31 (t, *J* = 6.4 Hz, 2H, OCH₂CH₂CH₂), 2.22 (s, 3H, CH₃), 2.21 (s, 3H, CH₃), 1.90 (dt, *J* = 8.8, 7.4, 6.4 Hz, 2H, OCH₂CH₂CH₂). ¹³C NMR (75 MHz, CDCl₃) δ 9.33, 27.72, 45.32, 56.38, 68.81, 107.00, 125.34, 128.76, 129.26, 134.00, 159.47, 159.67. HRMS *m/z* 277.1389 [M+H]⁺ (calcd 277.1375). Anal. Calcd for C₁₅H₂₀N₂O₃: C 65.18, H 7.29, N 10.14, S 11.60. Found: C 65.22, H 7.57, N 10.27, S 12.07.

5-Methyl-2-phenyl-4-(2-(piperidin-1-yl)methoxy)thiazole (9). Compound **9** was prepared according to procedure G from 5-methyl-2-phenylthiazol-4-ol and 1-(3-chloromethyl)piperidine to afford 59 mg of yellow solid (61%). ¹H NMR (CDCl₃, 300 MHz) δ 7.75 (dd, *J* = 8.1, 1.8 Hz, 2H, ph-2,6*H*), 7.33 – 7.22 (m, 3H, ph-3,4,5*H*), 4.40 (t, *J* = 6.1 Hz, 2H, OCH₂), 2.69 (t, *J* = 6.1 Hz, 2H, OCH₂CH₂), 2.45 (t, *J* = 5.6 Hz, 4H, pip-2,6*H*), 2.19 (s, 3H, CH₃), 1.63 – 1.42 (m, 4H, pip-3,5*H*), 1.36 (dt, *J* = 6.3, 3.3 Hz, 2H, pip-4*H*). ¹³C NMR (126 MHz, CDCl₃) δ 9.73, 24.63, 26.34, 55.33, 58.66, 68.65, 107.48, 125.73, 129.14, 129.62, 134.45, 159.81, 160.06. HRMS *m/z* 303.1533 [M+H]⁺ (calcd 303.1531). Anal. Calcd for C₁₇H₂₂N₂O₃: C 67.51, H 7.33, N 9.26, S 10.60. Found: C 67.89, H 7.48, N 9.18, S 10.63.

12

11

(CDCl₃, 300 MHz) δ 7.76 (dd, J = 7.9, 1.7 Hz, 2H, ph-2,6H), 7.37 – 7.26 (m, 3H, ph-3,4,5/H), 4.18 (d, J = 5.6 Hz, 2H, OC/H₂), 3.39 – 3.14 (m, 2H, pip-2,6/H_{eq}), 2.53 (s, 3H, CH₃), 2.48 – 2.40 (m, 2H, pip-2,6/H_{ax}), 2.21 (s, 3H, CH₃), 2.03 – 1.66 (m, 5H, pip-3,5/H_{axeq}), 1.47 (t, 3H, CH₃). HRMS m/z 303.1530 [M+H]⁺ (calcd 303.1531). Anal. Calcd for C₁₇H₂₂N₂O₃: C 67.51, H 7.33, N 9.26, S 10.60. Found: C 67.59, H 7.23, N 9.37, S 10.77.

5-Methyl-2-phenylthiazol-4-yl 4-methylpiperazine-1-carboxylate (13). Compound 13 was prepared according to procedure G from 5-methyl-2-phenylthiazol-4-ol and 4-methylpiperazine-1-carboxyl chloride to afford 88 mg of yellow solid (95%). ¹H NMR (CDCl₃, 300 MHz) δ 7.80 – 7.70 (m, 2H, ph-2,6H), 7.35 – 7.24 (m, 3H, ph-3,4,5H), 3.64 (dd, J = 6.6, 3.9 Hz, 2H, piperazine-2,6/H_{eq}), 3.51 (dd, J = 6.6, 3.9 Hz, 2H, piperazine-2,6/H_{ax}), 2.44 – 2.32 (m, 4H, piperazine-3,5H_{axeq}), 2.24 (s, 3H, CH₃), 2.21 (s, 3H, CH₃). ¹³C NMR (75 MHz, CDCl₃) δ 9.99, 43.94, 44.48, 46.06, 54.43, 54.62, 117.94, 125.67, 128.76, 129.83, 133.29, 151.60, 152.35, 161.21. ESI-MS m/z 318.1 [M+H]⁺ (calcd for C₁₆H₁₈N₄O₃, 318.1).

3-(2-(4-Chlorophenyl)-5-methylthiazol-4-yloxy)-N,N-dimethylpropan-1-amine (15). Compound 15 was prepared according to procedure G from 2-(4-chlorophenyl)-5-methylthiazol-4-ol and 3-chloro-N,N-dimethylpropan-1-amine to afford 56 mg of yellow solid (79%). ¹H NMR (CDCl₃, 300 MHz) δ 7.68 (dd, J = 8.5, 1.5 Hz, 2H, ph-2,6H), 7.26 (dd, J = 8.5, 1.6 Hz, 2H, ph-3,5H), 4.29 (td, J = 6.4, 1.1 Hz, 2H, OC/H₂), 2.53 – 2.36 (m, 2H, OC/H₂CH₃), 2.23 (s, 6H, N(CH₃)₂), 2.20 (s, 3H, CH₃), 2.00 – 1.77 (m, 2H, OC/H₂CH₂CH₃). ¹³C NMR (75 MHz, CDCl₃) δ 9.31, 27.64, 45.27, 56.33, 68.77, 107.37, 126.48, 128.93, 132.48, 134.99, 158.01, 159.78. HRMS m/z 311.0990 [M+H]⁺ (calcd

2-(4-Chlorophenyl)-5-methyl-4-(3-(pyrrolidin-1-yl)propoxy)thiazole (18). Compound 18 was prepared according to procedure G from 2-(4-chlorophenyl)-5-methylthiazol-4-ol and 1-(3-chloropropyl)pyrrolidine to afford 59 mg of yellow solid (74%). ¹H NMR (CDCl₃, 300 MHz) δ 7.67 (d, J = 8.6 Hz, 2H, ph-2,6H), 7.25 (d, J = 8.6 Hz, 2H, ph-3,5/H), 4.30 (t, J = 6.3 Hz, 2H, OC/H₂), 2.69 – 2.62 (m, 2H, OC/H₂CH₂CH₂), 2.61 – 2.54 (m, 4H, pyr-2,5H), 2.19 (s, 3H, CH₃), 2.03 – 1.91 (m, 2H, OC/H₂CH₂), 1.84 – 1.71 (m, 4H, pyr-3,4H), ¹³C NMR (75 MHz, CDCl₃) δ 9.33, 23.44, 28.73, 53.13, 54.10, 68.82, 107.35, 126.48, 128.93, 132.48, 135.00, 159.75. HRMS m/z 337.1137 [M+H]⁺ (calcd 337.1141). Anal. Calcd for C₁₇H₂₂N₂O₃: C 60.61, H 6.28, N 8.32, S 9.52. Found: C 60.86, H 6.34, N 8.27, S 9.62.

2-(4-Chlorophenyl)-5-methyl-4-(3-(piperidin-1-yl)propoxy)thiazole (19). Compound 19 was prepared according to procedure G from 2-(4-chlorophenyl)-5-methylthiazol-4-ol and 1-(3-chloropropyl)piperidine to afford 72 mg of yellow solid (88%). ¹H NMR (CDCl₃, 300 MHz) δ 7.69 (d, J = 8.7 Hz, 2H, ph-2,6H), 7.27 (d, J = 8.7 Hz, 2H, ph-3,5/H), 4.30 (t, J = 6.3 Hz, 2H, OC/H₂), 2.53 – 2.47 (m, 2H, pip-2,6/H_{eq}), 2.43 (t, J = 5.7 Hz, 6H, OC/H₂CH₂CH₃), 2.20 (s, 3H, CH₃), 2.03 – 1.88 (m, 2H, pip-2,6/H_{ax}), 1.68 – 1.51 (m, 4H, pip-3,5/H_{axeq}), 1.48 – 1.31 (m, 2H, pip-4,7/H_{axeq}). ¹³C NMR (75 MHz, CDCl₃) δ 9.34, 24.16, 25.54, 26.79, 54.48, 55.95, 69.03, 107.45, 126.51, 128.96, 132.50, 135.04, 158.06, 159.78. ESI-MS m/z 351.1 [M+H]⁺ (calcd 351.1). Anal. Calcd for C₁₈H₂₂N₂O₃: C 61.61, H 6.61, N 7.98, S 9.14. Found: C 61.85, H 6.60, N 7.73, S 9.57.

14

13

and 1-(3-chloropropyl)piperidine to afford 70 mg of yellow solid (76%). ¹H NMR (CDCl₃, 300 MHz) δ 7.76 – 7.75 (m, 1H, ph-2*H*), 7.56 (ddd, *J* = 5.0, 3.6, 1.7 Hz, 1H, ph-6*H*), 7.21 – 7.16 (m, 2H, ph-4,5*H*), 4.28 (t, *J* = 6.4 Hz, 2H, OCH₂), 2.51 – 2.28 (m, 6H, OCH₂CH₂CH₂, pip-2,6*H*_{2acq}), 2.18 (s, 3H, CH₃), 1.99 – 1.77 (m, 2H, OCH₂CH₂), 1.64 – 1.43 (m, 4H, pip-3,5*H*_{2acq}), 1.41 – 1.25 (m, 2H, pip-4*H*_{2acq}). ¹³C NMR (75 MHz, CDCl₃) δ 9.31, 24.31, 25.78, 26.98, 54.54, 55.97, 69.07, 107.65, 123.34, 125.15, 128.99, 129.95, 134.80, 135.61, 157.45, 159.90. HRMS *m/z* 351.1288 [M+H]⁺ (calcd 351.1298). Anal. Calcd for C₁₈H₂₅ClN₃O₈: C 61.61, H 6.61, N 7.98, S 9.14. Found: C 61.73, H 6.81, N 8.11, S 9.26.

***N,N*-Dimethyl-3-((5-methyl-2-(pyridin-4-yl)thiazol-4-yl)oxy)propan-1-amine (28).** Compound **28** was prepared according to procedure G from 5-methyl-2-(pyridin-4-yl)thiazol-4-ol and 3-chloro-*N,N*-dimethylpropan-1-amine to afford 125 mg of yellow solid (79%). ¹H NMR (CDCl₃, 300 MHz) δ 8.6 (dd, *J* = 3.7, 1.7 Hz, 2H, pyr-3,5*H*), 7.6 (dd, *J* = 3.7, 1.7 Hz, 2H, pyr-2,6*H*), 4.34 (t, *J* = 6.4 Hz, 2H, OCH₂), 2.55 – 2.40 (m, 2H, OCH₂CH₂CH₂), 2.25 (s, 3H, CH₃), 2.24 (s, 6H, N(CH₃)₂), 1.93, 1.99 – 1.84 (m, 2H, OCH₂CH₂), ¹³C NMR (126 MHz, CDCl₃) δ 9.82, 28.01, 45.66, 56.72, 69.24, 109.96, 119.46, 141.00, 150.83, 156.33, 160.97. HRMS *m/z* 278.1326 [M+H]⁺ (calcd 278.1327). Anal. Calcd for C₁₄H₁₆N₃O₃S: C 60.62, H 6.90, N 15.15, S 11.56. Found: C 60.85, H 7.24, N 15.27, S 11.84.

5-Methyl-2-(pyridin-4-yl)-4-(2-(pyrrolidin-1-yl)ethoxy)thiazole (29). Compound **29** was prepared according to procedure G from 5-methyl-2-(pyridin-4-yl)thiazol-4-ol and 1-(2-chloroethyl)pyrrolidine to afford 103 mg of yellow solid (86%). ¹H NMR (CDCl₃, 300

16

2-(3-Chlorophenyl)-5-methyl-4-(2-(piperidin-1-yl)ethoxy)thiazole (24). Compound **24** was prepared according to procedure G from 2-(3-chlorophenyl)-5-methylthiazol-4-ol and 1-(2-chloroethyl)piperidine to afford 73 mg of yellow solid (87%). ¹H NMR (CDCl₃, 300 MHz) δ 7.74 (m, 1H, ph-2*H*), 7.55 (ddd, *J* = 4.9, 3.4, 1.7 Hz, 1H, ph-6*H*), 7.22 – 7.15 (m, 2H, ph-4,5*H*), 4.38 (t, *J* = 6.1 Hz, 2H, OCH₂), 2.67 (t, *J* = 6.1 Hz, 2H, OCH₂CH₂), 2.44 (m, 4H, pip-2,6*H*_{2acq}), 2.17 (s, 3H, CH₃), 1.60 – 1.45 (m, 4H, pip-3,5*H*_{2acq}), 1.42 – 1.28 (m, 2H, pip-4*H*_{2acq}). ¹³C NMR (75 MHz, CDCl₃) δ 9.36, 24.20, 25.92, 54.92, 58.20, 68.21, 107.81, 123.32, 125.17, 129.00, 129.95, 134.81, 135.59, 157.44, 159.81. ESI-MS *m/z* 337.1 [M+H]⁺ (calcd 337.1). Anal. Calcd for C₁₇H₂₁ClN₃O₃S: C 60.61, H 6.28, N 8.32, S 9.52. Found: C 60.82, H 6.38, N 8.43, S 9.61.

2-(3-Chlorophenyl)-5-methyl-4-(3-(pyrrolidin-1-yl)propoxy)thiazole (25). Compound **25** was prepared according to procedure G from 2-(3-chlorophenyl)-5-methylthiazol-4-ol and 1-(3-chloropropyl)pyrrolidine to afford 73 mg of yellow solid (87%). ¹H NMR (CDCl₃, 300 MHz) δ 7.78 – 7.71 (m, 1H, ph-2*H*), 7.55 (ddd, *J* = 5.0, 3.6, 1.7 Hz, 1H, ph-6*H*), 7.22 – 7.16 (m, 2H, ph-4,5*H*), 4.30 (t, *J* = 6.4 Hz, 2H, OCH₂), 2.65 – 2.40 (m, 6H, OCH₂CH₂CH₂, pyr-2,5*H*), 2.18 (s, 3H, CH₃), 2.01 – 1.84 (m, 2H, OCH₂CH₂), 1.77 – 1.64 (m, 4H, pyr-3,4*H*), ¹³C NMR (75 MHz, CDCl₃) δ 9.31, 23.44, 29.00, 53.13, 54.19, 68.91, 107.61, 123.33, 125.14, 128.98, 129.95, 134.79, 135.60, 157.43, 159.88. ESI-MS *m/z* 337.1 [M+H]⁺ (calcd 337.1). Anal. Calcd for C₁₇H₂₁ClN₃O₃S: C 60.61, H 6.28, N 8.32, S 9.52. Found: C 60.80, H 6.34, N 8.44, S 9.67.

2-(3-Chlorophenyl)-5-methyl-4-(3-(piperidin-1-yl)propoxy)thiazole (26). Compound **26** was prepared according to procedure G from 2-(3-chlorophenyl)-5-methylthiazol-4-ol

15

24.58, 26.02, 27.23, 54.85, 56.22, 69.42, 109.83, 119.35, 140.91, 150.73, 156.18, 160.93, HRMS m/z 318.1632 [M+H]⁺ (calcd for C₁₇H₂₅N₃O₃: C 64.32, H 7.50, N 13.24, S 10.10. Found: C 64.57, H 7.72, N 13.35, S 10.28.

N,N-Dimethyl-3-((5-methyl-2-(pyrazin-2-yl)thiazol-4-yl)oxy)propan-1-amine (33). Compound **33** was prepared according to procedure G from 5-methyl-2-(pyrazin-2-yl)thiazol-4-ol and 3-chloro-N,N-dimethylpropan-1-amine to afford 84 mg of yellow solid (94%). ¹H NMR (CDCl₃, 300 MHz) δ 9.19 (d, J = 1.5 Hz, 1H, pyra-6H), 8.42 (d, J = 2.6 Hz, 1H, pyra-4H), 8.38 (dd, J = 2.6, 1.5 Hz, 1H, pyra-3H), 4.33 (t, J = 6.5 Hz, 2H, OCH₂), 2.41 (t, J = 7.7 Hz, 2H, OCH₂CH₂CH₂N), 2.25 (s, 3H, CH₃), 2.20 (s, 6H, N(CH₃)₂), 2.03 – 1.79 (m, 2H, OCH₂CH₂), ¹³C NMR (75 MHz, CDCl₃) δ 9.56, 27.78, 45.46, 56.35, 68.84, 111.49, 140.75, 143.62, 144.09, 146.94, 156.50, 160.69. ESI-MS m/z 279.1 [M+H]⁺ (calcd 279.1). Anal. Calcd for C₁₃H₁₈N₄O₃: C 56.09, H 6.52, N 20.13, S 11.52. Found: C 56.20, H 6.49, N 19.99, S 10.92.

5-Methyl-2-(prazin-2-yl)-4-2-(pyrrolidin-1-yl)ethoxythiazole (34). Compound **34** was prepared according to procedure G from 5-methyl-2-(pyrazin-2-yl)thiazol-4-ol and 1-(2-chloroethyl)pyrrolidine to afford 92 mg of yellow solid (71%). ¹H NMR (CDCl₃, 300 MHz) δ 9.18 (d, J = 1.5 Hz, 1H, pyra-6H), 8.40 (d, J = 2.6 Hz, 1H, pyra-4H), 8.36 (dd, J = 2.6, 1.5 Hz, 1H, pyra-3H), 4.43 (t, J = 6.1 Hz, 2H, OCH₂), 2.82 (t, J = 6.1 Hz, 2H, OCH₂CH₂N), 2.64 – 2.50 (m, 4H, pyr-2,5H₂), 2.24 (s, 3H, CH₃), 1.79 – 1.60 (m, 4H, pyr-3,4H₂), ¹³C NMR (75 MHz, CDCl₃) δ 9.60, 23.49, 54.68, 55.26, 69.51, 111.55, 140.72, 143.58, 144.06, 146.87, 156.48, 160.57. ESI-MS m/z 291.1 [M+H]⁺ (calcd 291.1). Anal.

18

MHz) δ 8.55 (d, J = 6.3 Hz, 2H, pyr-3,5H), 7.60 (d, J = 6.3 Hz, 1H, pyr-2,6H), 4.49 (t, J = 5.9 Hz, 2H, OCH₂), 2.92 (t, J = 5.9 Hz, 2H, OCH₂CH₂N), 2.73 – 2.59 (m, 4H, pyr-2,5H₂), 2.25 (s, 3H, CH₃), 1.85 – 1.68 (m, 4H, pyr-3,4H₂), ¹³C NMR (75 MHz, CDCl₃) δ 9.52, 23.47, 54.65, 55.13, 69.01, 109.76, 119.02, 140.49, 150.41, 155.96, 160.24. HRMS m/z 290.1327 [M+H]⁺ (calcd 290.1327). Anal. Calcd for C₁₄H₁₈N₄O₃: C 62.26, H 6.62, N 14.52, S 11.08. Found: C 62.49, H 6.72, N 14.58, S 11.17.

5-Methyl-2-(pyridin-4-yl)-4-(3-(pyrrolidin-1-yl)propoxy)thiazole (31). Compound **31** was prepared according to procedure G from 5-methyl-2-(pyridin-4-yl)thiazol-4-ol and 1-(3-chloropropyl)pyrrolidine to afford 72 mg of yellow solid (85%). ¹H NMR (CDCl₃, 300 MHz) δ 8.55 (dd, J = 4.5, 1.7 Hz, 2H, pyr-3,5H), 7.60 (dd, J = 4.3, 1.7 Hz, 2H, pyr-2,6H), 4.34 (t, J = 6.3 Hz, 2H, OCH₂), 2.77 – 2.50 (m, 6H, OCH₂CH₂CH₂ pyr-2,5H₂), 2.23 (s, 3H, CH₃), 2.11 – 1.92 (m, 2H, OCH₂CH₂), 1.86 – 1.70 (m, 4H, pyr-3,4H₂), ¹³C NMR (75 MHz, CDCl₃) δ 9.45, 23.42, 28.68, 55.11, 54.15, 68.81, 109.53, 119.01, 140.52, 150.40, 155.86, 160.45. ESI-MS m/z 304.12 [M+H]⁺ (calcd 304.2). Anal. Calcd for C₁₆H₂₁N₅O₃: C 63.33, H 6.98, N 13.85, S 10.57. Found: C 63.41, H 7.08, N 13.89, S 10.59.

5-Methyl-4-(3-(piperidin-1-yl)propoxy)-2-(pyridin-4-yl)thiazole (32). Compound **32** was prepared according to procedure G from 5-methyl-2-(pyridin-4-yl)thiazol-4-ol and 1-(3-chloropropyl)piperidine to afford 68 mg of yellow solid (84%). ¹H NMR (CDCl₃, 300 MHz) δ 8.6 (dd, J = 3.9, 1.8 Hz, 2H, pyr-3,5H), 7.6 (dd, J = 3.9, 1.8 Hz, 2H, pyr-2,6H), 4.33 (t, J = 6.4 Hz, 2H, OCH₂), 2.53 – 2.45 (m, 2H, OCH₂CH₂CH₂N), 2.44 – 2.37 (m, 4H, pip-2,6H₂), 2.24 (s, 3H, CH₃), 2.02 – 1.90 (m, 2H, OCH₂CH₂), 1.57 (p, J = 5.6 Hz, 4H, pip-3,5H₂), 1.45 – 1.36 (m, 2H, pip-4H₂), ¹³C NMR (126 MHz, CDCl₃) δ 9.76,

17

Calcd for C₁₄H₁₈N₄O₃S: C 52.65, H 5.37, N 21.93, S 10.04. Found: C 52.62, H 5.48, N 22.51, S 10.16.

4-(4-(4-(Bromomethyl)benzyl)oxy)-5-methylthiazol-2-yl)benzonitrile (38a). 38a was prepared according to procedure I to afford 0.87 g of yellow solid (86%). ¹H NMR (300 MHz, Chloroform-*d*) δ 7.86 (d, *J* = 8.8 Hz, 2H), 7.60 (d, *J* = 8.7 Hz, 2H), 7.37–7.33 (m, 4H), 5.34 (s, 2H), 4.43 (s, 2H), 2.24 (s, 3H).

4-(4-(4-(Bromomethyl)benzyl)oxy)-5-methyl-2-(pyrazin-2-yl)thiazole (38b). 38b was prepared according to procedure I to afford 0.72 g of yellow solid (74%). ¹H NMR (600 MHz, Chloroform-*d*) δ 9.21 (d, *J* = 1.1 Hz, 1H), 8.54 – 8.36 (m, 2H), 7.38 (d, *J* = 8.1 Hz, 2H), 7.33 (d, *J* = 8.1 Hz, 2H), 5.35 (s, 2H), 4.43 (s, 2H), 2.26 (s, 3H).

4-(5-Methyl-4-(4-(piperidin-1-yl)methyl)benzyl)oxy)thiazol-2-yl)benzonitrile (39). Compound 39 was prepared according to procedure J from 4-(4-(4-(bromomethyl)benzyl)oxy)-5-methylthiazol-2-yl)benzonitrile and piperidine to afford 92 mg of yellow solid (90%). ¹H NMR (CDCl₃, 300 MHz) δ 7.85 (d, *J* = 8.7 Hz, 2H, ph¹-2,6/*t*), 7.58 (d, *J* = 8.7 Hz, 2H, ph¹-3,5/*t*), 7.32 (d, *J* = 8.2 Hz, 2H, ph²-2,6/*t*), 7.24 (d, *J* = 8.2 Hz, 2H, ph²-3,5/*t*), 5.31 (s, 2H, OCH₂), 3.39 (s, 2H, phCCH₂N), 2.33 – 2.26 (m, 4H, pip-2,6/*t*_{aseq}), 2.22 (s, 3H, CH₃), 1.58 – 1.44 (m, 4H, pip-3,5/*t*_{aseq}), 1.39 – 1.25 (m, 2H, pip-4/*t*_{aseq}). ¹³C NMR (75 MHz, CDCl₃) δ 9.49, 24.35, 25.94, 54.50, 63.56, 72.16, 109.95, 112.15, 118.69, 125.55, 127.86, 129.31, 132.63, 135.99, 137.72, 138.44, 156.47, 160.32. HRMS *m/z* 404.1790 [M+H]⁺ (calcd for C₂₄H₂₅N₅O₃S, 404.1797).

20

Calcd for C₁₄H₁₈N₄O₃S: C 57.91, H 6.25, N 19.29, S 11.04. Found: C 57.95, H 6.29, N 19.00, S 10.76.

5-Methyl-4-(3-(piperidin-1-yl)propoxy)-2-(pyrazin-2-yl)thiazole (35). Compound 35 was prepared according to procedure G from 5-methyl-2-(pyrazin-2-yl)thiazol-4-ol and 1-(3-chloropropyl)piperidine to afford 91 mg of yellow solid (75%). ¹H NMR (CDCl₃, 300 MHz) δ 9.18 (d, *J* = 1.5 Hz, 1H, pyra-6/*t*), 8.41 (d, *J* = 2.6 Hz, 1H, pyra-4/*t*), 8.38 (dd, *J* = 2.6, 1.5 Hz, 1H, pyra-3/*t*), 4.32 (t, *J* = 6.4 Hz, 2H, OCH₂), 2.51 – 2.45 (m, 4H, pip-2,6/*t*_{aseq}), 2.40 (t, *J* = 5.6 Hz, 2H, OCH₂CH₂CH₂Cl), 2.24 (s, 3H, CH₃), 2.03 – 1.87 (m, 2H, OCH₂CH₂), 1.62 – 1.50 (m, 4H, pip-3,5/*t*_{aseq}), 1.43 – 1.31 (m, 2H, pip-4/*t*_{aseq}). ¹³C NMR (75 MHz, CDCl₃) δ 9.55, 24.19, 25.63, 26.81, 54.48, 55.89, 68.98, 111.50, 140.71, 143.61, 144.08, 146.89, 156.50, 160.63. ESI-MS *m/z* 319.2 [M+H]⁺ (calcd 319.2). Anal. Calcd for C₁₆H₂₂N₄O₃S: C 60.35, H 6.96, N 17.59, S 10.07. Found: C 59.45, H 6.75, N 17.82, S 9.62.

5-Methyl-2-(pyrazin-2-yl)thiazol-4-yl 4-methylpiperazine-1-carboxylate (36). Compound 36 was prepared according to procedure G from 5-methyl-2-(pyrazin-2-yl)thiazol-4-ol and 4-methylpiperazine-1-carboxyl chloride to afford 66 mg of yellow solid (75%). ¹H NMR (CDCl₃, 300 MHz) δ 9.23 (d, *J* = 1.5 Hz, 1H, pyra-6/*t*), 8.47 (d, *J* = 2.6 Hz, 1H, pyra-4/*t*), 8.42 (dd, *J* = 2.6, 1.5 Hz, 1H, pyra-3/*t*), 3.69 (dd, *J* = 6.6, 3.9 Hz, 2H, piperazine-2,6/*t*_{eq}), 3.58 – 3.52 (t, dd, *J* = 6.6, 3.9 Hz, 2H, piperazine-2,6/*t*_{ax}), 2.49 – 2.35 (m, 4H, piperazine-3,5/*t*_{aseq}), 2.29 (s, 2H, CH₃), 2.28 (s, 3H, CH₃). ¹³C NMR (75 MHz, CDCl₃) δ 10.24, 43.99, 44.53, 46.06, 54.41, 54.62, 122.42, 140.93, 143.65, 144.84, 146.24, 152.19, 152.41, 158.69. ESI-MS *m/z* 320.1 [M+H]⁺ (calcd 320.1). Anal. Calcd for

19

ethyl-*CH*₂), 1.88 – 1.66 (m, 4H, pyr-3,4*H*), 1.17 (t, *J* = 7.5 Hz, 3H, ethyl-*CH*₃). ¹³C NMR (75 MHz, CDCl₃) δ 15.81, 18.01, 23.51, 54.65, 55.23, 69.20, 115.24, 126.48, 128.94, 132.58, 135.00, 157.98, 158.81. ESI-MS *m/z* 351.1 [M+H]⁺ (calcd 351.1). Anal. Calcd for C₁₈H₂₃ClN₂O₈: C 61.61, H 6.61, N 7.98, S 9.14. Found: C 61.70, H 6.57, N 8.04, S 9.20.

2-(4-Chlorophenyl)-5-ethyl-4-(3-(piperidin-1-yl)propoxy)thiazole (46). Compound 46 was prepared according to procedure G from 4-chloro-2-(4-chlorophenyl)-5-ethylthiazole and 1-(3-chloropropyl)piperidine to afford 142 mg of yellow solid (94%). ¹H NMR (CDCl₃, 300 MHz) δ ¹H NMR (300 MHz, Chloroform-*d*) δ 7.70 (d, *J* = 8.8 Hz, 2H, ph-2,6*H*), 7.27 (d, *J* = 8.8 Hz, 2H, ph-3,5*H*), 4.30 (t, *J* = 6.3 Hz, 2H, OCH₂), 2.64 (q, *J* = 7.5 Hz, 2H, ethyl-*CH*₂), 2.55 – 2.33 (m, 6H, pip-2,6*H*₂_{seq}, OCH₂CH₂), 1.47 – 1.33 (m, 2H, pip-4*H*₂_{seq}), 1.17 (t, *J* = 6.3 Hz, 3H, ethyl-*CH*₃). ¹³C NMR (75 MHz, CDCl₃) δ 15.79, 17.99, 24.16, 25.55, 26.79, 54.47, 55.97, 68.93, 115.13, 126.49, 128.94, 132.61, 134.98, 157.97, 158.99. HRMS *m/z* 365.1445 [M+H]⁺ (calcd 365.1454). Anal. Calcd for C₁₉H₂₅ClN₂O₈: C 62.53, H 7.69, N 7.68, S 8.79. Found: C 62.42, H 6.98, N 7.74, S 8.70.

Table S.2) Compliance of the most active ligands to Lipinski's and Veber's rules.

Compound	MolP ^a (≤5)	MW ^b (≤500)	No. HBA ^a (≤10)	No. HBD ^b (≤5)	No. rotatable bonds (≤10)	Molecular PSA ^c (≤140 Å ²)
8	1.92	289.4	3	1	5	54
16	2.58	323.9	3	1	5	55
17	3.04	337.9	3	1	5	55
22	2.32	342.5	4	1	6	79
30	1.22	304.4	4	1	5	68
37	2.05	373.5	5	1	6	81
42	1.56	367.5	5	1	6	81

5-Ethyl-2-phenylthiazol-4-ol (43a). 43a was prepared according to procedure H to afford 0.71 g of yellow solid (89%). ¹H NMR (300 MHz, DMSO-*d*₆) δ 10.39 (s, 1H), 7.76 (dd, *J* = 8.1, 1.6 Hz, 2H, 7,34 – 7.23 (m, 3H), 2.66 (q, *J* = 7.5 Hz, 2H), 1.18 (t, *J* = 7.5 Hz, 3H).

2-(4-Chlorophenyl)-5-ethylthiazol-4-ol (43b). 43b was prepared according to procedure H to afford 0.73 g of yellow solid (76%). ¹H NMR (300 MHz, DMSO-*d*₆) δ 10.38 (s, 1H), 7.80 (d, *J* = 8.8 Hz, 2H), 7.51 (d, *J* = 8.8 Hz, 2H), 2.66 (q, *J* = 7.5 Hz, 2H), 1.18 (t, *J* = 7.5 Hz, 3H).

5-Ethyl-2-phenyl-4-(3-(piperidin-1-yl)propoxy)thiazole (44). Compound 44 was prepared according to procedure G from 5-ethyl-2-phenylthiazol-4-ol and 1-(3-chloropropyl)piperidine to afford 66 mg of yellow solid (71%). ¹H NMR (CDCl₃, 300 MHz) δ 7.76 (dd, *J* = 8.1, 1.6 Hz, 2H, ph-2,6*H*), 7.34 – 7.23 (m, 3H, ph-3,4,5*H*), 4.30 (t, *J* = 6.4 Hz, 2H, OCH₂), 2.64 (q, *J* = 7.5 Hz, 2H, ethyl-*CH*₂), 2.49 – 2.29 (m, 6H, pip-2,6*H*₂_{seq}, OCH₂CH₂CH₂N), 2.00 – 1.79 (m, 2H, OCH₂CH₂), 1.59 – 1.47 (m, 4H, pip-3,5*H*₂_{seq}), 1.46 – 1.28 (m, 2H, pip-4*H*₂_{seq}), 1.16 (t, *J* = 7.5 Hz, 3H, ethyl-*CH*₃). ¹³C NMR (75 MHz, CDCl₃) δ 15.83, 18.00, 24.35, 25.82, 27.03, 54.56, 56.06, 69.03, 114.65, 125.32, 128.73, 129.18, 134.13, 158.93, 159.35. ESI-MS *m/z* 331.2 [M+H]⁺ (calcd for C₁₉H₂₈N₂O₈, 331.2).

2-(4-chlorophenyl)-5-ethyl-4-(2-(pyrrolidin-1-yl)ethoxy)thiazole (45). Compound 45 was prepared according to procedure G from 4-chloro-2-(4-chlorophenyl)-5-ethylthiazole and 1-(3-chloropropyl)piperidine to afford 49 mg of yellow solid (62%). ¹H NMR (CDCl₃, 300 MHz) δ 7.69 (d, *J* = 8.6 Hz, 2H, ph-2,6*H*), 7.27 (d, *J* = 8.6 Hz, 2H, ph-3,5*H*), 4.44 (t, *J* = 6.0 Hz, 2H, OCH₂), 2.86 (t, *J* = 6.0 Hz, 2H, OCH₂CH₂), 2.75 – 2.54 (m, 6H, pyr-2,5*H*₂).

^aNumber of Hydrogen-bond acceptors (HBA); ^bN₅Number of Hydrogen-bond donors (HBD); ^cPolar Surface Area (PSA).

Table S.3) Predicted ADME profiles of further active ligands.					
Compound	BBB ^a	Absorption ^b	Solubility ^c	Hepatotoxicity ^d	CYP2D6 ^e
8	1	0	3	nontoxic	inhibitor
16	1	0	3	nontoxic	inhibitor
17	1	0	2	nontoxic	inhibitor
22	2	0	3	nontoxic	inhibitor
30	2	0	3	nontoxic	non-inhibitor
37	2	0	3	nontoxic	inhibitor
42	2	0	3	nontoxic	non-inhibitor

^aPredicts ability of the compound to penetrate the blood brain barrier (BBB). Levels 0, 1, 2, 3, or 4 correspond to very high, high, medium, low, or undetermined penetration, respectively. ^bPredicts human intestinal absorption for very high, high, medium, low, or undetermined penetration, respectively. ^cPredicts human intestinal absorption for extremely low, low, medium, high, or very high solubility, respectively. ^dPredicts the solubility of each compound in water at 25°C. Levels 0, 1, 2, 3, 4, 5, or 6 correspond to extremely low, very low, low, good, optimal, too soluble, or unknown solubility, respectively. ^ePredicts the occurrence of dose-dependent human hepatotoxicity. Levels 0 or 1 correspond to nontoxic or toxic effect, respectively. ^fPredicts cytochrome P450, 2D6 inhibition. Levels 0 or 1 correspond to non-inhibitor or inhibitor, respectively. ^gPredicts the likelihood that a compound will be highly bound to carrier proteins on the blood (PPBs, plasma protein binding). Levels 0, 1, or 2 correspond to binding < 90%, binding > 90%, or binding > 95%, respectively.

Compound	Aerobic biodegradability ^a	AMES mutagenicity ^b	Ocular Irritation ^c	Skin Irritation ^d	Skin Sensitizer ^e	Carcinogenicity ^f (SDA) ^g	
						Male Mouse	Female Rat
8	-	-	+	-	++	+	++
16	-	-	+	-	++	-	+
17	-	-	+	-	++	-	+
22	-	-	+	-	++	+	++
30	-	-	++	-	++	-	+
37	-	-	+	-	++	+	+
42	-	-	+	-	++	+	+

respectively. ^aPredicted autotoxicity in Ames with/without test. Indicators -, or - correspond to non-mutagenic, or mutagenic, respectively. ^bPrediction of organic toxicity. Indicators -, or - correspond to none, mild, or severe / strong toxic properties, respectively. ^cPrediction of carcinogenic properties. Indicators -, or - correspond to classification as Non-Carcinogen, Single-Carcinogen, or Multi-Carcinogen, respectively.

4. Multitarget-directed histamine H₃ receptor ligands in neurogenetic disorders

4.1. Profiling of LINS01 compounds at human dopamine D₂ and D₃ receptors

Michelle F. Correa¹⁾, David Reiner²⁾, Gustavo A. B. Fernandes¹⁾, Marina T. Varela¹⁾, Cecilia M. S. Q. Aranha¹⁾, Holger Stark²⁾ and Joao P. dos Santos Fernandes¹⁾

1) Department of Pharmaceutical Sciences, Universidade Federal de São Paulo, Rua São Nicolau 210, Diadema, SP 09913-030, Brazil

2) Institute of Pharmaceutical and Medicinal Chemistry, Heinrich Heine University Düsseldorf, Universitätsstr. 1, 40225 Duesseldorf, Germany

Published in: *Journal of Chemical Sciences*, 2020, 132:5.

DOI: 10.1007/s12039-019-1694-6

Contribution to research: DR was involved in cell-culture, prepared and conducted radioligand displacement experiments at dopamine D₂ and D₃ receptors, evaluated inhibition and affinity data, wrote pharmacological parts of the manuscript draft and reviewed the manuscript.

Abstract:

Histamine and dopamine neuronal pathways display interesting overlapping in the CNS, especially in the limbic areas, making them very attractive to designing drugs with synergistic and/or additive effects. The roles of these systems to treat schizophrenia, drug addiction, Parkinson's and Alzheimer's diseases, among others are widely known. The LINS01 compounds were previously reported as histamine H₃ receptor (H₃R) antagonists and some of them are under evaluation in rodent memory models. Considering their pharmacological potential and similarities to literature dopamine D₂ receptor (D₂R) and dopamine D₃ receptor (D₃R) ligands, this work aimed to evaluate these compounds as ligands these receptors by using [³H]spiperone displacement assays. A set of 11 compounds containing the dihydrobenzofuranyl-piperazine core with substituents at 5-position of dihydrobenzofuran ring and at the piperazine nitrogen was examined. The compounds showed low to moderate affinities at both, D₂R and D₃R. N-Phenyl compounds LINS01005 (1d), LINS01011 (1h), LINS01012 (1i) and LINS01016 (1k) showed the highest affinities in the set to D₃R (K_i 0.3–1.5 μM), indicating that N-phenylpiperazine moiety increases the affinity to this receptor subtype with some selectivity, since they showed lower affinities to D₂R (K_i 1.3–5.5 μM). With the LINS01 compounds showing moderate binding affinity, new lead structures for optimisation with regards to combined H₃R and D₂R/D₃R-ligands are provided.

Reproduced from Correa MF, Reiner D, Fernandes GAB, Varela MT, Aranha CMSQ, Stark H and dos Santos Fernandes JP, Profiling of LINS01 compounds at human dopamine D₂ and D₃ receptors, *J. Chem. Sci.*, 2020, 132:5. Reprinted with written permission from Springer Nature (Licence number: 4810140827557).

Copyright 2019 Springer Nature.



Profiling of LINS01 compounds at human dopamine D₂ and D₃ receptors

MICHELLE F CORRÊA^a, DAVID REINER^b, GUSTAVO A B FERNANDES^a,
MARINA T VARELA^a, CECÍLIA M S Q ARANHA^a, HOLGER STARK^{b,*} and
JOÃO PAULO S FERNANDES^{a,*}

^aDepartment of Pharmaceutical Sciences, Universidade Federal de São Paulo, Rua São Nicolau 210, Diadema, SP 09913-030, Brazil

^bInstitute of Pharmaceutical and Medicinal Chemistry, Heinrich Heine University Düsseldorf, Universitätsstr. 1, 40225 Duesseldorf, Germany
E-mail: stark@hhu.de; joao.fernandes@unifesp.br

MS received 4 June 2019; accepted 9 August 2019

Abstract. Histamine and dopamine neuronal pathways display interesting overlapping in the CNS, especially in the limbic areas, making them very attractive to designing drugs with synergistic and/or additive effects. The roles of these systems to treat schizophrenia, drug addiction, Parkinson's and Alzheimer's diseases, among others are widely known. The LINS01 compounds were previously reported as histamine H₃ receptor (H₃R) antagonists and some of them are under evaluation in rodent memory models. Considering their pharmacological potential and similarities to literature dopamine D₂ receptor (D₂R) and dopamine D₃ receptor (D₃R) ligands, this work aimed to evaluate these compounds as ligands these receptors by using [³H]spiperone displacement assays. A set of 11 compounds containing the dihydrobenzofuranyl-piperazine core with substituents at 5-position of dihydrobenzofuran ring and at the piperazine nitrogen was examined. The compounds showed low to moderate affinities at both, D₂R and D₃R. *N*-Phenyl compounds LINS01005 (**1d**), LINS01011 (**1h**), LINS01012 (**1i**) and LINS01016 (**1k**) showed the highest affinities in the set to D₃R (*K*_i 0.3–1.5 μM), indicating that *N*-phenylpiperazine moiety increases the affinity to this receptor subtype with some selectivity, since they showed lower affinities to D₂R (*K*_i 1.3–5.5 μM). With the LINS01 compounds showing moderate binding affinity, new lead structures for optimization with regards to combined H₃R and D₂R/D₃R-ligands are provided.

Keywords. Antihistamine; dopamine receptor ligand; D₂ receptor; D₃ receptor.

1. Introduction

Classically, the drug discovery process focuses on the “one drug, one target” paradigm, which means that a drug must interact specifically with a defined biological target in the organism, to assure the maximum efficacy (potency) and fewer side effects (selectivity). However, this philosophy has changed in the last years to a more comprehensive view of the diseases, coining a “one drug, multiple targets” paradigm, also known as polypharmacology.^{1,2} Several diseases have been treated using a polypharmacological approach with multitarget drugs that were not designed by purpose.

For example, schizophrenia is an affective disorder that has been treated with typical and atypical antipsychotics, targeting the dopamine receptors but far from being defined as “selective drugs”. The efficacy of the classical antipsychotics such as haloperidol is attributed to the dopamine receptor antagonism, leading to the desired therapeutic outcome, but also causing extrapyramidal side effects (EPS) and worsening the cognitive and negative symptoms.³ On the other hand, atypical antipsychotics display a better therapeutic profile (especially against the negative and cognitive symptoms of schizophrenia) possibly due to their additional actions on

*For correspondence

Electronic supplementary material: The online version of this article (<https://doi.org/10.1007/s12039-019-1694-6>) contains supplementary material, which is available to authorized users.

Published online: 19 December 2019

serotonin and histamine systems in the brain.⁴ Considering that most of these effects are attributed to the GPCR targeting, and taking advantage of the anatomy and physiology of the neural network of the synapses, CNS diseases have been explored for designing multi target GPCR ligands.¹

The histamine receptors are class-A GPCRs that are divided into 4 subtypes, H₁R to H₄R.⁵ The H₁R and H₂R are widely expressed in the brain and are related to the control of sleep, food intake, body temperature and cognition. The H₄R is expressed in glial cells and may play a role in the inflammatory processes in the CNS.⁶ The H₃R is mainly distributed in the CNS as an auto and/or heteroreceptor that regulates the production and releasing of histamine and other neurotransmitters, such as dopamine, and so it is a potential target for several CNS disorders.^{7,8}

The dopamine receptors are also class-A GPCRs which are expressed in 5 subtypes, D₁R-D₅R. Considering their signalling profile, they are grouped into D₁-like (coupled to G_s) and D₂-like (coupled to G_{i/o}) families.³ Classically, D₂-like receptors (D₂R, D₃R and possibly D₄R) have been widely explored to the treatment of schizophrenia. However, the distribution profile of the subtypes in CNS may lead to different applications. For instance, the high density of D₂R in the movement-related and cortical areas and the high density of both D₂R and D₃R in brain areas such as the limbic system may explain why non-selective D₂R antagonists lead to the motor-related EPS and cognitive decline as caused by the classical antipsychotics, but also the efficacy in the psychotic effects.^{9,10} D₃R blockade also increases the acetylcholine release in the cortex, related to the improvement in the cognitive processes.¹¹ In spite of this, selective D₃R antagonists would be effective drugs against conditions such as schizophrenia, drug addiction, AD, PD and depression.⁹

The histamine and dopamine systems in the brain are noteworthy due to very interesting common characteristics. Both systems are originated in the tuberomammillary nucleus (TMN), with projections to the cortex, (hypo)thalamus, hippocampus, striatum and amygdala. In particular, H₃R and D₃R present a considerable density distribution overlapping in the limbic areas, such as hippocampus, striatum and amygdala.¹² It is interesting to note that 95% of the neurons expressing dopamine D₁-like receptors and 89% of those expressing D₂-like receptors in the striatum also express H₃R leading to complex interactions between both neurotransmitter systems.¹³ Several results from pharmacological studies suggest that antagonists of both H₃R and D₃R can present additive and/or

synergistic effects, making them attractive multi-targeting tools for the treatment of schizophrenia, drug addiction, PD, AD, dementias and certain types of epilepsy.^{8,14,15}

The LINS01 compounds (e.g., **1c** and **1g**, Figure 1) were previously described as selective H₃R antagonists.^{16,17} However, these compounds present some similarity to dopamine D₂R/D₃R ligands, since the overlap between the H₃R and D₂R/D₃R pharmacophores can be noted.^{8,18} The *N*-phenylpiperazine motif present in some LINS01 compounds is found in several D₂R/D₃R ligands such as compounds **2**, **3** and **4** in Figure 1.^{19,20} Moreover, the similarity of LINS01 compounds to compound **4** and its analogue **5** is clearly evident, which are potent ligands of D₂R and D₃R.¹¹ Considering the potential of these compounds and the similarities, the present report intended to assess the affinity of the LINS01 compounds to the D₂R/D₃R.

2. Experimental

2.1 Preparation of the compounds LINS01

All chemicals were purchased with adequate purity from Sigma-Aldrich Co. (Brazil) and LabSynth (Brazil) and used as supplied. The compounds were prepared and characterized as described in previous reports from our group (Figure 2).^{16,17,21,22} The analytical characterization of the newly synthesized compounds **1j** and **1k** is stated below. All

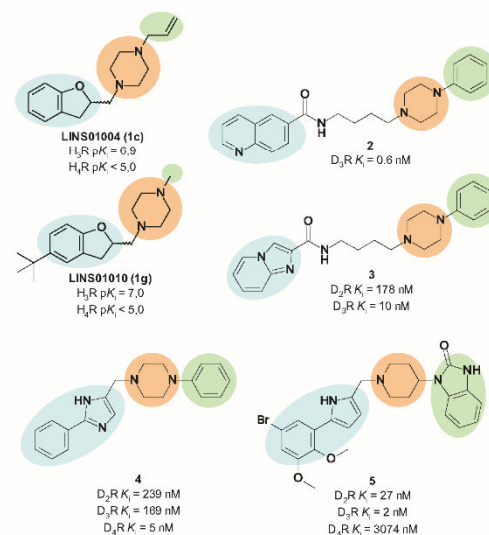


Figure 1. LINS01 compounds and literature ligands of D₂R/D₃R.

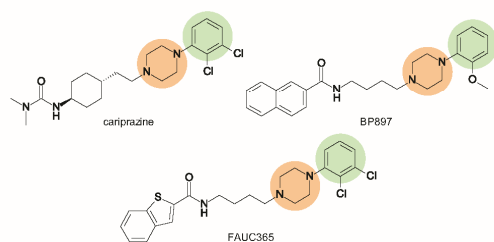


Figure 2. Ligands of D₂R and D₃R reported in the literature.

compounds were checked for purity through chromatography and considered adequate when purity was >95%.

1-Methyl-4-[(5-phenyl-2,3-dihydro-1-benzofuran-2-yl)methyl]piperazine (1j). The reaction between 1-methylpiperazine and prepared 2-(iodomethyl)-5-phenyl-2,3-dihydrobenzofuran yielded 45% of **1j**. ¹H NMR (300 MHz, CDCl₃): δ 2.31 (s, 3H), 2.41–2.74 (m, 9H), 2.82 (dd, 1H, *J* = 13.3, 7.7 Hz), 3.0 (dd, 1H, *J* = 15.7, 8.0 Hz), 3.32 (dd, 1H, *J* = 15.6, 9.1 Hz), 5.01 (dq, 1H, *J* = 8.2, 4.1 Hz), 6.85 (d, 1H, *J* = 8.3 Hz), 7.27–7.46 (m, 5H), 7.52 (d, 2H, *J* = 7.2 Hz). ¹³C NMR (75 MHz, CDCl₃): δ 34.2, 46.1, 53.8, 55.0, 63.2, 81.3, 109.8, 123.8, 126.5, 126.8, 127.1, 127.2, 128.9, 133.9, 141.3, 159.2.

1-Phenyl-4-[(5-phenyl-2,3-dihydro-1-benzofuran-2-yl)methyl]piperazine (1k). The reaction between 1-phenylpiperazine and prepared 2-(iodomethyl)-5-phenyl-2,3-dihydrobenzofuran yielded 78% of **1k**. ¹H NMR (300 MHz, CDCl₃): δ 2.67 (dd, 1H, *J* = 13.3, 4.1 Hz), 2.72–2.81 (m, 4H), 2.88 (dd, 1H, *J* = 13.4, 7.8 Hz), 2.98–3.10 (m, 2H), 3.26 (t, 4H, *J* = 4.9 Hz), 3.36 (dd, 1H, *J* = 15.8, 9.2 Hz), 5.00–5.13 (m, 1H), 6.83–6.91 (m, 2H), 6.95 (d, 2H, *J* = 8.2 Hz), 7.28–7.45 (m, 6H), 7.52 (d, 2H, *J* = 7.2 Hz). ¹³C NMR (75 MHz, CDCl₃): δ 34.2, 49.1, 53.9, 63.2, 77.3, 81.3, 109.8, 116.1, 119.7, 123.8, 126.5, 126.8, 127.2, 128.7, 129.1, 134.1, 141.3, 151.3, 159.2.

2.2 Binding assays on D₂R and D₃R

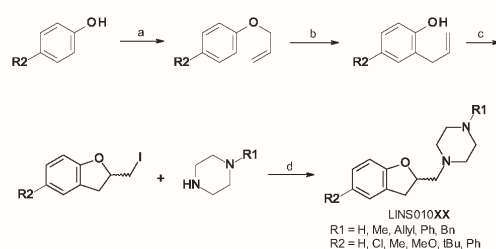
Membranes from CHO cells stably expressing either the short transcript of D₂ receptors or D₃ receptors were prepared as described previously.²³ For inhibition screening, freshly thawed membrane preparations (containing 25 and 20 µg/well of D₂R and D₃R, respectively) were incubated on microtiter plates with the indicated concentration of compounds and 0.2 nM [³H]spiperone in binding buffer [50 mM TRIS (pH = 7.4), 120 mM NaCl, 5 mM KCl, 1 mM CaCl₂ and 1 mM MgCl₂]. After an incubation period of 120 min, the mixture was harvested on glass-fiber mats, presoaked with 3% polyethylene-imine solution, followed by three wash-steps using cold demineralized water (approx. 1 mL/sample). The workup for scintillation-counting followed the standard procedure described before.²⁴ Non-specific binding was determined by an excess of unlabeled

haloperidol (10 µM). Inhibition was calculated as residual of specific binding of [³H]spiperone in presence of compound relative to specific binding in the absence of inhibitor. For affinity measurements, the same procedure as above was used but including a titration pattern of the investigated ligands (0.01–100,000 nM, final concentration). The finally determined specific binding was analyzed by non-linear least-square fitting to a four-parameter logistic equation. Conversion of the determined IC₅₀ to K_i values was performed as described elsewhere.²⁵

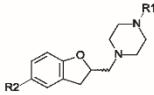
3. Results and Discussion

The LINS01 compounds (**1a–1k**, Scheme 1) were prepared as reported previously by our group.^{16,17} The derivatives **1a–1d** were prepared from 2-allylphenol through iodine-promoted cyclization, using water as a solvent.²¹ Finally, the iodinated heterocycle was used to alkylate the *N*-substituted piperazine in aprotic solvent (THF), with potassium carbonate as base, with moderate yield (~50%). The 5-phenyl derivatives **1j** and **1k** were prepared from the corresponding 4-phenyl-phenol following the same procedure, with moderate to good yields (45–78%). A novel microwave-assisted methodology¹⁷ was employed to avoid the considerable excess of 1-phenylpiperazine to obtain compounds **1h**, **1i** and **1k**, leading to good yields (>60%). Although this method gave comparable yields to the conventional methodology, it also saved reaction time and required less 1-phenylpiperazine (1.1 eq.) indeed, therefore comprising the green chemistry principles.²² The spectroscopic data for the final compounds and intermediates are in accordance with the literature reports.^{16,17,21, 26}

In an initial screening as shown in Table 1, the LINS01 compounds showed variable inhibition profiles at D₂R and D₃R, depending on the presence of certain groups. In general, a slight preference for



Scheme 1. Reagents and conditions. (a) Allyl bromide (2 eq.), K₂CO₃ (2 eq.), acetone, 60 °C, 2–4 h; (b) DMF, MW 200 °C (300 psi, 300 W), 1.5 h; (c) I₂ (1.1 eq.), water or EtOH/water, *r.t.*, 4–6 h; (d) K₂CO₃ (1.2 eq.), THF, reflux, 12–24 h or MW 120 °C (300 psi, 300 W), 1.5 h.

Table 1. Screening of the compounds LINS01 towards inhibition and affinity at the human dopamine D₂R and D₃R.

Compounds	R 1	R 2	% inhibition (10 μ M) \pm SD (n)		K_i (μ M) [95% CI]	
			D ₂ R	D ₃ R	D ₂ R	D ₃ R
1a (LINS01001)	H	H	0.0 \pm 0.0 (12)	9.0 \pm 6.4 (12)	n.d. (>10 μ M)	n.d. (>10 μ M)
1b (LINS01003)	Me	H	1.5 \pm 13.9 (15)	23.5 \pm 11.7 (15)	n.d. (>10 μ M)	n.d. (>10 μ M)
1c (LINS01004)	Allyl	H	33.6 \pm 9.7 (15)	62.3 \pm 14.4 (15)	5.5 [5.0–6.0]	1.5 [0.8–3.0]
1d (LINS01005)	Ph	H	34.1 \pm 10.5 (15)	55.1 \pm 10.3 (15)	2.4 [2.0–2.9]	0.89 [0.45–1.75]
1e (LINS01007)	Me	Cl	10.3 \pm 10.9 (15)	31.6 \pm 10.1 (15)	n.d. (>10 μ M)	n.d. (>10 μ M)
1f (LINS01008)	Me	Me	11.1 \pm 11.7 (15)	29.9 \pm 9.6 (15)	n.d. (>10 μ M)	n.d. (>10 μ M)
1g (LINS01010)	Me	<i>t</i> Bu	12.9 \pm 12.7 (15)	31.7 \pm 8.5 (15)	n.d. (>10 μ M)	n.d. (>10 μ M)
1h (LINS01011)	Ph	Cl	44.0 \pm 3.6 (6)	64.0 \pm 7.1 (6)	2.6 [1.2–6.1]	0.50 [0.10–2.66]
1i (LINS01012)	Ph	Me	45.1 \pm 4.2 (6)	60.9 \pm 10.7 (6)	2.4 [1.1–5.3]	1.5 [0.4–4.8]
1j (LINS01016)	Me	Ph	3.3 \pm 12.3 (15)	27.2 \pm 7.1 (15)	n.d. (>10 μ M)	n.d. (>10 μ M)
1k (LINS01017)	Ph	Ph	39.5 \pm 9.6 (6)	62.0 \pm 5.7 (6)	1.3 [0.6–3.0]	0.39 [0.04–3.40]
Haloperidol			100.0 \pm 2.5 (15)	99.3 \pm 2.6 (15)	n.d.	n.d.

inhibiting [³H]spiperone binding to D₃R was observed. Compounds **1a** to **1d** bear the 1-(2,3-dihydrobenzofuranyl)methylpiperazine core with different substituents attached to the nitrogen. Whereas **1a** did not show important inhibition at both D₂R and D₃R, compounds presenting bigger and/or aromatic substituents attached to the piperazine displayed increased inhibition at the dopamine receptors. The *N*-methylpiperazine analogues (**1e–1g**, **1j**) displayed inhibition below 50% at both receptors leading to affinities above the 10 μ M concentration range. There instead, substitution of *N*-allylpiperazine by *N*-phenylpiperazine (compounds **1c** and **1d**, respectively) showed comparable inhibition profiles at both receptors but a slight increase in affinity at D₂R. Furthermore, the results suggest that the presence of these groups drive the preference toward D₃R.

These results motivated us to further explore the affinities of the *N*-phenylpiperazine derivatives. The *N*-aryl piperazine group can be considered a privileged

group to design ligands of D₂-like receptors as embodied in the LINS01 series.^{10,11} The compounds **1d**, **1h**, **1i** and **1k** presented the highest inhibition at the investigated targets with affinities in the low micromolar concentration range at D₂R. Though only **1d** showing significant D₃R preference among them, even submicromolar K_i values were determined at the D₃R.

The influence of the groups attached in 5-position of dihydrobenzofuran (R2) on the affinity of the compounds seems minor. When comparing compounds with different substitution profiles in this part of the molecule, it can be noted that the inhibition did not significantly change among the *N*-methylpiperazine derivatives **1e**, **1f** and **1g**, as well as comparable affinities were observed among the *N*-phenylpiperazine compounds **1d**, **1h**, **1i** and **1k**.

The role of the 2,3-dihydrobenzofuran group in the affinity of the compounds remains unclear as this element originates from the initial H₃R design

strategy. A search in literature reveals that several compounds containing the aromatic benzofuran were already reported as dopamine receptor ligands, however, only few compounds containing the dihydro analogue were tested so far. The aromatic analogues of LINS01 compounds have been demonstrating activity as sigma- and serotonin receptor ligands,^{27,28} but usually with poor affinity to dopamine receptors,^{26,29} Despite a closely related aromatic *N*-benzylpiperazine analogue being reported in literature,²⁹ no compounds containing the unsubstituted *N*-allyl-, *N*-methyl- or *N*-phenylpiperazine moieties were found. On the other hand, homologues containing a longer linker between the benzofuran and the piperazine showed increased affinity to dopamine receptors,³⁰ suggesting that longer homologues of LINS01 compounds would shed light on the role of the dihydrobenzofuran in the D₂R and D₃R affinities, and should be considered in future evaluations. Secondly, derivatization of *N*-phenylpiperazine may be used for enhancing affinity at D₂R and D₃R. For instance, the substitution with a 2-methoxy or 2,3-dichloro groups in the phenyl ring usually leads to increased D₃R selectivity, as can be seen in cariprazine (a subnanomolar affinity D₃R ligand and nanomolar affinity at D₂R) and other compounds such as BP897 (bearing a 2-methoxyphenyl piperazine) and FAUC365 (bearing a 2,3-dichlorophenyl piperazine), indicating potential substitutions in this direction for designing improved ligands¹⁰ (Figure 2).

4. Conclusions

This is the first report exploring the histamine H₃R-targeting LINS01 compounds being ligands at dopamine receptors as well. Although these molecules showed low affinity to D₂R and D₃R, some of them show slight D₃R preference. The *N*-phenylpiperazine and *N*-benzylpiperazine fragments increased the binding of these compounds to D₂R and D₃R, although the latter reduces the selectivity. Additionally, the substitution in the dihydrobenzofuran seems not to influence the affinity of these compounds to D₂R or D₃R. The presented characterization of the LINS01 series lays the foundation for further profiling of the detected hits, profiling them towards attractive lead-compounds with combined dopaminergic and histaminergic activity.

Supplementary Information (SI)

Supplementary information is available at www.ias.ac.in/chemsci.

Acknowledgements

The authors would like to thank São Paulo Research Foundation - FAPESP (2016/25028-3) for providing financial support and to the scholarships to M.F.C. (2016/23139-2), G.A.B.F. (2017/05441-6), M.T.V. (2018/03918-2) and to C.M.S.Q.A. (2018/04488-1). J.P.S.F. is also thankful to the National Council for Scientific and Technological Development - CNPq (grant no. 306355/2018-3) for the scientific award. D.R. and H.S. acknowledge the financial support by the German Research Society (DFG INST 208/664-1 FUGG and GRK2158) and the EU COST Actions CA18133 and CA15135.

References

1. Anighoro A, Bajorath J and Rastelli G 2014 Polypharmacology: Challenges and Opportunities in Drug Discovery *J. Med. Chem.* **57** 7874
2. Reddy A S and Zhang S 2013 Polypharmacology: drug discovery for the future *Expert Rev. Clin. Pharmacol.* **6** 41
3. Rampino A, Marakhovskaia A, Soares-Silva T, Torretta S, Veneziani F and Beaulieu J M 2019 Antipsychotic Drug Responsiveness and Dopamine Receptor Signaling: Old Players and New Prospects *Front. Psychiatry* **9** 702
4. MacKenzie N E, Kowalchuk C, Agarwal S M, Costa-Dookhan K A, Caravaggio F, Gerretsen P, Chintoh A, Remington G J, Taylor V H, Müller D J, Graff-Guerrero A 2018 Antipsychotics, Metabolic Adverse Effects, and Cognitive Function in Schizophrenia *Front. Psychiatry* **9** 622
5. Tiligada E and Ennis M 2018 Histamine pharmacology: from Sir Henry Dale to the 21st century *Br. J. Pharmacol.* <https://doi.org/10.1111/bph.14524>
6. Corrêa M F and Fernandes J P S 2015 Histamine H₄ receptor ligands: Future applications and state of art *Chem. Biol. Drug Des.* **85** 461
7. Sadek B, Saad A, Sadeq A, Jalal F and Stark H 2016 Histamine H₃ receptor as a potential target for cognitive symptoms in neuropsychiatric diseases *Behav. Brain Res.* **312** 415
8. Khanfar M A, Affini A, Lutsenko K, Nikolic K, Butini S and Stark H 2016 Multiple Targeting Approaches on Histamine H₃ Receptor Antagonists *Front. Neurosci.* **10** 201
9. Moritz A E, Free R B and Sibley D R 2018 Advances and challenges in the search for D₂ and D₃ dopamine receptor-selective compounds *Cell. Signal.* **41** 75
10. Maramai S, Gemma S, Brogi S, Campiani G, Butini S, Stark H and Brindisi M 2016 Dopamine D₃ Receptor Antagonists as Potential Therapeutics for the Treatment of Neurological Diseases *Front. Neurosci.* **10** 451
11. Micheli F and Heidbreder C 2006 Selective Dopamine D₃ Receptor Antagonists: A Review 2001-2005 *Recent Pat. CNS Drug Discov.* **1** 271
12. Ellenbroek B A 2013 Histamine H₃ receptors, the complex interaction with dopamine and its implications for addiction *Br. J. Pharmacol.* **170** 46

13. Moreno E, Hoffmann H, Gonzalez-Sepúlveda M, Navarro G, Casadó V, Cortés A, Mallol J, Vignes M, McCormick P J, Canela E I, Lluís C, Moratalla R, Ferré S, Oritz J and Franco R 2011 Dopamine D1-histamine H₃ Receptor Heteromers Provide a Selective Link to MAPK Signaling in GABAergic Neurons of the Direct Striatal Pathway *J. Biol. Chem.* **286** 5846
14. Kononoff Vanhanen J, Nuutinen S, Tuominen M and Panula P 2016 Histamine H₃ Receptor Regulates Sensorimotor Gating and Dopaminergic Signaling in the Striatum *J. Pharmacol. Exp. Ther.* **357** 264
15. Ferrada C, Ferré S, Casadó V, Cortés A, Justinova Z, Barnes C, Canela E I, Goldberg S R, Leurs R, Lluís C and Franco R 2008 Interactions between histamine H₃ and dopamine D₂ receptors and the implications for striatal function *Neuropharmacology* **55** 190
16. Corrêa M F, Barbosa A J R, Teixeira L B, Duarte D A, Simões S C, Parreiras-e-Silva L T, Balbino A M, Landgraf R G, Costa-Neto C, Fernandes J P S 2017 Pharmacological Characterization of 5-Substituted 1-[(2,3-dihydro-1-benzofuran-2-yl)methyl]piperazines: Novel Antagonists for the Histamine H₃ and H₄ Receptors with Anti-inflammatory Potential *Front. Pharmacol.* **8** 825
17. Corrêa M F, Barbosa Á J R, Fernandes G A B, Baker J G and Fernandes J P S 2019 Pharmacological and SAR analysis of the LINS01 compounds at the human histamine H₁, H₂, and H₃ receptors *Chem. Biol. Drug Des.* **93** 89
18. von Coburg Y, Kottke T, Weizel L, Ligneau X and Stark H 2009 Potential utility of histamine H₃ receptor antagonist pharmacophore in antipsychotics *Bioorg. Med. Chem. Lett.* **19** 538
19. Brindisi M, Butini S, Franceschini S, Brogi S, Trotta F, Ros S, Cagnotto A, Salmona M, Casagni A, Andreassi M, Saponara S, Gorelli B, Weikop P, Mikkelsen J D, Scheel-Kruger J, Sandager-Nielsen K, Novellino E, Campiani G and Gemma S 2014 Targeting Dopamine D₃ and Serotonin 5-HT_{1A} and 5-HT_{2A} Receptors for Developing Effective Antipsychotics: Synthesis, Biological Characterization, and Behavioral Studies *J. Med. Chem.* **57** 9578
20. Ananthan S, Saini S K, Zhou G, Hobrath J V, Padmalayam I, Zhai L, Bostwick J R, Antonio T, Reith M E A, McDowell S, Cho E, McAleer L, Taylor M and Luedtke R R 2014 Design, Synthesis, and Structure-Activity Relationship Studies of a Series of [4-(4-Carboxamidobutyl)]-1-arylpiperazines: Insights into Structural Features Contributing to Dopamine D₃ versus D₂ Receptor Subtype Selectivity *J. Med. Chem.* **57** 7042
21. Corrêa M F, Varela M T, Balbino A M, Torrecilhas A C, Landgraf R G, Troncone L R P and Fernandes J P S 2017 1-[(2,3-Dihydro-1-benzofuran-2-yl) methyl]-piperazines as novel anti-inflammatory compounds: Synthesis and evaluation on H_{3R}/H_{4R} *Chem. Biol. Drug Des.* **90** 317
22. Corrêa M F, Barbosa Á J R, Sato R, Junqueira L O, Politi M J, Rando D G and Fernandes J P S 2016 Factorial design study to access the “green” iodocyclization reaction of 2-allylphenols *Green Process. Synth.* **5** 145
23. Frank A, Kiss D J, Keserü G M and Stark H 2018 Binding kinetics of cariprazine and aripiprazole at the dopamine D₃ receptor *Sci. Rep.* **8** 12509
24. Khanfar M A, Reiner D, Hagenow S and Stark H 2018 Design, synthesis, and biological evaluation of novel oxadiazole- and thiazole-based histamine H_{3R} ligands *Bioorg. Med. Chem.* **26** 4034
25. Cheng Y and Prusoff W H 1973 Relationship between the inhibition constant (K_i) and the concentration of inhibitor which causes 50 per cent inhibition (I₅₀) of an enzymatic reaction *Biochem. Pharmacol.* **22** 3099
26. Younes S, Labssita Y, Baziard-Mouysset G, Payard M, Rettori M C, Renard P, Pfeiffer B and Caignard D H 2000 Synthesis and structure-activity relationships of novel arylalkyl 4-benzyl piperazine derivatives as σ site selective ligands *Eur. J. Med. Chem.* **35** 107
27. Conroy T, Manohar M, Gong Y, Wilkinson S M, Webster M, Lieberman B P, Banister S D, Reekie T A, Mach R H, Rendina L M and Kassiou M 2016 A systematic exploration of the effects of flexibility and basicity on sigma (σ) receptor binding in a series of substituted diamines *Org. Biomol. Chem.* **14** 9388
28. Gu Z-S, Zhou A, Xiao Y, Zhang Q-W and Li J-Q 2018 Synthesis and antidepressant-like activity of novel aralkyl piperazine derivatives targeting SSR1/5-HT_{1A}/5-HT₇ *Eur. J. Med. Chem.* **144** 701
29. Moussa I A, Banister S D, Beinart C, Giboureau N, Reynolds A J and Kassiou M 2010 Design, Synthesis, and Structure—Affinity Relationships of Regioisomeric N -Benzyl Alkyl Ether Piperazine Derivatives as σ -1 Receptor Ligands *J. Med. Chem.* **53** 6228
30. Sampson D, Zhu X Y, Eyunni S V K, Etukala J R, Ofori E, Bricker B, Lamango N S, Setola V, Roth B L and Ablordepey S Y 2014 Identification of a new selective dopamine D₄ receptor ligand *Bioorg. Med. Chem.* **22** 3105

SUPPLEMENTARY INFORMATION

Profiling of LINS01 compounds at human dopamine D₂ and D₃ receptors

MICHELLE F CORRÊA,^a DAVID REINER,^b GUSTAVO A B FERNANDES,^a
MARINA T VARELA,^a CECÍLIA M S Q ARANHA,^a HOLGER STARK^{a,b} and JOÃO
PAULO S FERNANDES^{a,*}

^aDepartment of Pharmaceutical Sciences, Universidade Federal de São Paulo, Rua São
Nicolau 210, 09913-030 Diadema-SP, Brazil.

^bInstitute of Pharmaceutical and Medicinal Chemistry, Heinrich Heine University
Düsseldorf, Universitätsstr. 1, 40225 Düsseldorf, Germany.

Email: joao.fernandes@unifesp.br; stark@hhu.de

¹H-NMR copy of compound 1j.....S2

¹H-NMR copy of compound 1k.....S3

S2

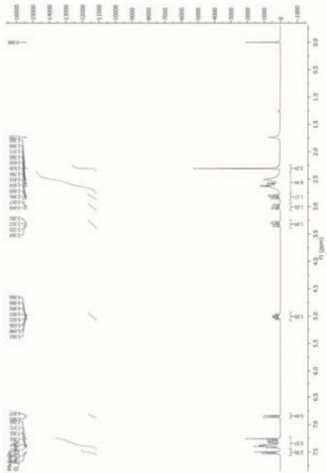


Figure S1. ¹H-NMR of compound 1j

S3

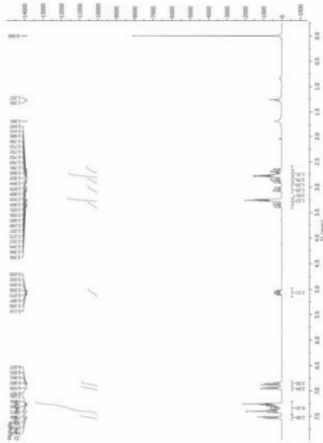


Figure S2. ¹H-NMR of compound 1k

4.2. Dual target ligands with 4-*tert*-butylphenoxy scaffold as histamine H₃ receptor antagonists and monoamine oxidase B inhibitors

Dorota Łazewska¹⁾, Agnieszka Olejarz-Maciej¹⁾, David Reiner²⁾, Maria Kaleta¹⁾, Gniewomir Latacz¹⁾, Małgorzata Zygmunt³⁾, Agata Doroz-Płonka¹⁾, Tadeusz Karcz¹⁾, Annika Frank²⁾, Holger Stark²⁾ and Katarzyna Kiec-Kononowicz¹⁾

1) Department of Technology and Biotechnology of Drugs, Jagiellonian University Medical College, 9 Medyczna Str, 30-688 Kraków, Poland

2) Institute of Pharmaceutical and Medicinal Chemistry, Heinrich Heine University Düsseldorf, Universitätsstr. 1, 40225 Duesseldorf, Germany

3) Department of Pharmacodynamics, Jagiellonian University Medical College, 9 Medyczna Str, 30-688 Kraków, Poland

Published in: *International Journal of Molecular Sciences*, 2020, 21:3411.

DOI: 10.3390/ijms21103411

Contribution to research: DR was involved in preparation, planning and conduction of cell-culture and radioligand displacement experiments, and evaluated corresponding data to determine H₃R affinity. DR wrote the pharmacological parts of and reviewed the manuscript.

Abstract:








Dual target ligands are a promising concept for the treatment of Parkinson's disease (PD). A combination of monoamine oxidase B (MAO B) inhibition with histamine H₃ receptor (H₃R) antagonism could have positive effects on dopamine regulation. Thus, a series of twenty-seven 4-*tert*-butylphenoxyalkoxyamines were designed as potential dual-target ligands for PD based on the structure of 1-(3-(4-*tert*-butylphenoxy)propyl)piperidine (DL76). Probed modifications included the introduction of different cyclic amines and elongation of the alkyl chain. Synthesized compounds were investigated for human H₃R (hH₃R) affinity and human MAO B (hMAO B) inhibitory activity. Most compounds showed good hH₃R affinities with *K_i* values below 400 nM, and some of them showed potent inhibitory activity for hMAO B with *IC*₅₀ values below 50 nM. However, the most balanced activity against both biological targets showed DL76 (hH₃R: *K_i* = 38 nM and hMAO B: *IC*₅₀ = 48 nM). Thus, DL76 was chosen for further studies, revealing the nontoxic nature of DL76 in HEK293 and neuroblastoma SH-SY5Y cells. However, no neuroprotective effect was observed for DL76 in hydrogen peroxide-treated neuroblastoma SH-SY5Y cells. Furthermore, *in vivo* studies showed antiparkinsonian activity of DL76 in haloperidol-induced catalepsy (Cross Leg Position Test) at a dose of 50 mg/kg body weight.

Reprinted with permission from Łazewska D, Olejarz-Maciej A, Reiner D, Kaleta M, Latacz G, Zygmunt M, Doroz-Płonka A, Karcz T, Frank A, Stark H and Kiec-Kononowicz K, Dual Target Ligands with 4-*tert*-Butylphenoxy Scaffold as Histamine H₃ Receptor Antagonists and Monoamine Oxidase B Inhibitors, *Int. J. Mol. Sci.*, 2020, 21:3411.

Copyright 2020 The Authors.

Article

Dual Target Ligands with 4-*tert*-Butylphenoxy Scaffold as Histamine H₃ Receptor Antagonists and Monoamine Oxidase B Inhibitors

Dorota Łażewska ^{1,*}, Agnieszka Olejarz-Maciej ¹, David Reiner ², Maria Kaleta ¹,
Gniewomir Latacz ¹, Małgorzata Zygmunt ³, Agata Doroz-Plonka ¹, Tadeusz Karcz ¹,
Annika Frank ², Holger Stark ² and Katarzyna Kieć-Kononowicz ^{1,*}

¹ Department of Technology and Biotechnology of Drugs, Jagiellonian University Medical College, 9 Medyczna Str, 30-688 Kraków, Poland; agnieszka.olejarz@uj.edu.pl (A.O.-M.); maria.kaleta@uj.edu.pl (M.K.); glatacz@cm-uj.krakow.pl (G.L.); a.doroz-plonka@uj.edu.pl (A.D.-P.); t.karcz@uj.edu.pl (T.K.)

² Institute of Pharmaceutical and Medicinal Chemistry, Heinrich Heine University Düsseldorf, Universitätsstr. 1, 40225 Düsseldorf, Germany; david.reiner@hhu.de (D.R.); a.frank@hhu.de (A.F.); stark@hhu.de (H.S.)

³ Department of Pharmacodynamics, Jagiellonian University Medical College, 9 Medyczna Str, 30-688 Kraków, Poland; malgorzata.zygmunt@uj.edu.pl

* Correspondence: dlażewska@cm-uj.krakow.pl (D.Ł.); mfkono@cyf-kr.edu.pl (K.K.-K.)

Received: 18 April 2020; Accepted: 9 May 2020; Published: 12 May 2020



Abstract: Dual target ligands are a promising concept for the treatment of Parkinson's disease (PD). A combination of monoamine oxidase B (MAO B) inhibition with histamine H₃ receptor (H₃R) antagonism could have positive effects on dopamine regulation. Thus, a series of twenty-seven 4-*tert*-butylphenoxyalkoxyamines were designed as potential dual-target ligands for PD based on the structure of 1-(3-(4-*tert*-butylphenoxy)propyl)piperidine (**DL76**). Probed modifications included the introduction of different cyclic amines and elongation of the alkyl chain. Synthesized compounds were investigated for human H₃R (hH₃R) affinity and human MAO B (hMAO B) inhibitory activity. Most compounds showed good hH₃R affinities with K_i values below 400 nM, and some of them showed potent inhibitory activity for hMAO B with IC₅₀ values below 50 nM. However, the most balanced activity against both biological targets showed **DL76** (hH₃R: K_i = 38 nM and hMAO B: IC₅₀ = 48 nM). Thus, **DL76** was chosen for further studies, revealing the nontoxic nature of **DL76** in HEK293 and neuroblastoma SH-SY5Y cells. However, no neuroprotective effect was observed for **DL76** in hydrogen peroxide-treated neuroblastoma SH-SY5Y cells. Furthermore, in vivo studies showed antiparkinsonian activity of **DL76** in haloperidol-induced catalepsy (Cross Leg Position Test) at a dose of 50 mg/kg body weight.

Keywords: dual-target ligands; histamine H₃ receptor; monoamine oxidase B; 4-*tert*-butylphenyl derivatives; antagonists; inhibitors; neurodegenerative disease; Parkinson's disease

1. Introduction

Parkinson's disease (PD) is a progressive neurodegenerative disorder characterized by motor problems. Although the entire pathology of PD is still unknown, several factors have been proposed to contribute to PD development, such as environmental toxins, neuroinflammation, genetic mutations, oxidative stress, or mitochondrial dysfunction [1]. Generally, PD is characterized by a severe lack of dopamine (DA) (80–90%) in *striatum* due to a progressive loss of dopaminergic neurons in the *substantia nigra* [1]. Current therapy for PD can only mitigate symptoms and slow the progress. However, there is no cure for the disease to date. Commonly administered drugs include levodopa

(as a DA precursor), DA agonists (e.g., pramipexole and rotigotine), and monoamine oxidase (MAO) B inhibitors (e.g., selegiline, rasagiline, or safinamide; Figure 1).

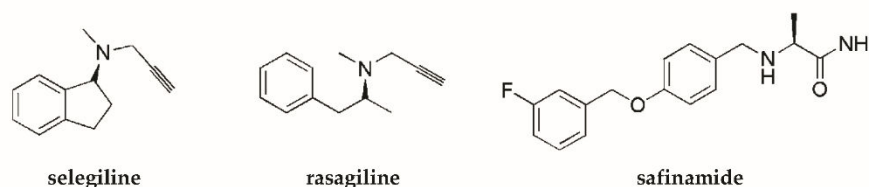


Figure 1. Structures of antiparkinsonian drugs—monoamine oxidase (MAO) B inhibitors.

MAO B plays a crucial role in the pathogenesis of PD. This enzyme belongs to the family of MAOs that catalyze the deamination of neurotransmitters (e.g., DA) and release reactive oxygen species as by-products. MAO B dominates in the human brain and deaminates β -phenylethylamine (PEA). PEA increases the synaptic levels of DA and blocks its reuptake into neurons. An increase in the activity of MAO B with age and some diseases as PD was observed in humans. Inhibitors of MAO B stop the activity of this enzyme and block the breakdown of DA. Moreover, MAO B inhibitors show neuroprotection and reduce oxidative stress [2]. Thus, MAO B inhibition is an important factor in the search for effective drugs in the treatment of PD. However, due to the multifactorial etiology of PD, it is thought that ligands acting on several targets at the same time (so-called Multi-Target-Directed Ligands (MTDL)) will be more effective in treatment than a one-target compound [3]. Thus, for improving the pharmacotherapy of PD, it is important to find MAO B inhibitors with combined activity at other targets.

Histamine H₃ receptors (H₃Rs) are widely distributed in the human brain and dominantly in areas connected with cognition (such as the striatum, cortex, or hippocampus). H₃Rs influence the release not only of histamine itself but also of other neurotransmitters, such as DA or acetylcholine [4], and increase the level of mentioned neurotransmitters in the synaptic cleft. Numerous pharmacological studies show that blocking H₃Rs provides beneficial effects in the treatment of various neurological diseases such as narcolepsy, neurodegenerative diseases (e.g., Alzheimer's disease and PD), attention deficit hyperactivity disorder, epilepsy, obesity, or neuropathic pain [5]. For years, many scientific centers and pharmaceutical companies have been involved in the search for active ligands of these receptors. Intensive synthetic work has led to a large number of structurally diverse compounds. Some of them have reached clinical trials, but so far, only one (pitolisant (Wakix[®]); Figure 2) has entered into the market as an orphan drug for narcolepsy [6].

One strategy to obtain MTDL is to combine two or more pharmacophores into a single molecule. Pharmacophores can be connected by linkers, attached directly (fused), or merged [7]. A propargylamine moiety is known to be important for MAO B inhibition [8], and it is present in the marketed drugs selegiline and rasagiline. The piperidinepropoxy motif is a part of many potent H₃R ligands, e.g., pitolisant (Figure 2). The idea to combine MAO B inhibition with H₃R antagonism is quite new. In 2017, the first of such compounds, contilisant (Figure 2), was described by Bautista-Aguilera et al. [9]. Contilisant not only proved to be a H₃R antagonist ($K_i = 11$ nM) and human MAO B (hMAO B) inhibitor ($IC_{50} = 78$ nM) but also showed moderate inhibition of cholinesterases (AChE $IC_{50} = 530$ nM; BuChE $IC_{50} = 1690$ nM). Further, this idea was continued by Lutsenko et al. [10] with the fused rasagiline derivative **1** as a dual-target ligand (DTL) with high hH₃R affinity ($K_i = 6.7$ nM) and good hMAO B inhibitory activity ($IC_{50} = 256$ nM) (Figure 2). Moreover, Affini et al. [11] described indanone derivatives as DTL for PD (compound **2**; hH₃R $K_i = 6.5$ nM; hMAO B $IC_{50} = 276$ nM; Figure 2). Recently, we have described a new group of DTL hMAO B inhibitors, *tert*-amylphenoxy derivatives [12]. These compounds showed also affinity for hH₃R (e.g., compound **3**; Figure 2). In contrast to the previously described DTL (contilisant, **1** and **2**), some of them showed an inhibitory activity for hMAO B that was higher than their affinity for hH₃R (**3**: hH₃R $K_i = 63$ nM; hMAO B $IC_{50} = 4.5$ nM).

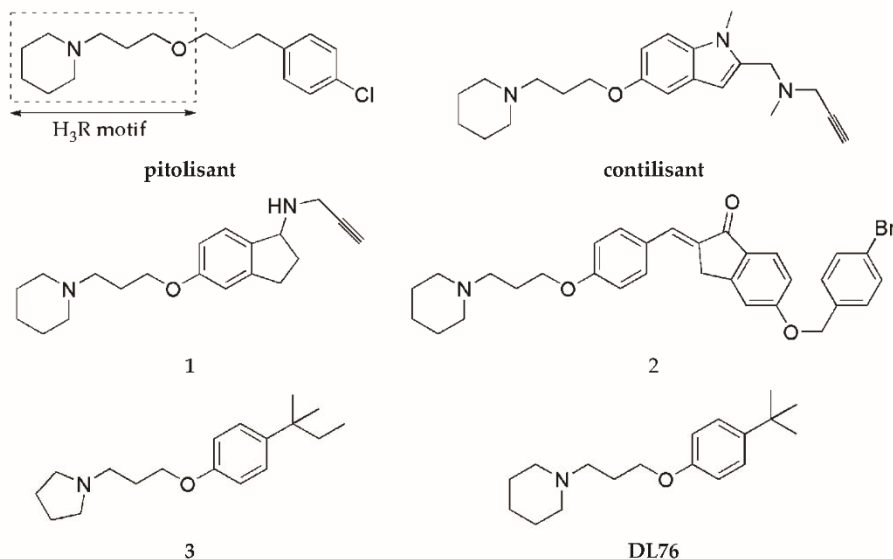


Figure 2. Structures of pitolisant and histamine H₃ receptor ligands with MAO B inhibitory activity.

To continue this work, we synthesized a series of 4-*tert*-butylphenoxy derivatives as analogues of histamine H₃R ligand **DL76** (hH₃R K_i = 22 nM in CHO K1 cells [13]; Figure 2) which showed also good inhibitory activity for hMAO B with an IC₅₀ of 48 nM. Encouraged by these results, we designed a series of novel 4-*tert*-butylphenoxy derivatives. Designed structural modifications included the following:

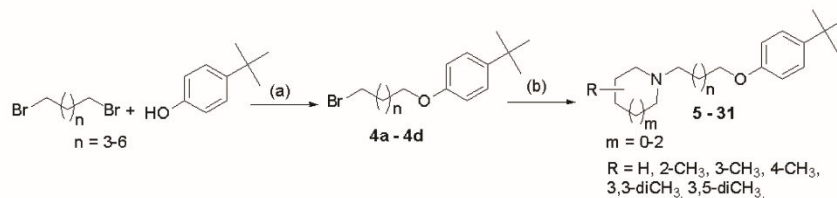
- exchange of piperidine moiety for other cyclic amines (pyrrolidine, substituted piperidine, or azepane)
- elongation of alkyl chain from three up to six atoms.

All compounds were evaluated for their affinity towards hH₃R and inhibition of hMAO B. Furthermore, we selected one of compounds for antiparkinsonian activity tests *in vivo* (in haloperidol-induced catalepsy) and neuroprotection studies *in vitro* (in neuroblastoma SH-SY5Y cells). Moreover, the toxicity of this compound in HEK293 cells and neuroblastoma SH-SY5Y cells was evaluated.

2. Results and Discussion

2.1. Synthesis of Compounds

Compounds were synthesized as shown in Scheme 1. Briefly, proper 4-*tert*-butylphenoxyalkyl bromides (**4a–4d**) were obtained by nucleophilic substitution of 4-*tert*-butylphenol with α,ω -dibromoalkanes in freshly prepared sodium propanolate as described previously [14]. Then, the bromides **4a–4d** were refluxed with corresponding amines in the mixture of ethanol–water (21:4) with powdered potassium carbonate and a catalytic amount of potassium iodide. The purified free bases were converted into hydrogen oxalates. Structures and purity of novel compounds **5–31** were confirmed by spectral analyses (¹H and ¹³C NMR spectra; see Supplementary Materials S1), mass spectrometry (MS), and elemental analysis.



Scheme 1. General synthetic pathway of synthesized compounds 5–31. Reagents and conditions: (a) sodium propanolate (0.05 mol Na in 50 mL), room temperature, 15'; 60 °C 3 h; reflux 3 h; 69–78%; (b) (i) amine, K₂CO₃, KI, EtOH:H₂O (21:4), and reflux 20 h and (ii) oxalic acid, EtOH, room temperature, 1 h; (Et)₂O; crystallization from EtOH, 5–53%.

2.2. Human Histamine H₃ Receptor Affinity

The affinity of compounds (5–31) for H₃R was evaluated in a radioligand-binding assay in HEK293 cells stably expressing hH₃R [14]. [³H]N^α-methylhistamine was used as a radioligand. Results are presented as K_i values in Table 1. The compounds showed variable affinities for hH₃R ranging from good (K_i < 100 nM) to weak (K_i > 1500 nM), depending on the kind of the introduced cyclic amine moiety and alkyl chain length. Analyzing the influence of a cyclic amine moiety on the affinity for hH₃R, it was noticed that derivatives of piperidine (DL76, 6–8), 3-methylpiperidine (12–15), and azepane (28–31) were the most active. On the other hand, 3,3-dimethylpiperidine derivatives (16–19) showed weaker affinities (K_i > 1600 nM). Unfortunately, none of the synthesized compounds (5–31) showed higher hH₃R affinity than the lead structure DL76 (K_i = 38 nM). The most potent was compound 9 with a K_i of 69 nM.

Table 1. Human histamine H₃ receptor affinity and human MAO B inhibition of tested compounds 5–31 and DL76.

Compounds	R	n	H ₃ R ^a	MAO B ^b	MAO A ^b
			K _i (nM) (95%CI)	IC ₅₀ (nM) (%Inh.) ^c	IC ₅₀ (nM) (%Inh.) ^d
5		1	371 (136, 1009)	2.7 ± 0.4	nt ^e
DL76		1	38 ^f (8, 181)	48 ± 15	>10,000 (9%)
6		2	309 (166, 574)	290 ± 7	>10,000 (10%)
7		3	252 (64, 990)	(28%)	nt ^e
8		4	225 (98, 519)	(13%)	nt ^e
9		1	69 (49, 96)	11 ± 1	>10,000 (5%)
10		2	153 (46, 505)	475 ± 38	>10,000 (2%)
11		3	1556 (349, 6941)	(36%)	nt ^e

4.2 Dual target ligands with 4-tert-butylphenoxy scaffold as histamine H₃ receptor antagonists and monoamine oxidase B inhibitors

Table 1. Cont.

Compounds	R	n	H ₃ R ^a K _i (nM) (95%CI)	MAO B ^b IC ₅₀ (nM) (%Inh.) ^c	MAO A ^b IC ₅₀ (nM) (%Inh.) ^d
12		1	98 (43, 226)	117 ± 12	>10,000 (10%)
13		2	102 (18, 571)	1405 ± 494	nt ^e
14		3	114 (33, 397)	(33%)	nt ^e
15		4	351 (223, 552)	(13%)	nt
16		1	1624 (1075, 2453)	476 ± 38	>10,000 (6%)
17		2	3437 (2701, 4374)	(38%)	nt ^e
18		3	3535 (2528, 4942)	2777 ± 66	>10,000 (19%)
19		4	2575 (542, 12227)	1953 ± 45	>10,000 (24%)
20		1	341 (49, 2388)	(37%)	nt ^e
21		2	1381 (923, 2066)	(35%)	nt ^e
22		3	2235 (1136, 4397)	(41%)	nt ^e
23		4	2083 (936, 4637)	(34%)	nt ^e
24		1	316 (123, 808)	(37%)	nt ^e
25		2	400 (152, 1050)	(33%)	nt ^e
26		3	531 (344, 822)	(39%)	nt ^e
27		4	1350 (651, 2798)	(10%)	nt ^e
28		1	111 (68, 180)	45 ± 4	>10,000 (10%)
29		2	299 (105, 855)	1627 ± 78	>10,000 (23%)
30		3	324 (121, 870)	(18%)	nt ^e
31		4	829 ^g (313, 2194)	(23%)	nt ^e
	rasagiline		nt ^e	15 ± 1	nt ^e
	pargiline		nt ^e	360 ± 138	nt ^e
	safinamide		nt ^e	7.7 ± 1.2	nt ^e
	clorgiline		nt ^e	nt ^e	1.76 ± 0.5 nM

^a [³H]N^α-Methylhistamine-binding assay in HEK293 cells stably expressing the human H₃R; mean value within the 95% confidence interval (CI); ^b fluorometricAmplex™ Red MAO assay [15]; mean ± SEM of 2–5 independent experiments; ^c the percent of inhibition at 1 μM, mean values of two independent experiments; ^d the percent of inhibition at 10 μM, mean values of two independent experiments; ^e nt = not tested; ^f K_i (±SEM) = 22 ± 3 nM in [¹²⁵I]iodoproxyfan binding assay in CHO K1 cells, data from Reference [13]; ^g data from Reference [16].

2.3. Human Monoamine Oxidase B Inhibitory Activity

2.3.1. Screening and Determination of IC₅₀

The inhibitory activity of the compounds against hMAO B was evaluated using Amplex Red[®] Monoamine Oxidase kits [15]. Rasagiline, pargyline, and safinamide were used as reference inhibitors. Following the initial screening of compounds at 1 μ M concentration, IC₅₀ values were determined for those which exhibited inhibitory activity greater than 50% (Table 1). Sixteen compounds out of the thirty-one showed a percentage of inhibition between 10% and 41%. Results of IC₅₀ determinations indicated the influence of both an amine moiety and a length of alkyl chain on hMAO B inhibition. Except the series of 3,5-dimethylpiperidine and 4-methylpiperidine derivatives, the inhibitory activity of the compounds was more pronounced with a shorter (three or four) alkyl linker. Thus, an elongation of alkyl chain caused a drop of activity. The highest activity was observed for the compounds with the propylene linker (**DL76**, **9**, **12**, **16**, **20**, **24**, and **28**). This observation is similar to our previous finding [12] concerning 4-*tert*-amylphenoxy derivatives as DTL ligands. Exchange of a cyclic amine group (piperidine in **DL76**) for other moieties (pyrrolidine, substituted piperidine, or azepane) caused variable influences: increased (pyrrolidine-**5** or 2-methylpiperidine-**9**), maintained (azepane-**28**), or decreased activity (3-methylpiperidine-**12**, 3,3-dimethylpiperidine-**16**, 3,5-dimethylpiperidine-**20**, or 4-methylpiperidine-**24**). The most potent inhibitor **5** (IC₅₀ = 2.7 nM) showed higher activity than the reference compounds rasagiline (IC₅₀ = 15 nM) and safinamide (IC₅₀ = 7.7 nM).

2.3.2. Reversibility Studies

To investigate the type of inhibition (reversible or irreversible) of hMAO B by 4-*tert*-butylphenoxy derivatives, experiments were performed with selected compounds (**DL76**, **5**, and **9**) and conducted as described previously [12]. Rasagiline (irreversible inhibitor) and safinamide (reversible inhibitor) were used as standards. Results from the experiment are shown in Figure 3A–C. All tested compounds presented a signal similar to the reversible reference inhibitor safinamide so they were considered as reversible. However, the signal for rasagiline was slightly higher than expected for the IC₈₀ concentration. High signal for rasagiline can be explained by the fact that irreversible inhibitors need more time to create the covalent bond with the enzyme. The used protocol for the reversibility testing did not contain the preincubation of enzyme with inhibitors. Lack of preincubation could also change the observed reversibility curves for reversible inhibitors because they could present different affinity towards the free enzyme and the enzyme that was bound to the substrate [17]. Thus, the experiment was modified and the reversibility of investigated inhibitors with and without the preincubation with the enzyme was performed (see Materials and Methods). Results from the experiments after the modification are shown in Figure 3D,E. Safinamide, **5**, and **9** did not show differences between experiments with and without the preincubation, suggesting that the inhibitors did not bind covalently to the enzyme. On the other hand, rasagiline (irreversible inhibitor) showed higher inhibition when preincubated with hMAOB.

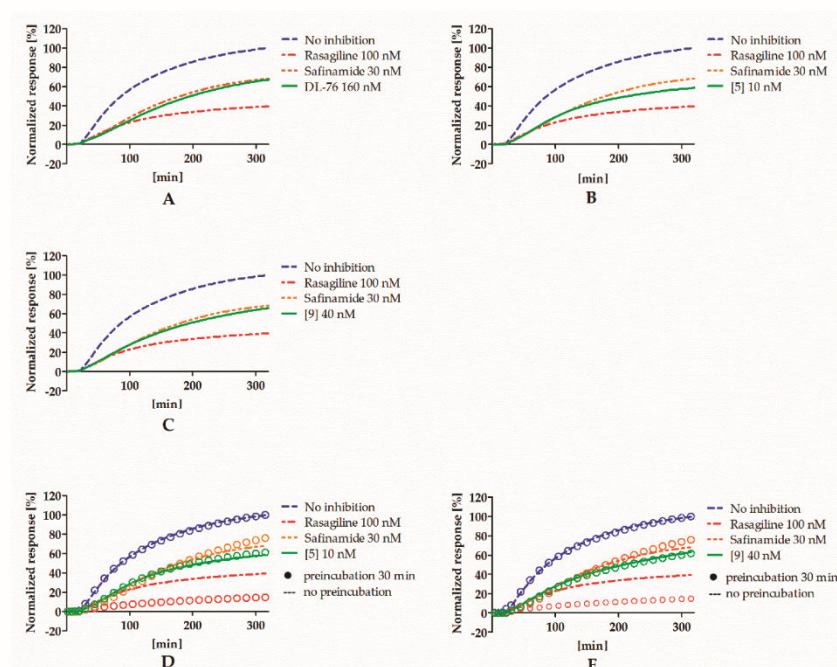


Figure 3. Reversibility of DL76 (A), 5 (B), 9 (C), and reference inhibitors without the preincubation and comparison of reversibility of 5 (D), 9 (E), and reference inhibitors that were (rings) or were not (lines) preincubated with hMAOB. Concentrations of compounds correspond to their IC₈₀ values.

2.3.3. Kinetic Studies

In order to determine the mode of hMAOB inhibition, compounds **9** and **DL76** were chosen and used in three concentrations corresponding to their IC₂₀, IC₅₀, and IC₈₀ values (0.2 nM, 10 nM, and 40 nM for **9** and 7 nM, 48 nM, and 164 nM for **DL76**). Results from the kinetic experiment were used for determination of Michaelis–Menten curves (Figure 4A,C). Later, data were transformed using the Lineweaver–Burk equation to double reciprocal plot (lines from different concentrations of both compound **9** and **DL76** converged to the left of *y*-axis and above *x*-axis; Figure 4B,D). From Michaelis–Menten curves, *V*_{max} and *K*_M values were fitted (Table 2). For both compounds, *V*_{max} values decreased curvilinearly and *K*_M values increased curvilinearly with the increased inhibitor concentrations. The behavior of these parameters suggested the mixed mode inhibition of **9** and **DL76** [17,18]. This observation was further confirmed by a value of calculated constant α ($\alpha = 1.6$ for **9** and $\alpha = 4.6$ for **DL76**) by GraphPad Prism software from the nonlinear regression (see Supplementary Materials S2). According to Copeland [18,19], $\alpha > 1$ is characteristic for the mixed mode of inhibition where an inhibitor is able to bind to both the free enzyme and the enzyme–substrate complex unequally and its affinity for binding to the free enzyme is higher (see Table S1, Supplementary Materials S2).

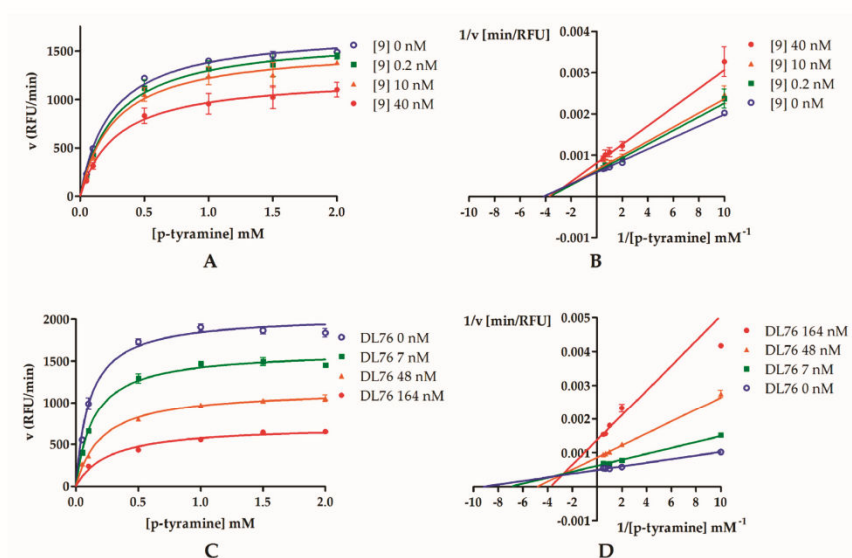


Figure 4. Michaelis–Menten curves for compound **9** (A) and **DL76** (C): Inhibitors were tested in three concentrations (0.2 nM, 10 nM, and 40 nM for **9** and 7 nM, 48 nM, and 164 nM for **DL76**) representing their IC₂₀, IC₅₀, and IC₈₀, respectively. Substrate (p-tyramine) was used in six concentrations: 0.05 mM, 0.1 mM, 0.5 mM, 1 mM, 1.5 mM, and 2 mM. (B,D) Double-reciprocal (Lineweaver–Burk) plots from enzyme kinetic studies.

Table 2. V_{max} and K_M calculated from Michaelis–Menten curves of compound **9** and **DL76**.

Parameters	Compound 9				DL76			
Concentration (nM)	0	0.2	10	40	0	7	48	164
V _{max} (RFU/min)	1713	1652	1544	1238	2046	1628	1165	726.3
K _M (mM)	0.24	0.27	0.27	0.28	0.11	0.14	0.21	0.27

2.4. Human Monoamine Oxidase A Inhibitory Activity

Selected compounds (**DL76**, **6**, **9**, **10**, **12**, **16**, and **28**) were screened for hMAO A inhibition using Amplex Red[®] Monoamine Oxidase kits [15]. Tested compounds showed a percentage of inhibition <25% at a concentration of 10 μM. Results indicated very weak or no inhibition of hMAO A by these compounds.

2.5. Toxicity and Neuroprotection Studies In Vitro

For toxicity and neuroprotection studies, **DL76** was chosen as the most promising DTL. The human embryonic kidney (HEK-293) cell line was used for the estimation of safety of **DL76**. As shown in Figure 5, the statistically significant decrease of HEK-293 cell viability in the presence of **DL76** was observed only at the highest doses of 125 μM and 250 μM. The used reference cytostatic drug doxorubicin (DX) decreased cell viability <50% under the same conditions at very low concentrations of 0.2 and 0.05 μM. The neuroprotection effect of **DL76** was investigated in vitro in the model of neuronal damage. Oxidative damage was induced by very high toxic levels of hydrogen peroxide (H₂O₂; 300 μM), the popular cell model for PD research, in neuroblastoma SH-SY5Y cell line. Compound **DL76** was tested at two doses, 10 μM and 50 μM, within two independent experiments. Salsolinol (SAL) was used at a concentration of 50 μM as the reference compound with the proven neuroprotection

activity [20]. **DL76** displayed no increase of cell survival either at 10 μ M (Figure 6A) or 50 μ M (Figure 6B), whereas SAL statistically significant increased cells viability in both experiments. However, the safety of **DL76** was confirmed here, as no toxic effect against SH-SY5Y cells was observed at both used concentrations 10 and 50 μ M (Figure 6A,B).

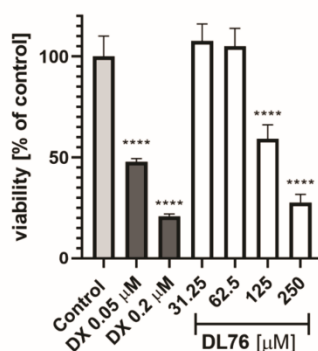


Figure 5. The effect of **DL76** and doxorubicin (DX) on HEK-293 viability: Statistical significance (**** $p < 0.0001$) was analyzed by GraphPadPrism™ 8 software using one-way ANOVA and Bonferroni's multiple comparison posttest in comparison with control (1% DMSO in cell culture medium).

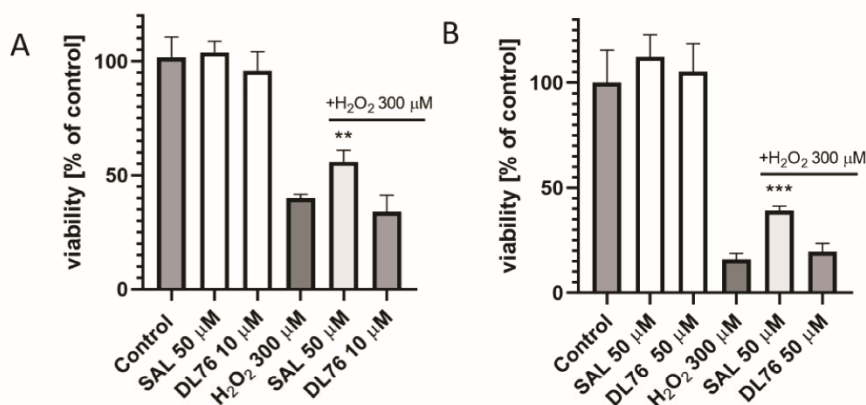


Figure 6. The effect of salsolinol (SAL) at 50 μ M and **DL76** at 10 μ M (A) or at 50 μ M (B) on SH-SY5Y neuroblastoma cells viability damaged by 300 μ M of H₂O₂ after 24 h of incubation: Statistical significance was set at *** $p < 0.001$ and ** $p < 0.01$ by GraphPadPrism™ 8 software using one-way ANOVA and Bonferroni's multiple comparison posttest in comparison with the positive control H₂O₂ (300 μ M).

2.6. Antiparkinsonian Activity in Haloperidol-Induced Catalepsy in Wistar Rats

Haloperidol (dopamine D₂ antagonist)-induced catalepsy in rodents is a popular model for screening of antiparkinsonian activity of compounds [21]. Caused symptoms in animals are similar to the inability of PD patients to initiate movements. We used this test to preliminary evaluate antiparkinsonian activity of **DL76**. Haloperidol (0.63 mg/kg; s.c.) was administered to induce catalepsy in Wistar rats; 5 min later, **DL76** was added at doses of 25 or 50 mg/kg (i.p.). The reversal of catalepsy was tested for 6 min (3 times in 3 min intervals) after 1 h of haloperidol administration. As the reference compound was used **MSX-3**, the adenosine A_{2A} receptor antagonist with confirmed ability to reverse

catalepsy mediated by D₁ and D₂ receptor antagonists [22]. To characterize the antiparkinsonian activity of **DL76**, two tests were performed: bar test and crossed-leg position test.

2.6.1. Bar Test

Haloperidol-induced catalepsy was not reduced by **DL-76** administrated at a dose of 25 mg/kg body weight (Table 3). After administration of **DL-76** at a dose of 50 mg/kg body weight, low antiparkinsonian activity in the bar test was observed. The compound reduced the duration of catalepsy by 36.4% compared to the control group, which was obtained after administration of haloperidol (16.4 versus 25.8). This effect was weaker than the anti-Parkinsonian activity of **MSX-3**.

Table 3. Antiparkinsonian activity of **DL76** in the bar test.

Compound	Dose (mg/kg; i.p.)	Times of Observation of Catalepsy (s) ¹		
		0 min	3 min	6 min
control	-	17.5 ± 5.3	30.0 ± 0	30.0 ± 0
DL-76	25	19.5 ± 4.2	26.5 ± 3.5	30.0 ± 0
	50	13.8 ± 5.9	13.5 ± 4.2 *	22.0 ± 5.0
MSX-3	25	0 ± 0 ***	0 ± 0 ***	0 ± 0 ***
	50	0 ± 0 ***	0 ± 0 ***	0 ± 0 ***

¹ mean ± SEM (n = 6); * p < 0.05; *** p < 0.001.

2.6.2. Crossed-Leg Position Test

The strongest, statistically significant antiparkinsonian activity was demonstrated by **DL-76** at a dose of 50 mg/kg body weight, which, compared to the control group, reduced the duration of haloperidol-induced catalepsy by 99.7% (0.053 versus 19.25) (Table 4). This effect was comparable to the antiparkinsonian activity of **MSX-3**.

The weaker, antiparkinsonian activity was demonstrated by **DL-76** administered at a dose of 25 mg/kg body weight. **DL76**, in comparison to the control group, reduced the duration of haloperidol-induced catalepsy by 54.5% (8.75 versus 19.25) (Table 4), but the effect was not statistically significant.

Table 4. Antiparkinsonian activity of **DL76** in the crossed-leg position test.

Compound	Dose (mg/kg)	Times of Observation of Catalepsy (s) ¹		
		0 min	3 min	6 min
control	-	4.2 ± 1.6	23.5 ± 6.5	30.0 ± 0
DL-76	25	0.66 ± 0.68	10.6 ± 6.1	15.0 ± 6.7
	50	0 ± 0 ***	0 ± 0 ***	0.16 ± 0.4 ***
MSX-3	25	0 ± 0 ***	0 ± 0 ***	0 ± 0 ***
	50	0 ± 0 ***	0 ± 0 ***	0 ± 0 ***

¹ mean ± SEM (n = 6); *** p < 0.001.

3. Materials and Methods

3.1. Chemistry

All reagents were purchased from commercial suppliers Alfa Aesar (Karlsruhe, Germany) or Sigma Aldrich (Darmstadt, Germany) and were used without further purification. TLC data were obtained with Merck silica gel 60F₂₅₄ aluminum sheets with UV light detection and evaluation with Dragendorff's reagent (solvent systems: methylene chloride: methanol 9:1 or methylene chloride). Melting points (m.p.) were determined on a MEL-TEMP II (LD Inc., Long Beach, CA, USA) melting

point apparatus and are uncorrected. Mass spectra (LC/MS) were performed on Waters TQ Detector (Water Corporation., Milford, CT, USA) mass spectrometer. Retention times (*t_R*) are given in minutes. The UPLC/MS purity of all final compounds was determined (%). All compounds (except **14**, **19**, and **26**) showed purity above 96%. ¹H NMR and ¹³C NMR spectra were recorded in DMSO-*d*₆ on a Mercury 300 MHz PFG spectrometer (Varian, Palo Alto, CA, USA), Avance III HD 400 MHz spectrometer (Bruker, Billerica, MA, USA), or FT-NMR 500 MHz spectrometer (Jeol Ltd., Akishima, Tokyo, Japan). Chemical shifts were expressed in parts per million (ppm) using the solvent signal as an internal standard. Data are reported in the following order: multiplicity (br, broad; d, doublet; m, multiplet; quin, quintet; s, singlet; and t, triplet), approximate coupling constants *J* expressed in Hertz (Hz), and number of protons. Elemental analyses were measured on analyzer Vario EL III 2 (Elementar, Langensfeld, Germany) and are within ±0.5% of the theoretical values (except carbon for **7** (±0.6%) and **28** (±0.7%).

4-*tert*-Butylphenoxyalkyl bromides (**4a–4d**) were synthesized according to the method described previously [14]. All of them are known and reported in Chemical Abstract Database:

1-(3-bromopropoxy)-4-*tert*-butylbenzene (**4a**): CAS3245-63-4; 1-(4-bromobutoxy)-4-*tert*-butylbenzene (**4b**): CAS53669-73-1;

1-(5-bromopentyloxy)-4-*tert*-butylbenzene (**4c**): CAS53669-74-2;

1-(6-bromohexyloxy)-4-*tert*-butylbenzene (**4d**): CAS53669-73-3.

Designed compounds **5–31** were synthesized according to the procedure described previously [12]. Briefly, to a proper 4-*tert*-butylphenylalkoxy bromide (2.5 mmol) in the mixture of C₂H₅OH (52.5 mL) and H₂O (10 mL) and in the presence of K₂CO₃ (7.5 mmol) with the catalytic amount of KI was added a proper amine (5 mmol), and the solution was refluxed from 10 to 48 h. Then, C₂H₅OH was evaporated, and to the residue were added 50 mL of CH₂Cl₂ and 40 mL of water. The organic solution was washed with 50 mL of 1% HCl, evaporated to dryness, dissolved in 3% HCl followed by washing with (C₂H₅)₂O, and neutralized with 5% NaOH. The final product was extracted with CH₂Cl₂, dried over Na₂SO₄, and evaporated. The oily residue was transformed into oxalic acid salt in absolute C₂H₅OH and precipitated (C₂H₅)₂O. The solid was crystallized from C₂H₅OH.

1-(3-(4-*tert*-Butylphenoxy)propyl)pyrrolidine hydrogen oxalate (**5**). White solid, yield 27%, m.p. 147–149 °C, C₁₇H₂₇NO × C₂H₂O₄ (MW = 351.43). ¹H NMR (400 MHz, DMSO-*d*₆) δ: 7.29 (d, *J* = 8.61 Hz, 2H), 6.86 (d, *J* = 8.61 Hz, 2H), 4.01 (t, *J* = 6.06 Hz, 2H), 3.20–3.31 (m, 6H), 2.05–2.14 (m, 2H), 1.93 (br s, 4H), 1.25 (s, 9H). ¹³C NMR (126 MHz, DMSO-*d*₆) δ: 165.3, 156.5, 143.4, 126.5, 114.4, 65.3, 53.5, 51.9, 34.2, 31.8, 25.9, 23.2. LC-MS: purity 100% *t_R* = 5.27, (ESI) *m/z* [M + H]⁺ 262.24. Anal. calcd. for C₁₉H₂₉NO₅: C, 64.93; H, 8.32; N, 3.99%. Found: C, 64.90; H, 8.35; N, 3.93%.

1-(4-(4-*tert*-Butylphenoxy)butyl)piperidine hydrogen oxalate (**6**). White solid, yield 52%, m.p. 150–152 °C, C₁₉H₃₁NO × C₂H₂O₄ (MW = 379.48). ¹H NMR (400 MHz, DMSO-*d*₆) δ: 7.28 (d, *J* = 9.00 Hz, 2H), 6.85 (d, *J* = 8.61 Hz, 2H), 3.95 (t, *J* = 5.87 Hz, 2H), 2.95–3.31 (m, 6H), 1.64–1.88 (m, 8H), 1.52 (br s., 2H), 1.25 (s, 9H). ¹³C NMR (101 MHz, DMSO-*d*₆) δ: 165.2, 156.7, 143.2, 126.5, 114.4, 67.2, 56.1, 52.4, 40.9, 34.2, 31.8, 26.5, 23.0, 22.0, 20.8. LC-MS: purity 100% *t_R* = 5.69, (ESI) *m/z* [M + H]⁺ 290.22. Anal. calcd. for C₂₁H₃₃NO₅: C, 66.46; H, 8.76; N, 3.69%. Found: C, 66.45; H, 8.48; N, 3.62%.

1-(5-(4-*tert*-Butylphenoxy)pentyl)piperidine hydrogen oxalate (**7**). White solid, yield 42%, m.p. 170–172 °C, C₂₀H₃₃NO × C₂H₂O₄ (MW = 393.51). ¹H NMR (400 MHz, DMSO-*d*₆) δ: 7.28 (d, *J* = 8.61 Hz, 2H), 6.84 (d, *J* = 8.61 Hz, 2H), 3.93 (t, *J* = 6.06 Hz, 1H), 2.89–3.39 (m, 6H), 1.72 (br s., 8H), 1.52 (br s., 2H), 1.37–1.48 (m, 2H), 1.25 (s, 9H). ¹³C NMR (101 MHz, DMSO-*d*₆) δ: 165.1, 156.8, 143.0, 126.5, 114.4, 67.5, 56.3, 52.4, 40.9, 34.2, 31.8, 28.7, 23.4, 23.3, 23.0, 22.0. LC-MS: purity 98.98% *t_R* = 5.98, (ESI) *m/z* [M + H]⁺ 304.18. Anal. calcd. for C₂₂H₃₅NO₅: C, 67.14; H, 8.96; N, 3.56%. Found: C, 66.50; H, 8.71; N, 3.42%.

1-(6-(4-*tert*-Butylphenoxy)hexyl)piperidine hydrogen oxalate (**8**). White solid, yield 16%, m.p. 156–158 °C, C₂₁H₃₅NO × C₂H₂O₄ (MW = 407.54). ¹H NMR (400 MHz, DMSO-*d*₆) δ: 7.27 (d, *J* = 9.00 Hz, 2H), 6.83 (d, *J* = 8.61 Hz, 2H), 3.92 (t, *J* = 6.26 Hz, 2H), 2.86–3.21 (m, 6H), 1.59–1.87 (m, 8H), 1.38–1.56 (m, 4H),

1.34 (d, $J = 7.04$ Hz, 2H), 1.25 (s, 9H). ¹³C NMR (101 MHz, DMSO-*d*₆) δ : 165.3, 156.9, 143.0, 126.5, 114.3, 67.6, 56.3, 52.4, 40.9, 34.2, 31.8, 29.0, 26.4, 25.6, 23.6, 22.9, 22.0. LC-MS: purity 96.38% $t_R = 6.39$, (ESI) m/z [M + H]⁺ 318.20. Anal. calcd. for C₂₃H₃₇NO₅: C, 67.78; H, 9.15; N, 3.44%. Found: C, 67.26; H, 9.13; N, 3.42%.

1-(3-(4-*tert*-Butylphenoxy)propyl)-2-methylpiperidine hydrogen oxalate (9). White solid, yield 19%, m.p. 114–116 °C, C₁₉H₃₁NO × C₂H₂O₄ (MW = 379.48). ¹H NMR (400 MHz, DMSO-*d*₆) δ : 7.30 (d, $J = 8.61$ Hz, 2H), 6.86 (d, $J = 9.00$ Hz, 2H), 3.93–4.12 (m, 2H), 3.18–3.44 (m, 3H), 3.06–3.17 (m, 1H), 2.92–3.05 (m, 1H), 2.01–2.20 (m, 2H), 1.78–1.91 (m, 1H), 1.53–1.76 (m, 4H), 1.38–1.52 (m, 1H), 1.28 (d, $J = 6.65$ Hz, 3H), 1.25 (s, 9H). ¹³C NMR (101 MHz, DMSO-*d*₆) δ : 165.2, 156.5, 143.4, 126.5, 114.5, 65.4, 57.3, 49.3, 40.9, 34.2, 31.8, 23.4, 22.8. LC-MS: purity 100% $t_R = 5.68$, (ESI) m/z [M + H]⁺ 290.22. Anal. calcd. for C₂₁H₃₃NO₅: C, 66.46; H, 8.76; N, 3.69%. Found: C, 66.29; H, 8.80; N, 3.64%.

1-(4-(4-*tert*-Butylphenoxy)butyl)-2-methylpiperidine hydrogen oxalate (10). White solid, yield 34%, m.p. 107–110 °C, C₂₀H₃₃NO × C₂H₂O₄ (MW = 393.51). ¹H NMR (400 MHz, DMSO-*d*₆) δ : 7.29 (d, $J = 9.00$ Hz, 2H), 6.85 (d, $J = 9.00$ Hz, 2H), 3.95 (m, 2H), 3.27 (br.s., 2H), 3.08–3.19 (m, 1H), 2.91–3.08 (m, 2H), 1.68–1.87 (m, 7H), 1.39–1.67 (m, 3H), 1.20–1.33 (m, 12H). ¹³C NMR (101 MHz, DMSO-*d*₆) δ : 165.2, 156.7, 143.2, 126.5, 114.4, 67.3, 51.6, 34.2, 31.8, 26.5, 22.7, 20.2. LC-MS: purity 100% $t_R = 5.94$, (ESI) m/z [M + H]⁺ 304.24. Anal. calcd. for C₂₂H₃₅NO₅: C, 67.14; H, 8.96; N, 3.56%. Found: C, 67.00; H, 8.95; N, 3.52%.

1-(5-(4-*tert*-Butylphenoxy)pentyl)-2-methylpiperidine hydrogen oxalate (11). White solid, yield 11%, m.p. 96–99 °C, C₂₁H₃₅NO × C₂H₂O₄ (MW = 407.54). ¹H NMR (400 MHz, DMSO-*d*₆) δ : 7.28 (d, $J = 6.81$ Hz, 2H), 6.84 (d, $J = 9.00$ Hz, 2H), 3.94 (t, $J = 6.26$ Hz, 2H), 3.26 (br.s., 2H), 3.03–3.13 (m, 1H), 2.91–3.02 (m, 2H), 1.56–1.86 (m, 9H), 1.40–1.50 (m, 3H), 1.23–1.30 (m, 12H). ¹³C NMR (101 MHz, DMSO-*d*₆) δ : 165.2, 156.8, 143.0, 126.5, 114.4, 67.5, 51.7, 34.2, 31.8, 28.7, 23.4, 22.9. LC-MS: purity 96.49% $t_R = 6.23$, (ESI) m/z [M + H]⁺ 318.27. Anal. calcd. for C₂₃H₃₇NO₅: C, 67.78; H, 9.15; N, 3.44%. Found: C, 67.50; H, 8.97; N, 3.41%.

1-(3-(4-*tert*-Butylphenoxy)propyl)-3-methylpiperidine hydrogen oxalate (12). White solid, yield 29%, m.p. 141–143 °C, C₁₉H₃₁NO × C₂H₂O₄ (MW = 379.48). ¹H NMR (500 MHz, DMSO-*d*₆) δ : 7.24 (d, $J = 8.88$ Hz, 2H), 6.80 (d, $J = 8.59$ Hz, 2H), 3.95 (t, $J = 5.87$ Hz, 2H), 3.24–3.43 (m, 2H), 3.07 (t, $J = 7.59$ Hz, 2H), 2.63–2.77 (m, 1H), 2.37–2.45 (m, 1H), 2.00–2.16 (m, 2H), 1.78–1.90 (m, 1H), 1.61–1.77 (m, 3H), 1.20 (s, 9H), 0.94–1.10 (m, 1H), 0.85 (d, $J = 6.59$ Hz, 3H). ¹³C NMR (126 MHz, DMSO-*d*₆) δ : 165.4, 156.6, 143.4, 126.6, 114.5, 65.5, 58.0, 54.0, 52.1, 34.3, 31.9, 30.6, 29.0, 24.1, 22.8, 19.1. LC-MS: purity 98.04% $t_R = 5.75$, (ESI) m/z [M + H]⁺ 290.22. Anal. calcd. for C₂₁H₃₃NO₅: C, 66.46; H, 8.76; N, 3.69%. Found: C, 66.44; H, 8.42; N, 3.65%.

1-(4-(4-*tert*-Butylphenoxy)butyl)-3-methylpiperidine hydrogen oxalate (13). White solid, yield 53%, m.p. 148–150 °C, C₂₀H₃₃NO × C₂H₂O₄ (MW = 393.51). ¹H NMR (400 MHz, DMSO-*d*₆) δ : 7.28 (d, $J = 8.61$ Hz, 2H), 6.85 (d, $J = 8.61$ Hz, 2H), 3.95 (t, $J = 6.06$ Hz, 2H), 3.24–3.45 (m, 2H), 2.94–3.11 (m, 2H), 2.67–2.78 (m, 2H), 1.62–1.97 (m, 8H), 1.25 (s, 9H), 1.06 (m, 1H), 0.89 (d, $J = 6.65$ Hz, 3H). ¹³C NMR (101 MHz, DMSO-*d*₆) δ : 165.2, 156.7, 143.1, 126.5, 114.4, 67.2, 57.9, 56.1, 51.9, 40.9, 34.2, 31.8, 30.6, 28.9, 26.5, 22.6, 20.8, 19.1. LC-MS: purity 99.46% $t_R = 6.13$, (ESI) m/z [M + H]⁺ 304.24. Anal. calcd. for C₂₂H₃₅NO₅: C, 67.14; H, 8.96; N, 3.56%. Found: C, 66.86; H, 8.62; N, 3.51%.

1-(5-(4-*tert*-Butylphenoxy)pentyl)-3-methylpiperidine hydrogen oxalate (14). White solid, yield 8%, m.p. 179–181 °C, C₂₁H₃₅NO × C₂H₂O₄ (MW = 407.54). ¹H NMR (400 MHz, DMSO-*d*₆) δ : 7.28 (d, $J = 8.22$ Hz, 2H), 6.84 (d, $J = 7.83$ Hz, 2H), 3.94 (br. s., 2H), 3.19–3.48 (m, 2H), 2.97 (br. s., 4H), 1.57–1.99 (m, 8H), 1.35–1.54 (m, 2H), 1.26 (br. s., 9H), 1.06 (d, $J = 9.39$ Hz, 1H), 0.69–0.97 (m, 3H). ¹³C NMR (101 MHz, DMSO-*d*₆) δ : 165.0, 156.8, 143.1, 126.5, 114.4, 67.5, 58.0, 56.4, 52.0, 41.0, 34.2, 31.8, 30.6, 28.7, 23.5, 23.3, 19.1. LC-MS: purity 93.40% $t_R = 6.40$, (ESI) m/z [M + H]⁺ 318.20. Anal. calcd. for C₂₃H₃₇NO₅: C, 67.78; H, 9.15; N, 3.44%. Found: C, 67.44; H, 8.90; N, 3.43%.

1-(6-(4-*tert*-Butylphenoxy)hexyl)-3-methylpiperidine hydrogen oxalate (15). White solid, yield 7%, m.p. 140–142 °C, C₂₂H₃₇NO × C₂H₂O₄ (MW = 421.56). ¹H NMR (400 MHz, DMSO-*d*₆) δ: 7.27 (d, *J* = 8.61 Hz, 2H), 6.83 (d, *J* = 9.00 Hz, 2H), 3.92 (t, *J* = 6.46 Hz, 2H), 3.23–3.43 (m, 2H), 2.88–3.04 (m, 2H), 2.68–2.76 (m, 2H), 1.57–1.95 (m, 8H), 1.43 (quin, *J* = 7.34 Hz, 2H), 1.33 (quin, *J* = 7.04 Hz, 2H), 1.25 (s, 9H), 0.97–1.14 (m, 1H), 0.89 (d, *J* = 6.65 Hz, 3H). ¹³C NMR (101 MHz, DMSO-*d*₆) δ: 165.2, 156.9, 143.0, 126.5, 114.3, 67.6, 57.8, 56.3, 51.9, 40.9, 34.2, 31.8, 30.6, 29.0, 28.9, 26.4, 25.6, 23.6, 22.6, 19.1. LC-MS: purity 100% *t*_R = 6.75, (ESI) *m/z* [M + H]⁺ 332.22. Anal. calcd. for C₂₄H₃₉NO₅: C, 68.37; H, 9.32; N, 3.32%. Found: C, 68.14; H, 9.20; N, 3.28%.

1-(3-(4-*tert*-Butylphenoxy)propyl)-3,3-dimethylpiperidine hydrogen oxalate (16). White solid, yield 44%, m.p. 183–186 °C, C₂₀H₃₃NO × C₂H₂O₄ (MW = 393.51). ¹H NMR (400 MHz, DMSO-*d*₆) δ: 7.30 (d, *J* = 8.61 Hz, 2H), 6.85 (d, *J* = 8.61 Hz, 2H), 3.99 (t, *J* = 5.67 Hz, 2H), 2.79–3.30 (m, 6H), 2.10 (br. s., 2H), 1.74 (br. s., 2H), 1.36 (br. s., 2H), 1.25 (s, 9H), 1.00 (s, 6H). ¹³C NMR (101 MHz, DMSO-*d*₆) δ: 164.7, 156.5, 143.4, 126.5, 114.4, 65.6, 62.1, 55.0, 52.8, 40.9, 35.3, 34.2, 31.8, 30.9, 24.2, 20.2. LC-MS: purity 100% *t*_R = 6.02, (ESI) *m/z* [M + H]⁺ 304.24. Anal. calcd. for C₂₂H₃₃NO₅: C, 67.14; H, 8.96; N, 3.56%. Found: C, 67.19; H, 8.50; N, 3.51%.

1-(4-(4-*tert*-Butylphenoxy)butyl)-3,3-dimethylpiperidine hydrogen oxalate (17). White solid, yield 23%, m.p. 140–142 °C, C₂₁H₃₅NO × C₂H₂O₄ (MW = 407.54). ¹H NMR (400 MHz, DMSO-*d*₆) δ: 7.28 (d, *J* = 8.61 Hz, 2H), 6.85 (d, *J* = 8.61 Hz, 2H), 3.95 (t, *J* = 5.87 Hz, 2H), 2.91–3.20 (m, 4H), 2.80 (br. s., 2H), 1.63–1.90 (m, 6H), 1.37 (d, *J* = 4.70 Hz, 2H), 1.25 (s, 9H), 0.99 (s, 6H). ¹³C NMR (101 MHz, DMSO-*d*₆) δ: 165.0, 156.7, 143.1, 126.5, 114.4, 67.2, 61.8, 57.1, 52.5, 40.9, 35.2, 34.2, 31.8, 30.9, 26.6, 20.8, 20.1. LC-MS: purity 100% *t*_R = 6.29, (ESI) *m/z* [M + H]⁺ 318.27. Anal. calcd. for C₂₃H₃₇NO₅: C, 67.78; H, 9.15; N, 3.44%. Found: C, 67.57; H, 9.03; N, 3.39%.

1-(5-(4-*tert*-Butylphenoxy)pentyl)-3,3-dimethylpiperidine hydrogen oxalate (18). White solid, yield 40%, m.p. 150–153 °C, C₂₂H₃₇NO × C₂H₂O₄ (MW = 421.56). ¹H NMR (400 MHz, DMSO-*d*₆) δ: 7.28 (d, *J* = 8.61 Hz, 2H), 6.84 (d, *J* = 9.00 Hz, 2H), 3.93 (t, *J* = 6.26 Hz, 2H), 2.88–3.24 (m, 4H), 2.81 (br. s., 2H), 1.61–1.83 (m, 6H), 1.30–1.45 (m, 4H), 1.25 (s, 9H), 0.99 (s, 6H). ¹³C NMR (101 MHz, DMSO-*d*₆) δ: 165.0, 156.8, 143.0, 126.5, 114.4, 67.4, 61.8, 57.3, 52.5, 40.9, 35.2, 34.2, 31.8, 30.9, 28.7, 23.4, 23.3, 20.0. LC-MS: purity 96.27% *t*_R = 6.58, (ESI) *m/z* [M + H]⁺ 332.29. Anal. calcd. for C₂₄H₃₉NO₅: C, 68.37; H, 9.32; N, 3.32%. Found: C, 67.94; H, 8.99; N, 3.24%.

1-(6-(4-*tert*-Butylphenoxy)hexyl)-3,3-dimethylpiperidine hydrogen oxalate (19). White solid, yield 21%, m.p. 122–125 °C, C₂₃H₃₉NO × C₂H₂O₄ (MW = 435.59). ¹H NMR (400 MHz, DMSO-*d*₆) δ: 7.27 (d, *J* = 8.61 Hz, 2H), 6.83 (d, *J* = 8.61 Hz, 2H), 3.83–4.01 (m, *J* = 6.46, 6.46 Hz, 2H), 2.75–3.13 (m, 6H), 1.57–1.83 (m, 6H), 1.29–1.54 (m, 6H), 1.25 (s, 9H), 0.99 (s, 6H). ¹³C NMR (101 MHz, DMSO-*d*₆) δ: 165.1, 156.9, 143.0, 126.5, 114.3, 67.6, 61.7, 57.3, 52.4, 40.9, 35.2, 34.2, 31.8, 30.9, 29.0, 26.4, 25.6, 23.5, 20.0. LC-MS: purity 94.18% *t*_R = 6.97, (ESI) *m/z* [M + H]⁺ 346.25. Anal. calcd. for C₂₅H₄₁NO₅: C, 68.93; H, 9.46; N, 3.22%. Found: C, 68.80; H, 9.26; N, 3.22%.

1-(3-(4-*tert*-Butylphenoxy)propyl)-3,5-dimethylpiperidine hydrogen oxalate (20). White solid, yield 43%, m.p. 143–145 °C, C₂₀H₃₃NO × C₂H₂O₄ (MW = 393.51). ¹H NMR (400 MHz, DMSO-*d*₆) δ: 7.29 (d, *J* = 9.00 Hz, 2H), 6.85 (d, *J* = 8.61 Hz, 2H), 4.00 (t, *J* = 5.67 Hz, 2H), 3.34 (d, *J* = 10.17 Hz, 2H), 2.97–3.23 (m, 2H), 2.40 (t, *J* = 11.93 Hz, 2H), 2.02–2.23 (m, 2H), 1.91 (d, *J* = 3.52 Hz, 2H), 1.73 (d, *J* = 12.91 Hz, 1H), 1.33–1.49 (m, 1H), 1.25 (s, 9H), 0.99 (d, *J* = 6.65 Hz, 6H). ¹³C NMR (101 MHz, DMSO-*d*₆) δ: 165.0, 156.5, 143.4, 126.5, 114.4, 65.5, 57.6, 53.9, 34.2, 31.8, 28.8, 24.1, 18.9. LC-MS: purity 15.62% *t*_R = 6.08, (ESI) *m/z* [M + H]⁺ 304.24 and purity 84.38% *t*_R = 6.15, (ESI) *m/z* [M + H]⁺ 304.24. Anal. calcd. for C₂₂H₃₅NO₅: C, 67.14; H, 8.96; N, 3.56%. Found: C, 67.03; H, 9.14; N, 3.52%.

1-(4-(4-*tert*-Butylphenoxy)butyl)-3,5-dimethylpiperidine hydrogen oxalate (21). White solid, yield 39%, m.p. 170–172 °C, C₂₁H₃₅NO × C₂H₂O₄ (MW = 407.54). ¹H NMR (400 MHz, DMSO-*d*₆) δ: 7.29 (d, *J* = 8.61 Hz, 2H), 6.85 (d, *J* = 8.61 Hz, 2H), 3.96 (t, *J* = 6.06 Hz, 2H), 3.31 (d, *J* = 9.78 Hz, 2H), 2.90–3.09 (m, 2H), 2.37 (t, *J* = 11.93 Hz, 2H), 1.61–2.02 (m, 7H), 1.13–1.44 (s, 10H), 0.87–1.04 (m, 6H). ¹³C NMR (101 MHz, DMSO-*d*₆) δ: 165.1, 156.9, 143.0, 126.5, 114.3, 67.6, 61.7, 57.3, 52.4, 40.9, 35.2, 34.2, 31.8, 30.9, 29.0, 26.4, 25.6, 23.5, 20.0. LC-MS: purity 94.18% *t*_R = 6.97, (ESI) *m/z* [M + H]⁺ 346.25. Anal. calcd. for C₂₃H₃₇NO₅: C, 67.78; H, 9.15; N, 3.44%. Found: C, 67.57; H, 9.03; N, 3.39%.

DMSO-*d*₆) δ: 165.0, 156.7, 143.2, 126.5, 114.4, 67.2, 57.4, 56.1, 34.2, 31.8, 28.7, 26.5, 20.8, 18.9. LC-MS: purity 11.21% *t*_R = 6.31, (ESI) *m/z* [M + H]⁺ 318.46 and purity 88.79% *t*_R = 6.37, (ESI) *m/z* [M + H]⁺ 318.46. Anal. calcd. for C₂₃H₃₇NO₅: C, 67.78; H, 9.15; N, 3.44%. Found: C, 68.14; H, 8.87; N, 3.40%.

1-(5-(4-tert-Butylphenoxy)pentyl)-3,5-dimethylpiperidine hydrogen oxalate (22). White solid, yield 31%, m.p. 175–178 °C, C₂₂H₃₇NO × C₂H₂O₄ (MW = 421.56). ¹H NMR (400 MHz, DMSO-*d*₆) δ: 7.28 (d, *J* = 8.61 Hz, 2H), 6.84 (d, *J* = 8.61 Hz, 2H), 3.94 (t, *J* = 6.06 Hz, 2H), 3.31 (d, *J* = 10.56 Hz, 2H), 2.80–3.06 (m, 2H), 2.36 (t, *J* = 11.74 Hz, 2H), 1.59–2.12 (m, 7H), 1.15–1.52 (m, 12H), 0.83–0.99 (m, 6H). ¹³C NMR (101 MHz, DMSO-*d*₆) δ: 164.9, 156.8, 143.1, 126.5, 114.4, 67.4, 57.5, 34.2, 31.8, 28.7, 23.5, 23.3, 18.9. LC-MS: purity 6.64% *t*_R = 6.73, (ESI) *m/z* [M + H]⁺ 332.29 and purity 93.36% *t*_R = 6.78, (ESI) *m/z* [M + H]⁺ 332.29. Anal. calcd. for C₂₄H₃₉NO₅: C, 68.37; H, 9.32; N, 3.32%. Found: C, 68.25; H, 9.06; N, 3.30%.

1-(6-(4-tert-Butylphenoxy)hexyl)-3,5-dimethylpiperidine hydrogen oxalate (23). White solid, yield 43%, m.p. 143–145 °C, C₂₃H₃₉NO × C₂H₂O₄ (MW = 345.56). ¹H NMR (400 MHz, DMSO-*d*₆) δ: 7.28 (d, *J* = 8.61 Hz, 2H), 6.84 (d, *J* = 8.61 Hz, 2H), 3.93 (t, *J* = 6.26 Hz, 2H), 3.30 (d, *J* = 10.17 Hz, 2H), 2.81–3.04 (m, 2H), 2.36 (t, *J* = 11.93 Hz, 2H), 1.88 (br. s., 2H), 1.60–1.78 (m, 5H), 1.20–1.53 (m, 14H), 0.89 (d, *J* = 6.65 Hz, 6H). ¹³C NMR (101 MHz, DMSO-*d*₆) δ: 164.9, 156.9, 143.0, 126.5, 114.4, 67.6, 57.5, 34.2, 31.8, 28.9, 26.4, 25.6, 23.7, 18.9. LC-MS: purity 5.30% *t*_R = 6.96, (ESI) *m/z* [M + H]⁺ 346.31 and purity 94.70% *t*_R = 7.00, (ESI) *m/z* [M + H]⁺ 346.31. Anal. calcd. for C₂₅H₄₁NO₅: C, 68.93; H, 9.49; N, 3.22%. Found: C, 68.74; H, 9.64; N, 3.19%.

1-(3-(4-tert-Butylphenoxy)propyl)-4-methylpiperidine hydrogen oxalate (24). White solid, yield 29%, m.p. 158–160 °C, C₁₉H₃₁NO × C₂H₂O₄ (MW = 379.48). ¹H NMR (500 MHz, DMSO-*d*₆) δ: 7.25 (d, *J* = 8.88 Hz, 2H), 6.81 (d, *J* = 8.59 Hz, 2H), 3.95 (t, *J* = 6.01 Hz, 8H), 3.35 (d, *J* = 11.74 Hz, 2H), 3.02–3.15 (m, 2H), 2.82 (t, *J* = 11.60 Hz, 2H), 2.00–2.11 (m, 2H), 1.72 (d, *J* = 13.17 Hz, 2H), 1.57 (d, *J* = 6.01 Hz, 1H), 1.29–1.43 (m, 2H), 1.20 (s, 9H), 0.88 (d, *J* = 6.59 Hz, 3H). ¹³C NMR (126 MHz, DMSO-*d*₆) δ: 165.2, 156.5, 143.4, 126.6, 114.5, 65.5, 53.8, 53.7, 52.2, 52.1, 52.1, 52.1, 34.3, 31.9, 31.2, 31.2, 31.1, 31.1, 31.1, 31.1, 31.0, 28.5, 24.2, 21.4, 21.4. LC-MS: purity 98.17% *t*_R = 5.84, (ESI) *m/z* [M + H]⁺ 290.22. Anal. calcd. for C₂₁H₃₃NO₅: C, 66.46; H, 8.76; N, 3.69%. Found: C, 65.97; H, 8.46; N, 3.63%.

1-(4-(4-tert-Butylphenoxy)butyl)-4-methylpiperidine hydrogen oxalate (25). White solid, yield 47%, m.p. 155–157 °C, C₂₀H₃₃NO × C₂H₂O₄ (MW = 393.51). ¹H NMR (400 MHz, DMSO-*d*₆) δ: 7.28 (d, *J* = 9.00 Hz, 2H), 6.85 (d, *J* = 9.00 Hz, 2H), 3.95 (t, *J* = 5.87 Hz, 2H), 3.37 (d, *J* = 11.74 Hz, 2H), 2.97–3.13 (m, 2H), 2.84 (t, *J* = 11.54 Hz, 2H), 1.67–1.90 (m, 6H), 1.61 (d, *J* = 5.87 Hz, 1H), 1.33–1.50 (m, 2H), 1.25 (s, 9H), 0.91 (d, *J* = 6.65 Hz, 3H). ¹³C NMR (101 MHz, DMSO-*d*₆) δ: 165.2, 156.7, 143.1, 126.5, 114.4, 67.2, 55.8, 51.8, 40.9, 34.2, 31.8, 30.9, 28.5, 26.5, 21.3, 20.9. LC-MS: purity 99.02% *t*_R = 6.07, (ESI) *m/z* [M + H]⁺ 304.24. Anal. calcd. for C₂₂H₃₅NO₅: C, 67.14; H, 8.96; N, 3.56%. Found: C, 67.41; H, 8.48; N, 3.56%.

1-(5-(4-tert-Butylphenoxy)pentyl)-4-methylpiperidine hydrogen oxalate (26). White solid, yield 8%, m.p. 167–170 °C, C₂₁H₃₅NO × C₂H₂O₄ (MW = 407.54). ¹H NMR (400 MHz, DMSO-*d*₆) δ: 7.28 (d, *J* = 8.61 Hz, 2H), 6.84 (d, *J* = 8.61 Hz, 2H), 3.94 (t, *J* = 6.26 Hz, 2H), 3.31–3.41 (m, 2H), 2.93–3.03 (m, 2H), 2.77–2.87 (m, 2H), 1.64–1.82 (m, 6H), 1.54–1.64 (m, 1H), 1.32–1.48 (m, 4H), 1.20–1.31 (m, 9H), 0.92 (d, *J* = 6.26 Hz, 3H). ¹³C NMR (101 MHz, DMSO-*d*₆) δ: 165.0, 156.8, 143.0, 126.5, 114.4, 67.4, 40.9, 34.2, 31.8, 28.7, 23.6, 23.3. LC-MS: purity 92.34% *t*_R = 6.34, (ESI) *m/z* [M + H]⁺ 318.20. Anal. calcd. for C₂₃H₃₇NO₅: C, 67.78; H, 9.15; N, 3.44%. Found: C, 67.65; H, 8.81; N, 3.42.

1-(6-(4-tert-Butylphenoxy)hexyl)-4-methylpiperidine hydrogen oxalate (27). White solid, yield 12%, m.p. 136–139 °C, C₂₂H₃₇NO × C₂H₂O₄ (MW = 421.56). ¹H NMR (400 MHz, DMSO-*d*₆) δ: 7.27 (d, *J* = 8.61 Hz, 2H), 6.83 (d, *J* = 9.00 Hz, 2H), 3.92 (t, *J* = 6.46 Hz, 2H), 3.36 (d, *J* = 11.74 Hz, 2H), 2.89–3.03 (m, 2H), 2.76–2.87 (m, 2H), 1.54–1.82 (m, 7H), 1.29–1.48 (m, 6H), 1.25 (s, 9H), 0.91 (d, *J* = 6.26 Hz, 3H). ¹³C NMR (101 MHz, DMSO-*d*₆) δ: 165.3, 156.9, 143.0, 126.5, 114.3, 67.6, 56.0, 51.8, 40.9, 34.2, 31.8, 30.9, 29.0, 28.5, 26.4, 25.6, 23.7, 21.3. LC-MS: purity 98.49% *t*_R = 6.77, (ESI) *m/z* [M + H]⁺ 332.22. Anal. calcd. for C₂₄H₃₉NO₅: C, 68.37; H, 9.32; N, 3.32%. Found: C, 68.51; H, 9.40; N, 3.30%.

1-(3-(4-tert-Butylphenoxy)propyl)-azepane hydrogen oxalate (28). White solid, yield 32%, m.p. 138–140 °C, C₁₉H₃₁NO × C₂H₂O₄ (MW = 379.48). ¹H NMR (500 MHz, DMSO-*d*₆) δ: 7.24 (d, *J* = 3.15 Hz, 2H), 6.81 (d, *J* = 2.86 Hz, 2H), 3.95 (br. s., 2H), 2.88–3.47 (m, 6H), 2.08 (br. s., 2H), 1.76 (br. s., 4H), 1.56 (br. s., 4H), 1.20 (br. s., 9H). ¹³C NMR (126 MHz, DMSO-*d*₆) δ: 165.5, 156.6, 143.4, 126.6, 114.5, 65.5, 54.3, 54.1, 34.3, 31.9, 26.6, 24.4, 23.6. LC-MS: purity 99.17% *t*_R = 5.82, (ESI) *m/z* [M + H]⁺ 290.22. Anal. calcd. for C₂₁H₃₃NO₅: C, 66.46; H, 8.76; N, 3.69%. Found: C, 65.74; H, 8.41; N, 3.65%.

1-(4-(4-tert-Butylphenoxy)butyl)-azepane hydrogen oxalate (29). White solid, yield 49%, m.p. 149–151 °C, C₂₀H₃₃NO × C₂H₂O₄ (MW = 393.51). ¹H NMR (400 MHz, DMSO-*d*₆) δ: 7.28 (d, *J* = 8.22 Hz, 2H), 6.85 (d, *J* = 7.82 Hz, 2H), 3.95 (t, *J* = 5.67 Hz, 2H), 3.16–3.32 (m, 4H), 3.11 (d, *J* = 7.04 Hz, 2H), 1.68–1.89 (m, 8H), 1.60 (br. s., 4H), 1.25 (s, 9H). ¹³C NMR (101 MHz, DMSO-*d*₆) δ: 165.3, 156.7, 143.1, 126.5, 114.4, 67.2, 56.4, 53.9, 40.9, 34.2, 31.8, 26.6, 26.5, 23.5, 21.2. LC-MS: purity 99.24% *t*_R = 6.01, (ESI) *m/z* [M + H]⁺ 304.24. Anal. calcd. for C₂₂H₃₅NO₅: C, 67.14; H, 8.96; N, 3.56%. Found: C, 67.40; H, 8.51; N, 3.55%.

1-(5-(4-tert-Butylphenoxy)pentyl)-azepane hydrogen oxalate (30). White solid, yield 38%, m.p. 151–153 °C, C₂₁H₃₅NO × C₂H₂O₄ (MW = 407.53). ¹H NMR (400 MHz, DMSO-*d*₆) δ: 7.28 (d, *J* = 8.61 Hz, 2H), 6.84 (d, *J* = 9.00 Hz, 2H), 3.93 (t, *J* = 6.26 Hz, 2H), 3.13–3.32 (m, 4H), 2.94–3.08 (m, 2H), 1.79 (br. s., 4H), 1.66–1.75 (m, 4H), 1.54–1.64 (m, 4H), 1.43 (d, *J* = 7.43 Hz, 2H), 1.25 (s, 9H). ¹³C NMR (101 MHz, DMSO-*d*₆) δ: 165.3, 156.8, 143.0, 126.5, 114.4, 67.5, 56.6, 53.9, 40.9, 34.2, 31.8, 28.7, 26.6, 23.8, 23.4, 23.3. LC-MS: purity 100% *t*_R = 6.27, (ESI) *m/z* [M + H]⁺ 366.25. Anal. calcd. for C₂₃H₃₇NO₅: C, 67.78; H, 9.15; N, 3.44%. Found: C, 67.47; H, 8.75; N, 3.39%.

1-(6-(4-tert-Butylphenoxy)hexyl)-azepane hydrogen oxalate (31). White solid, yield 5%, m.p. 130–132 °C, C₂₂H₃₇NO × C₂H₂O₄ (MW = 421.56). ¹H NMR (400 MHz, DMSO-*d*₆) δ: 7.27 (d, *J* = 8.61 Hz, 2H), 6.83 (d, *J* = 8.61 Hz, 2H), 3.92 (t, *J* = 6.46 Hz, 2H), 3.16–3.23 (m, 4H), 2.98–3.04 (m, 2H), 1.58–1.82 (m, 12H), 1.28–1.47 (m, 4H), 1.25 (s, 9H). ¹³C NMR (101 MHz, DMSO-*d*₆) δ: 165.3, 156.8, 143.0, 126.5, 114.3, 67.6, 56.7, 53.9, 40.9, 34.2, 31.8, 29.0, 26.6, 26.4, 25.6, 24.0, 23.4. LC-MS: purity 97.93% *t*_R = 6.79, (ESI) *m/z* [M + H]⁺ 332.22. Anal. calcd. for C₂₄H₃₉NO₅: C, 68.37; H, 9.32; N, 3.32%. Found: C, 68.46; H, 8.98; N, 3.32%.

3.2. Biological Studies In Vitro

3.2.1. Affinity for Human Histamine H₃ Receptor

The radioligand displacement binding assay was carried out in HEK-293 cells stably expressing the recombinant hH₃R as described by Kottke et al. [23] with slight modifications [14]. [³H]N^α-methylhistamine was used as radiolabeled tracer (2 nM, K_D = 3.08). Obtained data from at least three experiments (in at least duplicates) were analyzed with GraphPad Prism 6.1 (San Diego, CA, USA) using nonlinear regression (one-site competition on logarithmic scale), and K_i values were transformed from IC₅₀ according to Cheng-Prusoff [24]. Statistical analysis was performed on –log K_i values. Mean values and 95% confidence intervals were converted to nanomolar concentrations.

3.2.2. Human Monoamine Oxidase Inhibitory Activity

General Method for Determining Activity Against MAO Isoforms

Inhibitory potency of compounds on MAO isoenzymes were carried out by a fluorometric method with a commercial AmplexTM Red Monoamine Oxidase Assay Kit (ThermoFisher Scientific A12214, Waltham, MA, USA) as described previously [12,25]. For all tests, recombinant human MAO B and MAO A (from Sigma Aldrich M7441 and M7316, Darmstadt, Germany) were used. Inhibitors' activity was measured in the presence of p-tyramine (200 μM). In all experiments, reference inhibitors in the concentrations that fully inhibited the MAO isoform were included. Reference inhibitors for MAO-B were pargyline 10 μM, rasagiline 1 μM, and safinamide 1 μM and, for MAO-A, was clorgyline 1 μM.

Screening and Determination of IC₅₀

Firstly, inhibitors' activity was measured in a concentration of 1 μ M. The results were normalized (no inhibition = 0% and fully inhibited enzyme 100%). For compounds that inhibited the enzyme by more than 50%, further studies were conducted to obtain IC₅₀ from concentration–response curves. All calculations were made in Microsoft Excel and GraphPadPrism software. All experiments were performed in duplicate, and data are expressed as mean \pm SEM of 2–5 independent experiments.

Reversibility Studies

Reversibility of MAO B inhibitors was tested as described previously [12] with slight modification. Two experiments were performed simultaneously. In the first experiment, inhibitors (in concentrations corresponding to their IC₈₀ values) were incubated with the enzyme and p-tyramine (10 μ M) for 22 min (measuring fluorescence every two minutes). Next, the concentration of the substrate was increased to 1 mM and the fluorescence was measured every 5 min for 5 h. In the second experiment, inhibitors and enzyme were preincubated for 30 min in room temperature before addition of 10 μ M p-tyramine; then, continuation of the experiment was carried out identically as the first.

Kinetic Studies

The mode of the inhibition was tested according to the standard procedure described in Reversibility Studies using different concentrations of the substrate [12,26]. Inhibitors (compound 9 and DL76) were used in three concentrations corresponding to their IC₂₀, IC₅₀, and IC₈₀ values. Substrate was used in six concentrations: 0.05 mM, 0.1 mM, 0.5 mM, 1 mM, 1.5 mM, and 2 mM. After the experiment, velocities were calculated and put on the graph (*y*-axis) against the concentration of the substrate (*x*-axis). From the Michaelis–Menten plot V_{max} , K_M , and α values were calculated for different concentrations of the inhibitor. Double-reciprocal plot (Lineweaver–Burk plot) were prepared to display the data.

3.2.3. Toxicity and Neuroprotection Evaluation In Vitro

Cell Lines

SH-SY5Y CRL-2266™ neuroblastoma cell line was purchased directly from American Type Culture Collection (Manassas, VA, USA) and were cultured as described previously [20]. Human embryonic kidney HEK-293 cell line (ATCC CRL-1573) was kindly donated by Prof. Dr Christa Müller (Pharmaceutical Institute, Pharmaceutical Chemistry I, University of Bonn, Germany). The cells were cultured as described previously [27].

Toxicity Studies

The HEK-293 cells were seeded at a concentration of 1.5×10^4 cells/well in 200 μ L culture medium and incubated for 24 h at 37 °C and 5% CO₂. Next, the cytostatic reference doxorubicin (DX) or DL76 dissolved in DMSO were added at various concentrations into microplate (total concentration of DMSO in media was 1%) and incubated for 48 h at 37 °C and 5% CO₂. Then, 25 μ L EZ4U labelling mixture (Biomedica, Vienna, Austria) was added and the cells were incubated for 2 h. The spectrophotometric absorbance of the samples was measured using a microplate reader (EnSpire, PerkinElmer, Waltham, MA, USA) at 492 nm. All measurements were performed in triplicate, and results are shown as mean \pm SD.

Neuroprotection Studies

SH-SY5Y cells were seeded in microplate at a concentration of 2.5×10^4 cells/well in 100 μ L culture medium and cultured for 24 h at 37 °C and 5% CO₂ to reach 70% confluence. The cells were preincubated first for 1 h with DL76 (10 and 50 μ M) or with the reference neuroprotectant salsolinol.

(R,S)-salsolinol (purity $\geq 99\%$) was obtained from Cayman Chemical (Ann Arbor, MI, USA). Next, H₂O₂ was added at final concentration 300 μ M and the cells were placed into the incubator. After 24 h of compounds co-incubation with H₂O₂, the CellTiter 96[®] AQueous Non-Radioactive Cell Proliferation Assay (MTS) labeling mixture was added to each well, and the microplates were incubated under the same conditions for 5 h. The absorbance was measured using a microplate reader EnSpire (PerkinElmer, Waltham, MA USA) at 490 nm. All measurements were performed in triplicate, and results are shown as mean \pm SD.

3.3. Antiparkinsonian Activity in Haloperidol-Induced Catalepsy In Vivo

3.3.1. Animals

The experiments were carried out on male rats Wistar (180–220 g). Animals were housed in plastic cages in room at a constant temperature of 20 ± 2 °C with natural light–dark cycles. The animals had free access to standard pellet diet and water and were used after a minimum of 3 days of acclimatization to the housing conditions. Control and experimental groups consisted of 6 animals each. All experimental procedures were performed according to the European Union Directive of 22 September 2010 (2010/63/EU) and Polish legislation concerning animal care and use and was approved by the Local Ethics Committee for Experiments on Animals in Kraków, Poland (Resolution No. 70/2014, approval date: 20 May 2014). The examined compound was administered as the suspension in 0.5% methylcellulose in constant volume of 10 mL/kg.

3.3.2. Drugs

Haloperidol was purchased from Sigma Aldrich (Darmstadt, Germany). MSX-3 ((E)-phosphoric acid mono-[3-[8-[2-(3-methoxyphenyl)vinyl]-7-methyl-2,6-dioxo-1-prop-2-ynyl-1,2,6,7-tetrahydro-purin-3-yl]propyl] ester disodium salt) was synthesized in the laboratory of Pharmaceutical Institute, Pharmaceutical Chemistry I, University of Bonn, Germany and donated by Prof. Dr Christa Müller.

3.3.3. Statistical Analysis

The data are expressed as the means \pm SEM. All statistical calculations were carried out with the GraphPad Prism 5 program. The data were evaluated by one-way analysis of variance (ANOVA) followed by Duncan test; $p < 0.05$ was considered significant.

3.3.4. Determination of Antiparkinsonian Activity in Catalepsy Tests

Antiparkinsonian activity in catalepsy tests was performed as described in [28]. Haloperidol was administered s.c. at a dose of 0.63 mg/kg, which in 100% of control animals caused catalepsy. Tested compounds were administered i.p. at the doses 50 and 25 mg/kg body weight, 5 min after haloperidol injection. After 60 min from the injection of haloperidol, to assess the occurrence of catalepsy, the animals were placed in a forced position and the time they remained in this position was measured. Two tests were performed to determine the antiparkinsonian activity: crossed leg position test and bar test. In the first test, the animals were put on the hind paws behind the front (forced position); in the second, the animals were supported on a wooden block (the front paws were placed on a block suspended 10 cm above the ground). Then, the time that the animals remain is measured in a forced position (time was measured to a maximum of 60 s). Observation was carried out 3 times in 3-min intervals. The shortening of the time of catalepsy to the control group was adopted for the antiparkinsonian activity.

4. Conclusions

In summary, in this study, new potential DTL for PD have been designed and synthesized. As the lead structure, DL76 was chosen, the compound with proven high hH₃R affinity ($K_i = 22$ nM [13] in CHO K1 cells and $K_i = 38$ nM in HEK 293 cells) and hMAO B inhibitory activity in vitro ($IC_{50} = 48$ nM).

The introduced modifications were aimed at assessing the influence of cyclic amines and the length of the alkyl chain on hH₃R affinity and hMAO B inhibition. Most compounds showed nanomolar range affinities for hH₃R. The significant increase in the inhibitory effect for hMAO B occurred for pyrrolidine (5) and 2-methylpiperidine (9) derivatives. These results confirmed our previous observations concerning 4-*tert*-amylphenoxy derivatives [12] where such compounds were among the most potent hMAO B inhibitors.

In vitro toxicity studies with **DL76** in the HEK293 cells and neuroblastoma SH-SY5Y cells did not show risk of toxicity at the dose of 50 µM of this compound. However, no neuroprotection effect of **DL76** against very high toxic levels of hydrogen peroxide (300 µM) in neuroblastoma SH-SY5Y cells was observed.

Conducted in vivo studies showed that tested **DL76** caused just statistically significant antiparkinsonian activity in the crossed-leg position test. The tested compound, at the dose of 50 mg/kg body weight, practically completely reduced the duration of catalepsy, whereas in the bar test at this dose, a low positive effect was observed. Moreover, **DL76** did not show any cataleptic effects.

Considering the dual functional profile, the most valuable compound proved to be **DL76** with balanced activity against both biological targets (hH₃R K_i = 38 nM and hMAO B IC₅₀ = 48 nM). Structural modification in DTL is not easy as it requires optimization towards both targets. By direct exchange of a cyclic amine, it was possible to obtain a very potent hMAO B inhibitor, compound 5 with the IC₅₀ of 2.7 nM. However, this compound proved to be only a moderate hH₃R ligand (K_i = 371 nM). Generally, very potent hMAO B inhibitors (5, 9, and 28) showed higher strength to inhibit hMAO B than to block hH₃R. Thus, it seems that, in this class of compounds, a cyclic amine moiety in the western part of a molecule plays the very important role in the interaction with hMAO B, but further studies should be performed to confirm it. However, the presented compounds are promising starting materials in further search for new active DTL for PD.

Supplementary Materials: Supplementary Materials can be found at <http://www.mdpi.com/1422-0067/21/10/3411/s1>.

Author Contributions: Conceptualization, D.L. and K.K.-K.; synthesis of compounds: M.K.; in vitro hMAO B and A studies: A.O.-M., A.D.-P., and T.K.; in vitro hMAO B kinetic and reversibility studies: A.O.-M.; in vitro histamine H₃R affinity: D.R., A.F., and H.S.; supervision of in vitro H₃R studies: H.S.; in vivo studies: M.Z.; in vitro toxicity and neuroprotection studies: G.L.; writing—original draft preparation: D.L.; writing—review and editing: D.L. and K.K.-K.; project administration, D.L. All authors have read and agreed to the published version of the manuscript.

Funding: This research was funded by National Science Centre, Poland grant no. UMO-2016/23/B/NZ7/02327 (D.L.), UMO-2019/03/X/NZ7/00180 (G.L.), and DFG INST 208/664-1 FUGG (H.S.). Further, the authors acknowledge the contribution of EU-COST action CA18133 ERNEST (“European Research Network on Signal Transduction”).

Acknowledgments: The generous gift of MSX-3 and human embryonic kidney HEK-293 cell line (ATCC CRL-1573) by Christa Müller (University of Bonn, Germany) is gratefully acknowledged.

Conflicts of Interest: The authors declare no conflict of interest.

Abbreviations

AChE	Acetylcholinesterase
BuChE	Butyrylcholinesterase
DA	Dopamine
DMSO	Dimethyl sulfoxide
DTL	Dual Target Ligands
DX	Doxorubicin
H ₃ R	Histamine H ₃ receptor
HEK293	Human embryonic kidney
i.p.	Intraperitoneal
MAO B	Monoamine oxidase B
MTDL	Multi-Target-Directed Ligands
PD	Parkinson’s disease
PEA	β-phenylethylamine

SAL Salsolinol
s.c. Subcutaneous
TLC Thin-layer Chromatography

References

1. Draoui, A.; El Hiba, O.; Aimrane, A.; El Khat, A.; Gamrani, H. Parkinson's disease: From bench to bedside. *Rev. Neurol.* **2020**, in press. [\[CrossRef\]](#)
2. Szökő, É.; Tábi, T.; Riederer, P.; Vécsei, L.; Magyar, K. Pharmacological aspects of the neuroprotective effects of irreversible MAO-B inhibitors, selegiline and rasagiline, in Parkinson's disease. *J. Neural. Transm.* **2018**, *125*, 1735–1749. [\[CrossRef\]](#) [\[PubMed\]](#)
3. Proschak, E.J.; Stark, H.; Merk, D. Polypharmacology by Design: A Medicinal Chemist's Perspective on Multitargeting Compounds. *J. Med. Chem.* **2019**, *62*, 420–444. [\[CrossRef\]](#) [\[PubMed\]](#)
4. Panula, P.; Chazot, P.L.; Cowart, M.; Gutzmer, R.; Leurs, R.; Liu, W.L.; Stark, H.; Thurmond, R.L.; Haas, H.L. International Union of Basic and Clinical Pharmacology. XCVIII. Histamine Receptors. *Pharmacol. Rev.* **2015**, *67*, 601–655. [\[CrossRef\]](#) [\[PubMed\]](#)
5. Sadek, B.; Łażewska, D.; Hagenow, S.; Kieć-Kononowicz, K.; Stark, H. Histamine H₃R antagonists: From scaffold hopping to clinical candidates. In *Histamine Receptors*; Blandina, P., Passani, M.B., Eds.; Springer International Publishing: Cham, Switzerland, 2016; pp. 109–156.
6. Lamb, Y.N. Pitolisant: A Review in Narcolepsy with or without Cataplexy. *CNS Drugs.* **2020**, *34*, 207–218. [\[CrossRef\]](#)
7. Zhou, J.; Jiang, X.; He, S.; Jiang, H.; Feng, F.; Liu, W.; Qu, W.; Sun, H. Rational Design of Multitarget-Directed Ligands: Strategies and Emerging Paradigms. *J. Med. Chem.* **2019**, *62*, 8881–8914. [\[CrossRef\]](#)
8. Zindo, F.T.; Joubert, J.; Malan, S.F. Propargylamine as functional moiety in the design of multifunctional drugs for neurodegenerative disorders: MAO inhibition and beyond. *Future Med. Chem.* **2015**, *7*, 609–629. [\[CrossRef\]](#)
9. Bautista-Aguilera, Ó.M.; Hagenow, S.; Palomino-antolin, A.; Farré-Alins, V.; Ismaili, L.; Joffrin, P.L.; Jimeno, M.L.; Soukup, O.; Janočková, J.; Kalinowsky, L.; et al. Multitarget-directed ligands combining cholinesterase and monoamine oxidase inhibition with histamine H₃R antagonism for neurodegenerative diseases. *Angew. Chem. Int. Ed. Engl.* **2018**, *56*, 12765–12769. [\[CrossRef\]](#)
10. Lutsenko, K.; Hagenow, S.; Affini, A.; Reiner, D.; Stark, H. Rasagiline derivatives combined with histamine H₃ receptor properties. *Bioorg. Med. Chem. Lett.* **2019**, *29*, 126612. [\[CrossRef\]](#)
11. Affini, A.; Hagenow, S.; Zivkovic, A.; Marco-Contelles, J.; Stark, H. Novel indanone derivatives as MAO B/H₃R dual-targeting ligands for treatment of Parkinson's disease. *Eur. J. Med. Chem.* **2018**, *148*, 487–497. [\[CrossRef\]](#)
12. Łażewska, D.; Olejars-Maciej, A.; Kaleta, M.; Bajda, M.; Siwek, A.; Karcz, T.; Doroz-Płonka, A.; Cichor, U.; Kuder, K.; Kieć-Kononowicz, K. 4-tert-Pentylphenoxyalkyl derivatives—Histamine H₃ receptor ligands and monoamine oxidase B inhibitors. *Bioorg. Med. Chem. Lett.* **2018**, *28*, 3596–3600. [\[CrossRef\]](#) [\[PubMed\]](#)
13. Łażewska, D.; Ligneau, X.; Schwartz, J.C.; Schunack, W.; Stark, H.; Kieć-Kononowicz, K. Ether derivatives of 3-piperidinopropan-1-ol as non-imidazole histamine H₃ receptor antagonists. *Bioorg. Med. Chem.* **2006**, *14*, 3522–3529. [\[CrossRef\]](#) [\[PubMed\]](#)
14. Kuder, K.J.; Łażewska, D.; Latacz, G.; Schwed, J.S.; Karcz, T.; Stark, H.; Karolak-Wojciechowska, J.; Kieć-Kononowicz, K. Chlorophenoxyaminoalkyl derivatives as histamine H₃R ligands and antiseizure agents. *Bioorg. Med. Chem.* **2016**, *24*, 53–72. [\[CrossRef\]](#) [\[PubMed\]](#)
15. Zhou, M.; Panchuk-Voloshina, N. A one-step fluorometric method for the continuous measurement of monoamine oxidase activity. *Anal. Biochem.* **1997**, *253*, 169–174. [\[CrossRef\]](#)
16. Podlowska, S.; Latacz, G.; Łażewska, D.; Kieć-Kononowicz, K.; Handzlik, J. In silico and in vitro studies on interaction of novel non-imidazole histamine H₃R ligands with CYP3A4. *Bioorg. Med. Chem. Lett.* **2020**, *30*, 127147. [\[CrossRef\]](#) [\[PubMed\]](#)
17. Copeland, R.A. *Evaluation of Enzyme Inhibitors in Drug Discovery. A Guide for Medicinal Chemists and Pharmacologists*; John Wiley & Sons, Inc.: Hoboken, NJ, USA, 2005.
18. Ramsay, R.R.; Tipton, K.F. Assessment of Enzyme Inhibition: A Review with Examples from the Development of Monoamine Oxidase and Cholinesterase Inhibitory Drugs. *Molecules* **2017**, *22*, 1192. [\[CrossRef\]](#)

19. Copeland, R.A. *Enzymes: A Practical Introduction to Structure, Mechanism, and Data Analysis*, 2nd ed.; Wiley-VCH: New York, NY, USA, 2000; ISBN 0-471-22063-9.
20. Kurnik-Łucka, M.; Latacz, G.; Martyniak, A.; Bugajski, A.; Kieć-Kononowicz, K.; Gil, K. Salsolinol-neurotoxic or neuroprotective? *Neurotox. Res.* **2020**, *37*, 286–297. [[CrossRef](#)]
21. Duty, S.; Jenner, P. Animal models of Parkinson's disease: A source of novel treatments and clues to the cause of the disease. *Br. J. Pharmacol.* **2011**, *164*, 1357–1391. [[CrossRef](#)]
22. Hauber, W.; Neuscheler, P.; Nagel, J.; Müller, C.E. Catalepsy induced by a blockade of dopamine D1 or D2 receptors was reversed by a concomitant blockade of adenosine A(2A) receptors in the caudate-putamen of rats. *Eur. J. Neurosci.* **2001**, *14*, 1287–1293. [[CrossRef](#)]
23. Kottke, T.; Sander, K.; Weizel, L.; Schneider, E.H.; Seifert, R.; Stark, H. Receptor-specific functional efficacies of alkyl imidazoles as dual histamine H₃/H₄ receptor ligands. *Eur. J. Pharmacol.* **2011**, *654*, 200–208. [[CrossRef](#)]
24. Cheng, Y.C.; Prusoff, W. Relationship between the inhibition constant (KI) and the concentration of inhibitor which causes 50 per cent inhibition (I50) of an enzymatic reaction. *Biochem. Pharmacol.* **1973**, *22*, 3099–3108. [[CrossRef](#)] [[PubMed](#)]
25. Zaluski, M.; Schabikowski, J.; Schlenk, M.; Olejarsz-Maciej, A.; Kubas, B.; Karcz, T.; Kuder, K.; Latacz, G.; Zygmunt, M.; Synak, D.; et al. Novel multi-target directed ligands based on annelated xanthine scaffold with aromatic substituents acting on adenosine receptor and monoamine oxidase B. Synthesis, in vitro and in silico studies. *Bioorg. Med. Chem.* **2019**, *27*, 1195–1210. [[CrossRef](#)] [[PubMed](#)]
26. Tzvetkov, N.T.; Hinz, S.; Küppers, P.; Gastreich, M.; Müller, C.E. Indazole-and Indole-5-Carboxamides: Selective and Reversible Monoamine Oxidase B Inhibitors with Subnanomolar Potency. *J. Med. Chem.* **2014**, *57*, 6679–6703. [[CrossRef](#)] [[PubMed](#)]
27. Latacz, G.; Kechagioglou, P.; Papi, R.; Łażewska, D.; Wiecek, M.; Kamińska, K.; Wencel, P.; Karcz, T.; Schwed, J.S.; Stark, H.; et al. The Synthesis of 1,3,5-triazine Derivatives and JNJ7777120 Analogues with Histamine H₄ Receptor Affinity and Their Interaction with PTEN Promoter. *Chem. Biol. Drug Des.* **2016**, *88*, 254–263. [[CrossRef](#)] [[PubMed](#)]
28. Prinssen, E.P.M.; Kleven, M.S.; Koek, W. Interactions between neuroleptics and 5-HT_{1A} ligands in preclinical behavioral models for antipsychotic and extrapyramidal effects. *Psychopharmacology* **1999**, *144*, 20–29. [[CrossRef](#)] [[PubMed](#)]



© 2020 by the authors. Licensee MDPI, Basel, Switzerland. This article is an open access article distributed under the terms and conditions of the Creative Commons Attribution (CC BY) license (<http://creativecommons.org/licenses/by/4.0/>).

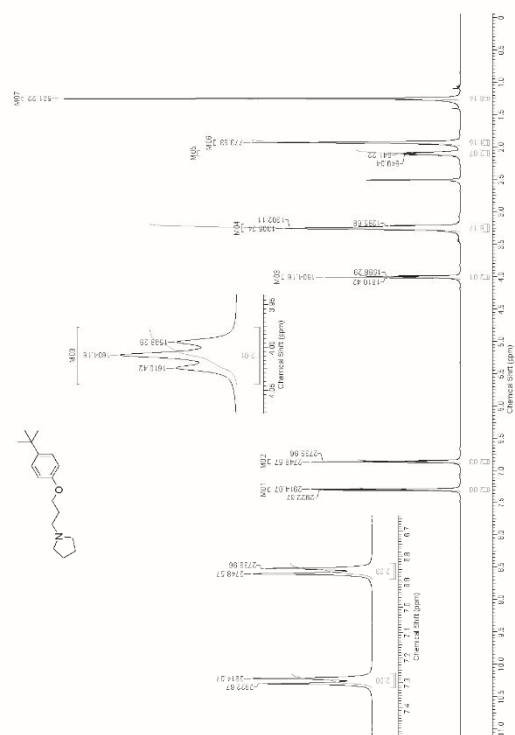


Fig S1. ¹H NMR spectrum of 5

Supplementary Materials S1

Dual target ligands with 4-*tert*-butylphenoxy scaffold as histamine H₃ receptor antagonists and monoamine oxidase B inhibitors

Dorota Łazewska¹, Agnieszka Olejarska-Maciej¹, David Reiner², Maria Kaleta¹, Gniewomir Łatacz¹, Małgorzata Zygmunt¹, Agata Dorosz-Płonka¹, Tadeusz Karcz¹, Annika Frank², Holger Stark² and Katarzyna Kieć-Kononowicz^{1*}

¹Department of Technology and Biotechnology of Drugs, Jagiellonian University Medical College, 9 Medyczna str, 30-688 Kraków, Poland; agnieszka.olejarska@um.edu.pl (A.O.-M); maria.kaleta@um.edu.pl (M.K.); glatacz@cm-sul.krakow.pl (G.L.); adorosz-plonka@um.edu.pl (A.D.-P); t.karcz@um.edu.pl (T.K.); mikonosieczny@krakow.pl (K.K.K.)

²Institute of Pharmaceutical and Medicinal Chemistry, Heinrich Heine University Düsseldorf, Universitätsstr. 1, 40225 Düsseldorf, Germany; david.reiner@hhu.de (D.R.); a.frank@hhu.de (A.F.); stark@hhu.de (H.S.)

³Department of Pharmacodynamics, Jagiellonian University Medical College, 9 Medyczna str, 30-688, Kraków, Poland; malgorzata.zygmunt@um.edu.pl (M.Z.)

*Correspondence: lazewska@cm-sul.krakow.pl (D.L.); mikonosieczny@krakow.pl (K.K.K.)

¹H NMR and ¹³C NMR data of synthesized compounds

4.2 Dual target ligands with 4-tert-butylphenoxy scaffold as histamine H₃ receptor antagonists and monoamine oxidase B inhibitors

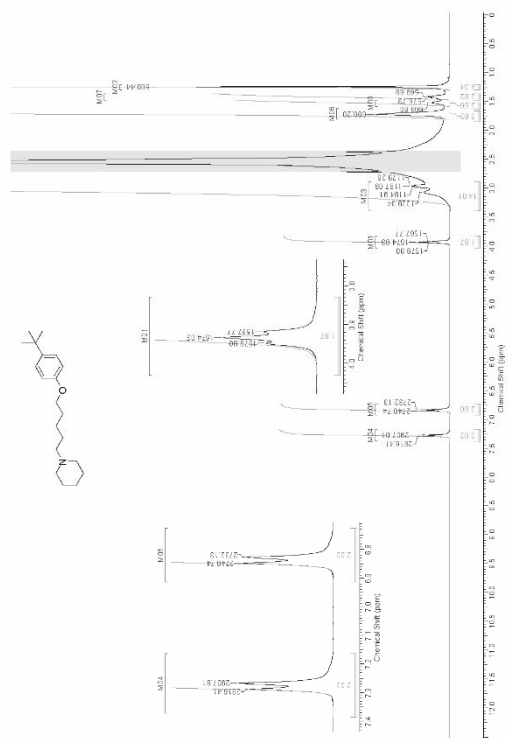
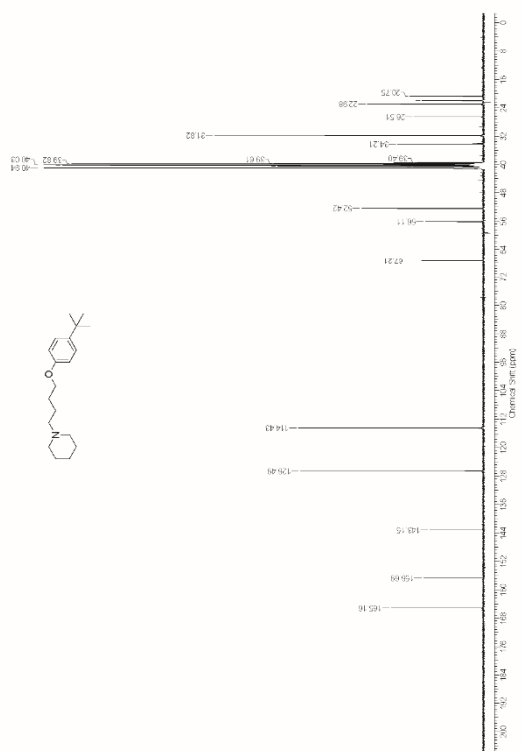


Fig S8. ¹³C NMR spectrum of 9

Fig S9. ^1H NMR spectrum of **9**

Fig S8. ^{13}C NMR spectrum of **8**

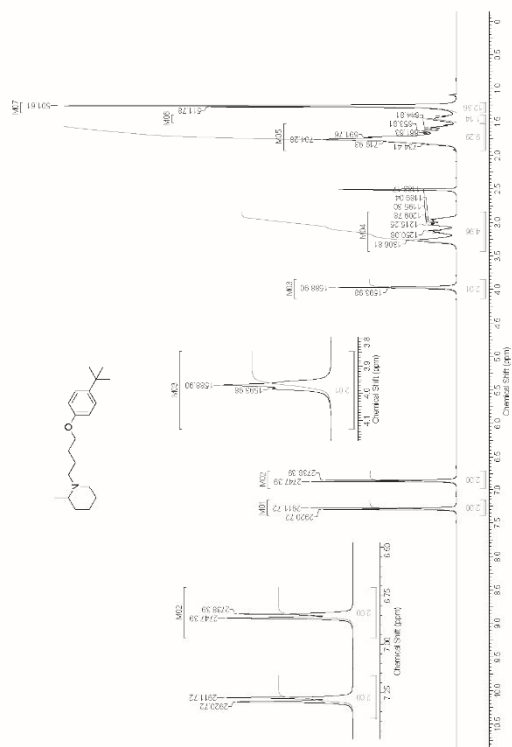


Fig S11. ¹H NMR spectrum of 10

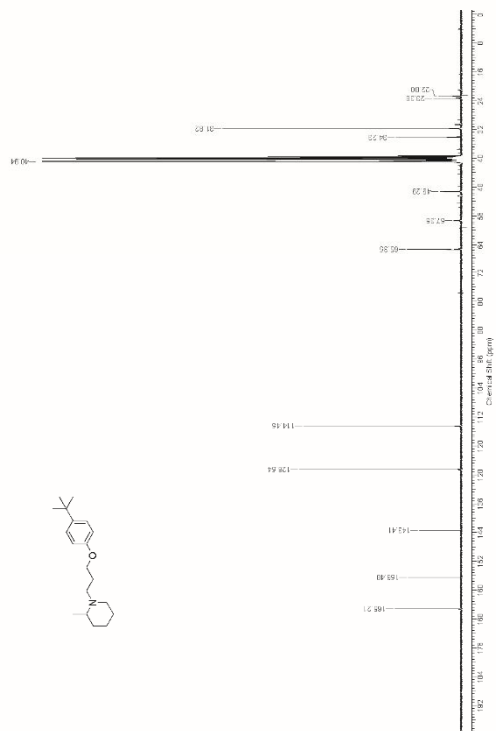


Fig S10. ¹³C NMR spectrum of 9

4.2 Dual target ligands with 4-tert-butylphenoxy scaffold as histamine H₃ receptor antagonists and monoamine oxidase B inhibitors

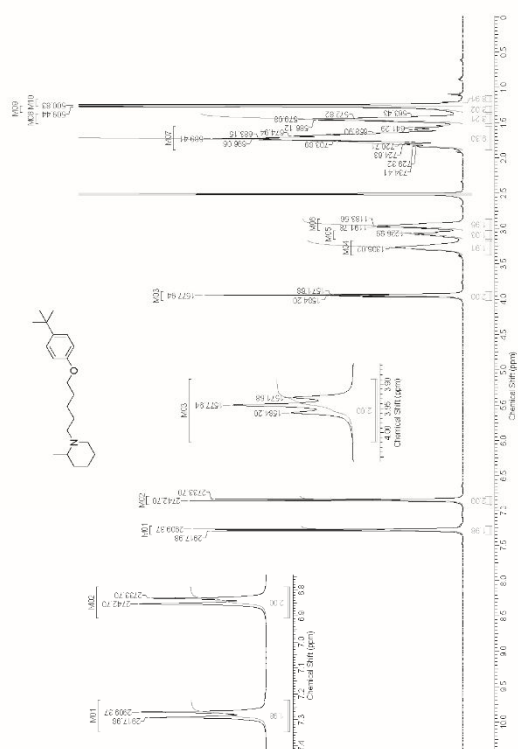


Fig S13. ¹H NMR spectrum of 11

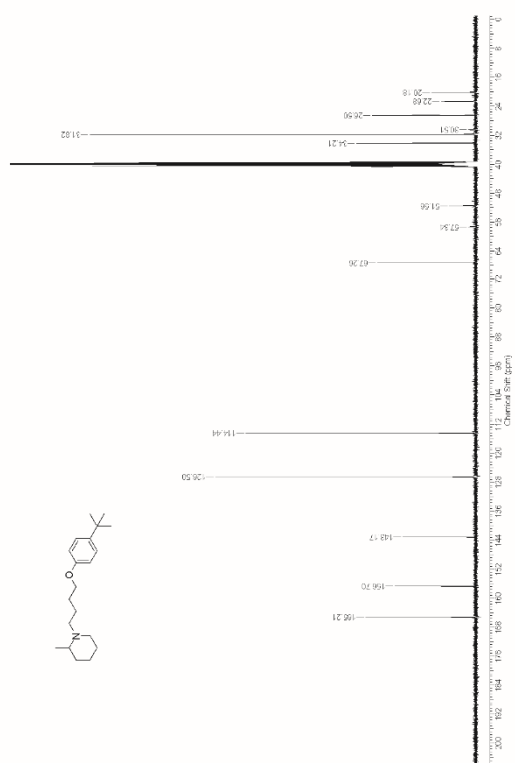


Fig S12. ¹³C NMR spectrum of 10

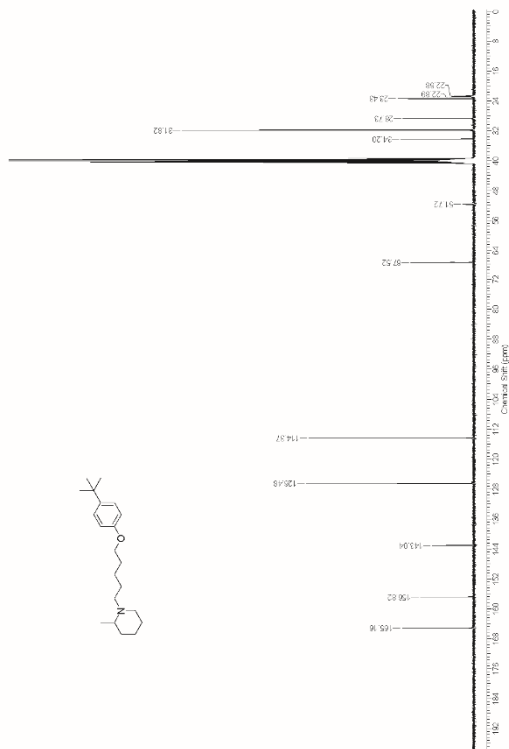


Fig S14. ¹³C NMR spectrum of 11

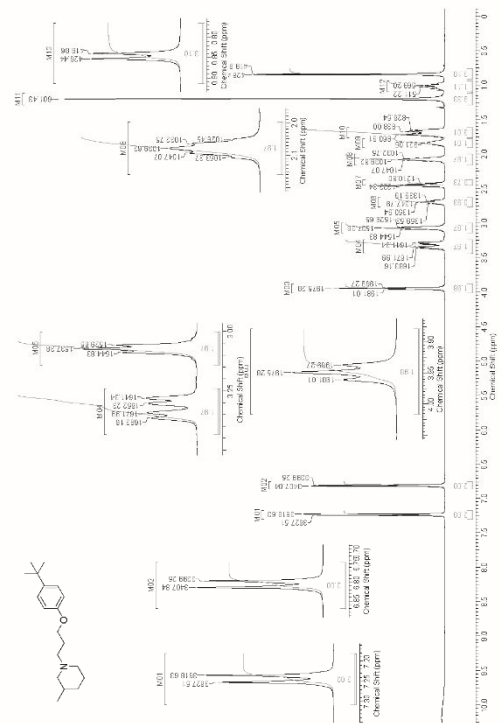


Fig S15. ¹H NMR spectrum of 12

4.2 Dual target ligands with 4-tert-butylphenoxy scaffold as histamine H₃ receptor antagonists and monoamine oxidase B inhibitors

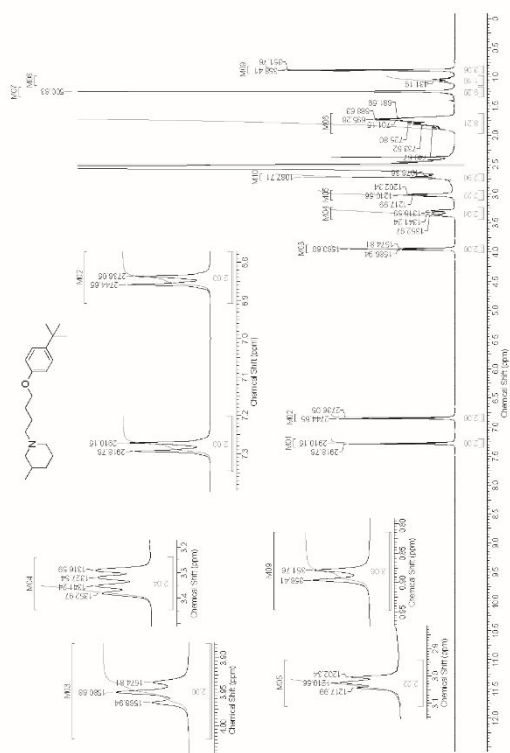


Fig S17. ^1H NMR spectrum of **13**

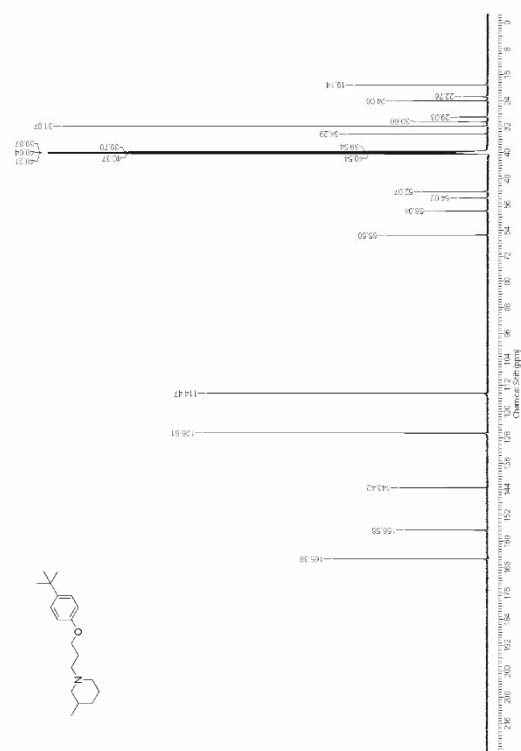


Fig S16. ^{13}C NMR spectrum of **12**

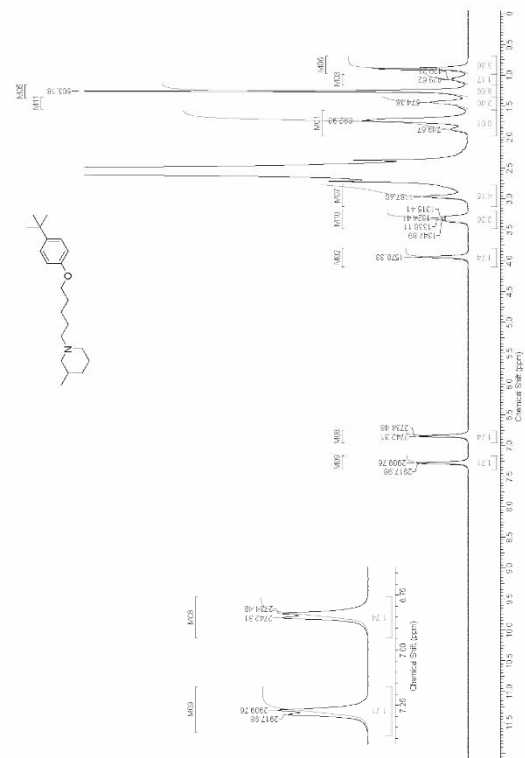


Fig S19. ¹H NMR spectrum of 14

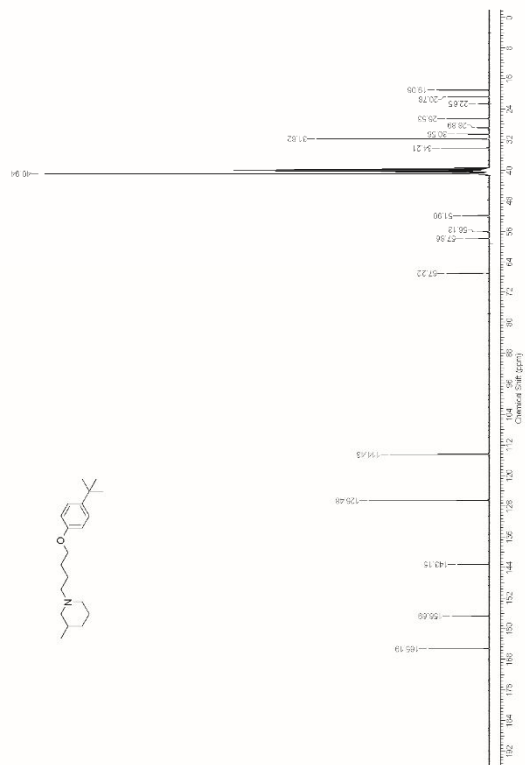


Fig S18. ¹³C NMR spectrum of 13

4.2 Dual target ligands with 4-tert-butylphenoxy scaffold as histamine H₃ receptor antagonists and monoamine oxidase B inhibitors

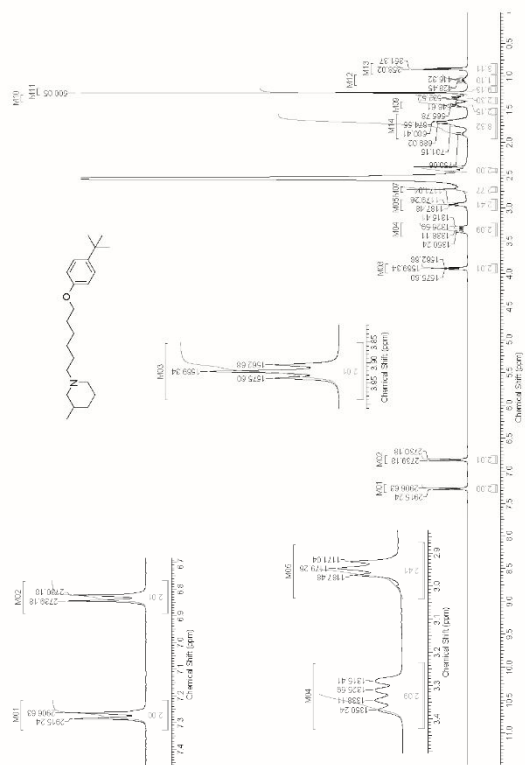
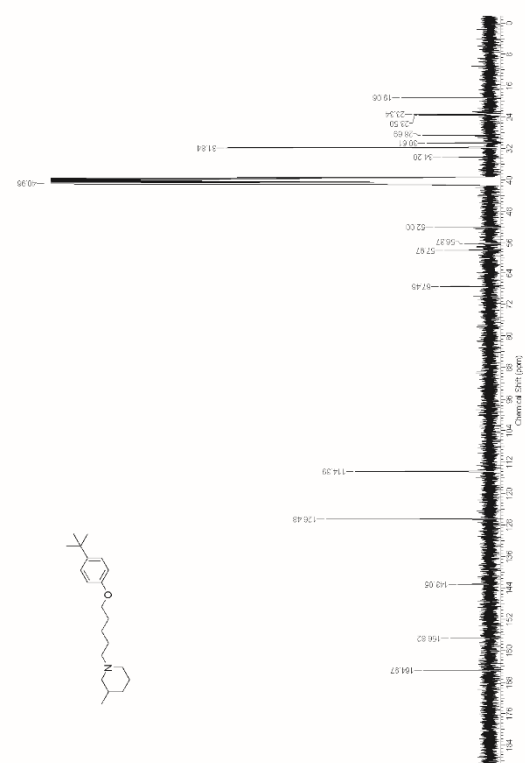


Fig S21. ¹H NMR spectrum of 15



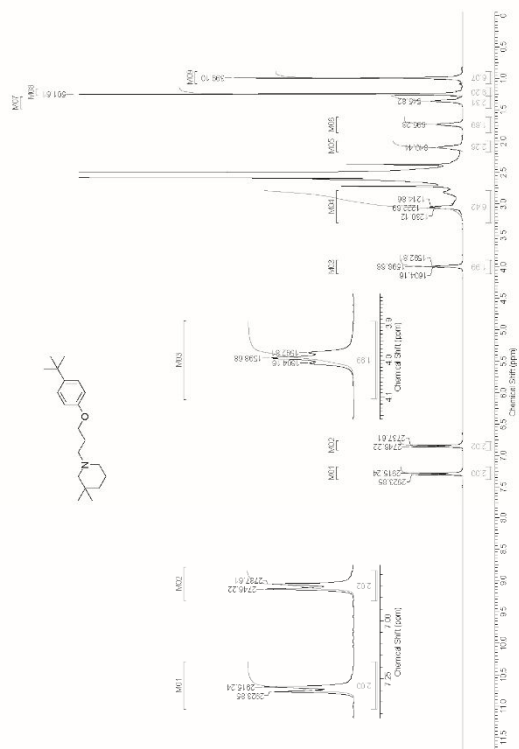


Fig S23. ¹H NMR spectrum of 16

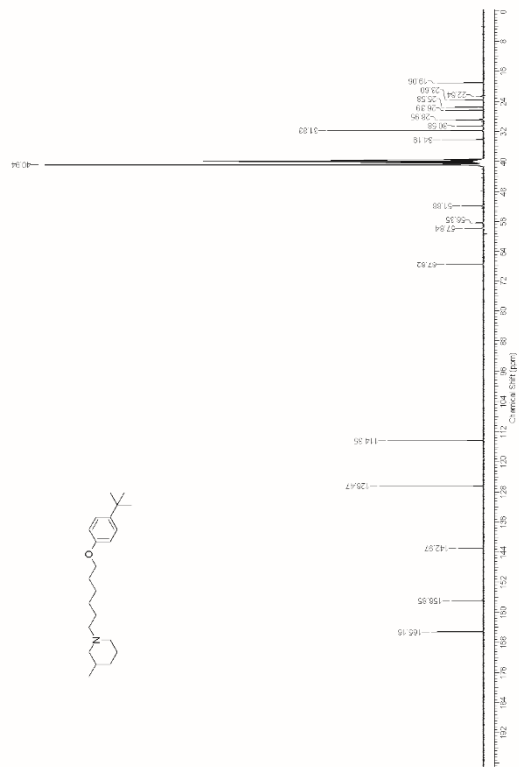
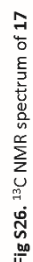
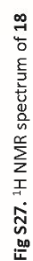


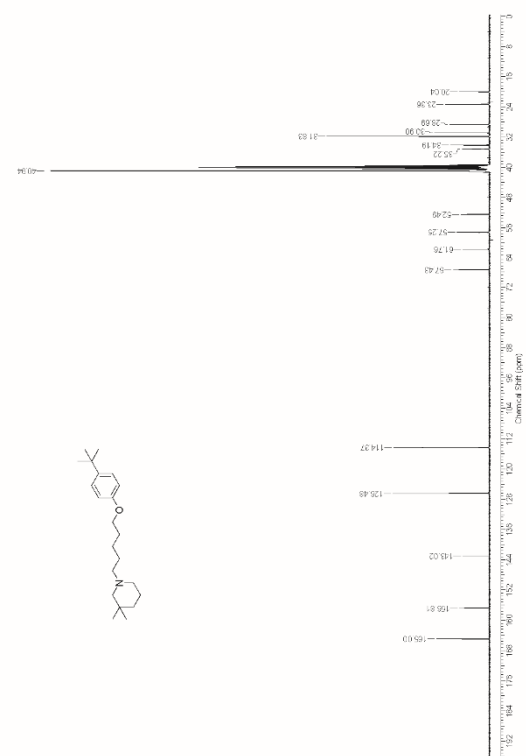
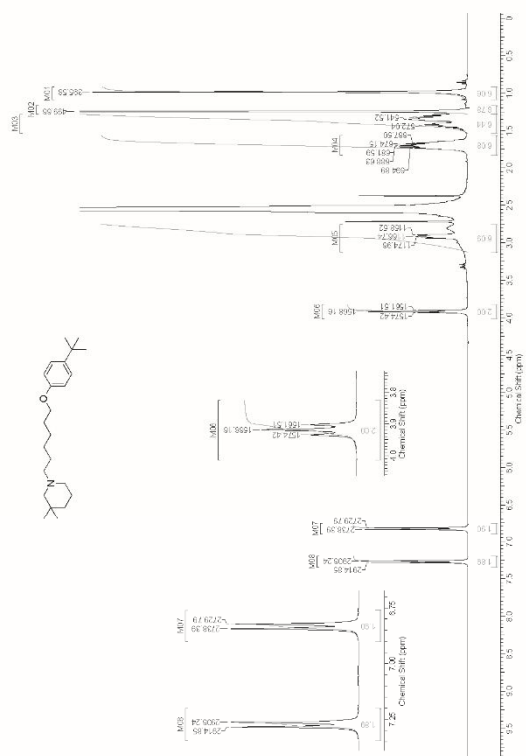
Fig S22. ¹³C NMR spectrum of 15

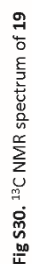
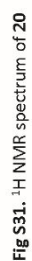
[illegible]

Fig S24. ^{13}C NMR spectrum of **16**



4.2 Dual target ligands with 4-tert-butylphenoxy scaffold as histamine H₃ receptor antagonists and monoamine oxidase B inhibitors





4.2 Dual target ligands with 4-tert-butylphenoxy scaffold as histamine H₃ receptor antagonists and monoamine oxidase B inhibitors

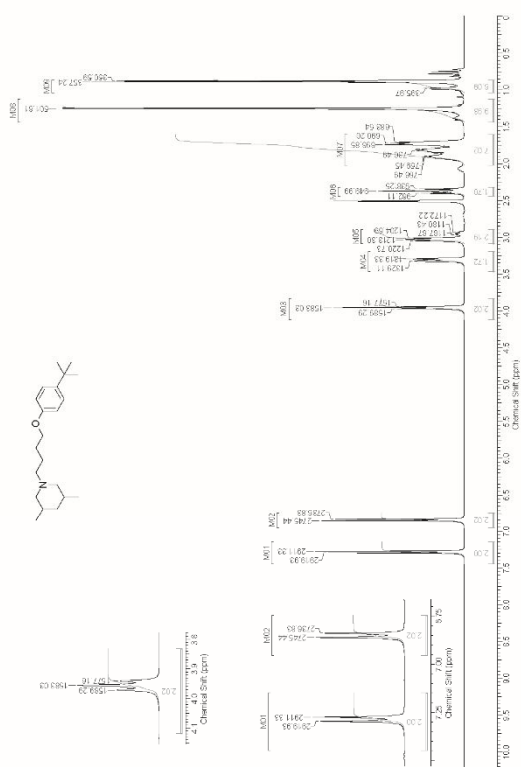


Fig S33. ¹H NMR spectrum of 21

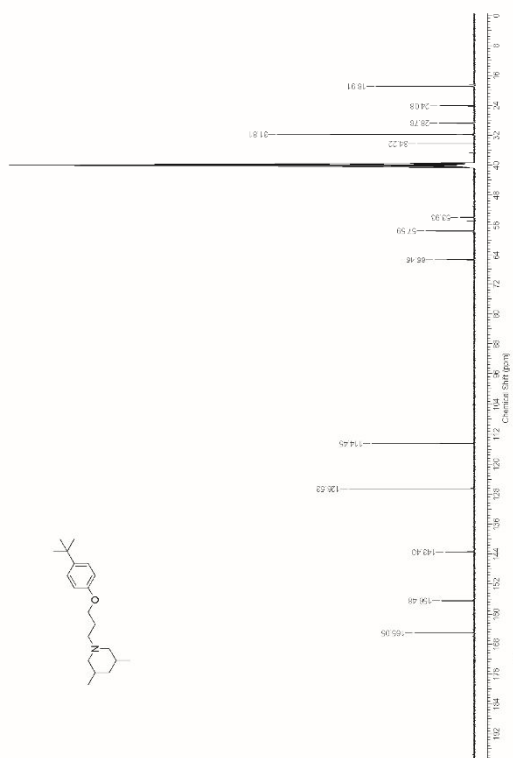


Fig S32. ¹³C NMR spectrum of 20

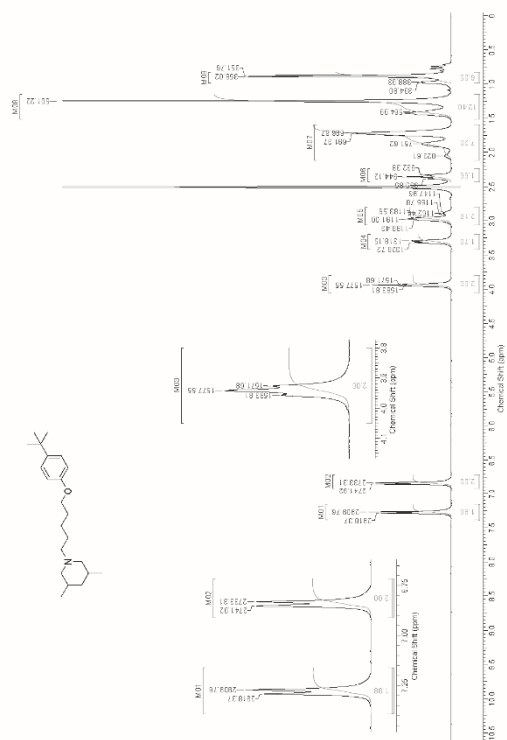


Fig S35. ¹H NMR spectrum of 22

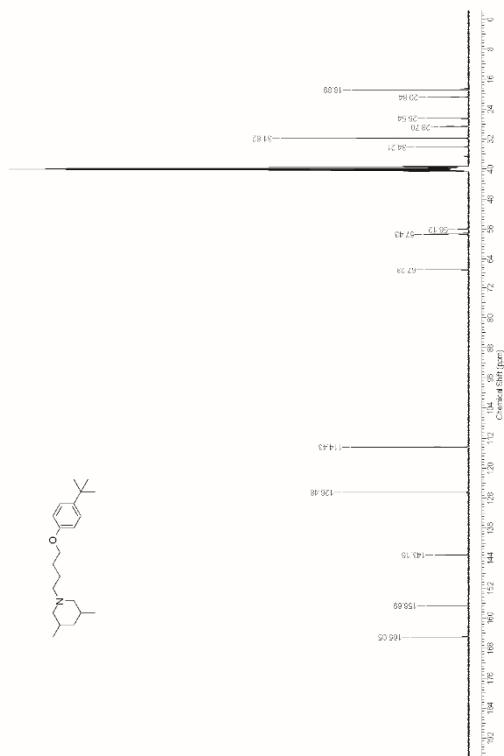


Fig S34. ¹³C NMR spectrum of 21

4.2 Dual target ligands with 4-tert-butylphenoxy scaffold as histamine H₃ receptor antagonists and monoamine oxidase B inhibitors

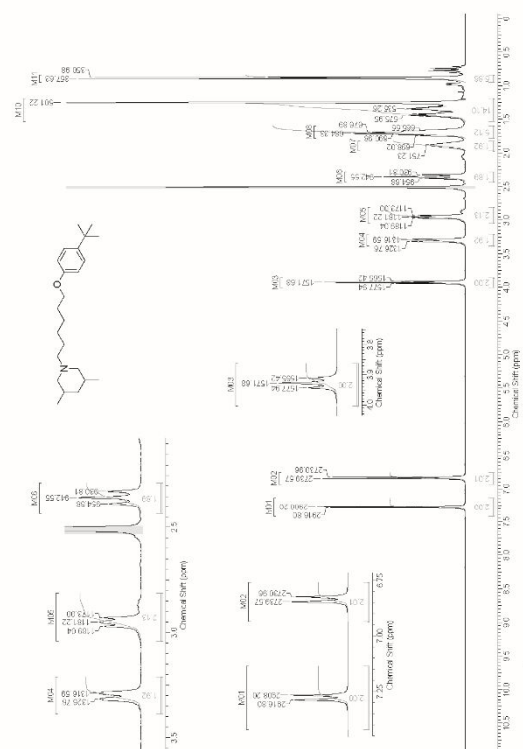


Fig S37. ¹H NMR spectrum of 23

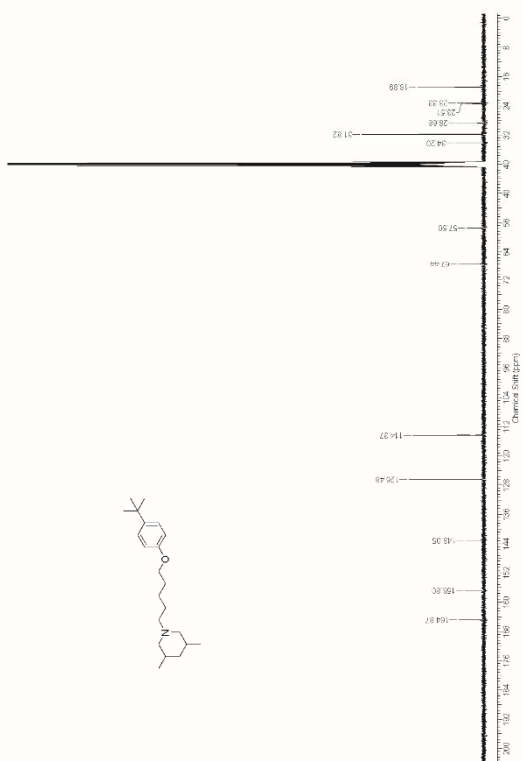
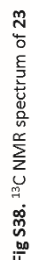
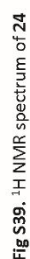


Fig S36. ¹³C NMR spectrum of 22



4.2 Dual target ligands with 4-tert-butylphenoxy scaffold as histamine H₃ receptor antagonists and monoamine oxidase B inhibitors

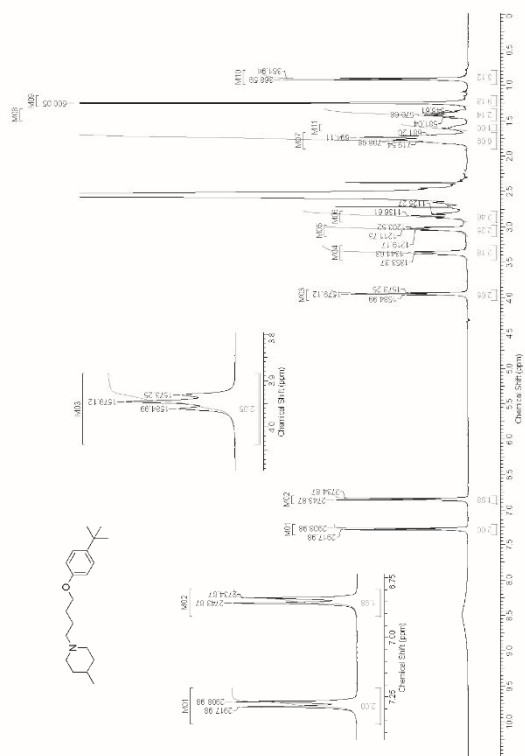


Fig S41. ¹H NMR spectrum of 25

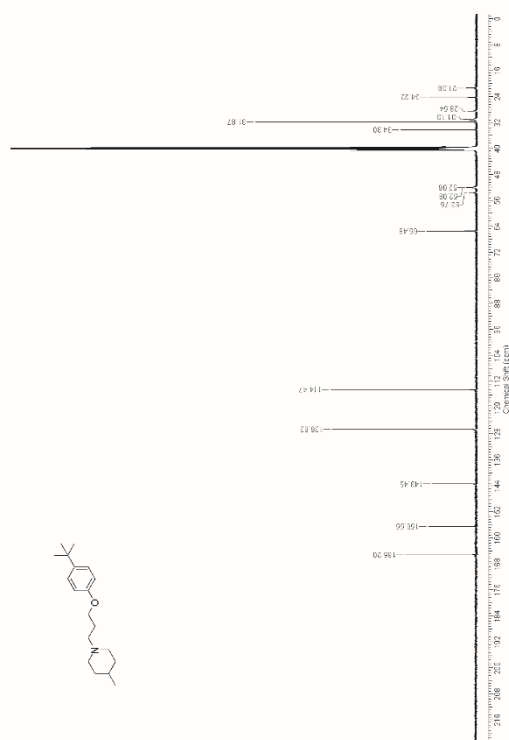


Fig S40. ¹³C NMR spectrum of 24

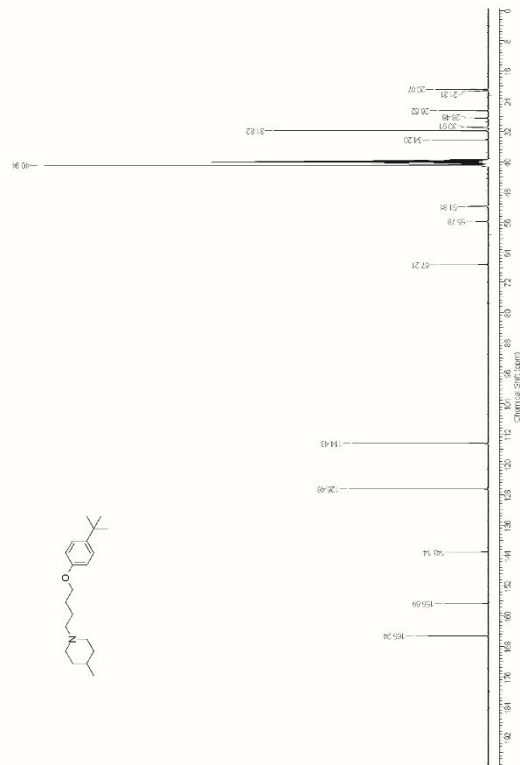


Fig S42. ¹³C NMR spectrum of 25

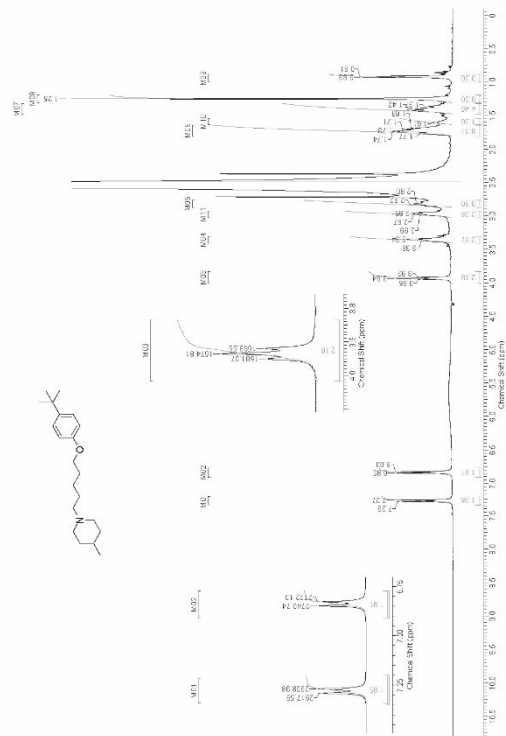


Fig S43. ¹H NMR spectrum of 26

4.2 Dual target ligands with 4-tert-butylphenoxy scaffold as histamine H₃ receptor antagonists and monoamine oxidase B inhibitors

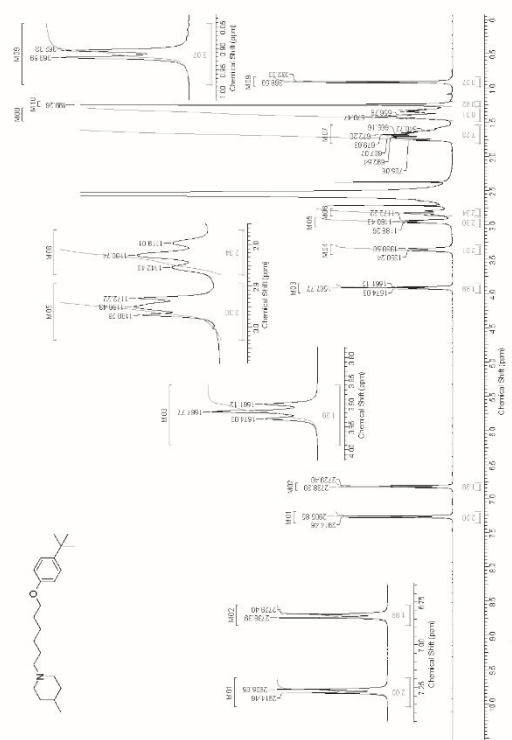


Fig S45. ¹H NMR spectrum of 27

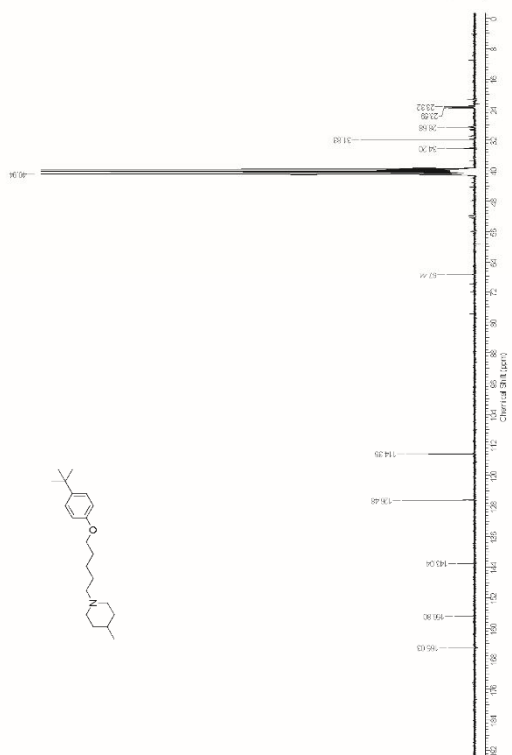


Fig S44. ¹³C NMR spectrum of 26

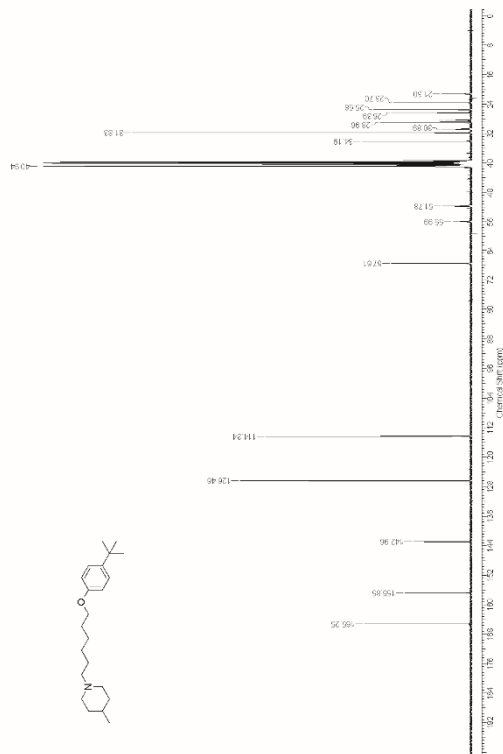


Fig S46. ¹³C NMR spectrum of 27

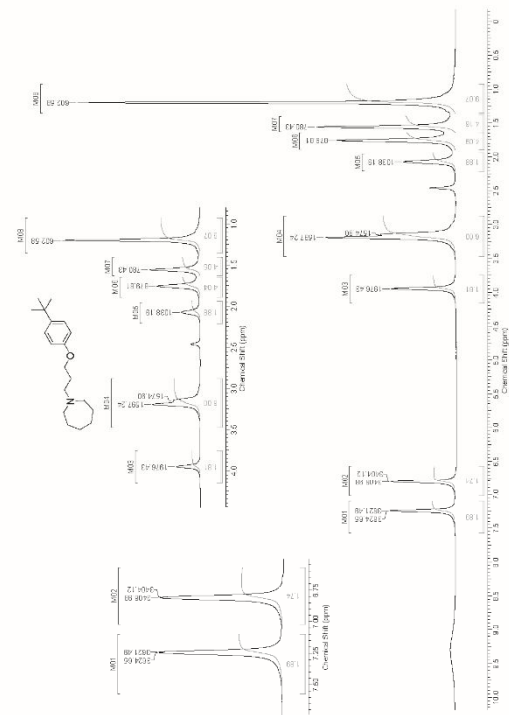
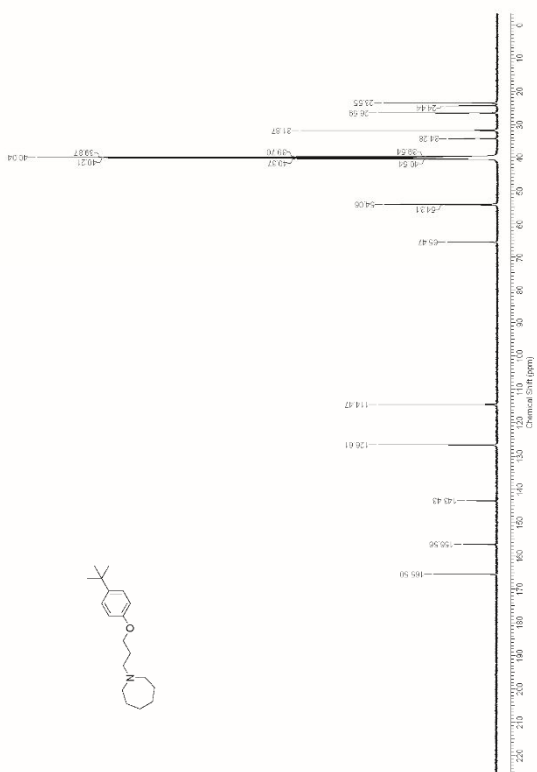
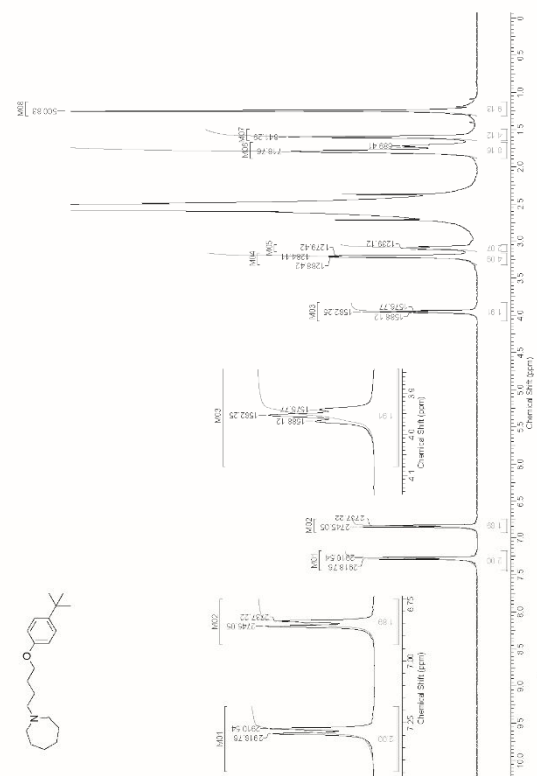
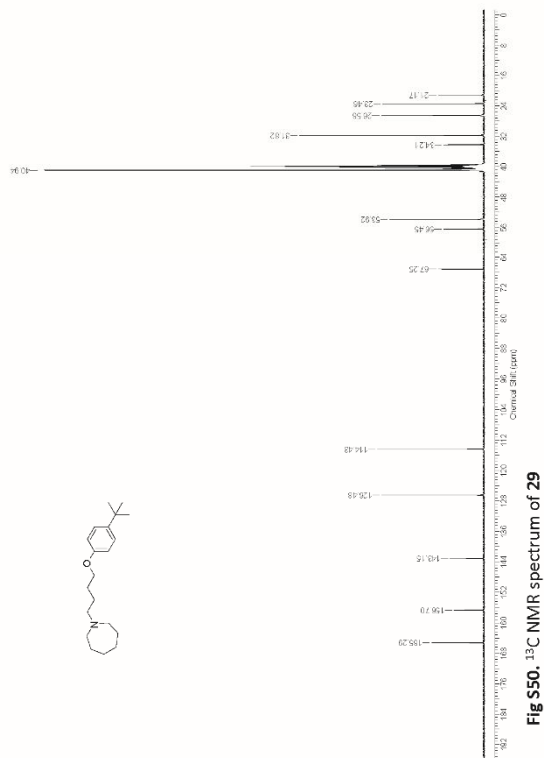
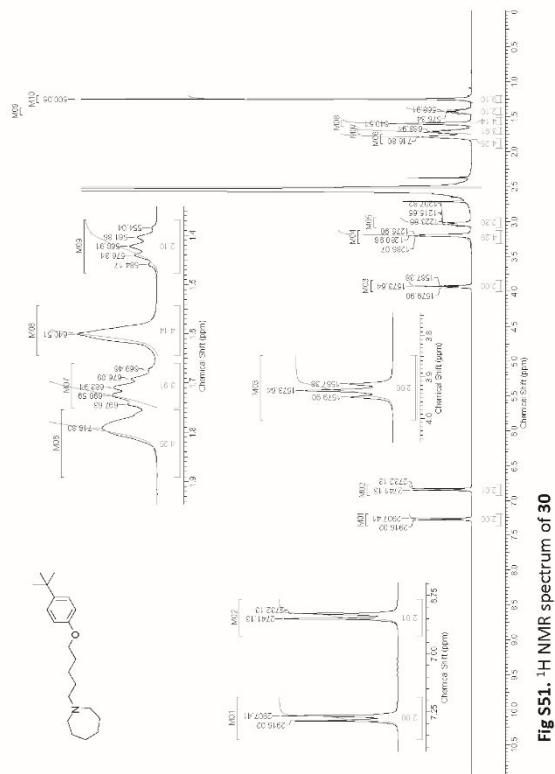


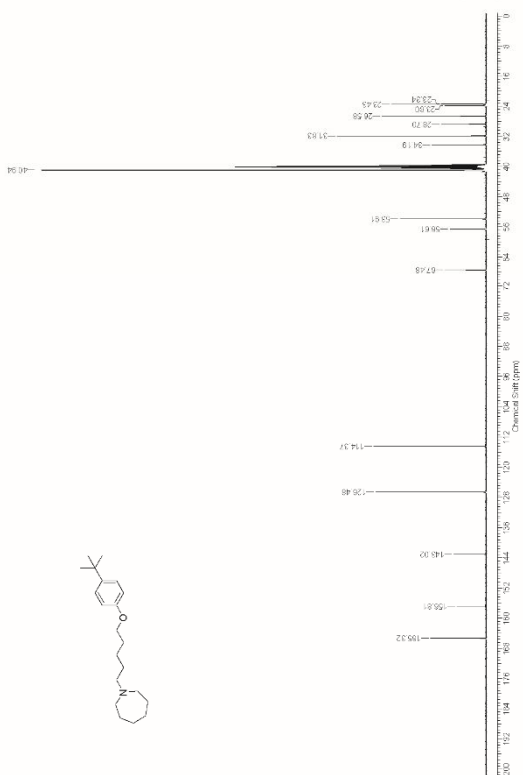
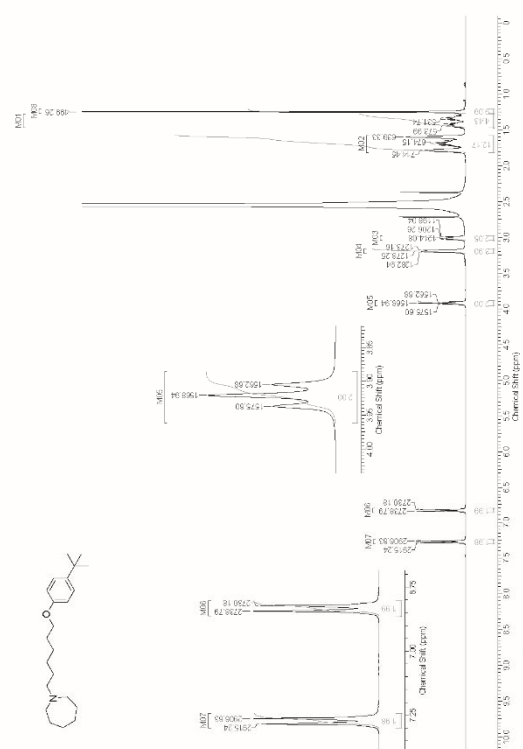
Fig S47. ¹H NMR spectrum of 28

4.2 Dual target ligands with 4-tert-butylphenoxy scaffold as histamine H₃ receptor antagonists and monoamine oxidase B inhibitors





4.2 Dual target ligands with 4-tert-butylphenoxy scaffold as histamine H₃ receptor antagonists and monoamine oxidase B inhibitors



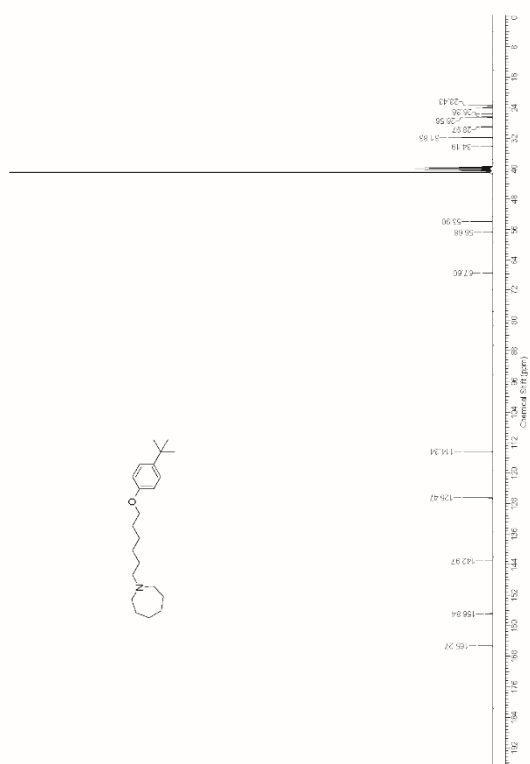


Fig S52. ¹³C NMR spectrum of 31

Supplementary Materials S2

Dual target ligands with 4-tert-butylphenoxy scaffold as histamine H₃ receptor antagonists and monoamine oxidase B inhibitors

Dorota Łazewska¹, Agnieszka Olejarska-Maciąg¹, David Reiner², Maria Kaleś¹, Grzegorz Łanecz¹, Małgorzata Zygmunt¹, Agata Dorosz-Plonka¹, Tadeusz Karcz¹, Annika Frank³, Holger Stark³ and Katarzyna Kieć-Kononowicz¹

¹ Department of Technology and Biotechnology of Drugs, Jagiellonian University Medical College, 9 Młyńska Str., 30-688 Kraków, Poland; agnieszka.olejarska@uj.edu.pl (A.O.-M.); maria.kales@uj.edu.pl (M.K.); grzegorz.lanecz@uj.edu.pl (G.L.); ad.dorosz@pion.katuj.edu.pl (A.D.-P.); lanecz@uj.edu.pl (T.K.); mkononowicz@uj.edu.pl (K.K.-K.)

² Institute of Pharmaceutical and Medicinal Chemistry, Heinrich Heine University Düsseldorf, Universitätsstr. 1, 40225 Düsseldorf, Germany; david.reiner@hhu.de (D.R.); a.frank@hhu.de (A.F.); stark@hhu.de (H.S.)

³ Department of Pharmacodynamics, Jagiellonian University Medical College, 9 Młyńska Str., 30-688 Kraków, Poland; malgorzata.zygmunt@uj.edu.pl (M.Z.)

* Correspondence: dlazewsk@em.uj.krakow.pl (D.L.); mkononowicz@uj.edu.pl (K.K.-K.)

hMAO B Kinetic studies

The α values for different modes of reversible inhibition as well as their diagnostic signature on double-reciprocal plot are shown in Table S1. The α value for compound **9** was calculated by GraphPad Prism software from the nonlinear regression curves using following equation for mixed-model of inhibition:

$$v = V_{max} \cdot [S] / ([S] \cdot (1 + [I] / \alpha K_i) + K_m \cdot (1 + [I] / K_i)) \quad (1)$$

v – velocity of enzyme reaction, V_{max} – maximum velocity (at infinite substrate concentration); K_i – dissociation constant for Enzyme-Inhibitor complex (in the enzymology literature other symbols can be used such as: K_i , K_i' , K_s etc.); αK_i – dissociation constant for Enzyme-Substrate-Inhibitor complex (in the literature also under the symbols: K_i' , K_s and K_{si}); K_m – Michaelis-Menten constant; $[I]$ – concentration of the inhibitor; $[S]$ – concentration of the substrate [Ref S1].

Table S1. Relation between inhibition modality, α value, and diagnostic signature on the double-reciprocal plots (cf. Lineweaver-Burk plot) [S2].

α	Inhibition modality	Diagnostic signature on double-reciprocal plot
$\alpha = 1$	noncompetitive (inhibitor binds to free enzyme and enzyme-substrate complex with equal affinity)	lines converge at the x-axis
$\alpha > 1$	mixed mode inhibitor (inhibitor can bind to free enzyme and enzyme-substrate complex unequally), inhibitor's affinity is higher for free enzyme	lines converge to the left of the y-axis and above the x-axis
$\alpha < 1$	mixed mode inhibitor (inhibitor can bind to free enzyme and enzyme-substrate complex unequally), inhibitor's affinity is higher for the enzyme-substrate complex)	lines converge to the left of the y-axis and below the x-axis
$\alpha \rightarrow \infty$	competitive (inhibitor and substrate compete for the same site of binding)	lines converge at the y-axis
$\alpha \rightarrow 0$ and $\alpha > 0$	uncompetitive (inhibitor binds only to the enzyme-substrate complex)	parallel lines

References:
S1. Copeland, R.A. *Enzymes: A Practical Introduction to Structure, Mechanism, and Data Analysis*, 2nd ed.; Wiley-VCH: New York / Chichester / Weinheim / Singapore / Toronto, 2000; ISBN 0-471-22063-9.
S2. Copeland, R.A. *Evaluation of Enzyme Inhibitors in Drug Discovery. A Guide for Medicinal Chemists and Pharmacologists*; John Wiley & Sons, Inc.: Hoboken, New Jersey, 2005.

4.3. Rasagiline derivatives combined with histamine H₃ receptor properties

Kiril Lutsenko¹⁾, Stefanie Hagenow¹⁾, Anna Affini¹⁾, David Reiner¹⁾ and Holger Stark¹⁾

1) Institute of Pharmaceutical and Medicinal Chemistry, Heinrich Heine University Düsseldorf, Universitätsstr. 1, 40225 Duesseldorf, Germany

Published in: *Bioorganic & Medicinal Chemistry Letters*, 2019, 29:126612.

DOI: 10.1016/j.bmcl.2019.08.016

Contribution to research: DR was involved in conduction of and data-evaluation from radioligand displacement experiments at histamine H₃ receptors, and reviewed the manuscript.

Abstract:

The irreversible monoamine oxidase B (MAO B) inhibitor rasagiline has been described with multiple disease modifying effects in vitro on models of Parkinson's disease. The combination of this established drug to recently developed histamine H₃ receptor (H₃R) antagonist elements gives new impetus to the design of multitargeting ligands. Surprisingly, the 5-substituted 3-piperidinopropoxy rasagiline derivative 1 was more potent on both targets than its 6-substituted isomer. It showed nanomolar affinities at the desired targets (MAO B IC_{50} = 256 nM; hH₃R K_i = 2.6 nM) with a high preference over monoamine oxidase A (MAO A) and negligible affinity at histamine H₁, H₄, dopamine D₂, D₃ receptors or acetyl-/butyrylcholinesterases.

Reprinted from Lutsenko K, Hagenow S, Affini A, Reiner D and Stark H, Rasagiline derivatives combined with histamine H₃ receptor properties, *Bioorg. Med. Chem. Lett.*, 2019, 29:126612, with permission for personal use from Elsevier.

Copyright 2018 Elsevier Ltd.



Contents lists available at ScienceDirect

Bioorganic & Medicinal Chemistry Letters

journal homepage: www.elsevier.com/locate/bmclRasagiline derivatives combined with histamine H₃ receptor propertiesK. Lutsenko^{a,b}, S. Hagenow^{a,b}, A. Affini^a, D. Reiner^a, H. Stark^{a,*}^aHeinrich Heine University Düsseldorf, Institute of Pharmaceutical and Medicinal Chemistry, Universitätsstr. 1, 40225 Düsseldorf, Germany

ARTICLE INFO

Keywords:

Multitarget-directed ligand
histamine H₃ receptor
Monoamine oxidase
MAO B inhibitor
Ladostigil
Parkinson's disease

ABSTRACT

The irreversible monoamine oxidase B (MAO B) inhibitor rasagiline has been described with multiple disease modifying effects in vitro on models of Parkinson's disease. The combination of this established drug to recently developed histamine H₃ receptor (H₃R) antagonist elements gives new impetus to the design of multitargeting ligands. Surprisingly, the 5-substituted 3-piperidinopropoxy rasagiline derivative **1** was more potent on both targets than its 6-substituted isomer. It showed nanomolar affinities at the desired targets (MAO B IC₅₀ = 256 nM; hH₃R K_i = 2.6 nM) with a high preference over monoamine oxidase A (MAO A) and negligible affinity at histamine H₁, H₄, dopamine D₂, D₃ receptors or acetyl-/butyrylcholinesterases.

Ligands simultaneously acting on a rational combination of target molecules, so called multitargeting ligands (MTLs), may be superior to target-selective drugs by triggering a number of positive synergistic effects. A meaningful target combination should address different pathophysiological pathways or different levels in one pathway. Still, optimizing structure-activity relationships (SARs) for combination of multiple targets of even different target families as well as assuring a balance in target affinities and maintaining drug-likeness at the same time is a high hanging fruit for medicinal chemists.^{1–3} This MTL approach is especially valuable when multiple targets have been described for a disease, e.g. for neurodegenerative diseases such as Parkinson's disease (PD).

In PD, patients suffer from progressive loss of dopaminergic neurons in the substantia nigra initiated by cellular oxidative stress and leading to the typical PD motor disorders but also associated non-motor symptoms.⁴ Monoamine oxidase B (MAO B) inhibitors are suitable medications in early PD or as add-on therapy, elevating striatal dopamine levels.⁵ Some representatives like rasagiline (Fig. 1) show efficacy in treatment of non-motor symptoms, like cognitive impairments and fatigue. Rasagiline is an irreversible propargyl amine-containing MAO B inhibitor, which covalently binds to the flavin adenine dinucleotide (FAD), acting as a cofactor of MAOs.⁶ It was shown to have neuroprotective and antiapoptotic effects in multiple studies, not least because it prevents the formation of reactive oxygen species (ROS), which are generated as second product during enzyme turnover.⁷ The combined cholinesterase (ChE)/MAO inhibitor ladostigil (Fig. 1),⁸ obtained by attaching a ChE active structural element at the 6-position of rasagiline, is currently under investigation for its therapeutic potential in

Alzheimer's disease.⁹ Also, its neuroprotective properties were tested in context of dementia associated with extrapyramidal disorders i.e. Parkinsonism and depression,¹⁰ which suggests the potential of MTLs in treatment of neurodegenerative diseases.

Based on previous designed indanone derivatives showing reversible MAO B inhibition,¹¹ we aimed to develop novel multitargeting rasagiline derivatives by introducing an accepted histamine H₃ receptor (H₃R) antagonist pharmacophore. The H₃R is a member of the GPCR receptor family, contributing to central neurotransmission of histamine and other neurotransmitters such as dopamine or acetylcholine. H₃R antagonists are currently investigated as potential drugs in sleep disorders having pitolisant with EMA market approval against narcolepsy, Alzheimer's disease (AD), PD or attention deficit hyperactivity disorder (ADHD).¹² Considering the previously described MAO inhibition properties of ciproxifan¹³, one of the most prominent H₃R antagonists/inverse agonist, and its non-imidazole analogues UCL2190¹¹ as well as DL77¹⁴ the 3-piperidinopropoxy moiety was chosen to be merged with rasagiline (Fig. 1).

The first series of compounds, **1a/2a**¹¹ were obtained from commercially available 5- and 6-methoxy-1-indanone via demethylation of phenol ethers¹⁵ following the Williamson ether reaction¹⁶ with 1-(3-chloropropyl)piperidine¹⁷ to alkylate 5- or 6-hydroxy-1-indanone.^{18,19} with a yield ranging from 81 to 85%. Compound **1** was synthesized via reductive amination using ammonium carbonate as amine source to give the intermediate **1b** with 47% yield²⁰ followed by nucleophilic substitution with propargyl bromide resulting in compound **1** in 55% yield (Scheme 1).²¹ For isomer **2** another reaction sequence was used starting from 6-hydroxy-1-indanone by performing Williamson ether

* Corresponding author.

E-mail address: stark@hhu.de (H. Stark).^bThese authors have contributed equally to this work.<https://doi.org/10.1016/j.bmcl.2019.08.016>

Received 30 July 2019; Received in revised form 7 August 2019; Accepted 8 August 2019

Available online 09 August 2019

0960-894X/ © 2019 Elsevier Ltd. All rights reserved.

K. Lutsenko, et al.

Bioorganic & Medicinal Chemistry Letters 29 (2019) 126612

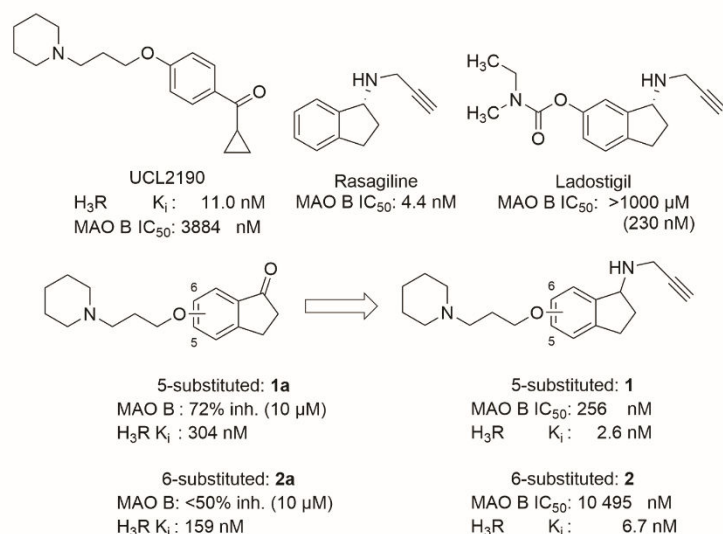
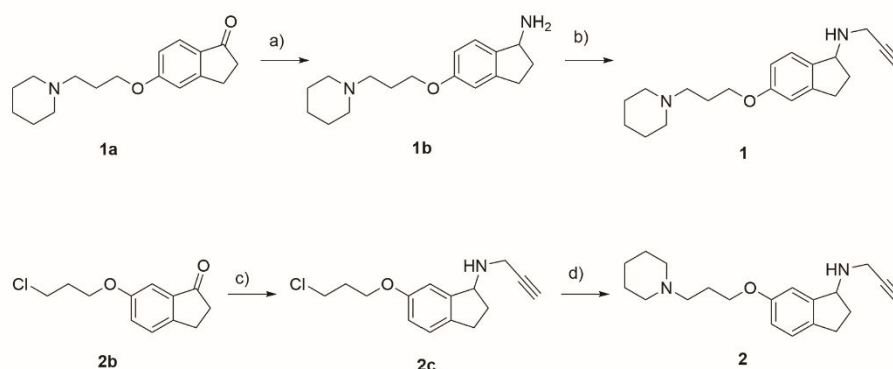


Fig. 1. MTL design of new irreversible MAO B/H₃R MTLs inspired by rasagiline,⁶ ladostigil (values for active metabolite are given in brackets),⁸ UCL2190¹¹ and previous described indanone lead compounds.¹¹



Scheme 1. Synthetic route for the design of indanamine MTLs **1** and **2**: (a) NaCNBH₃, NH₄OAc, EtOH, MW, 130 °C; (b) Propargyl bromide, K₂CO₃, DMF, 30 °C; (c) Propargyl amine, NaCNBH₃, AcOH, DCE, MW, 110 °C; (d) Piperidine, reflux.

reaction with 1-bromo-3-chloropropane to give the intermediate **2b** which was used without further purification for reductive amination with propargyl amine (yield 66% over two steps).²² The obtained intermediate **2c** was reacted with piperidine to give the final compound **2** in quantitative yield.²⁰ H₃R affinities of final compounds were determined in [³H]-N^α-methylhistamine radioligand displacement studies using crude membrane extracts from hH₃R-HEK293 cells.^{23,24} Monoamine oxidase A/B inhibition assays were performed using the discontinuous fluorimetric method with kynuramine as substrate for both isoforms (human recombinant MAO A/B).¹¹

Both indanamines (**1** and **2**) showed high affinities at H₃R (pK_i > 8) in a low nanomolar concentration range (Table 1), whereas at MAO B only compound **1** possessed inhibition in a nanomolar concentration range. However, our previously described indanone derivatives **1a** and **2a**, which are synthetic precursor molecules of MTLs **1** and **2** showed an inhibition < 80% at 10 μM for MAO B, respectively, and moderate affinities at H₃R (K_i > 100 nM).¹¹ Thus, concluding from SAR in these classes the introduction of the benzylic amine led to

improvement in H₃R affinity whereas the propargyl amine moiety increased MAO B inhibitory properties.

Interestingly, compound **1** showed an IC₅₀ shift to lower nanomolar concentrations with longer incubation times as expected for irreversible inhibitors. This suggests slow kinetics for the inactivation of MAO B by compound **1**, a time-dependency, which could also be verified by dilution method with excess of substrate (Fig. 2). The subtle but important variations are shown with compound **2** bearing the H₃R pharmacophore in C6 position failing to demonstrate irreversible mode of inhibition under conditions used despite the propargyl amino moiety. This lack of irreversibility together with its about 40-fold lower MAO B inhibition potency compared to **1** led to our assumption, that compound **2** might not or just barely reach the FAD in the active site of MAO B. A linear structure like in compound **1** might be favored to fit inside the MAO B cavity, while the non-linear and more rigid structure of compound **2** hampers binding to the active site.²⁵ Similar findings in styrylsatin compounds were published by Manley-King and colleagues, where the difference between C5 and C6 position lead to 68-fold

Table 1
Target affinities (expressed as K_i and IC₅₀ values) of novel MAO B/H₃R MTLs, UCL2190 and L-deprenyl (selegiline).

Compound	K _i [nM] ^a [CI 95%] (n) hH ₃ R	Pre-incubation at 37°	IC ₅₀ [nM] ^a [CI 95%] (n) hMAO B	IC ₅₀ [nM] ^a [CI 95%] (n) hMAO A	MAO SI ^b
1 	2.6 [1.3; 5.2] (3)	0 min	991 [461; 2130] (4)	> 100 000 (3)	> 100
		30 min	1052 [469; 2359] (3)	> 100 000 (1)	> 95
		60 min	256 [132; 497] (4)	> 10 000 (2)	> 39
2 	6.7 [2.3; 20] (3)	0 min	7920 [5521; 11363] (4)	> 100 000 (2)	> 13
		60 min	10 495 [8372; 13157] (3)	> 50 000 (3)	> 4.8
UCL2190 ^c	11 [3.5; 33] (3)	0 min	3884 [1816; 8311] (3)	> 50 000 (3)	> 12
L-Deprenyl ^c	nd	0 min	42 [23; 74] (4)	> 30 000 (4)	> 710
		30 min	3.9 [2.2; 6.8] (5)	nd	

^a Affinity values (expressed as K_i or IC₅₀) are given as mean values within the 95% confidence interval (CI) of n independent experiments each performed in duplicate.

^b Selectivity index (SI) = IC₅₀ (MAO A)/IC₅₀ (MAO B).

^c Data from Ref. 11, nd = not determined.

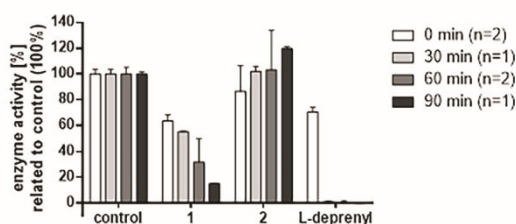


Fig. 2. Remained enzyme activity (%) of MAO B after pre-incubation with compound 1, 2 and the irreversible inhibitor L-deprenyl (10xIC₅₀). Data represent mean ± standard deviation of n independent experiments each performed in duplicates.

decrease of MAO B inhibition.²⁶ In case of the ChE/MAO inhibitor ladostigil, the ChE active structural motif was also attached at the unfavorable C6 position probably explaining its low binding to MAO B⁸. However, the active metabolite of ladostigil after ester cleavage show comparable MAO B inhibition to that of compound 1 (IC₅₀ = 230 nM vs. 256 nM for compound 1).¹³ Compared to contilisant, a combined H₃R/MAO/ChE MTL with similar irreversible MAO inhibition capacities,²⁷ compound 1 showed an improved preference for MAO B (MAO SI > 100 vs. SI = 0.5 for contilisant) as well as an improved selectivity for histamine H₃ over related histamine H₁, H₄, and dopamine D₂, D₃ receptor subtypes (K_i values > 10 μM; see Supporting information). Both compounds showed low cytotoxicity in a screening with neuroblastoma cells and compound 1 favorable ligand efficiency parameters (see Supporting information). This together with the effective structural pharmacophore overlap leading to a low molecular mass suggest high drug-like properties for compound 1. Additionally, introducing a second amino moiety improved the H₃R affinity for both indanamines compared to 1a and 2a. Nevertheless, enantiomeric separation of compound 1 was not taken into account because of higher nanomolar

MAO B affinity.

In conclusion, the substitution of the approved irreversible MAO B inhibitor rasagiline by a generally accepted H₃R antagonist pharmacophore led to design of two novel multitargeting H₃R/MAO B ligands. Whereas both compounds showed high H₃R affinities, interestingly they vary significantly in their inhibitory properties at MAO B. Only compound 1 bearing the H₃R pharmacophore in 5-position showed promising multitargeting properties in nanomolar concentration ranges with irreversible binding to MAO B for slow kinetics and for binding H₃R. Having this small molecule entity with its well-designed profile and suitable drug-likeness properties, it may serve as lead structure in prospective MTL drug design for the treatment of neurodegenerative diseases.

Acknowledgements

This work was kindly supported by COST action CM1103, CA15135 and CA18133 as well as DFG INST 208/664e1 FUGG (Germany). We thank J. Marco-Contelles for fruitful discussion on MTL design.

Appendix A. Supplementary data

Supplementary data to this article can be found online at <https://doi.org/10.1016/j.bmcl.2019.08.016>.

References

- Khanfar MA, Affini A, Lutsenko K, Nikolic K, Butini S, Stark H. Multiple targeting approaches on histamine H₃ receptor antagonists. *Front Neurosci*. 2016;10:1–17.
- Ramsay RR, Popovic-Nikolic MR, Nikolic K, Uliassi E, Bolognesi ML. A perspective on multi-target drug discovery and design for complex diseases. *Clin Transl Med*. 2018;7:3. <https://doi.org/10.1186/s40169-017-0181-2>.
- Proschak E, Stark H, Merk D. Polypharmacology by design: a medicinal chemist's perspective on multitargeting compounds. *J Med Chem*. 2019;62:420–444. <https://doi.org/10.1021/acs.jmedchem.8b00760>.
- Connolly BS, Lang AE. Pharmacological treatment of Parkinson disease: a review.

K. Lutsenko, et al.

Bioorganic & Medicinal Chemistry Letters 29 (2019) 126612

- JAMA. 2014;311:1670–1683. <https://doi.org/10.1001/jama.2014.3654>.
5. Finberg JPM, Wang J, Bankiewicz K, Harvey-White J, Kopin IJ, Goldstein DS. Increased striatal dopamine production from L-DOPA following selective inhibition of monoamine oxidase B by R (+)-N-propargyl-1-aminoindan (rasagiline) in the monkey. *MAO – The Mother of all Amine Oxidases*. Vienna: Springer; 1998:279–328.
6. Youdim MB, Gross A, Finberg JP. Rasagiline [N-propargyl-1R(+)-aminoindan], a selective and potent inhibitor of mitochondrial monoamine oxidase B. *Br J Pharmacol*. 2001;132:500–506.
7. Stocchi F, Fossati C, Torti M. Rasagiline for the treatment of Parkinson's disease: an update. *Expert Opin Pharmacother*. 2015;16:2231–2241. <https://doi.org/10.1517/14656566.2015.1086748>.
8. Sterling J, Herzig Y, Goren T, et al. Novel dual inhibitors of AChE and MAO derived from hydroxyl aminoindan and phenethylamine as potential treatment for Alzheimer's disease. *J Med Chem*. 2002;45:5260–5279.
9. Youdim MB. Multi target neuroprotective and neurorestorative anti-Parkinson and anti-Alzheimer drugs ladostigil and M30 derived from rasagiline. *Exp Neurobiol*. 2013;22:1–10. <https://doi.org/10.5607/en.2013.22.1.1>.
10. Weinreb O, Amit T, Bar-Am O, Youdim MB. Ladostigil: a novel multimodal neuro-protective drug with cholinesterase and brain-selective monoamine oxidase inhibitory activities for Alzheimer's disease treatment. *Curr Drug Targets*. 2012;13:483–494.
11. Affini A, Hagenow S, Zivkovic A, Marco-Contelles J, Stark H. Novel indanone derivatives as MAO B/H₃R dual-targeting ligands for treatment of Parkinson's disease. *Eur J Med Chem*. 2018;148:487–497. <https://doi.org/10.1016/j.ejmech.2018.02.015>.
12. Ghamari N, Zarei O, Arias-Montañón J-A, Reiner D, Dastmalchi S, Stark H, Hamzeh-Mivehroud M. Histamine H₃ receptor antagonists/inverse agonists: Where do they go? *Pharmacol Ther*. 2019;200:69–84.
13. Hagenow S, Stasiak A, Ramsay RR, Stark H. Ciprofloxan, a histamine H₃ receptor antagonist, reversibly inhibits monoamine oxidase A and B. *Sci Rep*. 2017;7:40541. <https://doi.org/10.1038/srep40541>.
14. Łazewska Dorota, Olejarz-Maciej Agnieszka, Kaleta Maria, et al. 4-tert-Pentylphenoxyalkyl derivatives – histamine H₃ receptor ligands and monoamine oxidase B inhibitors. *Bioorg Med Chem Lett*. 2018;28:3596–3600. <https://doi.org/10.1016/j.bmcl.2018.10.048>.
15. Weissman SA, Zewge D. Recent advances in ether dealkylation. *Tetrahedron*. 2005;61:7833–7863.
16. Williamson A. About the theory of the formation of ethers. *Ann Chem*. 1851;77:37–49.
17. Tomasch M, Schwed JS, Weizel L, Stark H. Novel chalcone-based fluorescent human histamine H₃ receptor ligands as pharmacological tools. *Front Syst Neurosci*. 2012;6:1–16.
18. Sander K, Von Coburg Y, Gamelin JC, et al. Acidic elements in histamine H₃ receptor antagonists. *Bioorg Med Chem Lett*. 2010;20:1581–1584.
19. Sadek B, Schwed JS, Subramanian D, et al. Non-imidazole histamine H₃ receptor ligands incorporating antiepileptic moieties. *Eur J Med Chem*. 2014;77:269–279. <https://doi.org/10.1016/j.ejmech.2014.03.014>.
20. Herzig Y, Lerman L, Goldenberg W, Lerner D, Gottlieb HE, Nudelman A. Hydroxy-1-aminoindans and derivatives: preparation, stability, and reactivity. *J Org Chem*. 2006;71:4130–4140.
21. Sander K, Kottke T, Hoffend C, et al. Metal-containing histamine H₃ receptor ligands. *Org Lett*. 2010;12:2578–2581.
22. Abdel-Magid AF, Carson KG, Harris BD, Maryanoff CA, Shah RD. Reductive amination of aldehydes and ketones with sodium triacetoxyborohydride. Studies on direct and indirect reductive amination procedures. *J Org Chem*. 1996;61:3849–3862.
23. Kottke T, Sander K, Weizel L, et al. Receptor-specific functional efficacies of alkyl imidazoles as dual histamine H₃/H₄ receptor ligands. *Eur J Pharmacol*. 2011;654:200–208.
24. Khanfar MA, Reiner D, Hagenow S, Stark H. Design, synthesis, and biological evaluation of novel oxadiazole- and thiazole-based histamine H₃R ligands. *Bioorg Med Chem*. 2018;26(14):4034–4046. <https://doi.org/10.1016/j.bmc.2018.06.028>.
25. Carradori S, Silvestri R. New Frontiers in selective human MAO-B inhibitors: mini-perspective. *J Med Chem*. 2015;58(17):6717–6732. <https://doi.org/10.1021/jm501690r>.
26. Manley-King CI, Bergh JJ, Petzer JP. Inhibition of monoamine oxidase by selected C5- and C6-substituted isatin analogues. *Bioorg Med Chem*. 2011;19(1):261–274. <https://doi.org/10.1016/j.bmc.2010.11.028>.
27. Bautista-Aguilera ÓM, Hagenow S, Palomino-Antolin A, et al. Multitarget-directed ligands combining cholinesterase and monoamine oxidase inhibition with histamine H₃R antagonism for neurodegenerative diseases. *Angew Chem Int Ed Engl*. 2017;56:12765–12769. <https://doi.org/10.1002/anie.201706072>.

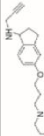

Supplementary Data

Rasagiline derivatives combined with histamine H₃ receptor properties

K. Lutsenko,³¹ S. Hagenow,³² A. Affini,³³ D. Reiner,³⁴ H. Stark³⁵
³¹Heinrich Heine University Düsseldorf, Institute of Pharmaceutical and Medicinal Chemistry, Universitätsstr. 1, 40225 Düsseldorf, Germany
³²corresponding author; e-mail: stark@hhu.de, Fax: +49 211 8113359, phone: +49 211 8110478
³³These authors have contributed equally to this work

Keywords: Multitarget-directed ligand, histamine H₃ receptor, monoamine oxidase, MAO B inhibitor, *l*-dopagilin, Parkinson's disease
Running title: Rasagiline with H₃R

Table 1. Off-target affinities for MTL1 and 2 at histamine/dopamine receptor subtypes and acetylcholinesterase.

Compound	K _i (μM)				% inhibition (global fit)	
	H ₃ R	H ₄ R	HD ₃ R	HD ₂ R	oeACHE	oeBUCHE
1 	>10	>100	>10	>10	57±1.4	32±1.1
	(2)	(3)	(2)	(2)	(2)	(2)
2 	nd	nd	nd	nd	47±4.4	47±2.5
	(2)	(2)	(2)	(2)	(2)	(2)

nd – not determined, oe – electric cell eq. – equine/horse serum

Table 2. Evaluation of Lipinski's rules and metric parameters for compound 1

Comp.	Lipinski's rules				H ₃ R		MAO B	
	HB donors	HB acceptors	M [g/mol]	clogP ^a	PSA ^b (Å ²)	LE ^c	LE ^d	LELP ^e
1	1	3	312.2	4.8	23.5	0.5	9.3	0.3
^a calculation with Marvin Sketch, ^b calculation with Molsoft, ^c HD ₃ R: LE = pK _a /H ₃ (heavy atoms), ^d MAO B: LE = pK _a /H ₃ (H ₃ R) = clogP/LE, ^e HB – hydrogen bond, PSA – polar surface areas, LE – ligand efficacy, LLEP – ligand efficacy dependent lipophilicity								

Table 3. Cell viability of SH-SY5Y after 24h treatment with test ligands (1 and 10 μM). Data are given as mean ± SD of % inhibition (related to 1% DMSO control; ns1, performed in triplicates).

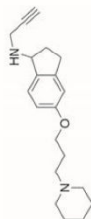
Compound	% cell viability ± SD	
1 2 Mpp⁺	10 μM	1 μM
	95.6 ± 9.7 100.5 ± 8.4	89.7 ± 12.3 84.0 ± 13.9
1.8 ± 0.6 (10 mV)		



6-(3-Chloropropoxy)-N-(prop-2-yn-1-yl)-2,3-dihydro-1H-inden-1-amine (**2c**)

(0.4 ml, 9.2 mmol) propargyl amine and (0.4 g, 6.9 mmol) sodium cyano borohydride were added to a solution of (0.4 ml, 4.6 mmol) glacial acetic acid and (1.1 g, 4.6 mmol) **4b** in absolute dichloro ethane in microwave vial. The mixture was stirred and heated at 110 °C for 10 min in a microwave reactor. The reaction mixture was concentrated to remove the solvent, treated with 2N NaOH until pH > 10, and extracted with dichloromethane. The organic phase was dried over magnesium sulfate, filtered, and concentrated under reduced pressure to give the crude product, which was purified with column chromatography (methylene chloride: methanol (NH₃ saturated) = 97:3).

Yield: 68%; ¹H NMR (600 MHz, CDCl₃) δ 7.12 (d, J = 8.3 Hz, 1H), 6.91 (d, J = 2.6 Hz, 1H), 6.78 (dd, J = 8.2, 2.5 Hz, 1H), 4.36 (t, J = 6.2 Hz, 1H), 4.10 (td, J = 6.1, 1.1 Hz, 2H), 3.74 (t, J = 6.4 Hz, 2H), 3.61 – 3.45 (m, 2H), 2.95 (ddd, J = 16.2, 8.4, 5.1 Hz, 1H), 2.83 – 2.67 (m, 1H), 2.42 (dddd, J = 12.4, 8.3, 6.9, 5.3 Hz, 1H), 2.27 – 2.26 (m, 1H), 2.22 (p, J = 6.2 Hz, 2H), 1.85 (dddd, J = 12.4, 8.4, 6.5, 5.6 Hz, 1H).



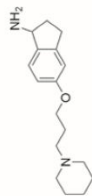
5-(3-(Piperidin-1-yl)propoxy)-N-(prop-2-yn-1-yl)-2,3-dihydro-1H-inden-1-amine hydrochloride (**1**)

Compound **4a** (0.3 g, 1.1 mmol), a propargyl bromide solution 80% wt. in toluene (0.1 ml, 1.1 mmol) and potassium carbonate (0.2 g, 1.1 mmol) were heated in DMF for 4 h. The crude product was purified by column chromatography (methylene chloride: methanol (NH₃ saturated) = 97:3) and crystallized as hydrochloride from 1,4-dioxane (0.2 g, 55%).

Yield: 55%; m.p. 162 °C; ¹H NMR (600 MHz, D₂O) δ 10.4 (br s, 1H, NH⁺), 7.44–7.36 (m, 1H, phind-7H), 6.96–6.90 (m, 1H, phind-4H), 6.89–6.82 (m, 1H, phind-6H), 4.87–4.80 (dd, 1H, J = 4.8, NHCH), 4.15–4.04 (t, 2H, J = 5.8, prop-1H), 3.88–3.82 (t, 2H, J = 3.9, NHCH₂C≡CH), 3.57–3.44 (m, 2H, prop-3H), 3.31–3.18 (m, 2H, NHCHCH₂), 3.14–2.99 (m, 1H, NHCHCH₂CH₂), 2.99–2.79 (m, 4H, pip-2,6H), 2.61–2.42 (m, 1H, NHCHCH₂CH₂), 2.30–2.08 (m, 3H, prop-2H, CH₂C≡CH), 1.96–1.32 (m, 6H, pip-3,5H, pip-4H) ¹³C NMR (150 MHz, D₂O) δ 157.02 (phind-5C), 144.95 (NHCHCH₂CH₂C), 125.89 (NHCHC), 123.95 (phind-7C), 111.21 (phind-4C), 108.42 (phind-6C), 75.20 (CH₂C≡CH), 70.54 (CH₂C≡CH), 62.74 (prop-1C), 58.82 (prop-3C), 51.77 (NHCH), 50.63 (pip-2,6C), 31.35 (NHCH₂C≡CH), 27.07 (NHCHCH₂), 26.11 (NHCHCH₂CH₂), 20.71 (prop-2C), 18.38 (pip-4C), 18.38 (pip-3C); ES-HRMS *m/z*: calc. for C₂₀H₂₈N₂O (MH⁺), 313.2274, found 313.2277. Anal. calcd.: C, 62.33; H, 7.85; N, 7.27. Found: C, 62.02; H, 8.07; N, 7.17.

4

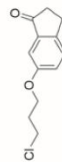
Demethylation of the 5- or 6-hydroxy-1-indanone was achieved as described previously.²¹ The corresponding 3-(piperidin-1-yl)propylchloride²¹ derivatives were synthesized according to already described methods.^{18–21} Synthesis of the indanone precursors **1a** and **2a** is described by Affini et al.²¹



5-(3-(Piperidin-1-yl)propoxy)-2,3-dihydro-1H-inden-1-amine (**1b**)

Ammonium acetate (2.5 g, 32.8 mmol) and sodium cyano borohydride (0.2 g, 2.6 mmol) were added to a solution of **3a** (0.6 g, 2.2 mmol) in absolute ethanol in microwave vial. The mixture was stirred and heated at 130 °C for 2 min in a microwave reactor. The reaction mixture was concentrated to remove the solvent, treated with 2N NaOH until pH > 10, and extracted with dichloromethane. The organic phase was dried over magnesium sulfate, filtered, and concentrated under reduced pressure to give the crude product, which was purified with column chromatography (methylene chloride: methanol (NH₃ saturated) = 97:3).

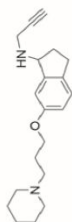
Yield: 47%; ¹H NMR (300 MHz, DMSO-d₆) δ 7.23–7.15 (m, 1H, phind-7H), 6.75–6.66 (m, 2H, phind-4,6H), 4.18–4.06 (t, 1H, J = 4.1, NH₂CHCH₂), 3.99–3.87 (t, 2H, J = 5.6, prop-1H), 2.87–2.74 (m, 1H, NH₂CHCH₂), 2.72–2.55 (m, 1H, NH₂CHCH₂), 2.40–2.17 (m, 7H, NH₂CHCH₂CH₂, pip-2,6H, prop-3H), 1.89–1.74 (g, 2H, J = 6.4, prop-2H), 1.64–1.43 (m, 5H, pip-3,5H, NH₂CHCH₂CH₂), 1.42–1.30 (m, 2H, pip-4H) ¹³C NMR (75 MHz, DMSO-d₆) δ 158.01 (phind-5C), 143.97 (NH₂CHCH₂CH₂C), 140.29 (NH₂CHC), 124.10 (phind-7C), 112.67 (phind-4C), 109.93 (phind-6C), 65.91 (prop-1C), 56.12 (prop-3C), 55.02 (NH₂CH), 54.10 (pip-2,6C), 37.27 (NH₂CHCH₂), 29.78 (NH₂CHCH₂CH₂), 26.39 (prop-2C), 25.61 (pip-3,5C), 24.15 (pip-4C); ES-HRMS *m/z*: calc. for C₁₇H₂₄N₂O (MH⁺), 275.2123, found 275.2120.



6-(3-Chloropropoxy)-2,3-dihydro-1H-inden-1-one (**2b**)

Compound **2b** (0.5 g, 3 mmol), 1-bromo-3-chloropropane (0.3 ml, 3.3 mmol) and potassium carbonate (1.0 g, 6.6 mmol) were heated in acetone in a microwave for 2 h. Reaction mixture was taken up in methylene chloride and the unreacted phenolic compound was washed out with 2N NaOH and the crude product was used for the next reaction without further purification.

3



6-(3-(4-piperidin-1-yl)propoxy)-N-(prop-2-yn-1-yl)-2,3-dihydro-1H-inden-1-amine dihydro oxalate (2)

Chloride precursor (4c) was refluxed in a large excess absolute piperidine. After 24 h, the reaction was cooled down. The solvent was concentrated under vacuum taken up in methylene chloride and washed with saturated NaHCO₃-solution. The organic phase was then washed with saturated NaCl-solution and water, dried over sodium sulfate, and concentrated under vacuum. The resulting oil was precipitated using oxalic acid and recrystallized from acetone.

Yield: 99%; ¹H NMR (600 MHz, CDCl₃) δ: 7.20 (d, J = 8.4 Hz, 1H), 7.13 (s, 1H), 6.91 (d, J = 8.5 Hz, 1H), 4.06 (q, J = 5.4 Hz, 2H), 3.97 (d, J = 2.7 Hz, 2H), 3.57 (dd, J = 21.3, 14.2, 11.0 Hz, 2H), 3.28–3.25 (m, 2H), 3.24 (t, J = 7.9 Hz, 2H), 3.16 (d, J = 2.8 Hz, 1H), 3.07 (dt, J = 15.2, 7.5 Hz, 1H), 2.98–2.80 (m, 2H), 2.53 (dd, J = 14.5, 8.0 Hz, 1H), 2.27 (ddt, J = 13.3, 8.7, 4.6 Hz, 1H), 2.19 (dt, J = 10.2, 5.8 Hz, 2H), 1.81 (s, 5H), 1.62–1.44 (m, 1H). ¹³C NMR (151 MHz, CDCl₃) δ: 166.59, 159.32, 139.13, 138.32, 127.26, 118.56, 111.88, 79.01, 75.00, 66.34, 63.42, 55.64, 54.42, 35.45, 30.24, 30.02, 25.03, 24.22, 22.77; ESI-HRMS *m/z*: calc. for C₂₁H₂₉N₂O (MH⁺), 313.2274, found 313.2274, LC-MS: 96.56% *m/z* 256.10.

Pharmacological testing

Radioligand displacement assay

Radioligand displacement studies for H₃R affinities were performed as described previously.^{16,17} Briefly, crude membrane extracts (20 mg/well) were incubated with [³H]-N-α-methylhistamine (2 nM, 78.3 Ci mmol⁻¹) and various concentrations of test compounds (10⁻¹¹ and 10⁻⁷ M) in a total volume of 0.2 mL binding buffer. The assay was partly automated by using a Tecan Freedom EVO pipetting robot. Data were analyzed using GraphPad PRISM 6 using the implemented non-linear regression fit “one-site competition”, where K_i values were calculated according to Cheng-Prusoff equation. Statistical analysis was performed on -log K_i values. Mean values and confidence intervals (95%) were converted to nanomolar concentrations.

Similar methods were used for determination of H₁, H₂, dopamine D₁ and D₂ receptor affinities using [³H]-pyrilamine (1 nM), [³H]-histamine (10 nM) and [³H]-loperone (0.2 nM), respectively.^{18,19}

Inhibition studies with human recombinant monoamine oxidases A and B

Monoamine oxidase A/B inhibition assays were performed as described previously using the discontinuous fluorimetric method.^{17,21} Briefly, for IC₅₀ determinations (without pre-incubation; 0 min) compounds (ten suitable concentrations between 10⁻¹¹ and 10⁻⁷ M) were incubated with kynuramine as substrate (2xK_m, K_m of 20 μM and 30 μM for MAO A and B, respectively) and MAO A (1.25 ng mL⁻¹, 900 units mL⁻¹) or MAO B (1.67 ng mL⁻¹, 375 units mL⁻¹) in a final assay volume of 100 μL. In case of pre-incubation experiments, IC₅₀ values were obtained after incubating inhibitors with enzyme for 30 or 60 min at 37 °C prior to addition of substrate. Reactions were conducted in pre-warmed potassium phosphate buffer (50 mM, pH 7.4). All data were analyzed with GraphPad PRISM 6. The IC₅₀ curves were fitted by non-linear regression fit (bottom set to zero).

Reversibility of inhibition was confirmed via pre-incubation of inhibitor (10xIC₅₀) with MAO B for 30, 60 and 90 min (37°C), followed by 50x dilution in potassium phosphate buffer and assayed with an excess of substrate (10xK_m).²¹ Data were calculated as percentage of control (DMSO) for each time point.

Inhibition studies with acetyl- and butyrylcholinesterases

Cholinesterase inhibition assays were performed according to a modified Ellman's assay.¹²¹ Compounds (10⁻⁶ and 10⁻⁹ M) were preincubated with electric eel acetylcholine esterase (eeACHE Type VI-S; 0.0025 U mL⁻¹) or equine serum butyrylcholine esterase (eqBuCHE; 0.002 U mL⁻¹) at 37°C for 30 min in a total assay volume of 200 μL (0.1 M potassium phosphate buffer pH 8). The enzyme reaction was started by adding a mixture of dithiois-nitrobenzolic acid (DTNB; 0.5 mM) and acetylthiocholine iodide (ATCI; 1 mM). Absorbance was monitored at 412 nm at 37°C over a period of 30 min in 40 sec intervals. Percentage values were calculated relative to control (no inhibitor) and physostigmine was used as positive control.

Cell viability assay

Cell viability of SH-SY5Y cells was assessed using resazurin fluorescent dye.¹²² Resazurin sodium salt was dissolved in NaCl/P_i buffer (1.05 mM KH₂PO₄, 154 mM NaCl, 3.77 mM Na₂HPO₄, pH = 7.4) to obtain a final concentration of 440 μM (Storage at 4°C, protected from light). Cells (8000 cells/well) were seeded in 96 wells plates (total volume 100 μL/well) and grown at 37°C in a 5% CO₂ atmosphere. After 24 h, media was removed and replaced by culture media containing test compounds in different concentrations (maximum of 1% DMSO per well). Cells were incubated with compounds and 1-methyl-4-phenylpyridinium iodide (YPP⁺, 10 mM) as positive control for 24h. For determination of remained cell viability, cells were incubated with resazurin working solution (44 μM in RPMI medium, 100 μL) for 2h. Fluorescence intensity (Excitation: 535 nm, Emission: 590 nm, bandwidth 5 nm) was measured using an Infinite M1000 Pro multimode reader (Tecan, Switzerland).

References

- 1: Hopkins AL, Keiseri GM, Leeson PD, Rees DC, Reynolds CH. The role of ligand efficiency metrics in drug discovery. *Nat Rev Drug Discov.* 13(2014):105-21. doi: 10.1038/nrd1465.
- 2: Weissman SA, Zewge D. Recent advances in ether dialkylation. *Tetrahedron.*, 61 (2005) 7833-7863.
- 3: Tomasch M, Schwed JS, Weizel L, Stark H. Novel chalcone-based fluorescent human histamine h₃ receptor ligands as pharmacological tools. *Front. Syst. Neurosci.*, 6 (2012) 1-16.
- 4: K. Sander, Y. Von Coburg, J.-C. Camelin, X. Ligneau, O. Rau, M. Schubert-Zolacek, J. Schwartz, H. Stark, Acidic elements in histamine H₃ receptor antagonists. *Bioorg. Med. Chem. Lett.*, 20 (2010) 1581-1584.
- 5: Sadek B, Schwed JS, Subramanian D, Weizel L, Walter M, Adem A, Stark H. Non-imidazole histamine H₃ receptor ligands incorporating antiepileptic moieties. *Eur. J. Med. Chem.*, 77 (2014): 269-79. doi: 10.1016/j.ejmech.2014.03.014.
- 6: Williamson, A. About the theory of the formation of ethers. *Ann. Chem.*, 77 (1851) 37-49.
- 7: Affini A, Hagenow S, Zivkovic A, Marco-Contelles J, Stark H. Novel indanone derivatives as MAO B/h₃h₄ dual-targeting ligands for treatment of Parkinson's disease. *Eur. J. Med. Chem.*, 148 (2018): 487-497. doi:10.1016/j.ejmech.2018.02.015.
- 8: Kottler T, Sander K, Weizel L, et al. Receptor-specific functional efficacies of alkyl imidazoles as dual histamine H₃/H₄ receptor ligands. *Eur J Pharmacol.* 654 (2011), 200-208
- 9: Kharifor MA, Reiner D, Hagenow S, Stark H. Design, synthesis, and biological evaluation of novel oxadiazole- and triazole-based histamine H₃R ligands. *Bioorg Med Chem.* 2018 Aug 7;26(14):4034-4046. doi: 10.1016/j.bmc.2018.06.028.
- 10: Bautista-Aguilera OM, Hagenow S, Palomino-Antolin A, Farré-Alins V, Ismail L, Joffrin PL, Jimeno ML, Soukup O, Janočková J, Kalinowski L, Proschak E, Irlepa I, Moraleda I, Schwed JS, Romero Martínez A, López-Muñoz F, Chioia M, Egea J, Ramsay RR, Marco-Contelles J, Stark H. Multitarget-Directed Ligands Combining Cholinesterase and Monoamine Oxidase Inhibition with Histamine H₃R Antagonism for Neurodegenerative Diseases. *Angew. Chem. Int. Ed. Engl.*, 56(2017),12765-12769. doi: 10.1002/anie.201706072.
- 11: Ellman GL, Courtney KD, Andres V, Featherstone RM, *Biochem. Pharmacol.*, 7 (1961), 88-95.
- 12: O'Brien J, Wilson I, Orton T, Pogran F. Investigation of the Alamar Blue (resazurin) Fluorescent Dye for the Assessment of Mammalian Cell Cytotoxicity. *Eur. J. Biochem.* 2000, 267, 5421-5426.

4.4. Histamine H₃ receptor ligands by hybrid virtual screening, docking, molecular dynamics simulations, and investigation of their biological effects

Nakisa Ghamari^{1),2)}, Omid Zarei^{3),4)}, David Reiner⁵⁾, Siavoush Dastmalchi^{1),2)}, Holger Stark⁵⁾, Maryam Hamzeh-Mivehroud^{1),2)}

1) Biotechnology Research Center, Tabriz, University of Medical Sciences, Tabriz, Iran

2) School of Pharmacy, Tabriz University of Medical Sciences, Tabriz, Iran

3) Neurosciences Research Center, Kurdistan, University of Medical Sciences, Sanandaj, Iran

4) Cellular and Molecular Research Center, Research Institute for Health Development, Kurdistan University of Medical Sciences, Sanandaj, Iran

5) Institute of Pharmaceutical and Medicinal Chemistry, Heinrich Heine University Duesseldorf, Duesseldorf, Germany

Published in: *Chemical Biology & Drug Design*, 2019, 93:832–843.

DOI: 10.1111/cbdd.13471.

Contribution to research: DR planned, conducted and supervised cell-culture. DR co-organised test-ligands, prepared, planned and conducted radioligand displacement experiments, and evaluated corresponding data to determine H₃R affinity. DR wrote pharmacological parts of and reviewed the manuscript.

Abstract:

Histamine H₃ receptors (H₃R), belonging to G protein-coupled receptors (GPCR) class-A superfamily, are responsible for modulating the release of histamine as well as of other neurotransmitters by a negative feedback mechanism mainly in the central nervous system (CNS). These receptors have gained increased attention as therapeutic target for several CNS related neurological diseases.

In the current study, we aimed to identify novel H₃R ligands using in silico virtual screening methods. To this end, a combination of ligand-and structure-based approaches was utilized for screening of ZINC database on the homology model of human H₃R. Structural similarity-and pharmacophore-based approaches were employed to generate compound libraries. Various molecular modelling methodologies such as molecular docking and dynamics simulation along with different drug-likeness filtering criteria were applied to select anti-H₃R ligands as promising candidate molecules based on different known parent lead compounds. In vitro binding assays of the selected molecules demonstrated three of them being active within the micromolar and submicromolar K_i range. The current integrated computational and experimental methods used in this work can provide new general insights for systematic hit identification for novel anti-H₃R agents from large compound libraries.

Reproduced from Ghamari N, Zarei O, Reiner D, Dastmalchi S, Stark H, Hamzeh-Mivehroud M, Histamine H₃ receptor ligands by hybrid virtual screening, docking, molecular dynamics simulations, and investigation of their biological effects, *Chem. Biol. Drug Des.*, 2019, 93:832-843. Reprinted with written permission from John Wiley & Sons (Licence number: 4810131416149).

Copyright 2018 John Wiley & Sons A/S

Received: 20 October 2018 | Revised: 28 November 2018 | Accepted: 17 December 2018
DOI: 10.1111/cbdd.13471

RESEARCH ARTICLE



Histamine H₃ receptor ligands by hybrid virtual screening, docking, molecular dynamics simulations, and investigation of their biological effects

Nakisa Ghamari^{1,2} | Omid Zarci^{3,4} | David Reiner⁵ | Siavoush Dastmalchi^{1,2} | Holger Stark⁵ | Maryam Hamzeh-Mivehroud^{1,2}

¹Biotechnology Research Center, Tabriz University of Medical Sciences, Tabriz, Iran

²School of Pharmacy, Tabriz University of Medical Sciences, Tabriz, Iran

³Neurosciences Research Center, Kurdistan University of Medical Sciences, Sanandaj, Iran

⁴Cellular and Molecular Research Center, Research Institute for Health Development, Kurdistan University of Medical Sciences, Sanandaj, Iran

⁵Institute of Pharmaceutical and Medicinal Chemistry, Heinrich Heine University Düsseldorf, Düsseldorf, Germany

Correspondence

Holger Stark, Heinrich Heine University Düsseldorf, Institute of Pharmaceutical and Medicinal Chemistry, Duesseldorf, Germany.

Email: stark@hhu.de

Maryam Hamzeh-Mivehroud, Biotechnology Research Center and School of Pharmacy, Tabriz University of Medical Sciences, Tabriz, Iran.

Emails: hamzehm@tbzmed.ac.ir, maryam_h_7860@yahoo.com

Funding information

Research Office and Biotechnology Research Center of Tabriz University of Medical Sciences, Grant/Award Number: 57572; German Research Society, Grant/Award Number: DFG INST 208/664-1 FUGG

Abstract

Histamine H₃ receptors (H₃R), belonging to G-protein coupled receptors (GPCR) class A superfamily, are responsible for modulating the release of histamine as well as of other neurotransmitters by a negative feedback mechanism mainly in the central nervous system (CNS). These receptors have gained increased attention as therapeutic target for several CNS related neurological diseases. In the current study, we aimed to identify novel H₃R ligands using in silico virtual screening methods. To this end, a combination of ligand- and structure-based approaches was utilized for screening of ZINC database on the homology model of human H₃R. Structural similarity- and pharmacophore-based approaches were employed to generate compound libraries. Various molecular modeling methodologies such as molecular docking and dynamics simulation along with different drug likeness filtering criteria were applied to select anti-H₃R ligands as promising candidate molecules based on different known parent lead compounds. In vitro binding assays of the selected molecules demonstrated three of them being active within the micromolar and submicromolar K_i range. The current integrated computational and experimental methods used in this work can provide new general insights for systematic hit identification for novel anti-H₃R agents from large compound libraries.

KEYWORDS

anti-H₃R agents, histamine H₃ receptor, molecular docking, molecular dynamics simulation, virtual screening

1 | INTRODUCTION

Histamine as a biogenic amine exerts its physiological effects via four different subtypes of G-protein coupled histamine receptors: H₁, H₂, H₃, and H₄ receptors (H₁R, H₂R, H₃R, and H₄R, respectively). Although blockade of H₁R and H₂R has

led to development of successful marketed drugs for treatment of allergy and gastric acid-related diseases, respectively, the H₃R- and H₄R-related therapeutics are under investigation or in early phases of clinical trials. The discovery of H₃R dates back to 1983 with the observation of regulated histamine release in depolarized slices of rat cerebral cortex by Arrang,

Garbarg, & Schwartz (1983). As presynaptic autoreceptors, they not only control the release of histamine, but also regulate the release of other neurotransmitters such as dopamine, norepinephrine, serotonin, and acetylcholine (Berlin, Boyce, & Ruiz, 2011). From sequence similarity point of view, H₃R shows the highest sequence homology to the H₄R (about ~37%) while less than 20% to H₁ and H₂ receptors (Mocking et al., 2016; Tiligada, Zampeli, Sander, & Stark, 2009). H₃R are mainly found in central nervous system (CNS) of human and animals. Induced signal transduction pathways upon H₃R activation are mediated through G_{i/o} proteins of GPCR, leading to the decrease of intracellular Ca²⁺ and cyclic adenosine monophosphate formation by inhibition of adenylyl cyclase and hence the release of histamine and related neurotransmitters are suppressed (Nieto-Alamilla, Marquez-Gomez, Garcia-Galvez, Morales-Figueroa, & Arias-Montano, 2016).

Since many CNS-related disorders are affected by intracellular level of histamine and other neurotransmitters, in this context, H₃R have gained considerable attention to be targeted. On the basis of several recent investigations, H₃R antagonists and inverse agonists would be effective in CNS-related diseases and neuronal abnormalities such as attention deficit hyperactivity disorder (ADHD), Alzheimer's disease, schizophrenia, learning and memory disorders, sleep disorders epilepsy, and obesity (Gemkow et al., 2009). Recently, pitolisant (also known as tipolisant and BF2.649) marketed under brand name of Wakix[®] was approved by European Medical Agency as an inverse agonist of H₃R used for treatment of narcolepsy with or without cataplexy in adults (Syed, 2016).

Accelerating rational drug design and development from bench to bed necessitates involvement of multidisciplinary efforts that are often costly and time-consuming. From this perspective, computer-aided drug design has emerged as invaluable tool significantly contributing in modern drug design pipeline with the major goal to introduce potential bioactive compounds, hit to lead optimization, and eliminating unnecessary experiments in early drug discovery research (Macalino, Gosu, Hong, & Choi, 2015).

Virtual screening is one of the attractive fields of computer-aided drug design which is subdivided into two categories: structure- and ligand-based virtual screening strategies. In structure-based virtual screening, structural information about the target protein (either obtained experimentally from X-ray crystallography and NMR or determined based on molecular modeling techniques) is utilized for screening the compounds through molecular docking. Given a defined pharmacophore model of the target binding site, candidate molecules from large libraries of commercially available compounds are ranked based on predicted interaction energies between molecules and complementary binding sites. In the case of ligand-based approach, the screening is performed according to the information of ligands known

to interact with a target molecule using chemical similarity, substructure searches, and three-dimensional pharmacophore shape matching. This approach is used in case of limited structural information regarding the target of interest (Chen et al., 2012; Scior et al., 2012; Sliwoski, Kothiwale, Meiler, & Lowe, 2014). Virtual screening can serve as an alternative to biological high-throughput screening owing to its potential for finding effective molecules in a timely and cost-effective manner. It provides a very limited set of commercially available candidate molecules for further biological evaluation and optimization achieved by purchasing ready-to-use compounds or synthesizing the compounds (Bielska et al., 2011; Lionta, Spyrou, Vassilatis, & Cournia, 2014).

In the current study, we tried to identify novel H₃R ligands using *in silico* methods. A combination of ligand-based and structure-based approaches was utilized for screening of databases oriented on the homology model of human H₃R. Structural similarity and pharmacophore-based approaches were employed to generate compound libraries. Various molecular modeling methodologies such as molecular docking and dynamics simulation along with different filtering criteria such as *in silico* pharmacokinetic properties were applied to select candidate molecules for further preliminary biological evaluation. *In vitro* binding assays conducted on the selected compounds examined their capability for binding to H₃R. The current synergistically applied computational and experimental methods used in this work provide a workflow for systematic evaluation of large compound libraries while identifying new hit structures for the development of novel anti-H₃R agents.

2 | METHODS AND MATERIALS

2.1 | Molecular docking and pharmacophore model generation

A homology-based model for histamine H₃ receptor was generated using M₃ muscarinic acetylcholine receptor (PDB code: 4DAJ, Supporting information Appendix S1). In the next step, flexible docking of pitolisant into binding site of the modeled H₃R was performed using GOLD program (version 5.0; CCDC Inc., Cambridge, UK) (Jones, Willett, & Glen, 1995; Jones, Willett, Glen, Leach, & Taylor, 1997) running under LINUX operating system. To define the binding site atoms of the receptor, a point was assigned based on the known residues involved in binding. Geometric center of the residues Asp¹¹⁴, Thr¹¹⁹, Tyr¹⁸⁹, Phe¹⁹⁸, Glu²⁰⁶, Trp³⁷¹, and Tyr³⁷⁴ (identified to be part of the binding site) was calculated and set as the center of the binding site. All atoms within a radius 10 Å were selected, and flexible docking was performed. Docking was carried out by applying two distance constraints (1.5–3.5 Å). The first constraint was between nitrogen atom of piperidine ring from pitolisant and oxygen atom of Glu²⁰⁶

side chain from protein. The second one imposed on the system was between phenyl ring of pitolisant and phenyl ring of Tyr¹⁸⁹ side chain of protein. The best solution was selected based on score fitness and used for generation of pharmacophore model.

For 3D pharmacophore model generation, LIGANDSCOUT program (version 4.1, Inteligand, GmbH, Vienna, Austria. <http://www.inteligand.com/ligandscout>) was used (Wolber & Langer, 2005). In this study, the complex of docked pitolisant and H₃R was introduced to LIGANDSCOUT for 3D pharmacophore generation using predefined features, such as hydrogen bond acceptor (HBA), hydrogen bond donor (HBD), hydrophobic (HY), negative ionizable (NI), positive ionizable (PI), aromatic ring (AR). The pharmacophore model was inspected for containing crucial chemical features and used as 3D query for virtual screening procedure.

2.2 | Ligand library preparation and virtual screening

Three approaches including structure- and ligand-based virtual screening or combination of them were used to find new ligands capable of binding to human H₃ receptor including: (a) In the first method, structure-based virtual screening was used through integration of LIGANDSCOUT (version 4.1) derived pharmacophore and ZINC^{PHARMER} database (Kocs & Camacho, 2012). Briefly, the obtained pharmacophore was subjected to ZINC^{PHARMER} web server to find hit compound(s) among the purchasable chemical space available in ZINC database. For filtering the compounds, some stringent criteria were applied: maximum 1 hit per conformation, maximum 1 hit per molecule, a maximum root-mean-square deviation (RMSD) of 0.2, a maximum of 10 rotatable bonds, and maximum molecular weight of 300 Da. (b) The second approach was based on ligand-based virtual screening through 2D/3D similarity-based search. For this purpose, pitolisant was used for similarity search in SWISS^{SIMILARITY} database (Zoete, Daina, Bovigny, & Michielin, 2016) using FP2 fingerprint as 2D and Electroshape and Spectrophores methods as 3D search methods. (c) In this approach, a hybrid of ligand- and structure-based methods was utilized for virtual screening. Results from a ligand-based search on ZINC15 library (Sterling & Irwin, 2015) using pitolisant structure were used for generation of a compound library using internal library preparation features implemented in LIGANDSCOUT. The prepared library was used as input for structure-based virtual screening based on pharmacophore of pitolisant in complex with model structure of H₃R in LIGANDSCOUT program. The hits were ranked according to the pharmacophore-fit score values.

Then, the identified hits from all of three above-mentioned methods were subjected to SWISS^{TARGETPREDICTION} web server for predicting the potential target candidates in a chemical-pharmacological space (Zoete et al., 2016). Accordingly, the

molecules with the most probable affinity to the H₃R were selected for further analyses.

2.3 | Drug-likeness and ADME/Tox properties of the identified virtual hits

For further filtering the obtained hit compounds, they were sorted based on drug-likeness properties. A comprehensive set of criteria implemented in SwissADME web server was considered (Daina, Michielin, & Zoete, 2017) including the following: Lipinski rule of five (Lipinski, Lombardo, Dominy, & Feeney, 2001), bioavailability criteria (Martin, 2005), Ghose filter (Ghose, Viswanadhan, & Wendoloski, 1999), Egan filter (Egan, Merz, & Baldwin, 2000) Muegge filter (Muegge, Heald, & Brittelli, 2001), Veber filter (Veber et al., 2002), and a lead-likeness criteria (Teague Simon, Davis Andrew, Leeson Paul, & Oprea, 1999). Ligands that successfully passed drug-likeness filters were kept for further evaluations. Moreover, SwissADME web server was used for predicting the pharmacokinetic profile of the selected compounds such as absorption, distribution, metabolism, and excretion (ADME) properties. For toxicity evaluation, OPEN^{VIRTUALTOXLAB} (version 5.8) was used for anticipating toxic potential (TP) by providing estimation of binding affinity profile of the candidate molecules to off-target proteins including nuclear receptors (AR, ER α , ER β , GR, MR, PR, LXR, PPAR γ , TR α , and TR β), cytochrome P450 enzyme family (1A2, 2C9, 2D6, 3A4), a cytosolic transcription factor (AhR) and a potassium ion channel (hERG) (Vedani, Dobler, Hu, & Smiesko, 2015; Vedani, Dobler, & Smiesko, 2012). Then, the selected candidate molecules were introduced to the next step of analyses.

2.4 | Molecular docking and binding free energy calculation

Ligands retrieved following rigorous and different filters in terms of drug-likeness, ADME and toxicity properties were subjected to molecular docking studies. GOLD software was used for flexible docking of the molecules on the modeled H₃R based on the same procedure conducted for pitolisant as parent lead compound. Similarly, two different sets of distance constraints including Tyr¹⁸⁹ and Glu²⁰⁶ residues were applied to the equivalent atoms in pitolisant structure. This is to simulate the presence of π - π stacking and ionic interactions reported for pitolisant structure. In case of π - π stacking corresponding phenyl groups available in Tyr¹⁸⁹ and pitolisant are involved, whereas ionic interaction is formed between oppositely charged oxygen atom from Glu²⁰⁶ and nitrogen atom of piperidine ring from pitolisant. Subsequently, the best pose among the docking solutions for each ligand was selected according to the used scoring function.

Following the molecular docking procedure, the molecular dynamics (MD) simulation was conducted for the

complex of candidate molecules and H₃R. Binding free energy was calculated for the complex of candidate ligands and H₃R for the simulation length of 10 ns using MM-Poisson-Boltzmann Surface Area (PBSA)/Generalized-Born Surface Area (GBSA) methods implemented in the AMBER package (Case et al., 2005; Kollman et al., 2000) as described in Supporting information (Appendix S4).

2.5 | Histamine H₃ receptor binding assay

Experimental H₃R affinity estimates were derived as described by Khanfar, Reiner, Hagenow, & Stark (2018). Therefore, a titration pattern of the purchased ligands (ranging from 1 nM to 100 µM) and pitolisant (0.01–1,000 nM) in duplicates was incubated with [³H]-N^α-methylhistamine (2 nM, K_D = 3.08 nM) and membrane preparations of HEK-293 cells stably expressing the human H₃ receptor (20 µg/well) on 96-well microplates, including a sample of pitolisant (10 µM) for estimation of non-specific binding. After 90 min, incubation was terminated upon filtration on glass-fiber mats

(presoaked with 3% (m/m) polyethylene-imine solution) using a cell-harvester (Inotech, Dottikon, Switzerland) and removing unbound radioligand by three washing steps with cold water. Subsequently dried filter mats were soaked with scintillation liquid, sealed and subjected to read out using a MicroBeta[®] TriLuxscintillation counter (Wallac, Turku, Finland). Specific binding data were analyzed using non-linear least squares fit module of GRAPHPAD PRISM[®] (2012, vers. 6.01, La Jolla, CA, USA) to yield IC₅₀ values, being converted to K_i constants (Cheng & Prusoff, 1973).

3 | RESULTS

3.1 | Molecular docking study and pharmacophore modeling

Following the modeling of H₃ receptor, pitolisant was docked into the model using GOLD program and Piecewise Linear Potential (PLP) fitness function (Korb, Stutzle, & Exner, 2009) to rank the docking solutions. The population size, number of

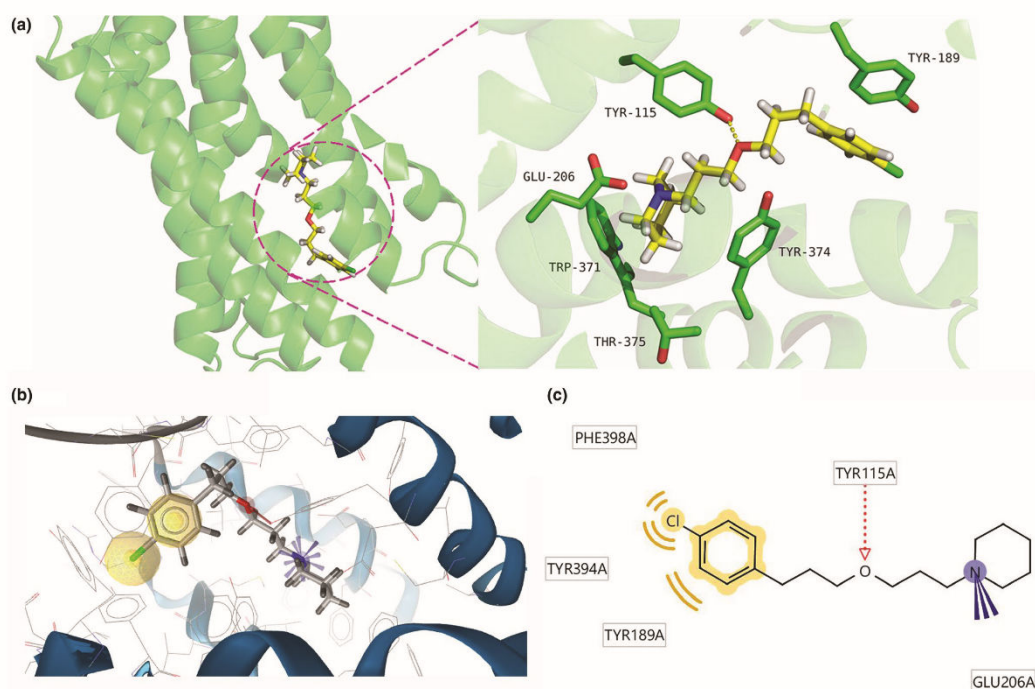


FIGURE 1 (a) 3D representation of the docked pitolisant into binding site of modeled H₃R generated by PyMol program (version 1.7.x). The ligands and the main interacting residues are illustrated as sticks. Only the side chains of the interacting residues from receptor are shown for further clarity. (b) The structure-based pharmacophore model of pitolisant-H₃R generated by LIGANDSCOUT program (version 4.1). (c) Chemical structures of pharmacophoric elements of pitolisant-H₃R complex used for structure-based virtual screening procedure. The yellow color indicates hydrophobic (HY) interaction, the red dashed arrow demonstrates hydrogen bond acceptor (HBA), and the purple color refers to positive ionizable (PI) area [Colour figure can be viewed at wileyonlinelibrary.com]

operations, and the number of islands were set to 100, 100,000, and 5, respectively. The best solution based on greater value of scoring function was selected and used for pharmacophore generation. Figure 1 illustrates the docked pitolisant in complex with histamine H₃ receptor. As shown, phenyl ring of pitolisant is sandwiched between Tyr¹⁸⁹ and Phe³⁹⁸. Piperidine nitrogen establishes an ionic bond with Glu²⁰⁶, and a hydrogen bond is observed between linker oxygen atom of pitolisant and Tyr¹¹⁵. The construction of the pharmacophore for structure-based virtual screening was based on the common features of already known active compounds utilizing LIGAND-SCOUT 4.1. Four chemical features including two hydrophobic regions, a positively ionizable moiety, and a hydrogen bond acceptor constituted the pharmacophore model (Figure 1). A π - π stacking interaction pointed to phenyl ring of Tyr¹⁸⁹, an ionic interaction oriented to Glu²⁰⁶, hydrophobic interactions through Phe³⁹⁸ and Tyr³⁹⁴ residues, and a hydrogen bond acceptor toward Tyr¹¹⁵ were considered as pharmacophoric elements and used as query for structure-based virtual screening procedure.

3.2 | Virtual screening of commercial libraries

Different approaches were employed for virtual screening of the ZINC database presented in Figure 2. In the structure-based virtual screening, 3D pharmacophoric features

generated for H₃R-pitolisant complex was used as input in the ZINCPhARMER web server to search purchasable chemical space available in ZINC database containing ~22 million commercially available compounds. Considering primary filtering criteria such as described above resulted to 56 chemical compounds. The remaining molecules were screened by applying additional lead-likeness filter (i.e. MW < 350 Da) leading to the selection of 16 hit compounds. The obtained compounds were subjected to SWISSTARGETPREDICTION web server for predicting the corresponding potential targets. The results showed that only one compound with drug-likeness properties is predicted to bind H₃R with the highest probability.

The structural similarity search based on pitolisant (FP2 fingerprint, Electroshape, and Spectrophores methods as 2D and 3D search methods) was employed for screening process among the ~10.6 million drug-like molecules of ZINC database. Similar to the previous method, the identified hits were inspected according to the possible binding affinity toward H₃R using SWISSTARGETPREDICTION web server. The findings resulted to introducing 18, 20, and 26 compounds for FP2 fingerprint, Electroshape, and Spectrophores search methods, respectively.

A combined ligand- and structure-based virtual screening protocol (hybrid method) was adopted as third approach in the current study. First, a library was prepared by applying

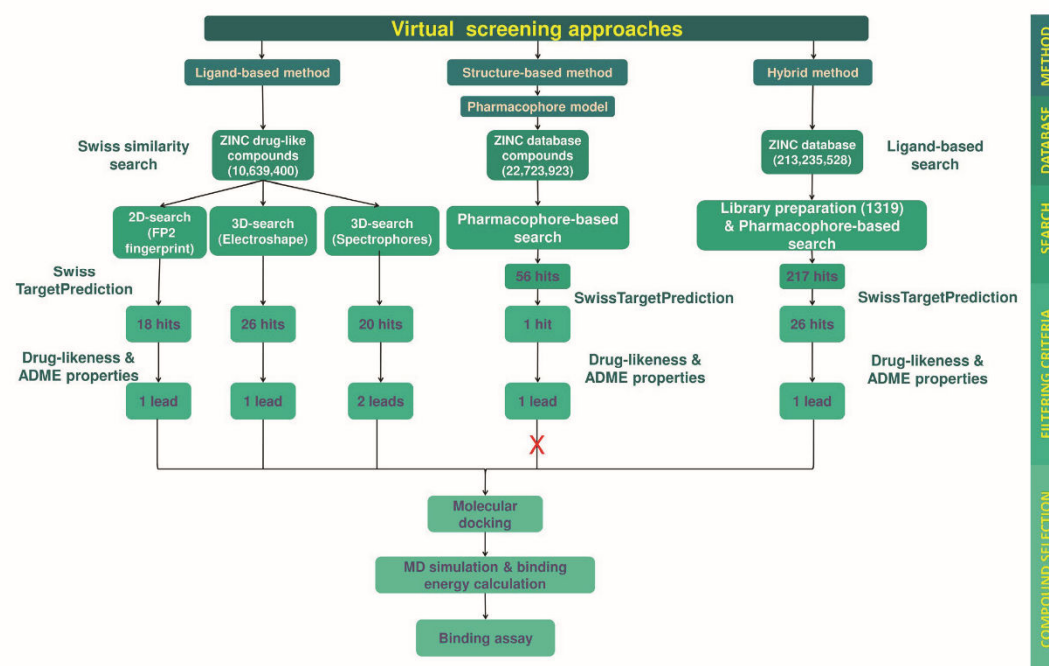
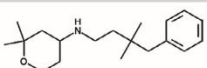
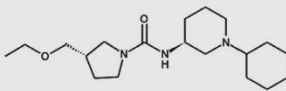
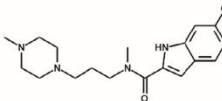
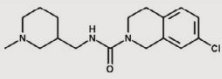
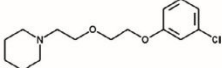


FIGURE 2 Overview of workflow used for virtual screening procedure [Colour figure can be viewed at wileyonlinelibrary.com]

TABLE 1 List of candidate molecules selected by virtual screening scheme

Compound	ZINC code	Structure	Search method
1	Zinc32124090		Ligand-based approach (FP2 fingerprint search method)
2	Zinc81494423		Ligand-based approach (Electroshape search method)
3	Zinc69700808		Ligand-based approach (Spectrophores search method)
4	Zinc90563066		Ligand-based approach (Spectrophores search method)
5	Zinc2895674		Hybrid approach

ligand-based virtual screening as performed with pitolisant as template structure within 50% Tanimoto similarity index. Following the creation of library composed of 1,319 compounds, structure-based virtual screening was performed by introducing the library to LIGANDSCOUT program. The number of compounds was narrowed down to 217 hits using screening of library against pharmacophore model of pitolisant-H₃R and ranked based on pharmacophore fit value. The included chemical features of the pharmacophore are as follows: two hydrophobic regions, a positive ionizable moiety, and a hydrogen bond acceptor (see Figure 1). These compounds were scrutinized using SWISSTARGETPREDICTION web server and 26 molecules with the highest probability of binding to H₃R were kept for further analyses.

All the selected hits obtained from different approaches were subjected to the additional assessments for selection of final drug-like compounds.

3.3 | Drug-likeness, ADME profiling, and toxicity risk assessment

To investigate the drug-likeness and pharmacokinetic properties of the retrieved hit compounds (shown in Table 1), different criteria were applied using SwissADME database. The pioneer of drug-likeness criteria corresponds to the study by Christopher A. Lipinski and his coworkers known as Lipinski's "rule-of-five." In this rule, an orally bioactive compound should pass the following criteria: MW of ≤ 500 Da, $\log P \leq 5$, hydrogen bond donor ≤ 5 , and hydrogen bond acceptor (N and O atoms) ≤ 10 . The other proposed criteria for drug-likeness property such as Ghose,

Egan, Muegge, and Veber are indicated in Supporting information Table S2.1. Furthermore, a variety of pharmacokinetic parameters such as blood–brain barrier (BBB) permeability, intestinal absorption, being substrate for P-glycoprotein (P-gp) or substrates, inhibitors or inducers of Cytochrome P-450 (CYP450) isoforms are also predicted (See Supporting information Table S2.1 for details). The analysis of the compounds obtained via the identification scheme presented in Figure 2 leads to identification of five drug candidates of which successfully passed those mentioned drug-likeness criteria as defined in Supporting information Table S2.1. One additional compound was identified from structure-based approach but excluded from further investigations due to contained imidazole moiety, since the latter showing detrimental biological properties. Compounds 1–4 originated from ligand-based search, with 1 and 2 detected by FP2 fingerprint and Electroshape methods of SWISSSIMILARITY, respectively, while compounds 3 and 4 were introduced as a result of the Spectrophores method of SWISSSIMILARITY. Compound 5 was obtained from hybrid method of virtual screening.

All the identified molecules have lead-likeness properties except compound 1 containing one violation (i.e. XLOGP3 > 3.5). Also, all the selected candidate molecules are predicted to be of desirable blood–brain barrier (BBB) permeability and of oral bioavailability, inferred from Abbott bioavailability score with potential synthetic accessibilities (Supporting information Table S2.1; Martin, 2005).

For toxicological risk assessment, OPENVIRTUALTOXLAB program was applied as a combination of automated and flexible molecular docking integrated with multi-dimensional

Compound	ZINC ID	$\Delta G_{\text{Binding (GB)}}$	$\Delta G_{\text{Binding (PB)}}$
Pitolisant	Zinc34045468	-38.85 (± 2.38)	-32.36 (± 3.23)
1	Zinc32124090	-35.56 (± 2.35)	-31.91 (± 3.08)
2	Zinc81494423	-35.32 (± 4.34)	-32.85 (± 3.77)
3	Zinc69700808	-36.88 (± 2.95)	-31.72 (± 3.69)
4	Zinc90563066	-28.72 (± 2.98)	-23.60 (± 3.89)
5	Zinc2895674	-23.62 (± 2.81)	-16.60 (± 3.37)

Note. Standard deviations are shown in parentheses.

quantitative structure–activity relationship (QSAR). Endocrine and metabolic disruption, some aspects of carcinogenicity and cardiotoxicity are evaluated in this approach, and the results are presented as an estimation of binding affinity (i.e. TP) toward 16 target proteins most likely to trigger adverse effect. Five classes (i.e. 0, I, II, III, and IV) are considered for assessing the toxic potential of the given compounds ranging from none to extreme in the scale of toxicity alert. The result of toxicity risk assessment for the selected candidate molecules is provided in Supporting information Table S2.2 with no toxic potential predicted for compounds **1** and **2**, moderate classification is found for compounds **4** and **5**, whereas **3** falls into class I (elevated toxic potential).

3.4 | Molecular docking and calculation of binding free energy for ligand–receptor complex

In an attempt for determining the binding mode of the selected candidate molecules with homology-based model of H₃R, the flexible docking was executed by GOLD program based on the procedure outlined for pitolisant structure. Supporting information Figure S3.1 illustrates the interactions between docked ligands and H₃R. For more comprehensive information on molecular docking analysis, see Supporting information S3. The best docked pose in complex with H₃R was subjected for MD simulation for 10 ns using AMBER package. Analysis of the RMSD trajectories and potential energy plot revealed that all systems in the simulation were well-equilibrated and remained stable throughout 10 ns simulation run (Supporting information Figure S4.1). During the simulation, the snapshots were extracted every 10 ps from the trajectory and used for estimation of binding free energy by applying MM-PBSA/GBSA methods implemented in AMBER package. Table 2 shows the binding free energy for the complexes with respect to pitolisant structure (as reference compound).

3.5 | Histamine H₃ receptor binding assay

In vitro human H₃R affinity determination using tritiated N^α-methylhistamine revealed three of the preselected

TABLE 2 Calculated mean values of binding free energies for the complex of docked candidate molecules and H₃R using Generalized-Born, $\Delta G_{\text{Binding (GB)}}$ and Poisson–Boltzmann, $\Delta G_{\text{Binding (PB)}}$ method for 10 ns MD simulation

TABLE 3 Affinity at human histamine H₃ receptor (H₃R) determined by [³H]-N^α-methylhistamine displacement assay

Compound	H ₃ R K _i (μM) [95% CI] ^a	n ^b
Pitolisant	0.0071 [0.0047;0.0106]	8
1	> 10	3
2	> 10	3
3	0.49 [0.12; 1.97]	4
4	0.54 [0.26; 1.16]	3
5	1.2 [0.7; 2.0]	3

^aValues represent affinity estimates at human H₃R as means and corresponding confidence interval (CI 95%).

^bNumber of independent experiments performed in duplicates.

structures being active within the screened concentration range (Table 3). Purity of purchased compounds was about 89.0%, determined by LC-MS as described in Supporting information (S5). No affinity estimates could be derived for compound **1** consisting of a secondary amine instead of tertiary amine as shown in Table 1. Compound **2**, lacking aromatic moiety appeared inactive as well. Thereinstead, micromolar and submicromolar K_i were detected for the remaining compounds without significant differences within this group. Each of the latter consists of chlorine substituted aromatic core in the eastern part of the molecule and a tertiary alicyclic amine on the facing part.

4 | DISCUSSION

Presynaptic histamine H₃ receptors (H₃R) act as auto- or heteroreceptors, modulating the release of histamine and other neuroactive substances in the central nervous system (CNS). The extracellular levels of several neurotransmitters are enriched by H₃R antagonists, and there is a great interest for brain-penetrating H₃ receptor antagonists/inverse agonists to compensate for the neurotransmitter deficiency existing in various neurological disorders. As a result of relevant investigations in animal models of CNS diseases, administration of anti-H₃R ligands enhances the synaptic neurotransmission and improves the

corresponding neurophysiological processes (Hancock & Fox, 2004). There are lines of evidence suggesting the usefulness of H₃-antagonists/inverse agonists in the treatment of neurological disorders (Haig et al., 2014; Herring et al., 2012; Jarskog et al., 2015; Passani, Cangioli, Bacciottini, Mannaioni, & Blandina, 2000; Schwartzbach et al., 2017). Due to the important physiological role of H₃R in controlling neurotransmitters, special attention has been dedicated to the development of novel H₃ antagonists for their potential therapeutic applicability in neurological diseases.

In spite of tremendous ongoing projects for identification of novel H₃ ligands, there is no crystallography or NMR derived solved 3D structure for H₃R due to obstacles and challenges dealing with solubilization, purification, and crystallization of GPCRs (Carpenter, Beis, Cameron, & Iwata, 2008; Loll, 2003; Zhao & Wu, 2012). By solving the 3D structure of bovine rhodopsin using crystallography technique in 2000, this protein was used for modeling of GPCRs as the only available template for several years as well as for H₃R. Following the introduction of crystal structure for histamine H₁ receptor in complex with doxepin by Shimamura et al. (2011), it was used for developing more realistic homology models for H₃R in comparison with bovine rhodopsin (Harusawa et al., 2013; Tang et al., 2013; Wen, Liu, Hu, Wang, & Wu, 2017). However, the structural features can be considered in addition to sequence similarity for alignment of target and template sequence for modeling purposes. In the current study, we modeled the H₃R using M₃ muscarinic acetylcholine receptor (PDB code: 4DAJ) as the template due to its high sequence similarity to H₃R. Although the similarity of M₃ muscarinic receptor is important for modeling of H₃R, the alignment was further improved according to the structure-based sequence alignment using proposed GPCR Sequence-Structure (GROSS) alignment of transmembrane (TM) regions for all experimentally solved structures for human GPCR (Cvick, Goddard, & Abrol, 2016; Kim, Fristrup, Abrol, & Goddard, 2011).

Molecular docking of pitolisant as reference molecule was performed based on the identified key residues in the binding site resulting in docking comparable to those reported elsewhere (Kuder et al., 2016; Łazewska et al., 2016; Levoine et al., 2008; Morini et al., 2006). These amino acids might be the key residues of the binding site of H₃R important for ligand binding as evidenced in several previously published reports (Axe, Bembenek, & Szalma, 2006; Kuder et al., 2016; Łazewska et al., 2016; Levoine et al., 2013; Morini et al., 2006; Schwartz, 2011). As structure-based virtual screening method, the pharmacophore model of the receptor complex outlined above was generated by LIGANDSCOUT and applied to online ZINCPharmer web server (Figure 1). Based on drug/lead-likeness filtering criteria and target prediction, only one imidazole-based compound was identified. This compound was excluded from further analyses due to its undesirable

properties such as binding to heme iron of cytochrome P450 enzymes (CYP450) as well as lack of selectivity toward histamine H₃/H₄ receptors (Łazewska et al., 2006; Sander, Kottke, & Stark, 2008).

The secondly applied ligand-based similarity search was carried out aiming to reach compounds with more than 50% similarity to pitolisant using ZINC drug-like of SWISSSIMILARITY database employing FP2 fingerprint, Electroshape, and Spectrophores search methods. As two-dimensional search method, descriptors originated from two-dimensional chemical structures are generated followed by computing similarities between descriptors of the molecular fingerprint (FP) and of chemical properties encoded in a vector, quantified using Tanimoto coefficient (Zoete et al., 2016). Thereinstead, as three-dimensional approaches, the 3D geometry of the molecules is considered such as Electroshape and Spectrophores search methods. The latter consist of multi-dimensional vectors considering the shape and molecular features while in Electroshape search methods, properties like atomic charge and partition coefficient are used for defining fourth and fifth coordinates of each atom. The retrieved compounds from each search methods were subjected to a second filtering in terms of drug/lead-likeness criteria and target prediction. Totally four candidate molecules were selected: one from FP2 fingerprint method (compound 1), one from Electroshape (compound 2), and two from Spectrophores (compounds 3 and 4) search methods (Table 1). The last virtual screening method utilized in the current study was a hybrid of ligand- and structure-based methods. Structural similarity- and pharmacophore-based approaches were employed to generate compound libraries to be screened according to the given pharmacophore. This approach led to identification of the fifth molecule (compound 5) having lead-likeness properties with probable H₃R affinity predicted. The embedded database in SWISSTARGETPREDICTION web server works based on a knowledge-based algorithm using 2D and 3D similarity measures in terms of chemical structure and molecular shape (Gfeller et al., 2014). To satisfy selectivity, H₃R was listed as first rank of target prediction with high probability for selected candidate molecules.

High attrition risk on late stage drug development necessitates early evaluation of pharmacokinetic profile, drug-likeness criteria, and toxicity risk. ADME properties such as absorption, distribution, metabolism, and excretion of drugs are studied on different clinical stages of development. In silico prediction of ADME properties has dramatically reduced high costs associated with labor-extensive experiments. The predicted ADME properties using SwissADME web server revealed all of the selected candidate molecules having high BBB penetration which is important for H₃R ligands. Moreover, high intestinal absorption was observed for all the compounds. From metabolic point of view, none of them inhibit the CYP3A4 and CYP2C9 as important



FIGURE 3 Schematic presentation of the pharmacophore model proposed for the selected candidate molecules as anti-H₃R ligands [Colour figure can be viewed at wileyonlinelibrary.com]

drug metabolizing isoforms of cytochrome P450 (CYP450) enzymes. Further, all the five selected compounds successfully passed the different drug-likeness criteria, and no violation was observed within the corresponding defined limits (Supporting information Table S2.1; Zanger & Schwab, 2013).

Preliminary potential “off-target” activity evaluation of the drug-like candidates such as endocrine and/or metabolic disruption, carcinogenicity, and cardiotoxicity is of great importance for toxicity assessment. The toxicity profile analysis using OPENVIRTUALTOXLAB program suggests the possible safety of the candidate molecules judged from low statistical probability (i.e. TP values assigned to class 0 and I; Supporting information Table S2.2).

Interestingly, the current selected molecules share a set of structural commonalities on the basis of given pharmacophore. Figure 3 shows the schematic representation of the main scaffold proposed for the selected candidate molecules comprised of a basic amine moiety connected to a hydrophobic/aromatic moiety through a linker. To investigate the mode of interactions of the compounds with H₃R and map pharmacophore features with key binding site residues, molecular docking was carried out. The results of docking indicate that the critical amino acids interacting with different parts of selected molecules are as follows: Glu²⁰⁶ (TM5) in the interaction with basic moiety, Tyr¹¹⁵ (TM3) and Tyr³⁷⁴ (TM6) residues interact with linker, and Tyr¹⁸⁹ (TM5) and Phe³⁹⁸ (TM7) forms the hydrophobic pocket with hydrophobic/aromatic moiety (Figure S3.1). These findings are in close agreement with the findings published previously (Axe et al., 2006; Bajda et al., 2012; Harusawa et al., 2013; Kuder et al., 2016; Łażewska et al., 2016; Lepailleur et al., 2014; Levoine et al., 2013; Morini et al., 2006; Sheng et al., 2015; Wen et al., 2017).

Affinity measurements revealed compounds **3–5** being active at H₃R. This is in contrast to the results obtained by MD simulations. Whereas the latter showing similar binding free energies between pitolisant and compounds **1–3** while presenting weaker ones for compounds **4** and **5**, affinity estimates in *N*^α-methylhistamine displacement indicate no affinity for **1** and **2** and similar binding affinities for the remaining compounds. To address these discrepancies, the use of H₃R agonist *N*^α-methylhistamine as radiolabeled species within the binding studies should be considered as the MD simulations were carried out using the receptor conformation while interacting with the H₃R inverse agonist pitolisant.

Structural differences presumably answering for the observations of the radioligand displacement studies comprise of

alternating substitution degree of basic amine in compound **1** (secondary instead of tertiary) and lacking aromatic cores in compound **2**. However, these are common structural features of H₃R ligands but no prerequisite to show activity. Namely the endogenous ligand histamine lacks tertiary amine and the sterically restricted steroid alkaloid conessine being active at H₃R without consisting of any aromatic core (Panula et al., 2015). Compound **3** shows structural resemblance to H₄R antagonist JNJ-7777120 with H₃R affinity ranging within the same order of magnitude whereas compound **5** appears as a pitolisant counterpart. In case of the latter pair, the decreased lipophilicity due to the bis-ethoxy linker and the shortage by one methylene group, thereby changing the spatial orientation of the aromatic core to the tertiary amine, may account for the reduced affinity.

5 | CONCLUSION

In the present investigation, novel anti-H₃R agents were introduced using ligand- and structure-based virtual screening approaches followed by in vitro binding assays. Biological evaluations revealed micromolar and submicromolar K_i values (i.e., 0.49–1.2 μM) for three of the identified molecules. The mode of interactions for the selected compounds was predicted using molecular modeling techniques. Taken together, the presented lead candidates may serve as starting points for further medicinal chemistry optimization for development of novel CNS selective H₃R antagonists to be used in neurodegenerative diseases.

ACKNOWLEDGEMENTS

This work forms part of the PhD thesis of Nakisa Ghamari at the School of Pharmacy, Tabriz University of Medical Sciences, Tabriz, Iran. The authors would like to thank the Research Office and Biotechnology Research Center of Tabriz University of Medical Sciences for providing financial support under the Postgraduate Research Grant scheme (Grant No. 57572) for the PhD thesis of NG. The authors also would like to thank for the technical support of Dr. Aleksandra Zivkovic and Kathrin Grau and for the financial support by German Research Society (DFG INST 208/664-1 FUGG).

CONFLICT OF INTEREST

The authors declare no conflict of interest.

ORCID

Holger Stark  <https://orcid.org/0000-0003-3336-1710>

Maryam Hamzeh-Mivehroud  <https://orcid.org/0000-0002-1257-0102>

REFERENCES

- Arrang, J. M., Garbarg, M., & Schwartz, J. C. (1983). Auto-inhibition of brain histamine release mediated by a novel class (H₃) of histamine receptor. *Nature*, 302(5911), 832–837. <https://doi.org/10.1038/302832a0>
- Axe, F. U., Bembenek, S. D., & Szalma, S. (2006). Three-dimensional models of histamine H₃ receptor antagonist complexes and their pharmacophore. *Journal of Molecular Graphics and Modelling*, 24(6), 456–464. <https://doi.org/10.1016/j.jmgm.2005.10.005>
- Bajda, M., Kuder, K. J., Łażewska, D., Kieć-Kononowicz, K., Więckowska, A., Ignasik, M., ... Malawska, B. (2012). Dual-acting diether derivatives of piperidine and homopiperidine with histamine H₃ receptor antagonistic and anticholinesterase activity. *Archiv der Pharmazie*, 345(8), 591–597. <https://doi.org/10.1002/ardp.201200018>
- Berlin, M., Boyce, C. W., & Ruiz, M. L. (2011). Histamine H₃ receptor as a drug discovery target. *Journal of Medicinal Chemistry*, 54(1), 26–53. <https://doi.org/10.1021/jm100064d>
- Bielska, E., Lucas, X., Czerwoniec, A., Kasprzak, J., Kaminska, K., & Bujnicki, J. (2011). Virtual screening strategies in drug design—methods and applications. *BioTechnologia*, 3(92), 249–264. <https://doi.org/10.5114/bta.2011.46542>
- Carpenter, E. P., Beis, K., Cameron, A. D., & Iwata, S. (2008). Overcoming the challenges of membrane protein crystallography. *Current Opinion in Structural Biology*, 18(5), 581–586. <https://doi.org/10.1016/j.sbi.2008.07.001>
- Case, D. A., Cheatham III, T. E., Darden, T., Gohlke, H., Luo, R., Merz Jr, K. M., ... Woods, R. J. (2005). The Amber biomolecular simulation programs. *Journal of Computational Chemistry*, 26(16), 1668–1688. [https://doi.org/10.1002/\(ISSN\)1096-987X](https://doi.org/10.1002/(ISSN)1096-987X)
- Chen, L., Morrow, J. K., Tran, H. T., Phatak, S. S., Du-Cuny, L., & Zhang, S. (2012). From laptop to benchtop to bedside: Structure-based drug design on protein targets. *Current Pharmaceutical Design*, 18(9), 1217–1239. <https://doi.org/10.2174/138161212799436386>
- Cheng, Y., & Prusoff, W. H. (1973). Relationship between the inhibition constant (K_i) and the concentration of inhibitor which causes 50 per cent inhibition (I₅₀) of an enzymatic reaction. *Biochemical Pharmacology*, 22(23), 3099–3108.
- Cvick, V., Goddard III, W. A., & Abrol, R. (2016). Structure-based sequence alignment of the transmembrane domains of all human GPCRs: Phylogenetic, structural and functional implications. *PLoS Computational Biology*, 12(3), e1004805. <https://doi.org/10.1371/journal.pcbi.1004805>
- Daina, A., Michielin, O., & Zoete, V. (2017). SwissADME: A free web tool to evaluate pharmacokinetics, drug-likeness and medicinal chemistry friendliness of small molecules. *Scientific Reports*, 7, 42717. <https://doi.org/10.1038/srnp42717>
- Egan, W. J., Merz Jr, K. M., & Baldwin, J. J. (2000). Prediction of drug absorption using multivariate statistics. *Journal of Medicinal Chemistry*, 43(21), 3867–3877. <https://doi.org/10.1021/jm000292e>
- Gemkow, M. J., Davenport, A. J., Harich, S., Ellenbroek, B. A., Cesura, A., & Hallett, D. (2009). The histamine H₃ receptor as a therapeutic drug target for CNS disorders. *Drug Discovery Today*, 14(9–10), 509–515. <https://doi.org/10.1016/j.drudis.2009.02.011>
- Gfeller, D., Grosdidier, A., Wirth, M., Daina, A., Michielin, O., & Zoete, V. (2014). SwissTargetPrediction: A web server for target prediction of bioactive small molecules. *Nucleic Acids Research*, 42(W1), W32–W38. <https://doi.org/10.1093/nar/gku293>
- Ghose, A. K., Viswanadhan, V. N., & Wendoloski, J. J. (1999). A knowledge-based approach in designing combinatorial or medicinal chemistry libraries for drug discovery. I. A Qualitative and quantitative characterization of known drug databases. *Journal of Combinatorial Chemistry*, 1(1), 55–68. <https://doi.org/10.1021/cc9800071>
- Haig, G. M., Bain, E., Robieson, W., Othman, A. A., Baker, J., & Lenz, R. A. (2014). A randomized trial of the efficacy and safety of the H₃ antagonist ABT-288 in cognitive impairment associated with schizophrenia. *Schizophrenia Bulletin*, 40(6), 1433–1442. <https://doi.org/10.1093/schbul/sbt240>
- Hancock, A. A., & Fox, G. B. (2004). Cognitive enhancing effects of drugs that target histamine receptors. In J. J. Buccafusco (Ed.), *Cognitive enhancing drugs* (pp. 97–114). Basel, Switzerland: Birkhäuser Basel. <https://doi.org/10.1007/978-3-0348-7867-8>
- Harusawa, S., Sawada, K., Magata, T., Yoneyama, H., Araki, L., Usami, Y., ... Yamatodani, A. (2013). Synthesis and evaluation of N-alkyl-S-[3-(piperidin-1-yl)propyl]isothioureas: High affinity and human/rat species-selective histamine H₃ receptor antagonists. *Bioorganic & Medicinal Chemistry Letters*, 23(23), 6415–6420. <https://doi.org/10.1016/j.bmcl.2013.09.052>
- Herring, W. J., Wilens, T. E., Adler, L. A., Baranak, C., Liu, K., Snavely, D. B., ... Michelson, D. (2012). Randomized controlled study of the histamine H₃ inverse agonist MK-0249 in adult attention-deficit/hyperactivity disorder. *Journal of Clinical Psychiatry*, 73(7), e891–e898. <https://doi.org/10.4088/JCP.11m07178>
- Jarskog, L. F., Lowy, M. T., Grove, R. A., Keefe, R. S., Horrigan, J. P., Ball, M. P., ... Peykamian, M. A. (2015). A Phase II study of a histamine H₃ receptor antagonist GSK239512 for cognitive impairment in stable schizophrenia subjects on antipsychotic therapy. *Schizophrenia Research*, 164(1), 136–142. <https://doi.org/10.1016/j.schres.2015.01.041>
- Jones, G., Willett, P., & Glen, R. C. (1995). Molecular recognition of receptor sites using a genetic algorithm with a description of desolvation. *Journal of Molecular Biology*, 245(1), 43–53. [https://doi.org/10.1016/S0022-2836\(95\)80037-9](https://doi.org/10.1016/S0022-2836(95)80037-9)
- Jones, G., Willett, P., Glen, R. C., Leach, A. R., & Taylor, R. (1997). Development and validation of a genetic algorithm for flexible docking. *Journal of Molecular Biology*, 267(3), 727–748. <https://doi.org/10.1006/jmbi.1996.0897>
- Khanfar, M. A., Reiner, D., Hagenow, S., & Stark, H. (2018). Design, synthesis, and biological evaluation of novel oxadiazole- and thiazole-based histamine H₃R ligands. *Bioorganic & Medicinal Chemistry*, 26(14), 4034–4046. <https://doi.org/10.1016/j.bmc.2018.06.028>
- Kim, S.-K., Fristrup, P., Abrol, R., & Goddard III, W. A. (2011). Structure-based prediction of subtype selectivity of histamine H₃ receptor selective antagonists in clinical trials. *Journal of Chemical Information and Modeling*, 51(12), 3262–3274. <https://doi.org/10.1021/ci200435b>
- Koes, D. R., & Camacho, C. J. (2012). ZINCPharmer: Pharmacophore search of the ZINC database. *Nucleic Acids Research*, 40(Web Server issue), W409–W414. <https://doi.org/10.1093/nar/gks378>

- Kollman, P. A., Massova, I., Reyes, C., Kuhn, B., Huo, S., Chong, L., ... Cheatham III, T. E. (2000). Calculating structures and free energies of complex molecules: Combining molecular mechanics and continuum models. *Accounts of Chemical Research*, 33(12), 889–897. <https://doi.org/10.1021/ar000033j>
- Korb, O., Stutzle, T., & Exner, T. E. (2009). Empirical scoring functions for advanced protein-ligand docking with PLANTS. *Journal of Chemical Information and Modeling*, 49(1), 84–96. <https://doi.org/10.1021/ci800298z>
- Kuder, K., Lazewska, D., Latacz, G., Schwed, J. S., Karcz, T., Stark, H., ... Kieć-Kononowicz, K. (2016). Chlorophenoxy aminoalkyl derivatives as histamine H₃R ligands and antiseizure agents. *Bioorganic & Medicinal Chemistry*, 24(2), 53–72. <https://doi.org/10.1016/j.bmc.2015.11.021>
- Łazewska, D., Jorńczyk, J., Bajda, M., Szałaj, N., Więckowska, A., Panek, D., ... Kieć-Kononowicz, K. (2016). Cholinesterase inhibitory activity of chlorophenoxy derivatives—Histamine H₃ receptor ligands. *Bioorganic & Medicinal Chemistry Letters*, 26(16), 4140–4145.
- Lazewska, D., Ligneau, X., Schwartz, J. C., Schunack, W., Stark, H., & Kieć-Kononowicz, K. (2006). Ether derivatives of 3-piperidinopropan-1-ol as non-imidazole histamine H₃ receptor antagonists. *Bioorganic & Medicinal Chemistry*, 14(10), 3522–3529. <https://doi.org/10.1016/j.bmc.2006.01.013>
- Lepailleur, A., Freret, T., Lemaitre, S., Boulouard, M., Fo, Dauphin, Hinschberger, A., ... Rault, S. (2014). Dual histamine H₃R/serotonin 5-HT₄R ligands with anti-anxiolytic properties: Pharmacophore-based virtual screening and polypharmacology. *Journal of Chemical Information and Modeling*, 54(6), 1773–1784. <https://doi.org/10.1021/ci500157n>
- Levoine, N., Calmels, T., Poupardin-Olivier, O., Labeeuw, O., Danvy, D., Robert, P., ... Capet, M. (2008). Refined docking as a valuable tool for lead optimization: Application to histamine H₃ receptor antagonists. *Archiv der Pharmazie*, 341(10), 610–623. <https://doi.org/10.1002/ardp.200800042>
- Levoine, N., Labeeuw, O., Krief, S., Calmels, T., Poupardin-Olivier, O., Berrebi-Bertrand, I., ... Capet, M. (2013). Determination of the binding mode and interacting amino-acids for dibasic H₃ receptor antagonists. *Bioorganic & Medicinal Chemistry*, 21(15), 4526–4529. <https://doi.org/10.1016/j.bmc.2013.05.035>
- Lionta, E., Spyrou, G., Vassilatis, D. K., & Cournia, Z. (2014). Structure-based virtual screening for drug discovery: Principles, applications and recent advances. *Current Topics in Medicinal Chemistry*, 14(16), 1923. <https://doi.org/10.2174/1568026614666140929124445>
- Lipinski, C. A., Lombardo, F., Dominy, B. W., & Feeney, P. J. (2001). Experimental and computational approaches to estimate solubility and permeability in drug discovery and development settings. *Advanced Drug Delivery Reviews*, 46(1–3), 3–26. [https://doi.org/10.1016/S0169-409X\(00\)00129-0](https://doi.org/10.1016/S0169-409X(00)00129-0)
- Loll, P. J. (2003). Membrane protein structural biology: The high throughput challenge. *Journal of Structural Biology*, 142(1), 144–153. [https://doi.org/10.1016/S1047-8477\(03\)00045-5](https://doi.org/10.1016/S1047-8477(03)00045-5)
- Macalino, S. J., Gosu, V., Hong, S., & Choi, S. (2015). Role of computer-aided drug design in modern drug discovery. *Archives of Pharmacological Research*, 38(9), 1686–1701. <https://doi.org/10.1007/s12272-015-0640-5>
- Martin, Y. C. (2005). A bioavailability score. *Journal of Medicinal Chemistry*, 48(9), 3164–3170. <https://doi.org/10.1021/jm0492002>
- Mocking, T. A. M., Bosma, R., Rahman, S. N., Verweij, E. W. E., McNaught-Flores, D. A., Vischer, H. F., & Leurs, R. (2016). Molecular aspects of histamine receptors. In P. Blandina, & M. B. Passani (Eds.), *Histamine receptors: Preclinical and clinical aspects. The receptors*. 28 (pp. 1–50). Berlin, Switzerland: Springer.
- Morini, G., Comini, M., Rivara, M., Rivara, S., Lorenzi, S., Bordin, F., ... Plazzi, P. V. (2006). Dibasic non-imidazole histamine H₃ receptor antagonists with a rigid biphenyl scaffold. *Bioorganic & Medicinal Chemistry Letters*, 16(15), 4063–4067. <https://doi.org/10.1016/j.bmcl.2006.04.092>
- Muegge, I., Heald, S. L., & Brittelli, D. (2001). Simple selection criteria for drug-like chemical matter. *Journal of Medicinal Chemistry*, 44(12), 1841–1846. <https://doi.org/10.1021/jm015507e>
- Nieto-Alamilla, G., Marquez-Gomez, R., Garcia-Galvez, A. M., Morales-Figueroa, G. E., & Arias-Montano, J. A. (2016). The histamine H₃ receptor: Structure, pharmacology, and function. *Molecular Pharmacology*, 90(5), 649–673. <https://doi.org/10.1124/mol.116.104752>
- Panula, P., Chazot, P. L., Cowart, M., Gutzmer, R., Leurs, R., Liu, W. L., & Haas, H. L. (2015). International union of basic and clinical pharmacology. XCVIII. Histamine Receptors. *Pharmacological Reviews*, 67(3), 601–655. <https://doi.org/10.1124/pr.114.010249>
- Passani, M. B., Cangioli, I., Bacciottini, L., Mannaioni, P. F., & Blandina, P. (2000). Thioperamide and cimetidine modulate acetylcholine release from the amygdala of freely moving rats. *Inflammation Research*, 49(Suppl 1), S43–S44. <https://doi.org/10.1007/PL00000175>
- Sander, K., Kottke, T., & Stark, H. (2008). Histamine H₃ receptor antagonists go to clinics. *Biological & Pharmaceutical Bulletin*, 31(12), 2163–2181.
- Schwartz, J. C. (2011). The histamine H₃ receptor: From discovery to clinical trials with pitolisant. *British Journal of Pharmacology*, 163(4), 713–721. <https://doi.org/10.1111/j.1476-5381.2011.01286.x>
- Schwartzbach, C. J., Grove, R. A., Brown, R., Tompson, D., Bergh, F. T., & Arnold, D. L. (2017). Lesion remyelinating activity of GSK239512 versus placebo in patients with relapsing-remitting multiple sclerosis: A randomised, single-blind, phase II study. *Journal of Neurology*, 264(2), 304–315. <https://doi.org/10.1007/s00415-016-8341-7>
- Scior, T., Bender, A., Tresadern, G., Medina-Franco, J. L., Martinez-Mayorga, K., Langer, T., ... Agrafiotis, D. K. (2012). Recognizing pitfalls in virtual screening: A critical review. *Journal of Chemical Information and Modeling*, 52(4), 867–881. <https://doi.org/10.1021/ci200528d>
- Sheng, R., Tang, L., Jiang, L., Hong, L., Shi, Y., Zhou, N., & Hu, Y. (2015). Novel 1-phenyl-3-hydroxy-4-pyridone derivatives as multifunctional agents for the therapy of Alzheimer's disease. *ACS Chemical Neuroscience*, 7(1), 69–81.
- Shimamura, T., Shiroishi, M., Weyand, S., Tsujimoto, H., Winter, G., Katritch, V., ... GPCR Network (2011). Structure of the human histamine H₁ receptor complex with doxepin. *Nature*, 475(7354), 65–70. <https://doi.org/10.1038/nature10236>
- Sliwoski, G., Kothiwale, S., Meiler, J., & Lowe Jr, E. W. (2014). Computational methods in drug discovery. *Pharmacological Reviews*, 66(1), 334–395.
- Sterling, T., & Irwin, J. J. (2015). ZINC 15 – Ligand discovery for everyone. *Journal of Chemical Information and Modeling*, 55(11), 2324–2337. <https://doi.org/10.1021/acs.jcim.5b00559>
- Syed, Y. Y. (2016). Pitolisant: First global approval. *Drugs*, 76(13), 1313–1318. <https://doi.org/10.1007/s40265-016-0620-1>

- Tang, L., Zhao, L., Hong, L., Yang, F., Sheng, R., Chen, J., ... Hu, Y. (2013). Design and synthesis of novel 3-substituted-indole derivatives as selective H₃ receptor antagonists and potent free radical scavengers. *Bioorganic & Medicinal Chemistry*, 21(19), 5936–5944. <https://doi.org/10.1016/j.bmc.2013.07.051>
- Teague Simon, J., Davis Andrew, M., Leeson Paul, D., & Oprea, T. (1999). The design of Leadlike combinatorial libraries. *Angewandte Chemie International Edition*, 38(24), 3743–3748. [https://doi.org/10.1002/\(ISSN\)1521-3773](https://doi.org/10.1002/(ISSN)1521-3773)
- Tiligada, E., Zampelli, E., Sander, K., & Stark, H. (2009). Histamine H₃ and H₄ receptors as novel drug targets. *Expert Opinion on Investigational Drugs*, 18(10), 1519–1531. <https://doi.org/10.1517/14728220903188438>
- Veber, D. F., Johnson, S. R., Cheng, H. Y., Smith, B. R., Ward, K. W., & Kopple, K. D. (2002). Molecular properties that influence the oral bioavailability of drug candidates. *Journal of Medicinal Chemistry*, 45(12), 2615–2623. <https://doi.org/10.1021/jm020017n>
- Vedani, A., Dobler, M., Hu, Z., & Smiesko, M. (2015). OpenVirtualToxLab—a platform for generating and exchanging in silico toxicity data. *Toxicology Letters*, 232(2), 519–532. <https://doi.org/10.1016/j.toxlet.2014.09.004>
- Vedani, A., Dobler, M., & Smiesko, M. (2012). VirtualToxLab - a platform for estimating the toxic potential of drugs, chemicals and natural products. *Toxicology and Applied Pharmacology*, 261(2), 142–153. <https://doi.org/10.1016/j.taap.2012.03.018>
- Wen, G., Liu, Q., Hu, H., Wang, D., & Wu, S. (2017). Design, synthesis, biological evaluation, and molecular docking of novel flavones as H₃ R inhibitors. *Chemical Biology & Drug Design*, 90(4), 580–589. <https://doi.org/10.1111/cbdd.12981>
- Wolber, G., & Langer, T. (2005). LigandScout: 3-D pharmacophores derived from protein-bound ligands and their use as virtual screening filters. *Journal of Chemical Information and Modeling*, 45(1), 160–169. <https://doi.org/10.1021/ci049885e>
- Zanger, U. M., & Schwab, M. (2013). Cytochrome P450 enzymes in drug metabolism: Regulation of gene expression, enzyme activities, and impact of genetic variation. *Pharmacology & Therapeutics*, 138(1), 103–141. <https://doi.org/10.1016/j.pharmthera.2012.12.007>
- Zhao, Q., & Wu, B.-L. (2012). Ice breaking in GPCR structural biology. *Acta Pharmacologica Sinica*, 33(3), 324–334. <https://doi.org/10.1038/aps.2011.187>
- Zoete, V., Daina, A., Bovigny, C., & Michielin, O. (2016). SwissSimilarity: A web tool for low to ultra high throughput ligand-based virtual screening. *Journal of Chemical Information and Modeling*, 56(8), 1399–1404. <https://doi.org/10.1021/acs.jcim.6b00174>

SUPPORTING INFORMATION

Additional supporting information may be found online in the Supporting Information section at the end of the article.

How to cite this article: Ghamari N, Zarei O, Reiner D, Dastmalchi S, Stark H, Hamzeh-Mivehroud M. Histamine H₃ receptor ligands by hybrid virtual screening, docking, molecular dynamics simulations, and investigation of their biological effects. *Chem Biol Drug Des*. 2019;93:832–843. <https://doi.org/10.1111/cbdd.13471>

Supplementary Material

Histamine H₃ Receptor Ligands By Hybrid Virtual Screening, Docking, Molecular Dynamics Simulations, and Investigation of Their Biological Effects

Nakisa Chamari^{1,2}, Omid Zareh^{3,4}, David Reiner⁵, Siavoush Dastmalchi^{1,2}, Holger Stark^{5,*}, and Maryam Hamzeh-Mivehroud^{1,2,*}

¹ Biotechnology Research Center, Tabriz University of Medical Sciences, Tabriz, Iran

² School of Pharmacy, Tabriz University of Medical Sciences, Tabriz, Iran

³ Neurosciences Research Center, Kurdistan University of Medical Sciences, Sanandaj, Iran

⁴ Cellular and Molecular Research Center, Research Institute for Health Development, Kurdistan University of Medical Sciences, Sanandaj, Iran

⁵ Heinrich Heine University Dusseldorf, Institute of Pharmaceutical and Medicinal Chemistry, Universitaetstr. Dusseldorf, Germany

* Corresponding Authors:

Holger Stark and Maryam Hamzeh-Mivehroud

Full address: Heinrich Heine University Dusseldorf, Institute of Pharmaceutical And Medicinal Chemistry, Universitaetstr. Dusseldorf, Germany. Tel: +49 211 81-10478, Fax: +49 211 81-13359, Email: stark@hhu.de, Biotechnology Research Center and School of Pharmacy, Tabriz University of Medical Sciences, Tabriz, Iran. Tel: +98 (41) 3336 400385, Fax: +98 (41) 3337 9420, E-mail: hamzehm@tbzmed.ac.ir, maryam_h_786@yahoo.com

S1. Homology modeling of human H₃ receptor

Comparative molecular modeling was used for modeling of human histamine H₃ receptor (Uniprot ID: Q9Y5N1). The BLAST search engine, publicly available at National Center for Biotechnology Information (NCBI), was used to find the homologous proteins with known structures as the templates for human H₃ receptor. Based on the obtained results, M₃ muscarinic acetylcholine receptor (PDB code: 4DAJ) (1) was selected as the template due to its highest similarity to human H₃ receptor. Clustal Omega from its website at European Bioinformatics Institute (<https://www.ebi.ac.uk/Tools/msa/clustalo/>) was used for sequence alignment of H₃ receptor and M₃ muscarinic acetylcholine receptor accepting default values for the alignment parameters. The alignment was manually adjusted guided by structure-based sequence alignment of all human GPCRs (2, 3). Initial model was built using Swiss PDB viewer (SPDBV, version 4.1, Swiss Institute of Bioinformatics, Lausanne, Switzerland) based on the obtained alignment and submitted to Swiss-Model server to generate energy minimized model structure (<https://swissmodel.expasy.org/>) (4). The quality of the generated model was evaluated using PROCHECK (5), Molprobability (6), and Verify 3D (7, 8), from their web servers.

The pharmacophore model required for structure-based virtual screening procedure consisted of a homology model of the histamine H₃ receptor based on the structure of M₃ muscarinic acetylcholine receptor (PDB ID: 4DAJ) as the template. The initial amino acid sequence alignment between H₃R and M₃ receptor by Clustal Omega resulted to 26.43% sequence identity. This alignment was further manually improved on the basis of structure-based sequence alignment of all human GPCRs. Figure S1.1 shows the sequence alignment and highlights the key conserved residues (red capitals) among GPCR superfamily. Analysis of the optimized final energy minimized model obtained from Swiss-Model server by Procheck program showed that backbone ϕ and ψ dihedral angles for more than 99% of residues are in the allowed region of the Ramachandran plot (Figure S1.2). The similar quality measure was estimated to be 97.5% using the MolProbability method (Figure 2B). The results are indicative of high quality of the generated model from geometrical perspective. Furthermore, to assess the folding properties of the model in terms of compatibility of proposed model structure (3D) with its sequence (1D), Verify-3D methodology was applied. The result revealed 71.65% of the residues in the 3D/1D profile showing an average score of > 0.2 (Figure S1.3) and those with 3D-1D scores lower than this value not being close to the binding site of the receptor.

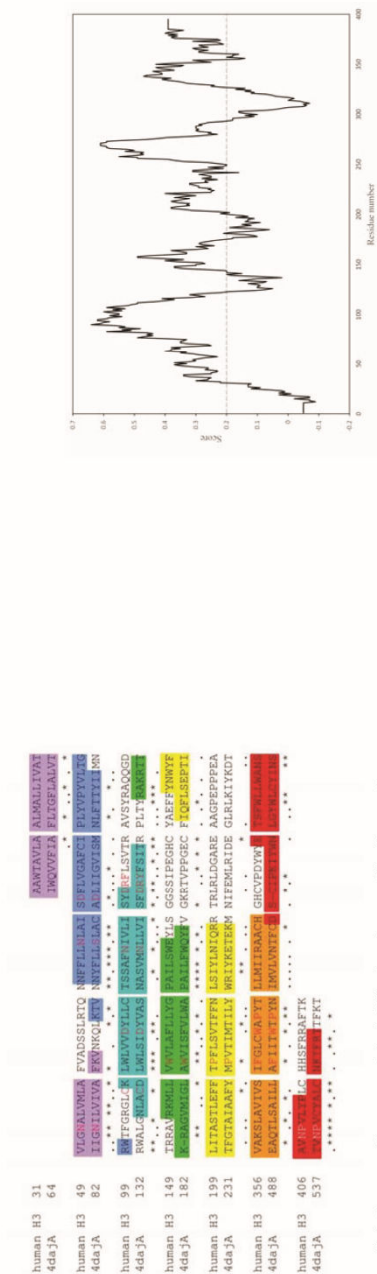


Figure S1. Sequence alignment used for building homology model of human H₃ receptor based on M1 muscarinic acetylcholine receptor (PDB ID: 4JAL). The alignment was manually adjusted guided by structure-based sequence alignment of all human GPCRs (2, 3). The symbols “+”, “-” and “.” represent identical, conserved and semi-conserved substitutions, respectively. The TM regions are shown in different colored boxes (TM1 in violet, TM2 in blue, TM3 in cyan, TM4 in green, TM5 in yellow, TM6 in orange, TM7 in red). Highly conserved amino acids are displayed in red in TM1–6 and white in TM7.

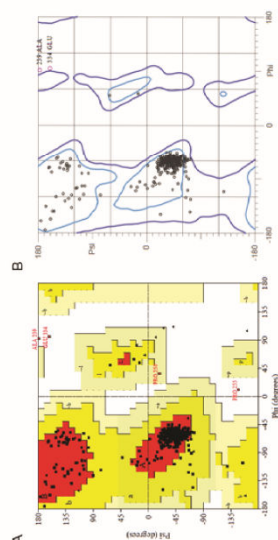


Figure S1.2. The Ramachandran plots for modeled H₂R obtained from (A) PROCHECK and (B) Molprobtity model evaluation web servers. Both calculations showed that more than 97% of amino acids are in the allowed regions.

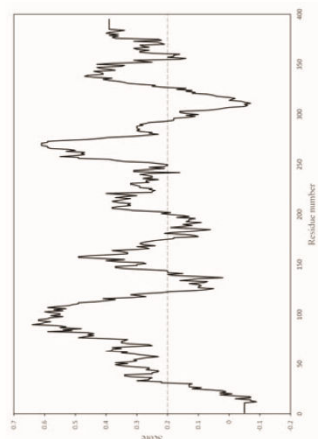


Figure S1.3. Sequence-structure compatibility assessment for H₃R model based on profiles-3D method calculated with verify-3D software from its website. The positive scores suggest that the residues are placed in a proper environment and the protein is folded appropriately.

S2. Drug-likeness, ADME profiling and toxicity risk assessment

Physicochemical, pharmacokinetic, drug-likeness, and medicinal chemistry properties of lead compounds is shown in Table S2.1. Table S2.2 provides the estimated toxic potential of candidate molecules.

4.4 Histamine H₃ receptor ligands by hybrid virtual screening, docking, molecular dynamics simulations, and investigation of their biological effects

Table S2.1 Physicochemical, pharmacokinetic, drug-likeness, and medicinal chemistry properties of lead compounds

Molecular Descriptor	1	2	3	4	5
Physicochemical Properties					
Formula	C ₁₂ H ₁₅ N	C ₁₂ H ₁₅ N	C ₁₂ H ₁₅ N	C ₁₂ H ₁₅ N	C ₁₂ H ₁₅ N
Molecular weight	209.46 g/mol	207.50 g/mol	246.87 g/mol	321.44 g/mol	283.79 g/mol
Num. rotatable bonds	5	3	5	4	7
Num. H-bond donors	1	1	1	1	0
Num. H-bond acceptors	6/0/1	10/2/0	100/3/0	97/1/3	82/1/8
Molar Refractivity	21.20 Å	46.61 Å	42.23 Å	35.58 Å	21.70 Å
Pharmacokinetic properties					
ADME prediction	High	High	High	High	High
BBB permeant	Yes	Yes	Yes	Yes	Yes
P-gp substrate	No	No	No	No	Yes
CYP2D6 inhibitor	No	No	Yes	No	Yes
CYP2C19 inhibitor	No	No	No	No	No
CYP2D6 inhibitor	No	No	No	No	No
CYP2C19 inhibitor	Yes	Yes	Yes	Yes	Yes
Log S ₇ (skin permeation)	-5.00 cm/s	-6.54 cm/s	-6.53 cm/s	-6.50 cm/s	-5.75 cm/s
Drug-likeness					
Lipinski	Yes	Yes	Yes	Yes	Yes
Glaxo	Yes	Yes	Yes	Yes	Yes
Veber	Yes	Yes	Yes	Yes	Yes
Egan	Yes	Yes	Yes	Yes	Yes
Morgan	Yes	Yes	Yes	Yes	Yes
Bioavailability Score	0.55	0.55	0.55	0.55	0.55
Medicinal Chemistry properties					
Lead-likeness ¹	No.1 violation: NLOPPS ≤ 2				
Lead-likeness ²	Yes				
Lead-likeness ³	Yes				
Lead-likeness ⁴	Yes				
Lead-likeness ⁵	Yes				
Lead-likeness ⁶	Yes				
Lead-likeness ⁷	Yes				
Lead-likeness ⁸	Yes				
Lead-likeness ⁹	Yes				
Lead-likeness ¹⁰	Yes				
Lead-likeness ¹¹	Yes				
Lead-likeness ¹²	Yes				
Lead-likeness ¹³	Yes				
Lead-likeness ¹⁴	Yes				
Lead-likeness ¹⁵	Yes				
Lead-likeness ¹⁶	Yes				
Lead-likeness ¹⁷	Yes				
Lead-likeness ¹⁸	Yes				
Lead-likeness ¹⁹	Yes				
Lead-likeness ²⁰	Yes				
Lead-likeness ²¹	Yes				
Lead-likeness ²²	Yes				
Lead-likeness ²³	Yes				
Lead-likeness ²⁴	Yes				
Lead-likeness ²⁵	Yes				
Lead-likeness ²⁶	Yes				
Lead-likeness ²⁷	Yes				
Lead-likeness ²⁸	Yes				
Lead-likeness ²⁹	Yes				
Lead-likeness ³⁰	Yes				
Lead-likeness ³¹	Yes				
Lead-likeness ³²	Yes				
Lead-likeness ³³	Yes				
Lead-likeness ³⁴	Yes				
Lead-likeness ³⁵	Yes				
Lead-likeness ³⁶	Yes				
Lead-likeness ³⁷	Yes				
Lead-likeness ³⁸	Yes				
Lead-likeness ³⁹	Yes				
Lead-likeness ⁴⁰	Yes				
Lead-likeness ⁴¹	Yes				
Lead-likeness ⁴²	Yes				
Lead-likeness ⁴³	Yes				
Lead-likeness ⁴⁴	Yes				
Lead-likeness ⁴⁵	Yes				
Lead-likeness ⁴⁶	Yes				
Lead-likeness ⁴⁷	Yes				
Lead-likeness ⁴⁸	Yes				
Lead-likeness ⁴⁹	Yes				
Lead-likeness ⁵⁰	Yes				
Lead-likeness ⁵¹	Yes				
Lead-likeness ⁵²	Yes				
Lead-likeness ⁵³	Yes				
Lead-likeness ⁵⁴	Yes				
Lead-likeness ⁵⁵	Yes				
Lead-likeness ⁵⁶	Yes				
Lead-likeness ⁵⁷	Yes				
Lead-likeness ⁵⁸	Yes				
Lead-likeness ⁵⁹	Yes				
Lead-likeness ⁶⁰	Yes				
Lead-likeness ⁶¹	Yes				
Lead-likeness ⁶²	Yes				
Lead-likeness ⁶³	Yes				
Lead-likeness ⁶⁴	Yes				
Lead-likeness ⁶⁵	Yes				
Lead-likeness ⁶⁶	Yes				
Lead-likeness ⁶⁷	Yes				
Lead-likeness ⁶⁸	Yes				
Lead-likeness ⁶⁹	Yes				
Lead-likeness ⁷⁰	Yes				
Lead-likeness ⁷¹	Yes				
Lead-likeness ⁷²	Yes				
Lead-likeness ⁷³	Yes				
Lead-likeness ⁷⁴	Yes				
Lead-likeness ⁷⁵	Yes				
Lead-likeness ⁷⁶	Yes				
Lead-likeness ⁷⁷	Yes				
Lead-likeness ⁷⁸	Yes				
Lead-likeness ⁷⁹	Yes				
Lead-likeness ⁸⁰	Yes				
Lead-likeness ⁸¹	Yes				
Lead-likeness ⁸²	Yes				
Lead-likeness ⁸³	Yes				
Lead-likeness ⁸⁴	Yes				
Lead-likeness ⁸⁵	Yes				
Lead-likeness ⁸⁶	Yes				
Lead-likeness ⁸⁷	Yes				
Lead-likeness ⁸⁸	Yes				
Lead-likeness ⁸⁹	Yes				
Lead-likeness ⁹⁰	Yes				
Lead-likeness ⁹¹	Yes				
Lead-likeness ⁹²	Yes				
Lead-likeness ⁹³	Yes				
Lead-likeness ⁹⁴	Yes				
Lead-likeness ⁹⁵	Yes				
Lead-likeness ⁹⁶	Yes				
Lead-likeness ⁹⁷	Yes				
Lead-likeness ⁹⁸	Yes				
Lead-likeness ⁹⁹	Yes				
Lead-likeness ¹⁰⁰	Yes				
Lead-likeness ¹⁰¹	Yes				
Lead-likeness ¹⁰²	Yes				
Lead-likeness ¹⁰³	Yes				
Lead-likeness ¹⁰⁴	Yes				
Lead-likeness ¹⁰⁵	Yes				
Lead-likeness ¹⁰⁶	Yes				
Lead-likeness ¹⁰⁷	Yes				
Lead-likeness ¹⁰⁸	Yes				
Lead-likeness ¹⁰⁹	Yes				
Lead-likeness ¹¹⁰	Yes				
Lead-likeness ¹¹¹	Yes				
Lead-likeness ¹¹²	Yes				
Lead-likeness ¹¹³	Yes				
Lead-likeness ¹¹⁴	Yes				
Lead-likeness ¹¹⁵	Yes				
Lead-likeness ¹¹⁶	Yes				
Lead-likeness ¹¹⁷	Yes				
Lead-likeness ¹¹⁸	Yes				
Lead-likeness ¹¹⁹	Yes				
Lead-likeness ¹²⁰	Yes				
Lead-likeness ¹²¹	Yes				
Lead-likeness ¹²²	Yes				
Lead-likeness ¹²³	Yes				
Lead-likeness ¹²⁴	Yes				
Lead-likeness ¹²⁵	Yes				
Lead-likeness ¹²⁶	Yes				
Lead-likeness ¹²⁷	Yes				
Lead-likeness ¹²⁸	Yes				
Lead-likeness ¹²⁹	Yes				
Lead-likeness ¹³⁰	Yes				
Lead-likeness ¹³¹	Yes				
Lead-likeness ¹³²	Yes				
Lead-likeness ¹³³	Yes				
Lead-likeness ¹³⁴	Yes				
Lead-likeness ¹³⁵	Yes				
Lead-likeness ¹³⁶	Yes				
Lead-likeness ¹³⁷	Yes				
Lead-likeness ¹³⁸	Yes				
Lead-likeness ¹³⁹	Yes				
Lead-likeness ¹⁴⁰	Yes				
Lead-likeness ¹⁴¹	Yes				
Lead-likeness ¹⁴²	Yes				
Lead-likeness ¹⁴³	Yes				
Lead-likeness ¹⁴⁴	Yes				
Lead-likeness ¹⁴⁵	Yes				
Lead-likeness ¹⁴⁶	Yes				
Lead-likeness ¹⁴⁷	Yes				
Lead-likeness ¹⁴⁸	Yes				
Lead-likeness ¹⁴⁹	Yes				
Lead-likeness ¹⁵⁰	Yes				
Lead-likeness ¹⁵¹	Yes				
Lead-likeness ¹⁵²	Yes				
Lead-likeness ¹⁵³	Yes				
Lead-likeness ¹⁵⁴	Yes				

S3. Molecular docking of selected candidate molecules

Analysis of molecular docking results demonstrates the key residues involved in the ligand-receptor interactions (see Table S3 and Figure S3.1). The important amino acids in the binding site of H₃R interacting with selected molecules are: Tyr¹¹⁵, Tyr¹⁸⁹, Phe¹⁹³, Leu¹⁹⁹, Glu²⁰⁶, Trp²⁷¹, Tyr²⁷⁴, Met²⁷⁸, Tyr³⁸⁴, Phe³⁸⁸. For all the selected molecules, π - π stacking and ionic interactions formed by Tyr¹⁸⁹ and Glu²⁰⁶, respectively, are the two important interactions observed. The main interactions observed for compound 1 bound to the H₃R are: a π - π stacking, two hydrophobic pockets, and an ionic interaction. The π - π stacking is established between Tyr¹⁸⁹ and phenyl group at the eastern part of molecule. One of hydrophobic pockets is composed of Phe¹⁹³, Leu¹⁹⁹, Tyr³⁸⁴, and Phe³⁸⁸ residues accommodating the phenyl and linker dimethyl moiety while the residues Tyr¹¹⁵, Trp²⁷¹, Tyr²⁷⁴, and Met²⁷⁸ consisting the other hydrophobic pocket to interact with tetrahydropyran ring in molecule 1. Additionally, the ionic interaction is established between Glu²⁰⁶ and basic amine of linker. In the case of molecule 2, the identified interactions include: an ionic interaction between Glu²⁰⁶ and nitrogen of pyrrolidine, a three centered hydrogen bond between NH in the proximity of piperidine ring and Tyr¹¹⁵ and Tyr²⁷⁴, and two hydrophobic pockets surrounding the endmost parts of molecule at both ends. Cyclohexyl and piperidine rings of molecule 2 interact hydrophobically with residues Tyr¹⁸⁹, Phe¹⁹³, Tyr³⁸⁴, and Phe³⁸⁸ from H₃R. It should be noted that Tyr¹⁸⁹ makes an interaction with cyclohexyl ring like π - π stacking observed for all compounds. Moreover, the other hydrophobic interactions are formed between Tyr²⁷¹, Thr²⁷⁵, Met²⁷⁸, and Leu¹⁰¹ of the H₃R and substituent of pyrrolidine at the distal end of molecule. The identified interactions observed for compound 3 are similar to those discussed above. Again π - π stacking is formed between Tyr¹⁸⁹ and phenyl group in the indole ring. In addition, indole ring makes hydrophobic interaction with Tyr³⁸⁴. A hydrogen bond is also seen between Tyr²⁷⁴ and oxygen of ketone group. Similar to other compounds, molecule 3 contains the ionic interaction between its piperazine nitrogen and Glu²⁰⁶. Furthermore, amino acids Tyr¹¹⁵, Phe¹⁹³, Leu¹⁹⁹, Tyr²⁷¹, and Met²⁷⁸ from H₃R hydrophobically interact with piperazine and alkyl part of linker in compound 3. The main interactions of molecule 4 resemble to those observed for other compounds. Similarly, a hydrophobic pocket formed by Tyr¹⁸⁹, Tyr²⁷⁴, and Phe³⁸⁸ and surrounds the tetrahydroisoquinoline moiety of the molecule and establishes hydrophobic interactions. The observed π - π stacking in this pocket is also related between Tyr¹⁸⁹ and phenyl ring of tetrahydroisoquinoline part. In addition, the other hydrophobic interactions are formed between piperidine ring and Tyr¹¹⁵, Phe¹⁹³, Leu¹⁹⁹, and Met²⁷⁸ from the receptor. Besides, Tyr²⁷⁴ of the H₃R is engaged in the hydrogen bond with linker amide NH of the compound 4. Moreover, the ionic interaction is also observed between Glu²⁰⁶ and nitrogen of piperidine at the end part of molecule. In the case of molecule 5 which is structurally similar to pibolisant, the observed interactions are as follows: ionic interaction between Glu²⁰⁶ and nitrogen of piperidine ring, hydrogen bond between Tyr²⁷⁴ and the central ether oxygen, as well as two hydrophobic contacts. The phenyl group is sandwiched in a hydrophobic pocket comprised of Tyr¹⁸⁹, Tyr³⁸⁴, and Phe³⁸⁸ residues from the receptor whereas piperidine ring and linker alkyl located in the hydrophobic pocket formed by Tyr¹¹⁵, Leu¹⁹⁹, and Met²⁷⁸.

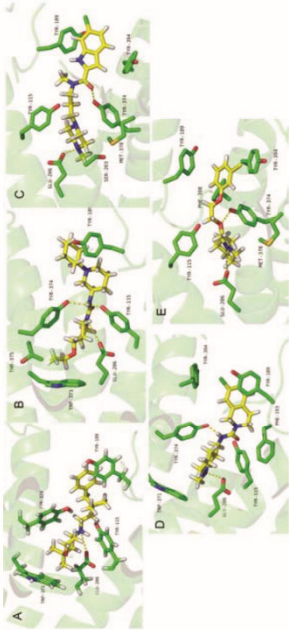


Figure S3.1. 3D representation of selected compounds 1-5 (Panels A to D) docked into the binding site of H₃R generated by PyMol program (version 1.7.x). The ligands and the main interacting residues are shown as sticks. Only the side chains of the interacting residues from receptor are shown for further clarity.

Table S3.1. Amino acids of H₃R involved in interactions with candidates.

Compound	Amino acids of H ₃ R
1	Tyr ¹⁵⁵ , Tyr ¹⁶² , Phe ¹⁶⁸ , Leu ¹⁶⁹ , Glu ¹⁸⁸ , Tyr ¹⁹¹ , Tyr ¹⁹³ , Thr ¹⁹⁵ , Met ¹⁹⁹ , Tyr ²⁰⁰ , Phe ²⁰⁶ , Leu ²¹⁰ , Tyr ²¹⁵ , Tyr ²¹⁶ , Phe ²¹⁸ , Glu ²¹⁹ , Tyr ²²¹ , Tyr ²²⁴ , Tyr ²²⁵ , Met ²²⁷ , Tyr ²³⁰ , Phe ²³² , Leu ²⁴¹
2	Tyr ¹⁵⁵ , Tyr ¹⁶² , Phe ¹⁶⁸ , Leu ¹⁶⁹ , Glu ¹⁸⁸ , Tyr ¹⁹¹ , Tyr ¹⁹³ , Thr ¹⁹⁵ , Met ¹⁹⁹ , Tyr ²⁰⁰ , Phe ²⁰⁶ , Leu ²¹⁰ , Tyr ²¹⁵ , Tyr ²¹⁶ , Phe ²¹⁸ , Glu ²¹⁹ , Tyr ²²¹ , Tyr ²²⁴ , Tyr ²²⁵ , Met ²²⁷ , Tyr ²³⁰ , Phe ²³² , Leu ²⁴¹
3	Tyr ¹⁵⁵ , Tyr ¹⁶² , Phe ¹⁶⁸ , Leu ¹⁶⁹ , Glu ¹⁸⁸ , Tyr ¹⁹¹ , Tyr ¹⁹³ , Thr ¹⁹⁵ , Met ¹⁹⁹ , Tyr ²⁰⁰ , Phe ²⁰⁶ , Leu ²¹⁰ , Tyr ²¹⁵ , Tyr ²¹⁶ , Phe ²¹⁸ , Glu ²¹⁹ , Tyr ²²¹ , Tyr ²²⁴ , Tyr ²²⁵ , Met ²²⁷ , Tyr ²³⁰ , Phe ²³² , Leu ²⁴¹
4	Tyr ¹⁵⁵ , Tyr ¹⁶² , Phe ¹⁶⁸ , Leu ¹⁶⁹ , Glu ¹⁸⁸ , Tyr ¹⁹¹ , Tyr ¹⁹³ , Thr ¹⁹⁵ , Met ¹⁹⁹ , Tyr ²⁰⁰ , Phe ²⁰⁶ , Leu ²¹⁰ , Tyr ²¹⁵ , Tyr ²¹⁶ , Phe ²¹⁸ , Glu ²¹⁹ , Tyr ²²¹ , Tyr ²²⁴ , Tyr ²²⁵ , Met ²²⁷ , Tyr ²³⁰ , Phe ²³² , Leu ²⁴¹
5	Tyr ¹⁵⁵ , Tyr ¹⁶² , Phe ¹⁶⁸ , Leu ¹⁶⁹ , Glu ¹⁸⁸ , Tyr ¹⁹¹ , Tyr ¹⁹³ , Thr ¹⁹⁵ , Met ¹⁹⁹ , Tyr ²⁰⁰ , Phe ²⁰⁶ , Leu ²¹⁰ , Tyr ²¹⁵ , Tyr ²¹⁶ , Phe ²¹⁸ , Glu ²¹⁹ , Tyr ²²¹ , Tyr ²²⁴ , Tyr ²²⁵ , Met ²²⁷ , Tyr ²³⁰ , Phe ²³² , Leu ²⁴¹

S4. MD simulation and calculation of binding free energy

All the MD calculations were performed using the Assisted Model Building with Energy Refinement (AMBER) suite of programs (version 14) (9, 10) operating on a Linux-based (Centos6.8) GPU work station consisting of four Nvidia40M (each has 12 GB RAM and 2880 cuda cores), 2X Intel Xeon E5-2697 v2, 2.7 GHz (total of 48 cores), total RAM = 128 GB. The usable coordinate files for AMBER (i.e. *.prmtop and *.inpcrd) were created by *leap* module followed by adding a correct number of counter ions for neutralizing the total charge of the system. The system was solvated with TIP3P water molecules in a rectangular box by the buffering distances set to 12 Å in all directions. Then the solvated system was subjected to an initial energy minimization process by applying *Sander* module (500 steps of steepest descent followed by 500 steps of conjugate gradient) followed by a 50 ps heating step where the temperature was gradually increased from 0 to 300 K. 50 ps of density equilibration was followed by 500 ps of constant pressure equilibration at 300 K with a time step of 2 fs. Only bond lengths involving hydrogen atoms were constrained using the SHAKE algorithm. A final 10 ns MD simulation was performed by applying the Particle Mesh Ewald (PME) method to calculate long-range electrostatic interactions. All calculations were carried out under periodic boundary conditions where no constraint was applied to either the protein or the ligand molecules. The trajectory of the simulation was obtained by writing out the coordinates every 10 ps. After MD simulation on receptor-ligand complex, snapshots were extracted from the 10 ns molecular dynamic trajectory with an interval of 10 ps. The dielectric constant values were set to 1.0 and 80 for the interior of solute and the surrounding solvent, respectively. Binding free energy was calculated for the complex of candidate ligands and H₃R using MM-Poisson-Boltzmann Surface Area (PBSA)/Generalized-Born Surface Area (GBSA) methods implemented in the AMBER package (9, 11). Ligand-receptor binding free energy is obtained by summing up the molecular mechanics energies, solvation-free energies, and entropic terms, averaged over a series of equilibrated snapshots from MD simulation trajectory. The interaction energies for the snapshots were calculated by excluding water molecules and counter ions and presented as the average value.

Binding free energy (ΔG_{bind}) is calculated using the following equation:

$$\Delta G_{bind} = G_{water}(complex) - G_{water}(protein) - G_{water}(ligand)$$

In this equation, $G_{water}(complex)$, $G_{water}(protein)$ and $G_{water}(ligand)$ are the free energies of the complex, protein, and ligand, respectively. Free energy, ΔG , for each species is calculated as follows:

$$G = E_{gas} + \Delta G_{solvation} - TS$$

9

$$\Delta G_{solvation} = \Delta G_{polar} - \Delta G_{non-polar}$$

$$E_{gas} = E_{int} + E_{solv} + E_{elec}$$

$$E_{int} = E_{bond} + E_{angle} + E_{tors}$$

G is the calculated average free energy, and E_{gas} is the standard force-field energy, including internal energy (E_{int}) in the gas phase as well as non-covalent van der Waals (E_{vdw}) and electrostatic (E_{elec}) energies. E_{bond} , E_{angle} and E_{tors} are the contributions to the internal energy caused by the strain from the deviation of the bonds, angle, and torsion angle from their equilibrium values. ΔG_{polar} and $\Delta G_{non-polar}$ are the polar and non-polar contributions to the solvation free energy. The polar contribution is achieved using Poisson-Boltzmann or Generalized Born model while the non-polar contributions are calculated by the solvent accessible surface area (SASA) using the LCPO method (12). TS indicates the vibrational entropy term which is neglected in this study assuming similar entropy contribution for all complexes to the binding free energy.

Analysis of the RMSD trajectories and potential energy plot demonstrated that all systems in the simulation were well-equilibrated and remained stable throughout 10 ns simulation run.

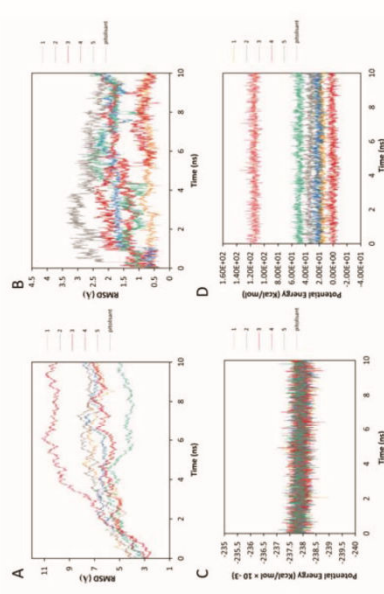


Figure S4.1. The results of molecular dynamics simulation analyses on ligand-H₃R complex. Panels A and B show the plot of root mean square deviation (RMSD) fluctuation in a 1 to 10 ns molecular dynamics simulation for ligand-H₃R complexes and ligands, respectively. Panels C and D indicate potential energies for the ligand-H₃ complexes and compounds 1 to 5 during 10 ns molecular dynamics simulation.

10

S5. Purity analytics of purchased compounds

Preslected compounds were purchased from various chemical suppliers listed within the MolPort database (Riga, Latvia) to evaluate binding behavior *in vitro*. Purity of supplied compounds was assessed by LC-MS using a Bruker Elute SP HPLC equipped with an Intensity Solo C18 RP column (100 × 2.1 mm) and connected to a Bruker ama/onspection-trap mass spectrometer (ESI) for detection. Used eluent consisted of water and acetonitrile (1 - 40% acetonitrile, 0.1% formic acid) at a flow of 0.3 ml/min. The purity of the ordered compounds was about 89.0% expressed as normalized fractional area (Supplementary Material S2).

Table S5.1 Purity of purchased compounds assessed by LC-MS

Compound	t _R ^{a)} [min]	m/z	Purity ^{b)} [%]
1	23.2	290.17	94.7
2	18.4	338.26	97.7
3	19.1	349.18	93.3
4	20.1	322.13	91.3
5	21.3	284.05	89.0

a) retention time.
b) HPLC analysis (Bruker Elute SP; Column: Intensity Solo C18 RP; column dimensions: 100x2.1 mm; eluent: acetonitrile (1-40%) in water, 0.1% formic acid; flow: 0.3 mL/min) combined with mass spectrometric detection (Bruker ama/onspection-trap; detection: ion-trap; ion-polarity: positive; scan: 100-600 m/z), expressed as normalized peak area (%) as approximated purity.

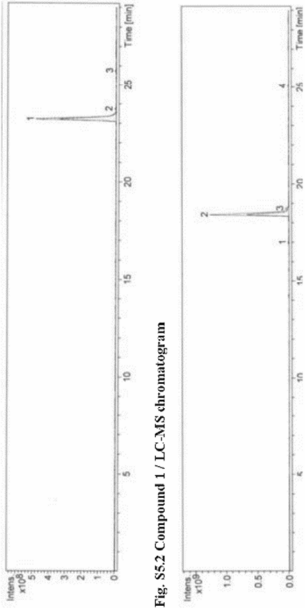


Fig. S5.2 Compound 1 / LC-MS chromatogram

Fig. S5.3 Compound 2 / LC-MS chromatogram

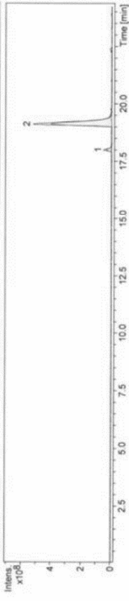


Fig. S5.4 Compound 3 / LC-MS chromatogram

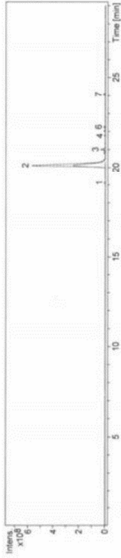


Fig. S5.5 Compound 4 / LC-MS chromatogram

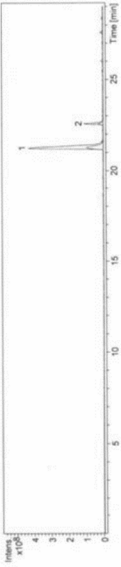


Fig. S5.6 Compound 5 / LC-MS chromatogram

References

1. Kruse AC, Hu J, Pan AC, Arlow DH, Rosenbaum JM, Rosenmond E, et al. Structure and dynamics of the M2 muscarinic acetylcholine receptor. *Nature*. 2012;482(7386):552.
2. Cvecek V, Goddard III W.A., Abrol R. Structure-based sequence alignment of the transmembrane domains of all human GPCRs: Phylogenetic, structural and functional implications. *PLoS Comput Biol*. 2016;12(3):e1004805.
3. Kim S-K, Fristrup P, Abrol R, Goddard III W.A. Structure-based prediction of subtype selectivity of histamine H₃ receptor selective antagonists in clinical trials. *J Chem Inf Model*. 2011;51(12):3262-74.
4. Waterhouse A, Bertoni M, Bienert S, Studer G, Tauriello G, Gumienny R, et al. SWISS-MODEL: homology modelling of protein structures and complexes. *Nucleic Acids Res*. 2018;46(W1):W296-w303.
5. Laskowski RA, Rullmann JA, MacArthur MW, Kaptein R, Thornton JM. AQUA and PROCHECK-NMR: programs for checking the quality of protein structures solved by NMR. *J Biomol NMR*. 1996;8(4):477-86.
6. Davis IW, Leaver-Fay A, Chen VB, Block JN, Kapral GJ, Wang X, et al. MolProbity: all-atom contacts and structure validation for proteins and nucleic acids. *Nucleic Acids Res*. 2007;35(Web Server issue):W375-83.
7. Bowie JU, Luthy R, Eisenberg D. A method to identify protein sequences that fold into a known three-dimensional structure. *Science* (New York, NY). 1991;253(5016):164-70.
8. Luthy R, Bowie JU, Eisenberg D. Assessment of protein models with three-dimensional profiles. *Nature*. 1992;356(6364):83-5.
9. Case DA, Cheatham TE, 3rd, Darden T, Gohlke H, Luo R, Merz KM, Jr., et al. The Amber biomolecular simulation programs. *J Comput Chem*. 2005;26(16):1668-88.
10. Pearlman DA, Case DA, Caldwell JW, Ross WS, Cheatham TE, DeBolt S, et al. AMBER, a package of computer programs for applying molecular mechanics, normal mode analysis, molecular dynamics and free energy calculations to simulate the structural and energetic properties of molecules. *Comput Phys Commun*. 1995;91(1):1-41.
11. Kollman PA, Massova I, Reyes C, Kuhn B, Huo S, Chong L, et al. Calculating Structures and Free Energies of Complex Molecules: Combining Molecular Mechanics and Continuum Models. *Acc Chem Res*. 2000;33(12):889-97.
12. Weiser J, Shenkin Peter S, Still WC. Approximate atomic surfaces from linear combinations of pairwise overlaps (LCPO). *J Comput Chem*. 1999;20(2):217-30.

4.5. In silico and in vitro studies of two non-imidazole multiple targeting agents at histamine H₃ receptors and cholinesterase enzymes

Nakisa Ghamari^{1), 2)}, Siavoush Dastmalchi^{1), 2)}, Omid Zarei^{3), 4)}, José-Antonio Arias-Montaña⁵⁾, David Reiner⁶⁾, Fulya Ustun-Alkan⁷⁾, Holger Stark⁶⁾, Maryam Hamzeh-Mivehroud^{1), 2)}

1) Biotechnology Research Center, Tabriz, University of Medical Sciences, Tabriz, Iran

2) School of Pharmacy, Tabriz University of Medical Sciences, Tabriz, Iran

3) Cellular and Molecular Research Center, Research Institute for Health Development, Kurdistan University of Medical Sciences, Sanandaj, Iran

4) Neurosciences Research Center, Kurdistan, University of Medical Sciences, Sanandaj, Iran

5) Departamento de Fisiología, Biofísica y Neurociencias, Centro de Investigación y de Estudios Avanzados del IPN, Ciudad de México, México

6) Institute of Pharmaceutical and Medicinal Chemistry, Heinrich Heine University Düsseldorf, Universitätsstr. 1, 40225 Duesseldorf, Germany

7) Department of Pharmacology and Toxicology, Faculty of Veterinary Medicine, Istanbul University-Cerrahpasa, Istanbul, Turkey

Published in: *Chemical Biology & Drug Design*, 2020, 195:279-290.

DOI: 10.1111/cbdd.13642

Contribution to research: Co-authorship. DR co-organised shipment of test-ligands, prepared, planned and conducted radioligand displacement experiments, and evaluated corresponding data to determine H₃R affinity. DR reviewed the manuscript.

Abstract:

Recently, multi-target directed ligands have been of research interest for multifactorial disorders such as Alzheimer's disease (AD). Since H₃ receptors (H₃Rs) and cholinesterases are involved in pathophysiology of AD, identification of dual-acting compounds capable of improving cholinergic neurotransmission is of importance in AD pharmacotherapy. In the present study, H₃R antagonistic activity combined with anticholinesterase properties of two previously computationally identified lead compounds, that is, compound 3 (6-chloro-N-methyl-N-[3-(4-methylpiperazin-1-yl)propyl]-1H-indole-2-carboxamide) and compound 4 (7-chloro-N-[(1-methylpiperidin-3-yl)methyl]-1,2,3,4-tetrahydroisoquinoline-2-carboxamide), was tested. Moreover, molecular docking and binding free energy calculations were conducted for binding mode and affinity prediction of studied ligands toward cholinesterases. Biological evaluations revealed inhibitory activity of ligands in nanomolar (compound 3: H₃R *EC*₅₀ = 0.73 nM; compound 4: H₃R *EC*₅₀ = 31 nM) and micromolar values (compound 3: AChE *IC*₅₀ = 9.09 μM, BuChE *IC*₅₀ = 21.10 μM; compound 4: AChE *IC*₅₀ = 8.40 μM, BuChE *IC*₅₀ = 4.93 μM) for H₃R antagonism and cholinesterase inhibition, respectively. Binding free energies yielded good consistency with cholinesterase inhibitory profiles. The results of this study can be used for lead optimisation where dual inhibitory activity on H₃R and cholinesterases is needed. Such ligands can exert their biological activity in a synergistic manner resulting in higher potency and efficacy.

Reproduced from Ghamari N, Dastmalchi S, Zarei O, Arias-Montaña JA, Reiner D, Ustun-Alkan F, Stark H, Hamzeh-Mivehroud M, In silico and in vitro studies of two non-imidazole multiple targeting agents at histamine H₃ receptors and cholinesterase enzymes, *Chem. Biol. Drug Des.*, 2020, 195:279-290. Reprinted with written permission from John Wiley & Sons (Licence number: 4810140373332).

Copyright 2019 John Wiley & Sons A/S

Received: 13 July 2019 | Revised: 4 September 2019 | Accepted: 29 September 2019

DOI: 10.1111/cbdd.13642



RESEARCH ARTICLE



In silico and in vitro studies of two non-imidazole multiple targeting agents at histamine H₃ receptors and cholinesterase enzymes

Nakisa Ghamari^{1,2} | Siavoush Dastmalchi^{1,2} | Omid Zarci^{3,4} |
 José-Antonio Arias-Montaña⁵ | David Reiner⁶ | Fulya Ustun-Alkan⁷ |
 Holger Stark⁶ | Maryam Hamzeh-Mivehroud^{1,2}

¹Biotechnology Research Center, Tabriz University of Medical Sciences, Tabriz, Iran

²School of Pharmacy, Tabriz University of Medical Sciences, Tabriz, Iran

³Cellular and Molecular Research Center, Research Institute for Health Development, Kurdistan University of Medical Sciences, Sanandaj, Iran

⁴Neurosciences Research Center, Kurdistan University of Medical Sciences, Sanandaj, Iran

⁵Departamento de Fisiología, Biofísica y Neurociencias, Centro de Investigación y de Estudios Avanzados del IPN, Ciudad de México, México

⁶Institute of Pharmaceutical and Medicinal Chemistry, Heinrich Heine University Düsseldorf, Düsseldorf, Germany

⁷Department of Pharmacology and Toxicology, Faculty of Veterinary Medicine, Istanbul University-Cerrahpasa, Istanbul, Turkey

Correspondence

Maryam Hamzeh-Mivehroud, Biotechnology Research Center and School of Pharmacy, Tabriz University of Medical Sciences, Tabriz, Iran.
 Emails: hamzehm@tbzmed.ac.ir, maryam_h_7860@yahoo.com

Funding information

European Cooperation in Science and Technology, Grant/Award Number: EU COST Actions CA15135 and CA18133; Tabriz University of Medical Sciences, Grant/Award Number: 57572

Abstract

Recently, multi-target directed ligands have been of research interest for multifactorial disorders such as Alzheimer's disease (AD). Since H₃ receptors (H₃Rs) and cholinesterases are involved in pathophysiology of AD, identification of dual-acting compounds capable of improving cholinergic neurotransmission is of importance in AD pharmacotherapy. In the present study, H₃R antagonistic activity combined with anticholinesterase properties of two previously computationally identified lead compounds, that is, compound **3** (6-chloro-*N*-methyl-*N*-[3-(4-methylpiperazin-1-yl)propyl]-1*H*-indole-2-carboxamide) and compound **4** (7-chloro-*N*-[1-methylpiperidin-3-yl)methyl]-1,2,3,4-tetrahydroisoquinoline-2-carboxamide), was tested. Moreover, molecular docking and binding free energy calculations were conducted for binding mode and affinity prediction of studied ligands toward cholinesterases. Biological evaluations revealed inhibitory activity of ligands in nanomolar (compound **3**: H₃R EC₅₀ = 0.73 nM; compound **4**: H₃R EC₅₀ = 31 nM) and micromolar values (compound **3**: AChE IC₅₀ = 9.09 μM, BuChE IC₅₀ = 21.10 μM; compound **4**: AChE IC₅₀ = 8.40 μM, BuChE IC₅₀ = 4.93 μM) for H₃R antagonism and cholinesterase inhibition, respectively. Binding free energies yielded good consistency with cholinesterase inhibitory profiles. The results of this study can be used for lead optimization where dual inhibitory activity on H₃R and cholinesterases is needed. Such ligands can exert their biological activity in a synergistic manner resulting in higher potency and efficacy.

KEYWORDS

anticholinesterase, anti-H₃R agents, histamine H₃ receptor, molecular docking, molecular dynamics simulation, multi-target directed ligands

1 | INTRODUCTION

Although much of medicinal chemistry efforts for drug discovery have been dedicated to “one-molecule-one-target” principle, this approach hardly meets the desired expectation in the case of certain diseases with complex pathophysiology (Chen & Decker, 2013; Geldenhuys & Van der Schyf, 2013; Prati, Uliassi, & Bolognesi, 2014). In this framework, the use of multi-target directed ligands (MTDLs) seems more effective compared to conventional targeting. MTDL is defined as a molecule capable of modulating different targets simultaneously (Chen & Decker, 2013; Geldenhuys & Van der Schyf, 2013; Lazewska et al., 2016). The main advantage associated with a given MTDL relies on enhancing the biological activity through different pharmacophores embedded in the given molecule that are required for interactions with multiple targets (Chen & Decker, 2013). Undoubtedly, such ligands can be beneficial in a more efficient way for the treatment of complex disorders with multifactorial nature. Alzheimer's disease (AD) is classified as neurological disorder with multifactorial etiology, which can be observed with high incidence in aged population. The major features of AD (as the most common form of dementia) are cognitive deficit, loss of memory, and language impairment leading to alterations in behavior and personality. Different abnormal neurological events are responsible for the pathophysiology of AD, such as misfolded and aggregated amyloid, tau protein hyperphosphorylation, oxidative stress, and cholinergic dysfunction (Bajda, Guzik, Ignasik, & Malawska, 2011; Rampa, Belluti, Gobbi, & Bisi, 2011). Based on the amyloid hypothesis, cerebral plaques are formed as a result of β -amyloid peptide aggregation. Formation of intracellular neurofibrillary tangles induced by tau hyperphosphorylation is another pathological initiator for AD development. The second important hypothesis in AD is oxidative stress arising from the accumulation of reactive oxygen species, which can cause cell injury and death. Lastly, cholinergic neurotransmission has a pivotal role in the pathology of AD. In AD patients, the brain acetylcholine levels are significantly reduced in hippocampus and cortex. This neurotransmitter plays a critical role in memory and learning, as well as in cognition. Its activity in the synaptic cleft is controlled by cholinesterase enzymes, responsible for the termination of acetylcholine biological activity through its hydrolysis in cholinergic synapses (Bajda et al., 2011; Darras et al., 2014; Lazewska et al., 2016). Currently, the pharmacotherapy of AD relies on the use of four marketed drugs, namely donepezil, rivastigmine and galantamine, as cholinesterase inhibitors, and the NMDA receptor antagonist memantine (Chen et al., 2012; Lalut et al., 2019; Sadek, Khan, Darras, Pockes, & Decker, 2016). However,

these disease-modifying agents only alleviate temporally the AD clinical symptoms, while their efficacy as monotherapy is one of today's controversial issues in AD.

In recent years, the histamine H₃ receptor (H₃R) has been highlighted as a potential target for the treatment of neurological disorders, including AD (Berlin, Boyce, & Ruiz Mde, 2011; Lazewska & Kiec-Kononowicz, 2014; Vohora & Bhowmik, 2012). These receptors are mainly located in different areas of CNS regulating the release of histamine and other neurotransmitter such as acetylcholine and dopamine through a negative feedback mechanism. The H₃R belongs to the superfamily of G protein-coupled receptors and is coupled to the G_q class of G proteins, leading to inhibition of the adenylyl cyclase with the subsequent decrease in the level of cAMP, among other actions (Nieto-Alamilla, Marquez-Gomez, Garcia-Galvez, Morales-Figueroa, & Arias-Montano, 2016). There are lines of evidence indicating that H₃R blockade enhances acetylcholine release, thereby leading to improved cognitive and behavioral symptoms (Brioni, Esbenshade, Garrison, Bitner, & Cowart, 2011; Medhurst et al., 2007; Raddatz, Tao, & Hudkins, 2010; Sadek, Saad, Sadeq, Jalal, & Stark, 2016).

According to the complexity and multifactorial characteristics of AD, the use of MTDLs may provide more promising results in terms of cognition enhancement in a more specific way. There are several reports in the literature introducing dual-acting ligands capable of improving cholinergic neurotransmission via simultaneous antagonistic activity at H₃Rs and cholinesterase inhibitory activity (Bajda et al., 2012; Bembenek et al., 2008; Incerti et al., 2010; Khanfar et al., 2016; Morini et al., 2008; Sadek, Khan, et al., 2016). In a previous study, we used *in silico* virtual screening for the identification of novel ligands at the H₃R from ZINC database. A variety of molecular modeling techniques such as molecular docking and dynamics simulation, as well as drug-likeness filtering criteria, were employed to select the candidate molecules. The selected compounds were experimentally evaluated using radioligand displacement studies, and the results revealed that two of them, obtained from the ligand-based search method, were capable of binding to H₃Rs in the sub-micromolar *K_i* range (Ghamari et al., 2018). In the current work, we aimed to evaluate H₃R antagonist/inverse agonist and anticholinesterase activity of the identified ligands with improved efficacy as a result of their synergistic activity.

2 | METHODS AND MATERIALS

2.1 | Chemicals and reagents

Compounds with ZINC IDs Zinc69700808 and Zinc90563066 were purchased from chemical suppliers of MolPort database

(Riga, Latvia). Purity of the supplied compounds was evaluated by LC-MS as described previously (Ghamari et al., 2018). Cyclic AMP XP Assay Kit (cat no. 4339) was obtained from Cell Signaling Technology. 3-isobutyl-1-methylxanthine (IBMX), (*R*)- α -methylhistamine, thioperamide, forskolin, G418 (Geneticin), acetylcholinesterase (AChE, E.C. 3.1.1.7, Type V-S, lyophilized powder, from electric eel), butyrylcholinesterase (BuChE, E.C. 3.1.1.8, from equine serum), and 3-(4,5-dimethyl-2-thiazolyl)-2,5-diphenyl-2H-tetrazolium bromide (MTT) were obtained from Sigma-Aldrich. CHO-K1 cells were purchased from the National Cell Bank of Iran, Pasteur Institute of Iran. Dulbecco's modified Eagle medium (DMEM) with L-glutamine and fetal bovine serum (FBS) were from Gibco® Life Technologies. Donepezil was purchased from Darou Pakhsh Pharma Chem Co. Acetylthiocholine iodide and 5,5'-Dithiobis(2-nitrobenzoic acid) (DTNB) from Sigma-Aldrich were kind gifts from Dr. Azarmi, Tabriz University of Medical Sciences.

2.2 | Cell culture and transfection

CHO-K1 cells were cultured in DMEM supplemented with 10% FBS and penicillin/streptomycin at 37°C and 5% CO₂ in a humidified incubator. CHO-K1 cells were grown to 50%–70% confluence and stably transfected with mammalian expression vector of pCI-neo encoding the full length of human H₃R (1,335 bp, 445 aa; Osorio-Espinoza, Escamilla-Sanchez, Aquino-Jarquin, & Arias-Montano, 2014) by electroporation. Briefly, after harvesting, cells were resuspended in 400 μ L DMEM and transferred to an electroporation cuvette with a 0.4-cm gap between electrodes. DNA (10 μ g/ml) was added and electroporation was conducted according to the Bio-Rad's preset protocol programmed in Gene Pulser Xcell. After electroporation, cells were transferred to a 6-well plate and incubated for 48 hr in complete media. Thereafter, the transfected cells were selected with geneticin (G-418; 600 μ g/ml). Stable transfectants were maintained in the presence of 400 μ g/ml geneticin.

2.3 | cAMP accumulation assay

CHO-K1 cells stably expressing the H₃R were plated in a 96-well plate (60,000 cells/well) and incubated overnight at 37°C. The medium was removed, and the cells were rinsed with 200 μ L prewarmed phosphate-buffered saline (PBS). The cells were then incubated with serum-free medium containing IBMX (1 mM) for 10 min at 37°C. The previously identified compounds (i.e., compounds **3** and **4**) and/or reference compounds ((*R*)- α -methylhistamine and thioperamide) were added at increasing concentrations (0.1 nM–10 μ M) and incubated for 5 min. Subsequently, forskolin (1 μ M) was added and incubated for additional 30 min at 37°C. Where required, for evaluating the effect

of the studied compounds in the presence of agonist, the fixed concentration of 15 nM was used for (*R*)- α -methylhistamine. The cyclic AMP XP Assay Kit (Cell Signaling Technology) was utilized for the determination of intracellular cAMP accumulation. For this purpose, the cells were rinsed twice with 200 μ L ice-cold PBS, followed by the addition of 100 μ L/well of 1X lysis buffer with an incubation on ice for 10 min. To the cAMP assay plate, 50 μ L of the HRP-linked cAMP solution and 50 μ L of the sample were added and plates were incubated at room temperature for 3 hr on a horizontal orbital plate shaker. The contents of the plates were discarded, and wells were washed four times with 200 μ L 1X wash buffer. TMB substrate (100 μ L) was added, and the wells were incubated for 30 min at room temperature. Finally, the reaction was terminated by adding of 100 μ L STOP solution and the absorbance was measured at 450 nm using ELISA reader (BioTek, US).

2.4 | Acetylcholinesterase and butyrylcholinesterase inhibition assay

In order to determine the inhibitory activity of the studied ligands, the spectrophotometric Ellman's test was conducted using AChE and BuChE from electric eel and horse serum, respectively (Ellman, Courtney, Andres, & Feather-Stone, 1961). The stock solutions of the tested compounds were prepared in DMSO. For each compound, different concentrations ranging from 0.1 nM to 100 μ M were prepared in 100 mM sodium phosphate buffer (pH = 8.0). The assay solution for the preincubation (5 min at room temperature) was sodium phosphate buffer containing 0.25 U/ml AChE or BuChE, 0.5 mM DTNB, and different concentrations of the tested compounds. The reaction was started by the addition of acetylthiocholine iodide (1 mM) as substrate, followed by absorbance measurement after 10 min at a wavelength of 412 nm. Donepezil was used as positive control. The percentage of inhibition was calculated using the following equation: % inhibition = $100 \times [(A_{\text{sample}} - A_{\text{blank}}) / (A_{\text{max}} - A_{\text{blank}})]$, where A_{sample} is the absorbance of each sample including the test compound, A_{blank} denotes the absorbance without enzyme, and A_{max} shows the absorbance without the test compound. Each concentration was examined in triplicate.

2.5 | Cell viability assay

For evaluation of the effects of the studied ligands on in vitro cell viability, the MTT assay was used (Mosmann, 1983). CHO-K1-hH₃R cells were seeded in triplicate in 96-well plates at a density of 1×10^4 cells/well and incubated for 24 hr at 37°C under a humidified atmosphere and 5% CO₂ saturation. Stock solutions of the studied compounds were prepared in DMSO, diluted in fresh medium and added to the wells in a range 0.1 nM–100 μ M. After 72 hr of incubation, the medium was discarded, followed by the addition

of 100 µl of filtered 3-(4,5-dimethylthiazol-2-yl)-2,5-diphenyltetrazolium bromide (MTT) solution (in a final concentration of 0.5 mg/ml) and incubation for 4 hr at 37°C in 5% CO₂ atmosphere. Then, the culture medium was carefully removed by tapping on paper towel followed by the addition of 100 µl solubilizing buffer containing Sorensen's phosphate buffer (12.5%) and DMSO (87.5%) for dissolving the produced formazan crystals. The plate was incubated for 40 min at room temperature with gentle shaking. Finally, the absorbance was measured at 570 nm. In this assay, doxorubicin (DX) was used as positive control. The percentage of cell viability was calculated using the following formula: % cell viability = $100 \times [(A_{\text{sample}} - A_{\text{Blank}})/(A_{\text{Control}} - A_{\text{Blank}})]$; in this equation, A_{sample} refers to the absorbance of tested compound, A_{Blank} shows well containing only medium and A_{Control} demonstrates untreated cells. All the experiments were conducted in triplicate. GraphPad Prism software (version 6.01) was utilized for the analysis of the results and determination of GI_{50} (concentration required for a 50%-inhibition of cell growth) based on a sigmoidal model using nonlinear regression analysis.

2.6 | Molecular docking and binding free energy calculation for ligand–enzyme complex

Molecular docking experiment was carried out to predict the mode of interactions between the ligands and cholinesterase enzymes. The experimental co-ordinates for AChE (PDB ID: 4EY7) (Cheung et al., 2012) and BuChE (PDB ID: 4TPK) (Brus et al., 2014) were retrieved from Protein Data Bank at the Research Collaboratory for Structural Bioinformatics (<http://www.RCSB.org>; Berman et al., 2000). Flexible docking of ligands into the binding site of enzymes was performed using GOLD program (version 5.0; CCDC Inc., Cambridge, UK) running under LINUX operating system. In order to determine the binding site, a geometric center was assigned based on the important residues in the active site of enzyme considering all atoms within a radius of 10 Å. By applying the default settings in GOLD, the best scoring function was selected based on re-docking experiment of donepezil into the binding site of AChE. Top-ranked docking pose in complex with corresponding enzyme was subjected to molecular dynamics (MD) simulation. Assisted Model Building with Energy Refinement (AMBER) suite of programs (version 14; Case et al., 2005; Pearlman et al., 1995) was used for MD calculation operating on a Linux-based (Centos 6.8) GPU work station consisting of four NvidiaK40M (each has 12 GB RAM and 2880 CUDA cores), 2X Intel Xeon E5-2697 v2, 2.7 GHz (total of 48 cores), total RAM = 128 GB. AMBER usable co-ordinate files (in the format of *.prmtop and *.inpcrd) were generated using *leap* module. Then, an appropriate number of counterions were added to the system for neutralizing the total charge and immersed into a rectangular box of explicit TIP3P water

molecules by the buffering distances set to 12 Å in all directions. Prior to MD simulation, the solvated system was energy minimized by 500 steps of steepest descent followed by 500 steps of conjugated gradient using *Sander* module of AMBER package. Subsequently, the system was heated for 50 ps with gradual increase in temperature from 0 to 300 K. Density equilibration was performed for additional 50 ps followed by 500 ps of constant pressure equilibration at 300 K with a time step of 2 fs. By applying SHAKE algorithm, all bonds involving hydrogen atoms were constrained. A 10 ns MD simulation was carried out using Particle Mesh Ewald method for calculation of long-range electrostatic interactions. Periodic boundary conditions were used for all the calculations without applying any constraint to either the protein or the ligand molecules. The trajectory of MD simulation was achieved by writing out the co-ordinates every 10 ps. Postprocessing the trajectory resulted to dynamically sampling of snapshots from simulation trajectory with an interval of 10 ps. The dielectric constant values for the interior of solute and the surrounding solvent were set to 1.0 and 80, respectively. Finally, the binding free energy was calculated for the complex of ligand–enzyme complex using molecular mechanics Poisson–Boltzmann surface area (MM-PBSA)/generalized Born–surface area (GBSA) methods implemented in the AMBER package (Case et al., 2005; Kollman et al., 2000). For obtaining binding free energy, sum of molecular mechanics energies, solvation free energies, and entropic terms were considered which was subsequently averaged over a series of equilibrated snapshots derived from MD simulation trajectory. For calculation of interaction energies, water molecules and counterions were excluded and presented as the average value.

For obtaining the binding free energy (ΔG_{bind}), the following equation was used:

$$\Delta G_{\text{bind}} = G_{\text{water}(\text{complex})} - G_{\text{water}(\text{protein})} - G_{\text{water}(\text{ligand})}$$

where $G_{\text{water}(\text{complex})}$, $G_{\text{water}(\text{protein})}$, and $G_{\text{water}(\text{ligand})}$ are the free energies of the complex, protein, and ligand, respectively. Free energy for each species is calculated as follows:

$$G = E_{\text{gas}} + \Delta G_{\text{solvation}} - TS$$

$$\Delta G_{\text{solvation}} = \Delta G_{\text{polar}} + \Delta G_{\text{non-polar}}$$

$$E_{\text{gas}} = E_{\text{int}} + E_{\text{vdw}} + E_{\text{elec}}$$

$$E_{\text{int}} = E_{\text{bond}} + E_{\text{angle}} + E_{\text{tors}}$$

G shows the calculated average free energy, and E_{gas} is the standard force-field energy, including internal energy (E_{int}) in the gas phase as well as non-covalent van der Waals (E_{vdw}) and electrostatic (E_{elec}) energies. E_{int} is composed of E_{bond} , E_{angle} , and E_{tors} , which are the contributors of internal energy originated

from the strain caused by deviation of the bonds, angle, and torsion angle from their equilibrium values. $\Delta G_{\text{solvation}}$ consists of ΔG_{polar} and $\Delta G_{\text{non-polar}}$ demonstrating the polar and non-polar contributions to the solvation free energy. The polar contribution is calculated by Poisson–Boltzmann or generalized Born model, while the non-polar contributions are achieved by the calculation of solvent accessible surface area using the linear combinations of pairwise overlaps method (Weiser, Shenkin, & Still, 1999). TS refers to the vibrational entropy term which is ignored in this study assuming similar entropy contribution for all complexes to the binding free energy.

3 | RESULTS

3.1 | H₃R antagonism in the cAMP accumulation assay

Functional properties of the selected compounds (i.e., compounds **3** and **4**) were determined in the forskolin-stimulated cAMP accumulation assay using hH₃R-expressing CHO-K1 cells. As shown in Figure 1a, the reference agonist (*R*)- α -methylhistamine decreased cAMP formation and when the cells were co-treated with the compounds and the reference agonist, the agonistic effect of (*R*)- α -methylhistamine was suppressed. Compounds **3** and **4** enhanced in a concentration-dependent manner cAMP levels in CHO-K1 expressing human H₃Rs that were incubated in the presence of (*R*)- α -methylhistamine and forskolin (Figure 1a), indicating the antagonistic activity of these compounds. Such antagonistic activity was more pronounced for compound **3** compared to compound **4** by means of changes in intrinsic activity of the receptor. Antagonistic potencies of compounds determined from sigmoidal dose–response curves in the functional assay are shown in Table 1. Moreover, in this cell system, a titration of these compounds in the absence of the reference agonist was performed and the results demonstrated that both compounds increased cAMP formation by themselves with maximal effect comparable to thioperamide as standard H₃R antagonist (Figure 1b). From similar concentration–response patterns in the literature and compared to thioperamide, it can be concluded that compounds **3** and **4** behave as inverse agonists at the human H₃R (Kuder et al., 2016; Lazewska et al., 2017; Sors et al., 2017).

3.2 | Cholinesterase inhibitory activity

The anticholinesterase activity of compounds **3** and **4** were evaluated according to the Ellman's method using AChE and BuChE from electric eel and horse serum, respectively. Donepezil was used as the reference compound in this assay, and the results are demonstrated in Table 1. As shown in Table 1, the compounds exhibited inhibitory activity on both AChE and BuChE in the micromolar range, indicative of moderate inhibition toward both cholinesterase enzymes. As the level of acetylcholine is of great importance in AD,

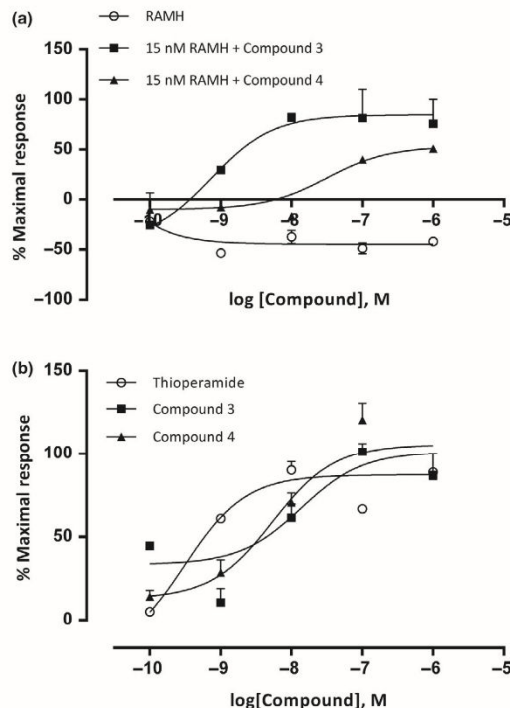


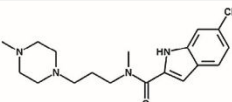
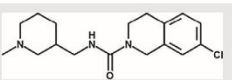
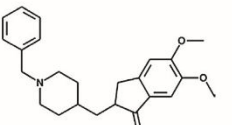
FIGURE 1 cAMP accumulation studies in CHO-K1 cells expressing human histamine H₃ receptor co-treated with forskolin and the studied compounds in the presence (a) and absence (b) of (*R*)- α -methylhistamine (RAMH). The response was calculated with the following formula: % maximal response = $100 \times [(A - A_{\text{basal}}) / (A_{\text{max}} - A_{\text{basal}})]$ where *A* is the absorbance of the sample, *A*_{max} is the absorbance at maximum stimulation, and *A*_{basal} is the absorbance at basal level. Data are represented as mean \pm SE from duplicate determinations

non-selective inhibition of both AChE and BuChE would therefore be beneficial from a therapeutic point of view. Based on the obtained results, the IC₅₀ values for inhibition of AChE were 9.09 and 8.40 μ M for compounds **3** and **4**, respectively, whereas in the case of BuChE, these values were achieved 21.10 and 4.93 μ M for compounds **3** and **4**, respectively. The results of cholinesterase inhibition assays are comparable with previously reported studies in which the inhibitory activity of the compounds and reference molecule (i.e., donepezil) is in micromolar and submicromolar concentration range for BuChE and AChE, respectively (Lalut et al., 2019; Lazewska et al., 2016; Li et al., 2014).

3.3 | Toxicity evaluation

To estimate potential cytotoxic effects of studied compounds and determine their influence on the viability of

TABLE 1 Chemical structures, antagonistic potencies to the human histamine H₃ receptor, and cholinesterase inhibitory activities of tested compounds

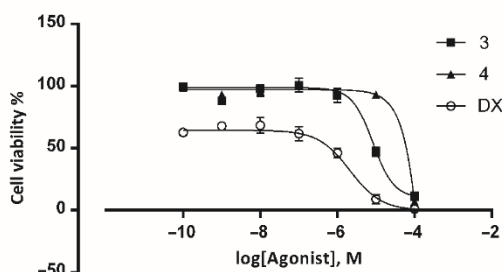
Compound	Structure	H ₃ R EC ₅₀ ± SE [nM]	AChE IC ₅₀ ± SE [μM]	BuChE IC ₅₀ ± SE [μM]
3		0.73 ± 0.016	9.09 ± 2.09	21.10 ± 4.8
4		31 ± 1.95	8.40 ± 1.93	4.93 ± 0.68
Donepezil		nt.	0.024 ± 0.002	2.50 ± 0.35

nt.: not tested.

hH₃R expressing CHO-K1 cells, the MTT assay was employed. Judged among the concentration corresponding to a 50% inhibition of growth (*GI*₅₀), the tested compounds did not exhibit significant cytotoxic influence on cell viability of the examined cell line in a concentration range from 0.1 nM to 100 μM compared to doxorubicin (DX) as reference compound (compound **3**, *GI*₅₀ = 8.38 ± 0.43 μM; compound **4**, *GI*₅₀ ≈ 100 μM, and DX, *GI*₅₀ = 2.1 ± 0.26 μM). As shown in Figure 2, following incubation of the studied compounds with hH₃R expressing CHO-K1 cells for 72 hr, the viability of the cells was intact up to 1 μM, whereas the cytotoxic effect is observed at higher concentrations of compounds (i.e., >10 μM). Based on the obtained results, it seems that they have no significant impact on cell viability which is more noticeable for compound **4** inferred from the corresponding *GI*₅₀. The results are comparable with those published previously in terms of toxicity of reference compound and selected compounds (Lazewska et al., 2018; Morini et al., 2008).

3.4 | Molecular docking and calculation of binding free energy for ligand–enzyme complex

In order to predict the mode of interactions between studied compounds and the cholinesterases, the molecular docking experiment was conducted. To this end, flexible docking of compounds **3** and **4** into active site of enzymes was performed using GOLD program based on the optimized condition set for re-docking of co-crystallized donepezil into active site of enzymes. Figure 3 and Table 2 illustrate the key residues in the active site of enzymes interacting with studied compounds. The main interactions observed for compound **3** bound to the active site of AChE include a π – π stacking, two

**FIGURE 2** MTT cytotoxicity assay. Anti-proliferative effects of the studied compounds on histamine H₃ receptor expressing CHO-K1 cells are shown as percentage of cell viability. Data are expressed as mean ± SE from a representative experiment performed in triplicate

hydrophobic pockets, and a hydrogen bond interaction. The π – π stacking is established between indole ring of compound **3** and Trp²⁸⁶. One of the hydrophobic interactions is formed between the alkyl part of the linker in compound **3** and Tyr³³⁷ and Tyr³⁴¹ from AChE, while the other hydrophobic interactions are observed between methylpiperazine moiety of the compound **3** and Trp⁸⁶ and His⁴⁴⁷ from the enzyme. Besides, Tyr¹²⁴ of the AChE is engaged in the hydrogen bond with nitrogen of indole ring in compound **3**. In case of molecule **4**, the main interactions are similar to those observed for compound **3** with the phenyl ring of tetrahydroisoquinoline moiety being involved in a π – π stacking interaction with Trp²⁸⁶. Additionally, the tetrahydroisoquinoline part hydrophobically interacts with Tyr³⁴¹ of enzyme. Furthermore, a hydrophobic pocket composed of Trp⁸⁶, Tyr³³⁷, and His⁴⁴⁷ surrounds the methylpiperidine at the endmost part of molecule **4**. A hydrogen bond is also seen between Tyr¹²⁴ and nitrogen of tetrahydroisoquinoline. Such similar interactions

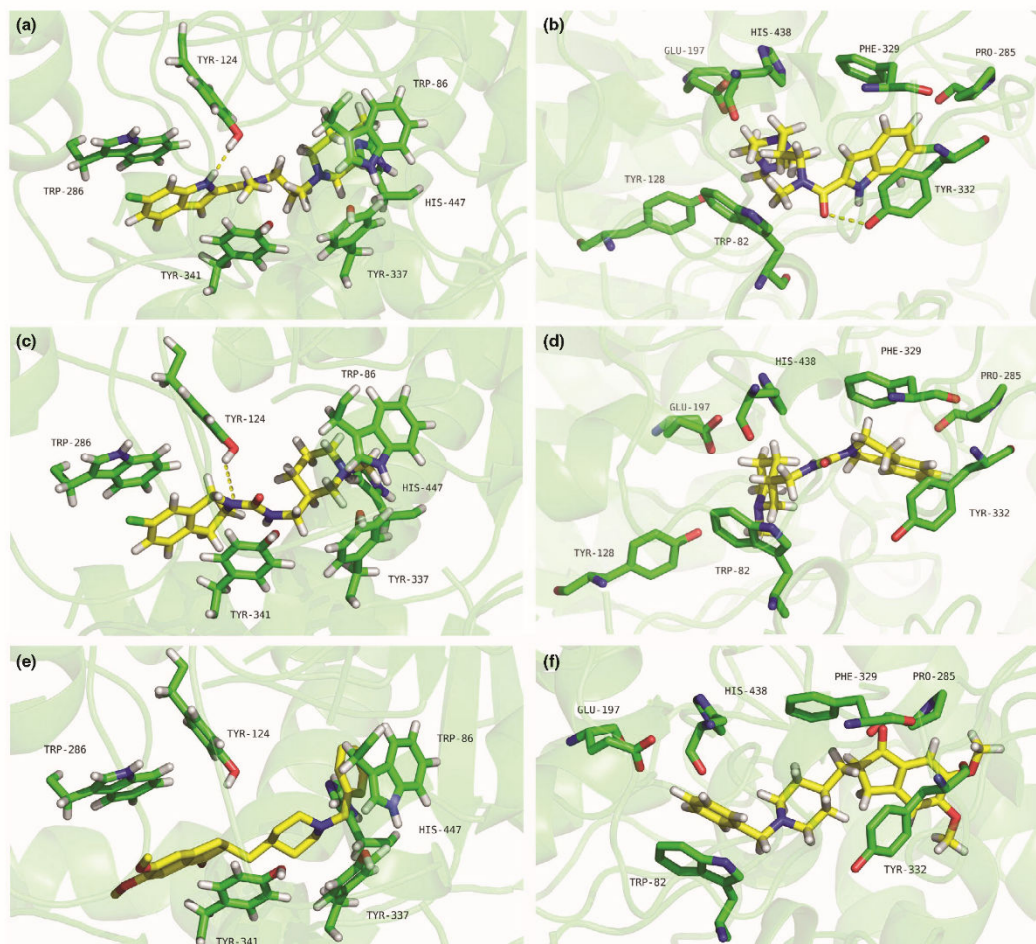


FIGURE 3 3D representation of compounds **3**, **4**, and donepezil (Panels (a) to (f)) docked onto the binding site of cholinesterase enzymes generated by PyMOL program (version 1.7.x). Panels (a), (c), and (e) show the interactions of the compounds **3**, **4**, and donepezil with AChE, respectively. Panels (b), (d), and (f) indicate the interactions of compounds **3**, **4**, and donepezil in complex with BuChE, respectively. The ligands and the main interacting residues are shown as sticks. Only the side chains of the interacting residues from the receptor are shown for further clarity [Colour figure can be viewed at wileyonlinelibrary.com]

have been detected for the complex of donepezil and AChE enzyme.

The interactions observed for the complex of inhibitor BuChE resemble those seen for AChE. The identified interactions for compound **3** consist of hydrophobic interactions and a hydrogen bond. A hydrophobic pocket formed by Trp⁸², Tyr¹²⁸, and Glu¹⁹⁷ of the BuChE accommodates the methylpiperazine part of compound **3**. Alkyl part of linker in compound **3** makes hydrophobic interaction with His⁴³⁸. Furthermore, the other hydrophobic interactions are observed between indole ring of compound **3** and Pro²⁸⁵, Phe³²⁹, and Tyr³³². Moreover, oxygen of amide linker in compound **3**

makes a hydrogen bond with Tyr³³². Compound **4** binds into the active site of BuChE predominantly via hydrophobic interactions. One of the hydrophobic interactions is established by contribution of Trp⁸², Tyr¹²⁸, Ser¹⁹⁸, and His⁴³⁸ from the enzyme and methylpiperidine part of compound **4**, whereas the tetrahydroisoquinoline part of compound **4** is surrounded by a hydrophobic pocket formed by Pro²⁸⁵, Phe³²⁹, and Tyr³³² of the enzyme.

In the current study, binding free energy for the ligand–enzyme complexes was calculated using AMBER package. To this end, MD simulation was performed for the best docked pose for 10 ns. The snapshots were extracted from the MD

trajectory every 10 ps to be used for calculation of binding free energy using MM-PBSA/GBSA methods. The analysis of the MD trajectory based on root-mean-square deviation (RMSD) and potential energy indicated that all systems in the simulation process were well equilibrated and stable during the simulation period (Figure S1). Table 3 provides the results of binding free energy calculations for the complexes with respect to donepezil (as reference compound).

4 | DISCUSSION

The complex and multifaceted pathophysiological nature of AD necessitates the identification and development of novel therapeutic agents. For several decades of research, H₃R antagonists have gained much attention in the field of neurological disorders (Brioni et al., 2011; Esbenshade et al., 2008; Sadek, Saad, et al., 2016; Shan, Bao, & Swaab, 2015; Tiligada, Kyriakidis, Chazot, & Passani, 2011; Vohora & Bhowmik, 2012). There are some H₃R antagonists in clinical trial studies for which their effectiveness in AD is being evaluated as mono- or add-on therapy. The examples of such clinical candidates are ABT-288, AZD-5213, GSK-239512, GSK-1004723, MK-0249, and S 38093 (for more details, see Ghamari et al., 2019). Recently, several studies have focused on developing ligands targeting both H₃Rs and cholinesterase enzymes (Bajda et al., 2012; Bembenek et al., 2008; Darras et al., 2014; Incerti et al., 2010; Lazewska et al., 2016; Sadek, Khan, et al., 2016), since the synergistic effect of these agents leads to enhance cholinergic neurotransmission through different mechanisms.

Previously, we identified novel anti-H₃R agents using in silico virtual screening methods. Briefly, a combination of structure- and ligand-based approaches was applied to search

compounds from ZINC library on the homology model of the human H₃R. Following the screening, the molecules were also inspected for drug-likeness and ADME properties. Furthermore, the results of binding assays on selected compounds demonstrated that two compounds (i.e., compounds **3** and **4**) were capable of binding to histamine H₃Rs with K_i values in submicromolar concentration range (Ghamari et al., 2018). In the current study, dual inhibitory activity of these compounds on H₃Rs and cholinesterase enzymes was investigated. The analysis of cAMP accumulation within CHO-K1 cells expressing recombinant hH₃Rs revealed that compounds **3** and **4** elevate cAMP levels by themselves and antagonize the effect (*R*)- α -methylhistamine, implying the compounds to be classified as H₃R antagonists/inverse agonists.

The anticholinesterase activity of such compounds was also assessed, showing moderate inhibition on both, AChE and BuChE, with IC₅₀ values in the micromolar range. Both compounds were approximately equipotent toward AChE, whereas compound **4** exhibited higher potency on BuChE compared to compound **3**. In addition to AChE, targeting BuChE is of great importance in AD pharmacotherapy as several studies indicate that the activity and levels of acetylcholine in the CNS are modulated by AChE as well as by BuChE (Darvesh, Hopkins, & Geula, 2003; Mesulam et al., 2002). Furthermore, BuChE activity is enhanced in hippocampus and cerebral cortex along AD progression (Perry, Perry, Blessed, & Tomlinson, 1978). Therefore, this can be a driving force for designing non-selective inhibitors with superior efficiency to selective AChE inhibitors in advanced stages of AD. In this context, compounds **3** and **4** were able to target both of cholinesterase enzymes. Similar to the ligands presented herein, there are several reports in which dual-acting cholinesterase inhibitors and H₃R antagonists were designed and experimentally evaluated. Darras et al. (2014) designed and synthesized the hybrid molecules containing piperdinyloxyphenyl moiety and related H₃R pharmacophores with nitrogen-bridgehead moieties as AChE inhibition pharmacophore. The most potent compound of this study, that is, compound **41** (named UW-MD-71), showed high potency at both targets (hH₃R: K_i = 76.2 nM and hAChE: IC₅₀ = 33.9 nM) (Darras et al., 2014). Subsequently, the effect of this compound on memory retrieval and precognitive enhancement was also assessed in an in vivo study. The findings of this investigation demonstrated promising

TABLE 2 The key amino acids of cholinesterase enzymes involved in the interactions with the studied compounds

Enzyme	Amino acids
AChE	Trp ⁸⁶ , Tyr ¹²⁴ , Trp ²⁸⁶ , Tyr ³³⁷ , Tyr ³⁴¹ , His ⁴⁴⁷
BuChE	Trp ⁸² , Tyr ¹²⁸ , Glu ¹⁹⁷ , Ser ¹⁹⁸ , Pro ²⁸⁵ , Phe ³²⁹ , Tyr ³³² , His ⁴³⁸

Compound	AChE		BuChE	
	$\Delta G_{\text{Binding (GB)}}$	$\Delta G_{\text{Binding (PB)}}$	$\Delta G_{\text{Binding (GB)}}$	$\Delta G_{\text{Binding (PB)}}$
3	-37.11 (± 2.41)	-23.93 (± 3.75)	-29.91 (± 3.84)	-25.75 (± 4.34)
4	-30.4 (± 4.72)	-24.24 (± 4.46)	-30.85 (± 2.47)	-26.92 (± 3.97)
Donepezil	-42.6 (± 3.06)	-28.34 (± 6.14)	-35.98 (± 3.06)	-26.17 (± 3.95)

Note: Energy values are dimensioned as kcal/mol. Standard deviations are shown in parentheses.

TABLE 3 Calculated mean values of binding free energies for the complex of docked lead molecules using generalized Born, $\Delta G_{\text{Binding (GB)}}$, and Poisson–Boltzmann, $\Delta G_{\text{Binding (PB)}}$, methods for 10 ns MD simulation

results in improving retrieval processes in rat memory models (Khan et al., 2016). The similar in vivo results were also observed for another, structurally related compound named UW-MD-72 (Sadek, Khan, et al., 2016). In another study, the dual inhibitory activities of diether derivatives of homo- or substituted piperidines were investigated. The most potent compound of this series (i.e., compound **13**) exhibited high affinity to H₃R ($K_i = 3.48$ nM) and moderate inhibitory activity to cholinesterase enzymes (EeAChE: $IC_{50} = 7.91$ μ M and EqAChE: $IC_{50} = 4.97$ μ M; Bajda et al., 2012). Extending the previous work, a novel series of compounds was designed with chlorophenoxyalkylamine scaffold inspired from the structure of compound **13**. This structural modification led to identification of the most potent compound of this set (1-(7-(4-chlorophenoxy)heptyl)homopiperidine) with increased affinity toward cholinesterase enzymes (EeAChE: $IC_{50} = 1.93$ μ M and EqAChE: $IC_{50} = 1.64$ μ M); however, the antagonistic potency of H₃R was not improved (hH₃R: $K_i = 203$ nM; Lazewska et al., 2016). More structurally different compounds as dual-acting cholinesterase inhibitors and H₃R antagonists were designed based on a 4,4'-biphenyl scaffold with mono- and dibasic moieties at distal ends. The findings of this study showed a dibasic piperidine containing compound (1-[2-(4'-piperidinomethyl-biphenyl-4-yl)ethyl]piperidine), revealing high H₃R binding affinity (hH₃R: $K_i = 1.9$ nM) and moderate inhibition on rat cholinesterase (rAChE: $IC_{50} = 1.096$ μ M; Morini et al., 2008). Moreover, among a series of piperidinoalkyl derivatives with different length of linker and terminal heterocyclic ring, an analogue containing a tetrahydroaminoacridine moiety at distal end of molecule showed promising results with H₃R affinity corresponding to $K_i = 1.8$ nM and inhibitory activity of $IC_{50} = 0.26$ nM at rat cholinesterase (Incerti et al., 2010). In a recent study, a series of MDTLs acting at H₃Rs and cholinesterases as well as on monoamine oxidases was developed (Bautista-Aguilera et al., 2017). Based on a MDTL with AChE and BuChE targeting properties (ASS234), the author demonstrates that a 1-Benzylpiperidin-4-yl alkyl motif as found as pharmacophore in donepezil can be shifted toward a 1-piperidinylalkyl pharmacophore leading to a pharmacophoric overlap of H₃R and AChE/BuChE targeting motif. Collectively, by structural inspection of mentioned dual inhibitors and the ligands disclosed here, it seems that the presence of basic moiety such as piperidine ring connecting to aromatic/heteroaromatic moiety through a linker is necessary for exerting inhibitory activity on either targets. The results of such studies can motivate medicinal chemists to rational design of novel dual-acting ligands of H₃R and cholinesterase enzymes.

The cell viability estimation of the studied compounds showed no significant cytotoxic effect on CHO-K1 cells up to micromolar concentrations. According to the GI_{50} values, the cytotoxic effect is more evident for compound **3** compared to

the reference compound DX and therefore in agreement with the previously predicted in silico toxic potential. Based on the scale of toxicity alert, compound **4** was predicted to be a safe compound in comparison with compound **3** (Ghamari et al., 2018).

In order to gain insight into the possible mode of interactions between ligands and cholinesterase enzymes, docking studies were performed. The analysis of the proposed interactions shows similarity in the binding mode to that of donepezil co-crystallized with AChE (Cheung et al., 2012). The indole and tetrahydroisoquinoline rings of compounds **3** and **4** can be considered to be equivalent to indanone ring of donepezil in establishing π - π interaction with Trp²⁸⁶ of AChE. Similarly, methylpiperazine and methylpiperidine moieties of compounds **3** and **4** resemble the benzyl ring of donepezil which stack against Trp⁸⁶. The Tyr³³⁷ and Tyr³⁴¹ from AChE are additional key residues for the interactions with the studied ligands as observed in donepezil-AChE complex. Such interactions were also predicted for the complex of inhibitor BuChE due to high similarity of the residues located in the active sites of both enzymes. For example, amino acids Trp⁸², Tyr³³², and His⁴³⁸ from BuChE are equivalent to Trp⁸⁶, Tyr³⁴¹, and His⁴⁴⁷ from AChE in terms of interactions with the ligand. The results of molecular docking studies are in line with formerly published findings (Bajda et al., 2012; Darras et al., 2014; Jang et al., 2018; Lazewska et al., 2016; Morini et al., 2008). In addition, the results of binding affinity prediction for the complexes of ligand-cholinesterase are consistent with the experimentally determined anticholinesterase activity of compounds **3** and **4**. The calculated binding energy for donepezil demonstrated that this therapeutic agent strongly inhibits the cholinesterase enzymes (Table 3) which is in close agreement with the experimental results (Table 1). Although in the case of AChE inhibition, there is no significant difference in the inhibitory potency of compounds **3** and **4**, the results of binding affinity calculations correlate well with IC_{50} values. It can be deduced from comparison of ΔG values obtained from MM-PBSA and MM-GBSA methods. This consistency implies the reliability of MM-PBSA/GBSA methods in predicting binding affinities of studied ligands to cholinesterase enzymes.

Although compounds **3** and **4** showed antagonistic activity at the human H₃R combined with cholinesterase inhibitory properties, compound **3** was more potent in terms of H₃R blockade with approximate equipotency in cholinesterase inhibition compared to compound **4**. On the other hand, by considering the results obtained from toxicity evaluation, it seems that compound **4** has greater safety compared to compound **3**. Moreover, it appears that structural modification of both compounds can be beneficial for developing dual-acting compounds with improved efficacy and lower toxicity. To reach this goal, the use of medicinal chemistry-oriented

strategies such as scaffold hopping or bioisosteric replacement is highly recommended. Additionally, more preclinical biological assays both in vitro and in vivo paradigms are needed to elucidate the potential effect of the designed compounds.

5 | CONCLUSIONS

According to the special place of in silico methods in modern drug discovery, remarkable advances have been achieved in the last decades at the early stages of the drug design and discovery pipeline. In this study, the anti-H₃R ligands identified through previous in silico virtual screening approaches were functionally evaluated and found as dual-acting H₃R antagonists and cholinesterase inhibitors. Collectively, the presented lead compounds can serve as promising starting points for further development of novel anti-AD agents through medicinal chemistry aided structural modification and optimization.

ACKNOWLEDGMENTS

This work forms part of the PhD thesis of Nakisa Ghamari at the School of Pharmacy, Tabriz University of Medical Sciences, Tabriz, Iran. The authors would like to thank the Research Office and Biotechnology Research Center of Tabriz University of Medical Sciences for providing financial support under the Postgraduate Research Grant scheme for the PhD thesis of NG (Grant Number: 57572). Additional support was given by EU COST Actions CA15135 and CA18133 (HS).

CONFLICT OF INTEREST

The authors declare no conflict of interest.

ORCID

Nakisa Ghamari  <https://orcid.org/0000-0002-8515-3326>

Siavoush Dastmalchi  <https://orcid.org/0000-0001-9427-0770>

Omid Zarei  <https://orcid.org/0000-0002-9362-9240>

José-Antonio Arias-Montaña  <https://orcid.org/0000-0002-0791-8397>

David Reiner  <https://orcid.org/0000-0003-1514-2215>

Fulya Ustun-Alkan  <https://orcid.org/0000-0003-1782-9467>

Holger Stark  <https://orcid.org/0000-0003-3336-1710>

Maryam Hamzeh-Mivehroud  <https://orcid.org/0000-0002-1257-0102>

DATA AVAILABILITY STATEMENT

The data that support the findings of this study are available from the corresponding author upon reasonable request.

REFERENCES

- Bajda, M., Guziar, N., Ignasik, M., & Malawska, B. (2011). Multi-target-directed ligands in Alzheimer's disease treatment. *Current Medicinal Chemistry*, 18, 4949–4975. <https://doi.org/10.2174/092986711797535245>
- Bajda, M., Kuder, K. J., Łażewska, D., Kieć-Kononowicz, K., Wieckowska, A., Ignasik, M., ... Malawska, B. (2012). Dual-acting diether derivatives of piperidine and homopiperidine with histamine H₃ receptor antagonistic and anticholinesterase activity. *Archiv Der Pharmazie (Weinheim)*, 345, 591–597. <https://doi.org/10.1002/ardp.201200018>
- Bautista-Aguilera, O. M., Hagenow, S., Palomino-Antolin, A., Farre-Alins, V., Ismaili, L., Joffrin, P. L., ... Stark, H. (2017). Multitarget-directed ligands combining cholinesterase and monoamine oxidase inhibition with histamine H₃ R antagonism for neurodegenerative diseases. *Angewandte Chemie, International Edition in English*, 56, 12765–12769. <https://doi.org/10.1002/anie.201706072>
- Bembenek, S. D., Keith, J. M., Letavice, M. A., Apodaca, R., Barbier, A. J., Dvorak, L., ... Carruthers, N. I. (2008). Lead identification of acetylcholinesterase inhibitors-histamine H₃ receptor antagonists from molecular modeling. *Bioorganic and Medicinal Chemistry*, 16, 2968–2973. <https://doi.org/10.1016/j.bmc.2007.12.048>
- Berlin, M., Boyce, C. W., & Ruiz Mde, L. (2011). Histamine H₃ receptor as a drug discovery target. *Journal of Medicinal Chemistry*, 54, 26–53. <https://doi.org/10.1021/jm100064d>
- Berman, H. M., Westbrook, J., Feng, Z., Gilliland, G., Bhat, T. N., Weissig, H., ... Bourne, P. E. (2000). The Protein Data Bank. *Nucleic Acids Research*, 28, 235–242. <https://doi.org/10.1093/nar/28.1.235>
- Brioni, J. D., Esbenshade, T. A., Garrison, T. R., Bitner, S. R., & Cowart, M. D. (2011). Discovery of histamine H₃ antagonists for the treatment of cognitive disorders and Alzheimer's disease. *Journal of Pharmacology and Experimental Therapeutics*, 336, 38–46. <https://doi.org/10.1124/jpet.110.166876>
- Brus, B., Kořak, U., Turk, S., Pišlar, A., Coquelle, N., Kos, J., ... Gobec, S. (2014). Discovery, biological evaluation, and crystal structure of a novel nanomolar selective butyrylcholinesterase inhibitor. *Journal of Medicinal Chemistry*, 57, 8167–8179. <https://doi.org/10.1021/jm501195e>
- Case, D. A., Cheatham, T. E., Darden, T., Gohlke, H., Luo, R., Merz, K. M., ... Woods, R. J. (2005). The Amber biomolecular simulation programs. *Journal of Computational Chemistry*, 26, 1668–1688. <https://doi.org/10.1002/jcc.20290>
- Chen, P.-Y., Tsai, C.-T., Ou, C.-Y., Hsu, W.-T., Jhuo, M.-D., Wu, C.-H., ... Chung, J.-G. (2012). Computational analysis of novel drugs designed for use as acetylcholinesterase inhibitors and histamine H₃ receptor antagonists for Alzheimer's disease by docking, scoring and de novo evolution. *Molecular Medicine Reports*, 5, 1043–1048. <https://doi.org/10.3892/mmr.2012.757>
- Chen, X., & Decker, M. (2013). Multi-target compounds acting in the central nervous system designed from natural products. *Current Medicinal Chemistry*, 20, 1673–1685. <https://doi.org/10.2174/0929867311320130007>

- Cheung, J., Rudolph, M. J., Burshteyn, F., Cassidy, M. S., Gary, E. N., Love, J., ... Height, J. J. (2012). Structures of human acetylcholinesterase in complex with pharmacologically important ligands. *Journal of Medicinal Chemistry*, 55, 10282–10286. <https://doi.org/10.1021/jm300871x>
- Darras, F. H., Pockes, S., Huang, G., Wehle, S., Strasser, A., Wittmann, H. J., ... Decker, M. (2014). Synthesis, biological evaluation, and computational studies of Tri- and tetracyclic nitrogen-bridgehead compounds as potent dual-acting AChE inhibitors and hH₃ receptor antagonists. *ACS Chemical Neuroscience*, 5, 225–242. <https://doi.org/10.1021/cn4002126>
- Darvesh, S., Hopkins, D. A., & Geula, C. (2003). Neurobiology of butyrylcholinesterase. *Nature Reviews Neuroscience*, 4, 131–138. <https://doi.org/10.1038/nrn1035>
- Ellman, G. L., Courtney, K. D., Andres, V. Jr., & Feather-Stone, R. M. (1961). A new and rapid colorimetric determination of acetylcholinesterase activity. *Biochemical Pharmacology*, 7, 88–95. [https://doi.org/10.1016/0006-2952\(61\)90145-9](https://doi.org/10.1016/0006-2952(61)90145-9)
- Esbenshade, T. A., Browman, K. E., Bitner, R. S., Strakhova, M., Cowart, M. D., & Brioni, J. D. (2008). The histamine H₃ receptor: An attractive target for the treatment of cognitive disorders. *British Journal of Pharmacology*, 154, 1166–1181. <https://doi.org/10.1038/bjp.2008.147>
- Geldenhuys, W. J., & Van der Schyf, C. J. (2013). Designing drugs with multi-target activity: The next step in the treatment of neurodegenerative disorders. *Expert Opinion on Drug Discovery*, 8, 115–129. <https://doi.org/10.1517/17460441.2013.744746>
- Ghamari, N., Zarei, O., Arias-Montano, J. A., Reiner, D., Dastmalchi, S., Stark, H., & Hamzeh-Mivehroud, M. (2019). Histamine H₃ receptor antagonists/inverse agonists: Where do they go? *Pharmacology & Therapeutics*, 200, 69–84. <https://doi.org/10.1016/j.pharmthera.2019.04.007>
- Ghamari, N., Zarei, O., Reiner, D., Dastmalchi, S., Stark, H., & Hamzeh-Mivehroud, M. (2018). Histamine H₃ receptor ligands by hybrid virtual screening, docking, molecular dynamics simulations, and investigation of their biological effects. *Chemical Biology & Drug Design*, 93, 832–843. <https://doi.org/10.1111/cbdd.13471>
- Incerti, M., Flammini, L., Saccani, F., Morini, G., Comini, M., Coruzzi, M., ... Berton, S. (2010). Dual-acting drugs: An in vitro study of nonimidazole histamine H₃ receptor antagonists combining anticholinesterase activity. *ChemMedChem*, 5, 1143–1149. <https://doi.org/10.1002/cmdc.201000008>
- Jang, C., Yadav, D. K., Subedi, L., Venkatesan, R., Venkanna, A., Afzal, S., ... Kim, M.-H. (2018). Identification of novel acetylcholinesterase inhibitors designed by pharmacophore-based virtual screening, molecular docking and bioassay. *Scientific Reports*, 8, 14921. <https://doi.org/10.1038/s41598-018-33354-6>
- Khan, N., Saad, A., Nurulain, S. M., Darras, F. H., Decker, M., & Sadek, B. (2016). The dual-acting H₃ receptor antagonist and AChE inhibitor UW-MD-71 dose-dependently enhances memory retrieval and reverses dizocilpine-induced memory impairment in rats. *Behavioural Brain Research*, 297, 155–164. <https://doi.org/10.1016/j.bbr.2015.10.022>
- Khanfar, M. A., Affini, A., Lutsenko, K., Nikolic, K., Butini, S., & Stark, H. (2016). Multiple targeting approaches on histamine H₃ receptor antagonists. *Frontiers in Neuroscience*, 10, 201. <https://doi.org/10.3389/fnins.2016.00201>
- Kollman, P. A., Massova, I., Reyes, C., Kuhn, B., Huo, S., Chong, L., ... Cheatham, T. E. (2000). Calculating structures and free energies of complex molecules: Combining molecular mechanics and continuum models. *Accounts of Chemical Research*, 33, 889–897. <https://doi.org/10.1021/ar000033j>
- Kuder, K., Łazewska, D., Latacz, G., Schwed, J. S., Karcz, T., Stark, H., ... Kieć-Kononowicz, K. (2016). Chlorophenoxy aminoalkyl derivatives as histamine H(3)R ligands and antiseizure agents. *Bioorganic and Medicinal Chemistry*, 24, 53–72. <https://doi.org/10.1016/j.bmc.2015.11.021>
- Lalut, J., Santoni, G., Karila, D., Lecoutey, C., Davis, A., Nachon, F., ... Rochais, C. (2019). Novel multitarget-directed ligands targeting acetylcholinesterase and sigma1 receptors as lead compounds for treatment of Alzheimer's disease: Synthesis, evaluation, and structural characterization of their complexes with acetylcholinesterase. *European Journal of Medical Chemistry*, 162, 234–248. <https://doi.org/10.1016/j.ejmech.2018.10.064>
- Łazewska, D., Jorńczyk, J., Bajda, M., Szałaj, N., Więckowska, A., Panek, D., ... Kieć-Kononowicz, K. (2016). Cholinesterase inhibitory activity of chlorophenoxy derivatives-Histamine H₃ receptor ligands. *Bioorganic and Medicinal Chemistry Letters*, 26, 4140–4145. <https://doi.org/10.1016/j.bmcl.2016.04.054>
- Łazewska, D., Kaleta, M., Hagenow, S., Mogiński, S., Latacz, G., Karcz, T., ... Kieć-Kononowicz, K. (2018). Novel naphthoxy derivatives—potent histamine H₃ receptor ligands. Synthesis and pharmacological evaluation. *Bioorganic and Medicinal Chemistry*, 26, 2573–2585. <https://doi.org/10.1016/j.bmc.2018.04.023>
- Łazewska, D., Kaleta, M., Schwed, J. S., Karcz, T., Mogiński, S., Latacz, G., ... Kieć-Kononowicz, K. (2017). Biphenyloxy-alkyl-piperidine and azepane derivatives as histamine H₃ receptor ligands. *Bioorganic and Medicinal Chemistry*, 25, 5341–5354. <https://doi.org/10.1016/j.bmc.2017.07.058>
- Lazewska, D., & Kieć-Kononowicz, K. (2014). New developments around histamine H(3) receptor antagonists/inverse agonists: A patent review (2010–present). *Expert Opinion on Therapeutic Patents*, 24, 89–111. <https://doi.org/10.1517/13543776.2014.848197>
- Li, Y., Peng, P., Tang, L., Hu, Y., Hu, Y., & Sheng, R. (2014). Design, synthesis and evaluation of rivastigmine and curcumin hybrids as site-activated multitarget-directed ligands for Alzheimer's disease therapy. *Bioorganic and Medicinal Chemistry*, 22, 4717–4725. <https://doi.org/10.1016/j.bmc.2014.07.009>
- Medhurst, A. D., Atkins, A. R., Beresford, I. J., Brackenborough, K., Briggs, M. A., Calver, A. R., ... Wilson, D. M. (2007). GSK189254, a novel H₃ receptor antagonist that binds to histamine H₃ receptors in Alzheimer's disease brain and improves cognitive performance in preclinical models. *Journal of Pharmacology and Experimental Therapeutics*, 321, 1032–1045. <https://doi.org/10.1124/jpet.107.120311>
- Mesulam, M. M., Guillozet, A., Shaw, P., Levey, A., Duysen, E. G., & Lockridge, O. (2002). Acetylcholinesterase knockouts establish central cholinergic pathways and can use butyrylcholinesterase to hydrolyze acetylcholine. *Neuroscience*, 110, 627–639. [https://doi.org/10.1016/S0306-4522\(01\)00613-3](https://doi.org/10.1016/S0306-4522(01)00613-3)
- Morini, G., Comini, M., Rivara, M., Rivara, S., Bordini, F., Plazzi, P. V., ... Mor, M. (2008). Synthesis and structure-activity relationships for biphenyl H₃ receptor antagonists with moderate anti-cholinesterase activity. *Bioorganic and Medicinal Chemistry*, 16, 9911–9924. <https://doi.org/10.1016/j.bmc.2008.10.029>
- Mosmann, T. (1983). Rapid colorimetric assay for cellular growth and survival: Application to proliferation and cytotoxicity assays. *Journal of Immunological Methods*, 65, 55–63. [https://doi.org/10.1016/0022-1759\(83\)90303-4](https://doi.org/10.1016/0022-1759(83)90303-4)
- Nieto-Alamilla, G., Marquez-Gomez, R., Garcia-Galvez, A. M., Morales-Figueroa, G. E., & Arias-Montano, J. A. (2016). The

- histamine H₃ receptor: Structure, pharmacology, and function. *Molecular Pharmacology*, 90, 649–673. <https://doi.org/10.1124/mol.116.104752>
- Osorio-Espinoza, A., Escamilla-Sanchez, J., Aquino-Jarquin, G., & Arias-Montano, J. A. (2014). Homologous desensitization of human histamine H₃ receptors expressed in CHO-K1 cells. *Neuropharmacology*, 77, 387–397. <https://doi.org/10.1016/j.neuropharm.2013.09.011>
- Pearlman, D. A., Case, D. A., Caldwell, J. W., Ross, W. S., Cheatham, T. E., DeBolt, S., ... Kollman, P. (1995). AMBER, a package of computer programs for applying molecular mechanics, normal mode analysis, molecular dynamics and free energy calculations to simulate the structural and energetic properties of molecules. *Computer Physics Communications*, 91, 1–41. [https://doi.org/10.1016/0010-4655\(95\)00041-D](https://doi.org/10.1016/0010-4655(95)00041-D)
- Perry, E. K., Perry, R. H., Blessed, G., & Tomlinson, B. E. (1978). Changes in brain cholinesterases in senile dementia of Alzheimer type. *Neuropathology and Applied Neurobiology*, 4, 273–277. <https://doi.org/10.1111/j.1365-2990.1978.tb00545.x>
- Prati, F., Uliassi, E., & Bolognesi, M. L. (2014). Two diseases, one approach: Multitarget drug discovery in Alzheimer's and neglected tropical diseases. *MedChemComm*, 5, 853–861. <https://doi.org/10.1039/C4MD00069B>
- Raddatz, R., Tao, M., & Hudkins, R. L. (2010). Histamine H₃ antagonists for treatment of cognitive deficits in CNS diseases. *Current Topics in Medicinal Chemistry*, 10, 153–169. <https://doi.org/10.2174/156802610790411027>
- Rampa, A., Belluti, F., Gobbi, S., & Bisi, A. (2011). Hybrid-based multi-target ligands for the treatment of Alzheimer's disease. *Current Topics in Medicinal Chemistry*, 11, 2716–2730. <https://doi.org/10.2174/156802611798184409>
- Sadek, B., Khan, N., Darras, F. H., Pockes, S., & Decker, M. (2016). The dual-acting AChE inhibitor and H₃ receptor antagonist UW-MD-72 reverses amnesia induced by scopolamine or dizocilpine in passive avoidance paradigm in rats. *Physiology & Behavior*, 165, 383–391. <https://doi.org/10.1016/j.physbeh.2016.08.022>
- Sadek, B., Saad, A., Sadeq, A., Jalal, F., & Stark, H. (2016). Histamine H₃ receptor as a potential target for cognitive symptoms in neuropsychiatric diseases. *Behavioural Brain Research*, 312, 415–430. <https://doi.org/10.1016/j.bbr.2016.06.051>
- Shan, L., Bao, A. M., & Swaab, D. F. (2015). The human histaminergic system in neuropsychiatric disorders. *Trends in Neurosciences*, 38, 167–177. <https://doi.org/10.1016/j.tins.2014.12.008>
- Sors, A., Panayi, P., Bert, L., Favale, D., Nosjean, O., Audinot, V., ... Lestage, P. (2017). Mechanistic characterization of S 38093, a novel inverse agonist at histamine H₃ receptors. *European Journal of Pharmacology*, 803, 11–23. <https://doi.org/10.1016/j.ejphar.2017.03.013>
- Tiligada, E., Kyriakidis, K., Chazot, P. L., & Passani, M. B. (2011). Histamine pharmacology and new CNS drug targets. *CNS Neuroscience & Therapeutics*, 17, 620–628. <https://doi.org/10.1111/j.1755-5949.2010.00212.x>
- Vohora, D., & Bhowmik, M. (2012). Histamine H₃ receptor antagonists/inverse agonists on cognitive and motor processes: Relevance to Alzheimer's disease, ADHD, schizophrenia, and drug abuse. *Frontiers in Systems Neuroscience*, 6, 72–72. <https://doi.org/10.3389/fnsys.2012.00072>
- Weiser, J., Shenkin, P. S., & Still, W. C. (1999). Approximate atomic surfaces from linear combinations of pairwise overlaps (LCPO). *Journal of Computational Chemistry*, 20, 217–230. [https://doi.org/10.1002/\(SICI\)1096-987X\(19990130\)20:2<217::AID-JCC4>3.0.CO;2-A](https://doi.org/10.1002/(SICI)1096-987X(19990130)20:2<217::AID-JCC4>3.0.CO;2-A)

SUPPORTING INFORMATION

Additional supporting information may be found online in the Supporting Information section.

How to cite this article: Ghamari N, Dastmalchi S, Zarei O, et al. In silico and in vitro studies of two non-imidazole multiple targeting agents at histamine H₃ receptors and cholinesterase enzymes. *Chem Biol Drug Des*. 2020;95:279–290. <https://doi.org/10.1111/cbdd.13642>

Supplementary Material

In Silico and In Vitro Studies of Two Non-Imidazole Multiple Targeting Agents at Histamine H₃ Receptors and Cholinesterase Enzymes

Nakisa Ghamari^{1,2}, Siavoush Dasamulahi^{1,2}, Omid Zare^{3,4}, José Antonio Arias-Montañón⁵, David Reiner⁶, Fulya Ustaun-Alkan⁷, Holger Stark⁶ and Maryam Hamzeh-Mivehroud^{1,2,*}

¹Biotechnology Research Center, Tabriz University of Medical Sciences, Tabriz, Iran

²School of Pharmacy, Tabriz University of Medical Sciences, Tabriz, Iran

³Cellular and Molecular Research Center, Research Institute for Health Development, Kurdistan University of Medical Sciences, Sanandaj, Iran

⁴Neurosciences Research Center, Kurdistan University of Medical Sciences, Sanandaj, Iran

⁵Departamento de Fisiología, Biofísica y Neurociencias, Centro de Investigación y de Estudios Avanzados del IPN, Av. Instituto Politécnico Nacional 2508, Zacatenco, 07360 Ciudad de México, México

⁶Heinrich Heine University Düsseldorf, Institute of Pharmaceutical and Medicinal Chemistry, Universitätsstr. 1, 40225 Düsseldorf, Germany

⁷Department of Pharmacology and Toxicology, Faculty of Veterinary Medicine, Istanbul University-Cerrahpasa, Istanbul, Turkey.

*Corresponding Author:

Maryam Hamzeh-Mivehroud

Full address: Biotechnology Research Center and School of Pharmacy, Tabriz University of Medical Sciences, Tabriz, Iran. Tel: +98 (41) 3336 4038, Fax: +98 (41) 3337 9420, E-mail: hamzehm@tbzmed.ac.ir, maryam_h.786@yahoo.com

S1. The results of molecular dynamics simulation analyses on ligand-cholinesterase complexes

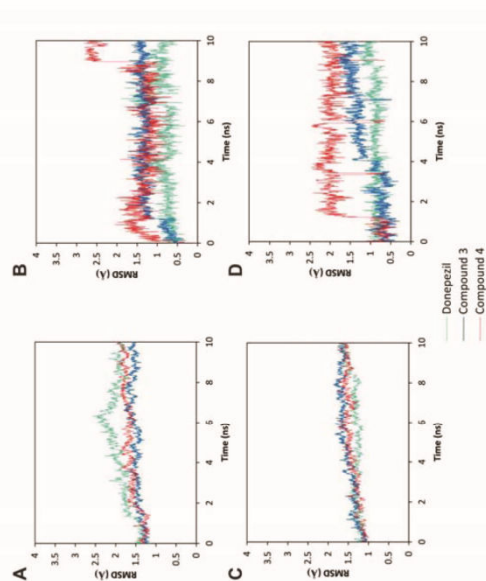


Figure S1.1. The results of molecular dynamics simulation analyses on ligand-cholinesterase complexes. Panels A to D show the plots of root mean square deviation (RMSD) fluctuation in a 1 to 10 ns molecular dynamics simulation for ligand-cholinesterase complexes (panels A and C) and ligands (panels B and D). Panels A and B refer to the RMSD results when AChE used as cholinesterase enzyme while C and D indicate RMSD results where BuChE was used during molecular dynamics simulation.

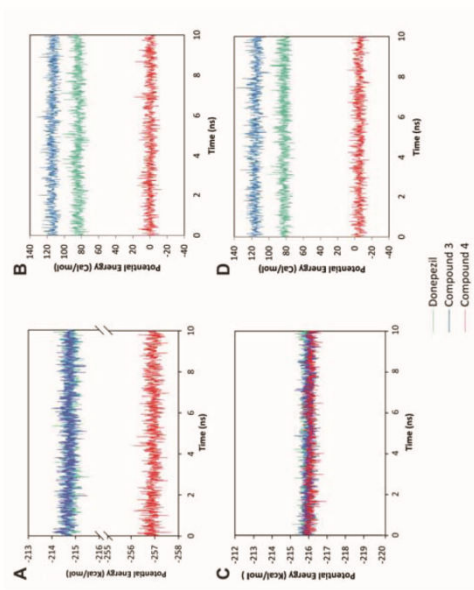


Figure S1.2. The results of molecular dynamics simulation analyses on ligand-cholinesterase complexes. Panels A to D show the plots of potential energies fluctuation in a 1 to 10 ns molecular dynamics simulation for ligand-cholinesterase complexes (panels A and C) and ligands (panels B and D). Panels A and B refer to the potential energy results when AChE used as cholinesterase enzyme while C and D indicate potential energy results where BuChE was used during molecular dynamics simulation.

4.6. The dual-active histamine H3 receptor antagonist and acetylcholine esterase inhibitor E100 ameliorates stereotyped repetitive behavior and neuroinflammation in sodium valproate-induced autism in mice

Nermin Eissa¹⁾, Sheikh Azimullah¹⁾, Petrilla Jayaprakash¹⁾, Richard L. Jayaraj¹⁾, David Reiner²⁾, Shreesh K. Ojha¹⁾, Rami Beiram¹⁾, Holger Stark²⁾, Dorota Łażewska³⁾, Katarzyna Kieć-Kononowicz³⁾, Bassem Sadek¹⁾

1) Department of Pharmacology & Therapeutics, College of Medicine and Health Sciences, United Arab Emirates University, P.O. Box 17666, Al Ain, United Arab Emirates

2) Institute of Pharmaceutical and Medicinal Chemistry, Heinrich Heine University Düsseldorf, Universitätsstr. 1, 40225 Düsseldorf, Germany

3) Jagiellonian University-Medical College, Faculty of Pharmacy, Department of Technology and Biotechnology of Drugs, Medyczna 9 St., 30-688, Kraków, Poland

Published in: *Chemico-Biological Interactions*, 2019, 312:108775.
DOI: 10.1016/j.cbi.2019.108775

Contribution to research: Co-authorship. DR co-organised shipment of test-ligands, prepared, planned and conducted radioligand selectivity screenings at H₁R and H₄R, and evaluated corresponding data. DR proof-edited the manuscript.

Abstract:

Postnatal exposure to valproic acid (VPA) in rodents induces autism-like neurobehavioral defects which are comparable to the motor and cognitive deficits observed in humans with autism-spectrum disorder (ASD). Histamine H3 receptor (H3R) and acetylcholine esterase (AChE) are involved in several cognitive disorders such as Alzheimer's disease, schizophrenia, anxiety, and narcolepsy, all of which are comorbid with ASD. Therefore, the present study aimed at evaluating effect of the novel dual-active ligand E100 with high H3R antagonist affinity and balanced AChE inhibition on autistic-like repetitive behavior, anxiety parameters, locomotor activity, and neuroinflammation in a mouse model of VPA-induced ASD in C57BL/6 mice. E100 (5, 10, and 15 mg/kg) dose-dependently and significantly ameliorated repetitive and compulsive behaviors by reducing the increased percentages of nestlets shredded (all $P < 0.05$). Moreover, pretreatment with E100 (10 and 15 mg/kg) attenuated disturbed anxiety levels ($P < 0.05$) but failed to restore the hyperactivity observed in the open field test. Furthermore, pretreatment with E100 (10 mg/kg) the increased microglial activation, proinflammatory cytokines and expression of NF- κ B, iNOS, and COX-2 in the cerebellum as well as the hippocampus (all $P < 0.05$). These results demonstrate the ameliorative effects of E100 on repetitive compulsive behaviors in a mouse model of ASD. To our knowledge, this is the first in vivo demonstration of the effectiveness of a potent dual-active H3R antagonist and AChE inhibitor against autistic-like repetitive compulsive behaviors and neuroinflammation, and provides evidence for the role of such compounds in treating ASD.

Reprinted from Eissa N, Azimullah S, Jayaprakash P, Jayaraj RL, Reiner D, Ojha SK, Beiram R, Stark H, Łażewska D, Kieć-Kononowicz K, Sadek B, The dual-active histamine H3 receptor antagonist and acetylcholine esterase inhibitor E100 ameliorates stereotyped repetitive behavior and

neuroinflammation in sodium valproate-induced autism in mice, *Chem.-Biol. Interact.*, 2019, 312:108775, with permission for personal use from Elsevier.

Copyright 2018 Elsevier B.V.

4.6 The dual-active histamine H₃ receptor antagonist and acetylcholine esterase inhibitor E100 ameliorates stereotyped repetitive behavior and neuroinflammation in sodium valproate induced autism in mice

Chemico-Biological Interactions 312 (2019) 108775



Contents lists available at ScienceDirect

Chemico-Biological Interactions

journal homepage: www.elsevier.com/locate/chembioint



The dual-active histamine H₃ receptor antagonist and acetylcholine esterase inhibitor E100 ameliorates stereotyped repetitive behavior and neuroinflammation in sodium valproate induced autism in mice

Nermin Eissa^a, Sheikh Azimullah^a, Petrilla Jayaprakash^a, Richard L. Jayaraj^a, David Reiner^b, Shreesh K. Ojha^a, Rami Beiram^a, Holger Stark^b, Dorota Łażewska^c, Katarzyna Kieć-Kononowicz^c, Bassem Sadek^{a,*}

^a Department of Pharmacology & Therapeutics, College of Medicine and Health Sciences, United Arab Emirates University, P.O. Box 17666, Al Ain, United Arab Emirates

^b Institute of Pharmaceutical and Medicinal Chemistry, Heinrich Heine University Düsseldorf, Universitätsstr. 1, 40225, Düsseldorf, Germany

^c Jagiellonian University Medical College, Faculty of Pharmacy, Department of Technology and Biotechnology of Drugs, Medyczna 9 St., 30 688, Kraków, Poland

ARTICLE INFO

Keywords:

VPA-Induced repetitive compulsive behaviors
Mice
Histamine
Acetylcholine
E100
Neuroinflammation
Protein expression

ABSTRACT

Postnatal exposure to valproic acid (VPA) in rodents induces autism-like neurobehavioral defects which are comparable to the motor and cognitive deficits observed in humans with autism spectrum disorder (ASD). Histamine H₃ receptor (H₃R) and acetylcholine esterase (AChE) are involved in several cognitive disorders such as Alzheimer's disease, schizophrenia, anxiety, and narcolepsy, all of which are comorbid with ASD. Therefore, the present study aimed at evaluating effect of the novel dual-active ligand E100 with high H₃R antagonist affinity and balanced AChE inhibition on autistic-like repetitive behavior, anxiety parameters, locomotor activity, and neuroinflammation in a mouse model of VPA-induced ASD in C57BL/6 mice. E100 (5, 10, and 15 mg/kg) dose-dependently and significantly ameliorated repetitive and compulsive behaviors by reducing the increased percentages of nestlets shredded (all $P < 0.05$). Moreover, pretreatment with E100 (10 and 15 mg/kg) attenuated disturbed anxiety levels ($P < 0.05$) but failed to restore the hyperactivity observed in the open field test. Furthermore, pretreatment with E100 (10 mg/kg) the increased microglial activation, proinflammatory cytokines and expression of NF- κ B, iNOS, and COX-2 in the cerebellum as well as the hippocampus (all $P < 0.05$). These results demonstrate the ameliorative effects of E100 on repetitive compulsive behaviors in a mouse model of ASD. To our knowledge, this is the first *in vivo* demonstration of the effectiveness of a potent dual-active H₃R antagonist and AChE inhibitor against autistic-like repetitive compulsive behaviors and neuroinflammation, and provides evidence for the role of such compounds in treating ASD.

1. Introduction

Autism spectrum disorder (ASD) is a common neurobehavioral disorder with limited treatment options [1,2]. Despite its increasing prevalence, the pathophysiological background of ASD is not fully understood [3]. Accordingly, no specific treatment can have potential effect for all autistic children [4,5]. Consequently, recent developments of new agents with multiple pharmacological effects have become promising strategy for novel treatment options of multifactorial disorders such as ASD [6–8]. In search of studying the etiology of ASD, the role of several central neurotransmitters, e.g., serotonin (5-HT), acetylcholine (ACh), dopamine (DA), γ -aminobutyric acid (GABA),

glutamate (Glu), and histamine (HA), in early brain development encourage to be a significant area of research, and accumulation of evidences suggest that several numerous neurotransmitters such as ACh, 5-HT, DA, GABA, Glu, and HA are involved in the onset and progression of ASD [9–19]. The involvement of histamine receptors (HRs) in the cognitive functions has long been confirmed, notably of H₃Rs which are mainly expressed in the CNS [20–23]. While activation of H₁R and H₂R facilitates slow excitatory postsynaptic potentials, H₃Rs are coupled to Gi/Go-proteins that control the biosynthesis and release of histamine with high constitutive activity, as an auto-receptors. Moreover, H₃Rs functioning as hetero-receptors can also regulate the release of other numerous brain neurotransmitters like ACh, Glu, GABA, 5-HT, DA in

* Corresponding author. United Arab Emirates University, College of Medicine & Health Sciences, Department of Pharmacology and Therapeutics, PO Box 17666, Al Ain, United Arab Emirates.

E-mail address: bassem.sadek@uaeu.ac.ae (B. Sadek).

<https://doi.org/10.1016/j.cbi.2019.108775>

Received 23 April 2019; Received in revised form 17 July 2019; Accepted 29 July 2019

Available online 30 July 2019

0009-2797/ © 2019 Elsevier B.V. All rights reserved.

various brain regions [24,25]. Accordingly, blocking central H₃Rs has been projected to improve the cortical fast rhythms closely associated with cognitive behaviors [25], and numerous preclinical studies indicated particularly that H₃R antagonists/inverse agonists have been found to exhibit a unique feature by their potential cognition-enhancing property [22,23,26,27]. Furthermore, several drug candidates with H₃R antagonist properties have shown to increase the release of brain ACh, therefore alleviating symptomatic features and progression of Alzheimer's disease (AD) in clinical trials [28,29]. In addition, a previous report demonstrated lower ACh level in the prefrontal cortex region of mice which showed attention deficit and impulsive behavior [30]. Interestingly, cholinergic deficit was, also, found in BTBR T + tf/J mice, an animal model that displays behaviors consistent with the three diagnostic categories for ASD, namely impaired social interaction and communication as well as increased repetitive behaviors [31–35]. Based on the high level of attention generated by these preclinical experimental outcomes, the central H₃Rs are an attractive target for developing novel H₃R antagonists/inverse agonists with the potential role in neuropsychiatric multi-neurotransmitter disorders, e.g., Alzheimer's disease, cognitive deficit associated with schizophrenia and recently on ASD [1,22,27,36–39]. In view of that both acetylcholine esterase (AChE) and H₃Rs (auto- and heteroreceptors) are involved in the regulation of numerous brain neurotransmitters including ACh and HA, dual-active AChEs and H₃R antagonists have been developed by several groups [40–43]. Therefore, in present study we describe the effects of a recently developed dual-active AChEI and H₃R antagonist, namely E100 [1-(7-(4-chlorophenoxy) heptyl) homo-piperidine] with histamine H₃ receptor (H₃R) antagonist affinity ($hH_3R K_i = 203$ nM) and acetylcholine esterase inhibitory effect ($EeAChE IC_{50} = 2$ μ M and $Eg-BuChE IC_{50} = 2$ μ M) in male C57BL/6 mice model of ASD-like repetitive compulsive behaviors induced by prenatal exposure to valproic acid (VPA, 500 mg/kg, i.p.). The effects of E100 on locomotor activity and anxiety-like behaviors of the same animals were evaluated in open field test, since anxiety and motor activity could misperceive performance of animals in behavioral tests [44]. Moreover, neuroinflammation was assessed in cerebellum and hippocampus, as several studies showed that cerebellar inflammation may alter social behavior in adult mice, as cerebellum is involved in executive and cognitive functions [45–48], whereas hippocampus is involved in memory, learning and recently in cognition including social cognition [49]. In addition, abrogative studies were carried out co-administering CNS penetrant H₁R antagonist mepyramine (MPA), H₂R antagonist zolantidine (ZLT), H₃R agonist (R)- α -methyl histamine (RAM), and cholinergic muscarinic antagonist scopolamine (SCO) to test whether brain histaminergic as well as cholinergic neurotransmission are involved in the effects provided by E100.

2. Materials and methods

2.1. Animals

C57BL/6 mice (aged 8–12 weeks, weighing 20–25 g) (Jackson Laboratory, Bar Harbor, USA) bred in the local central animal facility of the College of Medicine and Health Sciences, United Arab Emirates University [50] were used in this study. All mice were housed in plastic cages under a standard light/dark cycle (12-h light/dark cycle, lights on at 6 a.m.) at a constant temperature of 22–25 °C, with free access to tap water and a standard rodent chow diet. Mice were kept in separate cages for mating. Female mice were observed daily and placed in a separate cage when pregnancy was confirmed by the presence of a vaginal plug. This day was considered embryonic day 0 (E0). On E12.5, pregnant females were i.p. injected with 500 mg/kg VPA dissolved in isotonic 0.9% sodium chloride solution, and control mice were injected with saline, as described previously [51,52]. The day of delivery was defined as postnatal day 0 (P0). All offspring were weaned and sex-grouped (5–6 mice/cage) at P21. Pups from VPA-exposed mothers were

considered the VPA-exposed model mice for ASD, and were used for the experiments at the age of 8 weeks. On the other hand, the pups of mothers treated with saline were used as control mice. All procedures were carried out in accordance with the recommendations of the European Communities Council Directive of 24 November 1986 (86/609/EEC), and were approved by the Institutional Animal Ethics Committee in the College of Medicine and Health Sciences/United Arab Emirates (Approval No. ERA-2017-5603). All authors confirm that all methods were carried out in accordance with relevant guidelines and regulations.

2.2. Drugs and biochemical reagents

The H₃R antagonist E100 was designed and synthesized in the Department of Technology and Biotechnology of Drugs, Krakow, Poland, according to a previously described procedure [53,54].

The H₃R antagonist E100 belongs to the chlorophenoxyalkylamine derivatives which were synthetically achievable through two-step synthetic pathway. In the first step, the precursor 1-(7-bromoheptyl)-4-chlorobenzene was obtained in simple one-step alkylation of 4-chlorophenol with 1,7-dibromoheptane refluxed in sodium propanolate. Obtained 1-(7-bromoheptyl)-4-chlorobenzene was then reacted with homopiperidine in the mixture of ethanol/water with powdered potassium carbonate and a catalytic amount of potassium iodide. The desired product E100 was obtained as a free base and crystallized as salt of oxalic acid. The structure of E100 was confirmed by several elemental and spectral analyses. For estimation of the levels of proinflammatory cytokines (IL-1 β , IL-6, TNF- α , and TGF- β), commercially available enzyme-linked immunosorbent assay (ELISA) kits were purchased from R&D Systems (Minneapolis, MN, USA). Rabbit anti-NF- κ B p65 antibody was purchased from Abcam (Cambridge, MA, USA) and Rabbit anti-COX2 and rabbit anti-iNOS antibodies were purchased from Sigma-Aldrich (St. Louis, MO, USA). Anti-actin antibody was obtained from MERCK (Millipore, USA), while the goat anti-mouse and goat anti rabbit secondary immunoglobulin G antibodies conjugated to horseradish peroxidase were purchased from Santa Cruz Biotechnology (Dallas, TX, USA). Anti-Iba-1 polyclonal rabbit was purchased from Wako Chemicals (Richmond, VA, USA). Alexa Fluor 488-conjugated secondary goat anti-rabbit antibodies were purchased from Life Technologies (Grand Island, NY, USA). Protease and phosphatase inhibitors were obtained from Thermo Scientific (Waltham, MA, USA). The Pierce® BCA Protein Assay Reagent Kit and the SuperSignal® West Pico PLUS chemiluminescence substrate kit were purchased from Thermo Fisher Scientific, Inc. (Rockford, IL, USA). Mini-Protein TGX® precast electrophoresis gels were obtained from Bio-Rad Laboratories, Inc. (USA). Vectashield® fluorescent mounting media was procured from Vector Laboratories (Burlingame, CA, USA). All the reagents used in the study were of analytical grade and were purchased from Sigma-Aldrich. All test compounds were suspended in 1% aqueous solution of Tween 80. All mice were i.p. injected at a volume of 10 mL/kg, and all doses are expressed in terms of the free base.

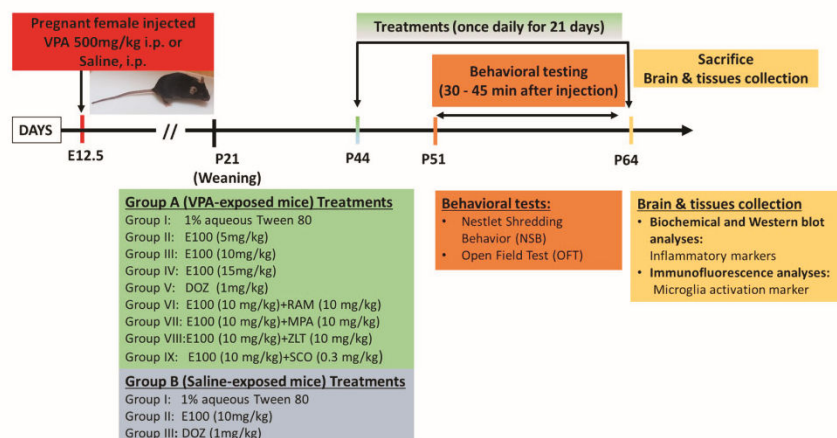
2.3. Study design and drug treatment

Pregnant C57 mice were monitored and day of birth was recorded as postnatal day 0 (P0). All offspring were weaned, sex-grouped at P 21 (Scheme 1). Then only male offspring were divided into 2 groups where Group A served as prenatally VPA-exposed mice and Group B served as prenatally saline-exposed mice. All mice started receiving treatments daily from P44 for 21 days. Group A were further subdivided where Group I received only 1% aqueous solution of Tween 80, i.p., Group II received E100 5 mg/kg, i.p, Group III received E100 10 mg/kg, i.p, Group IV received E100 15 mg/kg, i.p, Group V received donepezil (DOZ, 1 mg/kg, i.p.), the acetylcholine esterase inhibitor as a reference drug, Group VI were VPA-exposed mice co-administered with E100 10 mg/kg, i.p and RAM 10 mg/kg, i.p, Group VII were VPA-exposed

4.6 The dual-active histamine H₃ receptor antagonist and acetylcholine esterase inhibitor E100 ameliorates stereotyped repetitive behavior and neuroinflammation in sodium valproate induced autism in mice

N. Eissa, et al.

Chemico Biological Interactions 312 (2019) 108775



Scheme 1. Schematic illustration of prenatally VPA-induced ASD, drug treatments, behavioral studies, and biochemical assessments with VPA mice. Pregnant mice were administered with VPA (500 mg/kg, i.p.) at embryonic day 12.5 (E12.5). Systemic treatments started from postnatal day (P44). Daily injections continued for a duration of 21 days until P64. Behavioral studies were conducted starting from P51. All mice were then sacrificed at P64 for biochemical, western blot and immunofluorescence analyses. Modified after Eissa et al., 2018 [58].

mice co-administered with E100 10 mg/kg, i.p and MPA 10 mg/kg, i.p., Group VIII were VPA-exposed mice co-administered with E100 10 mg/kg, i.p and ZLT 10 mg/kg, i.p and Group IX were VPA-exposed mice co-administered with E100 10 mg/kg, i.p and SCO 0.3 mg/kg, i.p. Group B were subdivided where Group I received only 1% aqueous solution of Tween 80, i.p., Group II received E100 10 mg/kg, i.p and Group III received DOZ 1 mg/kg, i.p. One week after starting the treatments, that is from P51, mice were subjected to behavioral testing in a sequence to assess stereotyped repetitive and compulsive like-behaviours, locomotion, and anxiety, by conducting nestlet shredding behavioral test (NSB) and open field test (OFT) (Scheme 1). On P64 all the animals were sacrificed; brains were isolated for biochemical estimations (IL-1 β , IL-6, TNF- α , TGF- β), Western blot analyses (NF- κ B, iNOS and COX-2) and Immunofluorescence analyses for microglial activation. All doses were selected based on the results of our previous studies on strongly related dual-active compounds, and are expressed in terms of the free bases [39,55] (Scheme 1). E100 and DOZ or 1% aqueous of Tween 80 were administered 30–45 min before each behavioral test. All the behavioral studies were performed in the light phase between 09:00 and 15:00. To reduce the number of animals used, the biochemical analysis, western blotting, and immunofluorescence staining were performed in the same group of animals that were subjected to behavioral tests (Scheme 1). The doses of MPA, ZLT, and SCO were injected 30–45 min before behavioral assessments, while the CNS penetrant H3R agonist RAM was administered 15–20 min before the start of behavioral tests to ensure its presence in the CNS, as RAM was described to show fast metabolism [56]), and were selected according to previous studies [55,57–60].

2.4. Brain collection and tissue preparation for biochemical studies

For further biochemical assessments, brain collection and tissue preparation experiments were carried out following 21 days of drug treatment (Scheme 1). The animals were deeply anesthetized with pentobarbital (40 mg/kg, i.p.), and cardiac perfusion was performed using 1 \times PBS (0.01 M phosphate buffer, 0.0027 M potassium chloride and 0.137 M sodium chloride) at pH 7.4 to wash out the blood. The animals were injected with the inflammatory stimulus lipopolysaccharide (LPS, 25 μ g/kg, i.p., from *E. coli* serotype 0111:B4) 2 h before the sacrifice. Accordingly, the inflammatory stimulus LPS demonstrate a significant LPS-induced exacerbated rise in the expression of

proinflammatory cytokines (IL-1 β , IL-6, TNF- α , and TGF- β) in cerebellum of VPA-exposed mice [47,58]. The brains were then quickly removed and placed on an ice plate, where the two hemispheres were separated. The cerebellum and hippocampus were excised from the brain and snap-frozen in liquid nitrogen for biochemical tests [61]. On the day of assay, the tissues were homogenized on ice in the extraction buffer recommended by the manufacturer, radioimmunoprecipitation assay buffer (50 mM Tris HCl, pH 7.4, 140 mM NaCl, 1 mM EDTA, 0.5% Triton X-100, and 0.5% sodium deoxycholate) with protease and phosphatase inhibitors. The homogenates were sonicated and centrifuged for 30 min at 14000 rpm at 4 $^{\circ}$ C to remove tissue debris, and the resulting supernatant was used for the pro-inflammatory cytokine assessment and Western blot analysis. After being transcardially perfused with PBS, four animals from each group were further perfused with 4% paraformaldehyde (cold) in 0.1 M phosphate buffer (pH 7.2). After removing the brains from the skulls, they were post-fixed in the same fixative (4% paraformaldehyde) for 48 h at 4 $^{\circ}$ C. The brains were then immersed in 10% sucrose solution for three consecutive days at 4 $^{\circ}$ C. Finally, the brains were stored at -80° C for cryostat sectioning [61,62]. All experimenters who performed the behavioral, biochemical tests, and immunofluorescence analysis were blinded to the experimental groups.

2.5. Behavioral tests

2.5.1. Nestlet shredding behavior (NSB)

The test to evaluate NSB was performed by placing commercially available cotton fiber (nestlets) (5 cm \times 5 cm, 5-mm thick, \sim 2.5 g each), after weighing it on an analytical balance, into a cage (19 cm \times 29 cm \times 13 cm) filled with fresh, unscented mouse bedding material to a depth of 0.5 cm. One nestlet was placed on top of the bedding in each test cage, and the filter-top cover was placed on the cage. No food and water were provided during the test. One mouse was added to each cage and left undisturbed with the nestlet for 30 min. After test completion, the remaining intact nestlet was removed from the cage using forceps and allowed to dry overnight. The remaining unshredded nestlet was weighed, and then the percentage of nestlet shredded was calculated. The remaining shredded nestlet material and bedding were discarded [58,63].

2.5.2. Open field test (OFT)

Open field test (OFT) is an exploratory activity performed in a novel environment, assessed in an open field box (45 × 45 × 30 cm) [47]. This test systematically assesses novel environment exploration, general locomotor activity, and anxiety-related behavior in rodents. The centre region was defined as the central 23 × 23 cm area. Mice were introduced into the centre area of the arena and given 5 min habituation before actual behaviors recording. The total distance moved in the whole arena, time spent in the centre and periphery were recorded for 10 min using CCD camera-assisted motion tracking apparatus and software (EthoVision 3.1, Noldus Information Technology, the Netherlands). After each trial, apparatus was cleaned using 70% ethanol and allowed to dry [64,65]. When evaluating the results, longer time spent in the centre indicated lower levels of anxiety-like behaviors and total distance travelled reflected locomotor activity.

2.6. Biochemical assessments

2.6.1. Pro-inflammatory cytokine estimations using ELISA

We performed ELISA to quantify the levels of pro-inflammatory cytokines (IL-1 β , IL-6, TNF- α , and TGF- β) in the cerebellum. Commercially available ELISA kits for IL-1 β , IL-6, TNF- α , and TGF- β were purchased from R&D Systems. The levels of IL-1 β , IL-6, TNF- α , and TGF- β were estimated following the manufacturer's instructions and as described earlier [58,61,62,66]. The optical density was determined at 450 nm using a microplate absorbance reader (Sunrise, TECAN). The results were expressed as pg/mg protein.

2.7. Western blot analysis

Western blot analysis was conducted to measure the levels of expression of COX-2, iNOS, and NF- κ B p65 in the cerebellum and hippocampus of different animal groups, as described previously [61,62]. As mentioned earlier, the prepared cell lysates containing the extracted protein from the mouse brain tissues were used. The protein content in the sample was estimated using the Pierce® BCA Protein Assay Reagent Kit. The protein samples containing equal amounts of protein (30 μ g), adjusted using radioimmunoprecipitation assay buffer and 4 × Laemmli sample buffer, were loaded and separated in Mini-Protean TGX® precast electrophoresis gels. The proteins were then transferred onto polyvinylidene difluoride membranes that were first activated by soaking in 100% methanol. Subsequently, the membranes were incubated for 1 h with the blocking buffer (non-fat dry milk) and then washed to avoid non-specific binding. The membranes were then incubated overnight at 4 °C with the specific primary rabbit polyclonal antibodies against COX-2 (1:1000), iNOS (1:5000), and NF- κ B p65 (1:50000), followed by the horseradish peroxidase-conjugated secondary anti-rabbit antibody (1:20000) on the second day. The bands of proteins detected by the antibodies were visualized using an enhanced chemiluminescence Pico kit as substrate. Subsequently, the blots were stripped and re-probed for actin (1:7000) (used as a loading control) using horseradish peroxidase-conjugated anti-mouse secondary antibody (1:20000). The intensity of the band was measured using densitometry and quantified using the ImageJ software (National Institutes of Health, Bethesda, MD, USA).

2.8. Immunofluorescence labelling of Iba-1

Brains were collected, post-fixed, and stored at −80 °C, as mentioned earlier. On the day of sectioning, the brains were sliced using a cryostat into 20- μ m sections. Immunofluorescence staining was performed with the coronal sections of the cerebellum to examine the Iba-1-positive microglia (activated) and according to previously described methods [67]. Brain sections were washed twice with PBS (500 μ l/well) and incubated with a blocking reagent (10% normal goat serum in PBS 0.3% Triton-X 100) for 1 h at room temperature. The sections were then

washed and incubated with the primary polyclonal rabbit antibody against Iba-1 (1:700) overnight at 4 °C. On the second day, the sections were washed twice with PBS and incubated with fluorescent anti-rabbit secondary antibody (Alexa Fluor 488) (1:1000) for 1 h at room temperature. Subsequently, the sections were washed again and mounted using Vectashield® mounting media. The images were then captured using the fluorescent microscope EVOS FL (Thermo Fisher Scientific). A minimum of three sections per brain from four animals were used (three sections per brain) to analyze microglial activation. From each section, the activated microglia were evaluated by measuring the integrated density of the Iba-1 marker signal from three different randomly selected fields of equal areas using the Image J software. The expression levels of Iba-1 were detected by the green fluorescence emitted by Alexa Fluor 488. The total corrected cellular fluorescence (TCCF) was then calculated using the following equation: TCCF = integrated density-(area of selected cell × mean fluorescence of the background) [67]. This TCCF was calculated and normalized against the mean of the control, with results presented as percentage fold increase from the control level.

2.9. Inhibition of radioligand-binding by E100 at H1R and H4R

Inhibition of [³H]-pyrilamine and [³H]-histamine binding to human isoforms of H1R and H4R was determined for E100, as previously described [68,69]. Briefly, binding assays conducted on CHO-K1 cells stably expressing the hH1R were used to determine the antagonist affinity of the respective test compound for hH1Rs. The experimental assays were carried out in triplicates with at least four appropriate concentrations in the range of 100 nM–100 μ M of the test compound E100. The resulting nonspecific binding was evaluated in the presence of the standard H1R antagonist chlorpheniramine hydrogenmaleate at a concentration of 10 mM. In addition, the unbound radioligand was removed with four washes of 5 mL of ice-cold HEPES buffer. Liquid scintillation counting using a PerkinElmer MicroBeta Trilux scintillation counter was used to determine the amount of radioactivity collected on the filter used in the current experiment. Accordingly, competition binding data were analyzed using the software GraphPad Prism 5.01 (GraphPad Software, Inc.) using nonlinear least squares fit, and K_i values were calculated from the IC₅₀ values according to the Cheng–Prusoff equation [68–70]. For the measurement of antagonist affinity of the test compound E100 to hH4Rs and as described previously, binding assay experiments were carried out [68,69]. Briefly, the competition binding experiments were run on incubating membranes, 35 μ g/well (prepared from Sf9 cells expressing hH4R, coexpressed with G protein G γ i2 and G β 1 γ 2 subunits) in a final volume of 0.2 mL containing binding buffer and [³H]histamine (10 nM, 15.3 Ci/mmol) in a 96-well microtiterplate. Assays were conducted in triplicates with seven appropriate concentrations in the range of 0.1 nM–100 μ M of E100. Nonspecific binding, bound radioligand, and free radioligand were determined as described previously [68,69], and competition binding data were analyzed using the software GraphPad Prism 5.01 (GraphPad Software, Inc.) using nonlinear least squares fit. K_i values were calculated from the IC₅₀ values according to the Cheng–Prusoff equation [68–70].

2.10. Statistical analysis

For the NSB and OFT tests, statistical significance was assessed with a group (Control, VPA) × drug (SAL, E100) analysis of variance. The data were analyzed for normality by assessing the sample distribution or skewness (−1.5 to +1.5 considered normally distributed). The source of the detected significances was determined by Bonferroni's multiple comparison post hoc test. *P* values less than 0.05 were considered statistically significant. The number of mice per group is indicated in the figures. Statistical significance for Western blot and immunofluorescence analyses was calculated using one-way analysis of

4.6 The dual-active histamine H₃ receptor antagonist and acetylcholine esterase inhibitor E100 ameliorates stereotyped repetitive behavior and neuroinflammation in sodium valproate induced autism in mice

N. Eissa, et al.

Chemico Biological Interactions 312 (2019) 108775

variance followed by post hoc Tukey's multiple comparison test. For statistical comparisons, the software package SPSS 25.0 (IBM Middle East, Dubai, UAE) was used. The results are expressed as the means and standard errors of the means (SEM).

3. Results

3.1. In Vitro affinities at hH1Rs, hH3Rs, and hH4Rs

The novel dual-active ligand E100 was tested for its H₃R affinity by [³H]N^α-methylhistamine displacement assays on membrane preparations of HEK-293 cells, stably expressing the hH₃R. The results showed that E100 displayed histamine H₃ receptor (H₃R) antagonist affinity with a K_i value of 203 ± 48 at hH₃Rs. E100 was further evaluated for its affinity at human histamine H₁ (hH₁R) and H₄ (hH₄R) receptors. The results showed that test compound E100 exhibited (> 10,000 nM for H₁R, 203 nM for H₃R, > 10,000 nM for H₄R) a selectivity profile toward H₃Rs with at least 10-fold lower affinity at hH₁- and H₄Rs.

3.2. In Vivo behavioral models

3.2.1. Effects of E100 on stereotyped repetitive behavior of VPA-exposed mice in nestlet-shredding behavior test

The effect of subchronic systemic administration of E100 (5, 10, or 15 mg/kg, i.p.) or DOZ (1 mg/kg, i.p.) on the percentage increase of shredded nestlet was evaluated in the nestlet-shredding behavior (NSB) test (Fig. 1). Post hoc analyses showed that VPA-exposed mice shredded significantly more nestlets than the saline-exposed mice ($F_{(1,8)} = 44.09$, $P < 0.01$). However, VPA-exposed mice pre-treated with test compound E100 (5, 10, or 15 mg/kg, i.p.) or the reference drug DOZ (1 mg/kg, i.p.) exhibited a significantly lower percentage of shredded nestlets than VPA-exposed mice pre-treated with saline ($F_{(1,8)} = 20.92$, $P < 0.05$; $F_{(1,8)} = 33.26$, $P < 0.01$; $F_{(1,8)} = 38.78$, $P < 0.01$, and $F_{(1,8)} = 42.56$, $P < 0.01$, respectively) (Fig. 1). Moreover, the effects observed with 10 or 15 mg/kg E100 were significantly higher than that observed with 5 mg/kg E100 ($F_{(1,8)} = 6.62$, $P < 0.05$ and $F_{(1,8)} = 9.60$, $P < 0.05$, respectively). Notably, no significant difference in the E100-induced effect on the percentage of shredded nestlets was detected

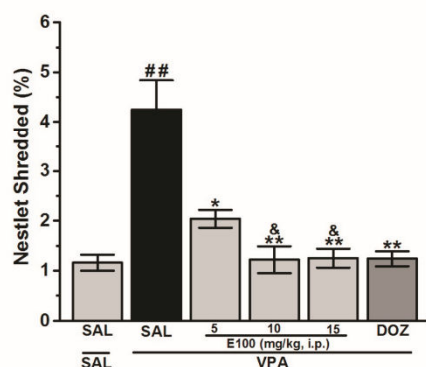


Fig. 1. E100 attenuated increased obsessive compulsive features in nestlet shredding test. Obsessive compulsive nestlet shredding behavior was measured after a 30-min testing session. VPA-exposed mice treated with saline (VPA group) demonstrated elevated stereotyped, repetitive behaviors that were significantly increased compared to Saline-exposed mice (SAL group). E100 (at a dose of 5, 10, or 15 mg/kg, i.p.) or DOZ (1 mg/kg, i.p.) were administered subchronically for 21 days in VPA-exposed mice. Data are expressed as the mean ± SEM (n = 5). ** $P < 0.01$ vs. Saline-treated Saline-exposed mice. * $P < 0.05$ vs. Saline-treated VPA-exposed mice. ** $P < 0.01$ vs. Saline-treated VPA-exposed mice. * $P < 0.05$ vs. E100(5 mg)-treated VPA-exposed mice.

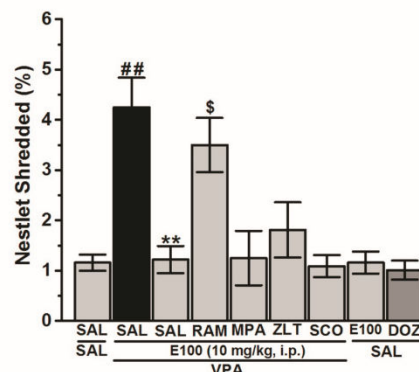


Fig. 2. Effects of RAM, MPA, ZLT, and SCO on E100-provided attenuation of obsessive compulsive behavior of VPA-exposed mice. Obsessive compulsive nestlet shredding behavior was measured after a 30-min testing session. VPA-exposed mice treated with saline (VPA group) demonstrated elevated stereotyped, repetitive behaviours that were significantly increased compared to Saline-exposed mice (SAL group). E100 (10 mg/kg, i.p.) was administered subchronically for 21 days in VPA-exposed mice. Effects of subchronic (21 days) systemic co-injection of RAM (10 mg/kg, i.p. for RAM group), MPA (10 mg/kg, i.p. for MPA group), ZLT (10 mg/kg, i.p. for ZLT group), or SCO (0.3 mg/kg, i.p. for SCO group) on the E100(10 mg)-provided attenuation of stereotyped repetitive and compulsive behavior of VPA-exposed mice were assessed in NSB. Effects of subchronic (21 days) systemic injection of E100 (10 mg/kg) and DOZ (1 mg/kg) on the Saline-exposed mice (SAL group) were assessed in NSB. Data are expressed as the mean ± SEM (n = 5). ** $P < 0.01$ vs. Saline-treated Saline-exposed mice. * $P < 0.05$ vs. E100(10 mg)-treated VPA-exposed mice.

between the 10 mg/kg and 15 mg/kg doses ($F_{(1,8)} = 0.01$, $P = 0.93$) (Fig. 1). Also, no significant difference in the E100-induced effect on the percentage of shredded nestlets was detected between the 10 mg/kg and 15 mg/kg doses and DOZ (1 mg/kg), with ($F_{(1,8)} = 0.003$, $p = 0.96$) and ($F_{(1,8)} = 0.002$, $p = 0.95$), respectively (Fig. 1).

3.2.2. Effects of RAM, MPA, ZLT, and SCO on E100-provided attenuation of stereotyped repetitive behavior in VPA-exposed mice in nestlet-shredding behavior test

Subchronic systemic administration of E100 (10 mg/kg, i.p.) significantly lowered the percentage of shredded nestlets in VPA-exposed mice ($F_{(1,8)} = 33.26$, $P < 0.01$). As shown in Fig. 2 and observed in the post hoc analyses, the E100 (10 mg/kg)-induced decrease in the percentage of shredded nestlets was countered following subchronic systemic co-administration of RAM (10 mg/kg, i.p.) ($F_{(1,8)} = 11.45$, $P < 0.05$) compared with E100 (10 mg)-treated VPA-exposed mice (Fig. 2). However, MPA, ZLT, and SCO failed to reverse this E100-induced decrease in the percentage of shredded nestlets, as they showed no significant effect compared with VPA-exposed mice treated with E100 (10 mg/kg, i.p.) ($F_{(1,8)} = 0.003$, $P = 0.96$; $F_{(1,8)} = 0.74$, $P = 0.41$, and $F_{(1,8)} = 0.11$, $P = 0.75$, respectively) (Fig. 2).

3.2.3. Effects of E100 on anxiety levels and locomotor activity of VPA-exposed mice in open field test

The observed effects of subchronic systemic injection of saline or E100 (5, 10, or 15 mg/kg, i.p.) on the time spent in the centre (Fig. 3A), time spent in the periphery (Fig. 3B) and total distance travelled (Fig. 3C) of VPA-exposed mice tested in the OFT are shown in Fig. 3A–C. As shown in Fig. 3B&C, there were no significant effects of subchronic systemic exposure of VPA-exposed mice to E100 (5, 10, and 15 mg/kg, i.p.) and DOZ (1 mg/kg, i.p.) on time spent in the periphery and total distance travelled vs. saline-treated VPA-exposed mice (all

N. Eissa, et al.

Chemico Biological Interactions 312 (2019) 108775

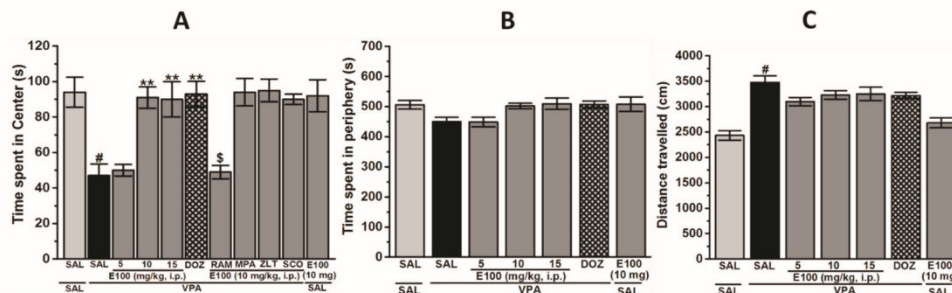


Fig. 3. E100 ameliorated fear-related behavior without affecting locomotor activity in open field test. VPA-exposed mice demonstrated elevated anxiety and deficits in cognition behaviours that were significantly increased compared to Saline-exposed mice. E100 (5, 10 or 15 mg/kg, i.p.) or DOZ (1 mg/kg, i.p.) was administered subchronically for 21 days in VPA-exposed mice. E100 (10 and 15 mg/kg, i.p.) and DOZ (1 mg/kg, i.p.) attenuated the decreased time spent in the central arena (Fig. 3A), however, failed to modify the decreased time spent in the periphery (Fig. 3B) as well as the increased total distance travelled (Fig. 3C) in the OFT in VPA-exposed mice. Effects of subchronic (21 days) systemic co-injection of RAM (10 mg/kg, i.p. for RAM group), MPA (10 mg/kg, i.p. for MPA group), ZLT (10 mg/kg, i.p. for ZLT group), or SCO (0.3 mg/kg, i.p. for SCO group) on the E100(10 mg)-provided amelioration of time spent in the centre as well as time spent of VPA-exposed mice were assessed in OFT (Fig. 3A). Data are expressed as the mean \pm SEM (n = 5). #*P* < 0.05 vs. Saline-treated VPA-exposed mice. **P* < 0.05 vs. Saline-treated saline exposed mice. ***P* < 0.01 vs. Saline-treated VPA-exposed mice. ⁵*P* < 0.05 vs. E100(10 mg)-treated VPA-exposed mice.

P > 0.01) (Fig. 3B&C). In contrast, analysis of variance demonstrated that VPA-exposed mice pretreated with E100 (10 and 15 mg/kg, i.p.) and DOZ (1 mg/kg, i.p.) spent a significantly higher percentage of time in the centre of the arena, with [$F_{(1,8)} = 19.95$; *P* < 0.01], [$F_{(1,8)} = 10.31$; *P* < 0.05], and [$F_{(1,8)} = 18.24$; *P* < 0.01], respectively (Fig. 3A). As shown in Fig. 3A and observed in the post hoc analyses, the E100 (10 mg)-provided increase in the time spent in the centre of arena was abrogated following subchronic systemic co-administration of RAM (10 mg/kg, i.p.), with [$F_{(1,8)} = 28.93$; *P* < 0.05] compared with E100 (10 mg)-treated VPA-exposed mice. However, MPA, ZLT, and SCO failed to counteract this E100-provided increase in time spent in central arena, as they had no significant effect compared to VPA-exposed mice treated with E100 (10 mg/kg, i.p.), with [$F_{(1,8)} = 0.05$; *p* = 0.82], [$F_{(1,8)} = 0.18$; *p* = 0.69], and [$F_{(1,8)} = 0.03$; *p* = 0.86], respectively (Fig. 3A). Notably, subchronic treatment of Saline-exposed mice with E100 (10 mg/kg, i.p.) had no significant influence on time spent in the central arena, time spent in the periphery, and total distance travelled when compared to saline-pretreated Saline-exposed mice, with [$F_{(1,8)} = 0.01$; *p* = 0.92], [$F_{(1,8)} = 0$; *p* = 0.95], and [$F_{(1,8)} = 2.65$; *p* = 0.14], respectively (Fig. 3A–C).

3.3. Biochemical assessments

3.3.1. Effects of E100 pre-treatment on the levels of proinflammatory cytokines in the brain tissue of VPA-exposed mice

The effects of E100 on the exacerbated levels of proinflammatory cytokines (interleukin [IL]-1 β , IL-6, tumor necrosis factor [TNF]- α , and tumor growth factor [TGF]- β) following lipopolysaccharide (LPS) challenge in the brain tissue of VPA-exposed mice were evaluated (Fig. 4A–D). The results revealed that a systemic prenatal injection of VPA (500 mg/kg, i.p.) induced ASD-like behaviors in VPA-exposed mice and significantly increased the levels of IL-1 β (Fig. 4A), IL-6 (Fig. 4B), TNF- α (Fig. 4C), and TGF- β (Fig. 4D) compared with the saline-exposed mice (all *P* < 0.001). However, subchronic systemic administration of E100 (10 mg/kg, i.p.) or DOZ (1 mg/kg, i.p.) significantly mitigated the increase in the levels of these proinflammatory cytokines in VPA-exposed mice (all *P* < 0.01) (Fig. 4A–D). Notably, subchronic systemic co-administration of RAM (10 mg/kg, i.p.) partially abrogated (*P* < 0.01) the protective effects of E100 (10 mg/kg, i.p.) against VPA-induced elevation of IL-1 β (Fig. 4A) and TNF- α (Fig. 4C) levels, but entirely reversed the E100 (10 mg/kg)-induced protection against increase in IL-6 (Fig. 4B) and TGF- β (Fig. 4D) levels (all *P* < 0.01).

3.3.2. Effects of E100 on the protein expression of NF- κ B p65, iNOS, and COX-2 in the brain tissue of VPA-exposed mice

The expressions of nuclear factor kappa-light-chain-enhancer of activated B cells p65 subunit (NF- κ B p65), induced nitric oxide synthase (iNOS), and cyclooxygenase-2 (COX-2) were also tested using western blotting of lysates from the cerebellum (Fig. 5A) and hippocampus (Fig. 5B). A significant increase in the expression of NF- κ B p65 (*P* < 0.01), iNOS (*P* < 0.001), and COX-2 (*P* < 0.01) was observed in the cerebellum of VPA-exposed mice compared with that of the saline-exposed mice (Fig. 5AII–III). However, following subchronic systemic pretreatment of VPA-exposed mice with E100 (10 mg/kg), a remarkable reduction in the levels of NF- κ B p65, iNOS, and COX-2 was observed compared with the VPA-exposed mice (all *P* < 0.05) (Fig. 5AII–III). Similarly, hippocampal tissues of VPA-exposed mice also showed a significant increase in the expression of NF- κ B p65 (*P* < 0.001), iNOS (*P* < 0.01), and COX-2 (*P* < 0.01) (Fig. 5BII–III) compared with the saline-exposed mice. However, following subchronic systemic pretreatment of VPA-exposed mice with E100 (10 mg/kg), a remarkable reduction in the levels of NF- κ B p65, iNOS, and COX-2 was observed compared with the VPA-exposed mice (all *P* < 0.05) (Fig. 5BII–III). Interestingly, subchronic systemic co-administration of RAM (10 mg/kg, i.p.) reversed the mitigating effects of E100 (10 mg/kg, i.p.) on the expression of NF- κ B p65, iNOS, and COX-2 in the cerebellum. Similarly, subchronic systemic co-administration of RAM (10 mg/kg, i.p.) reversed the mitigating effects of E100 (10 mg/kg, i.p.) on the expression of NF- κ B p65, iNOS and COX-2 in the hippocampus of VPA-exposed mice (all *P* < 0.05).

3.4. Immunofluorescence

3.4.1. Effects of E100 on the activation of Iba-1 in the cerebellum of VPA-exposed mice

Activation of glial cells (microglia) in VPA-exposed mice is considered an index of inflammatory responses [62], and was also observed in this study (Fig. 6A&B). The observed results showed that VPA-exposed mice exhibited a significant increase in the expression of ionized calcium-binding adaptor molecule-1 (Iba-1) in microglia, which is a marker of their activation (*P* < 0.05) (Fig. 6A&B). Immunofluorescence staining revealed a significant increase (*P* < 0.05) in the number of activated microglia in VPA-exposed mice compared with the saline-exposed mice (Fig. 6A&B). However, subchronic systemic treatment of VPA-exposed mice with E100 (10 mg/kg, i.p.) significantly decreased the number of activated microglia compared with the saline-

4.6 The dual-active histamine H₃ receptor antagonist and acetylcholine esterase inhibitor E100 ameliorates stereotyped repetitive behavior and neuroinflammation in sodium valproate induced autism in mice

N. Eissa, et al.

Chemico Biological Interactions 312 (2019) 108775

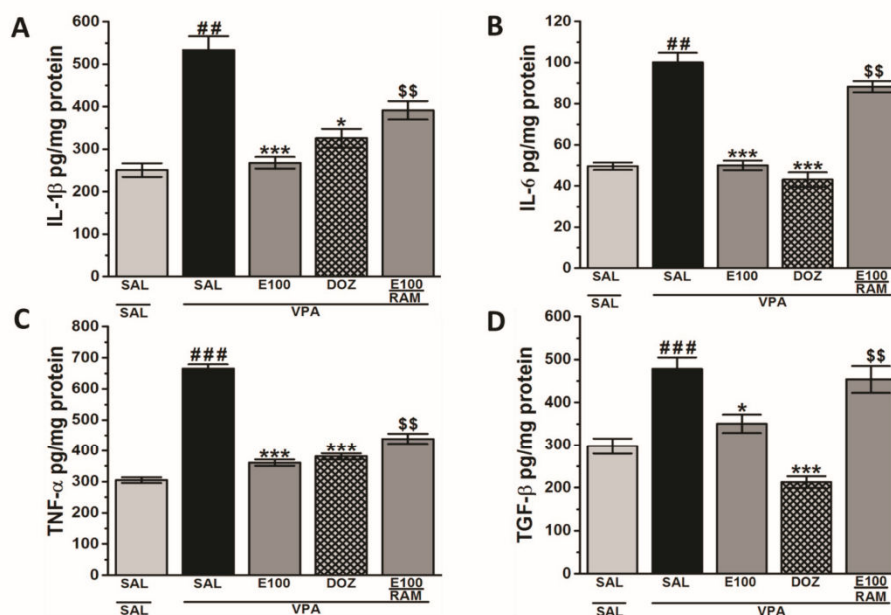


Fig. 4. E100 restored levels of proinflammatory cytokines in the cerebellum of the experimental animals. Modulated Interleukins (IL-1 β , IL-6), Tumor Necrosis Factor (TNF- α), and Transforming Growth Factor (TGF- β) were assessed. VPA-exposed mice showed a significant increase in IL-1 β (Fig. 4A), IL-6 (Fig. 4B), TNF- α (Fig. 4C), and TGF- β (Fig. 4D), compared to Saline-exposed mice. E100 (5, 10, or 15 mg/kg, i.p.) or DOZ (1 mg/kg, i.p.) were administered subchronically for 21 days in VPA-exposed mice. E100 (10 mg/kg, i.p.) or DOZ (1 mg/kg, i.p.) significantly decreased IL-1 β , IL-6, TNF- α , TGF- β (Fig. 4A–D). Effects of subchronic (21 days) systemic co-injection RAM (10 mg/kg, i.p.) on E100(10 mg)-provided modulation of proinflammatory cytokines levels were assessed (Fig. 4A–D). Saline-exposed mice were injected with saline. Data are expressed as the mean \pm SEM (n = 5). ^{###} P < 0.001 vs. SAL-exposed mice. ^{*} P < 0.05 vs. Saline-treated VPA-exposed mice. ^{***} P < 0.001 vs. Saline-treated VPA-exposed mice. ^{\$\$} P < 0.01 vs. E100 (10 mg)-treated VPA-exposed mice.

exposed mice (P < 0.05) (Fig. 6C). Moreover, subchronic systemic co-administration of RAM (10 mg/kg, i.p.) entirely reversed the effects of E100 (10 mg/kg, i.p.) on the number of activated microglia compared with the E100 (10 mg)-treated VPA-exposed mice (P < 0.05) (Fig. 6D).

4. Discussion

In search of sensitive and specific markers of ASD as well as potential therapeutic interventions, the study of brain neurotransmitters has attracted considerable attention. Along with the genetic and environmental factors, accumulated evidence suggests that a variety of several brain neurotransmitters, such as ACh, 5-HT, DA, GABA, Glu, and HA, are implicated in the onset and progression of ASD, substantiating the significance of this research area in the study of ASD etiology [9–14,16–19,71]. As alterations in histaminergic as well as cholinergic neurotransmission are thought to play a crucial role in the phenotypic outcomes of ASD-related behavioral features [1,72,73], the aim of the current study was to examine the effects of the pharmacological modulation of brain HA and ACh using the novel dual-active AChEI and H3R antagonist E100 on a mouse model of ASD-like stereotyped repetitive behaviors induced by prenatal exposure to VPA, as stereotypy, repetitive behavior, and restricted interests are considered core features of ASD. Moreover, recent studies have suggested that histaminergic signaling abnormalities may contribute to rare diseases such as Tourette syndrome [74], a condition reported to be among the most prevalently comorbid neurodevelopmental disorders with ASD and characterized by stereotypies [75–77]. Furthermore, Rapanelli et al. have reported the implication of H3R in repetitive behavior-related pathology [77]. In the current study, VPA-exposed mice

subchronically pretreated with E100 (10 or 15 mg/kg, i.p.) or with the reference drug DOZ (1 mg/kg, i.p.) showed comparable reduction in stereotyped repetitive behavior in the NSB test (Fig. 1). Numerous previous studies showed that H3Rs functioning as hetero-receptors can also regulate the release of several other brain neurotransmitters, e.g. ACh, Glu, GABA, 5-HT, DA in different brain regions [24,25]. Consequently, blocking central H3Rs has been projected to improve the cortical fast rhythms closely associated with cognitive behaviors [25], and numerous preclinical studies indicated particularly that H3R antagonists exhibited a unique feature by their potential cognition-enhancing property [22,23,26,27]. Furthermore, several drug candidates with H3R antagonist properties have shown to increase the release of brain ACh, therefore alleviating symptomatic features and progression of Alzheimer's disease (AD) in clinical trials [28,29]. In addition, a recent report demonstrated lower ACh level in the prefrontal cortex region of mice which showed attention deficit and impulsive behavior [30]. Interestingly, deficit in cholinergic neurotransmission was, also, found in BTBR T + tf/J mice, an idiopathic animal model with the three diagnostic categories for ASD, namely impaired social interaction and communication as well as increased repetitive behaviors [31–35]. Additionally, the E100 (10 mg/kg)-induced effects observed in the NSB test were nullified when mice were administered RAM, but not MPA, ZLT, or SCO (Fig. 2). The mechanism by which the repetitive/compulsive behavior is improved following systemic administration with E100 may involve its capability, as a potent dual-active H3R antagonist and AChE inhibitor, to modulate the release of different neurotransmitters besides HA and ACh, such as DA and 5-HT, in several specific brain areas. Interestingly, the results observed for E100 in NSB are in agreement with previous studies in which subchronic systemic

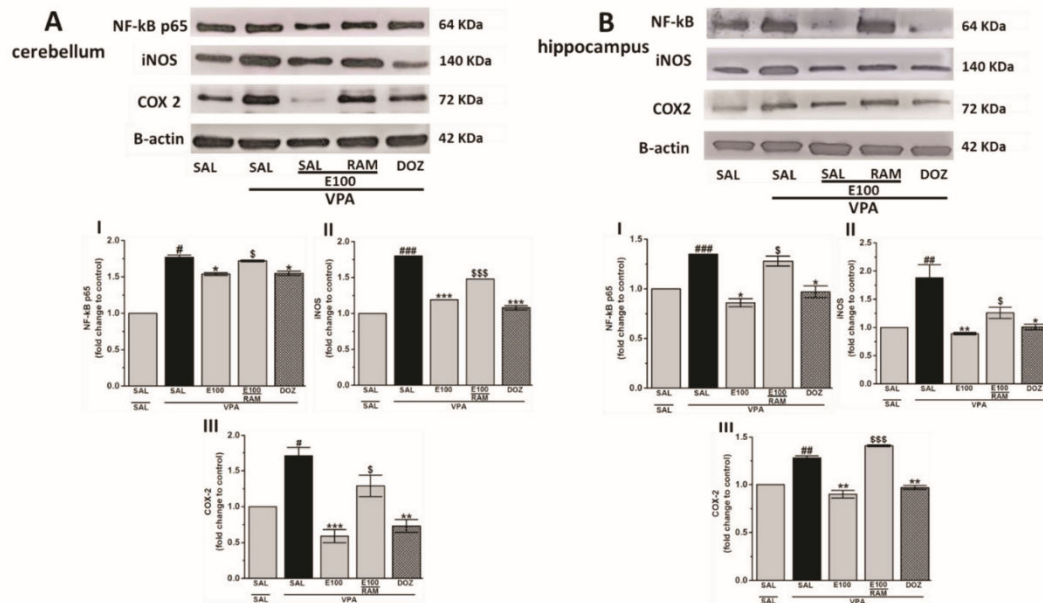


Fig. 5. Representative immunoblots of NF-kB p65, iNOS & COX-2 expression in cerebellum and hippocampus of the experimental animals. NF-kBp65, iNOS and COX-2 are modulated by subchronic treatment with E100 (10 mg) in cerebellum and hippocampus of prenatally VPA treated mice. (A) Cerebellum tissues of VPA-exposed group were subjected to immunoreactions with anti-NF-kB p65 (I), anti-iNOS (II), and anti-COX2 (III). (B) Hippocampal tissues of VPA-exposed group were subjected to immunoreactions with anti-NF-kB p65 (I), anti-iNOS (II), and anti-COX2 (III). Expression levels were determined using western blotting in both the cerebellum and hippocampus. The VPA-exposed mice showed significant increase in NF-kBp65, iNOS and COX-2 compared to Saline-exposed mice in both brain regions (Fig. 5A&B I-III). Subchronic treatment with E100 (10 mg/kg, i.p.) or DOZ (1 mg/kg, i.p.) to VPA-exposed mice remarkably decreased the expression levels of NF-kBp65, iNOS and COX-2 in both brain regions (Fig. 5A&B I-III). However, subchronic (21 days) systemic co-injection of RAM (10 mg/kg, i.p.) reversed the E100(10 mg)-provided suppressed expression in NF-kBp65, iNOS and COX-2 in cerebellum (Fig. 5A I-III), and in NF-kBp65, iNOS and COX-2 in hippocampus (Fig. 5B I-III). Blots were quantified using Image J and corresponding results were represented as fold change of control. Data are expressed as mean \pm SEM (n = 3). #*p* < 0.05, ##*p* < 0.01, ###*p* < 0.001 vs Saline-exposed mice; **p* < 0.05, ***p* < 0.01, ****p* < 0.001 vs VPA-exposed mice and \$*p* < 0.05, \$\$\$*p* < 0.001 vs E100(10 mg)-treated VPA-exposed mice.

administration of the non-imidazole H₃R antagonist DL77 significantly and dose-dependently (5, 10, 15 mg/kg, i.p.) mitigated the increased percentage of shredded nestlet in adult male Tuck-Ordinary mice of VPA-induced ASD features, comprehending the current observations in NSB with E100 capability to facilitate the release of several brain neurotransmitters besides HA and ACh that are of crucial function in repetitive/compulsive behaviors in different animal species [58]. Consequently, assessing the levels of different brain neurotransmitters, including HA and ACh, in different brain areas of the VPA-exposed mice with ASD-like behaviors as well as after pre-treatment with E100 would further help to understand which neural circuits may be involved in this observed behavioral improvement.

The effects of E100 on locomotor activity as well as anxiety levels were examined as ligands modulating anxiety levels or locomotion may give rise to a false-positive effect in these behavioral tests. Therefore, locomotor activity was examined to simultaneously rule out possible intrinsic impairment of spontaneous locomotor activity since reduced activity could otherwise wrongfully be interpreted as increased measures of anxiety hence give rise to a false-positive effect in behavioral tests. The results observed indicated that E100 (10 and 15 mg) significantly increased time spent in the central area, confirming the ability of E100 to modulate anxiety-associated fear levels. In contrast, E100 failed to restore hyperactivity, as no effect was exhibited with all doses on total distance travelled (Fig. 3). Thus, the improvements in repetitive/compulsive behaviours observed for E100 in NSB appeared

unlikely to be connected with a modulating effect in locomotor activity of the tested mice. Moreover, the failure of E100 (at all doses) and DOZ in alleviating the hyperactivity observed in VPA-exposed mice may have been due to the well-known existing imbalance of excitatory (Glu) and inhibitory (GABA) neurotransmitters, as such an imbalance was observed in several clinical trials in patients with ASD [78–81].

Previous studies have found that several proinflammatory cytokines, including TNF- α , IL-1 β , IL-6, and TGF- β , are elevated in the autistic brain [82–85]. Consistent with these findings, our study showed that the levels of TNF- α , IL-1 β , IL-6, and TGF- β were significantly increased in the cerebellum of VPA-exposed mice compared with age-matched control mice (Fig. 4A–D). However, systemic administration of E100 (10 mg/kg, i.p.) significantly modulated the levels of the proinflammatory cytokines in VPA-exposed mice (Fig. 4A–D). In addition, when co-administered with E100, the CNS-penetrant H₃R agonist abrogated the E100-induced protective effects against increased levels of proinflammatory cytokines (Fig. 4), indicating the involvement of brain HA in facilitating the neuroprotective action of E100 in VPA-exposed mice with ASD-like features. The regulation of immune response is mediated by NF-kB via induction of the expression of inflammatory cytokines and chemokines, establishing a feedback mechanism that can produce chronic or excessive inflammation. Activation of NF-kB is significantly increased in children with ASD [86,87]. Young et al. also observed elevated levels of NF-kB in the blood and brain of patients with ASD [88]. Moreover, neuroinflammation is characterized by

4.6 The dual-active histamine H₃ receptor antagonist and acetylcholine esterase inhibitor E100 ameliorates stereotyped repetitive behavior and neuroinflammation in sodium valproate induced autism in mice

N. Eissa, et al.

Chemico Biological Interactions 312 (2019) 108775

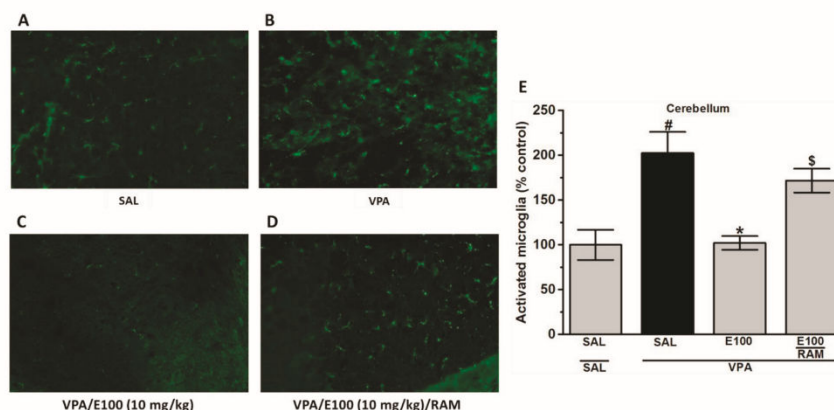


Fig. 6. Effects of E100 on Iba-1 in cerebellum tissues of VPA-exposed mice. Profound expression of Iba-1-positive microglia (Fig. 6B) was found in the VPA-exposed mice compared to the Saline-exposed mice (Fig. 6A). In contrast, subchronic treatment with E100 (10 mg/kg, i.p.) to the VPA-exposed mice showed significantly lower staining of Iba-1 compared to the VPA-exposed mice (Fig. 6C). Subchronic (21 days) systemic co-injection of RAM (10 mg/kg, i.p.) counteracted the E100(10 mg)-provided amelioration of Iba-1 expression of VPA-exposed mice ($P < 0.05$) (Fig. 6D) (scale bar 1000 μ m). Quantitative analysis of activated microglia (Fig. 6E) revealed a significant increase ($P < 0.05$) in the number of activated microglia in the VPA-exposed mice compared to the Saline-exposed mice. However, subchronic treatment with E100 (10 mg/kg, i.p.) to the VPA-exposed mice significantly reduced ($P < 0.05$) the number of activated microglia in the E100-treated VPA-exposed mice compared to the saline-treated VPA-exposed mice group. $^{\#}P < 0.05$ vs. E100(10 mg)-treated VPA-exposed mice. Data are expressed as the percent mean \pm SEM ($n = 3$).

reactivity of microglia and astrocytes, activation of iNOS signaling, and increased expression and release of cytokines and chemokines [89]. Evidence indicates that patients with ASD exhibit ongoing neuroinflammatory processes in various regions of the brain involving microglial activation [82,90]; consequently, aberrant expression of cytokines and their signaling intermediaries are often observed. Furthermore, recent findings have shown that mice exhibiting disrupted COX-2 signaling might serve as a novel animal model to assess ASD [91]. In the current study, the expression of NF- κ B, iNOS, and COX-2 were significantly higher in the cerebellum as well as the hippocampus of VPA-exposed mice compared with saline-exposed mice (Fig. 5A&B). However, systemic administration of E100 (10 mg/kg, i.p.) significantly reduced the increased levels of NF- κ B, iNOS, and COX-2, and the CNS-penetrant H₃R agonist, when co-administered with E100, reversed the E100-induced neuroprotection in both brain regions (Fig. 5A&B). The latter observations indicate that brain HA is strongly involved in facilitating the neuroprotective action of E100 in VPA-exposed mice with ASD-like features.

Growing evidence suggests a crucial role for immune dysregulation in patients with ASD. Several ASD risk-related genes are linked to the immune system- and maternal immune system-related risk factors of ASD [92,93]. Microglia, a representative immune cell in the brain, plays an important role in synaptic refinement [92,93], and are also supposed to be associated with the pathogenesis of ASD [92,93]. Moreover, previous reports have also shown changes in the activation, number, and distribution of microglia in the brains of patients with ASD [94,95]. In the current study, the results showed that expression of Iba-1-positive microglia was significantly higher in the cerebellum of VPA-exposed mice than in that of the saline-exposed control mice (Fig. 6A–D). Further, immunofluorescence staining revealed a significant increase in the number of activated microglia in VPA-exposed mice compared with the saline-exposed mice (Fig. 6A&B). However, systemic pre-treatment of VPA-exposed mice with E100 (10 mg/kg, i.p.) significantly decreased the number of activated microglia compared with the saline-exposed control mice (Fig. 6C), and the E100-induced effect on activated microglia was entirely counteracted by co-administration of RAM (Fig. 6D). The latter result signifies the involvement of brain HA in facilitating the neuroprotective effects of E100 against the

disrupted microglia of VPA-exposed mice.

5. Conclusion

The novel dual-active H₃R antagonist and AChE inhibitor E100 ameliorates ASD-like stereotyped repetitive behaviors induced by prenatal exposure of C57BL/6 mice to VPA. Moreover, E100 modulates the levels of central HA and ACh in an inflammatory context, mitigating the increase in the levels of proinflammatory cytokines and expression of NF- κ B, iNOS, and COX-2 in the cerebellum as well as the hippocampus. To our knowledge, this is the first in vivo demonstration of the effectiveness of a potent dual-active H₃R antagonist and AChE inhibitor in palliating stereotypes of ASD-like features induced by prenatal exposure to VPA, and provides evidence for the role of such compounds in treating ASD.

Conflicts of interest

The authors declare no competing interests.

Acknowledgments

The Office of Graduate Studies and Research of UAE University as well as the ADEK Award for Research Excellence 2017 are thanked for the support provided to B.S. in the form of the intramural College of Medicine and Health Sciences (Zayed-Center for Health Sciences) as well as extramural funds from ADEK. The authors also acknowledge the partial support of Jagiellonian University statutory funds (K/ZDS/007121). Support was kindly provided by the EU COST Action MuTaLig CA15135 to H.S., K.K.-K., and D.L.

Appendix A. Supplementary data

Supplementary data to this article can be found online at <https://doi.org/10.1016/j.cbi.2019.108775>.

References

- [1] D. Baronio, K. Castro, T. Gonchoroski, G.M. de Melo, G.D. Nunes, V. Bambini-Junior, C. Gottfried, R. Riesgo, Effects of an H3R antagonist on the animal model of autism induced by prenatal exposure to valproic acid, *PLoS One* 10 (2015) e0116363.
- [2] O. Arvidsson, C. Gillberg, P. Lichtenstein, S. Lundstrom, Secular changes in the symptom level of clinically diagnosed autism, *JCPP (J. Child Psychol. Psychiatry)* 59 (2018) 744–751.
- [3] E.J. Nestler, S.E. Hyman, Animal models of neuropsychiatric disorders, *Nat. Neurosci.* 13 (2010) 1161–1169.
- [4] R.C. Sheldrick, A.S. Carter, State-level trends in the prevalence of autism spectrum disorder (ASD) from 2000 to 2012: a reanalysis of findings from the autism and developmental disabilities network, *J. Autism Dev. Disord.* 48 (2018) 3086–3092.
- [5] G. Xu, L. Strathearn, B. Liu, W. Bao, Prevalence of autism spectrum disorder among US children and adolescents, 2014–2016, *J. Am. Med. Assoc.* 319 (2018) 81–82.
- [6] A. Cavalli, M.L. Bolognesi, A. Minarini, M. Rosini, V. Tumiatti, M. Recanatini, C. Melchiorre, Multi-target-directed ligands to combat neurodegenerative diseases, *J. Med. Chem.* 51 (2008) 347–372.
- [7] M. Decker, Recent advances in the development of hybrid molecules/designed multiple compounds with anti-amnesic properties, *Mini Rev. Med. Chem.* 7 (2007) 221–229.
- [8] P. Karimi, E. Kamali, S.M. Mousavi, M. Karahmadi, Environmental factors influencing the risk of autism, *J. Res. Med. Sci.* 22 (2017) 27.
- [9] B.A. Ellenbroek, B. Ghiabi, Do Histamine receptor 3 antagonists have a place in the therapy for schizophrenia? *Curr. Pharmaceut. Des.* 21 (2015) 3760–3770.
- [10] E. Bacchelli, A. Battaglia, C. Cameli, S. Lomartire, R. Tancredi, S. Thomson, J.S. Sutcliffe, Analysis of CHRNA7 rare variants in autism spectrum disorder susceptibility, *Am. J. Med. Genet.* 167A (2015) 715–723.
- [11] J.A. Helligs, L.E. Arnold, J.C. Han, Dopamine antagonists for treatment resistance in autism spectrum disorders: review and focus on BDNF stimulators loxapine and amitriptyline, *Expert Opin. Pharmacother.* 18 (2017) 581–588.
- [12] J. Naajien, J. Braiten, G. Poelmans, I. consortium, J.C. Glennon, B. Franke, J.K. Builtealer, Glutamatergic and GABAergic gene sets in attention-deficit/hyperactivity disorder: association to overlapping traits in ADHD and autism, *Transl. Psychiatry* 7 (2017) e999.
- [13] N. Nakai, M. Nagano, F. Saitow, Y. Watanabe, Y. Kawamura, A. Kawamoto, K. Tamada, H. Mizuma, H. Onoe, Y. Watanabe, H. Monai, H. Hirase, J. Nakatani, H. Inagaki, T. Kawada, T. Miyazaki, M. Watanabe, Y. Sato, S. Okabe, K. Kitamura, M. Kano, K. Hashimoto, H. Suzuki, T. Takumi, Serotonin rebalances cortical tuning and behavior linked to autism symptoms in 15q11-13 CNV mice, *Sci Adv* 3 (2017) e1603001.
- [14] D. Paval, A dopamine hypothesis of autism spectrum disorder, *Dev. Neurosci.* 39 (2017) 355–360.
- [15] D. Paval, F. Rad, R. Rusu, A.S. Niculae, H.A. Colosi, I. Dobrescu, E. Dronca, Low retinal dehydrogenase 1 (RALDH1) level in prepubertal boys with autism spectrum disorder: a possible link to dopamine dysfunction? *Clin Psychopharmacol Neurosci* 15 (2017) 229–236.
- [16] A. Shah, L. Wing, Psychological approaches to chronic catatonia-like deterioration in autism spectrum disorders, *Int. Rev. Neurobiol.* 72 (2006) 245–264.
- [17] L. Wang, L.E. Almeida, N.A. Spornick, N. Kenyon, S. Kamimura, A. Khaibullina, M. Nouraei, Z.M. Quezada, Modulation of social deficits and repetitive behaviors in a mouse model of autism: the role of the nicotinic cholinergic system, *Psychopharmacology (Berlin)* 232 (2015) 4303–4316.
- [18] R. Chen, L.K. Davis, S. Guter, Q. Wei, S. Jacob, M.H. Potter, N.J. Cox, E.H. Cook, J.S. Sutcliffe, B. Li, Leveraging blood serotonin as an endophenotype to identify de novo and rare variants involved in autism, *Mol. Autism* 8 (2017) 14.
- [19] K. Hellmer, P. Nystrom, Infant acetylcholine, dopamine, and melatonin dysregulation: neonatal biomarkers and causal factors for ASD and ADHD phenotypes, *Med. Hypotheses* 100 (2017) 64–66.
- [20] P. Panula, P.L. Chazot, M. Cowart, R. Gutzmer, R. Leurs, W.L. Liu, H. Stark, R.L. Thurmond, H.L. Haas, International union of basic and clinical pharmacology. XCVIII. Histamine receptors, *Pharmacol. Rev.* 67 (2015) 601–655.
- [21] P. Panula, J. Rinne, K. Kuokkanen, K.S. Eriksson, T. Sallinen, H. Kalimo, M. Relja, Neuronal histamine deficit in Alzheimer's disease, *Neuroscience* 82 (1998) 993–997.
- [22] B. Sadek, H. Stark, Cherry-picked ligands at histamine receptor subtypes, *Neuropharmacology* 106 (2016) 56–73.
- [23] B. Sadek, A. Saad, A. Sadeq, F. Jalal, H. Stark, Histamine H3 receptor as a potential target for cognitive symptoms in neuropsychiatric diseases, *Behav. Brain Res.* 312 (2016) 415–430.
- [24] M. Berlin, C.W. Boyce, L. Ruiz Mde, Histamine H3 receptor as a drug discovery target, *J. Med. Chem.* 54 (2011) 26–53.
- [25] R. Parmentier, C. Anacleit, C. Guhenec, E. Brousseau, D. Bricout, T. Giboulot, D. Bozyczko-Coyne, K. Spiegel, H. Ohtsu, M. Williams, J.S. Lin, The brain H3-receptor as a novel therapeutic target for vigilance and sleep-wake disorders, *Biochem. Pharmacol.* 73 (2007) 1157–1171.
- [26] M.B. Passani, P. Blandina, Histamine receptors in the CNS as targets for therapeutic intervention, *Trends Pharmacol. Sci.* 32 (2011) 242–249.
- [27] J.M. Witkin, D.L. Nelson, Selective histamine H3 receptor antagonists for treatment of cognitive deficiencies and other disorders of the central nervous system, *Pharmacol. Ther.* 103 (2004) 1–20.
- [28] J.D. Brioni, T.A. Esbenshade, T.R. Garrison, S.R. Bitner, M.D. Cowart, Discovery of histamine H3 antagonists for the treatment of cognitive disorders and Alzheimer's disease, *J. Pharmacol. Exp. Ther.* 336 (2011) 38–46.
- [29] A.D. Medhurst, A.R. Atkins, L.J. Beresford, K. Brackenborough, M.A. Briggs, A.R. Calver, J. Cilia, J.E. Cluderay, B. Crook, J.B. Davis, R.K. Davis, R.P. Davis, L.A. Dawson, A.G. Foley, J. Gartlon, M.I. Gonzalez, T. Heslop, W.D. Hirst, C. Jennings, D.N. Jones, L.P. Lacroix, A. Martyn, S. Ociepka, A. Ray, C.M. Regan, J.C. Roberts, J. Schogger, E. Southam, T.O. Stean, B.K. Trail, N. Upton, G. Wadsworth, J.A. Wald, T. White, J. Witherington, M.L. Woolley, A. Worby, D.M. Wilson, GSK189254, a novel H3 receptor antagonist that binds to histamine H3 receptors in Alzheimer's disease brain and improves cognitive performance in preclinical models, *J. Pharmacol. Exp. Ther.* 321 (2007) 1032–1045.
- [30] S.M. McTighe, S.J. Neal, Q. Lin, Z.A. Hughes, D.G. Smith, The BTBR mouse model of autism spectrum disorders has learning and attentional impairments and alterations in acetylcholine and kynurenic acid in prefrontal cortex, *PLoS One* 8 (2013) e62189.
- [31] K.Z. Meyza, E.B. Defensor, A.L. Jensen, M.J. Corley, B.L. Pearson, R.L. Pobbe, V.J. Bolivar, D.C. Blanchard, R.J. Blanchard, The BTBR T+ tf/J mouse model for autism spectrum disorders-in search of biomarkers, *Behav. Brain Res.* 251 (2013) 25–34.
- [32] M.L. Scattoni, S.U. Gandhi, L. Ricceri, J.N. Crawley, Unusual repertoire of vocalizations in the BTBR T+ tf/J mouse model of autism, *PLoS One* 3 (2008) e3067.
- [33] J.L. Silverman, S.S. Tolu, C.L. Barkan, J.N. Crawley, Repetitive self-grooming behavior in the BTBR mouse model of autism is blocked by the mGluR5 antagonist MPEP, *Neuropsychopharmacology* 35 (2010) 976–989.
- [34] H.G. McFarlane, G.K. Kusek, M. Yang, J.L. Phoenix, V.J. Bolivar, J.N. Crawley, Autism-like behavioral phenotypes in BTBR T+ tf/J mice, *Genes Brain Behav.* 7 (2008) 152–163.
- [35] M. Yang, V. Zhodzishsky, J.N. Crawley, Social deficits in BTBR T+ tf/J mice are unchanged by cross-fostering with C57BL/6J mothers, *Int. J. Dev. Neurosci.* 25 (2007) 515–521.
- [36] H. Yokoyama, K. Onodera, K. Iinuma, T. Watanabe, Effect of thioperamide, a histamine H3 receptor antagonist, on electrically induced convulsions in mice, *Eur. J. Pharmacol.* 234 (1993) 129–133.
- [37] M. Bhowmik, R. Khanam, D. Vohora, Histamine H3 receptor antagonists in relation to epilepsy and neurodegeneration: a systemic consideration of recent progress and perspectives, *Br. J. Pharmacol.* 167 (2012) 1398–1414.
- [38] N. Khan, A. Saad, S.M. Nurulain, F.H. Darras, M. Decker, B. Sadek, The dual-acting H3 receptor antagonist and AChE inhibitor UW-MD-71 dose-dependently enhances memory retrieval and reverses dizocilpine-induced memory impairment in rats, *Behav. Brain Res.* 297 (2016) 155–164.
- [39] B. Sadek, N. Khan, F.H. Darras, S. Pockes, M. Decker, The dual-acting AChE inhibitor and H3 receptor antagonist UW-MD-72 reverses amnesia induced by scopolamine or dizocilpine in passive avoidance paradigm in rats, *Physiol. Behav.* 165 (2016) 383–391.
- [40] G. Morini, M. Couini, M. Rivara, S. Rivara, F. Bordini, P.V. Plazzi, L. Flaminio, F. Saccani, S. Bertoni, V. Ballabeni, E. Barocelli, M. Mor, Synthesis and structure-activity relationships for biphenyl H3 receptor antagonists with moderate anticholinesterase activity, *Bioorg. Med. Chem.* 16 (2008) 9911–9924.
- [41] K. Nikolic, S. Filipic, D. Aghaba, H. Stark, Pro-cognitive properties of drugs with single and multitargeting H3 receptor antagonist activities, *CNS Neurosci. Ther.* 20 (2014) 613–623.
- [42] G. Petroianu, K. Ararat, B.C. Sasse, H. Stark, Multiple enzyme inhibitions by histamine H3 receptor antagonists as potential pro-cognitive agents, *Die Pharmazie* 61 (2006) 179–182.
- [43] S.D. Bembek, J.M. Keith, M.A. Letavic, R. Apodaca, A.J. Barbier, L. Dvorak, L. Aluisio, K.L. Miller, T.W. Lovenberg, N.J. Carruthers, Lead identification of acetylcholinesterase inhibitors-histamine H3 receptor antagonists from molecular modeling, *Bioorg. Med. Chem.* 16 (2008) 2968–2973.
- [44] B. Sadek, A. Saad, D. Subramanian, M. Shafullah, D. Lazewska, K. Kiec-Kononowicz, Anticonvulsant and pro-cognitive properties of the non-imidazole histamine H3 receptor antagonist DL77 in male adult rats, *Neuropharmacology* 106 (2016) 46–55.
- [45] S.S.H. Wang, A.D. Kloth, A. Badura, The cerebellum, sensitive periods, and autism, *Neuron* 83 (2014) 518–532.
- [46] L.F. Koziol, D. Budding, N. Andreasen, S. D'Arrigo, S. Bulgheroni, H. Imamizu, M. Ito, M. Manto, C. Marvel, K. Parker, G. Pezzulo, N. Ramnani, D. Riva, J. Schmähmann, L. Vandervort, T. Yamazaki, Consensus paper: the cerebellum's role in movement and cognition, *Cerebellum* 13 (2014) 151–177.
- [47] L. Lucchina, A.M. Depino, Altered peripheral and central inflammatory responses in a mouse model of autism, *Autism Res.* 7 (2014) 273–289.
- [48] L. Shi, S.E. Smith, N. Malkova, D. Tse, Y. Su, P.H. Patterson, Activation of the maternal immune system alters cerebellar development in the offspring, *Brain Behav. Immun.* 23 (2009) 116–123.
- [49] R.D. Rubin, P.D. Watson, M.C. Duff, N.J. Cohen, The role of the hippocampus in flexible cognition and social behavior, *Front. Hum. Neurosci.* 8 (2014) 742.
- [50] S.M. Bastaki, Y.M. Abdulrazzaq, M. Shafullah, M. Wiecek, K. Kiec-Kononowicz, B. Sadek, Anticonvulsant and reproductive toxicological studies of the imidazole-based histamine H3R antagonist 2-18 in mice, *Drug Des. Dev. Ther.* 12 (2018) 179–194.
- [51] S. Kataoka, K. Takuma, Y. Hara, Y. Maeda, Y. Ago, T. Matsuda, Autism-like behaviours with transient histone hyperacetylation in mice treated prenatally with valproic acid, *Int. J. Neuropsychopharmacol.* 16 (2013) 91–103.
- [52] K. Takuma, Y. Hara, S. Kataoka, T. Kawanai, Y. Maeda, R. Watanabe, E. Takano, A. Hayata-Takano, H. Hashimoto, Y. Ago, T. Matsuda, Chronic treatment with valproic acid or sodium butyrate attenuates novel object recognition deficits and hippocampal dendritic spine loss in a mouse model of autism, *Pharmacol. Biochem. Behav.* 126 (2014) 43–49.
- [53] K. Kuder, D. Lazewska, G. Latacz, J.S. Schwed, T. Karcz, H. Stark, J. Karolak-

4.6 The dual-active histamine H₃ receptor antagonist and acetylcholine esterase inhibitor E100 ameliorates stereotyped repetitive behavior and neuroinflammation in sodium valproate induced autism in mice

N. Eissa, et al.

Chemico-Biological Interactions 312 (2019) 108775

- Wojciechowska, K. Kieć-Kononowicz, Chlorophenoxy aminoalkyl derivatives as histamine H₃R ligands and antiepileptic agents, *Bioorg. Med. Chem.* 24 (2016) 53–72.
- [54] D. Lazewska, J. Jonczyk, M. Bajda, N. Szalaj, A. Wieckowska, D. Panek, C. Moore, K. Kuder, B. Malawska, K. Kieć-Kononowicz, Cholinesterase inhibitory activity of chlorophenoxy derivatives-Histamine H₃ receptor ligands, *Bioorg. Med. Chem. Lett.* 26 (2016) 4140–4145.
- [55] N. Khan, A. Saad, S.M. Nurulain, F.H. Darras, M. Decker, B. Sadek, The dual-acting H₃ receptor antagonist and AChE inhibitor UW-MD-71 dose-dependently enhances memory retrieval and reverses dizocilpine-induced memory impairment in rats, *Behav. Brain Res.* 297 (2015) 155–164.
- [56] M. Krause, H. Stark, W. Schunack, Azomethine prodrugs of (R)-alpha-methylhistamine, a highly potent and selective histamine H₃-receptor agonist, *Curr. Med. Chem.* 8 (2001) 1329–1340.
- [57] A. Alachkar, D. Lazewska, K. Kieć-Kononowicz, B. Sadek, The histamine H₃ receptor antagonist E159 reverses memory deficits induced by dizocilpine in passive avoidance and novel object recognition paradigm in rats, *Front. Pharmacol.* 8 (2017) 709.
- [58] N. Eissa, P. Jayaprakash, S. Azimullah, S.K. Ojha, M. Al-Houqani, F.Y. Jalal, D. Lazewska, K. Kieć-Kononowicz, B. Sadek, The histamine H₃R antagonist DL77 attenuates autistic behaviors in a prenatal valproic acid-induced mouse model of autism, *Sci. Rep.* 8 (2018) 13077.
- [59] A. Alachkar, N. Khan, D. Lazewska, K. Kieć-Kononowicz, B. Sadek, Histamine H₃ receptor antagonist E177 attenuates amnesia induced by dizocilpine without modulation of anxiety-like behaviors in rats, *Neuropsychiatric Dis. Treat.* 15 (2019) 531–542.
- [60] M. Orsetti, P. Ghi, G. Di Carlo, H. Histamine, (3)-receptor antagonism improves memory retention and reverses the cognitive deficit induced by scopolamine in a two-trial place recognition task, *Behav. Brain Res.* 124 (2001) 235–242.
- [61] S. Ojha, H. Javed, S. Azimullah, S.B. Abul Khair, M.E. Haque, Neuroprotective potential of ferulic acid in the rotenone model of Parkinson's disease, *Drug Des. Dev. Ther.* 9 (2015) 5499–5510.
- [62] H. Javed, S. Azimullah, S.B. Abul Khair, S. Ojha, M.E. Haque, Neuroprotective effect of nerolidol against neuroinflammation and oxidative stress induced by rotenone, *BMC Neurosci.* 17 (2016) 58.
- [63] M. Angoa-Perez, M.J. Kane, D.I. Briggs, D.M. Francescutti, D.M. Kuhn, Marble burying and nestlet shredding as tests of repetitive, compulsive-like behaviors in mice, *J. Vis. Exp.* (2013) 50978.
- [64] J.W. Kim, H. Seung, K.J. Kwon, M.J. Ko, E.J. Lee, H.A. Oh, C.S. Choi, K.C. Kim, E.L. Gonzales, J.S. You, D.H. Choi, J. Lee, S.H. Han, S.M. Yang, J.H. Cheong, C.Y. Shin, G.H. Bahn, Subchronic treatment of donepezil rescues impaired social, hyperactive, and stereotypic behavior in valproic acid-induced animal model of autism, *PLoS One* 9 (2014) e104927.
- [65] L. Prut, C. Belzung, The open field as a paradigm to measure the effects of drugs on anxiety-like behaviors: a review, *Eur. J. Pharmacol.* 463 (2003) 3–33.
- [66] A.A. Tyrtshynaia, L.V. Lysenko, F. Madamba, I.V. Manzhulo, M.Y. Khotimchenko, A.M. Kleschnevnikov, Acute neuroinflammation provokes intracellular acidification in mouse hippocampus, *J. Neuroinflammation* 13 (2016) 283.
- [67] R.A. McCloy, S. Rogers, C.E. Caldon, T. Lorca, A. Castro, A. Burgess, Partial inhibition of Gdki in G 2 phase overrides the SAC and decouples mitotic events, *Cell Cycle* 13 (2014) 1400–1412.
- [68] M.J. Smit, H. Timmerman, J.C. Hijzelendoorn, H. Fukui, R. Leurs, Regulation of the human histamine H₁ receptor stably expressed in Chinese hamster ovary cells, *Br. J. Pharmacol.* 117 (1996) 1071–1080.
- [69] E.H. Schneider, R. Seifert, Histamine H₄(4) receptor-RGS fusion proteins expressed in Sf9 insect cells: a sensitive and reliable approach for the functional characterization of histamine H₄(4) receptor ligands, *Biochem. Pharmacol.* 78 (2009) 607–616.
- [70] Y. Cheng, W.H. Prusoff, Relationship between the inhibition constant (K_i) and the concentration of inhibitor which causes 50 per cent inhibition (I₅₀) of an enzymatic reaction, *Biochem. Pharmacol.* 22 (1973) 3099–3108.
- [71] D. Paval, A dopamine hypothesis of autism spectrum disorder, *Dev. Neurosci.* 100 (2017) 64–66.
- [72] G. Karvat, T. Kimchi, Acetylcholine elevation relieves cognitive rigidity and social deficiency in a mouse model of autism, *Neuropsychopharmacology* 39 (2014) 831–840.
- [73] C. Wright, J.H. Shin, A. Rajpurohit, A. Deep-Soboslay, L. Collado-Torres, N.J. Brandon, T.M. Hyde, J.E. Kleinman, A.E. Jaffe, A.J. Cross, D.R. Weinberger, Altered expression of histamine signaling genes in autism spectrum disorder, *Transl. Psychiatry* 7 (2017) e1126.
- [74] P. Paschou, T.V. Fernandez, F. Sharp, G.A. Heiman, P.J. Hoekstra, Genetic susceptibility and neurotransmitters in tourette syndrome, *Int. Rev. Neurobiol.* 112 (2013) 155–177.
- [75] C. Gillberg, E. Billstedt, Autism and Asperger syndrome: coexistence with other clinical disorders, *Acta Psychiatr. Scand.* 102 (2000) 321–330.
- [76] I. Karagiannidis, S. Dehning, P. Sandor, Z. Tarnok, R. Rizzo, T. Wolanczyk, M. Madruga-Garrido, J. Hebebrand, M.M. Nothen, G. Lehmkuhl, L. Farkas, P. Nagy, U. Szymanska, Z. Anastasiou, V. Stathias, C. Androustos, V. Tsironi, A. Koumoula, C. Barta, P. Zill, P. Mir, N. Muller, C. Barr, P. Paschou, Support of the histaminergic hypothesis in Tourette syndrome: association of the histamine decarboxylase gene in a large sample of families, *J. Med. Genet.* 50 (2013) 760–764.
- [77] M. Rapanelli, L. Frick, V. Pogorelov, H. Ohtsu, H. Bito, C. Pittenger, Histamine H₃R receptor activation in the dorsal striatum triggers stereotypies in a mouse model of tic disorders, *Transl. Psychiatry* 7 (2017) e1013.
- [78] E.V. Orekhova, T.A. Stroganova, A.O. Prokofyev, G. Nygren, C. Gillberg, M. Elam, Sensory gating in young children with autism: relation to age, IQ, and EEG gamma oscillations, *Neurosci. Lett.* 434 (2008) 218–223.
- [79] M.F. Casanova, D. Buxhoeveden, J. Gomez, Disruption in the inhibitory architecture of the cell minicolumn: implications for autism, *The Neuroscientist* 9 (2003) 496–507.
- [80] J.L. Rubenstein, M.M. Merzenich, Model of autism: increased ratio of excitation/inhibition in key neural systems, *Genes Brain Behav.* 2 (2003) 255–267.
- [81] D.F. Mabung, E.L. Gonzales, J.W. Kim, K.C. Kim, C.Y. Shin, Exploring the validity of valproic acid animal model of autism, *Exp. Neurobiol.* 24 (2015) 285–300.
- [82] D.L. Vargas, C. Nascimbene, C. Krishnan, A.W. Zimmerman, C.A. Pardo, Neuroglial activation and neuroinflammation in the brain of patients with autism, *Ann. Neurol.* 57 (2005) 67–81.
- [83] P.E. Goines, P. Ashwood, Cytokine dysregulation in autism spectrum disorders (ASD): possible role of the environment, *Neurotoxicol. Teratol.* 36 (2013) 67–81.
- [84] I. Deckmann, G.B. Schwingel, M. Fontes-Dutra, V. Bambini-Junior, C. Gottfried, Neuroimmune alterations in autism: a translational analysis focusing on the animal model of autism induced by prenatal exposure to valproic acid, *Neuroimmunomodulation* 25 (2018) 285–299.
- [85] A.M. Depino, Peripheral and central inflammation in autism spectrum disorders, *Mol. Cell. Neurosci.* 53 (2013) 69–76.
- [86] U.S. Naik, C. Gangadharan, K. Abbagani, B. Nagalla, N. Dasari, S.K. Manna, A study of nuclear transcription factor-kappa B in childhood autism, *PLoS One* 6 (2011) e19488.
- [87] A. Nadeem, S.F. Alimad, S.A. Bakheet, N.O. Al-Harbi, L.Y. Al-Ayadli, S.M. Attia, K.M.A. Zoheir, Toll-like receptor 4 signaling is associated with upregulated NADPH oxidase expression in peripheral T cells of children with autism, *Brain Behav. Immun.* 61 (2017) 146–154.
- [88] A.M. Young, E. Campbell, S. Lynch, J. Suckling, S.J. Powis, Aberrant NF-kappaB expression in autism spectrum condition: a mechanism for neuroinflammation, *Front. Psychiatry* 2 (2011) 27.
- [89] F. Monnet-Tschudi, A. Defaux, O. Braissant, L. Cagnon, M.G. Zurich, Methods to assess neuroinflammation, *Curr. Protoc. Toxicol.* 12 (2011) Unit12.19.
- [90] J.I. Rodriguez, J.K. Kern, Evidence of microglial activation in autism and its possible role in brain underconnectivity, *Neuron Glia Biol.* 7 (2011) 205–213.
- [91] C.T. Wong, I. Bestard-Lorigados, D.A. Crawford, Autism-related behaviors in the cyclooxygenase-2-deficient mouse model, *Genes Brain Behav.* 18 (2019) e12506.
- [92] H.J. Kim, M.H. Cho, W.H. Shim, J.K. Kim, E.Y. Jeon, D.H. Kim, S.Y. Yoon, Deficient autophagy in microglia impairs synaptic pruning and causes social behavioral defects, *Mol. Psychiatry* 22 (2017) 1576–1584.
- [93] R. Koyama, Y. Ikegaya, Microglia in the pathogenesis of autism spectrum disorders, *Neurosci. Res.* 100 (2015) 1–5.
- [94] J.T. Morgan, G. Chana, C.A. Pardo, C. Achim, K. Semendeferi, J. Buckwalter, E. Courchesne, I.P. Everall, Microglial activation and increased microglial density observed in the dorsolateral prefrontal cortex in autism, *Biol. Psychiatry* 68 (2010) 368–376.
- [95] C.A. Pardo, D.L. Vargas, A.W. Zimmerman, Immunity, neuroglia and neuroinflammation in autism, *Int. Rev. Psychiatry* 17 (2005) 485–495.

Supplementary Information

The dual-active histamine H₃ receptor antagonist and acetylcholine esterase inhibitor E100 ameliorates stereotyped repetitive behavior and neuroinflammation in sodium valproate-induced autism in mice

Normin Eissa¹, Sheikh Azimullah¹, Patrilla Jayaprakash¹, Richard L. Jayaram¹, David Reiner², Sheesh K. Ojha³, Rami Beiram¹, Holger Stark², Dorota Lazewska², Katarzyna Kiec-Kononowicz², Bassem Sadek^{1*}

¹Department of Pharmacology & Therapeutics, College of Medicine and Health Sciences, United Arab Emirates University, P.O. Box 17666, Al Ain, UAE.
²Institute of Pharmaceutical and Medicinal Chemistry, Heinrich Heine University Düsseldorf, Universitätsstr. 1, 40225 Düsseldorf, Germany.
³Jagiellonian University-Medical College, Faculty of Pharmacy, Department of Technology and Biotechnology of Drugs, Medyczna 9 St., 30-688 Kraków, Poland.

*Corresponding address:

Dr. Bassem Sadek
United Arab Emirates University
College of Medicine & Health Sciences
Department of Pharmacology and Therapeutics
PO Box 17666, Al Ain, UAE
Tel + 971 3 7137 512
Fax + 971 3 7672 033
Email bassem.sadek@uaeu.ac.ae

S.1) Supplementary Methods

S.1.1) Cell culture & membrane preparations of histamine H₁- and H₄-receptor expressing cells

Membrane preparations from Sf9-insect cells transiently expressing the human H₄ receptor were carried out as described previously [1, 2].

For generating cell membrane preparations of histamine H₁-receptors (H₁R), CHO-cells stably expressing the human isoform of the H₁R were cultured in Dulbecco's Modified Eagles Medium (Sigma-Aldrich, Taufkirchen, Germany) supplemented with 10% fetal bovine serum (PAN Biotech, Aldenhach, Germany), 1% L-Glutamine solution (200 mM, Sigma-Aldrich), Penicillin-Streptomycin (100 units/0.1 mg/mL; Sigma-Aldrich) and 1% non-essential aminoacid solution (100x) on cell-culture flasks (175 cm², Sarstedt, Nümbrecht, Germany) upon confluence, maintaining the culture flasks at 37 °C in atmosphere at absolute humidity and 5% CO₂. Upon confluence, medium was removed and cells were detached using membrane buffer (HEPES 20 mM, pH = 7.4; MgCl₂ 10 mM; NaCl 100 mM). The suspension was sonicated for three cycles (15 sec, each) and centrifugated for 30 min at 50,000 × g and 4 °C. The remaining pellet was re-suspended in fresh membrane buffer and homogenized using a hand-potter. Protein content was determined by the method of Bradford [3].

S.1.2) Inhibition of radioligand-binding by E100 at histamine H₁ and H₄ receptors

Activity of E100 at the H₁R and H₄R was determined by incubation of 10 μM or 1 μM of compound for either 120 min with [³H]-pyrilamine and H₁R-membrane preparations (40 μg/well) or for 60 min with [³H]-histamine dihydrochloride and H₄R-membrane preparations (40 μg/well), respectively. Radiolabeled ligands were purchased from PerkinElmer (Boston, MA, USA). Therefore, E100 was diluted from DMSO-based stock solution (10 mM) in either membrane

References:

[1]Kottke T, Sander K, Weizel L, Schneider EH, Seifert R, Stark H. Receptor-specific functional efficacies of alkyl imidazoles as dual histamine H₃/H₄ receptor ligands. *Eur J Pharmacol.* 2011;654:200-208.

[2]Schneider EH, Seifert R. S19 cells: a versatile model system to investigate the pharmacological properties of G protein-coupled receptors. *Pharmacol Ther.* 2010;128:387-418.

[3]Bradford MM. A rapid and sensitive method for the quantitation of microgram quantities of protein utilizing the principle of protein-dye binding. *Anal Biochem.* 1976;72:248-254.

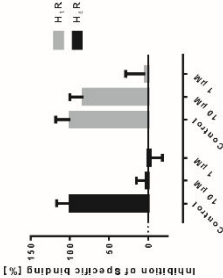
[4]Khanfar MA, Reiner D, Hagenow S, Stark H. Design, synthesis, and biological evaluation of novel oxadiazole- and thiazole-based histamine H₃ ligands. *Bioorg Med Chem.* 2018;26:4034-4046.

buffer for H₁R (as described above) or in membrane buffer for H₄R (TRIS 75 mM, EDTA 1 mM, pH = 7.4; MgCl₂ 12.5 mM). The procedure for harvesting and scintillation counting was as described previously [4]. Percentage of inhibition was calculated based on total (TB) and non-specific (NSB) binding levels of radioligand, according to:

$$\text{Inhibition}(\%) = [1 - (\text{remained binding} - \text{NSB}) / (\text{TB} - \text{NSB})] * 100\%$$

S.2) Results

S.2.1) Inhibition of radioligand-binding by E100 at histamine H₁ and H₄ receptors



4.7. The dual-active histamine H₃ receptor antagonist and acetylcholine esterase inhibitor E100 alleviates autistic-like behaviors and oxidative stress in valproic acid induced autism in mice

Nermin Eissa^{1),2)}, Sheikh Azimullah^{1),2)}, Petrilla Jayaprakash^{1),2)}, Richard L. Jayaraj^{1),2)}, David Reiner²⁾, Shreesh K. Ojha^{1),2)}, Rami Beiram^{1),2)}, Holger Stark²⁾, Dorota Łażewska³⁾, Katarzyna Kieć-Kononowicz³⁾, Bassem Sadek^{1),2)}

1) Department of Pharmacology & Therapeutics, College of Medicine and Health Sciences, United Arab Emirates University, P.O. Box 17666, Al Ain, United Arab Emirates

2) Zayed Center for Health Sciences, United Arab Emirates University, Al Ain P.O. Box 17666, UAE

3) Institute of Pharmaceutical and Medicinal Chemistry, Heinrich Heine University Düsseldorf, Universitätsstr. 1, 40225 Duesseldorf, Germany

4) Jagiellonian University-Medical College, Faculty of Pharmacy, Department of Technology and Biotechnology of Drugs, Medyczna 9 St., 30-688, Kraków, Poland

Published in: *International Journal of Molecular Sciences*, 2020, 21:3996.

DOI: 10.3390/ijms21113996

Contribution to research: Co-authorship. DR co-organised shipment of test-ligands, prepared, planned and conducted radioligand selectivity screenings at H₁R and H₄R, and evaluated corresponding data. DR proof-edited the manuscript.

Abstract:

The histamine H₃ receptor (H₃R) functions as auto- and hetero-receptors, regulating the release of brain histamine (HA) and acetylcholine (ACh), respectively. The enzyme acetylcholine esterase (AChE) is involved in the metabolism of brain ACh. Both brain HA and ACh are implicated in several cognitive disorders like Alzheimer's disease, schizophrenia, anxiety, and narcolepsy, all of which are comorbid with autistic spectrum disorder (ASD). Therefore, the novel dual-active ligand E100 with high H₃R antagonist affinity (hH₃R: K_i = 203 nM) and balanced AChE inhibitory effect (EeAChE: IC₅₀ = 2 M and EqBuChE: IC₅₀ = 2 M) was investigated on autistic-like sociability, repetitive/compulsive behaviour, anxiety, and oxidative stress in male C57BL/6 mice model of ASD induced by prenatal exposure to valproic acid (VPA, 500 mg/kg, intraperitoneal (i.p.)). Subchronic systemic administration with E100 (5, 10, and 15 mg/kg, i.p.) significantly and dose-dependently attenuated sociability deficits of autistic (VPA) mice in three-chamber behaviour (TCB) test (all p < 0.05). Moreover, E100 significantly improved repetitive and compulsive behaviors by reducing the increased percentage of marbles buried in marble-burying behaviour (MBB) (all p < 0.05). Furthermore, pre-treatment with E100 (10 and 15 mg/kg, i.p.) corrected decreased anxiety levels (p < 0.05), however, failed to restore hyperactivity observed in elevated plus maze (EPM) test. In addition, E100 (10 mg/kg, i.p.) mitigated oxidative stress status by increasing the levels of decreased glutathione (GSH), superoxide dismutase (SOD), and catalase (CAT), and decreasing the elevated levels of malondialdehyde (MDA) in the cerebellar tissues (all p < 0.05). Additionally, E100 (10 mg/kg, i.p.) significantly reduced the elevated levels of AChE activity in VPA mice (p < 0.05). These results demonstrate

the promising effects of E100 on in-vivo VPA-induced ASD-like features in mice, and provide evidence that a potent dual-active H₃R antagonist and AChE inhibitor (AChE-I) is a potential drug candidate for future therapeutic management of autistic-like behaviours.

Reprinted with permission from Eissa N, Azimullah S, Jayaprakash P, Jayaraj RL, Reiner D, Ojha SK, Beiram R, Stark H, Łażewska D, Kieć-Kononowicz K, Sadek B, The Dual-Active Histamine H₃ Receptor Antagonist and Acetylcholine Esterase Inhibitor E100 Alleviates Autistic-Like Behaviors and Oxidative Stress in Valproic Acid Induced Autism in Mice, *Int. J. Mol. Sci.*, 2020, 21:3996.

Copyright 2020 The Authors.

Article

The Dual-Active Histamine H₃ Receptor Antagonist and Acetylcholine Esterase Inhibitor E100 Alleviates Autistic-Like Behaviors and Oxidative Stress in Valproic Acid Induced Autism in Mice

Nermin Eissa ^{1,2}, Sheikh Azimullah ^{1,2}, Petrilla Jayaprakash ^{1,2}, Richard L. Jayaraj ^{1,2}, David Reiner ³, Shreesh K. Ojha ^{1,2}, Rami Beiram ^{1,2}, Holger Stark ³, Dorota Łażewska ⁴, Katarzyna Kieć-Kononowicz ⁴ and Bassem Sadek ^{1,2,*}

¹ Department of Pharmacology & Therapeutics, College of Medicine and Health Sciences, United Arab Emirates University, Al Ain P.O. Box 17666, UAE; 201690014@uaeu.ac.ae (N.E.); azim.sheikh@uaeu.ac.ae (S.A.); petrilla.jp@uaeu.ac.ae (P.J.); richardlj@uaeu.ac.ae (R.L.J.); shreeshojha@uaeu.ac.ae (S.K.O.); rbeiram@uaeu.ac.ae (R.B.)

² Zayed Center for Health Sciences, United Arab Emirates University, Al Ain P.O. Box 17666, UAE

³ Institute of Pharmaceutical and Medicinal Chemistry, Heinrich Heine University Düsseldorf, Universitätsstr. 1, 40225 Düsseldorf, Germany; David.Reiner@uni-duesseldorf.de (D.R.); stark@hhu.de (H.S.)

⁴ Department of Technology and Biotechnology of Drugs, Faculty of Pharmacy, Jagiellonian University-Medical College, Medyczna 9 St., 30-688 Kraków, Poland; dlazewska@cm-uj.krakow.pl (D.Ł.); mfkono@cyf-kr.edu.pl (K.K.-K.)

* Correspondence: bassem.sadek@uaeu.ac.ae; Tel.: +971-3-7137-512; Fax: +971-3-7672-033

Received: 22 April 2020; Accepted: 27 May 2020; Published: 3 June 2020



Abstract: The histamine H₃ receptor (H₃R) functions as auto- and hetero-receptors, regulating the release of brain histamine (HA) and acetylcholine (ACh), respectively. The enzyme acetylcholine esterase (AChE) is involved in the metabolism of brain ACh. Both brain HA and ACh are implicated in several cognitive disorders like Alzheimer's disease, schizophrenia, anxiety, and narcolepsy, all of which are comorbid with autistic spectrum disorder (ASD). Therefore, the novel dual-active ligand E100 with high H₃R antagonist affinity (hH₃R: K_i = 203 nM) and balanced AChE inhibitory effect (EeAChE: IC₅₀ = 2 μM and EqBuChE: IC₅₀ = 2 μM) was investigated on autistic-like sociability, repetitive/compulsive behaviour, anxiety, and oxidative stress in male C57BL/6 mice model of ASD induced by prenatal exposure to valproic acid (VPA, 500 mg/kg, intraperitoneal (i.p.)). Subchronic systemic administration with E100 (5, 10, and 15 mg/kg, i.p.) significantly and dose-dependently attenuated sociability deficits of autistic (VPA) mice in three-chamber behaviour (TCB) test (all *p* < 0.05). Moreover, E100 significantly improved repetitive and compulsive behaviors by reducing the increased percentage of marbles buried in marble-burying behaviour (MBB) (all *p* < 0.05). Furthermore, pre-treatment with E100 (10 and 15 mg/kg, i.p.) corrected decreased anxiety levels (*p* < 0.05), however, failed to restore hyperactivity observed in elevated plus maze (EPM) test. In addition, E100 (10 mg/kg, i.p.) mitigated oxidative stress status by increasing the levels of decreased glutathione (GSH), superoxide dismutase (SOD), and catalase (CAT), and decreasing the elevated levels of malondialdehyde (MDA) in the cerebellar tissues (all *p* < 0.05). Additionally, E100 (10 mg/kg, i.p.) significantly reduced the elevated levels of AChE activity in VPA mice (*p* < 0.05). These results demonstrate the promising effects of E100 on in-vivo VPA-induced ASD-like features in mice, and provide evidence that a potent dual-active H₃R antagonist and AChE inhibitor (AChEI) is a potential drug candidate for future therapeutic management of autistic-like behaviours.

Keywords: VPA-induced autism-like behaviors; mice; sociability; repetitive behaviors; anxiety histamine H₃R; antagonist; acetylcholine esterase inhibitor; E100; oxidative stress; cerebellum

1. Introduction

Autistic spectrum disorder (ASD) is a neurodevelopmental disorder with a large population prevalence, characterized by impairments in social interaction and restricted/repetitive behavioral pattern or interest [1,2]. Despite its increasing prevalence, the pathophysiology of ASD is still poorly understood [3,4]. The difficulty in understanding the pathophysiology of ASD lies in the complex involvement of several clinical and behavioral symptoms, making clinically accessible specific treatments for ASD often less effective [5,6]. Recent advances in drug developments focus on novel agents with multiple pharmacological effects for multifactorial diseases, such as ASD [7–9]. In search of sensitive and specific markers of ASD, numerous research efforts have focused on the study of various brain neurotransmitters [4]. Hence, assessment of the function of numerous brain neurotransmitters, e.g., histamine (HA), acetylcholine (ACh), serotonin (5-HT), dopamine (DA), γ -aminobutyric acid (GABA), and glutamate (Glu) in initial brain growth encourages to be an important area of research in the field of developing newer therapeutics [4,10–20]. Accordingly, the brain cholinergic neurotransmitter system with ACh has an essential role in controlling ASD-related behavioral features including attention [19], cognitive flexibility [20], social interaction [21], and stereotypical behaviors [9,16,18,22]. Preclinical as well as clinical evidences reveal the involvement of cholinergic system dysfunction in the phenotypic outcomes of ASD-related behavioral features, in both humans and animal models [23]. In ASD patients, there are significant irregularities in the brain cholinergic system. Anatomically there is abnormality in the number and structure of neurons in a basal forebrain cholinergic nucleus of patients diagnosed with ASD [24]. Additionally, a remarkable reduction in the level of choline, a precursor of the neurotransmitter ACh and agonist for nicotinic-cholinergic receptor, was reported in individuals diagnosed with ASD [25]. In addition, abnormalities in the levels of nicotinic ACh receptors were observed in several brain regions, e.g., neocortex, cerebellum, thalamus, and striatum, of patients diagnosed with ASD, with the chief abnormalities being the reduced levels of muscarinic receptors (M1 type) [26–28].

Several essential physiological functions e.g., sleep–wake cycle, energy and endocrine homeostasis, sensory and motor functions, cognition, and attention, are controlled by the brain histaminergic system, and as such, are all severely affected in neuropsychiatric disorders [4,29–32]. Histamine mediates its effects through binding to four known histamine receptor (HR) subtypes belonging to the family of G-protein-coupled receptors, and designated H1 to H4 receptors (H1R–H4R). The histamine H3 receptor (H3R) initially described in 1983 was found to be a constitutively active receptor mostly expressed in the brain and was evaluated pharmacologically to negatively regulate histamine synthesis and release, acting as presynaptic auto-receptors [33,34]. In addition, H3Rs functioning as hetero-receptors can also control the release of other neurotransmitters like ACh, Glu, GABA, 5-HT, and DA in various brain regions [35–39]. Moreover, it has been revealed that H3Rs are predominantly expressed in the central nervous system (CNS), while activation of H1R and H2R mediates slow excitatory postsynaptic potentials. Interestingly, few studies projected the use of HR antagonists in the therapeutic management of autistic behavior. Consequently, famotidine (a histamine H2R antagonist) was projected to be a possible treatment for ASD children [12], since famotidine was revealed to alleviate sociability deficits in a patient with schizophrenia [13], a brain disorder that shares various genetic factors and symptoms with ASD [14,15]. In addition, niaprazine (a histamine H1R antagonist) has weakened features such as unbalanced attention, resistance to alteration, and frustration in patients with ASD [40]. Furthermore, it has been proposed that histamine H3R antagonists are of potential therapeutic future for the treatment of several brain disorders, e.g., Alzheimer’s disease (AD), schizophrenia, and narcolepsy [29–32]. Accordingly and in an animal model of schizophrenia, H3R antagonist was found to ameliorate behavioral deficiencies, including spatial working memory deficit, an abnormality also found in ASD patients [32]. Besides, antagonism of histamine H3Rs was found to reduce social behavior deficits in rodents exposed to phencyclidine, signifying the promising potential use of H3R antagonist in the therapeutic management of ASD [31,32]. Additionally, ciproxifan, an old-generation H3R antagonist,

4.7 The dual-active histamine H₃ receptor antagonist and acetylcholine esterase inhibitor E100 alleviates autistic-like behaviors and oxidative stress in valproic acid induced autism in mice

Int. J. Mol. Sci. 2020, 21, 3996

3 of 22

was found to attenuate impaired sociability and stereotypies in animal model of ASD in which rodents were exposed to valproic acid (VPA) [1].

During pregnancy, environmental risk factors may affect the inflammatory response of new-borns, hence altering postnatal brain development [41]. VPA as an environmental risk factor showed activation in different brain regions, with evidence of long-lasting glia activation in the hippocampus and the cerebellum [42], which are two brain regions associated with autism-related features, namely social interaction and repetitive behaviours [41,43]. Moreover, numerous preclinical experiments indicated that inflammation in the cerebellum may change social behaviours in adult mice, since cerebellum was found to be involved in executive and cognitive behavioural functions [43–45]. Interestingly and based on neuropathological findings of several studies on autism post-mortem brains, cerebellum has been identified as one of the key brain regions that can play role in autistic features [46], and substantial accumulating evidence has linked the cerebellum with higher cognitive functions [47]. Moreover, the cerebellum is being considered a key structure within the social circuitry [48]. Furthermore, valproic acid as an environmental risk factor showed activation in different brain regions, with evidence of long-lasting glia activation in the hippocampus and the cerebellum [49], which are two brain regions linked to autism-related behaviour, namely social interaction and repetitive behaviours [46–52].

Considering the aforementioned preclinical as well as clinical results, H₃Rs represent a promising target for developing new dual-active compounds with the potential role in neuropsychiatric multi-neurotransmitter disorders, e.g., AD, cognitive deficit accompanying schizophrenia and ASD [1,29,53–55]. Given the involvement of AChE and H₃-auto- and hetero-receptors in the modulation of several central neurotransmitters including ACh and H₃A, dual-active AChE inhibitors (AChEIs) and H₃R antagonists have been developed by several groups [56–62]. Therefore, we describe the effects of a novel dual-active AChE inhibitor and H₃R antagonist E100 (1-(7-(4-chlorophenoxy) heptyl) homo-piperidine) with balanced acetylcholine esterase inhibitory effect (*Ee*AChE: IC₅₀ = 2 µM and *Eq*BuChE: IC₅₀ = 2 µM), histamine H₃ receptor (H₃R) antagonist affinity (*h*H₃R K_i = 203 nM), and high selectivity profile towards H₃R subtype (Figure 1) in male C57BL/6 mice model of ASD, induced by prenatal exposure to VPA (500 mg/kg, i.p.). Moreover, the effects of E100 on locomotor activity and anxiety-like behaviors of the same animals were tested in the elevated plus-maze (EPM), since anxiety and motor activity can influence the performance of animals [62]. Furthermore, the effects of E100 on AChE activity and oxidative stress markers were assessed in the cerebellum, as it is involved in executive and cognitive functions and exaggerated oxidative stress may alter social behavior in adult mice [4,46]. In addition, the ability of the H₁R antagonist mepyramine (MPA), H₂R antagonist zolantidine (ZLT), H₃R agonist (*R*)-α-methylhistamine (RAM), and cholinergic muscarinic antagonist scopolamine (SCO) to reverse the effects provided by E100 were evaluated to clarify whether brain HA and ACh are involved in the effects exhibited by E100.

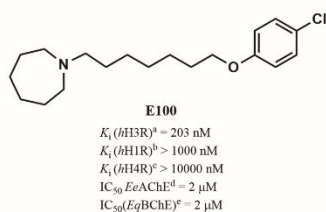


Figure 1. Chemical structure of the dual-acting human H₃R (*h*H₃R) antagonist and AChE inhibitor E100 and in vitro data with regard to *h*H₁-, *h*H₃-, and *h*H₄R, *Ee*AChE, and *Eq*BuChE. ^{a,b,c} Binding assays to determine affinity to H₁-, H₃-, and H₄Rs were performed in differently expressed cells as previously described n = 3 [59]. ^d AChE: Acetylcholine esterase; *Ee*: electric eel; ^e BuChE: Butyrylcholinesterase; *Eq*: equine [63–65].

2. Results

2.1. Effects of E100 on Sociability Impairments in Three-Chamber Behaviour (TCB) Test and Stereotyped Repetitive Behavior in Marble-Burying Behaviour (MBB)

The effect of systemic injection of E100 (5, 10, and 15 mg/kg, i.p.) and donepezil (DOZ; 1 mg/kg, i.p.) on ASD-like sociability impairments in the three-chamber behaviour (TCB) task and stereotyped repetitive behavior in marble burying behavior (MBB) in VPA-exposed mice (VPA mice) are shown in Figure 2A,B. There was a statistically significant difference between groups as determined by statistical analyses ($F_{(7,48)} = 5.118$, $p < 0.01$). As observed in the Tukey post hoc analyses, VPA mice exhibited significantly lower sociability expressed as sociability index (SI) when compared to saline-exposed control mice (CNT), with SIs of (-0.07 ± 0.05) and (0.40 ± 0.07) , respectively ($p < 0.01$) (Figure 2A). However, E100 (5, 10, and 15 mg/kg) significantly increased SI of VPA mice with SI values of (0.22 ± 0.08) , (0.44 ± 0.08) , and (0.40 ± 0.09) when compared to VPA mice with a SI of (-0.07 ± 0.05) (all $p < 0.05$) (Figure 2A). The results revealed that the enhancement in SI observed with E100 (10 mg/kg, SI = 0.44 ± 0.08) was statistically comparable to that shown with DOZ (1 mg/kg, SI = 0.39 ± 0.07 , $p = 0.99$) (Figure 2A). Moreover, there was a statistically significant difference between tested groups in the abrogative study ($F_{(10,66)} = 5.454$, $p < 0.01$) (Figure 2B). Interestingly, the E100-provided improvement of sociability was counteracted following co-administration with RAM (10 mg/kg, i.p.), ZLT (10 mg/kg, i.p.), or SCO (0.3 mg/kg, i.p.), with SI values of (0.05 ± 0.04) , (0.16 ± 0.03) , and (0.18 ± 0.05) , respectively ($p < 0.05$). However, co-administration of the CNS-penetrant H1R antagonist MPA (10 mg/kg, i.p.) with SI value of (0.40 ± 0.10) , $p = 1.00$ failed to reverse the E100 (10 mg/kg)-provided sociability enhancement observed in the E100 (10 mg/kg)-treated VPA animals (Figure 2B). Notably, subchronic treatment of CNT mice with E100 (10 mg/kg, i.p.), RAM (10 mg/kg, i.p.), MPA (10 mg/kg, i.p.), ZLT (10 mg/kg, i.p.), or SCO (0.3 mg/kg, i.p.) had no significant influence on SI compared to saline-pretreated CNT mice, with SI values of (0.36 ± 0.06) , $p = 1.00$, (0.42 ± 0.08) , $p = 1.00$, (0.38 ± 0.07) , $p = 1.00$, (0.39 ± 0.07) , $p = 1.00$, and (0.35 ± 0.06) , $p = 1.00$, respectively (Figure 2B).

In the marble-burying behaviour (MBB) and as determined by statistical analyses, there was a significant difference between all groups assessed ($F_{(7,32)} = 5.797$, $p < 0.01$). Statistical post hoc analyses showed that VPA mice ($58.00 \pm 4.81\%$, $p < 0.01$) buried significantly more marbles compared to the CNT animals ($26.00 \pm 4.55\%$) tested in MBB (Figure 2C). However, E100 (10 or 15 mg/kg, i.p.) and DOZ (1 mg/kg, i.p.) significantly reduced the increased percentage of marbles buried by VPA mice when compared to saline-treated VPA mice, with $(27.00 \pm 4.60\%)$, $p < 0.01$, $(27.00 \pm 3.34\%)$, $p < 0.01$, and $(37.00 \pm 4.37\%)$, $p < 0.01$, respectively (Figure 2C). Moreover, there was a statistically significant difference between tested groups in the abrogative study with ($F_{(10,44)} = 5.935$, $p < 0.01$) (Figure 2D). The E100 (10 mg)-provided a decrease in the percentage of buried marbles ($27.00 \pm 4.60\%$) was entirely abrogated by co-administration of RAM ($60.00 \pm 5.28\%$, $p < 0.05$), ZLT ($53.00 \pm 8.30\%$, $p < 0.05$), and SCO ($52.00 \pm 7.94\%$, $p < 0.05$), respectively (Figure 2D). However, MPA ($29.00 \pm 3.84\%$, $p = 1.000$) failed to counteract the E100 (10 mg)-provided effect ($27.00 \pm 4.60\%$) on VPA (Figure 2D). Notably, subchronic treatment of CNT mice with E100 (10 mg/kg, i.p.), RAM (10 mg/kg, i.p.), MPA (10 mg/kg, i.p.), ZLT (10 mg/kg, i.p.), or SCO (0.3 mg/kg, i.p.) had no significant influence on percentage of buried marbles compared to saline-pretreated CNT mice, with $(24.00 \pm 2.96\%)$, $p = 1.00$, $(27.20 \pm 4.63\%)$, $p = 1.00$, $(25.80 \pm 4.22\%)$, $p = 1.00$, $(28.40 \pm 5.04\%)$, $p = 1.00$, and $(27.40 \pm 3.00\%)$, $p = 1.00$, respectively (Figure 2D).

4.7 The dual-active histamine H₃ receptor antagonist and acetylcholine esterase inhibitor E100 alleviates autistic-like behaviors and oxidative stress in valproic acid induced autism in mice

Int. J. Mol. Sci. 2020, 21, 3996

5 of 22

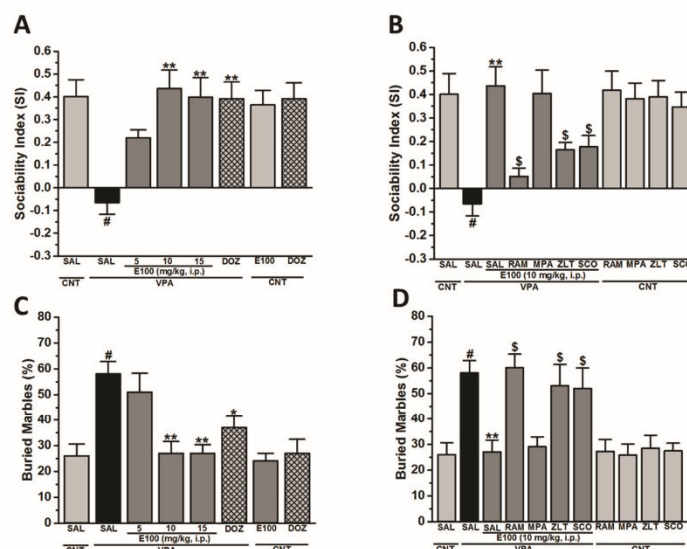


Figure 2. E100 improved sociability in three-chamber behaviour (TCB) and repetitive behavior in marble-burying behaviour (MBB) paradigms. **(A,B)** Following acclimatization for a duration of 10 min, male mice were allowed to explore all three chambers for 10 min. The obtained results were expressed in form of Sociability index (SI). Control (CNT) mice received systemic injections of saline (group 1), E100 (10 mg/kg) (group 7), and donepezil (DOZ) (1 mg/kg) (group 8), whereas VPA mice were injected with saline (group 2), E100 (5, 10, and 15 mg/kg) (groups 3–5), or DOZ (1 mg/kg, i.p.) (group 6) subchronically for 21 days **(A)**. Abrogative studies of subchronic (21 days) systemic co-injection of RAM (10 mg/kg, i.p. for group 9), mepyramine (MPA) (10 mg/kg, i.p. group 10), zolantidine (ZLT) (10 mg/kg, i.p., for group 11), or scopolamine (SCO) (0.3 mg/kg, i.p., for group 12) on the E100 (10 mg)-provided improvement of sociability of VPA mice were assessed **(B)**. Marble-burying behavior (MBB) was measured after a 30-min testing session applying the same treatments. VPA mice treated with saline (group 2) displayed significantly increased repetitive behaviors when compared to CNT mice (group 1). E100 (5, 10, or 15 mg/kg, i.p.) or DOZ (1 mg/kg, i.p.) were injected systemically and subchronically for 21 days in VPA mice **(C)**. Effects of subchronic (21 days) systemic co-administration of RAM (10 mg/kg, i.p., group 9), MPA (10 mg/kg, i.p., group 10), ZLT (10 mg/kg, i.p., group 11), or SCO (0.3 mg/kg, i.p., group 12) on the E100(10 mg)-provided attenuation of stereotyped repetitive behavior of VPA mice were assessed MBB **(D)**. CNT mice were injected with saline, E100 (10 mg/kg, i.p.), DOZ (1 mg/kg, i.p.), RAM (10 mg/kg, i.p.), MPA (10 mg/kg, i.p.), ZLT (10 mg/kg, i.p.), or SCO (0.3 mg/kg, i.p.) **(D)**. Data are expressed as the mean \pm standard errors of the means (SEM) ($n = 7$ for TCB and $n = 5$ for MBB). 8 groups of 7 mice per group in TCB **(A,B)** and 8 groups of 5 mice per group in MBB **(C,D)** were used. The effects of E100 were analyzed using two-way analysis of variance (ANOVA) with dose of drugs and animals (either VPA or CNT mice) as the between-subjects factor, and post hoc comparisons were performed with Tukey's test in case of a significant main effect. # $p < 0.05$ vs. CNT mice. ** $p < 0.01$ vs. saline-treated VPA mice. $^{\$}$ $p < 0.05$ vs. E100 (10mg)-treated VPA mice.

2.2. Effects of E100 on Anxiety Levels and Locomotor Activity of Valproic Acid (VPA)-Exposed Mice in Elevated Plus Maze (EPM) Test

Figure 3A–F shows the observed effects of E100 (5, 10, or 15 mg/kg, i.p.) on the anxiety levels (the time spent (Figure 3A) and the number of entries into open arms (Figure 3B) of VPA mice assessed in the EPM test. Additionally, the locomotor activity expressed as the number of entries into closed arms (Figure 3C) was simultaneously evaluated in the same EPM test. Moreover, the abrogative effects of systemic co-administration of RAM, MPA, ZLT, or SCO on the E100-provided effects were tested

(Figure 3D–F). The studies have been conducted for 5 min each. The results observed for the time spent and number of entries into open arms revealed a statistically significant difference between groups with ($F_{(10,55)} = 5.505$, $p < 0.01$) for time spent and ($F_{(10,55)} = 7.339$, $p < 0.01$) for number of entries (Figure 3A,B). Statistical post hoc analyses showed that VPA mice spent significantly less time (19.00 ± 4.46 s, $p < 0.05$) and displayed a lower number of entries (1.60 ± 0.37 , $p < 0.01$) in open arms when compared to CNT mice with time spent (60.00 ± 7.02 s) and number of entries (5.50 ± 0.66) (Figure 3A,B). However, subsequent post hoc analyses revealed that E100 when administered at 10 or 15 mg/kg significantly altered the time spent exploring the open arms of the maze during a 5 min session compared to saline-treated VPA mice, with (50.17 ± 4.21 s, $p < 0.05$) and (54.67 ± 8.00 s, $p < 0.05$), respectively (Figure 3A). Moreover, post hoc evaluation revealed that E100 when administered at 10 or 15 mg/kg i.p. significantly increased the number of entries into the open arms of the maze during a 5 min session compared to saline-treated VPA mice, with (3.67 ± 0.54 , $p < 0.05$) and (4.33 ± 0.51 , $p < 0.05$), respectively (Figure 3B). However, E100 (5 mg/kg) failed to alter time spent and number for entries into open arms of VPA mice, with (20.98 ± 3.00 s, $p = 0.57$) and (2.41 ± 0.37), respectively, and as compared with VPA mice with (19.00 ± 4.46 s) and (1.60 ± 0.37) for time spent and number of entries, respectively (Figure 3A,B). Interestingly, VPA mice pretreated with DOZ (1 mg) spent significantly longer time exploring the open arms compared to saline-treated VPA mice, with (47.17 ± 4.46 s, $p < 0.01$) (Figure 3A). Further analyses of data describing the number of entries into the open arms of the maze yielded practically the same results for DOZ (1 mg/kg, i.p.), with (4.67 ± 0.73 , $p < 0.01$) (Figure 3B). On the other hand, VPA mice entered the closed arms significantly more often than CNT mice, with (11.83 ± 1.22 , $p < 0.01$) (Figure 3C). Besides, subchronic treatment of CNT mice with E100 (10 mg/kg, i.p.) or DOZ (1 mg/kg, i.p.) had no significant influence on time spent in open arms (Figure 3A), number of entries into open (Figure 3B) or into closed arms (Figure 3C) compared to saline-pretreated CNT mice (all $p > 0.05$). Interestingly, the E100 (10 mg)-provided increase in the time spent in open arms (Figure 3D), and the number of entries into open arms (Figure 3E) was entirely abrogated by co-administration of RAM ($p < 0.05$). However, MPA, ZLT, and SCO failed to counteract the E100 (10 mg)-provided effect on VPA mice (Figure 3D,E). Notably, the number of closed arm entries following subchronic systemic injection of E100 (5, 10, or 15 mg/kg) and DOZ (1 mg/kg, i.p.) was not significantly different as compared to saline-treated VPA mice, with (10.50 ± 0.75 , $p = 0.99$), (9.50 ± 0.81 , $p = 0.88$), (10.50 ± 1.45 , $p = 0.99$), and (11.33 ± 1.24 , $p = 1.00$), respectively (Figure 3C,F).

2.3. Effect of E100 on Oxidative Stress Levels in Cerebellar Tissues of VPA-Exposed Mice

As determined by statistical analysis, there was a significant difference between all groups assessed on the levels of MDA (malondialdehyde, $F_{(4,20)} = 5.505$, $p < 0.01$), GSH (glutathione, $F_{(4,20)} = 7.399$, $p < 0.01$), SOD (superoxide dismutase, $F_{(4,20)} = 8.586$, $p < 0.01$), and CAT (catalase, $F_{(4,20)} = 8.057$, $p < 0.01$) of VPA mice and following subchronic systemic administration of saline, E100 (10 mg/kg, i.p.), or DOZ (1 mg/kg, i.p.) (Figure 4A–D). The results showed that MDA was significantly increased (109.14 ± 10.84 µg/mg protein, $p < 0.05$) and GSH (16.16 ± 1.19 µg/mg protein, $p < 0.05$), SOD (8.66 ± 1.43 U/mg protein, $p < 0.05$), and CAT (13.24 ± 0.96 nmol/min/mg protein, $p < 0.05$) were significantly reduced in the cerebellum of VPA mice compared to CNT mice, with (57.66 ± 8.79 µg/mg protein) for MDA, (54.30 ± 5.59 µg/mg protein) for GSH, (35.72 ± 3.44 U/mg protein) for SOD, and (20.01 ± 0.37 nmol/min/mg protein) for CAT (Figure 4A–D). However, cerebellum of VPA mice pretreated with E100 (10 mg/kg, i.p.) displayed a significant reduction of MDA (39.69 ± 3.89 µg/mg protein, $p < 0.001$) as well as significant elevation of GSH (57.88 ± 8.23 µg/mg protein, $p < 0.001$), SOD (28.15 ± 4.82 U/mg protein, $p < 0.01$), and CAT (20.51 ± 0.73 nmol/min/mg protein, $p < 0.05$), and as compared with saline-treated VPA mice (Figure 4A–D). Similarly, cerebellum of VPA mice pretreated with DOZ (1 mg/kg, i.p.) showed a significant reduction of MDA (58.43 ± 14.00 µg/mg protein, $p < 0.05$) as well as significant increase of GSH (51.59 ± 7.51 µg/mg protein, $p < 0.001$), SOD (23.12 ± 3.66 U/mg protein, $p < 0.05$), and CAT (18.77 ± 0.84 nmol/min/mg protein, $p < 0.05$), and as compared with saline-treated VPA mice (Figure 4A–D). Moreover, systemic co-administration of RAM (10 mg/kg,

4.7 The dual-active histamine H₃ receptor antagonist and acetylcholine esterase inhibitor E100 alleviates autistic-like behaviors and oxidative stress in valproic acid induced autism in mice

Int. J. Mol. Sci. 2020, 21, 3996

7 of 22

i.p.) partially abrogated the E100 (10 mg)-provided decrease against the VPA-induced increase in the level of MDA ($82.26 \pm 10.80 \mu\text{g}/\text{mg}$ protein, $p = 0.01$) (Figure 4A), and it also partially reversed the E100 (10 mg)-provided increases in GSH ($32.18 \pm 3.22 \mu\text{g}/\text{mg}$ protein, $p = 0.03$), SOD concentrations ($12.32 \pm 3.08 \text{ U}/\text{mg}$ protein, $p = 0.04$), and CAT ($15.05 \pm 1.68 \text{ nmol}/\text{min}/\text{mg}$ protein, $p = 0.02$) in VPA mice (Figure 4B–D).

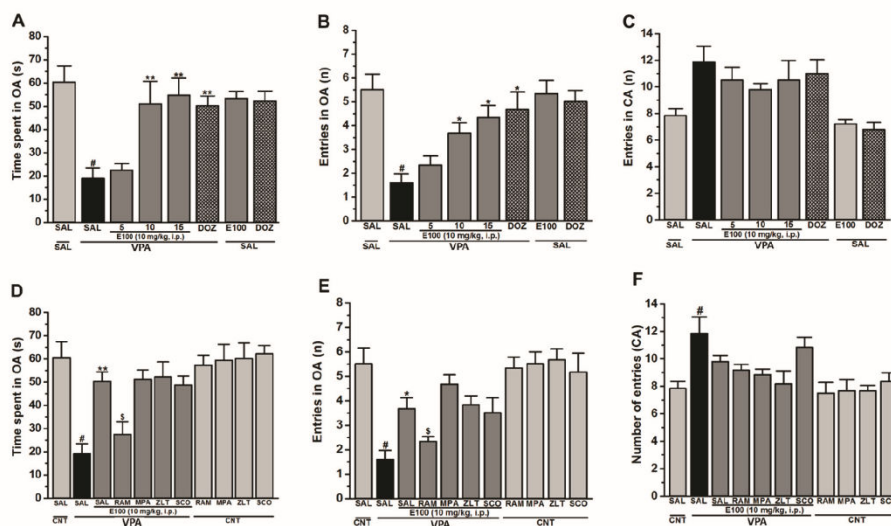


Figure 3. E100 ameliorated fear-related behavior without affecting locomotor activity in elevated plus maze (EPM). VPA mice injected with saline (group 2) displayed significantly increased deficits in cognitive behaviors compared to CNT mice (group 1). Test compound E100 (5, 10, or 15 mg/kg, i.p.) or DOZ (1 mg/kg) were injected for 21 days to VPA mice (subchronic). E100 (10 and 15 mg/kg, groups 4 and 5) and DOZ (1 mg/kg, group 6) attenuated the decreased time spent on the open arms, however, failed to modify the increased number of entries into the closed arms of the EPM (A–C). Abrogative effects of subchronic (21 days) systemic co-administration of RAM (10 mg/kg, group 9), MPA (10 mg/kg, group 10), ZLT (10 mg/kg, group 11), or SCO (0.3 mg/kg, group 12) on the E100 (10 mg)-provided improvement in number and time spent for open arms of VPA mice were measured (D,E). Number of entries into closed arms was elevated in saline-treated VPA mice (group 2) when compared to saline-treated CNT mice (group 1). E100 (5, 10, and 15 mg/kg) and DOZ failed to modulate the increased number of entries into closed arms (C,F). Additionally, CNT mice treated with E100 (10 mg/kg, group 7) did not show significant difference in number of entries into closed arms when compared with saline-treated CNT mice (group 1). Data are expressed as the mean \pm SEM ($n = 6$). # $p < 0.05$ vs. CNT mice. * $p < 0.05$ vs. Saline-treated VPA mice. ** $p < 0.01$ vs. saline-treated VPA mice. \$ $p < 0.05$ vs. E100 (10mg)-treated VPA mice. In the EPM test, 8 groups of 6 mice per group were used. The effects of E100 were analyzed using two-way analysis of variance (ANOVA) with dose of drugs and animals (either VPA or CNT mice) as the between-subjects factor, and post hoc comparisons were performed with Tukey's test in case of a significant main effect (A–D).

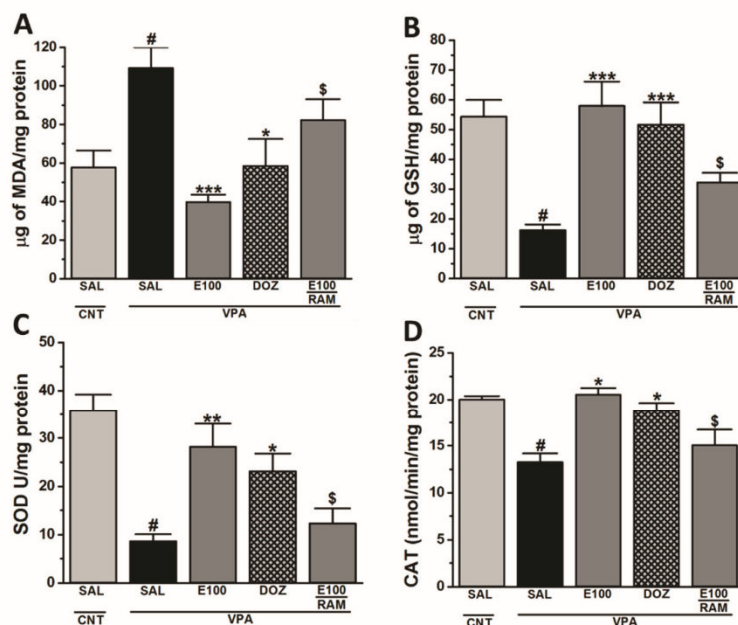


Figure 4. E100 restored levels of oxidative stress markers in the cerebellum. Modulated malondialdehyde (MDA), glutathione (GSH), catalase (CAT), and superoxide dismutase (SOD) were assessed. VPA mice showed a significant increase in MDA (A) and significant decrease in GSH (B), SOD (C), and CAT (D) compared to CNT mice. Subchronic systemic administration of E100 (10 mg/kg) or DOZ (1 mg/kg) were assessed in VPA mice. E100 (10 mg/kg) or DOZ (1 mg/kg) significantly reduced the increased levels of MDA (A) and significantly increased the reduced levels of GSH, SOD and CAT (A–D). Abrogative effects of subchronic (21 days) systemic co-administration with RAM (10 mg/kg) on modulation of oxidative stress levels provided by E100 (10 mg) were assessed (A–D). Data are expressed as the mean \pm SEM ($n = 5$). [#] $p < 0.05$ vs. VPA mice. ^{*} $p < 0.05$ vs. VPA mice. ^{**} $p < 0.01$ vs. VPA mice. ^{***} $p < 0.001$ vs. VPA mice. ^{\$} $p < 0.01$ vs. E100 (10 mg)-treated VPA mice. In biochemical assessments, 5 groups of 5 mice per group were used. The effects of E100 were analyzed using two-way analysis of variance (ANOVA) with dose of drugs and animals (either VPA or CNT mice) as the between-subjects factor, and post hoc comparisons were performed with Tukey's test in case of a significant main effect (A–D).

2.4. Effect of E100 on Acetylcholine Esterase Activity in Cerebellum Tissues of VPA-Exposed Mice

As determined by statistical analyses, there was a significant difference between groups assessed on the levels of AChE ($F_{(3,15)} = 4.176$, $p < 0.05$) (Figure 5). The observed results showed that VPA mice exhibited a significant increase in the activity of AChE enzyme in cerebellum (426.72 ± 31.20 nmol/min/mg protein, $p < 0.05$) when compared to CNT mice (291.87 ± 33.34 nmol/min/mg protein) (Figure 5). However, subchronic systemic treatment of VPA mice with E100 (10 mg/kg, i.p.) significantly decreased the AChE activity of VPA mice (282.87 ± 36.13 nmol/min/mg protein, $p < 0.05$) when compared with the saline-treated VPA mice (426.72 ± 31.20 nmol/min/mg protein) (Figure 5). Similarly, subchronic systemic pretreatment with the reference drug DOZ (1 mg/kg, i.p.) significantly decreased the AChE activity of VPA mice (326.16 ± 24.09 nmol/min/mg protein, $p < 0.05$) when compared with the saline-treated VPA mice (426.72 ± 31.20 nmol/min/mg protein) (Figure 5).

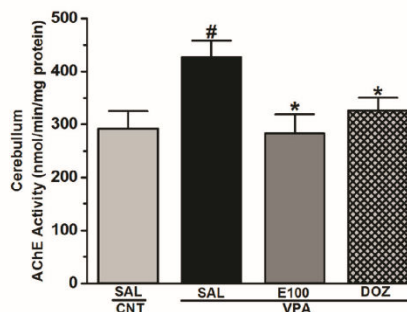


Figure 5. Effects of E100 on acetylcholine esterase activity in cerebellum tissues of valproic acid (VPA)-exposed mice. Inhibitory effects of E100 (10 mg/kg, i.p.) on acetylcholine esterase enzyme in the cerebellum of VPA mice. Quantitative analysis revealed a significant increase ($^{\#} p < 0.05$) in the acetylcholine esterase enzyme activity in cerebellum of VPA mice compared to the CNT mice. However, subchronic treatment with E100 (10 mg/kg, i.p.) or DOZ (1 mg/kg, i.p.) to the VPA mice significantly reduced ($* p < 0.05$) this activity compared to the VPA mice. Values are expressed as the percent mean \pm SEM. For assessment of AChE activity 4 groups were used. 4 CNT mice were used for saline group and 5 VPA mice were used for each treatment group. The effects of E100 were analyzed using two-way analysis of variance (ANOVA) with dose of drugs and animals (either VPA or CNT mice) as the between-subjects factor, and post hoc comparisons were performed with Tukey's test in case of a significant main effect.

3. Discussion

Alteration in brain histaminergic and cholinergic neurotransmissions is supposed play a critical role in the clinical results of ASD-related behavioural features [1,25,66]. Consequently, the aim of the current study was to assess the modulating effects of the novel dual-acting AChEI and H₃R antagonist E100 on brain HA and ACh applying a mouse model VPA-induced ASD-like behaviors. Our findings show that E100 significantly and dose-dependently improved sociability deficits in TCB paradigm and stereotypies in MBB paradigm in VPA mice. In the TCB paradigm, systemic pretreatment with E100 ameliorated the impairment in sociability demonstrated by VPA mice, since these animals, when pretreated with E100, showed significantly higher SI, with observed levels similar to the CNT mice. Various previous studies have focused on the procognitive effects of several H₃R antagonists on social memory [67–70], a behavioral feature that is also altered in ASD [69]. Moreover, previous reports suggested that an impaired cholinergic system causes cognitive problems that may include social problems, which were reversed by donepezil treatments [71,72]. Importantly, the sociability-enhancing effect observed for E100 was dose-dependent, since E100 (10 mg/kg) showed an optimum effect comparable to that provided by the reference drug DOZ. Contrarily, a dose of 15 mg/kg E100 did not further improve upon the E100 (10mg)-provided sociability enhancement. The observations for the dose-dependent effects of E100 are in line with our recent studies observed with a non-imidazole-based H₃R antagonist on VPA-induced ASD in Tuck-Ordinary mice [73], and an imidazole-based H₃R antagonist in preclinical experiments in different rodents [1]. Moreover, the observations of sociability-enhancing effects for E100 aligns with earlier experimental results observed with the imidazole based H₃R antagonist ciproxifan in Swiss mice [1], and comprehend our previously observations in which E100 enhanced social novelty in mice [63]. The mechanism behind E100-provided sociability improvement is unclear. Still, it might be explained by its dual action with the capability of H₃R antagonists to mediate the release of different neurotransmitters other than histamine, such as DA, 5-HT, and ACh, in specific brain regions [74], together with its AChE inhibitory property that results in correction of abnormal cholinergic transmission. Interestingly, the E100-provided enhancing effects on sociability were reversed when mice were co-administered the H₃R agonist RAM, the H₂R antagonist ZLT, or with muscarinic

cholinergic antagonist SCO, but not with the centrally acting H₁R antagonist MPA, indicating that HA and ACh, through activation of postsynaptically located H₂Rs (but not H₁Rs) and muscarinic cholinergic receptors, respectively, obviously contribute to neuronal pathways important for alteration of sociability processes in the TCB paradigm in VPAmice. Therefore, considering the levels of different brain neurotransmitters, including HA and ACh, in various brain areas of the VPA-exposed mice with ASD-like behaviors as well as when pretreated with E100 would further assist in understanding the neural intersections involved in the observed behavioral enhancement. This is *in vivo* evidence that a simultaneous interaction with the above two targets leads to symptomatic *in vivo* enhancements of behavioral autistic-like parameters in mice. However, the mitigating effects observed for the dual-acting compound E100 are not due to either its AChE-inhibiting or to its H₃R-blocking properties alone, since it neither acts purely as an H₃R antagonist DL77 (non-imidazole based H₃R antagonist [73]) or ciproxifan (an imidazole-based H₃R antagonist [1]) nor as an AChEI such as DOZ (used as a reference drug in the current study). Notably, the postulated advantage of a dual-acting compound (e.g., E100) with combined affinities at the required targets over co-administration of two drugs are the straightforward single-compound pharmacokinetics. Thereby, putative drug–drug interactions occurring with combination therapy might be avoided. Conclusively, the dose-finding for co-application of two different drugs can be bypassed which would become necessary since the effective doses might be considerably different from the ones applied in the case of monotherapy, especially in multifactorial disorders like ASD. Whether the above mitigation of autistic-like behaviors is also induced after administration of H₃R antagonist or co-administration of an H₃R antagonist and an AChEI was beyond the scope of this project and will require dose-finding experiments for several ratios of the combination of AChEIs and H₃R antagonist.

Repetitive behavior and restricted interests are considered as core features of patients with ASD [75,76]. In previous preclinical studies, abnormalities in histaminergic signalling was found to contribute to rare diseases such as Tourette syndrome [77], a condition featured by stereotypies and described to be among the most commonly comorbid neurodevelopmental disorders with ASD [1,63,73]. The results observed in the present study showed that VPA mice pretreated with E100 (10 or 15 mg) or with the reference drug DOZ (1 mg) demonstrated similar decreases in repetitive behavior when tested in MBB test, and the E100 (10 mg)-provided effects in MBB were nullified when mice were co-administered with RAM, ZLT, or SCO, but not with MPA. The mechanism by which the repetitive/compulsive behavior is improved following systemic administration with E100 could be explained with the capability of E100 to modulate the brain levels of different neurotransmitters in several specific brain areas besides HA and ACh, such as DA and 5-HT, through antagonist interaction of E100 with histamine H₃ heteroreceptors expressed on dopaminergic and serotonergic neurons [78–80]. Furthermore, the results observed for E100 in MBB mirror a previous study in which acute systemic administration of the non-imidazole H₃R antagonist DL77 significantly decreased the number of buried marbles in adult male Tuck-Ordinary mice of VPA-induced ASD features [73]. Interestingly, the results observed for E100 on repetitive behavior in MBB comprehend our previously observations for E100 in nestlet shredding behavioral test, a test that also evaluates repetitive/obsessive compulsive paradigm in rodents [63].

The effects of systemic administration with E100 on locomotion as well as anxiety levels were tested as pharmacological compounds that are able to modulate anxiety levels or locomotor activity may give rise to a false-positive effect in these behavioral paradigms. Therefore, locomotor activity was assessed simultaneously to exclude possible intrinsic deficits of spontaneous locomotor activity. Consequently, the numbers of entries into the closed arms were used as indicators of locomotor activity, while time spent and number of entries into open arms provided indications about anxiety levels in the EPM test. The results showed that E100 (10 or 15 mg) reduced elevated anxiety levels in VPA mice, similarly as DOZ (1 mg), measured by the time spent in open arms and number of open arms entries. However, pretreatment of VPA mice with E100 (5, 10, or 15 mg) or DOZ (1 mg/kg) did not alter a locomotor activity as measured by number of entries into closed arms. Moreover,

subchronic co-administration of VPA mice with the most promising dose E100 (10 mg/kg, i.p.) and RAM, MPA, ZLT, or SCO had no significant influence on the number of closed arm entries compared to saline-pretreated CNT mice. Furthermore, subchronic systemic injection of CNT mice with the most promising dose E100 (10 mg/kg, i.p.) failed to modify locomotor activity of CNT mice in EPM test. These results comprehend our previously observations for E100 in open field assessment [63]. Thus, the improvements in sociability and repetitive/compulsive behaviors observed for E100 in TCB and MBB, respectively, appear unlikely to be associated with a modulating effect in locomotor activity of the tested mice. Moreover, the E100 (10 mg)-provided effects on anxiety-like behaviors of treated mice were nullified when mice were co-administered with RAM, but not with MPA, ZLT, or SCO, indicating that postsynaptic histaminergic receptor subtypes (H1Rs and H2Rs) and postsynaptic muscarinic cholinergic receptors are not involved in the E100-provided effects on anxiety-like behavior of VPA mice. However, the H3R agonist RAM abrogated the effects provided by E100, demonstrating that E100 may exerted its effects on anxiety-like behaviors VPA mice through modulation of several other neurotransmitters, such as serotonin [80,81], glutamate, and GABA [82–84], that are reported to be imbalanced in ASD patients. These results were in accordance with previous results that revealed anxiolytic-like effects of a non-imidazole-based H3R antagonist as well as UW-MD-71 with no differences in spontaneous locomotor activity [56,57,85].

Previous studies revealed that imidazole-based H3R antagonists, namely clobenpropit and ciproxifan, mitigated several oxidative stress markers (e.g., MDA and GSH) in amphetamine- or dizocilpine-augmented oxidative stress in a preclinical mice model of schizophrenia, signifying the protective effects of H3R antagonists in such conditions [86,87]. In the current study, the results showed that VPA mice with ASD-like behavioral features displayed significant increase in MDA, with a concomitant decline in GSH, SOD, and CAT in the cerebellum tissues, and several previous studies showed that cerebellum is significantly involved in executive and cognitive functions [39,42,43,83]. The observed results for E100 (10 mg/kg) and DOZ (1 mg/kg) showed a significant reduction of MDA as well as a significant elevation of GSH, SOD, and CAT. Moreover, systemic co-administration with RAM (10 mg) reversed the E100 (10 mg)-provided modulating effects on MDA, GSH, SOD, and CAT in VPA mice. The latter results indicate that modulation of brain histamine provided by E100 may have contributed to the correction of an unbalanced ratio of radical oxygen species through the generation of endogenous cellular antioxidant defensive mechanisms.

The ability of E100 to enhance cholinergic activity in VPA mice and to exert its potential effect on cognitive deficit associated with sociability impairments was confirmed by measuring AChE activity in the cerebellum. The results revealed that the activity of AChE in E100 (10 mg)-treated mice was significantly reduced compared to VPA mice, and comparable to the DOZ. Considering the role of this enzyme which is responsible in degrading the ACh, it has been reported in a previous study that AChE inhibition augmented ACh in the synapse, therefore, relieving the cognitive rigidity and ameliorating the social deficiency in VPA mice [25].

4. Materials and Methods

4.1. Animals

Bred in the local central animal facility of the College of Medicine and Health Sciences, United Arab Emirates University, C57BL/6 (C57) mice (aged 8–12 weeks, weighing 20–25 g) (Jackson Laboratory, Bar Harbor, ME, USA) were used in this study [88]. All mice were kept in plastic cages under a standard light/dark cycle, namely 12 h light cycle, and lights were switched on at 6:00 a.m. Additionally, animals were housed at constant temperature 22–25 °C, and with free access to tap water and a standard rodent chow diet. For mating, male and female mice were housed together, and female mice were observed daily. The day was considered as embryonic day 0 (E0) on which the vaginal plug was detected. Each pregnant female was then kept in a separate cage until delivery, the day of delivery was defined as postnatal day 0 (P0). The Institutional Animal Ethics Committee in the College of Medicine and

Health Sciences/United Arab Emirates (Approval No. ERA-2017-5603) approved all procedures that were carried out in accordance with the recommendations of the European Communities Council Directive of 24 November 1986 (86/609/EEC).

4.2. Drugs

The dual-active AChE inhibitor and H₃R antagonist E100, namely 1-(7-(4-chlorophenoxy)heptyl)azepane, was designed and synthesized in the Department of Technology and Biotechnology of Drugs Kraków, Poland, according to previously published procedures [65]. All chemical reagents used in the current study, including sodium valproate (VPA) (500 mg/kg, i.p.), donepezil hydrochloride (DOZ, 1 mg/kg, i.p.), the CNS-penetrant H₃R agonist (*R*)- α -methylhistamine (RAM, 10 mg/kg, i.p.), the CNS-penetrant H₁R antagonist pyrilamine (MPA) (10 mg/kg, i.p.), the CNS-penetrant H₂R antagonist zolantidine (ZLT) (10 mg/kg, i.p.), and Scopolamine hydrochloride (SCO) (0.3 mg/kg, i.p.) were obtained from Sigma-Aldrich (St. Louis, MO, USA). The assay kit for reduced glutathione (GSH, Assay Kit, Lot no: 095M4114V, Product code: 1002170877) was obtained from Sigma-Aldrich (St. Louis, MO, USA). The lipid peroxidation assay kit for estimation of malondialdehyde (MDA, Lot no: MDA-2409, Product code: NWK-MDA01) was purchased from North West Life Science (Vancouver, WA, USA). The assay kits for superoxide dismutase (SOD, Batch no: 0538703, Item: 706002) and catalase (CAT, Batch no: 0539007, Item: 707002) were purchased from Cayman chemical (Ann Arbor, MI, USA). Acetylcholinesterase activity colorimetric assay kit (Lot no: GR 3295454-2, Product: ab65345) was purchased from BioVision (Milpitas, CA, USA). All the reagents used in the study were of analytical grade and were dissolved in 1% aqueous Tween 20 solution (saline) and administered intraperitoneally (i.p.) at a volume of 10 mL/kg adjusted to body weight, and all doses are expressed in terms of the free base. All the reagents used in the experiments were of analytical grade.

4.3. Study Design and Treatments

4.3.1. Prenatal Treatment

On E12.5, pregnant females were intraperitoneally (i.p.) injected with either VPA 500 mg/kg [89,90], or saline and returned to their home cages, as described previously [63,73,89,90]. After the injection of VPA few pregnant mice died, and some gave still birth or underwent desorption. From the successfully delivered pups, only male offspring were used in the study. Pups delivered from VPA-exposed mothers were considered as VPA mice and were used for the experiments when they reached age of 8 weeks. On the other hand, pups delivered from mothers exposed to saline were used as CNT mice. All obtained offspring were weaned and gender-grouped (5–6 mice/cage) at P21.

4.3.2. Postnatal Treatments

On P21, male offspring (VPA mice with autistic features) from VPA-exposed mothers and from mothers that received saline (CNT, control mice) were divided into 16 subgroups (number of mice per group is provided in the following respective experimental sections), and received intraperitoneally (i.p.) the following treatment groups and as shown in experimental design (Figure 6): 1: CNT mice injected with saline, 2: VPA mice injected with saline (1% aqueous Tween 20), 3: VPA mice injected with E100 (5 mg/kg, i.p.), 4: VPA mice injected with E100 (10 mg/kg, i.p.), 5: VPA mice injected with E100 (15 mg/kg, i.p.), 6: VPA mice injected with DOZ (1 mg/kg, i.p.), 7: CNT mice injected with E100 (10 mg/kg, i.p.), 8: CNT mice injected with DOZ (1 mg/kg, i.p.), 9: E100 (10 mg/kg, i.p.) was co-administered with RAM (10 mg/kg, i.p.), 10: E100 (10 mg/kg, i.p.) was co-administered with MPA (10 mg/kg, i.p.), 11: E100 (10 mg/kg, i.p.) was co-administered with ZLT (10 mg/kg, i.p.), 12: E100 (10 mg/kg, i.p.) was co-administered with SCO (0.3 mg/kg, i.p.), 13: CNT mice injected with RAM (10 mg/kg), 14: CNT mice injected with MPA (10 mg/kg, i.p.), 15: CNT mice injected with ZLT (10 mg/kg, i.p.), and 16: CNT mice injected with RAM (10 mg/kg, i.p.). All co-administrations were carried out as separate injections with 5-min interval following administration of the test compound

4.7 The dual-active histamine H₃ receptor antagonist and acetylcholine esterase inhibitor E100 alleviates autistic-like behaviors and oxidative stress in valproic acid induced autism in mice

Int. J. Mol. Sci. 2020, 21, 3996

13 of 22

(E100). E100 (5, 10, and 15 mg/kg), or DOZ 1 mg/kg or vehicle (saline) were injected once daily for 21 days, from postnatal day (P44). All doses were selected based on the results of our previous studies of strongly related dual-active compounds and are expressed in terms of the free bases [57,85]. E100 and DOZ or saline were administered 30–45 min before each behavioral test, followed by a series of behavioral tests which began one week after starting the treatments and according to previously published works [63,73]. Doses for RAM, MPA, ZLT, and SCO were carefully selected according to previous experimental protocols from our laboratories. The behavioural experiments of the study were carried out between 9:00 a.m. and 3:00 p.m., and were conducted in the following sequence once the animals were 50 days old: three-chamber behaviour test (TCB), marble burying behaviour (MBB), and elevated plus maze (EPM). The behavioural assessments were carried out in the morning (8:00 a.m. and 12:00 p.m.) in a calm and sealed off area that was illuminated with four 60 V light-emitting diodes (LEDs). Before starting the behavioural tests, animals were habituated in the study place at least for one hour. To reduce the number of animals used, the levels of oxidative stress and AChE activity were studied in the same groups of animals that were subjected to behavioral tests.

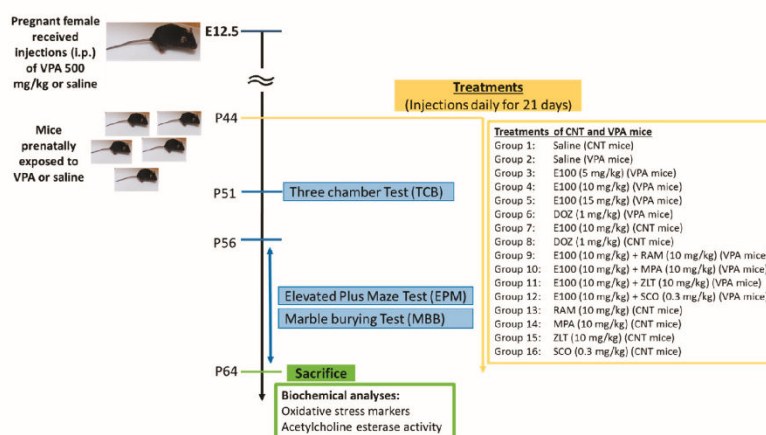


Figure 6. Schematic illustration of systemic treatments, behavioral experiments, and biochemical measurements with VPA and CNT mice. At embryonic day 12.5 (E12.5), pregnant mice were administered intraperitoneally with VPA (500 mg/kg) or Saline. After delivery of pups and starting from postnatal day (P44), treatments of VPA mice and CNT mice were carried out. The systemic administrations continued for 21 days until VPA and CNT mice reached P64. Starting from P51, behavioral assessments were conducted. Following behavioral assessments, all mice were sacrificed at P64 for biochemical and immunofluorescence analyses. VPA and CNT treatment groups (8–12 mice/group) were subdivided into 16 subgroups and received intraperitoneally (i.p.) the following treatments and as shown in experimental design: VPA offspring (mice with autistic features; VPA) Group 1: CNT mice injected with saline, group 2: VPA mice injected with saline, group 3: VPA mice injected with E100 (5 mg/kg, i.p.), group 4: VPA mice injected with E100 (10 mg/kg, i.p.), group 5: VPA mice injected with E100 (15 mg/kg, i.p.), group 6: VPA mice injected with DOZ (1 mg/kg, i.p.), group 7: CNT mice injected with E100 (10 mg/kg, i.p.), group 8: CNT mice injected with DOZ (1 mg/kg, i.p.), group 9: E100 (10 mg/kg, i.p.) was co-administered with RAM (10 mg/kg, i.p.), group 10: E100 (10 mg/kg, i.p.) was co-administered with MPA (10 mg/kg, i.p.), group 11: E100 (10 mg/kg, i.p.) was co-administered with ZLT (10 mg/kg, i.p.), group 12: E100 (10 mg/kg, i.p.) was co-administered with SCO (0.3 mg/kg, i.p.), group 13: CNT mice injected with RAM (10 mg/kg), group 14: CNT mice injected with MPA (10 mg/kg, i.p.), group 15: CNT mice injected with ZLT (10 mg/kg, i.p.), and group 16: CNT mice injected with SCO (0.3 mg/kg, i.p.). All co-administrations were carried out in separate injections with 5-min interval following the test compound (E100) administration. CNT; control mice delivered from saline-exposed mice. VPA; autistic mice delivered from VPA-exposed mice.

4.4. Behavioral Tests

4.4.1. Three-Chamber Behavior (TCB)

As previously described, the sociability test was performed [63,73,91,92]. It is a rectangular three chambered transparent polycarbonate cage (homemade), with one center chamber (40 cm × 20 cm × 22 cm) and two side chambers (40 cm × 20 cm × 22 cm) separated by two sliding doors. In the first session, a test mouse was habituated for 5 min in the center chamber with the two side doors closed. In the second session and following habituation, the doors were opened to allow the test mouse to explore all three chambers for a duration of 5 min. Before starting the third session, a stranger mouse of similar age, gender, and strain with no previous contact with the test mouse (referred to as a novel mouse (NM)), was positioned in a small plastic cage in the either left or right chamber, chosen randomly to avoid side preference, while the other cage was kept empty in the opposite chamber and was referred to as a novel object (NO). In the third session, the test mouse was allowed to explore all three chambers and cages for 10 min sociability test, and the time spent exploring the NM and NO (sniffing) was automatically recorded during the experiment using EthoVision® Software (Noldus, Netherlands). Finally, the time spent in the chamber with NM and around the cage was compared with the time spent in the chamber with NO. Eight groups of 7 mice/group were used for the TCB assessment. As previously described, sociability index (SI) was calculated by applying a mathematical equation to allow the direct comparison of social behavior of the treated groups [63,73], and was calculated with the following formula:

$$SI = \frac{\text{Time exploring novel mouse 1} - \text{Time exploring novel object}}{\text{Time exploring novel mouse 1} + \text{Time exploring novel object}}$$

4.4.2. Marble Burying Behavior (MBB)

The test was performed as previously reported with slight modifications [63,93–96]. Briefly, each mouse was individually kept in a polycarbonate cage (26 cm × 48 cm × 20 cm) with fitted filter-top covers, and filled with fresh, unscented mouse bedding material to a depth of 5 cm, for habituation. After habituation for 10 min, the mouse was removed, and 20 glass marbles (15 mm diameter) were carefully overlaid equidistantly in a 4 × 5 arrangement in the cage. Each mouse was returned to its designated test cage and was allowed to explore for a duration of 30 min. The percentage of marbles buried (a marble was considered to be covered when >50% was covered by the bedding) was recorded and calculated as previously described [63]. Eight groups of 5 mice/group were used for the MBB assessment.

4.4.3. Elevated Plus Maze (EPM) Test

The EPM test was performed as previously described with slight modifications [97–100]. Briefly, the maze is composed of two opposite open arms (30 cm × 6 cm), two opposite closed arms (30 cm × 6 cm × 15 cm) and a central area (6 cm × 6 cm) constructed from plexiglas. An animal was placed in the center of the maze facing an open arm. Mice entries as well as time spent into each arm were measured for 5 min using EthoVision® Software (Noldus, Netherlands). The maze was carefully cleaned using a, with alcohol dampened, tissue (70%, *v/v*) to eliminate the odor of the previously assessed mouse. Eight groups of 6 mice/group were used in the EPM test.

4.5. Biochemical Assessments

4.5.1. Brain Collection and Tissue Preparation for Biochemical Studies

Following behavioral assessments, the animals were sacrificed according to previously published protocols [63,73]. Deep anesthesia of the treated animals was achieved with pentobarbital (40 mg/kg, *i.p.*). Cardiac perfusion was carried out using 1× PBS (0.01 M phosphate buffer, 0.0027 M potassium chloride and 0.137 M sodium chloride) at pH 7.4 to wash out the blood. The perfusion

was carried out manually by using a 50 mL syringe with 20 G needle. The optimal pressure was obtained by slowly flowing 1× PBS (approximately 5 mL/minute). The mice were observed until liver, heart, and kidney were blood free and gave a whitish color, an indication of blood removal. The brains were quickly removed and placed on an ice plate. The cerebellum was excised from the brain and snap-frozen in liquid nitrogen for further use in biochemical tests [63,73]. On the day of biochemical assessment, the tissues were homogenized and placed on ice in the extraction buffer recommended by the manufacturer, radioimmunoprecipitation assay (RIPA) buffer (50 mM Tris HCl, pH 7.4, 140 mM NaCl, 1 mM EDTA, 0.5% Triton X-100 and 0.5% sodium deoxycholate) with protease and phosphatase inhibitors. The homogenates were sonicated and centrifuged for a duration of 30 min at 14,000 rpm and at 4 °C to eliminate tissue debris, and the resulting supernatant was used for the assessments of oxidative stress levels and AChE activity [88,89]. Five groups of 5 mice/group were used for oxidative stress marker estimations.

4.5.2. Oxidative Stress Marker Estimations

Lipid Peroxidation Estimation

Malondialdehyde (MDA) detection kit was used to estimate the amount of lipid peroxidation after the manufacturer's instructions, as previously described in our laboratories [63,101,102]. Briefly, samples or calibrators (250 µL) were incubated in the presence of acid reagent and thiobarbituric acid (250 µL). Then butylated hydroxytoluene in ethanol (10 µL) was added and vortexed vigorously. Samples were then incubated for 60 min at 60 °C and centrifuged at 10,000× g for 2–3 min. The reaction mixture was transferred to a cuvette aseptically and the absorbance was measured at 532 nm using VersaMax™ Microplate Reader (Molecular devices, San José, CA, USA). The ELISA reader was used from, tunable Microplate Reader with a SoftMax Pro reading software, wavelength range 340 nm to 850 nm. The protein estimation was performed by using BCA 96 well microplate method. Kits from Thermo Fisher Scientific (Waltham, MA, USA) (product number #23225) were obtained and the kits protocols were followed. Nunc MaxiSorp™ high protein-binding capacity 96 well ELISA plates were purchased from Thermo Fisher Scientific (product number #439454). The results are expressed as µM MDA/mg protein.

Glutathione (GSH) Estimation

The estimation of GSH levels were carried out according to the manufacturer's instructions of the commercially available GSH kit purchased, and as reported earlier [63,101,102]. The reduced glutathione was estimated in the samples that were first deproteinized with 5% 5-sulfosalicylic acid solution and centrifuged to remove the precipitated protein. The obtained supernatant was used to assess the levels of GSH by measuring the absorbance of test samples at 412 nm with the kinetics for 5 min applying the microplate reader. The results are expressed as µM GSH/mg protein.

Estimation of Antioxidant Enzymes Activity

For estimation of the activity of antioxidant enzymes Superoxide dismutase (SOD) and Catalase (CAT), manufacturer's instructions of commercially available kits were followed, and as previously reported [101,102]. CAT absorbance was read using a micro plate reader at 540 nm, and activity was expressed as nmol/min/mg protein. The protein estimation was carried out using the same devices and in similarity to the experimental protocol described under the Lipid Peroxidation Estimation Section. SOD absorbance was read at 450 nm using a microplate reader and activity was expressed as unit/mg protein.

Determination of Acetylcholinesterase (AChE) Activity in VPA-Exposed Mice Cerebellum

The acetylcholine assay kit was used, and the procedure followed was according to the manufacturer. The assay relates the hydrolysis of ACh to choline by AChE enzyme. Briefly, 5 µL of supernatant of homogenate (cerebellum tissue) was placed into the plate. Then, 45 µL of working reagent that consists of AChE assay buffer, and 50 µL reaction mix were added into each well.

After incubation for 20–30 min at 37 °C, absorbance was read in a kinetic mode, and choosing two time points in a linear range to calculate the AChE activity of the sample, using VersaMax™ MicroplateReader with a tunneable reader ranged from 340–850 nm wavelength.

4.6. Statistics

For behavioral studies and biochemical assessments, data were expressed as means ± SEM. The data were analyzed for normality by assessing the sample distribution or skewness (−1.8 to +1.8 considered normally distributed). After the results had passed the tests for normality, the effects of E100 were analyzed using two-way analysis of variance (ANOVA) with dose of drugs and animals (either VPA or CNT mice) as the between-subjects factor, and post hoc comparisons were performed with Tukey's test in case of a significant main effect. For statistical comparisons, the software package SPSS 25.0 (IBM Middle East, Dubai, UAE) was used. The *p* values less than 0.05 were considered statistically significant.

5. Conclusions

The novel dual-active H₃R antagonist and AChE inhibitor E100 alleviated sociability deficits in TCB and stereotypies in MBB. In addition, E100 reduced elevated AChE activity and mitigated oxidative stress levels in cerebellum of mice with ASD-like behaviors induced by prenatal exposure to VPA (Figure 7). These results demonstrate the alleviating effects of E100 in different behavioural and biochemical assays following *in vivo* VPA-induced ASD in mice, and are to our knowledge the first *in vivo* demonstration that a potent dual-active H₃R antagonist and AChE inhibitor is effective in improving sociability deficits and stereotypies of ASD-like features induced by prenatal exposure to VPA, and provide evidence to such dual-active compound to be used as a potential template for further drug design towards novel therapeutic entities for the treat ASD. However, additional trials with newer developed agents of this class and in different autistic animal models and in other species are warranted to clarify the pharmacological profile of the current class to develop proper, clinically potential candidates with balanced inhibitory affinities at both targets, namely the AChE and the H₃Rs. Additionally, further investigations assessing pharmacokinetics/pharmacodynamics analysis for E100 are warranted to comprehend the provided ameliorating effects on ASD-like features and to exclude possible off-target effects.

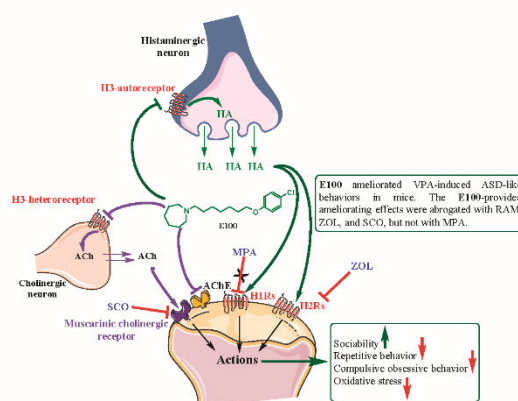


Figure 7. Putative mode of action of E100 by blocking the acting auto- and hetero histamine H₃ receptors (H₃Rs) and inhibition of the acetylcholine esterase enzyme (AChE). Regulating the release of brain histamine (HA) and acetylcholine (ACh), respectively and inhibiting the metabolism of ACh.

4.7 The dual-active histamine H₃ receptor antagonist and acetylcholine esterase inhibitor E100 alleviates autistic-like behaviors and oxidative stress in valproic acid induced autism in mice

Int. J. Mol. Sci. 2020, 21, 3996

17 of 22

Author Contributions: B.S. was responsible for the study concept, design, and acquisition and analysis of animal data. N.E. and P.J. conducted behavioral experiments. N.E., S.A., R.L.J., S.K.O., and R.B. were responsible for biochemical analyses. K.K.-K. and D.L. were responsible for the generation and synthesis of test compound E100. H.S. and D.R. were responsible for pharmacological in vitro characterization of test compound E100. N.E. drafted the manuscript. K.K.-K., D.L., H.S., S.K.O., R.B., and B.S. provided critical revision of the manuscript. All authors have read and agreed to the published version of the manuscript.

Funding: The Office of Graduate Studies and Research of UAE University as well as Zayed-Center for Health Sciences are thanked for the support provided to BS with funds (31R077, 31R223, and 31R224). The authors also acknowledge the partial support of Jagiellonian University statutory funds (N42/DBS/000039). Support was kindly provided by the EU COST Action MuTaliG CA1513 5 to D.L., H.S. and K.K.-K.

Conflicts of Interest: The authors declare no competing interests.

References

1. Baronio, D.; Castro, K.; Gonchoroski, T.; de Melo, G.M.; Nunes, G.D.; Bambini-Junior, V.; Gottfried, C.; Riesgo, R. Effects of an H₃R antagonist on the animal model of autism induced by prenatal exposure to valproic acid. *PLoS ONE* **2015**, *10*, e0116363. [CrossRef] [PubMed]
2. Arvidsson, O.; Gillberg, C.; Lichtenstein, P.; Lundstrom, S. Secular changes in the symptom level of clinically diagnosed autism. *J. Child. Psychol. Psychiatry* **2018**, *59*, 744–751. [CrossRef] [PubMed]
3. Nestler, E.J.; Hyman, S.E. Animal models of neuropsychiatric disorders. *Nat. Neurosci.* **2010**, *13*, 1161–1169. [CrossRef] [PubMed]
4. Eissa, N.; Al-Houqani, M.; Sadeq, A.; Ojha, S.K.; Sasse, A.; Sadek, B. Current Enlightenment about etiology and pharmacological treatment of autism spectrum disorder. *Front. Neurosci.* **2018**, *12*, 304. [CrossRef] [PubMed]
5. Sheldrick, R.C.; Carter, A.S. State-level trends in the prevalence of Autism Spectrum Disorder (ASD) from 2000 to 2012: A reanalysis of findings from the autism and developmental disabilities network. *J. Autism Dev. Disord.* **2018**, *48*, 3086–3092. [CrossRef]
6. Xu, G.; Strathearn, L.; Liu, B.; Bao, W. Prevalence of Autism Spectrum Disorder among US children and adolescents, 2014–2016. *JAMA* **2018**, *319*, 81–82. [CrossRef]
7. Cavalli, A.; Bolognesi, M.L.; Minarini, A.; Rosini, M.; Tumiatto, V.; Recanatini, M.; Melchiorre, C. Multi-target-directed ligands to combat neurodegenerative diseases. *J. Med. Chem.* **2008**, *51*, 347–372. [CrossRef]
8. Decker, M. Recent advances in the development of hybrid molecules/designed multiple compounds with antiamnesic properties. *Mini Rev. Med. Chem.* **2007**, *7*, 221–229. [CrossRef]
9. Karimi, P.; Kamali, E.; Mousavi, S.M.; Karahmadi, M. Environmental factors influencing the risk of autism. *Off. J. Isfahan Univ. Med. Sci.* **2017**, *22*, 27. [CrossRef]
10. Ellenbroek, B.A.; Ghiabi, B. Do H₃ histamine receptor 3 antagonists have a place in the therapy for schizophrenia? *Curr. Pharm. Des.* **2015**, *21*, 3760–3770. [CrossRef]
11. Bacchelli, E.; Battaglia, A.; Cameli, C.; Lomartire, S.; Tancredi, R.; Thomson, S.; Sutcliffe, J.S.; Maestrini, E. Analysis of CHRNA7 rare variants in autism spectrum disorder susceptibility. *Am. J. Med. Genet. A* **2015**, *167A*, 715–723. [CrossRef] [PubMed]
12. Hellings, J.A.; Arnold, L.E.; Han, J.C. Dopamine antagonists for treatment resistance in autism spectrum disorders: Review and focus on BDNF stimulators loxapine and amitriptyline. *Expert Opin. Pharmacother.* **2017**, *18*, 581–588. [CrossRef] [PubMed]
13. Naaijen, J.; Bralten, J.; Poelmans, G.; Glennon, J.C.; Franke, B.; Buitelaar, J.K. Glutamatergic and GABAergic gene sets in attention-deficit/hyperactivity disorder: Association to overlapping traits in ADHD and autism. *Transl. Psychiatry* **2017**, *7*, e999. [CrossRef] [PubMed]
14. Nakai, N.; Nagano, M.; Saitow, F.; Watanabe, Y.; Kawamura, Y.; Kawamoto, A.; Tamada, K.; Mizuma, H.; Onoe, H.; Watanabe, Y.; et al. Serotonin rebalances cortical tuning and behavior linked to autism symptoms in 15q11-13 CNV mice. *Sci. Adv.* **2017**, *3*, e1603001. [CrossRef]
15. Pavál, D. Dopamine hypothesis of autism spectrum disorder. *Dev. Neurosci.* **2017**, *39*, 355–360. [CrossRef]
16. Pavál, D.; Rad, F.; Rusu, R.; Niculae, A.S.; Colosi, H.A.; Dobrescu, I.; Dronca, E. Low retinal dehydrogenase 1 (RALDH1) Level in prepubertal boys with autism spectrum disorder: A Possible link to dopamine dysfunction? *Clin. Psychopharmacol. Neurosci.* **2017**, *15*, 229–236. [CrossRef]

17. Shah, A.; Wing, L. Psychological approaches to chronic catatonia-like deterioration in autism spectrum disorders. *Int. Rev. Neurobiol.* **2006**, *72*, 245–264. [\[CrossRef\]](#)
18. Wang, L.; Almeida, L.E.; Spornick, N.A.; Kenyon, N.; Kamimura, S.; Khaibullina, A.; Nouraie, M.; Quezado, Z.M. Modulation of social deficits and repetitive behaviors in a mouse model of autism: The role of the nicotinic cholinergic system. *Psychopharmacology* **2015**, *232*, 4303–4316. [\[CrossRef\]](#)
19. Chen, R.; Davis, L.K.; Guter, S.; Wei, Q.; Jacob, S.; Potter, M.H.; Cox, N.J.; Cook, E.H.; Sutcliffe, J.S.; Li, B. Leveraging blood serotonin as an endophenotype to identify de novo and rare variants involved in autism. *Mol. Autism* **2017**, *8*, 14. [\[CrossRef\]](#)
20. Hellmer, K.; Nystrom, P. Infant acetylcholine, dopamine, and melatonin dysregulation: Neonatal biomarkers and causal factors for ASD and ADHD phenotypes. *Med. Hypotheses* **2017**, *100*, 64–66. [\[CrossRef\]](#)
21. Arnold, H.M.; Burk, J.A.; Hodgson, E.M.; Sarter, M.; Bruno, J.P. Differential cortical acetylcholine release in rats performing a sustained attention task versus behavioral control tasks that do not explicitly tax attention. *Neuroscience* **2002**, *114*, 451–460. [\[CrossRef\]](#)
22. Ragozzino, M.E.; Pal, S.N.; Unick, K.; Stefani, M.R.; Gold, P.E. Modulation of hippocampal acetylcholine release and spontaneous alternation scores by intrahippocampal glucose injections. *J. Neurosci.* **1998**, *18*, 1595–1601. [\[CrossRef\]](#) [\[PubMed\]](#)
23. Avale, M.E.; Chabaut, J.; Pons, S.; Serreau, P.; De Chaumont, F.; Olivo-Marin, J.C.; Bourgeois, J.P.; Maskos, U.; Changeux, J.P.; Granon, S. Prefrontal nicotinic receptors control novel social interaction between mice. *FASEB J.* **2011**, *25*, 2145–2155. [\[CrossRef\]](#) [\[PubMed\]](#)
24. McConville, B.J.; Sanberg, P.R.; Fogelson, M.H.; King, J.; Cirino, P.; Parker, K.W.; Norman, A.B. The effects of nicotine plus haloperidol compared to nicotine only and placebo nicotine only in reducing tic severity and frequency in Tourette's disorder. *Biol. Psychiatry* **1992**, *31*, 832–840. [\[CrossRef\]](#)
25. Karvat, G.; Kimchi, T. Acetylcholine elevation relieves cognitive rigidity and social deficiency in a mouse model of autism. *Neuropsychopharmacology* **2014**, *39*, 831–840. [\[CrossRef\]](#)
26. Kemper, T.L.; Bauman, M. Neuropathology of infantile autism. *J. Neuropathol. Exp. Neurol.* **1998**, *57*, 645–652. [\[CrossRef\]](#)
27. Friedman, S.D.; Shaw, D.W.; Artru, A.A.; Dawson, G.; Petropoulos, H.; Dager, S.R. Gray and white matter brain chemistry in young children with autism. *Arch. Gen. Psychiatry* **2006**, *63*, 786–794. [\[CrossRef\]](#)
28. Mukaetova-Ladinska, E.B. Silent lives: Why do we fail community-dwelling people with dementia? *Age Ageing* **2017**, *46*, 341–343. [\[CrossRef\]](#)
29. Panula, P.; Chazot, P.L.; Cowart, M.; Gutzmer, R.; Leurs, R.; Liu, W.L.; Stark, H.; Thurmond, R.L.; Haas, H.L. International union of basic and clinical pharmacology. XCVIII. Histamine receptors. *Pharmacol. Rev.* **2015**, *67*, 601–655. [\[CrossRef\]](#) [\[PubMed\]](#)
30. Panula, P.; Rinne, J.; Kuokkanen, K.; Eriksson, K.S.; Sallmen, T.; Kalimo, H.; Relja, M. Neuronal histamine deficit in Alzheimer's disease. *Neuroscience* **1998**, *82*, 993–997. [\[CrossRef\]](#)
31. Sadek, B.; Stark, H. Cherry-picked ligands at histamine receptor subtypes. *Neuropharmacology* **2016**, *106*, 56–73. [\[CrossRef\]](#) [\[PubMed\]](#)
32. Sadek, B.; Saad, A.; Sadeq, A.; Jalal, F.; Stark, H. Histamine H₃ receptor as a potential target for cognitive symptoms in neuropsychiatric diseases. *Behav. Brain Res.* **2016**, *312*, 415–430. [\[CrossRef\]](#) [\[PubMed\]](#)
33. Arrang, J.M.; Garbarg, M.; Schwartz, J.C. Auto-inhibition of brain histamine release mediated by a novel class (H₃) of histamine receptor. *Nature* **1983**, *302*, 832–837. [\[CrossRef\]](#)
34. Lovenberg, T.W.; Roland, B.L.; Wilson, S.J.; Jiang, X.; Pyati, J.; Huvar, A.; Jackson, M.R.; Erlander, M.G. Cloning and functional expression of the human histamine H₃ receptor. *Mol. Pharmacol.* **1999**, *55*, 1101–1107. [\[CrossRef\]](#)
35. Berlin, M.; Boyce, C.W.; Ruiz Mde, L. Histamine H₃ receptor as a drug discovery target. *J. Med. Chem.* **2011**, *54*, 26–53. [\[CrossRef\]](#) [\[PubMed\]](#)
36. Parmentier, R.; Anaclet, C.; Guhenec, C.; Brousseau, E.; Bricout, D.; Giboulot, T.; Bozyczko-Coyne, D.; Spiegel, K.; Ohtsu, H.; Williams, M.; et al. The brain H₃-receptor as a novel therapeutic target for vigilance and sleep-wake disorders. *Biochem. Pharmacol.* **2007**, *73*, 1157–1171. [\[CrossRef\]](#) [\[PubMed\]](#)
37. Alachkar, A.; Khan, N.; Lazewska, D.; Kiec-Kononowicz, K.; Sadek, B. Histamine H₃ receptor antagonist E177 attenuates amnesia induced by dizocilpine without modulation of anxiety-like behaviors in rats. *Neuropsychiatr. Dis. Treat.* **2019**, *15*, 531–542. [\[CrossRef\]](#)

4.7 The dual-active histamine H₃ receptor antagonist and acetylcholine esterase inhibitor E100 alleviates autistic-like behaviors and oxidative stress in valproic acid induced autism in mice

38. Alachkar, A.; Lazewska, D.; Kiec-Kononowicz, K.; Sadek, B. The histamine H₃ Receptor antagonist E159 Reverses memory deficits induced by dizocilpine in passive avoidance and novel object recognition paradigm in rats. *Front. Pharmacol.* **2017**, *8*, 709. [\[CrossRef\]](#)
39. Alachkar, A.; Azimullah, S.; Ojha, S.K.; Beiram, R.; Lazewska, D.; Kiec-Kononowicz, K.; Sadek, B. The neuroprotective effects of histamine H₃ Receptor antagonist E177 on pilocarpine-induced status epilepticus in rats. *Molecules* **2019**, *24*. [\[CrossRef\]](#)
40. Rossi, P.G.; Posar, A.; Parmeggiani, A.; Pipitone, E.; D'Agata, M. Niaprazine in the treatment of autistic disorder. *J. Child Neurol.* **1999**, *14*, 547–550. [\[CrossRef\]](#)
41. Adams-Chapman, I.; Stoll, B.J. Neonatal infection and long-term neurodevelopmental outcome in the preterm infant. *Curr. Opin. Infect. Dis.* **2006**, *19*, 290–297. [\[CrossRef\]](#) [\[PubMed\]](#)
42. Lucchina, L.; Depino, A.M. Altered peripheral and central inflammatory responses in a mouse model of autism. *Autism Res.* **2014**, *7*, 273–289. [\[CrossRef\]](#) [\[PubMed\]](#)
43. DeLorey, T.M.; Sahbaie, P.; Hashemi, E.; Homanics, G.E.; Clark, J.D. Gabrb3 gene deficient mice exhibit impaired social and exploratory behaviors, deficits in non-selective attention and hypoplasia of cerebellar vermal lobules: A potential model of autism spectrum disorder. *Behav. Brain Res.* **2008**, *187*, 207–220. [\[CrossRef\]](#)
44. Martin, L.A.; Goldowitz, D.; Mittleman, G. Repetitive behavior and increased activity in mice with Purkinje cell loss: A model for understanding the role of cerebellar pathology in autism. *Eur. J. Neurosci.* **2010**, *31*, 544–555. [\[CrossRef\]](#)
45. Koziol, L.F.; Budding, D.; Andreassen, N.; D'arrigo, S.; Bulgheroni, S.; Imamizu, H.; Ito, M.; Manto, M.; Marvel, C.; Parker, K.; et al. Consensus paper: The cerebellum's role in movement and cognition. *Cerebellum* **2014**, *13*, 151–177. [\[CrossRef\]](#) [\[PubMed\]](#)
46. Wang, S.S.H.; Kloth, A.D.; Badura, A. The cerebellum, sensitive periods, and autism. *Neuron* **2014**, *83*, 518–532. [\[CrossRef\]](#) [\[PubMed\]](#)
47. Shi, L.; Smith, S.E.; Malkova, N.; Tse, D.; Su, Y.; Patterson, P.H. Activation of the maternal immune system alters cerebellar development in the offspring. *Brain Behav. Immun.* **2009**, *23*, 116–123. [\[CrossRef\]](#)
48. Miller, H.L.; Ragozzino, M.E.; Cook, E.H.; Sweeney, J.A.; Mosconi, M.W. Cognitive set shifting deficits and their relationship to repetitive behaviors in autism spectrum disorder. *J. Autism Dev. Disord.* **2015**, *45*, 805–815. [\[CrossRef\]](#)
49. Gadad, B.S.; Hewitson, L.; Young, K.A.; German, D.C. Neuropathology and animal models of autism: Genetic and environmental factors. *Autism Res. Treat.* **2013**, *2013*, 731935. [\[CrossRef\]](#)
50. Fernández, M.; Sierra-Arregui, T.; Peñagarikano, O. The Cerebellum and autism: More than motor control. *Behav. Neurosci.* **2019**. [\[CrossRef\]](#)
51. Li, B.; Zhu, J.N.; Wang, J.J. Histaminergic afferent system in the cerebellum: Structure and function. *Cerebellum Ataxias* **2014**, *1*, 5. [\[CrossRef\]](#)
52. Depino, A.M.; Lucchina, L.; Pitossi, F. Early and adult hippocampal TGF- β 1 overexpression have opposite effects on behavior. *Brain Behav. Immun.* **2011**, *25*, 1582–1591. [\[CrossRef\]](#) [\[PubMed\]](#)
53. Witkin, J.M.; Nelson, D.L. Selective histamine H₃ receptor antagonists for treatment of cognitive deficiencies and other disorders of the central nervous system. *Pharmacol. Ther.* **2004**, *103*, 1–20. [\[CrossRef\]](#) [\[PubMed\]](#)
54. Yokoyama, H.; Onodera, K.; Iinuma, K.; Watanabe, T. Effect of thioperamide, a histamine H₃ receptor antagonist, on electrically induced convulsions in mice. *Eur. J. Pharmacol.* **1993**, *234*, 129–133. [\[CrossRef\]](#)
55. Bhowmik, M.; Khanam, R.; Vohora, D. Histamine H₃ receptor antagonists in relation to epilepsy and neurodegeneration: A systemic consideration of recent progress and perspectives. *Br. J. Pharmacol.* **2012**, *167*, 1398–1414. [\[CrossRef\]](#) [\[PubMed\]](#)
56. Khan, N.; Saad, A.; Nurulain, S.M.; Darras, F.H.; Decker, M.; Sadek, B. The dual-acting H₃ receptor antagonist and AChE inhibitor UW-MD-71 dose-dependently enhances memory retrieval and reverses dizocilpine-induced memory impairment in rats. *Behav. Brain Res.* **2016**, *297*, 155–164. [\[CrossRef\]](#)
57. Sadek, B.; Khan, N.; Darras, F.H.; Pockes, S.; Decker, M. The dual-acting AChE inhibitor and H₃ receptor antagonist UW-MD-72 reverses amnesia induced by scopolamine or dizocilpine in passive avoidance paradigm in rats. *Physiol. Behav.* **2016**, *165*, 383–391. [\[CrossRef\]](#)
58. Morini, G.; Comini, M.; Rivara, M.; Rivara, S.; Bordini, F.; Plazzi, P.V.; Flammini, L.; Sacconi, F.; Bertoni, S.; Ballabeni, V.; et al. Synthesis and structure-activity relationships for biphenyl H₃ receptor antagonists with moderate anti-cholinesterase activity. *Bioorganic Med. Chem.* **2008**, *16*, 9911–9924. [\[CrossRef\]](#)

59. Nikolic, K.; Filipic, S.; Agbaba, D.; Stark, H. Procognitive properties of drugs with single and multitargeting H₃ receptor antagonist activities. *CNS Neurosci. Ther.* **2014**, *20*, 613–623. [\[CrossRef\]](#)
60. Petroianu, G.; Arafat, K.; Sasse, B.C.; Stark, H. Multiple enzyme inhibitions by histamine H₃ receptor antagonists as potential procognitive agents. *Pharmazie* **2006**, *61*, 179–182.
61. Bembenek, S.D.; Keith, J.M.; Letavic, M.A.; Apodaca, R.; Barbier, A.J.; Dvorak, L.; Aluisio, L.; Miller, K.L.; Lovenberg, T.W.; Carruthers, N.I. Lead identification of acetylcholinesterase inhibitors-histamine H₃ receptor antagonists from molecular modeling. *Bioorganic Med. Chem.* **2008**, *16*, 2968–2973. [\[CrossRef\]](#)
62. Sadek, B.; Saad, A.; Subramanian, D.; Shafiullah, M.; Lazewska, D.; Kiec-Kononowicz, K. Anticonvulsant and procognitive properties of the non-imidazole histamine H₃ receptor antagonist DL77 in male adult rats. *Neuropharmacology* **2016**, *106*, 46–55. [\[CrossRef\]](#)
63. Eissa, N.; Azimullah, S.; Jayaprakash, P.; Jayaraj, R.L.; Reiner, D.; Ojha, S.K.; Beiram, R.; Stark, H.; Lazewska, D.; Kiec-Kononowicz, K.; et al. The dual-active histamine H₃ receptor antagonist and acetylcholine esterase inhibitor E100 ameliorates stereotyped repetitive behavior and neuroinflammation in sodium valproate induced autism in mice. *Chem. Biol. Interact.* **2019**, *312*, 108775. [\[CrossRef\]](#) [\[PubMed\]](#)
64. Lazewska, D.; Jonczyk, J.; Bajda, M.; Szalaj, N.; Wieckowska, A.; Panek, D.; Moore, C.; Kuder, K.; Malawska, B.; Kiec-Kononowicz, K. Cholinesterase inhibitory activity of chlorophenoxy derivatives-Histamine H₃ receptor ligands. *Bioorganic Med. Chem. Lett.* **2016**, *26*, 4140–4145. [\[CrossRef\]](#) [\[PubMed\]](#)
65. Kuder, K.; Lazewska, D.; Latacz, G.; Schwed, J.S.; Karcz, T.; Stark, H.; Karolak-Wojciechowska, J.; Kiec-Kononowicz, K. Chlorophenoxy aminoalkyl derivatives as histamine H(3)R ligands and antiseizure agents. *Bioorganic Med. Chem.* **2016**, *24*, 53–72. [\[CrossRef\]](#) [\[PubMed\]](#)
66. Wright, C.; Shin, J.H.; Rajpurohit, A.; Deep-Soboslay, A.; Collado-Torres, L.; Brandon, N.J.; Hyde, T.M.; Kleinman, J.E.; Jaffe, A.E.; Cross, A.J.; et al. Altered expression of histamine signaling genes in autism spectrum disorder. *Transl. Psychiatry* **2017**, *7*, e1126. [\[CrossRef\]](#) [\[PubMed\]](#)
67. Fox, G.B.; Esbenshade, T.A.; Pan, J.B.; Radek, R.J.; Krueger, K.M.; Yao, B.B.; Browman, K.E.; Buckley, M.J.; Ballard, M.E.; Komater, V.A.; et al. Pharmacological properties of ABT-239 [4-(2-[(2R)-2-Methylpyrrolidinyl]ethyl)-benzofuran-5-yl]benzonitrile]: II. Neurophysiological characterization and broad preclinical efficacy in cognition and schizophrenia of a potent and selective histamine H₃ receptor antagonist. *J. Pharmacol. Exp. Ther.* **2005**, *313*, 176–190. [\[CrossRef\]](#) [\[PubMed\]](#)
68. Fox, G.B.; Pan, J.B.; Esbenshade, T.A.; Bennani, Y.L.; Black, L.A.; Faghhi, R.; Hancock, A.A.; Decker, M.W. Effects of histamine H(3) receptor ligands GT-2331 and ciproxifan in a repeated acquisition avoidance response in the spontaneously hypertensive rat pup. *Behav. Brain Res.* **2002**, *131*, 151–161. [\[CrossRef\]](#)
69. Fox, G.B.; Pan, J.B.; Esbenshade, T.A.; Bitner, R.S.; Nikkel, A.L.; Miller, T.; Kang, C.H.; Bennani, Y.L.; Black, L.A.; Faghhi, R.; et al. Differential in vivo effects of H₃ receptor ligands in a new mouse dipsogenia model. *Pharmacol. Biochem. Behav.* **2002**, *72*, 741–750. [\[CrossRef\]](#)
70. Fox, G.B.; Pan, J.B.; Radek, R.J.; Lewis, A.M.; Bitner, R.S.; Esbenshade, T.A.; Faghhi, R.; Bennani, Y.L.; Williams, M.; Yao, B.B.; et al. Two novel and selective nonimidazole H₃ receptor antagonists A-304121 and A-317920: II. In vivo behavioral and neurophysiological characterization. *J. Pharmacol. Exp. Ther.* **2003**, *305*, 897–908. [\[CrossRef\]](#)
71. Noland, J.S.; Steven Reznick, J.; Stone, W.L.; Walden, T.; Sheridan, E.H. Better working memory for non-social targets in infant siblings of children with Autism Spectrum Disorder. *Dev. Sci.* **2010**, *13*, 244–251. [\[CrossRef\]](#) [\[PubMed\]](#)
72. Riedel, G.; Kang, S.H.; Choi, D.Y.; Platt, B. Scopolamine-induced deficits in social memory in mice: Reversal by donepezil. *Behav. Brain Res.* **2009**, *204*, 217–225. [\[CrossRef\]](#) [\[PubMed\]](#)
73. Eissa, N.; Jayaprakash, P.; Azimullah, S.; Ojha, S.K.; Al-Houqani, M.; Jalal, F.Y.; Lazewska, D.; Kiec-Kononowicz, K.; Sadek, B. The histamine H₃R antagonist DL77 attenuates autistic behaviors in a prenatal valproic acid-induced mouse model of autism. *Sci. Rep.* **2018**, *8*, 13077. [\[CrossRef\]](#) [\[PubMed\]](#)
74. Brioni, J.D.; Esbenshade, T.A.; Garrison, T.R.; Bitner, S.R.; Cowart, M.D. Discovery of histamine H₃ antagonists for the treatment of cognitive disorders and Alzheimer's disease. *J. Pharmacol. Exp. Ther.* **2011**, *336*, 38–46. [\[CrossRef\]](#) [\[PubMed\]](#)
75. Paschou, P.; Fernandez, T.V.; Sharp, F.; Heiman, G.A.; Hoekstra, P.J. Genetic susceptibility and neurotransmitters in tourette syndrome. *Int. Rev. Neurobiol.* **2013**, *112*, 155–177. [\[CrossRef\]](#)
76. Gillberg, C.; Billstedt, E. Autism and Asperger syndrome: Coexistence with other clinical disorders. *Acta Psychiatr. Scand.* **2000**, *102*, 321–330. [\[CrossRef\]](#)

4.7 The dual-active histamine H₃ receptor antagonist and acetylcholine esterase inhibitor E100 alleviates autistic-like behaviors and oxidative stress in valproic acid induced autism in mice

77. Karagiannidis, I.; Dehning, S.; Sandor, P.; Tarnok, Z.; Rizzo, R.; Wolanczyk, T.; Madruga-Garrido, M.; Hebebrand, J.; Nothen, M.M.; Lehmkuhl, G.; et al. Support of the histaminergic hypothesis in Tourette syndrome: Association of the histamine decarboxylase gene in a large sample of families. *J. Med. Genet.* **2013**, *50*, 760–764. [\[CrossRef\]](#)
78. Haas, H.L.; Sergeeva, O.A.; Selbach, O. Histamine in the nervous system. *Physiol. Rev.* **2008**, *88*, 1183–1241. [\[CrossRef\]](#)
79. Hagenow, S.; Stasiak, A.; Ramsay, R.R.; Stark, H. Ciproxifan, a histamine H₃ receptor antagonist, reversibly inhibits monoamine oxidase A and B. *Sci. Rep.* **2017**, *7*, 40541. [\[CrossRef\]](#)
80. Chugani, D.C. Role of altered brain serotonin mechanisms in autism. *Mol. Psychiatry* **2002**, *7* (Suppl. 2), S16–S17. [\[CrossRef\]](#)
81. Mabunga, D.F.N.; Gonzales, E.L.T.; Kim, J.W.; Kim, K.C.; Shin, C.Y. Exploring the validity of valproic acid animal model of autism. *Exp. Neurobiol.* **2015**, *24*, 285–300. [\[CrossRef\]](#) [\[PubMed\]](#)
82. Orekhova, E.V.; Stroganova, T.A.; Prokofyev, A.O.; Nygren, G.; Gillberg, C.; Elam, M. Sensory gating in young children with autism: Relation to age, IQ, and EEG gamma oscillations. *Neurosci. Lett.* **2008**, *434*, 218–223. [\[CrossRef\]](#) [\[PubMed\]](#)
83. Casanova, M.F.; Buxhoeveden, D.; Gomez, J. Disruption in the inhibitory architecture of the cell minicolumn: Implications for autism. *Neuroscientist* **2003**, *9*, 496–507. [\[CrossRef\]](#) [\[PubMed\]](#)
84. Rubenstein, J.L.R.; Merzenich, M.M. Model of autism: Increased ratio of excitation/inhibition in key neural systems. *Genes Brain Behav.* **2003**, *2*, 255–267. [\[CrossRef\]](#)
85. Bahi, A.; Schwed, J.S.; Walter, M.; Stark, H.; Sadek, B. Anxiolytic and antidepressant-like activities of the novel and potent non-imidazole histamine H₃ receptor antagonist ST-1283. *Drug Des. Dev. Ther.* **2014**, *8*, 627–637. [\[CrossRef\]](#)
86. Mahmood, D. Histamine H₃ receptors and its antagonism as a novel mechanism for antipsychotic effect: A current preclinical & clinical perspective. *Int. J. Health Sci.* **2016**, *10*, 564–575.
87. Mahmood, D.; Khanam, R.; Pillai, K.K.; Akhtar, M. Reversal of oxidative stress by histamine H₃ receptor-ligands in experimental models of schizophrenia. *Arzneimittelforschung* **2012**, *62*, 222–229. [\[CrossRef\]](#)
88. Bastaki, S.M.; Abdulrazzaq, Y.M.; Shafiullah, M.; Wiecek, M.; Kiec-Kononowicz, K.; Sadek, B. Anticonvulsant and reproductive toxicological studies of the imidazole-based histamine H₃R antagonist 2-18 in mice. *Drug Des. Dev. Ther.* **2018**, *12*, 179–194. [\[CrossRef\]](#)
89. Kataoka, S.; Takuma, K.; Hara, Y.; Maeda, Y.; Ago, Y.; Matsuda, T. Autism-like behaviours with transient histone hyperacetylation in mice treated prenatally with valproic acid. *Int. J. Neuropsychopharmacol.* **2013**, *16*, 91–103. [\[CrossRef\]](#)
90. Takuma, K.; Hara, Y.; Kataoka, S.; Kawanai, T.; Maeda, Y.; Watanabe, R.; Takano, E.; Hayata-Takano, A.; Hashimoto, H.; Ago, Y.; et al. Chronic treatment with valproic acid or sodium butyrate attenuates novel object recognition deficits and hippocampal dendritic spine loss in a mouse model of autism. *Pharmacol. Biochem. Behav.* **2014**, *126*, 43–49. [\[CrossRef\]](#)
91. Silverman, J.L.; Yang, M.; Lord, C.; Crawley, J.N. Behavioural phenotyping assays for mouse models of autism. *Nat. Rev. Neurosci.* **2010**, *11*, 490–502. [\[CrossRef\]](#)
92. Bambini-Junior, V.; Zanatta, G.; Della Flora Nunes, G.; Mueller de Melo, G.; Michels, M.; Fontes-Dutra, M.; Nogueira Freire, V.; Riesgo, R.; Gottfried, C. Resveratrol prevents social deficits in animal model of autism induced by valproic acid. *Neurosci. Lett.* **2014**, *583*, 176–181. [\[CrossRef\]](#) [\[PubMed\]](#)
93. Thomas, A.; Burant, A.; Bui, N.; Graham, D.; Yuva-Paylor, L.A.; Paylor, R. Marble burying reflects a repetitive and perseverative behavior more than novelty-induced anxiety. *Psychopharmacology* **2009**, *204*, 361–373. [\[CrossRef\]](#)
94. Theoharides, T.C.; Tsilioni, I.; Patel, A.B.; Doyle, R. Atopic diseases and inflammation of the brain in the pathogenesis of autism spectrum disorders. *Transl. Psychiatry* **2016**, *6*, e844. [\[CrossRef\]](#)
95. Angoa-Perez, M.; Kane, M.J.; Briggs, D.I.; Francescutti, D.M.; Kuhn, D.M. Marble burying and nestlet shredding as tests of repetitive, compulsive-like behaviors in mice. *J. Vis. Exp.* **2013**. [\[CrossRef\]](#) [\[PubMed\]](#)
96. Kim, J.W.; Seung, H.; Kwon, K.J.; Ko, M.J.; Lee, E.J.; Oh, H.A.; Choi, C.S.; Kim, K.C.; Gonzales, E.L.; You, J.S.; et al. Subchronic treatment of donepezil rescues impaired social, hyperactive, and stereotypic behavior in valproic acid-induced animal model of autism. *PLoS ONE* **2014**, *9*, e104927. [\[CrossRef\]](#)
97. Bahi, A. Individual differences in elevated plus-maze exploration predicted higher ethanol consumption and preference in outbred mice. *Pharmacol. Biochem. Behav.* **2013**, *105*, 83–88. [\[CrossRef\]](#) [\[PubMed\]](#)

98. Bahi, A. Increased anxiety, voluntary alcohol consumption and ethanol-induced place preference in mice following chronic psychosocial stress. *Stress* **2013**, *16*, 441–451. [[CrossRef](#)]
99. Bahi, A.; Dreyer, J.L. Hippocampus-specific deletion of tissue plasminogen activator “tPA” in adult mice impairs depression- and anxiety-like behaviors. *Eur. Neuropsychopharmacol.* **2012**, *22*, 672–682. [[CrossRef](#)]
100. Bahi, A.; Dreyer, J.L. Chronic psychosocial stress causes delayed extinction and exacerbates reinstatement of ethanol-induced conditioned place preference in mice. *Psychopharmacology* **2014**, *231*, 367–377. [[CrossRef](#)]
101. Ojha, S.; Javed, H.; Azimullah, S.; Khair, S.B.A.; Haque, M.E. Neuroprotective potential of ferulic acid in the rotenone model of Parkinson’s disease. *Drug Des. Dev. Ther.* **2015**, *9*, 5499–5510. [[CrossRef](#)]
102. Javed, H.; Azimullah, S.; Abul Khair, S.B.; Ojha, S.; Haque, M.E. Neuroprotective effect of nerolidol against neuroinflammation and oxidative stress induced by rotenone. *BMC Neurosci.* **2016**, *17*, 58. [[CrossRef](#)] [[PubMed](#)]



© 2020 by the authors. Licensee MDPI, Basel, Switzerland. This article is an open access article distributed under the terms and conditions of the Creative Commons Attribution (CC BY) license (<http://creativecommons.org/licenses/by/4.0/>).

4.8. Epigenetics meets GPCR – Inhibition of histone H3 methyltransferase (G9a) and histamine H₃ receptor for Prader-Willi syndrome

David Reiner¹⁾, Ludwig Seifert²⁾, Caroline Deck²⁾, Roland Schüle³⁾, Manfred Jung²⁾, Holger Stark¹⁾

1) Institute of Pharmaceutical and Medicinal Chemistry, Heinrich Heine University Düsseldorf, Universitätsstr. 1, 40225 Düsseldorf, Germany

2) Institute of Pharmaceutical Sciences, University of Freiburg, 79104 Freiburg, Germany

3) Department of Urology, Center for Clinical Research, Medical Center, Signalling Research Centres BIOS and CIBSS, University of Freiburg, 79106 Freiburg, Germany

Published in: *Scientific Reports*, 2020, 10:13558.

DOI: 10.1038/s41598-020-70523-y

Contribution to research: DR designed, planned, and conducted radioligand displacement assays and functional studies. DR organised CRE-Luc cell lines, organised and established functional assays and conducted cell-culture. DR organised the shipment of test-ligands, and evaluated corresponding data. DR wrote the manuscript and was involved in processing the review.

Abstract:

The role of epigenetic regulation is in large parts connected to cancer, but additionally, its therapeutic claim in neurological disorders has emerged. Inhibition of histone H3 lysine N-methyltransferase, especially G9a, has been recently shown to restore candidate genes from silenced parental chromosomes in the imprinting disorder Prader–Willi syndrome (PWS). In addition to this epigenetic approach, pitolisant as G-protein coupled histamine H₃ receptor (H₃R) antagonist has demonstrated promising therapeutic effects for Prader–Willi syndrome. To combine these pioneering principles of drug action, we aimed to identify compounds that combine both activities, guided by the pharmacophore blueprint for both targets. However, pitolisant as selective H₃R inverse agonist with FDA and EMA-approval did not show the required inhibition at G9a. Pharmacological characterization of the prominent G9a inhibitor A-366, that is as well an inhibitor of the epigenetic reader protein Spindlin1, revealed its high affinity at H₃R while showing subtype selectivity among subsets of the histaminergic and dopaminergic receptor families.

This work moves prominent G9a ligands forward as pharmacological tools to prove for a potentially combined, symptomatic and causal, therapy in PWS by bridging the gap between drug development for G-protein coupled receptors and G9a as an epigenetic effector in a multi-targeting approach.

Reprinted with permission from Reiner D, Seifert L, Deck C, Schüle R, Jung M, Stark H, Epigenetics meets GPCR – Inhibition of histone H3 methyltransferase (G9a) and histamine H₃ receptor for Prader-Willi syndrome, *Sci. Rep.* 2020, 10:13558.

Copyright 2020 The Authors.



OPEN

Epigenetics meets GPCR: inhibition of histone H3 methyltransferase (G9a) and histamine H₃ receptor for Prader–Willi Syndrome

David Reiner¹, Ludwig Seifert², Caroline Deck², Roland Schüle³, Manfred Jung² & Holger Stark¹✉

The role of epigenetic regulation is in large parts connected to cancer, but additionally, its therapeutic claim in neurological disorders has emerged. Inhibition of histone H3 lysine *N*-methyltransferase, especially G9a, has been recently shown to restore candidate genes from silenced parental chromosomes in the imprinting disorder Prader–Willi syndrome (PWS). In addition to this epigenetic approach, pitolisant as G-protein coupled histamine H₃ receptor (H₃R) antagonist has demonstrated promising therapeutic effects for Prader–Willi syndrome. To combine these pioneering principles of drug action, we aimed to identify compounds that combine both activities, guided by the pharmacophore blueprint for both targets. However, pitolisant as selective H₃R inverse agonist with FDA and EMA-approval did not show the required inhibition at G9a. Pharmacological characterization of the prominent G9a inhibitor A-366, that is as well an inhibitor of the epigenetic reader protein Spindlin1, revealed its high affinity at H₃R while showing subtype selectivity among subsets of the histaminergic and dopaminergic receptor families. This work moves prominent G9a ligands forward as pharmacological tools to prove for a potentially combined, symptomatic and causal, therapy in PWS by bridging the gap between drug development for G-protein coupled receptors and G9a as an epigenetic effector in a multi-targeting approach.

Prader–Willi syndrome (PWS) is a rare neurogenetic disorder that affects approximately 1 of 15,000–30,000 newborn infants^{1,2}. Clinically, the disease manifests in a marked hypotonia that presents as earliest symptoms in reduced fetal movement, in sucking weakness of neonates and further limits motoric development in early childhood³. Following a period of reduced nutrition due to decreased muscle tone, the disease proceeds with a bland feeling of satiety, leading to a massive urge for eating (hyperphagia). If not controlled by exogenic dietary limitation through caregivers, PWS leads to obesity during adolescence and adulthood, that is the common reason for increased morbidity and mortality of such patients^{1,3}. Next to behavioral disorders, patients often show mild mental retardation such as restraints in executing complex tasks and/or mildly reduced intelligence, short stature, hypogonadism, a general delayed development and sleeping issues that demonstrate as hypersomnia and excessive daytime sleepiness (EDS)^{3–5}.

PWS is referred to as a neurogenetic disorder that has been associated with a loss of genetic information between loci q11 and q13 on the chromosome 15 where several SNORD clusters and the genes SNURF-SNRPN, NDN, MKRN3 and MAGEL2 are located⁶. However, it is hard to correlate their loss with specific symptoms of the phenotype. On the one hand, their specific functions have not been elucidated yet, on the other hand, not many PWS or PWS-like phenotypes could be attributed to the loss of a single of such genes⁷. The function of the small nucleolar RNA (snoRNA) expressed by SNORD116 has not been elucidated yet, though, the deletion of this cluster suggests a critical role for determining the PWS phenotype^{8,9}. Progress of knowledge about the organization of genes led to an understanding of the molecular origin of PWS. It is caused by a loss of the paternally inherited genes within the depicted loci, either due to deletion or uniparental disomy. At the same

¹Institute of Pharmaceutical and Medicinal Chemistry, Heinrich Heine University Duesseldorf, Universitaetsstr. 1, 40225 Duesseldorf, Germany. ²Institute of Pharmaceutical Sciences, University of Freiburg, 79104 Freiburg, Germany. ³Department of Urology, Center for Clinical Research, Medical Center, Signalling Research Centres BIOSS and CIBSS, University of Freiburg, 79106 Freiburg, Germany. ✉email: stark@hhu.de

www.nature.com/scientificreports/

	G9a methyltransferase inhibition at 10 μ M ^a (n)	Spindlin1 inhibition ^b	hH ₃ R affinity K _i [CI _{95%}] ^c (n)
Ciproxifan	-1.9 \pm 4.9% (2)	No inhibition	320 [250–430] nM ⁴⁷ (3)
UCL-2190	13.9 \pm 9.3% (2)	No inhibition	11 [3.5–33] nM ⁴⁸ (3)
Pitolisant	-2.6 \pm 12.2% (4)	No inhibition	12 [11–13] nM ⁴⁹ (5)
A-366	100.00 \pm 0.04% (6) IC ₅₀ = 2.5 nM ¹⁸	IC ₅₀ = 182.6 nM ²⁷	17 [8–37] nM (6)
UNC-0642	99.90 \pm 0.09% (4)	IC ₅₀ = 2.7 \pm 6.7 μ M	1.8 [0.6–5.5] nM (4)

Table 1. Representative ligands and their G9a inhibition, Spindlin1 inhibition and H₃R affinity. ^aAlphaLISA based CLOT (Chemiluminescence-based oxygen tunnelling) assay; results are expressed as means \pm s.d. from the indicated number of replicates (n). ^bScreening for inhibition of the epigenetic reader protein Spindlin1 in a fluorescence polarization-based approach. ^cAffinity to the human isoform of histamine H₃ receptor (hH₃R) as determined by [³H]N^a-methylhistamine displacement studies.

time, the copy of information remains on the corresponding maternal chromosome¹⁰. However, the genes on this opposite parental chromosome are silenced by epigenetic mechanisms, such as DNA methylation or post-translational histone modifications that lead to imprinting of the corresponding alleles. Thus, PWS is referred to as an “imprinting disorder”, a group of disorders that shares many clinical manifestations such as affected growth, development, metabolism or behavior¹¹.

The current pharmacotherapeutic interventions in PWS involve substitution of Growth Hormone that has shown to improve body composition and motoric strength. It can and should be applied before the first birthday of infants¹. Additionally, the application of sexual hormones, antipsychotics and antidepressants in the disease is reported in the literature¹. Among the psychiatric drugs, modafinil demonstrated effectiveness to relieve the impulsive behavior of PWS patients and has been approved for the treatment of EDS or narcolepsy¹². Similarly, application of pitolisant as novel inverse agonist/antagonist at the G-protein coupled histamine H₃ receptor (H₃R) by children suffering from PWS is known to us^{13–15}. The drug obtained market-approval by the European Medicines Agency of the European Union (EMA) in 2016 for narcolepsy with or without cataplexy, recently followed by the FDA (U.S. Food and Drug Administration) approval. In clinical studies, the drug displayed significant improvement of EDS determined by the Epworth Scale of Sleepiness (ESS) and non-inferiority towards the therapeutically established modafinil¹⁶. Additionally, pitolisant is currently examined for effects in pediatric narcoleptic patients (ClinicalTrials.gov database of the U.S. National Institutes of Health, Identifier: NCT02611687, <https://www.clinicaltrials.gov/>). Though highly significant clinical studies for pitolisant in PWS patients are missing to date, recent patient-based case reports suggest benefits of this H₃R targeting drug. It shows improved activity of patients, reduction of daytime-sleepiness as well as improvements in mental clarity and processing speed^{13–15}. Moreover, preclinical in vivo examination in SNORD116-deficient PWS mice showed abolished baseline changes in REM sleep after administration of pitolisant¹⁷ that has emphasized the role of H₃R in the pathophysiology of PWS.

The outlined therapeutic options are mainly linked to decrease behavioral and endocrinal symptoms; however, without clear evidence for each of them. Therefore, appropriate and causal pharmacotherapy for PWS is still demanded.

On this search, the demonstration of an epigenetic approach to PWS by Kim and co-workers in 2017 has got our attention^{10,18}. The group shows that at least two inhibitors of the histone H3 lysine-9 (H3K9) methyltransferase G9a (syn. Euchromatic histone N-methyltransferase 2, EHMT-2) are capable of restoring the expression of candidate PWS genes from the maternally inherited chromosome. While the group found no alterations in the level of DNA-methylation within the imprinted region and genes were still restored, the role of methylation for gene silencing seems less important in PWS. Therefore, the relevance of histone H3 methylation as a regulator of the expression of the imprinted genes during imprinting has been highlighted¹⁸. Further unknown roles of G9a to gene expression may contribute¹⁹, and involvement of additional regulators of gene expression seems likely. For example, some G9a inhibitors have shown inhibition of Spindlin1 that belongs to the epigenetic “reader” proteins and has been studied for its role in cancer progression²⁰. It can detect H3K4 trimethylation (H3K4me3) and trigger downstream signalling²¹ as well as the expression of rRNA genes²².

Inspired by the recent progress of pitolisant in PWS, we aimed to accelerate the preclinical and clinical investigation by the discovery of further H₃R inverse agonists/antagonists with improved profiles. The reported potential of the G9a inhibitors UNC-0642 and UNC-0638 to restore the expression of candidate genes in PWS prompted us to identify H₃R antagonists among compounds with inhibitory activity for G9a. Additionally, we took identified lead-compounds for a selectivity screening among histamine H₄ receptors that possess high structural similarity to H₃R²³ as well as towards dopaminergic receptor subtypes that have been associated with the regulation of food intake²⁴. Finally, relevant queries were made for Spindlin1 inhibition to identify congeners for further pharmacological elucidation of involvement of this target in PWS.

Results

Cross-over screening of H₃R ligands and dual G9a/Spindlin1 inhibitors. Testing of the H₃R ligands pitolisant and ciproxifan did not reveal remarkable inhibition of G9a and Spindlin1. UCL-2190 showed only slight G9a inhibition when compared to negative control (buffer only, $P = 0.035$). In contrast, known G9a inhibitors potently diminished H3K9 dimethylation (Table 1). Additionally, UNC-0642 inhibited Spindlin1 to interact

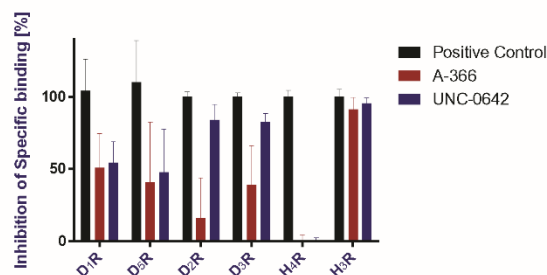


Figure 1. Screening for selectivity of G9a-inhibitors at 1 μ M among dopamine D₁, D₅, D₂ and D₃ receptors (D₁R, D₂R, D₃R, D₅R, respectively) and at the histamine H₄ receptor (H₄R). For comparison, the figure depicts the inhibition of specific binding to H₃R that was extracted from affinity screening data. Bars represent means \pm s.d. of the inhibition of radioligand binding to the respective receptor by either A-366, UNC-0642 or control compound (100 μ M fluphenazine for D₁R and D₂R, 10 μ M haloperidol for D₃R and D₅R, 100 μ M JNJ-7777120 for H₄R or 10 μ M pitolisant for H₃R). [³H]-SCH23390, [³H]-spiperone, [³H]-histamine and [³H]N^a-methylhistamine were used as radiolabelled tracers at D₁R/D₂R, D₂R/D₃R, H₄R and H₃R, respectively, each at approx. $1 \times K_D$.

with trimethylated H3K4 at 10 μ M. Interestingly, such dual G9a/Spindlin1 inhibitors were as well able for potent displacement of [³H]N^a-methylhistamine from human isoform of H₃R (hH₃R) in the nanomolar concentration range. While A-366 exerted its action at a concentration similar to the prominent H₃R inverse agonist/antagonist pitolisant, UNC-0642 was more active by about an order of magnitude.

Selectivity screening of G9a inhibitors at other GPCR subtypes. The G9a inhibitors A-366 and UNC-0642 were screened for their ability to inhibit binding of radiolabeled ligands to dopamine D₁, D₂, D₃, D₅ receptors (D₁R, D₂R, D₃R, D₅R) and histamine H₄ receptor (H₄R) (Fig. 1). For both compounds, significant differences to the respective positive controls were observed ($P < 0.05$; positive controls: 10 μ M haloperidol for dopaminergic receptor subtypes, 100 μ M JNJ-7777120 for histamine H₄ receptor, 10 μ M pitolisant for H₃R). Such differences were slight with regards to H₃R (A-366: Δ between means = 9%, UNC-0642: Δ between means = 5%). However, differences in inhibition were significantly more pronounced when comparing their activity between H₃R and the other GPCR subtypes ($P < 0.02$), suggesting lower receptor affinity for the latter. A-366 and UNC-0642 did not differ from each other for their exerted radioligand displacement at H₃R, H₄R, D₁R and D₂R ($P > 0.22$). In contrast, a higher susceptibility to displace [³H]-spiperone from D₂R and D₃R was observed for UNC-0642 than for A-366 ($P < 0.01$).

Mode of antagonism of A-366 at rat isoform of H₃R. Additionally, A-366 was investigated in a cAMP-response element driven luciferase reporter gene (CRE-Luc) assay at another isoform of H₃R. At the *Rat Norvegicus* isoform of H₃R (rH₃R), A-366 potently shifted receptor activation by histamine ($EC_{50} = 2.3$ [0.4–14.9] nM). As determined from fitting data of Fig. 2a, the resulting affinity was in line with the observations above that used the human isoform of H₃R (hH₃R, $K_a = 15$ [2–150] nM). Subsequent Schild-plot showed that A-366 shifts the affinity of histamine in a rather equipotent manner (Fig. 2b) with a slightly reduced slope (0.79 ± 0.45 , mean \pm 95% confidence interval) but not significantly different from unity.

Discussion

Among our search for novel H₃R ligands with combined G9a inhibitory activity, relevant progress could be made in this study to define a novel mode of action in the pharmacotherapy of PWS. Particularly guided by the recent clinical effects of pitolisant, we started with the search for a potential epigenetic mechanism of action for pitolisant as well as ciproxifan and UCL-2190. However, such could not be delineated based on our data. Ciproxifan serves as an advanced pharmacological tool on preclinical investigation stage and a standard tool in various rodent models²⁵, despite that included imidazole moiety²⁶. Some drawbacks associated with the susceptibility of imidazole to inhibit CYP enzymes led to the derivative UCL-2190 that belongs to the second, nonimidazole-based generation of H₃R antagonists²⁷. Whereas a slight G9a inhibition in low percentile range was observed for UCL-2190, the corresponding affinity estimate would be far apart from such observed for potent G9a inhibitors. Crystal structures of some G9a inhibitors in complex with the enzyme suggest the necessity of protonated heterocyclic element for ionic interaction with the Asp1088 residue of the enzyme^{28–30}. We attribute the lack of G9a inhibition by our scrutinized H₃R inverse agonists to the absence of this structural feature.

In contrast, we could identify potent H₃R ligands among G9a inhibitors. Therefore, we examined UNC-0642, bearing a quinazoline-core motif and A-366 as a spirocyclic 2-amino-3*H*-indole-based G9a-pharmacophore. The latter is suggested to be protonated at physiological pH-value due to variation towards an inherent amidine or aromatic guanidine functionality^{30,31}. Further aliphatic and amino group-containing moieties are tolerated. Interestingly, for some G9a inhibitors, the core bears substituents like a 3-pyrrolidinopropoxy moiety as present in

www.nature.com/scientificreports/

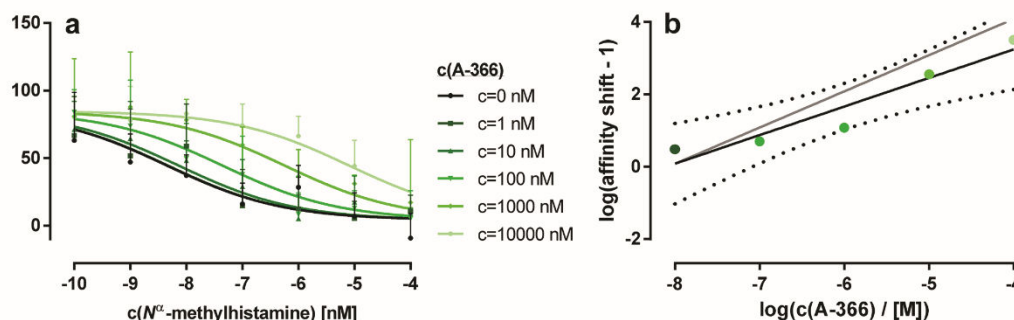


Figure 2. Schild-assay revealing antagonist properties of A-366 at rat isoform of H₃R. **(a)** Effects of the H₃R agonist N^α-methylhistamine on formation of cAMP concentrations were studied in a cAMP response element-driven luciferase reporter gene (CRE-Luc) assay in HEK-293 T cells that were stably transfected with the receptor as described by Nordemann et al.^{44,45} Evaluated data originated from two independent experiments performed in duplicate and are stated as means ± s.d. **(b)** Data from panel a were transformed to a Schild-plot that resulted in a regression of R² = 0.91 (black line, with 95% confidence band depicted with small dots). The slope was not different from unity (grey line).

A-366 and UNC-0642. As enlightened from the crystal structures, the latter motif could be linked to an increased potency at G9a due to substrate mimicking of lysine in position 9 of histone H3K9 and therefore a blocking of the lysine binding tunnel in the histone H3 binding pocket³⁰. Additionally, this variation draws the basis for an H₃R pharmacophore that can constitute of a basic moiety, linked by an alkyl-spacer towards a substitutable aromatic central core³². The high binding affinity of the G9a inhibitors can be explained as such features have already been incorporated into UNC-0642 and A-366. For the former tool compound, the findings are in line with its previous characterization as a G9a inhibitor with selectivity over a broad range of kinases, transporters, ion channels as well as GPCR's, except an affinity at histamine H₃R²⁸.

To search for potential discriminants between both pharmacological tools at GPCRs, we extended our in vitro profiling with selectivity studies against a small set of dopamine receptors (D₁R, D₂R, D₃R, D₄R) as well as the histamine H₄ receptor that shows the highest structural similarity to H₃R among GPCRs²³. In all cases, inhibition of radioligand binding to the off-targets was lower for UNC-0642 and A-366 when compared with the respective positive controls at such receptors and also lower when compared to their inhibitory activity at H₃R. In essence, one could hypothesize an additional action of agonists at D₂R would have beneficial effects for PWS due to a suppressed food-intake in vivo²⁴. Consequently, antagonists could compromise such an effect³³. Thus, we see the selectivity against D₂R and D₃R, that was slightly more pronounced for A-366 than for UNC-0642, as an essential property for our desired pharmacological tools.

As a consequence of the well-documented interspecies differences of H₃R affinity, we decided to determine A-366 binding at the rH₃R. Due to the G_{12/13} coupling nature of H₃R, agonists as N^α-methylhistamine lead to a reduced intracellular cAMP content compared to untreated cells³⁴. In a Schild-based³⁵ characterization of A-366 as depicted in Fig. 2, we observed a potency that was consistent with such at hH₃R and an equipotent affinity shift of agonist with increasing antagonist concentrations. This result creates a basis for exploitability of H₃R mediated effects in preclinical PWS in vivo studies, although we are aware that mouse models have been predominantly used in the past. However, some reports move for extended usage of animal models other than PWS mouse models as such do usually not present obesity and hyperphagia simultaneously³⁶.

Together with the previously presented data^{30,37}, our results indicate that both G9a standard ligands have low nanomolar H₃R binding affinities with required selectivity among further GPCR subtypes and that they exert potent inhibition of G9a and Spindlin1. Besides the effectiveness of UNC-0642 in PWS mice that was mentioned previously, this compound has already been subjected for further neurological examination, showing amelioration of autism-like social deficits in Shank3-deficient mice³⁸ and reduction of anxiety-related behavior in adult mice³⁹. In the latter study, effects similar to those of UNC-0642 could be demonstrated for A-366³⁹. This implies both compounds to be tolerated in mouse or rat models and that they possess essential features for neurological drugs such as blood-brain barrier permeability and metabolic stability^{18,28,30,40}. Therefore, both ligands will be suitable pharmacological tools for potential in vivo investigation.

Concluding our search for potential dual G9a inhibitors/H₃R antagonists for the treatment of PWS in future, significant prerequisites for applying the preclinical candidate A-366 in PWS studies could be identified. With the identification of H₃R antagonizing properties of A-366, our in vitro characterization presents this compound as a multi-target ligand that has a high potential to show symptomatic effects in the neurogenetic PWS, congruent to those described for pitolisant (Fig. 3). Secondly, the recently demonstrated gene restoration from maternal chromosomes by UNC-0642 mediated G9a inhibition should allow for a potential causal intervention by A-366. Besides, the advanced preclinical development stage of this drug makes it very attractive for further clinical characterization, promising a symptomatic and causal approach in the pharmacotherapy of PWS.

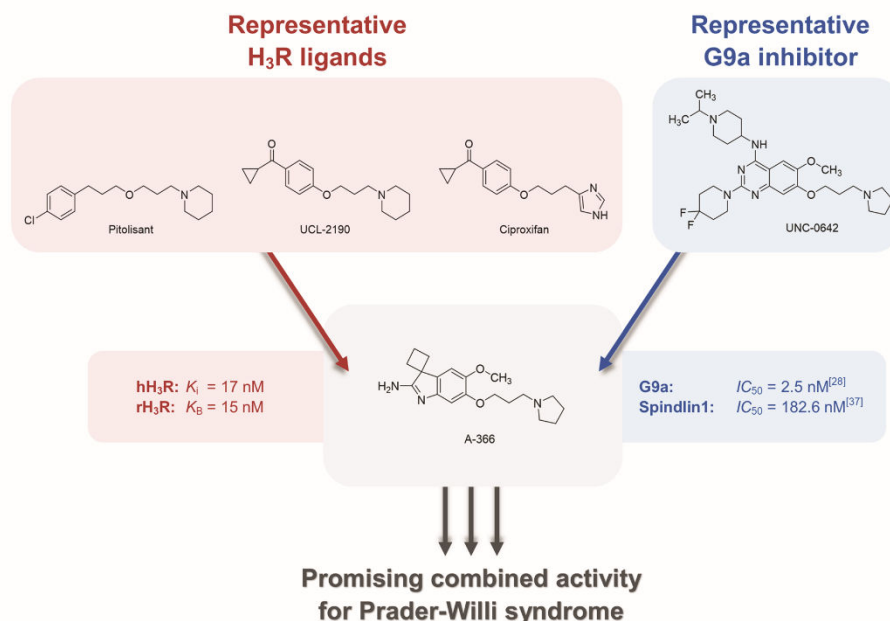


Figure 3. Promising combined H₃R antagonist, G9a- and Spindlin1-inhibitor activity of A366 for pharmacotherapy of Prader-Willi syndrome (PWS).

Methods

Materials. UCL-2190⁴¹, Ciproxifan⁴² and Pitolisant²⁷ were from own laboratory stocks of which synthesis and analytics have been described previously. G9a-inhibitors A-366 and UNC-0642 as well as G9a enzyme, S-adenosylmethionine (SAM), (2S)-2-amino-4-[[[(2S,3S,4R,5R)-5-(6-amino-9H-purin-9-yl)-3,4-dihydroxytetrahydrofuran-2-yl]methyl-methylsulfonio]butanoate], biotinylated histone H3 (1–21) fragment and Dulbecco's modified eagle medium (DMEM, article no. D5671) were purchased from Sigma-Aldrich, Taufkirchen, Germany. Fetal bovine serum albumin (FBS Good-Forte) and Dulbecco's Phosphate Buffered Saline (DPBS) were provided by PAN biotech (Aidenbach, Germany). The radioligands [³H]N^α-methylhistamine, [³H]histamine, [³H]spiperone and [³H]SCH23390 were purchased from PerkinElmer (Rodgau, Germany) as well as AlphaLISA materials such as AlphaLISA H3K9me2 acceptor beads, streptavidin-coated donor beads, detection buffer (5x) and white 384-well microplates (OptiPlate). Human or animal blood/tissue/cell samples have not been used in this study.

Cell culture and membrane preparations. Cell culture and membrane preparations for radioligand displacement assays were performed according to the protocols provided by Bautista-Aguilera et al.⁴³

HEK-293T cells were used for cAMP-response element driven luciferase reporter gene (CRE-Luc) assays, that were stably transfected with cDNA of the H₃R isoform of *Rattus Norvegicus* (rH₃R, NCBI sequence code: NC_005102.4) and a vector containing the *Photinus pyralis* luciferase with a cAMP-response element in its promoter region⁴⁴. Cells were cultured in DMEM supplemented with 1% FBS in the presence of hygromycin (250 µg/mL) and geneticin (1,000 µg/mL) under culture conditions of 37.0 °C, 5.0% CO₂-saturation and 95.0% humidity (for source of cell lines see Supplementary Information).

Radioligand displacement assays at GPCRs. The affinity of A-366 and UNC-0642 at human isoform of H₃R (NCBI sequence code: NM_007232.3) was determined in radioligand displacement studies at membrane preparations of transfected HEK-293 T cells. Therefore, titration schemes ranging from 0.003 to 1,000 nM were prepared in duplicates and incubated with 20 µg/200 µL protein and [³H]N^α-methylhistamine (c = 2 nM) for 90 min. To determine non-specific binding, additional samples of pitolisant 10 µM were prepared. For off-target activity screenings, 1 µM of G9a inhibitors were incubated with receptors at the conditions that are described in Table 2. Therefore, triplicates were examined in the case of dopaminergic or histaminergic receptor subtypes, respectively.

The workflow to terminate incubation and measurement of bound radioligand was identical for both experimental set-ups. Briefly, samples were filtrated from microplates onto GF/B filters presoaked with 0.3% polyethyleneimine solution using a 96-well cell harvester. Filter mats were washed three times with water at 4 °C,

Receptor NCBI sequence code (protein content)	Cell line	Radioligand (concentration)	Control (concentration)	Incubation time
Dopamine D ₁ NM_000794.5 (10 µg/200 µL)	HEK-293 T	[³ H]SCH23390 (0.3 nM)	Fluphenazine (100 µM)	120 min
Dopamine D ₂ NM_016574.3 (25 µg/200 µL)	CHO-K1	[³ H]spiperone (0.2 nM)	Haloperidol (10 µM)	120 min
Dopamine D ₃ NM_000796.6 (20 µg/200 µL)	CHO-K1	[³ H]spiperone (0.2 nM)	Haloperidol (10 µM)	120 min
Dopamine D ₅ NM_000798.5 (5 µg/200 µL)	HEK-293 T	[³ H]SCH23390 (0.3 nM)	Fluphenazine (100 µM)	120 min
Histamine H ₃ NM_021624.4 (60 µg/200 µL)	SH9	[³ H]histamine (10 nM)	NIJ-7777120 (100 µM)	60 min

Table 2. Conditions for screening of A-366 for off-target activity (dopamine D₁, D₂, D₃, D₅ and histamine H₃ receptors).

dried for 60 min (54 °C), soaked with scintillation liquid (Betaplate Scint, PerkinElmer), sealed and subjected to scintillation counting.

G9a-inhibition screening. Inhibition of G9a was examined in an AlphaLISA based format with protocols provided by PerkinElmer. In brief, compounds were incubated for 30 min on white 384-well microplates at the indicated concentration and with 5 nM G9a (Supplementary Information, Figure S1), 100 nM histone H3 (1–21) fragment and 15 µM SAM in assay buffer (50 mM Tris-HCl (pH=9.0); 50 mM NaCl, 1 mM dithiothreitol, 0.01% Tween-20). Incubation was terminated by addition of anti-H3K9me2 acceptor beads in provided detection buffer. After incubating the mixture for 60 min, streptavidin-coated donor beads were added to the mix for additional 30 min. Luminescence was then measured using the AlphaLISA luminescence filter of an Infinite M1000pro multiplate reader (Tecan, Maennedorf, Switzerland) for 1,000 ms (integration time).

Spindlin1 inhibition screening. Spindlin1 inhibition was determined using the fluorescence polarization displacement assay described by Wagner et al.³⁷ For the IC₅₀ values, 12 concentrations were measured in triplicates.

CRE-Luc assays at rH₃R. CRE-Luc assays were conducted by following the protocol provided by Nordemann et al.^{44,45}, with slight modifications: For functional-based Schild⁴⁶ studies in HEK-293T cells, such were seeded into polyethylenimine-coated 96-well tissue culture plates (TPP) at 2 × 10⁵ cells/200 µL/well in assay medium (DMEM without phenol-red, 1% FBS) and allowed to attach for 24–48 h. Afterwards, forskolin (c_{final} = 3 µM) and serially-diluted N^α-methylhistamine (10,000–0.01 nM) were added to the reaction cells in absence or presence of A-366 (10–100,000 nM) using a Freedom EVO[®] liquid handling robot (Tecan). The mixture was incubated for 5 h under culture conditions.

Subsequently, the medium was removed and replaced by 80 µL lysis buffer (25 µM tricine, 10% glycerol, 2 µM egtazic acid, 1% Triton X-100, 5 µM MgSO₄·7H₂O and 1 µM dithiothreitol) for 30 min while shaking at 300 rpm. Lysed homogenate was transferred into white microplates. Luminescence was recorded using an Infinite M1000pro multiplate reader (Tecan) in luminescence mode (3,000 ms integration time, no filter) immediately after addition of 40 µL assay-buffer (25 mM glycylglycine, 15 mM MgSO₄·7H₂O, 15 mM KH₂PO₄, 4 mM egtazic acid, 2 mM dithiothreitol, 1 mM ATP, 50 µM coenzyme A, 0.02 mg/mL D-luciferin potassium salt) by the injector module.

Data handling and statistics. For experiments employing radiolabeled ligands, raw data that were measured as counts-per-minute [c.p.m.] were reduced by non-specific binding. For affinity measurements, such results were fitted to least-squares method “One site competition” of GraphPad Prism version 7.0 (La Jolla, CA, United States) and final values were calculated as means [95% confidence interval]. In case of selectivity experiments, inhibition of specific binding [%] was calculated from raw data according to $[1 - (SM - NSB) / (TB - NSB)] \times 100\%$, where SM, NSB and TB refer to binding in the presence of ligand, non-specific binding and total binding, respectively. Data were stated as means ± s.d. For G9a inhibition studies, results were calculated from luminescence according to: $100\% \times [1 - (SM - NC) / (PC - NC)]$, where SM, NC and PC refer to luminescence in samples including test compound, water and A-366 at 10 µM, respectively. Data were stated as means ± s.d. with the indicated number of replicates. For CRE-Luc assays, data were normalized to luminescence derived by forskolin containing samples (= 100%) and minimum luminescence measured in samples containing forskolin + N^α-methylhistamine (10 µM) (= 0%). Data from both experiments were globally fit to the “Gaddum/Schild EC₅₀ shift” model of GraphPad Prism and were stated as means [95% confidence interval].

Where appropriate, non-parametric tests or parametric t-tests were conducted utilizing GraphPad Prism to test for differences between data, while assuming significance if $P < 0.05$.

Data availability

Data for the conducted studies will be provided by the corresponding author upon reasonable request.

4.8 Epigenetics meets GPCR - Inhibition of histone H3 methyltransferase (G9a) and histamine H₃ receptor for Prader-Willi syndrome

www.nature.com/scientificreports/

Received: 29 May 2020; Accepted: 28 July 2020
Published online: 11 August 2020

References

1. Duijs, J. *et al.* A multidisciplinary approach to the clinical management of Prader–Willi syndrome. *Mol. Genet. Genom. Med.* **7**, e514 (2019).
2. Cassidy, S. B. & Driscoll, D. J. Prader–Willi syndrome. *Eur. J. Hum. Genet.* **17**, 3–13 (2009).
3. Holm, V. A. *et al.* Prader–Willi Syndrome: Consensus Diagnostic Criteria. *Pediatrics* **91**, 398–402 (1993).
4. Cassidy, S. B. Prader–Willi syndrome. *J. Med. Genet.* **34**, 917–923 (1997).
5. Ward, O. C. Down's 1864 case of Prader–Willi syndrome: A follow-up report. *J. R. Soc. Med.* **90**, 694–696 (1997).
6. Beygo, J. *et al.* Update of the EMQN/ACGS best practice guidelines for molecular analysis of Prader–Willi and Angelman syndromes. *Eur. J. Hum. Genet.* **27**, 1326–1340 (2019).
7. Kanber, D. *et al.* A paternal deletion of MKRN3, MAGEL2 and NDN does not result in Prader–Willi syndrome. *Eur. J. Hum. Genet.* **17**, 582 (2008).
8. Buiting, K. Prader–Willi syndrome and Angelman syndrome. *Am. J. Med. Genet. C Semin. Med. Genet.* **154**, 365–376 (2010).
9. Bieth, E. *et al.* Highly restricted deletion of the SNORD116 region is implicated in Prader–Willi Syndrome. *Eur. J. Hum. Genet.* **23**, 252–255 (2015).
10. Kim, Y., Wang, S. E. & Jiang, Y.-h. Epigenetic Therapy of Prader–Willi syndrome. *Transl. Res.* (2019).
11. Eggermann, T. *et al.* Imprinting disorders: a group of congenital disorders with overlapping patterns of molecular changes affecting imprinted loci. *Clin. Epigenetics* **7**, 1 (2015).
12. De Cock, V. C. *et al.* Efficacy of modafinil on excessive daytime sleepiness in Prader–Willi syndrome. *Am. J. Med. Genet. Part A* **155**, 1552–1557 (2011).
13. Pullen, L. C., Picone, M., Tan, L., Johnston, C. & Stark, H. Cognitive Improvements in Children with Prader–Willi Syndrome Following Pitolisant Treatment—Patient Reports. *J. Pediatr. Pharmacol. Ther.* **24**, 166–171 (2019).
14. Pullen, L., Picone, M., Tan, L., Johnston, C. & Stark, H. Pitolisant treatment improves multiple clinical symptoms of Prader–Willi syndrome (PWS) in children (P36–024). *Neurology* **92**, 6–024 (2019).
15. Pullen, L. C., Picone, M., Tan, L., Johnston, C. & Stark, H. 0771 pitolisant is a safe and effective treatment for children with Prader–Willi syndrome (pws). *Sleep* **42**, A309–A310 (2019).
16. Dauvilliers, Y. *et al.* Pitolisant versus placebo or modafinil in patients with narcolepsy: A double-blind, randomised trial. *Lancet Neurol.* **12**, 1068–1075 (2013).
17. Balzani, E., Pace, M., Falappa, M. & Tucci, V. A pre-clinical investigation into the potential use of pitolisant as new intervention for sleep problems in Prader–Willi syndrome. *Sleep Med.* **40**, e23 (2017).
18. Kim, Y. *et al.* Targeting the histone methyltransferase G9a activates imprinted genes and improves survival of a mouse model of Prader–Willi syndrome. *Nat. Med.* **23**, 213–222 (2017).
19. Purcell, D. J., Jeong, K. W., Bittencourt, D., Gerke, D. S. & Stallcup, M. R. A distinct mechanism for Coactivator versus corepressor function by histone methyltransferase g9a in transcriptional regulation. *J. Biol. Chem.* **286**, 41963–41971 (2011).
20. Fagan, V. *et al.* A chemical probe for tudor domain protein spindlin1 to investigate chromatin function. *J. Med. Chem.* **62**, 9008–9025 (2019).
21. Robaa, D. *et al.* Identification and structure-activity relationship studies of small-molecule inhibitors of the methyllysine reader protein spindlin1. *ChemMedChem* **11**, 2327–2338 (2016).
22. Wang, W. *et al.* Nucleolar protein Spindlin1 recognizes H3K4 methylation and stimulates the expression of rRNA genes. *EMBO Rep.* **12**, 1160–1166 (2011).
23. Liu, C. *et al.* Cloning and pharmacological characterization of a fourth histamine receptor (H₄) Expressed in bone marrow. *Mol. Pharmacol.* **59**, 420–426 (2001).
24. Kern, A., Grande, C. & Smith, R. G. Apo-ghrelin receptor (apo-GHSR1a) regulates dopamine signaling in the brain. *Front. Endocrinol.* **5**, 129 (2014).
25. Hagenow, S., Stasiak, A., Ramsay, R. R. & Stark, H. Ciproxifan, a histamine H₃ receptor antagonist, reversibly inhibits monoamine oxidase A and B. *Sci. Rep.* **7**, 40541 (2017).
26. Alves-Rodrigues, A. *et al.* [³H]-thioperamide as a radioligand for the histamine H₃ receptor in rat cerebral cortex. *Br. J. Pharmacol.* **118**, 2045–2052 (1996).
27. Meier, G. *et al.* Influence of imidazole replacement in different structural classes of histamine H(3)-receptor antagonists. *Eur. J. Pharm. Sci.* **13**, 249–259 (2001).
28. Liu, F. *et al.* Discovery of an in vivo chemical probe of the Lysine Methyltransferases G9a and GLP. *J. Med. Chem.* **56**, 8931–8942 (2013).
29. Liu, F. *et al.* Protein lysine methyltransferase G9a inhibitors: Design, synthesis, and structure activity relationships of 2,4-Diamino-7-aminoalkoxy-quinazolines. *J. Med. Chem.* **53**, 5844–5857 (2010).
30. Sweis, R. F. *et al.* Discovery and development of potent and selective inhibitors of histone methyltransferase g9a. *ACS Med. Chem. Lett.* **5**, 205–209 (2014).
31. Rabal, O. *et al.* Discovery of reversible DNA methyltransferase and lysine methyltransferase G9a inhibitors with antitumoral in vivo efficacy. *J. Med. Chem.* **61**, 6518–6545 (2018).
32. Celanire, S., Wijtman, M., Talaga, P., Leurs, R. & de Esch, I. J. P. Keynote review: Histamine H₃ receptor antagonists reach out for the clinic. *Drug Discov. Today* **10**, 1613–1627 (2005).
33. Kalyanasundar, B. *et al.* D₁ and D₂ antagonists reverse the effects of appetite suppressants on weight loss, food intake, locomotion, and rebalance spiking inhibition in the rat NAc shell. *J. Neurophysiol.* **114**, 585–607 (2015).
34. Panula, P. *et al.* International union of basic and clinical pharmacology. XCVIII. Histamine receptors. *Pharmacol. Rev.* **67**, 601–655 (2015).
35. Hall, D. A. & Langmead, C. J. Matching models to data: A receptor pharmacologist's guide. *Br. J. Pharmacol.* **161**, 1276–1290 (2010).
36. Resnick, J. L., Nicholls, R. D. & Wevrick, R. Prader–Willi Syndrome animal models working. G recommendations for the investigation of animal models of Prader–Willi syndrome. *Mamm. Genome* **24**, 165–178 (2013).
37. Wagner, T. *et al.* Identification of a small-molecule ligand of the epigenetic reader protein Spindlin1 via a versatile screening platform. *Nucleic Acids Res.* **44**, e88–e88 (2016).
38. Wang, Z.-J. *et al.* Amelioration of autism-like social deficits by targeting histone methyltransferases EHMT1/2 in Shank3-deficient mice. *Mol. Psychiatry* (2019).
39. Wang, D.-Y. *et al.* Inhibition of the G9a/GLP histone methyltransferase complex modulates anxiety-related behavior in mice. *Acta Pharmacol. Sin.* **39**, 866–874 (2018).
40. Khanban, H., Fattahi, E. & Talkhabi, M. In vivo administration of G9a inhibitor A366 decreases osteogenic potential of bone marrow-derived mesenchymal stem cells. *EXCLI J.* **18**, 300–309 (2019).
41. Affini, A., Hagenow, S., Zivkovic, A., Marco-Contelles, J. & Stark, H. Novel indanone derivatives as MAO B/H3R dual-targeting ligands for treatment of Parkinson's disease. *Eur. J. Med. Chem.* **148**, 487–497 (2018).
42. Schwartz, J.-C. *et al.* Imidazole derivatives as histamine receptor H₃ (ant) agonists. Intl. Pat. Appl. WO9629315 (1996).

www.nature.com/scientificreports/

43. Bautista-Aguilera, O.M. *et al.* Multitarget-directed ligands combining cholinesterase and monoamine oxidase inhibition with histamine H₃R antagonism for Neurodegenerative diseases. *Angew. Chem. Int. Ed.* **56**, 12765–12769 (2017).
44. Nordemann, U. *Radioligand binding and reporter gene assays for histamine H₃ and H₄ receptor species orthologs* (University of Regensburg, Regensburg, 2013).
45. Nordemann, U. *et al.* Luciferase reporter gene assay on human, murine and rat histamine H₄ receptor orthologs: Correlations and discrepancies between distal and proximal readouts. *PLoS ONE* **8**, e73961–e73961 (2013).
46. Lazareno, S. & Birdsall, N. J. M. Estimation of antagonist K_b from inhibition curves in functional experiments: Alternatives to the Cheng-Prusoff equation. *Trends Pharmacol. Sci.* **14**, 237–239 (1993).
47. Reiner, D. & Stark, H. Ligand binding kinetics at histamine H₃ receptors by fluorescence-polarization with real-time monitoring. *Eur. J. Pharmacol.* **848**, 112–120 (2019).
48. Lutsenko, K., Hagenow, S., Affini, A., Reiner, D. & Stark, H. Rasagiline derivatives combined with histamine H₃ receptor properties. *Bioorg. Med. Chem. Lett.* **29**, 126612 (2019).

Acknowledgements

We acknowledge the kind provision of HEK-293T cells for CRE-Luc-measurements by Prof. Dr Bernhard, Mrs Edith Bartole and Mrs Maria Beer-Kroehn (University of Regensburg, Germany). As well, we would like to thank Prof. Dr Lehmann (Jena, Germany), Prof. Dr Shine (Garvan Institute, Australia), Prof. Dr Sokoloff (Centre Paul Broca de l'INSERM, France), Prof. Dr Schwartz (Bioprojet, France) and Prof. Dr Seifert (Hannover, Germany) for gifting the cell-lines. Special thanks are dedicated to the Deutsche Forschungsgemeinschaft (DFG) for funding within CRC992 (Medical Epigenetics) and DFG INST 208/664-1 FUGG. We also thank the EU-COST Actions CA15135, CA18133, CA18240 and CM1406. D.R. acknowledges the Bursary Award of the 49th Annual Meeting of the European Histamine Research Society (online meeting), 2020. Open access funding provided by Projekt DEAL.

Author contributions

D.R. designed, conducted and evaluated radioligand-based affinity and selectivity experiments, G9a inhibition screening, CRE-Luc assays and drafted the manuscript. L.S. & C.D. designed, conducted and assessed relevant Spindlin1 inhibition studies. R.S., M.J. & H.S. provided materials. M.J. & H.S. created and supervised the project, and they maintained the collaboration. All authors thoroughly reviewed and accepted the manuscript.

Competing interests

H.S. contributed to the discovery of pitolisant. The authors declare to have no financial conflicts of interest.


Additional information

Supplementary information is available for this paper at <https://doi.org/10.1038/s41598-020-70523-y>.

Correspondence and requests for materials should be addressed to H.S.

Reprints and permissions information is available at www.nature.com/reprints.

Publisher's note Springer Nature remains neutral with regard to jurisdictional claims in published maps and institutional affiliations.

 **Open Access** This article is licensed under a Creative Commons Attribution 4.0 International License, which permits use, sharing, adaptation, distribution and reproduction in any medium or format, as long as you give appropriate credit to the original author(s) and the source, provide a link to the Creative Commons license, and indicate if changes were made. The images or other third party material in this article are included in the article's Creative Commons license, unless indicated otherwise in a credit line to the material. If material is not included in the article's Creative Commons license and your intended use is not permitted by statutory regulation or exceeds the permitted use, you will need to obtain permission directly from the copyright holder. To view a copy of this license, visit <http://creativecommons.org/licenses/by/4.0/>.

© The Author(s) 2020

Supplementary Information

Epigenetics meets GPCR – Inhibition of histone H3 methyltransferase (G9a) and histamine H₃ receptor for Prader-Willi Syndrom

David Reiner¹, Ludwig Seifert², Caroline Deck², Roland Schüle³, Manfred Jung², Holger Stark^{1,*}

¹ Institute of Pharmaceutical and Medicinal Chemistry, Heinrich Heine University
Duesseldorf, Universitaetsstr. 1, 40225 Duesseldorf, Germany;

² Institute of Pharmaceutical Sciences, University of Freiburg, 79104 Freiburg, Germany

³ Department of Urology, Center for Clinical Research, Medical Center, Signalling Research
Centres BIOS and CIBS, University of Freiburg, 79106 Freiburg, Germany

*Corresponding author: Holger Stark, Tel.: +49 211 81 10478, Fax: +49 211 81 13359,
Email: stark@hhu.de.

AlphaLISA™ based G9a inhibition

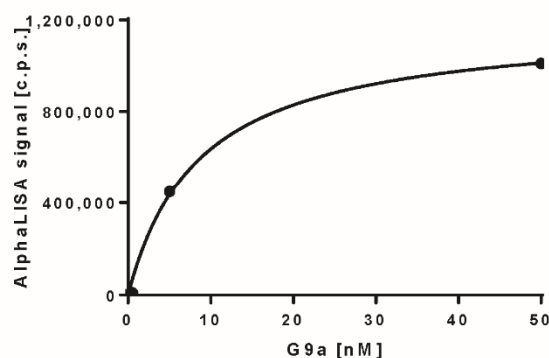


Figure S1. G9a enzyme titration (0.05, 0.5, 5 and 50 nM) at fixed concentrations of recombinant histone H3 fragment 1-21 (c = 100 nM) and *S*-adenosylmethionine (SAM, c = 15 μ M). Incubation was carried out once for 30 min. Data represent means \pm s.d. from an initial experiment performed in duplicates. For further tests, 5 nM G9a were used.

5. Summary & perspectives

Tremendous efforts have been made in molecular pharmacology within the last decades, aiming for identification of novel potent H₃R inverse agonists with effectiveness on clinical investigation stage. Despite the multiple involvements of H₃R in physiological regulation of not only the histaminergic neurotransmitter system, but as well of GABAergic, glutamatergic, dopaminergic and adrenergic ones, only one H₃R inverse agonist has succeeded on its way throughout the drug development, with market authorisation in the European Union and, in 2019, within the U.S.A (Syed, 2016; Kumar et al., 2019). Given this discrepancy between multiple efforts in drug design and drugs approved after almost 40 years of H₃R research, this research aimed to identify potential pitfalls in the molecular pharmacology of H₃R ligands. The second objective was dedicated to the identification of novel hit and lead structures with multitarget directed profile for complex neurogenetic disorders such as schizophrenia and Gilles de la Tourette syndrome, Alzheimer's disease and Parkinson's disease, ASD and the PWS.

In order to increase throughput in an automated screening environment, an FP-based homogenous method to investigate drug-target binding kinetics was developed. Bodilisant was chosen due to the outlined initial considerations of fluorescent, non-imidazole-based antagonists as chemical probes and to elucidate their binding behaviour (Reiner et al., 2019). Another reason in favour of bodilisant was its detectability in even nanomolar concentration range. This observation was a practical prerequisite to obtain a signal in FP, which requires binding of a significant amount of bodilisant. Furthermore, employing novel fluorescence-labelled chemical probes in screening methods can unveil pharmacologic features of the target in interest. The observations made in the study in section 3.1 highlights the importance of reaching out for novel tracers and to motivate further exploration of receptor binding behaviour of H₃R ligands (Reiner et al., 2019). Most attractively, the method enabled for distinguishing association kinetics of the standard antagonists **ciproxifan**, **clobenpropit**, **thiopramide**, **pitolisant** (cf. page 29) and the agonist **NAMH** (cf. page 24) while measuring comparable dissociation kinetics. This observation points towards differences in the mechanism of receptor binding but similarities in unbinding events, the latter being an inherent property of the drug-target complex. Besides, the observed affinities were in marked contrast to such observed with the standard-tracer [³H]NAMH, for all investigated ligands except for pitolisant. Employing a classical molecular pharmacological model, the displacement behaviour of [³H]NAMH against bodilisant was characteristic for a competitive binding behaviour including secondary binding sites for NAMH and consequently for bodilisant. However, the location of this secondary binding site could not be elucidated to date. Certain probability for this binding occurring elsewhere could not be ruled out. However, it was considered low as a result of study design, that relied on experimentation with purified membrane extracts derived from a receptor-overexpressing recombinant cell line. Furthermore,

non-specific binding in such measurements was determined with the H₃R antagonist pitolisant, representing a drug which underwent thorough selectivity screening during development. However, comparison with screening techniques that consider the spatial proximity between the receptor and a given ligand (such as F/BRET techniques) will help to rule out this uncertainty, while deciphering the receptor structure in complex with bodilisant will provide final evidence for the binding mode (Goulding et al., 2018).

As an orthogonal method to [³H]NAMH displacement assays, it was subsequently used in an attempt to characterise receptor binding of the novel non-imidazole-based H₃R agonist **6-k** (cf. page 26) that was previously reported by Ghoshal et al. (2018b). This group identified **6-k** in a functional assay, applying a biosensor consisting of an engineered luciferase, which restores luciferin-oxidation upon conformational shift after cAMP-complexation. The effects were indirectly attributed to H₃R, upon antagonism of signal in the presence of a selective H₃R antagonist (Ghoshal et al., 2018b), while the determination of receptor binding was not performed. The non-imidazole nature which was apart from previously known H₃R pharmacophores prompted us for further elucidation on level of receptor binding. As within our [³H]NAMH displacement assay, an unambiguous receptor binding was not observed for **6-k**, the novel FP-method was employed to screen the agonist against potential secondary binding sites. However, even this method did not show displacement of bodilisant (section 3.2, (Reiner et al., 2020b)). As such behaviour might not only occur from off-target activity but as well occur for partial agonists in an overexpressing system, a subset of consecutive functional assays within the Gα_i/AC/cAMP cascade were performed by our collaboration partners, each without effect that was in accordance with previously published results.

In conclusion, the novel FP-based methods delivered important hints for the molecular pharmacology of H₃R ligands and was able to differentiate between distinct receptor binding modes of potent receptor ligands. Additionally, it was able to identify compounds with H₃R affinity while not showing results for compounds with an apparent off-target activity.

Given such insights, using drug-target binding experiments were chosen as a suitable strategy for all subsequent projects to identify novel hit and lead compounds with multitargeting properties, in order to expand pharmacotherapeutic strategies for neurogenetic disorders. While the novel FP-based method using bodilisant will be an element of future characterisation but not the desired substitute for radioligand displacement assays, the latter were chosen for further purposes in order to achieve comparability of my results with the literature and functional assays were considered as a second-line option for more detailed characterisation.

The purpose of the work described in section 3.3, was to explore novel H₃R ligands based on five-membered multi-heterocycles such as oxadiazoles and thiazole (Khanfar et al., 2018). We have focussed on the introduction of heteroaromatic elements into the standard pharmacophore of H₃R ligands, proving for bioisosteric replacement of the central aromatic core. This design was rationalised by improved drug-like properties that focussed such nuclei within several recent drug development campaigns and resulted in lead structures against a plethora of disorders (Saha et al., 2013; Chhabria et al., 2016). However, the previously outlined pharmacophore model for H₃R ligands (Figure 8) was not uniformly applicable to draft potent 1,2,4- or 1,3,4-oxadiazole-based H₃R ligands.

For ligands incorporating 1,3-thiazoles, an easier strategy was chosen based on previous works that presented a highly affine H₃R ligand (Figure 18). ST-979 can be seen as a result of bioisosteric replacement of the central phenyl core within the compound 1-(3-([1,1'-biphenyl]-3-yloxy)propyl)piperidine, by a 5-methyl-1,3-thiazole core. Interestingly, the corresponding ligand ST-2088, which was derived by the same strategy but showed a different orientation of the central methyl thiazole, showed an essential drop in affinity as compared to that of ST-979 (Figure 18, upper panel). This observation might be rationalised mainly for two reasons. First, as of the substituents, only the methyl scaffold attached to the central nucleus is changing its spatial orientation, this observation might be due to a steric repulsive effect. Secondly, if this discrepancy in affinity may be due to thermodynamic stability of a rotamer of ST-2088 different to that as drawn in Figure 4, the interactions of the functionalised thiazole with the receptor may change additionally.

Within our studies, we have shown that derivatisation of the substituents was suitable to obtain highly affine H₃R ligands. Concomitantly, a series of 38 derivatives with affinities ranging from micromolar to single-digit nanomolar concentration range were characterised in this project. The amelioration of the impaired affinity of ST-2088 was mainly attributable to two strategies,

- i. functionalisation of the phenyl-moiety with H-bond acceptors within the “arbitrary region” (see ST-2114 and MAK-84, Figure 18), or
- ii. rigidification of the linker to the alicyclic amine leading to a spatial constraint in the eastern part of the pharmacophore (see ST-2111 and MAK-84, Figure 18).

Interestingly, ABT-239 (cf. page 32) represents a well-characterised drug candidate that underwent clinical investigation and which contains both design features as well.

Regarding potential lead structures with applicability as H₃R inverse agonists, the group consists of easily accessible H₃R ligands with promising lead-like properties. They comply to Lipinski's and Veber's rules, and they possess good toxicity profile according to structure-based prediction (Khanfar et al., 2018).

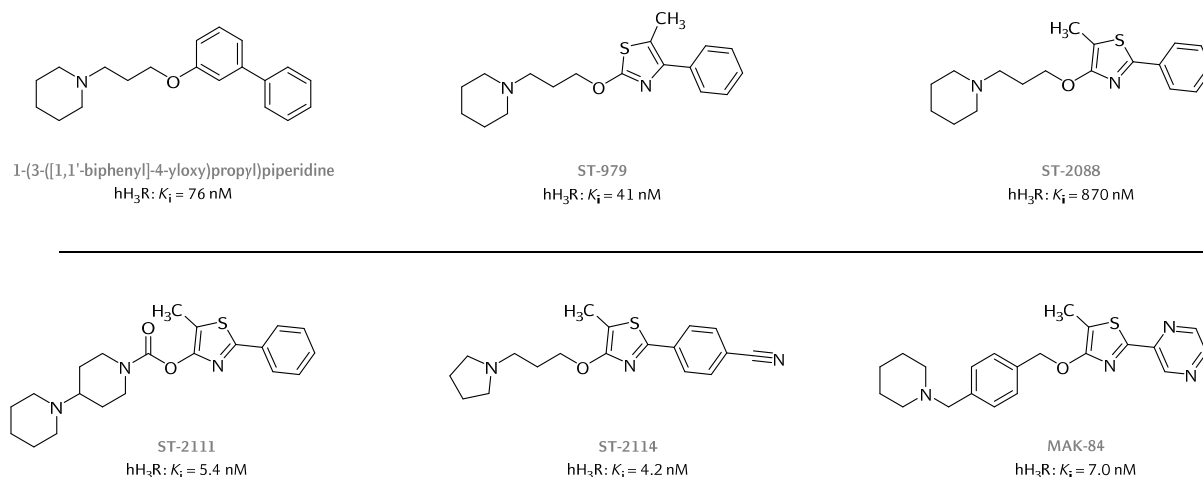


Figure 18. Novel 1,3-thiazole-based H₃R ligands, taken from Khanfar et al. (2018) (section 3.3). All affinity estimates were derived within the same experimental setup.

Overall, the derived compound series will be of importance and a guide for future chemico-biological efforts to 1,3-thiazole-based H₃R ligands and the understanding of drug-target interaction with the H₃R. This study constrains the simplicity of ligand design guided by the general H₃R pharmacophore, in particular, constrained the replaceability of the central aromatic core by a 5-methyl-1,3-thiazole moiety in an attempt to improve drug-likeness.

MTDLs have emerged as promising drug candidates with superior activity in multifactorial diseases such as neurogenetic disorders (section 1.6). Given the numerous involvements of H₃R in neurological processes and the corresponding value for not only a single but two or more diseases, the search was conducted among targets with numerous pharmacotherapeutic implications. Thereby, the multitargeting concept could be expanded from the ‘one disease – multiple targets’ paradigm to a ‘multiple targets – multiple diseases’ strategy.

Thus, the scope of the first approach was the identification of novel hit compounds among pharmacophore fragments with known H₃R affinity from recent studies, but with potential usefulness for future medicinal chemistry efforts for drugs against **schizophrenia** and **Gilles de la Tourette syndrome**. Both represent diseases of high inheritability but without clear genetic aetiology (section 1.5) and in both, DA receptor antagonists have provided some therapeutic effects, but not uniformly. Therefore, combined **H₃R/D₂R/D₃R ligands** may have superior effects. Currently available H₃R ligands with D₂ and D₃ antagonism are of large molecular size. Therefore, I have focussed on the characterisation of the LINS01 series with previously published affinities at HA receptor subtypes H₁, H₂ and H₃ (Corrêa et al., 2019). The compounds were subjected for [³H]-spiperone displacement at the short and full-length isoform of D₂R and D₃R, respectively. As depicted in **Table 9**, **LINS01004**, **LINS01005** and **LINS01012** fulfilled the desired

properties with affinities in (sub)micromolar concentration range, while showing comparability among their D₃R affinity measures (Corrêa et al., 2020)(section 4). Only LINS01004 showed slight discrepancies in receptor binding to each investigated receptor subtype (affinity profile: hH₃R > hD₃R > hD₂R), while LINS01012 was showing higher affinity at hH₃R without differentiation between hD₂R and hD₃R. Interestingly, all compounds were different in terms of their H₃R affinity (Corrêa et al., 2019), suggesting further exploration of modifications of the motif attached to the piperazine and 5-position of dihydro benzofuran moiety. The latter insights will, therefore, be crucial in hit-to-lead optimisation of this series of MTDLs to candidate structures for the application in **schizophrenia** and likewise, in **GTS**.

Table 9. Hit compounds with combined activity at either HA hH₁R or hH₃R from (Corrêa et al., 2019), or at hH₃R, hD_{2,s}R and hD₃R from (Corrêa et al., 2020).

	R ¹	R ²	hH ₁ R ¹⁾ <i>K_D</i> [μM]	hH ₂ R ¹⁾ <i>K_D</i> [μM]	hH ₃ R ¹⁾ <i>K_D</i> [μM]	hD _{2,s} R <i>K_i</i> [μM]	hD ₃ R <i>K_i</i> [μM]
LINS01001	H	H	5.4 [2.5;11.2]	> 10	> 10	> 10	> 10
LINS01003	Me	H	2.2 [1.1;4.6]	> 10	0.21 [0.13;0.33]	> 10	> 10
LINS01004	Allyl	H	> 10	> 10	0.14 [0.09;0.21]	5.5 [5.0;6.0]	1.5 [0.8;3.0]
LINS01005	Ph	H	> 10	> 10	2.5 [0.9;6.4]	2.4 [2.0;2.9]	0.89 [0.45;1.75]
LINS01007	Me	Cl	> 10	> 10	0.50 [0.35;0.68]	> 10	> 10
LINS01008	Me	Me	> 10	> 10	0.16 [0.09;0.29]	> 10	> 10
LINS01010	Me	<i>t</i> Bu	> 10	> 10	0.10 [0.09;0.11]	> 10	> 10
LINS01012	Ph	Me	> 10	> 10	0.51 [0.44;0.60]	2.4 [1.1;5.3]	1.5 [0.4;4.8]

all affinity values are stated as means [95 % confidence-interval]

¹⁾ Affinities converted from p*K_i* values, taken from (Correa et al., 2017; Corrêa et al., 2019)

The discovery of H₃R ligands with putative modulation of striatal DA levels aiming for application in PD models, prompted screening of previously designed **H₃R ligands with combined MAO B inhibition**. A first study with the previously known H₃R antagonist, with the capability to enhance cortical HA turnover, **DL76** (Lazewska et al., 2006), revealed potent MAO B inhibition (Łazewska et al., 2020)(section 4.2).

Concerning the previously made assumption for the responsible MAO B pharmacophore in ciproxifan and UCL-2190 (section 1.6), the *tert*-butyl substituted phenyl scaffold elicited a considerably higher enzyme inhibition compared to the cyclopropylmethanone substituted one. These findings point towards a preference of MAO B for unpolar groups in the eastern part of the H₃R pharmacophore.

Proving for a pharmacophoric relevance of the piperidinoalkoxy scaffold on the MAO binding capacities, the results from collaborators from the Medical College of Jagiellonian University Krakow (Poland) pointed more towards a direct involvement of the whole H₃R pharmacophore into MAO B binding. Intolerability towards mono- and dimethylation of piperidine in 3-,4- and 5-position as well as towards increased linker length was demonstrated. In contrast, monomethylation in 2-position of piperidine seemed to improve MAO B binding for the piperidinopropoxy-based ligand. Screening for the H₃R affinities of this compound series showed some, but less sensitivity towards dimethylation in combination with increased linker length, compared to the behaviour against MAO B. Such results from a first larger series of dual H₃R/MAO B ligands provide evidence for a complete overlap of H₃R and MAO B pharmacophore. Thus, it prompts for including MAO B assay into the standard selectivity screening of future H₃R ligands. With a focus on the identification of a combined H₃R/MAO B inhibitors within this series, DL76 depicted the most interesting candidate within this series, not representing a novel ligand but being re-characterised as a dual-targeting ligand with good preclinical profile. Fulfilling the aim to prove for potential applicability in an *in vivo* model of PD, DL76 exhibited profound and dose-dependent reduction of neuroleptics-induced catalepsy in Cross Leg Position test, besides showing ambiguous results in the bar test (section 4.2).

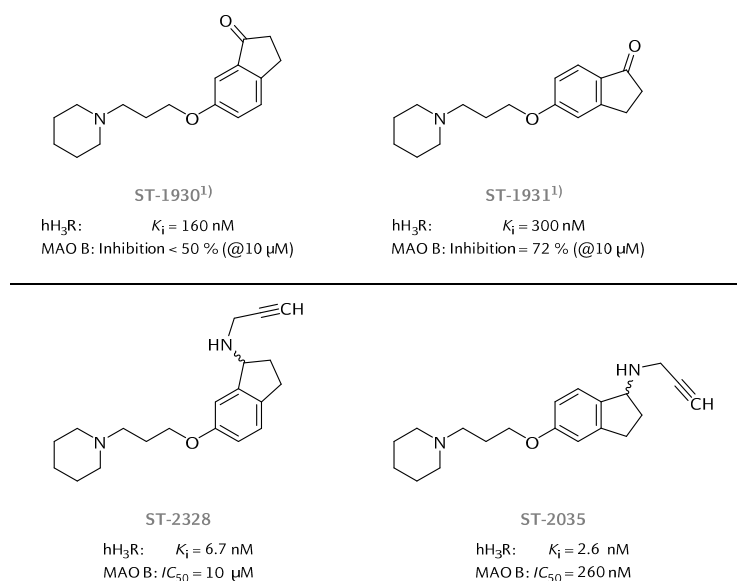


Figure 19. Rasagiline inspired MAO B inhibitors with H₃R affinities from section 4.3 (Lutsenko et al., 2019). ¹⁾Depicted indanone-derivatives (ST-1930, ST-1931) were taken from a previous study (Affini et al., 2018).

Furthermore, H₃R binding properties were investigated for two derivatives of the previously published H₃R/MAO B inhibitors ST-1930 and ST-1931 (**Figure 19**), with structural resemblance to the approved irreversible and selective MAO B inhibitor rasagiline (Lutsenko et al., 2019)(section 4.3). Within this study, the propargyl aminoindane derivative ST-2328 showed less potent and reversible MAO B inhibition compared to the 5-substituted congener ST-2035, which irreversibly and selectively inhibited MAO B in the nanomolar concentration range. In contrast, both candidates did not differ in their low nanomolar K_i for H₃R (section 4.3). This affinity pattern emphasised the assumption that was raised for the DL76 congeners (section 4.2), that whole H₃R pharmacophore is involved in MAO B binding. The latter is supported by the binding behaviour, where MAO B showed a higher tolerability of a contralateral substitution at the indane scaffold than for an ipsilateral one.

With regards to extensive studies by Yogev-Falach et al. (2002; 2003; 2006), both drug-like give rise for a probable MAO-independent neuroprotective mechanism as shown by rasagiline, ladostigil and even propargylamine. This structural feature is not included in DL-76 (Łażewska et al., 2020)(section 4.2). Therefore, they may suit as promising lead candidates for further exploration in models of AD and PD.

The discovery of MAO B inhibition exerted by the pharmacophore of H₃R was a motivator for a novel approach towards **combined H₃R inverse agonist/ChE inhibitors** in order to achieve additive effects by enhancement of ACh release and decelerated degradation. In contrast to previous approaches (e.g., by Petroianu et al. (2006) or Bautista-Aguilera et al. (2018)), this search was not conducted upon rational design using the piperidinoalkoxyphenyl pharmacophore for H₃R, but among databases of commercially available ligands with unknown binding properties towards the receptor and the enzymes of interest (section 4.4 and 4.5). Therefore, a set of computational screening methods was set up by our collaborators from Tabriz University of Medical Sciences (Iran) with subsequent application towards libraries of commercially available ligands. In more detail, they consisted of either ligand-based structural similarity approach guided by the structure of **pitolisant** among the SwissSimilarity database (Zoete et al., 2016), or a search method using a pharmacophore model that was based on a generated H₃R homology model in complex with pitolisant among the ZINCPharmer dataset (Koes et al., 2012). Both methods could be used for screening among smaller libraries of < 11 Mio and < 23 Mio compounds.

Moreover, a hybrid approach consisting of both, pitolisant structure-based library generation and subsequent pharmacophore-based virtual screening was undertaken among the larger ZINC15 database (>210 Mio compounds, (Sterling et al., 2015)). In summary, four commercially available ligands were derived from ligand-based structural similarity approach, one from the hybrid-method. In contrast, no structure from the pharmacophore-based approach was able to pass the preset parameters for drug-

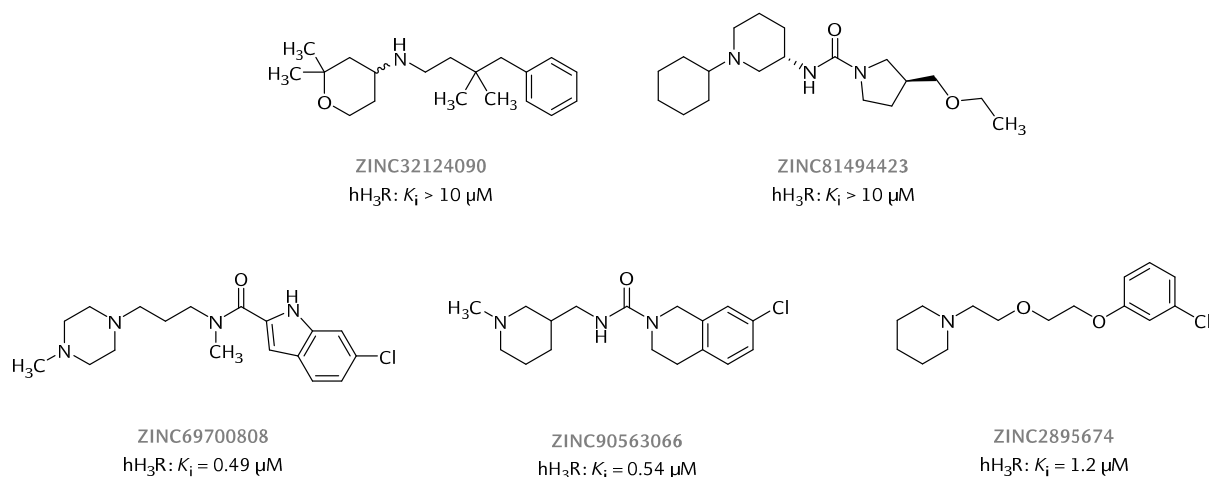


Figure 20. Novel H₃R pharmacophores identified from combined virtual screening and molecular pharmacological analysis, taken from (section 4.4)(Ghamari et al., 2019b).

likeness and predicted absorption, distribution, metabolism and excretion (ADME) properties (Ghamari et al., 2019b). The affinity at H₃R was determined again using the [³H]NAMH displacement approach to rule out false positives among such screening results (Figure 20). Thereby, three out of five screenings hits resulted in novel H₃R ligands in micromolar and submicromolar concentration range. While ZIN2895674 resemble fragments of pitolisant but consisting of a more hydrophilic linker, ZINC69700808 and ZINC90563066 compose of methyl piperazine and methyl piperidine as basic moieties, and bear 6-chloro-1*H*-indole and 7-chloro-1,2,3,4-tetrahydroisochinoline as aromatic core moieties, respectively. Subsequent functional investigation of the latter two compounds revealed H₃R inverse agonist efficacy, and both were even more potent than expected from H₃R affinity alone. These findings argue for a strong decoupling of the G $\alpha_{i/o}$ /AC/cAMP pathway, exerted by such compounds. Concerning our search for combined H₃R/AChE inhibitors, both compounds were able to inhibit cholinesterases in micromolar concentration range, slightly less active than the previously presented contilisant, which was yield by rational drug design approach. Both lead compounds were similar in their capabilities to inhibit AChE and differed marginally in their preference for BuChE, with ZINC69700808 showing somewhat lower and ZINC90563066 somewhat higher affinity in comparison to AChE (Ghamari et al., 2020) (section 4.5). This combined strategy of computational and molecular pharmacological methods for the discovery of potent MTDL with H₃R inverse agonism/AChE provided us with two lead structures based on novel pharmacophore motifs to serve as a starting point for future lead optimisation on the one hand, but for the application in *in vivo* models of neurogenetic disorders such as Alzheimer's disease on the other.

Not only AD represents a condition where combined H₃R inverse agonist/ChE inhibitors emerged as potential drugs to ameliorate decreased cortical AChE levels. Similar aberrations have been found in the BTBR mouse models for ASD. Consequently, this was a motivator for testing the effects of a known H₃R

Table 10. Changes in behavioural paradigms of autism in C57BL/6 mice with or without valproate-induced autistic-like behaviours, upon several pharmacotherapeutic interventions (E100 or donepezil), and reversal tests by BBB-permeable H₁R, H₂R, H₃R and M₁R-M₅R antagonists (mepyramine, zolantadine, RAMH and scopolamine). Each drugs were administered i.p. (section 4.6 and 4.7).

	Phenotype	Intervention	Reversal	Healthy (controls)				Autism-like deficits (valproate-induced)								
				E100	donepezil	mepyramine	zolantadine	RAMH	scopolamine		donepezil		E100			
													mepyramine	zolantadine	RAMH	scopolamine
Anxiety	Open-field test ¹⁾	C	~	nd	nd	nd	nd	nd	↑ sC	↓	↓ sC	~	~	↑	~	
	Elevated-plus maze ²⁾	C	~	~	~	~	~	~	↑ sC	↓	↓ sC	~	~	↑	~	
Sociability	Three-chamber behaviour ²⁾	C	~	~	~	~	~	~	↓ sC	↑	↑ sC	~	↓	↓	↓	
Repetitive behaviour	Nestlet-shredding behaviour ¹⁾	C	~	~	nd	nd	nd	nd	↑ sC	↓	↓ sC	~	~	↑	~	
	Marble-burying behaviour ²⁾	C	~	~	~	~	~	~	↑ sC	↓	↓ sC	~	↑	↑	↑	
Locomotion	Elevated-plus maze ²⁾	C	~	~	~	~	~	~	↑ sC	~	~	~	~	~	~	

C = control; sC = subgroup control; nd = not determined; ↑ = increased; ~ = not altered; ↓ = decreased.

¹⁾ Ref. (Eissa et al., 2019), section 4.6.

²⁾ Ref. (Eissa et al., 2020), section 4.7.

inverse agonist/AChE & BuChE inhibitor in C57BL/6 mice with induced autism-like behaviour upon prenatal exposure to valproate. On the one hand, valproate treatment resulted in neuroinflammation that was characterised by increased levels of proinflammatory cytokines in cerebellum and hippocampus, both areas involved in either executive or cognitive tasks, E100 was able to ameliorate such levels, to decrease elevated expression of enzymes linked to inflammation processes (Eissa et al., 2019), and to reduce increased markers of oxidative stress (Eissa et al., 2020).

Moreover and focussing on behavioural effects, E100 (10 mg/kg or 15 mg/kg) was efficient in abrogation of valproate-induced autistic deficits in terms of anxiety, sociability and repetitive or compulsive-obsessive behaviour. As depicted in **Table 10**, such effects were comparable with such exerted by the approved AChE inhibitor donepezil. Determination of involved neuronal circuitries was conducted by abrogation groups, where each effect was diminished upon H₃R agonism (RAMH), but not by H₁R antagonism (mepyramine). This prompted for *in vitro* selectivity screening to exclude inherent H₁R antagonism of E100. This was confirmed for concentrations up to 1 μ M while some inhibition was seen at 10 μ M. Thus, a contribution of H₁R to the observed effects seems unlikely but cannot be completely ruled out. H₄R-mediated distortions in inflammatory processes, however, seem not to participate in the observed effects due to unambiguous absence of effect in a physiologic concentration range.

Moreover, H₂R receptors (as indicated by zolantadine-antagonism), together with muscarinergic receptors (as indicated by scopolamine-antagonism), showed involvement in sociability and the marble-burying paradigm for repetitive behaviour but not in the nestlet shredding paradigm (Eissa et al., 2019; 2020). At first sight, the results obtained from donepezil might be surprising, which indicate a cholinergic triggered but non-muscarinergic effect. However, this can be rationalised by a potential involvement of nicotinic ACh receptors, of which $\alpha 4\beta 2$ and $\alpha 7$ heteromers in the forebrain, have shown a contribution to cognitive performance (Dineley et al., 2015) and of which the $\alpha 7$ receptor has shown to activate histaminergic TMN neurons. Thus, E100 joins the group of combined H₃R inverse agonists/ChE inhibitors as a drug candidate with promising *in vivo* effects for the complex ASD.

My work on H₃R inhibitors with combined effects at other targets terminates with some outlook on the problem of whether modulating the genetic basis might provide us with better strategies for neurogenetic disorders. Fortunately, auspicious efforts in the field of G9a inhibitors have been recently dedicated to neurogenetic disorders such as AD, ASD and PWS (section 1.6). This progress supports multitargeting properties apart from specific neurotransmitter levels and moves towards the most intracellular source of neurologic pathophysiology, that usually falls out of sight in the daily business of a histaminologist. A straightforward approach to a multi-faceted neurogenetic disease will be an MTDL combining targets with

numerous physiological indications. This theorem was the motivator for the last project, dedicated to the rare-disorder PWS and novel MTDLs for the rare-disorder PWS. More precisely, the H₃R and the histone H3 methyltransferase G9a were chosen not due to their coincidental linguistic comparability but due to their apparent engagement in various neurogenetic disorders.

Initially, we could rule out inherent G9a inhibition properties of H₃R ligands that often seem to bind desired co-targets, as shown previously (section 4.8)(Reiner et al., 2020a). Conversely, the study revealed potent H₃R antagonism of A-366, which was exclusively investigated in models of cancer so far, and UNC-0642 which evolved as a candidate drug for neurogenetic diseases. Whereas some H₃R affinity was ascribed for UNC-0642 before (Liu et al., 2013), this important property was neglected in the interpretation of recent results from mouse models of AD, ASD and PWS (Kim et al., 2017; Griñán-Ferré et al., 2019; Wang et al., 2019). Also, A-366 was identified as an MTDL with previously known high potency at G9a (Sweis et al., 2014). The compound displayed high affinity at hH₃R, high selectivity over other dopaminergic and histaminergic receptor subtypes, fulfils multiple drug-like properties due to exceptionally low molecular weight of a MTDL and shows no affinity difference to a rodent H₃R isoform (Figure 21). Such prominent drug candidates with extensive preclinical characterisation have appeared as potent H₃R ligands, which is

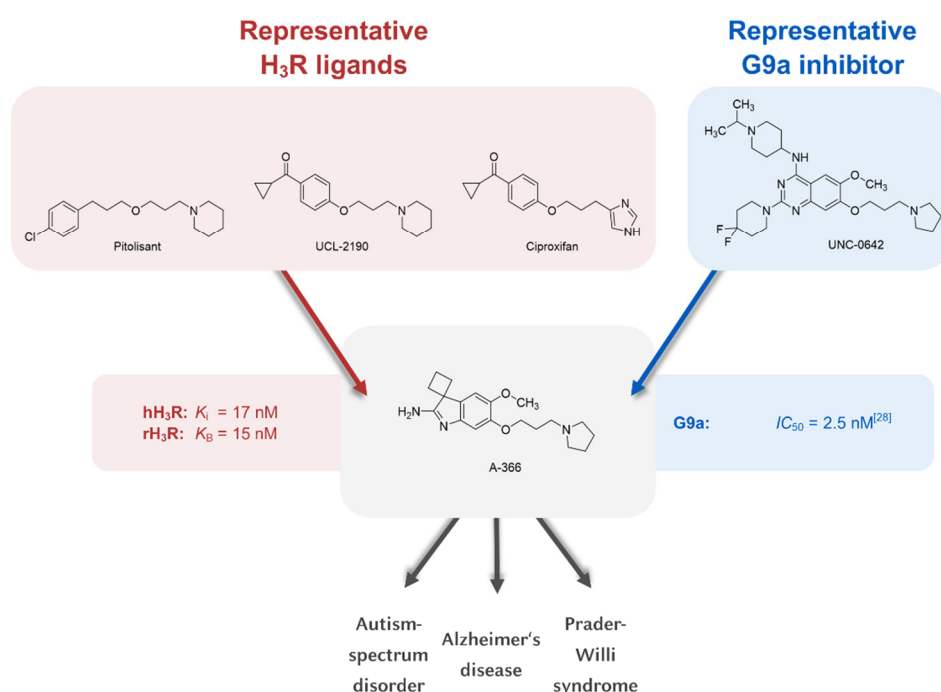


Figure 21. A-366 as MTDL with G9a inhibitory and H₃R-antagonist properties as a paradigmatic shift of pharmacotherapy in neurogenetic disorders (section 4.8). Figure is a derivative from Figure 3 in (Reiner et al., 2020a), used under CC BY 4.0.

attributable to an inherent H₃R pharmacophore of such ligands.

Concluding such findings, A366 and UNC-0642 are promising tools of which a pivotal mode of action can be expected. Due to the involvement of G9a in many neurogenetic disorders where H₃R inverse agonists have emerged as well, these drug candidates will be of relevance for the future pharmacotherapy of neurogenetic disorders. Thus, combined H₃R antagonists/G9a inhibitors represent MTDLs with an excellent profile, which strike the path from a neurotransmission-focussed strategy outlined in the anterior studies of this thesis, towards a single but versatile pharmacotherapeutic approach to numerous neurogenetic disorders (Figure 21).

6. References

- Abdul Majeed, A. B., Mani, V., Jaafar, S. M., Azahan, N. S. M., Ramasamy, K., et al. (2017). Ciproxifan improves cholinergic transmission, attenuates neuroinflammation and oxidative stress but does not reduce amyloid level in transgenic mice. *Life Sci.* 180:23-35.
- Affini, A., Hagenow, S., Zivkovic, A., Marco-Contelles, J. and Stark, H. (2018). Novel indanone derivatives as MAO B/H3R dual-targeting ligands for treatment of Parkinson's disease. *Eur. J. Med. Chem.* 148:487-497.
- Albin, R. L. and Mink, J. W. (2006). Recent advances in Tourette syndrome research. *Trends Neurosci.* 29(3):175-182.
- Alexander, S. P. H., Christopoulos, A., Davenport, A. P., Kelly, E., Mathie, A., et al. (2019a). The concise guide to pharmacology 2019/20: G protein-coupled receptors. *Br. J. Pharmacol.* 176(S1):S21-S141.
- Alexander, S. P. H., Fabbro, D., Kelly, E., Mathie, A., Peters, J. A., et al. (2019b). The concise guide to pharmacology 2019/20: Enzymes. *Br. J. Pharmacol.* 176:S297-S396.
- Alves-Rodrigues, A., Leurs, R., Wu, T.-S., Prell, G. D., Foged, C., et al. (1996). [3H]-thioperamide as a radioligand for the histamine H3 receptor in rat cerebral cortex. *Br. J. Pharmacol.* 118(8):2045-2052.
- American Psychiatric Association (2013a). Autism Spectrum Disorder. In: Diagnostic and statistical manual of mental disorders, 5th edition: 50 - 59, Washington, DC, USA.
- American Psychiatric Association (2013b). Major or Mild Neurocognitive Disorder due to Alzheimer's Disease. In: Diagnostic and statistical manual of mental disorders, 5th edition: 611 - 614, Washington, DC, USA.
- American Psychiatric Association (2013c). Major or Mild Neurocognitive Disorder due to Parkinson's Disease. In: Diagnostic and statistical manual of mental disorders, 5th edition: 636 - 638, Washington, DC, USA.
- American Psychiatric Association (2013d). Schizophrenia. In: Diagnostic and statistical manual of mental disorders, 5th edition: 99 - 105, Washington, DC, USA.
- Amon, M., Ligneau, X., Schwartz, J. C. and Stark, H. (2006). Fluorescent non-imidazole histamine H-3 receptor ligands with nanomolar affinities. *Bioorg. Med. Chem. Lett.* 16(7):1938-1940.
- Andrews, J. R., Filer, C. N., Maniscalco, M., Becknell, N. C. and Hudkins, R. L. (2012). High specific activity tritiation of the pyridazin-3-one histamine H3 receptor inverse agonist CEP-27088. *Appl. Radiat. Isot.* 70(3):512-514.
- Anichtchik, O. V., Peitsaro, N., Rinne, J. O., Kalimo, H. and Panula, P. (2001). Distribution and Modulation of Histamine H3 Receptors in Basal Ganglia and Frontal Cortex of Healthy Controls and Patients with Parkinson's Disease. *Neurobiol. Dis.* 8(4):707-716.
- Apelt, J., Ligneau, X., Pertz, H. H., Arrang, J. M., Ganellin, C. R., et al. (2002). Development of a new class of nonimidazole histamine H(3) receptor ligands with combined inhibitory histamine N-methyltransferase activity. *J. Med. Chem.* 45(5):1128-1141.
- Arrang, J.-M., Devaux, B., Chodkiewicz, J.-P. and Schwartz, J.-C. (1988). H3-Receptors Control Histamine Release in Human Brain. *J. Neurochem.* 51(1):105-108.
- Arrang, J.-M., Garbarg, M. and Schwartz, J.-C. (1983). Auto-inhibition of brain histamine release mediated by a novel class (H3) of histamine receptor. *Nature* 302:832.
- Arrang, J. M., Garbarg, M., Lancelo, J. C., Lecomte, J. M., Pollard, H., et al. (1987a). Highly potent and selective ligands for histamine H3-receptors. *Nature* 327(6118):117-123.
- Arrang, J. M., Garbarg, M. and Schwartz, J. C. (1985). Autoregulation of histamine release in brain by presynaptic H3-receptors. *Neurosci.* 15(2):553-562.
- Arrang, J. M., Garbarg, M. and Schwartz, J. C. (1987b). Autoinhibition of histamine synthesis mediated by presynaptic H3-receptors. *Neurosci.* 23(1):149-157.
- Arrang, J. M., Culat-Marnay, C., Defontaine, N. and Schwartz, J. C. (1991). Regulation of histamine release in rat hypothalamus and hippocampus by presynaptic galanin receptors. *Peptides* 12(5):1113-1117.

- Axe, F. U., Bembenek, S. D. and Szalma, S. (2006). Three-dimensional models of histamine H₃ receptor antagonist complexes and their pharmacophore. *J. Mol. Graph. Model.* 24(6):456-464.
- Bahi, A., Sadek, B., Nurulain, S. M., Lazewska, D. and Kiec-Kononowicz, K. (2015). The novel non-imidazole histamine H₃ receptor antagonist DL77 reduces voluntary alcohol intake and ethanol-induced conditioned place preference in mice. *Physiol. Behav.* 151:189-197.
- Baker, J. G. (2009). A study of antagonist affinities for the human histamine H₂ receptor. *Br. J. Pharmacol.* 153(5):1011-1021.
- Baker, J. G. and Hill, S. J. (2007). Multiple GPCR conformations and signalling pathways: implications for antagonist affinity estimates. *Trends Pharmacol. Sci.* 28(8):374-381.
- Baldwin, J. M. (1993). The probable arrangement of the helices in G protein-coupled receptors. *EMBO J.* 12(4):1693-1703.
- Ballesteros, J. A. and Weinstein, H. (1995). Integrated methods for the construction of three-dimensional models and computational probing of structure-function relations in G protein-coupled receptors. In: Receptor Molecular Biology. S. C. Sealfon. Academic Press, Cambridge, MA, USA. 25: 366-428.
- Barnes, W. G. and Hough, L. B. (2002). Membrane-bound histamine N-methyltransferase in mouse brain: possible role in the synaptic inactivation of neuronal histamine. *J. Neurochem.* 82(5):1262-1271.
- Bartole, E., Grätz, L., Littmann, T., Wifling, D., Seibel, U., et al. (2020). UR-DEBa242: A Py-5-Labeled Fluorescent Multipurpose Probe for Investigations on the Histamine H₃ and H₄ Receptors. *Journal of Medicinal Chemistry* 63(10):5297-5311.
- Bautista-Aguilera, Ó. M., Budni, J., Mina, F., Medeiros, E. B., Deuther-Conrad, W., et al. (2018). Contilisant, a Tetratarget Small Molecule for Alzheimer's Disease Therapy Combining Cholinesterase, Monoamine Oxidase Inhibition, and H₃R Antagonism with S1R Agonism Profile. *J. Med. Chem.* 61(15):6937-6943.
- Bautista-Aguilera, Ó. M., Hagenow, S., Palomino-Antolin, A., Farré-Alins, V., Ismaili, L., et al. (2017). Multitarget-Directed Ligands Combining Cholinesterase and Monoamine Oxidase Inhibition with Histamine H₃R Antagonism for Neurodegenerative Diseases. *Angew. Chem. Int. Ed.* 56(41):12765-12769.
- Bettens, K., Slegers, K. and Van Broeckhoven, C. (2013). Genetic insights in Alzheimer's disease. *Lancet Neurol.* 12(1):92-104.
- Beygo, J., Buiting, K., Ramsden, S. C., Ellis, R., Clayton-Smith, J., et al. (2019). Update of the EMQN/ACGS best practice guidelines for molecular analysis of Prader-Willi and Angelman syndromes. *Eur. J. Hum. Genet.* 27(9):1326-1340.
- Bieth, E., Eddiry, S., Gaston, V., Lorenzini, F., Buffet, A., et al. (2015). Highly restricted deletion of the SNORD116 region is implicated in Prader-Willi Syndrome. *Eur. J. Hum. Genet.* 23(2):252-255.
- Bird, T. D. (2009). Neurogenetic Diseases. In: Encyclopedia of Neuroscience. M. D. Binder, N. Hirokawa and U. Windhorst. Springer Berlin Heidelberg, Berlin, Heidelberg: 2680-2681.
- Birks, J. S. and Harvey, R. J. (2018). Donepezil for dementia due to Alzheimer's disease. *Cochrane Database Syst. Rev.*(6).
- Birnbaum, R. and Weinberger, D. R. (2017). Genetic insights into the neurodevelopmental origins of schizophrenia. *Nat. Rev. Neurosci.* 18(12):727-740.
- Blauwendraat, C., Nalls, M. A. and Singleton, A. B. (2020). The genetic architecture of Parkinson's disease. *Lancet Neurol.* 19(2):170-178.
- Bongers, G., Bakker, R. A. and Leurs, R. (2007). Molecular aspects of the histamine H₃ receptor. *Biochem. Pharmacol.* 73(8):1195-1204.
- Bosma, R., Moritani, R., Leurs, R. and Vischer, H. F. (2016). BRET-based beta-arrestin2 recruitment to the histamine H₁ receptor for investigating antihistamine binding kinetics. *Pharmacol. Res.* 111:679-687.

- Bouley, R., Sun, T.-X., Chenard, M., McLaughlin, M., McKee, M., et al. (2003). Functional role of the NPxxY motif in internalization of the type 2 vasopressin receptor in LLC-PK1 cells. *Am. J. Physiol. Cell Physiol.* 285(4):C750-C762.
- Brown, R. E. and Reymann, K. G. (1996). Histamine H3 receptor-mediated depression of synaptic transmission in the dentate gyrus of the rat in vitro. *J. Physiol.* 496(1):175-184.
- Brown, R. E., Stevens, D. R. and Haas, H. L. (2001). The physiology of brain histamine. *Prog. Neurobiol.* 63(6):637-672.
- Buiting, K. (2010). Prader-Willi syndrome and Angelman syndrome. *Am. J. Med. Genet. C Semin. Med. Genet.* 154C(3):365-376.
- Burkard, W. P., Gey, K. F. and Pletscher, A. (1963). Diamine oxidase in the brain of vertebrates. *J. Neurochem.* 10(3):183-186.
- Butini, S., Nikolic, K., Kassel, S., Brückmann, H., Filipic, S., et al. (2016). Polypharmacology of dopamine receptor ligands. *Prog. Neurobiol.* 142:68-103.
- Calik, M. W. (2017). Update on the treatment of narcolepsy: clinical efficacy of pitolisant. *Nat. Sci. Sleep* 9:127-133.
- Canet-Avilés, R. M., Wilson, M. A., Miller, D. W., Ahmad, R., McLendon, C., et al. (2004). The Parkinson's disease protein DJ-1 is neuroprotective due to cysteine-sulfinic acid-driven mitochondrial localization. *Proc. Natl. Acad. Sci. U.S.A.* 101(24):9103-9108.
- Cardno, A. G. and Gottesman, I. I. (2000). Twin studies of schizophrenia: from bow-and-arrow concordances to star wars Mx and functional genomics. *Am. J. Med. Genet. Part A* 97(1):12-17.
- Cassidy, S. B. (1997). Prader-Willi syndrome. *J. Med. Genet.* 34(11):917-923.
- Cassidy, S. B. and Driscoll, D. J. (2009). Prader-Willi syndrome. *Eur. J. Hum. Genet.* 17(1):3-13.
- Cassidy, S. B., Schwartz, S., Miller, J. L. and Driscoll, D. J. (2012). Prader-Willi syndrome. *Gen. Med.* 14(1):10-26.
- Castellani, C. A. and Arking, D. E. (2020). High-Risk, High-Reward Genetics in ASD. *Neuron* 105(3):407-410.
- Celanire, S., Wijtmans, M., Talaga, P., Leurs, R. and de Esch, I. J. P. (2005). Keynote review: Histamine H3 receptor antagonists reach out for the clinic. *Drug Discov. Today* 10(23-24):1613-1627.
- Chazot, P., Cowart, M., Fukui, H., Ganellin, C. R., Gutzmer, R., et al. (2019). Histamine receptors (version 2019.4) in the IUPHAR/BPS Guide to Pharmacology Database. *IUPHAR/BPS Guide to Pharmacology CITE* 2019(4).
- Chhabria, M. T., Patel, S., Modi, P. and Brahmshatriya, P. S. (2016). Thiazole: A Review on Chemistry, Synthesis and Therapeutic Importance of its Derivatives. *Curr. Top. Med. Chem.* 16(26):2841-2862.
- Chiavegatto, S., Nasello, A. G. and Bernardi, M. M. (1998). Histamine and spontaneous motor activity: Biphasic changes, receptors involved and participation of the striatal dopamine system. *Life Sci.* 62(20):1875-1888.
- Clapham, J. and Kilpatrick, G. (1992). Histamine H3 receptors modulate the release of [3H]-acetylcholine from slices of rat entorhinal cortex: evidence for the possible existence of H3 receptor subtypes. *Br. J. Pharmacol.* 107(4):919-923.
- Clark, E. A. and Hill, S. J. (1996). Sensitivity of histamine H3 receptor agonist-stimulated [35S]GTP γ [S]binding to pertussis toxin. *Eur. J. Pharmacol.* 296(2):223-225.
- Coge, F., Guenin, S. P., Audinot, V., Renouard-Try, A., Beauverger, P., et al. (2001). Genomic organization and characterization of splice variants of the human histamine H3 receptor. *Biochem. J.* 355(Pt 2):279-288.
- Colquhoun, D. (1968). The rate of equilibration in a competitive n drug system and the auto-inhibitory equations of enzyme kinetics: some properties of simple models for passive sensitization. *Proc. Royal Soc. B* 170(1019):135-154.
- Copeland, R. A. (2010). The dynamics of drug-target interactions: drug-target residence time and its impact on efficacy and safety. *Expert Opin. Drug. Discov.* 5(4):305-310.

- Copeland, R. A. (2016). The drug-target residence time model: a 10-year retrospective. *Nat. Rev. Drug Discov.* 15(2):87-95.
- Copeland, R. A., Pompliano, D. L. and Meek, T. D. (2006). Drug-target residence time and its implications for lead optimization. *Nat. Rev. Drug Discov.* 5(9):730-739.
- Corder, E., Saunders, A., Strittmatter, W., Schmechel, D., Gaskell, P., et al. (1993). Gene dose of apolipoprotein E type 4 allele and the risk of Alzheimer's disease in late onset families. *Sci.* 261(5123):921-923.
- Corder, E. H., Saunders, A. M., Risch, N. J., Strittmatter, W. J., Schmechel, D. E., et al. (1994). Protective effect of apolipoprotein E type 2 allele for late onset Alzheimer disease. *Nat. Genet.* 7(2):180-184.
- Corrêa, M. F., Barbosa, Á. J. R., Fernandes, G. A. B., Baker, J. G. and dos Santos Fernandes, J. P. (2019). Pharmacological and SAR analysis of the LINS01 compounds at the human histamine H₁, H₂, and H₃ receptors. *Chem. Biol. Drug Des.* 93:98-95.
- Corrêa, M. F., Reiner, D., Fernandes, G. A. B., Varela, M. T., Aranha, C. M. S. Q., et al. (2020). Profiling of LINS01 compounds at human dopamine D₂ and D₃ receptors. *J. Chem. Sci.* 132(5):5.
- Correa, M. F., Varela, M. T., Balbino, A. M., Torrecilhas, A. C., Landgraf, R. G., et al. (2017). 1-[(2,3-Dihydro-1-benzofuran-2-yl) methyl]piperazines as novel anti-inflammatory compounds: Synthesis and evaluation on H₃ R/H₄ R. *Chem. Biol. Drug Des.* 90(2):317-322.
- Cowart, M., Pratt, J. K., Stewart, A. O., Bennani, Y. L., Esbenshade, T. A., et al. (2004). A new class of potent non-imidazole H₃ antagonists: 2-aminoethylbenzofurans. *Bioorg. Med. Chem. Lett.* 14(3):689-693.
- Dahl, G. and Akerud, T. (2013). Pharmacokinetics and the drug-target residence time concept. *Drug Discov. Today* 18(15-16):697-707.
- Dahl, K., Nakao, R., Amini, N., Moein, M. M., Finnema, S., et al. (2018). Development of [Carbonyl-¹¹C]AZ13198083, a Novel Histamine Type-3 Receptor Radioligand with Favorable Kinetics. *ACS Chemical Neuroscience* 9(5):906-911.
- Dastmalchi, S., Hamzeh-Mivehroud, M., Ghafourian, T. and Hamzeiy, H. (2008). Molecular modeling of histamine H₃ receptor and QSAR studies on arylbenzofuran derived H₃ antagonists. *J. Mol. Graph. Model.* 26(5):834-844.
- Dauvilliers, Y., Bassetti, C., Lammers, G. J., Arnulf, I., Mayer, G., et al. (2013). Pitolisant versus placebo or modafinil in patients with narcolepsy: a double-blind, randomised trial. *Lancet Neurol.* 12(11):1068-1075.
- Davenas, E., Rouleau, A., Morisset, S. and Arrang, J. M. (2008). Autoregulation of McA-RH7777 hepatoma cell proliferation by histamine H₃ receptors. *J. Pharmacol. Exp. Ther.* 326(2):406-413.
- De Lecea, L., Kilduff, T. S., Peyron, C., Gao, X. B., Foye, P. E., et al. (1998). The hypocretins: Hypothalamus-specific peptides with neuroexcitatory activity. *Proc. Natl. Acad. Sci. U.S.A.* 95(1):322-327.
- de Witte, W. E. A., Danhof, M., van der Graaf, P. H. and de Lange, E. C. M. (2016). In vivo Target Residence Time and Kinetic Selectivity: The Association Rate Constant as Determinant. *Trends Pharmacol. Sci.* 37(10):831-842.
- de Witte, W. E. A., Danhof, M., van der Graaf, P. H. and de Lange, E. C. M. (2018). The implications of target saturation for the use of drug-target residence time. *Nat. Rev. Drug Discov.* 18:82.
- Deng, H., Wang, P. and Jankovic, J. (2018). The genetics of Parkinson disease. *Ageing Res. Rev.* 42:72-85.
- Dessalew, N. and Mikre, W. (2008). On the Paradigm Shift Towards Multitarget Selective Drug Design. *Curr. Comput. Aid. Drug Des.* 4(2):76-90.
- Deupi, X. and Standfuss, J. (2011). Structural insights into agonist-induced activation of G-protein-coupled receptors. *Curr. Opin. Struct. Biol.* 21(4):541-551.
- Dineley, K. T., Pandya, A. A. and Yakel, J. L. (2015). Nicotinic ACh receptors as therapeutic targets in CNS disorders. *Trends Pharmacol. Sci.* 36(2):96-108.
- Doreulee, N., Yanovsky, Y., Flagmeyer, I., Stevens, D. R., Haas, H. L., et al. (2001). Histamine H₃ receptors depress synaptic transmission in the corticostriatal pathway. *Neuropharmacol.* 40(1):106-113.

- Dorsey, E. R., Elbaz, A., Nichols, E., Abd-Allah, F., Abdelalim, A., et al. (2018). Global, regional, and national burden of Parkinson's disease, 1990–2016: a systematic analysis for the Global Burden of Disease Study 2016. *Lancet Neurol.* 17(11):939-953.
- Dosier, L., Vaughn, B. and Fan, Z. (2017). Sleep Disorders in Childhood Neurogenetic Disorders. *Children* 4(9):82.
- Driver, A. G. and Mustafa, S. J. (1987). Correlation of histamine H1 receptor function and [3H]mepyramine binding in porcine tracheal tissue. *Eur. J. Pharmacol.* 139(3):287-295.
- Drutel, G., Peitsaro, N., Karlstedt, K., Wieland, K., Smit, M. J., et al. (2001). Identification of Rat H3 Receptor Isoforms with Different Brain Expression and Signaling Properties. *Mol. Pharmacol.* 59(1):1-8.
- Eberling, J. L., Jagust, W. J., Christine, C. W., Starr, P., Larson, P., et al. (2008). Results from a phase I safety trial of hAADC gene therapy for Parkinson disease. *Neurol.* 70(21):1980-1983.
- Edlow, B. L., Takahashi, E., Wu, O., Benner, T., Dai, G., et al. (2012). Neuroanatomic connectivity of the human ascending arousal system critical to consciousness and its disorders. *J. Neuropathol. Exp. Neurol.* 71(6):531-546.
- Einfeld, S. L., Kavanagh, S. J., Smith, A., Evans, E. J., Tonge, B. J., et al. (2006). Mortality in Prader-Willi Syndrome. *Am. J. Ment. Retard.* 111(3):193.
- Eissa, N., Azimullah, S., Jayaprakash, P., Jayaraj, R. L., Reiner, D., et al. (2019). The dual-active histamine H3 receptor antagonist and acetylcholine esterase inhibitor E100 ameliorates stereotyped repetitive behavior and neuroinflammation in sodium valproate induced autism in mice. *Chem. Biol. Interact.* 312:108775.
- Eissa, N., Azimullah, S., Jayaprakash, P., Jayaraj, R. L., Reiner, D., et al. (2020). The Dual-Active Histamine H3 Receptor Antagonist and Acetylcholine Esterase Inhibitor E100 Alleviates Autistic-Like Behaviors and Oxidative Stress in Valproic Acid Induced Autism in Mice. *Int. J. Mol. Sci.* 21(11).
- Eissa, N., Jayaprakash, P., Azimullah, S., Ojha, S. K., Al-Houqani, M., et al. (2018). The histamine H3R antagonist DL77 attenuates autistic behaviors in a prenatal valproic acid-induced mouse model of autism. *Sci. Rep.* 8(1):13077.
- Ellenbroek, B. A. and Ghiabi, B. (2014). The other side of the histamine H3 receptor. *Trends Neurosci.* 37(4):191-199.
- Elsworth, J. D., Glover, V. and Sandler, M. (1980). Tele-methylhistamine is a specific MAO B substrate in man. *Psychopharmacol.* 69(3):287-290.
- Ericson, H., Blomqvist, A. and Köhler, C. (1989). Brainstem afferents to the tuberomammillary nucleus in the rat brain with special reference to monoaminergic innervation. *J. Comp. Neurol.* 281(2):169-192.
- Eriksson, K. S., Stevens, D. R. and Haas, H. L. (2000). Opposite modulation of histaminergic neurons by nociceptin and morphine. *Neuropharmacol.* 39(12):2492-2498.
- Esbenshade, T. A., Browman, K. E., Bitner, R. S., Strakhova, M., Cowart, M. D., et al. (2008). The histamine H3 receptor: an attractive target for the treatment of cognitive disorders. *Br. J. Pharmacol.* 154(6):1166-1181.
- Esbenshade, T. A., Krueger, K. M., Miller, T. R., Kang, C. H., Denny, L. I., et al. (2003). Two Novel and Selective Nonimidazole Histamine H3 Receptor Antagonists A-304121 and A-317920: I. In Vitro Pharmacological Effects. *J Pharmacol Exp Ther* 305(3):887-896.
- Faucard, R., Armand, V., Héron, A., Cochois, V., Schwartz, J. C., et al. (2006). N-methyl-d-aspartate receptor antagonists enhance histamine neuron activity in rodent brain. *J. Neurochem.* 98(5):1487-1496.
- Fernandez, T. V., Sanders, S. J., Yurkiewicz, I. R., Ercan-Sencicek, A. G., Kim, Y.-S., et al. (2012). Rare Copy Number Variants in Tourette Syndrome Disrupt Genes in Histaminergic Pathways and Overlap with Autism. *Biol. Psychiatry* 71(5):392-402.
- Ferrada, C., Ferré, S., Casadó, V., Cortés, A., Justinova, Z., et al. (2008). Interactions between histamine H3 and dopamine D2 receptors and the implications for striatal function. *Neuropharmacol.* 55(2):190-197.

- Ferrada, C., Moreno, E., Casadó, V., Bongers, G., Cortés, A., et al. (2009). Marked changes in signal transduction upon heteromerization of dopamine D1 and histamine H₃ receptors. *Br. J. Pharmacol.* 157(1):64-75.
- Flores-Clemente, C., Osorio-Espinoza, A., Escamilla-Sánchez, J., Leurs, R., Arias, J. M., et al. (2013). A single-point mutation (Ala280Val) in the third intracellular loop alters the signalling properties of the human histamine H₃ receptor stably expressed in CHO-K1 cells. *Br. J. Pharmacol.* 170(1):127-135.
- Folmer, R. H. A. (2018). Drug target residence time: a misleading concept. *Drug Discov. Today* 23(1):12-16.
- Fox, G. B., Esbenshade, T. A., Pan, J. B., Radek, R. J., Krueger, K. M., et al. (2005). Pharmacological properties of ABT-239 [4-(2-{2-[(2R)-2-Methylpyrrolidinyl]ethyl}-benzofuran-5-yl)benzonitrile]: II. Neurophysiological characterization and broad preclinical efficacy in cognition and schizophrenia of a potent and selective histamine H₃ receptor antagonist. *J. Pharmacol. Exp. Ther.* 313(1):176-190.
- Fredriksson, R., Lagerström, M. C., Lundin, L.-G. and Schiöth, H. B. (2003). The G-Protein-Coupled Receptors in the Human Genome Form Five Main Families. Phylogenetic Analysis, Paralogon Groups, and Fingerprints. *Mol. Pharmacol.* 63(6):1256-1272.
- Frymarkiewicz, A. and Walczyński, K. (2009). Non-imidazole histamine H₃ ligands, Part IV: SAR of 1-[2-thiazol-5-yl-(2-aminoethyl)]-4-n-propylpiperazine derivatives. *Eur. J. Med. Chem.* 44(4):1674-1681.
- Fu, H., Hardy, J. and Duff, K. E. (2018). Selective vulnerability in neurodegenerative diseases. *Nat. Neurosci.* 21(10):1350-1358.
- Galés, C., Kowalski-Chauvel, A., Dufour, M. N., Seva, C., Moroder, L., et al. (2000). Mutation of Asn-391 within the Conserved NPXXY Motif of the Cholecystokinin B Receptor Abolishes Gq Protein Activation without Affecting Its Association with the Receptor. *J. Biol. Chem.* 275(23):17321-17327.
- Ganellin, C. R., Fkyerat, A., BangAndersen, B., Athmani, S., Tertiuk, W., et al. (1996). A novel series of (phenoxyalkyl)imidazoles as potent H₃-receptor histamine antagonists. *J. Med. Chem.* 39(19):3806-3813.
- Ganellin, C. R., Hosseini, S. K., Khalaf, Y. S., Tertiuk, W., Arrang, J. M., et al. (1995). Design of Potent Non-Thiourea H₃ Receptor Histamine-Antagonists. *J. Med. Chem.* 38(17):3342-3350.
- Ganellin, C. R., Jayes, D., Khalaf, Y. S., Tertiuk, W., Arrang, J.-M., et al. (1991). Synthesis of pyridyl isosteres of thioperamide as H₃-receptor histamine antagonists. *Collect. Czech. Chem. Commun.* 56(11):2448-2455.
- Ganellin, C. R., Leurquin, F., Piripitsi, A., Arrang, J. M., Garbarg, M., et al. (1998). Synthesis of potent non-imidazole histamine H₃-receptor antagonists. *Arch. Pharm.* 331(12):395-404.
- Garbarg, M., Arrang, J. M., Rouleau, A., Ligneau, X., Tuong, M. D., et al. (1992). S-[2-(4-imidazolyl)ethyl]isothiourea, a highly specific and potent histamine H₃ receptor agonist. *J. Pharmacol. Exp. Ther.* 263(1):304-310.
- Gaulton, A., Hersey, A., Nowotka, M., Bento, A. P., Chambers, J., et al. (2016). The ChEMBL database in 2017. *Nucleic Acids Research* 45(D1):D945-D954.
- Gbahou, F., Rouleau, A., Morisset, S., Parmentier, R., Crochet, S., et al. (2003). Protean agonism at histamine H(3) receptors in vitro and in vivo. *Proc. Natl. Acad. Sci. U.S.A.* 100(19):11086-11091.
- Gbahou, F., Vincent, L., Humbert-Claude, M., Tardivel-Lacombe, J., Chabret, C., et al. (2006). Compared pharmacology of human histamine H₃ and H₄ receptors: structure-activity relationships of histamine derivatives. *Br. J. Pharmacol.* 147(7):744-754.
- Gemkow, M. J., Davenport, A. J., Harich, S., Ellenbroek, B. A., Cesura, A., et al. (2009). The histamine H₃ receptor as a therapeutic drug target for CNS disorders. *Drug Discov. Today* 14(9):509-515.
- Ghamari, N., Dastmalchi, S., Zarei, O., Arias-Montano, J. A., Reiner, D., et al. (2020). In silico and in vitro studies of two non-imidazole multiple targeting agents at histamine H₃ receptors and cholinesterase enzymes. *Chem. Biol. Drug Des.* 95(2):279-290.

- Ghamari, N., Zarei, O., Arias-Montaña, J.-A., Reiner, D., Dastmalchi, S., et al. (2019a). Histamine H3 receptor antagonists/inverse agonists: Where do they go? *Pharmacol. Ther.* 200:69-84.
- Ghamari, N., Zarei, O., Reiner, D., Dastmalchi, S., Stark, H., et al. (2019b). Histamine H3 receptor ligands by hybrid virtual screening, docking, molecular dynamics simulations, and investigation of their biological effects. *Chem. Biol. Drug Des.* 93(5):832-843.
- Ghoshal, A., Kumar, A., Yugandhar, D., Sona, C., Kuriakose, S., et al. (2018a). Corrigendum to "Identification of novel β -lactams and pyrrolidinone derivatives as selective Histamine-3 receptor (H3R) modulators as possible anti-obesity agents" [Eur. J. Med. Chem. 152 (2018) 148–159]. *Eur. J. Med. Chem.* 156:628-630.
- Ghoshal, A., Kumar, A., Yugandhar, D., Sona, C., Kuriakose, S., et al. (2018b). Identification of novel β -lactams and pyrrolidinone derivatives as selective Histamine-3 receptor (H3R) modulators as possible anti-obesity agents. *Eur. J. Med. Chem.* 152:148-159.
- Gillberg, C. (1998). Chromosomal Disorders and Autism. *J. Autism Dev. Disord.* 28(5):415-425.
- González-Sepúlveda, M., Rosell, S., Hoffmann, H. M., Castillo-Ruiz, M. D. M., Mignon, V., et al. (2013). Cellular distribution of the histamine H3 receptor in the basal ganglia: Functional modulation of dopamine and glutamate neurotransmission. *Basal Ganglia* 3(2):109-121.
- Goodearl, A. D. J. and Glucksmann, M. A. (1999). G-protein coupled receptors and uses therefore. WO 99/28470.
- Gotter, A. L., Webber, A. L., Coleman, P. J., Renger, J. J. and Winrow, C. J. (2012). International Union of Basic and Clinical Pharmacology. LXXXVI. Orexin Receptor Function, Nomenclature and Pharmacology. *Pharmacolog. Rev.* 64(3):389-420.
- Goulding, J., May, L. T. and Hill, S. J. (2018). Characterisation of endogenous A2A and A2B receptor-mediated cyclic AMP responses in HEK 293 cells using the GloSensor™ biosensor: Evidence for an allosteric mechanism of action for the A2B-selective antagonist PSB 603. *Biochem. Pharmacol.* 147:55-66.
- Griñán-Ferré, C., Marsal-García, L., Bellver-Sanchis, A., Kondengaden, S. M., Turga, R. C., et al. (2019). Pharmacological inhibition of G9a/GLP restores cognition and reduces oxidative stress, neuroinflammation and β -Amyloid plaques in an early-onset Alzheimer's disease mouse model. *Aging* 11(23):11591-11608.
- Grove, J., Ripke, S., Als, T. D., Mattheisen, M., Walters, R. K., et al. (2019). Identification of common genetic risk variants for autism spectrum disorder. *Nat. Genet.* 51(3):431-444.
- Gulat-Marnay, C., Lafitte, A., Arrang, J.-M. and Schwartz, J.-C. (1990). Modulation of Histamine Release in the Rat Brain by K-Opioid Receptors. *J. Neurochem.* 55(1):47-53.
- Gulat-Marnay, C., Lafitte, A., Arrang, J. M. and Schwartz, J. C. (1989a). Modulation of histamine release and synthesis in the brain mediated by α 2-adrenoceptors. *J. Neurochem.* 53(2):519-524.
- Gulat-Marnay, C., Lafitte, A., Arrang, J. M. and Schwartz, J. C. (1989b). Regulation of histamine release and synthesis in the brain by muscarinic receptors. *J. Neurochem.* 52(1):248-254.
- Guo, R., Anaclet, C., Roberts, J., Parmentier, R., Zhang, M., et al. (2009). Differential effects of acute and repeat dosing with the H3 antagonist GSK189254 on the sleep-wake cycle and narcoleptic episodes in Ox-/- mice. *Br. J. Pharmacol.* 157(1):104-117.
- Gur, R. E., Bassett, A. S., McDonald-McGinn, D. M., Bearden, C. E., Chow, E., et al. (2017). A neurogenetic model for the study of schizophrenia spectrum disorders: the International 22q11.2 Deletion Syndrome Brain Behavior Consortium. *Mol. Psychiatry* 22(12):1664-1672.
- Haas, H. L., Sergeeva, O. A. and Selbach, O. (2008). Histamine in the Nervous System. *Physiol. Rev.* 88(3):1183-1241.
- Habibi, E., Masoudi-Nejad, A., Abdolmaleky, H. M. and Haggarty, S. J. (2011). Emerging roles of epigenetic mechanisms in Parkinson's disease. *Funct. Integr. Genomics* 11(4):523-537.
- Hagenow, S., Stasiak, A., Ramsay, R. R. and Stark, H. (2017). Ciproxifan, a histamine H3 receptor antagonist, reversibly inhibits monoamine oxidase A and B. *Sci. Rep.* 7:40541.

- Hainmueller, T. and Bartos, M. (2020). Dentate gyrus circuits for encoding, retrieval and discrimination of episodic memories. *Nat. Rev. Neurosci.* 21(3):153-168.
- Hallmayer, J. (2011). Genetic Heritability and Shared Environmental Factors Among Twin Pairs With Autism. *Arch. Gen. Psychiatry* 68(11):1095.
- Hamill, T. G., Sato, N., Jitsuoka, M., Tokita, S., Sanabria, S., et al. (2009). Inverse agonist histamine H₃ receptor PET tracers labelled with carbon-11 or fluorine-18. *Synapse* 63(12):1122-1132.
- Hancock, A. A., Esbenshade, T. A., Krueger, K. M. and Yao, B. B. (2003). Genetic and pharmacological aspects of histamine H₃ receptor heterogeneity. *Life Sci.* 73(24):3043-3072.
- Handen, B. L., Johnson, C. R., McAuliffe-Bellin, S., Murray, P. J. and Hardan, A. Y. (2011). Safety and Efficacy of Donepezil in Children and Adolescents with Autism: Neuropsychological Measures. *J. Child Adolesc. Psychopharmacol.* 21(1):43-50.
- Hasselmo, M. E. (2006). The role of acetylcholine in learning and memory. *Curr. Opin. Neurobiol.* 16(6):710-715.
- Hauser, A. S., Chavali, S., Masuho, I., Jahn, L. J., Martemyanov, K. A., et al. (2018). Pharmacogenomics of GPCR Drug Targets. *Cell* 172(1-2):41-54 e19.
- Hibino, H., Inanobe, A., Furutani, K., Murakami, S., Findlay, I., et al. (2010). Inwardly Rectifying Potassium Channels: Their Structure, Function, and Physiological Roles. *Physiol. Rev.* 90(1):291-366.
- Hill, S. J. (1990). Distribution, Properties, and Functional Characteristics of Three Classes of Histamine Receptor. *Pharmacol. Rev.* 42(1):45-83.
- Hill, S. J., Ganellin, C. R., Timmerman, H., Schwartz, J. C., Shankley, N. P., et al. (1997). International Union of Pharmacology. XIII. Classification of Histamine Receptors. *Pharmacol. Rev.* 49(3):253-278.
- Hirschhorn, J. N. and Daly, M. J. (2005). Genome-wide association studies for common diseases and complex traits. *Nat. Rev. Genet.* 6(2):95-108.
- Holm, V. A., Cassidy, S. B., Butler, M. G., Hanchett, J. M., Greenswag, L. R., et al. (1993). Prader-Willi Syndrome: Consensus Diagnostic Criteria. *Pediatrics* 91(2):398-402.
- Hu, W. and Chen, Z. (2017). The roles of histamine and its receptor ligands in central nervous system disorders: An update. *Pharmacol. Ther.* 175:116-132.
- Hutchinson, M. and Fazzini, E. (1996). Cholinesterase inhibition in Parkinson's disease. *J. Neurol. Neurosurg. Psychiatry* 61(3):324-325.
- Igel, P., Schnell, D., Bernhardt, G., Seifert, R. and Buschauer, A. (2009). Tritium-labeled N(1)-[3-(1H-imidazol-4-yl)propyl]-N(2)-propionylguanidine ([³H]UR-PI294), a high-affinity histamine H(3) and H(4) receptor radioligand. *ChemMedChem* 4(2):225-231.
- Inoue, A., Raimondi, F., Kadji, F. M. N., Singh, G., Kishi, T., et al. (2019). Illuminating G-protein-coupling selectivity of GPCRs. *Cell* 177(7):1933-1947. e1925.
- Ishikawa, M., Watanabe, T., Kudo, T., Yokoyama, F., Yamauchi, M., et al. (2010). Investigation of the Histamine H₃ Receptor Binding Site. Design and Synthesis of Hybrid Agonists with a Lipophilic Side Chain. *J. Med. Chem.* 53(17):6445-6456.
- Johnson, C. Y. and Dennis, B. (2015). Gene therapies offer dramatic promise but shocking costs. *Washington Post*, published online: 11/11/2015. Retrieved: 27/08/2020, from <http://wapo.st/1QwkATp>.
- Jończyk, J., Lodarski, K., Staszewski, M., Godyń, J., Zaręba, P., et al. (2019). Search for multifunctional agents against Alzheimer's disease among non-imidazole histamine H₃ receptor ligands. In vitro and in vivo pharmacological evaluation and computational studies of piperazine derivatives. *Bioorg. Chem.* 90:103084.
- Jończyk, J., Malawska, B. and Bajda, M. (2017). Hybrid approach to structure modeling of the histamine H₃ receptor: Multi-level assessment as a tool for model verification. *PLoS One* 12(10):e0186108.
- Jones, B. E. and Hassani, O. K. (2013). The role of Hcrt/Orx and MCH neurons in sleep-wake state regulation. *Sleep* 36(12):1769-1772.

- Kalia, L. V. and Kalia, S. K. (2015). α -Synuclein and Lewy pathology in Parkinson's disease. *Curr. Opin. Neurol.* 28(4):375-381.
- Kalia, L. V. and Lang, A. E. (2016). Parkinson disease in 2015: evolving basic, pathological and clinical concepts in PD. *Nat. Rev. Neurol.* 12(2):65.
- Kallmann, F. J. (1938). The genetics of schizophrenia. Oxford, England, J. J. Augustin.
- Kanber, D., Giltay, J., Wieczorek, D., Zogel, C., Hochstenbach, R., et al. (2008). A paternal deletion of MKRN3, MAGEL2 and NDN does not result in Prader–Willi syndrome. *Eur. J. Hum. Genet.* 17:582.
- Kang, D., Jing, Z., Li, R., Hei, G., Shao, T., et al. (2018). Effect of Betahistine and Metformin on Antipsychotic-Induced Weight Gain: An Analysis of Two Clinical Trials. *Front. Psychiatry* 9(620).
- Karagiannidis, I., Dehning, S., Sandor, P., Tarnok, Z., Rizzo, R., et al. (2013). Support of the histaminergic hypothesis in Tourette Syndrome: association of the histamine decarboxylase gene in a large sample of families. *J. Med. Genet.* 50(11):760-764.
- Karvat, G. and Kimchi, T. (2014). Acetylcholine Elevation Relieves Cognitive Rigidity and Social Deficiency in a Mouse Model of Autism. *Neuropsychopharmacol.* 39(4):831-840.
- Kenakin, T. (2001). Inverse, protean, and ligand-selective agonism: matters of receptor conformation. *FASEB J.* 15(3):598-611.
- Kenakin, T. (2010). The Evolution of Receptors: From On–Off Switches to Microprocessors. In: GPCR Molecular Pharmacology and Drug Targeting: Shifting Paradigms and New Directions. A. Gilchrist. John Wiley & Sohns, New Jersey.
- Kenakin, T. and Christopoulos, A. (2013). Signalling bias in new drug discovery: detection, quantification and therapeutic impact. *Nat. Rev. Drug Discov.* 12(3):205-216.
- Khanfar, M. A., Affini, A., Lutsenko, K., Nikolic, K., Butini, S., et al. (2016). Multiple Targeting Approaches on Histamine H3 Receptor Antagonists. *Front. Neurosci.* 10:201.
- Khanfar, M. A., Reiner, D., Hagenow, S. and Stark, H. (2018). Design, synthesis, and biological evaluation of novel oxadiazole- and thiazole-based histamine H3R ligands. *Bioorg. Med. Chem.* 26(14):4034-4046.
- Kim, Y., Lee, H. M., Xiong, Y., Sciaky, N., Hulbert, S. W., et al. (2017). Targeting the histone methyltransferase G9a activates imprinted genes and improves survival of a mouse model of Prader-Willi syndrome. *Nat. Med.* 23(2):213-222.
- Kim, Y., Wang, S. E. and Jiang, Y.-h. (2019). Epigenetic therapy of Prader–Willi syndrome. *Transl. Res.* 208:105-118.
- Kitbunnadaj, R., Hashimoto, T., Poli, E., Zuiderveld, O. P., Menozzi, A., et al. (2005). N-Substituted Piperidinyll Alkyl Imidazoles: Discovery of Methimepip as a Potent and Selective Histamine H3 Receptor Agonist. *J. Med. Chem.* 48(6):2100-2107.
- Kitbunnadaj, R., Zuiderveld, O. P., De Esch, I. J. P., Vollinga, R. C., Bakker, R., et al. (2003). Synthesis and Structure–Activity Relationships of Conformationally Constrained Histamine H3 Receptor Agonists. *J. Med. Chem.* 46(25):5445-5457.
- Kobilka, B. (2013). The Structural Basis of G-Protein-Coupled Receptor Signaling (Nobel Lecture). *Angew. Chem. Int. Ed.* 52(25):6380-6388.
- Koes, D. R. and Camacho, C. J. (2012). ZINCPharmer: pharmacophore search of the ZINC database. *Nucleic Acids Res.* 40(W1):W409-W414.
- Kononoff Vanhanen, J., Nuutinen, S., Tuominen, M. and Panula, P. (2016). Histamine H3 Receptor Regulates Sensorimotor Gating and Dopaminergic Signaling in the Striatum. *J. Pharmacol. Exp. Ther.* 357(2):264-272.
- Kornum, B. R., Knudsen, S., Ollila, H. M., Pizza, F., Jennum, P. J., et al. (2017). Narcolepsy. *Nat. Rev. Dis. Primers* 3(1):16100.
- Kottke, T., Sander, K., Weizel, L., Schneider, E. H., Seifert, R., et al. (2011). Receptor-specific functional efficacies of alkyl imidazoles as dual histamine H3/H4 receptor ligands. *Eur. J. Pharmacol.* 654(3):200-208.

- Krause, M., Ligneau, X., Stark, H., Garbarg, M., Schwartz, J. C., et al. (1998). 4-alkynylphenyl imidazolylpropyl ethers as selective histamine H₃-receptor antagonists with high oral central nervous system activity. *J. Med. Chem.* 41(21):4171-4176.
- Krueger, K. M., Witte, D. G., Ireland-Denny, L., Miller, T. R., Baranowski, J. L., et al. (2005). G Protein-Dependent Pharmacology of Histamine H₃ Receptor Ligands: Evidence for Heterogeneous Active State Receptor Conformations. *J. Pharmacol. Exp. Ther.* 314(1):271-281.
- Kumar, A. and Sinha, R. I. (2019). Pitolisant for Narcolepsy. *J. Rational Pharmacother. Res.* 5(2):29-31.
- Labeeuw, O., Levoine, N., Billot, X., Danvy, D., Calmels, T., et al. (2016). Synthesis and evaluation of a 2-benzothiazolylphenylmethyl ether class of histamine H₄ receptor antagonists. *Bioorg. Med. Chem. Lett.* 26(21):5263-5266.
- Lambert, J.-C., Ibrahim-Verbaas, C. A., Harold, D., Naj, A. C., Sims, R., et al. (2013). Meta-analysis of 74,046 individuals identifies 11 new susceptibility loci for Alzheimer's disease. *Nat. Genet.* 45(12):1452-1458.
- Lanzi, C., Lucarini, L., Durante, M., Sgambellone, S., Pini, A., et al. (2019). Role of histamine H₃ receptor antagonists on intraocular pressure reduction in rabbit models of transient ocular hypertension and glaucoma. *Int. J. Mol. Sci.* 20(4):981.
- Latorraca, N. R., Venkatakrishnan, A. J. and Dror, R. O. (2017). GPCR Dynamics: Structures in Motion. *Chem. Rev.* 117(1):139-155.
- Lau, C. I., Wang, H. C., Hsu, J. L. and Liu, M. E. (2013). Does the dopamine hypothesis explain schizophrenia? *Rev. Neurosci.* 24(4):389-400.
- Łazewska, D., Kaleta, M., Schwed, J. S., Karcz, T., Mogilski, S., et al. (2017). Biphenyloxy-alkyl-piperidine and azepane derivatives as histamine H₃ receptor ligands. *Bioorg. Med. Chem.* 25(20):5341-5354.
- Lazewska, D., Ligneau, X., Schwartz, J. C., Schunack, W., Stark, H., et al. (2006). Ether derivatives of 3-piperidinopropan-1-ol as non-imidazole histamine H₃ receptor antagonists. *Bioorg. Med. Chem.* 14(10):3522-3529.
- Lazewska, D., Olejarz-Maciej, A., Kaleta, M., Bajda, M., Siwek, A., et al. (2018). 4-tert-Pentylphenoxyalkyl derivatives - Histamine H₃ receptor ligands and monoamine oxidase B inhibitors. *Bioorg. Med. Chem. Lett.* 28(23-24):3596-3600.
- Łazewska, D., Olejarz-Maciej, A., Reiner, D., Kaleta, M., Latacz, G., et al. (2020). Dual Target Ligands with 4-tert-Butylphenoxy Scaffold as Histamine H₃ Receptor Antagonists and Monoamine Oxidase B Inhibitors. *Int. J. Mol. Sci.* 21(10).
- Lee, Y. J., Oh, S. H., Park, C., Hong, M., Lee, A. R., et al. (2014). Advanced Pharmacotherapy Evidenced by Pathogenesis of Autism Spectrum Disorder. *Clin. Psychopharmacol. Neurosci.* 12(1):19-30.
- Lefkowitz, R. J. (2013). A Brief History of G-Protein Coupled Receptors (Nobel Lecture). *Angew. Chem. Int. Ed.* 52(25):6366-6378.
- Lefkowitz, R. J., Cotecchia, S., Samama, P. and Costa, T. (1993). Constitutive activity of receptors coupled to guanine nucleotide regulatory proteins. *Trends Pharmacol. Sci.* 14(8):303-307.
- Levoine, N., Calmels, T., Poupardin-Olivier, O., Labeeuw, O., Danvy, D., et al. (2008). Refined Docking as a Valuable Tool for Lead Optimization: Application to Histamine H₃ Receptor Antagonists. *Arch. Pharm.* 341(10):610-623.
- Levoine, N., Labeeuw, O., Calmels, T., Poupardin-Olivier, O., Berrebi-Bertrand, I., et al. (2011). Novel and highly potent histamine H₃ receptor ligands. Part 1: withdrawing of hERG activity. *Bioorg. Med. Chem. Lett.* 21(18):5378-5383.
- Lichtenstein, P., Carlström, E., Råstam, M., Gillberg, C. and Anckarsäter, H. (2010). The Genetics of Autism Spectrum Disorders and Related Neuropsychiatric Disorders in Childhood. *Am. J. Psychiatr.* 167(11):1357-1363.
- Liedtke, S., Flau, K., Kathmann, M., Schlicker, E., Stark, H., et al. (2003). Replacement of imidazole by a piperidine moiety differentially affects the potency of histamine H₃-receptor antagonists. *Naunyn-Schmiedeberg's Arch. Pharmacol.* 367(1):43-50.

- Ligneau, X., Landais, L., Perrin, D., Piriou, J., Uquen, M., et al. (2007a). Brain histamine and schizophrenia: Potential therapeutic applications of H₃-receptor inverse agonists studied with BF2.649. *Biochem. Pharmacol.* 73(8):1215-1224.
- Ligneau, X., Morisset, S., Tardivel-Lacombe, J., Gbahou, F., Ganellin, C. R., et al. (2000). Distinct pharmacology of rat and human histamine H₃ receptors: role of two amino acids in the third transmembrane domain. *Br. J. Pharmacol.* 131(7):1247-1250.
- Ligneau, X., Perrin, D., Landais, L., Camelin, J. C., Calmels, T. P. G., et al. (2007b). BF2.649 [1-{3-[3-(4-chlorophenyl)propoxy]propyl}piperidine, hydrochloride], a nonimidazole inverse agonist/antagonist at the human histamine H₃ receptor: Preclinical pharmacology. *J. Pharmacol. Exp. Ther.* 320(1):365-375.
- Liguori, C., Placidi, F., Izzi, F., Mercuri, N. B., Stefani, A., et al. (2020). Pitolisant for treating narcolepsy comorbid with Parkinson's disease. *Sleep Med.* 69:86-87.
- Lin, J.-S., Sakai, K., Vanni-Mercier, G., Arrang, J.-M., Garbarg, M., et al. (1990). Involvement of histaminergic neurons in arousal mechanisms demonstrated with H₃-receptor ligands in the cat. *Brain Res.* 523(2):325-330.
- Lin, J. S., Fort, P., Kitahama, K., Panula, P., Denney, R. M., et al. (1991). Immunohistochemical evidence for the presence of type B monoamine oxidase in histamine-containing neurons in the posterior hypothalamus of cats. *Neurosci. Lett.* 128(1):61-65.
- Lippert, U., Artuc, M., Grützkau, A., Babina, M., Guhl, S., et al. (2004). Human Skin Mast Cells Express H₂ and H₄, but not H₃ Receptors. *J. Invest. Dermatol.* 123(1):116-123.
- Liu, F., Barsyte-Lovejoy, D., Li, F., Xiong, Y., Korboukh, V., et al. (2013). Discovery of an in Vivo Chemical Probe of the Lysine Methyltransferases G9a and GLP. *J. Med. Chem.* 56(21):8931-8942.
- Liu, Y., Zeng, H., Pediani, J. D., Ward, R. J., Chen, L. Y., et al. (2018). Visualization of the activation of the histamine H₃ receptor (H₃R) using novel fluorescence resonance energy transfer biosensors and their potential application to the study of H₃R pharmacology. *FEBS J.* 285(12):2319-2336.
- Lord, C., Cook, E. H., Leventhal, B. L. and Amaral, D. G. (2000). Autism spectrum disorders. *Neuron* 28(2):355-363.
- Lovenberg, T. W., Pyati, J., Chang, H., Wilson, S. J. and Erlander, M. G. (2000). Cloning of Rat Histamine H₃ Receptor Reveals Distinct Species Pharmacological Profiles. *J. Pharmacol. Exp. Ther.* 293(3):771-778.
- Lovenberg, T. W., Roland, B. L., Wilson, S. J., Jiang, X., Pyati, J., et al. (1999). Cloning and Functional Expression of the Human Histamine H₃ Receptor. *Mol. Pharmacol.* 55(6):1101-1107.
- Lozeva, V., Tuomisto, L., Tarhanen, J. and Butterworth, R. F. (2003). Increased concentrations of histamine and its metabolite, tele-methylhistamine and down-regulation of histamine H₃ receptor sites in autopsied brain tissue from cirrhotic patients who died in hepatic coma. *J. Hepatol.* 39(4):522-527.
- Luo, W., Yu, Q.-S., Kulkarni, S. S., Parrish, D. A., Holloway, H. W., et al. (2006). Inhibition of Human Acetyl- and Butyrylcholinesterase by Novel Carbamates of (-)- and (+)-Tetrahydrofurobenzofuran and Methanobenzodioxepine. *J. Med. Chem.* 49(7):2174-2185.
- Lutsenko, K., Hagenow, S., Affini, A., Reiner, D. and Stark, H. (2019). Rasagiline derivatives combined with histamine H₃ receptor properties. *Bioorg. Med. Chem. Lett.* 29(19):126612.
- Malkki, H. (2015). NGF gene therapy activates neurons in the AD patient brain. *Nat. Rev. Neurol.* 11(10):548-548.
- Márquez-Gómez, R., Robins, M. T., Gutiérrez-Rodelo, C., Arias, J.-M., Olivares-Reyes, J.-A., et al. (2018). Functional histamine H₃ and adenosine A_{2A} receptor heteromers in recombinant cells and rat striatum. *Pharmacol. Res.* 129:515-525.
- McCutcheon, R. A., Reis Marques, T. and Howes, O. D. (2020). Schizophrenia—An Overview. *JAMA Psychiatry* 77(2):201-210.
- McDougle, C. J., Goodman, W. K. and Price, L. H. (1993). The Pharmacotherapy of Obsessive-Compulsive Disorder. *Pharmacopsychiatry* 26(S 1):24-29.

- McFarlane, H. G., Kusek, G., Yang, M., Phoenix, J., Bolivar, V., et al. (2008). Autism-like behavioral phenotypes in BTBR T+ tf/J mice. *Genes Brain Behav.* 7(2):152-163.
- Mehler, M. F. (2008). Epigenetics and the nervous system. *Ann. Neurol.* 64(6):602-617.
- Meier, G., Apelt, J., Reichert, U., Grassmann, S., Ligneau, X., et al. (2001). Influence of imidazole replacement in different structural classes of histamine H(3)-receptor antagonists. *Eur. J. Pharm. Sci.* 13(3):249-259.
- Meier, G., Ligneau, X., Pertz, H. H., Ganellin, C. R., Schwartz, J. C., et al. (2002). Piperidino-hydrocarbon compounds as novel non-imidazole histamine H-3-receptor antagonists. *Bioorg. Med. Chem.* 10(8):2535-2542.
- Meyza, K. Z., Defensor, E. B., Jensen, A. L., Corley, M. J., Pearson, B. L., et al. (2013). The BTBR T+tf/J mouse model for autism spectrum disorders—in search of biomarkers. *Behav. Brain Res.* 251:25-34.
- Mignot, E., Hayduk, R., Black, J., Grumet, F. C. and Guilleminault, C. (1997). HLA DQB1*0602 is Associated With Cataplexy in 509 Narcoleptic Patients. *Sleep* 20(11):1012-1020.
- Mikó, T., Ligneau, X., Pertz, H. H., Arrang, J.-M., Robin Ganellin, C., et al. (2004). Structural variations of 1-(4-(phenoxyethyl)benzyl)piperidines as nonimidazole histamine H₃ receptor antagonists. *Bioorg. Med. Chem.* 12(10):2727-2736.
- Mirzahassemi, A., Kovacs, M., Kanai, K., Csutora, P. and Dalmadi, B. (2015). BODIPY((R)) FL histamine as a new modality for quantitative detection of histamine receptor upregulation upon IgE sensitization in murine bone marrow-derived mast cells. *Cytometry A* 87(1):23-31.
- Miyazaki, S., Onodera, K., Imaizumi, M. and Timmerman, H. (1997). Effects of clobenpropit (VUF-9153), a histamine H₃-receptor antagonist, on learning and memory, and on cholinergic and monoaminergic systems in mice. *Life Sci.* 61(4):355-361.
- Mocking, T. A. M., Verweij, E. W. E., Vischer, H. F. and Leurs, R. (2018). Homogeneous, Real-Time NanoBRET Binding Assays for the Histamine H₃ and H₄ Receptors on Living Cells. *Mol. Pharmacol.* 94(6):1371-1381.
- Moghaddam, B. and Krystal, J. H. (2012). Capturing the Angel in "Angel Dust": Twenty Years of Translational Neuroscience Studies of NMDA Receptor Antagonists in Animals and Humans. *Schizophr. Bull.* 38(5):942-949.
- Molina-Hernández, A., Nuñez, A., Sierra, J.-J. and Arias-Montaña, J.-A. (2001). Histamine H₃ receptor activation inhibits glutamate release from rat striatal synaptosomes. *Neuropharmacol.* 41(8):928-934.
- Moreno, E., Hoffmann, H., Gonzalez-Sepúlveda, M., Navarro, G., Casadó, V., et al. (2011). Dopamine D1-histamine H₃Receptor Heteromers Provide a Selective Link to MAPK Signaling in GABAergic Neurons of the Direct Striatal Pathway. *J. Biol. Chem.* 286(7):5846-5854.
- Moreno, E., Moreno-Delgado, D., Navarro, G., Hoffmann, H. M., Fuentes, S., et al. (2014). Cocaine Disrupts Histamine H₃ Receptor Modulation of Dopamine D1 Receptor Signaling: 1-D1-H₃ Receptor Complexes as Key Targets for Reducing Cocaine's Effects. *J. Neurosci.* 34(10):3545-3558.
- Morini, G., Comini, M., Rivara, M., Rivara, S., Bordi, F., et al. (2008). Synthesis and structure–activity relationships for biphenyl H₃ receptor antagonists with moderate anti-cholinesterase activity. *Bioorg. Med. Chem.* 16(23):9911-9924.
- Morisset, S., Rouleau, A., Ligneau, X., Gbahou, F., Tardivel-Lacombe, J., et al. (2000). High constitutive activity of native H₃ receptors regulates histamine neurons in brain. *Nature* 408(6814):860-864.
- Morisset, S., Sasse, A., Gbahou, F., Heron, A., Ligneau, X., et al. (2001). The rat H-3 receptor: Gene organization and multiple isoforms. *Biochem. Biophys. Res. Commun.* 280(1):75-80.
- Morphy, R. and Rankovic, Z. (2005). Designed Multiple Ligands. An Emerging Drug Discovery Paradigm. *J. Med. Chem.* 48(21):6523-6543.
- Motulsky, H. J. and Mahan, L. C. (1984). The kinetics of competitive radioligand binding predicted by the law of mass action. *Mol. Pharmacol.* 25(1):1-9.

- Müller, U., Graeber, M. B., Haberhausen, G. and Köhler, A. (1994). Molecular basis and diagnosis of neurogenetic disorders. *J. Neurol. Sci.* 124(2):119-140.
- Munari, L., Provensi, G., Passani, M. B. and Blandina, P. (2013). Selective brain region activation by histamine H(3) receptor antagonist/inverse agonist ABT-239 enhances acetylcholine and histamine release and increases c-Fos expression. *Neuropharmacol.* 70:131-140.
- Murdin, L., Hussain, K. and Schilder, A. G. M. (2016). Betahistine for symptoms of vertigo. *Cochrane Database of Sys. Rev.*(6).
- Nathan, P. J., Boardley, R., Scott, N., Berges, A., Maruff, P., et al. (2013). The safety, tolerability, pharmacokinetics and cognitive effects of GSK239512, a selective histamine H3 receptor antagonist in patients with mild to moderate Alzheimer's disease: A preliminary investigation. *Curr. Alzheimer Res.* 10(3):240-251.
- Neale, B. M., Kou, Y., Liu, L., Ma'Ayan, A., Samocha, K. E., et al. (2012). Patterns and rates of exonic de novo mutations in autism spectrum disorders. *Nat.* 485(7397):242-245.
- Nelson, E. B. and Sallee, F. R. (2012). Treatment methods employing histamine h3 receptor antagonists, including betahistine. US8119668B2.
- Nichols, E., Szeke, C. E. I., Vollset, S. E., Abbasi, N., Abd-Allah, F., et al. (2019). Global, regional, and national burden of Alzheimer's disease and other dementias, 1990–2016: a systematic analysis for the Global Burden of Disease Study 2016. *Lancet Neurol.* 18(1):88-106.
- Nieto-Alamilla, G., Escamilla-Sanchez, J., Lopez-Mendez, M.-C., Molina-Hernandez, A., Guerrero-Hernandez, A., et al. (2018). Differential expression and signaling of the human histamine H3 receptor isoforms of 445 and 365 amino acids expressed in human neuroblastoma SH-SY5Y cells. *J. Recept. Signal Transduction* 38(2):141-150.
- Nieto-Alamilla, G., Márquez-Gómez, R., García-Gálvez, A.-M., Morales-Figueroa, G.-E. and Arias-Montaña, J.-A. (2016). The Histamine H3 Receptor: Structure, Pharmacology, and Function. *Mol. Pharmacol.* 90(5):649-673.
- Nishino, S., Fujiki, N., Ripley, B., Sakurai, E., Kato, M., et al. (2001). Decreased brain histamine content in hypocretin/orexin receptor-2 mutated narcoleptic dogs. *Neurosci. Lett.* 313(3):125-128.
- Nomenclature, I.-I. J. C. o. B. (1984). Nomenclature and symbolism for amino acids and peptides. Recommendations 1983. *Biochem. J.* 219(2):345-373.
- O'Rourke, J. A., Scharf, J. M., Yu, D. and Pauls, D. L. (2009). The genetics of Tourette syndrome: A review. *J. Psychosom. Res.* 67(6):533-545.
- Obara, I., Telezhkin, V., Alrashdi, I. and Chazot, P. L. (2020). Histamine, histamine receptors, and neuropathic pain relief. *Br. J. Pharmacol.* 177(3):580-599.
- Okakura-Mochizuki, K., Mochizuki, T., Yamamoto, Y., Horii, A. and Yamatodani, A. (1996). Endogenous GABA Modulates Histamine Release from the Anterior Hypothalamus of the Rat. *J. Neurochem.* 67(1):171-176.
- Onodera, K., Miyazaki, S., Imaizumi, M., Stark, H. and Schunack, W. (1998). Improvement by FUB 181, a novel histamine H3-receptor antagonist, of learning and memory in the elevated plus-maze test in mice. *Naunyn-Schmiedeberg's Arch. Pharmacol.* 357(5):508-513.
- Ornitz, E. M. (1969). Disorders of perception common to early infantile autism and schizophrenia. *Compr. Psychiatry* 10(4):259-274.
- Palczewski, K., Kumasaka, T., Hori, T., Behnke, C. A., Motoshima, H., et al. (2000). Crystal Structure of Rhodopsin: A G Protein-Coupled Receptor. *Sci.* 289(5480):739-745.
- Panayi, F., Sors, A., Bert, L., Martin, B., Rollin-Jego, G., et al. (2017). In vivo pharmacological profile of S 38093, a novel histamine H3 receptor inverse agonist. *Eur. J. Pharmacol.* 803:1-10.
- Pandy-Szekeres, G., Munk, C., Tsonkov, T. M., Mordalski, S., Harpsoe, K., et al. (2018). GPCRdb in 2018: adding GPCR structure models and ligands. *Nucleic Acids Res.* 46(D1):D440-D446.
- Panula, P., Chazot, P. L., Cowart, M., Gutzmer, R., Leurs, R., et al. (2015). International Union of Basic and Clinical Pharmacology. XCVIII. Histamine Receptors. *Pharmacol. Rev.* 67(3):601-655.

- Panula, P., Yang, H. Y. and Costa, E. (1984). Histamine-containing neurons in the rat hypothalamus. *Proc. Natl. Acad. Sci. U.S.A.* 81(8):2572-2576.
- Parks, G. S., Olivas, N. D., Ikrar, T., Sanathara, N. M., Wang, L., et al. (2014). Histamine inhibits the melanin-concentrating hormone system: implications for sleep and arousal. *J. Physiol.* 592(10):2183-2196.
- Parmentier, R., Zhao, Y., Perier, M., Akaoka, H., Lintunen, M., et al. (2016). Role of histamine H1-receptor on behavioral states and wake maintenance during deficiency of a brain activating system: A study using a knockout mouse model. *Neuropharmacol.* 106:20-34.
- Peedicayil, J. (2019). Pharmacoepigenetics and Pharmacoepigenomics: An Overview. *Curr. Drug Discov. Technol.* 16(4):392-399.
- Peter, D., Jimenez, J., Liu, Y., Kim, J. and Edwards, R. H. (1994). The chromaffin granule and synaptic vesicle amine transporters differ in substrate recognition and sensitivity to inhibitors. *J. Biol. Chem.* 269(10):7231-7237.
- Petroianu, G., Arafat, K., Sasse, B. C. and Stark, H. (2006). Multiple enzyme inhibitions by histamine H₃ receptor antagonists as potential procognitive agents. *Pharm.* 61(3):179-182.
- Peyron, C., Faraco, J., Rogers, W., Ripley, B., Overeem, S., et al. (2000). A mutation in a case of early onset narcolepsy and a generalized absence of hypocretin peptides in human narcoleptic brains. *Nat. Med.* 6(9):991-997.
- Pillot, C., Heron, A., Cochois, V., Tardivel-Lacombe, J., Ligneau, X., et al. (2002). A detailed mapping of the histamine H-3 receptor and its gene transcripts in rat brain. *Neurosci.* 114(1):173-193.
- Pittenger, C. (2020). The histidine decarboxylase model of tic pathophysiology: a new focus on the histamine H₃ receptor. *Br. J. Pharmacol.* 177(3):570-579.
- Poewe, W., Seppi, K., Tanner, C. M., Halliday, G. M., Brundin, P., et al. (2017). Parkinson disease. *Nat. Rev. Dis. Primers* 3(1):17013.
- Posey, D. J., Stigler, K. A., Erickson, C. A. and McDougle, C. J. (2008). Antipsychotics in the treatment of autism. *J. Clin. Invest.* 118(1):6-14.
- Poulet, J. F. A. and Crochet, S. (2019). The Cortical States of Wakefulness. *Frontiers in Systems Neuroscience* 12(64).
- Prader, A., Labhart, A. and Willi, H. (1956). Ein Syndrom von Adipositas, Kleinwuchs, Kryptorchismus und Oligophrenie nach myatonieartigem Zustand im Neugeborenenalter. *Schweiz. Med. Wochenschr.* 86:1260-1261.
- Prast, H., Fischer, H. and Philippu, A. (1994). Release of acetylcholine in the ventral striatum is influenced by histamine receptors. *Agents Actions* 41(S1):C85-C86.
- Proschak, E., Stark, H. and Merk, D. (2018). Polypharmacology by Design: A Medicinal Chemist's Perspective on Multitargeting Compounds. *J. Med. Chem.*
- Provensi, G., Blandina, P. and Passani, M. B. (2016a). The histaminergic system as a target for the prevention of obesity and metabolic syndrome. *Neuropharmacol.* 106:3-12.
- Provensi, G., Costa, A., Passani, M. B. and Blandina, P. (2016b). Donepezil, an acetylcholine esterase inhibitor, and ABT-239, a histamine H₃ receptor antagonist/inverse agonist, require the integrity of brain histamine system to exert biochemical and procognitive effects in the mouse. *Neuropharmacol.* 109:139-147.
- Pullen, L., Picone, M., Tan, L., Johnston, C. and Stark, H. (2019a). Pitolisant Treatment Improves Multiple Clinical Symptoms of Prader-Willi Syndrome (PWS) in Children (P3.6-024). *Neurol.* 92(15 Supplement):P3.6-024.
- Pullen, L. C., Picone, M., Tan, L., Johnston, C. and Stark, H. (2019b). 0771 Pitolisant Is A Safe And Effective Treatment For Children With Prader-Willi Syndrome (PWS). *Sleep* 42(Supplement_1):A309-A310.
- Pullen, L. C., Picone, M., Tan, L., Johnston, C. and Stark, H. (2019c). Cognitive Improvements in Children with Prader-Willi Syndrome Following Pitolisant Treatment -Patient Reports. *J. Pediatr. Pharmacol. Ther.* 24(2):166-171.

- Qanbar, R. and Bouvier, M. (2003). Role of palmitoylation/depalmitoylation reactions in G-protein-coupled receptor function. *Pharmacol. Ther.* 97(1):1-33.
- Rai, B. K., Tawa, G. J., Katz, A. H. and Humblet, C. (2010). Modeling G protein-coupled receptors for structure-based drug discovery using low-frequency normal modes for refinement of homology models: application to H3 antagonists. *Proteins* 78(2):457-473.
- Rapanelli, M., Frick, L. R., Pogorelov, V., Ota, K. T., Abbasi, E., et al. (2014). Dysregulated intracellular signaling in the striatum in a pathophysiologically grounded model of Tourette syndrome. *Eur. Neuropsychopharmacol.* 24(12):1896-1906.
- Rapanelli, M. and Pittenger, C. (2016). Histamine and histamine receptors in Tourette syndrome and other neuropsychiatric conditions. *Neuropharmacol.* 106:85-90.
- Raymer, B. and Bhattacharya, S. K. (2018). Lead-like Drugs: A Perspective. *J. Med. Chem.* 61(23):10375-10384.
- Reiner, D., Seifert, L., Deck, C., Schüle, R., Jung, M., et al. (2020a). Epigenetics meets GPCR: inhibition of histone H3 methyltransferase (G9a) and histamine H3 receptor for Prader–Willi Syndrome. *Sci. Rep.* 10(1):13558.
- Reiner, D. and Stark, H. (2019). Ligand binding kinetics at histamine H3 receptors by fluorescence-polarization with real-time monitoring. *Eur. J. Pharmacol.* 848:112-120.
- Reiner, D., Zivkovic, A., Labeeuw, O., Krief, S., Capet, M., et al. (2020b). Novel pyrrolidinone derivative lacks claimed histamine H3 receptor stimulation in receptor binding and functional studies. *Eur. J. Med. Chem.* 191:112150.
- Reitz, C., Brayne, C. and Mayeux, R. (2011). Epidemiology of Alzheimer disease. *Nat. Rev. Neurol.* 7(3):137-152.
- Riddy, D. M., Cook, A. E., Diepenhorst, N. A., Bosnyak, S., Brady, R., et al. (2017). Isoform-Specific Biased Agonism of Histamine H3 Receptor Agonists. *Mol. Pharmacol.* 91(2):87-99.
- Riddy, D. M., Cook, A. E., Shackelford, D. M., Pierce, T. L., Mocaer, E., et al. (2019). Drug-receptor kinetics and sigma-1 receptor affinity differentiate clinically evaluated histamine H3 receptor antagonists. *Neuropharmacol.* 144:244-255.
- Riley, J. F. (1965). Histamine and Sir Henry Dale. *Br. Med. J.* 1(5448):1488-1490.
- Rizzo, R. and Gulisano, M. (2019). Treatment resistance in Tourette syndrome. In: *Treatment Resistance in Psychiatry*. Springer: 237-252.
- Rocca, W. A. (2018). The burden of Parkinson's disease: a worldwide perspective. *Lancet Neurol.* 17(11):928-929.
- Roche, O., Nettekoven, M., Vifian, W. and Sarmiento, R. M. R. (2008). Refinement of histamine H3 ligands pharmacophore model leads to a new class of potent and selective naphthalene inverse agonists. *Bioorg. Med. Chem. Lett.* 18(15):4377-4379.
- Roessner, V., Plessen, K. J., Rothenberger, A., Ludolph, A. G., Rizzo, R., et al. (2011). European clinical guidelines for Tourette syndrome and other tic disorders. Part II: pharmacological treatment. *Eur. Child Adolesc. Psychiatry* 20(4):173-196.
- Rouleau, A., Garbarg, M., Ligneau, X., Manton, C., Lavie, P., et al. (1997). Bioavailability, antinociceptive and antiinflammatory properties of BP 2-94, a histamine H-3 receptor agonist prodrug. *J. Pharmacol. Exp. Ther.* 281(3):1085-1094.
- Rouleau, A., Ligneau, X., Tardivel-Lacombe, J., Morisset, S., Gbahou, F., et al. (2002). Histamine H-3-receptor-mediated [³⁵S]GTP gamma[S] binding: evidence for constitutive activity of the recombinant and native rat and human H-3 receptors. *Br. J. Pharmacol.* 135(2):383-392.
- Rovati, G. E., Capra, V. and Neubig, R. R. (2007). The highly conserved DRY motif of class A G protein-coupled receptors: beyond the ground state. *Mol. Pharmacol.* 71(4):959-964.
- Sadek, B., Saad, A., Subramanian, D., Shafiullah, M., Łażewska, D., et al. (2016a). Anticonvulsant and procognitive properties of the non-imidazole histamine H3 receptor antagonist DL77 in male adult rats. *Neuropharmacol.* 106:46-55.

- Sadek, B. and Stark, H. (2016b). Cherry-picked ligands at histamine receptor subtypes. *Neuropharmacol.* 106:56-73.
- Saha, R., Tanwar, O., Marella, A., Mumtaz Alam, M. and Akhter, M. (2013). Recent Updates on Biological Activities of Oxadiazoles. *Mini Rev. Med. Chem.* 13(7):1027-1046.
- Sakurai, E., Sakurai, E., Orelund, L., Nishiyama, S., Kato, M., et al. (2006). Evidence for the Presence of Histamine Uptake into the Synaptosomes of Rat Brain. *Pharmacol.* 78(2):72-80.
- Sander, K., Kottke, T. and Stark, H. (2008). Histamine H₃ Receptor Antagonists Go to Clinics. *Biol. Pharm. Bull.* 31(12):2163-2181.
- Sander, K., Kottke, T., Weizel, L. and Stark, H. (2010). Kojic Acid Derivatives as Histamine H₃ Receptor Ligands. *Chem. Pharm. Bull.* 58(10):1353-1361.
- Saper, C. B., Scammell, T. E. and Lu, J. (2005). Hypothalamic regulation of sleep and circadian rhythms. *Nat.* 437(7063):1257-1263.
- Sarter, M. and Bruno, J. P. (1997). Cognitive functions of cortical acetylcholine: toward a unifying hypothesis. *Brain Res. Rev.* 23(1):28-46.
- Scammell, T. E. (2015). Narcolepsy. *N. Engl. J. Med.* 373(27):2654-2662.
- Schaller, D., Hagenow, S., Stark, H. and Wolber, G. (2019). Ligand-guided homology modeling drives identification of novel histamine H₃ receptor ligands. *PLoS One* 14(6):e0218820.
- Schayer, R. W. and Reilly, M. A. (1973). Metabolism of [¹⁴C]histamine in brain. *J. Pharmacol. Exp. Ther.* 187(1):34-39.
- Schihada, H., Ma, X., Zabel, U., Vischer, H. F., Schulte, G., et al. (2020). Development of a conformational histamine H₃ receptor biosensor for the synchronous screening of agonists and inverse agonists. *ACS Sens.* 5:1734-1742.
- Schlegel, B., Stark, H., Sippl, W. and Hölting, H.-D. (2005). Model of a specific human histamine H₃ receptor (hH₃R) binding pocket suitable for virtual drug design. *Inflamm. Res.* 54(1):S50-S51.
- Schlicker, E., Betz, R. and Göthert, M. (1988). Histamine H₃ receptor-mediated inhibition of serotonin release in the rat brain cortex. *Naunyn-Schmiedeberg's Arch. Pharmacol.* 337(5).
- Schlicker, E., Fink, K., Detzner, M. and Göthert, M. (1993). Histamine inhibits dopamine release in the mouse striatum via presynaptic H₃ receptors. *J. Neural Transm. Gen. Sect.* 93(1):1-10.
- Schlicker, E., Fink, K., Hinterthaler, M. and Göthert, M. (1989). Inhibition of noradrenaline release in the rat brain cortex via presynaptic H₃ receptors. *Naunyn-Schmiedeberg's Arch. Pharmacol.* 340(6):633-638.
- Schneider, C., Risser, D., Kirchner, L., Kitzmüller, E., Nigel, C., et al. (1997). Similar deficits of central histaminergic system in patients with Down syndrome and Alzheimer disease. *Neurosci. Lett.* 222(3):183-186.
- Schneider, E. H. and Seifert, R. (2016). The histamine H₄-receptor and the central and peripheral nervous system: A critical analysis of the literature. *Neuropharmacol.* 106:116-128.
- Schneider, L. S., Geffen, Y., Rabinowitz, J., Thomas, R. G., Schmidt, R., et al. (2019). Low-dose lisdextroamphetamine for mild cognitive impairment. A phase 2 placebo-controlled clinical trial. *Neurol.* 93(15):e1474-e1484.
- Schönrock, B., Büsselberg, D. and Haas, H. L. (1991). Properties of tuberomammillary histamine neurones and their response to galanin. *Agents Actions* 33(1-2):135-137.
- Schuetz, D. A., de Witte, W. E. A., Wong, Y. C., Knasmueller, B., Richter, L., et al. (2017). Kinetics for Drug Discovery: an industry-driven effort to target drug residence time. *Drug Discov. Today* 22(6):896-911.
- Schwartz, J.-C. (2011). The histamine H₃ receptor: from discovery to clinical trials with pitolisant. *Br. J. Pharmacol.* 163(4):713-721.
- Schwartz, J.-C. and Lecomte, J.-M. (2016). Clinical trials with H₃-receptor inverse agonists: What they tell us about the role of histamine in the human brain. *Neuropharmacol.* 106:35-36.

- Schwartz, J. C., Lampart, C. and Rose, C. (1970). Properties and regional distribution of histidine decarboxylase in rat brain. *J. Neurochem.* 17(11):1527-1534.
- Scialò, C. and Legname, G. (2020). How would defining Parkinson's as a prion disease impact the search of a cure? *Expert Review of Neurotherapeutics* 20(5):417-420.
- Sergeeva, O. A., Amberger, B. T., Eriksson, K. S., Scherer, A. and Haas, H. L. (2003). Co-ordinated expression of 5-HT_{2C} receptors with the NCX1 Na⁺/Ca²⁺ exchanger in histaminergic neurones. *J. Neurochem.* 87(3):657-664.
- Shah, R. R., Maison-Blanche, P., Robert, P., Denis, E. and Duvauchelle, T. (2016). Can an early phase clinical pharmacology study replace a thorough QT study? Experience with a novel H₃-receptor antagonist/inverse agonist. *Eur. J. Clin. Pharmacol.* 72(5):533-543.
- Shan, L., Bao, A. M. and Swaab, D. F. (2015a). The human histaminergic system in neuropsychiatric disorders. *Trends Neurosci.* 38(3):167-177.
- Shan, L., Dauvilliers, Y. and Siegel, J. M. (2015b). Interactions of the histamine and hypocretin systems in CNS disorders. *Nat. Rev. Neurol.* 11(7):401-413.
- Sharma, R. N., Xavier, F. P., Vasu, K. K., Chaturvedi, S. C. and Pancholi, S. S. (2009). Synthesis of 4-benzyl-1,3-thiazole derivatives as potential anti-inflammatory agents: An analogue-based drug design approach. *J. Enzyme Inhib. Med. Chem.* 24(3):890-897.
- Sherin, J. E., Shiromani, P. J., McCarley, R. W. and Saper, C. B. (1996). Activation of Ventrolateral Preoptic Neurons During Sleep. *Sci.* 271(5246):216-219.
- Silverman, J. L., Tolu, S. S., Barkan, C. L. and Crawley, J. N. (2010). Repetitive Self-Grooming Behavior in the BTBR Mouse Model of Autism is Blocked by the mGluR5 Antagonist MPEP. *Neuropsychopharmacol.* 35(4):976-989.
- Smits, R. P. J. M. and Mulder, A. H. (1991). Inhibitory effects of histamine on the release of serotonin and noradrenaline from rat brain slices. *Neurochem. Int.* 18(2):215-220.
- Southan, C., Sharman, J. L., Benson, H. E., Faccenda, E., Pawson, A. J., et al. (2015). The IUPHAR/BPS Guide to PHARMACOLOGY in 2016: towards curated quantitative interactions between 1300 protein targets and 6000 ligands. *Nucleic Acids Res.* 44(D1):D1054-D1068.
- Sridharan, R., Zuber, J., Connelly, S. M., Mathew, E. and Dumont, M. E. (2014). Fluorescent approaches for understanding interactions of ligands with G protein coupled receptors. *Biochim. Biophys. Acta* 1838(1 Pt A):15-33.
- Stark, H., Purand, K., Huls, A., Ligneau, X., Garbarg, M., et al. (1996). [I-125]iodoproxyfan and related compounds: A reversible radioligand and novel classes of antagonists with high affinity and selectivity for the histamine H₃ receptor. *J. Med. Chem.* 39(6):1220-1226.
- Stark, H., Sippl, W., Ligneau, X., Arrang, J.-M., Ganellin, C. R., et al. (2001). Different antagonist binding properties of human and rat histamine H₃ receptors. *Bioorg. Med. Chem. Lett.* 11(7):951-954.
- Stasiak, A., Mussur, M., Unzeta, M., Lazewska, D., Kiec-Kononowicz, K., et al. (2011). The central histamine level in rat model of vascular dementia. *J. Physiol. Pharmacol.* 62(5):549-558.
- Sterling, J., Herzig, Y., Goren, T., Finkelstein, N., Lerner, D., et al. (2002). Novel Dual Inhibitors of AChE and MAO Derived from Hydroxy Aminoindan and Phenethylamine as Potential Treatment for Alzheimer's Disease. *J. Med. Chem.* 45(24):5260-5279.
- Sterling, T. and Irwin, J. J. (2015). ZINC 15–ligand discovery for everyone. *J. Chem. Inf. Model.* 55(11):2324-2337.
- Stevens, D. R., Kuramasu, A., Eriksson, K. S., Selbach, O. and Haas, H. L. (2004). α 2-Adrenergic receptor-mediated presynaptic inhibition of GABAergic IPSPs in rat histaminergic neurons. *Neuropharmacol.* 46(7):1018-1022.
- Stevens, D. R., Kuramasu, A. and Haas, H. L. (1999). GABA B -receptor-mediated control of GABAergic inhibition in rat histaminergic neurons in vitro. *Neurosci. Lett.* 11(4):1148-1154.

- Stoddart, L. A., White, C. W., Nguyen, K., Hill, S. J. and Pflieger, K. D. G. (2016). Fluorescence- and bioluminescence-based approaches to study GPCR ligand binding. *Br. J. Pharmacol.* 173(20):3028-3037.
- Sweis, R. F., Pliushchev, M., Brown, P. J., Guo, J., Li, F., et al. (2014). Discovery and development of potent and selective inhibitors of histone methyltransferase g9a. *ACS Med. Chem. Lett.* 5(2):205-209.
- Syed, Y. Y. (2016). Pitolisant: First Global Approval. *Drugs* 76(13):1313-1318.
- Sykes, D. A., Dowling, M. R., Leighton-Davies, J., Kent, T. C., Fawcett, L., et al. (2012). The Influence of Receptor Kinetics on the Onset and Duration of Action and the Therapeutic Index of NVA237 and Tiotropium. *J. Pharmacol. Exp. Ther.* 343(2):520-528.
- Sykes, D. A., Stoddart, L. A., Kilpatrick, L. E. and Hill, S. J. (2019). Binding kinetics of ligands acting at GPCRs. *Mol. Cell. Endocrinol.* 485:9 - 19.
- Szafarz, M., Kryczyk, A., Lazewska, D., Kiec-Kononowicz, K. and Wyska, E. (2015). Pharmacokinetics and tissue distribution of the new non-imidazole histamine H₃ receptor antagonist 1-[3-(4-tert-butylphenoxy) propyl]piperidine in rats. *Xenobiotica* 45(10):912-920.
- Szymura-Oleksiak, J., Kryczyk, A., Szafarz, M., Jawien, W., Lazewska, D., et al. (2012). Binding of 1-[3-(4-tert-butyl-phenoxy)propyl]piperidine, a new non imidazole histamine H₃ receptor antagonist to bovine serum albumin. *Acta Pol. Pharm.* 69(6):1043-1047.
- Tejjido, O. and Cacabelos, R. (2018). Pharmacoeepigenomic Interventions as Novel Potential Treatments for Alzheimer's and Parkinson's Diseases. *Int. J. Mol. Sci.* 19(10).
- Tellechea, P., Pujol, N., Esteve-Belloch, P., Echeveste, B., García-Eulate, M. R., et al. (2018). Early- and late-onset Alzheimer disease: Are they the same entity? *Neurología (English Edition)* 33(4):244-253.
- Thomas, R. and Cavanna, A. E. (2013). The pharmacology of Tourette syndrome. *J Neural Transm (Vienna)* 120(4):689-694.
- Tiligada, E. and Ennis, M. (2020). Histamine pharmacology: from Sir Henry Dale to the 21st century. *Br. J. Pharmacol.* 177(3):469-489.
- Tiligada, E., Zampeli, E., Sander, K. and Stark, H. (2009). Histamine H₃ and H₄ receptors as novel drug targets. *Expert Opin. Investig. Drugs* 18(10):1519-1531.
- Timmins, P. (2019). Industry update: the latest developments in the field of therapeutic delivery, 1–31 December 2018. *Ther. Deliv.* 10(4):215-226.
- Tomasch, M., Schwed, J. S., Paulke, A. and Stark, H. (2013). Bodilisant-a novel fluorescent, highly affine histamine h₃ receptor ligand. *ACS Med. Chem. Lett.* 4(2):269-273.
- Tomasch, M., Schwed, J. S., Weizel, L. and Stark, H. (2012). Novel chalcone-based fluorescent human histamine h(3) receptor ligands as pharmacological tools. *Front. Syst. Neurosci.* 6:14.
- Trzaskowski, B., Latek, D., Yuan, S., Ghoshdastider, U., Debinski, A., et al. (2012). Action of molecular switches in GPCRs-theoretical and experimental studies. *Curr. Med. Chem.* 19(8):1090-1109.
- Udvardi, P. T., Nespoli, E., Rizzo, F., Hengerer, B. and Ludolph, A. G. (2013). Chapter Four - Nondopaminergic Neurotransmission in the Pathophysiology of Tourette Syndrome. In: *Int. Rev. Neurobiol.* D. Martino and A. E. Cavanna. Academic Press, Cambridge, MA, USA. 112: 95-130.
- Uteshev, V. V., Stevens, D. R. and Haas, H. L. (1996). α -bungarotoxin-sensitive nicotinic responses in rat tuberomammillary neurons. *Pflugers Arch.* 432(4):607-613.
- Uveges, A. J., Kowal, D., Zhang, Y., Spangler, T. B., Dunlop, J., et al. (2002). The Role of Transmembrane Helix 5 in Agonist Binding to the Human H₃ Receptor. *J. Pharmacol. Exp. Ther.* 301(2):451-458.
- Valente, E. M. (2004). Hereditary Early-Onset Parkinson's Disease Caused by Mutations in PINK1. *Sci.* 304(5674):1158-1160.
- Van Cauwenberghe, C., Van Broeckhoven, C. and Sleegers, K. (2016). The genetic landscape of Alzheimer disease: clinical implications and perspectives. *Genet. Med.* 18(5):421-430.
- van der Velden, W., Heitman, L. H. and Rosenkilde, M. M. (2020). Implications of Ligand-Receptor Binding Kinetics for Therapeutic Targeting of G Protein-Coupled Receptors. *ACS Pharmacol. Translat. Sci.*

- van der Vliet, A., van der Werf, I. F., Bast, A. and Timmerman, H. (1988). Frequency-dependent autoinhibition of histamine release from rat cortical slices: a possible role for H3 receptor reserve. *J. Pharm. Pharmacol.* 40(8):577-579.
- Vollinga, R. C., de Koning, J. P., Jansen, F. P., Leurs, R., Menge, W. M., et al. (1994). A new potent and selective histamine H3 receptor agonist, 4-(1H-imidazol-4-ylmethyl) piperidine. *J. Med. Chem.* 37(3):332-333.
- von Coburg, Y., Kottke, T., Weizel, L., Ligneau, X. and Stark, H. (2009). Potential utility of histamine H(3) receptor antagonist pharmacophore in antipsychotics. *Bioorg. Med. Chem. Lett.* 19(2):538-542.
- Wágner, G., Mocking, T., Arimont, M., Provensi, G., Rani, B., et al. (2019). 4-(3-Aminoazetidin-1-yl)pyrimidin-2-amines as high-affinity non-imidazole histamine H3 receptor agonists with in vivo central nervous system activity. *J. Med. Chem.* (in press).
- Wallis, J. D. (2019). Chapter 15 - Reward. In: Handbook of Clinical Neurology. M. D'Esposito and J. H. Grafman. Elsevier. 163: 281-294.
- Walter, M., von Coburg, Y., Isensee, K., Sander, K., Ligneau, X., et al. (2010). Azole derivatives as histamine H-3 receptor antagonists, Part I: Thiazol-2-yl ethers. *Bioorg. Med. Chem. Lett.* 20(19):5879-5882.
- Wang, C., Wang, Q., Ji, B., Pan, Y., Xu, C., et al. (2018). The Orexin/Receptor System: Molecular Mechanism and Therapeutic Potential for Neurological Diseases. *Front. Mol. Neurosci.* 11(220).
- Wang, Z.-J., Zhong, P., Ma, K., Seo, J.-S., Yang, F., et al. (2019). Amelioration of autism-like social deficits by targeting histone methyltransferases EHMT1/2 in Shank3-deficient mice. *Mol. Psychiatry*.
- Ward, O. C. (1997). Down's 1864 Case of Prader-Willi Syndrome: A Follow-up Report. *J. R. Soc. Med.* 90(12):694-696.
- Weinreb, O., Amit, T., Bar-Am, O. and B.H. Youdim, M. (2012). Ladostigil: A Novel Multimodal Neuroprotective Drug with Cholinesterase and Brain-Selective Monoamine Oxidase Inhibitory Activities for Alzheimers Disease Treatment. *Curr. Drug Targets* 13(4):483-494.
- Weinstock, M., Goren, T. and Youdim, M. B. (2000). Development of a novel neuroprotective drug (TV3326) for the treatment of Alzheimer's disease, with cholinesterase and monoamine oxidase inhibitory activities. *Drug Dev. Res.* 50(3-4):216-222.
- Weinstock, M., Gorodetsky, E., Poltyrev, T., Gross, A., Sagi, Y., et al. (2003). A novel cholinesterase and brain-selective monoamine oxidase inhibitor for the treatment of dementia comorbid with depression and Parkinson's disease. *Prog. Neuropsychopharmacol. Biol. Psychiatry* 27(4):555-561.
- Weisgraber, K. H. and Mahley, R. W. (1996). Human apolipoprotein E: the Alzheimer's disease connection. *FASEB J.* 10(13):1485-1494.
- Wellendorph, P., Goodman, M. W., Burstein, E. S., Nash, N. R., Brann, M. R., et al. (2002). Molecular cloning and pharmacology of functionally distinct isoforms of the human histamine H3 receptor. *Neuropharmacol.* 42(7):929-940.
- West, R. E., Zweig, A., Granzow, R. T., Siegel, M. I. and Egan, R. W. (1990). Biexponential Kinetics of (R)- α -[3H]Methylhistamine Binding to the Rat Brain H3 Histamine Receptor. *J. Neurochem.* 55(5):1612-1616.
- Witte, D. G., Yao, B. B., Miller, T. R., Carr, T. L., Cassar, S., et al. (2006). Detection of multiple H3 receptor affinity states utilizing [3H]A-349821, a novel, selective, non-imidazole histamine H3 receptor inverse agonist radioligand. *Br. J. Pharmacol.* 148(5):657-670.
- Wulff, B. S., Hastrup, S. and Rimvall, K. (2002). Characteristics of recombinantly expressed rat and human histamine H3 receptors. *Eur. J. Pharmacol.* 453(1):33-41.
- Yamamoto, Y., Mochizuki, T., Okakura-Mochizuki, K., Uno, A. and Yamatodani, A. (1997). Thioperamide, a histamine H3 receptor antagonist, increases GABA release from the rat hypothalamus. *Methods Find. Exp. Clin. Pharmacol.* 19(5):289-298.
- Yamanaka, A., Tsujino, N., Funahashi, H., Honda, K., Guan, J.-I., et al. (2002). Orexins Activate Histaminergic Neurons via the Orexin 2 Receptor. *Biochem. Biophys. Res. Commun.* 290(4):1237-1245.

- Yamasaki, M., Miyagawa, T., Toyoda, H., Khor, S.-S., Liu, X., et al. (2016). Evaluation of polygenic risks for narcolepsy and essential hypersomnia. *J. Hum. Genet.* 61(10):873-878.
- Yang, Q. Z. and Hatton, G. I. (1997). Electrophysiology of excitatory and inhibitory afferents to rat histaminergic tuberomammillary nucleus neurons from hypothalamic and forebrain sites. *Brain Res.* 773(1-2):162-172.
- Yao, B. B., Hutchins, C. W., Carr, T. L., Cassar, S., Masters, J. N., et al. (2003). Molecular modeling and pharmacological analysis of species-related histamine H₃ receptor heterogeneity. *Neuropharmacol.* 44(6):773-786.
- Yin, J., Chen, K. M., Clark, M. J., Hijazi, M., Kumari, P., et al. (2020). Structure of a D2 dopamine receptor-G-protein complex in a lipid membrane. *Nature* 584(7819):125-129.
- Yogev-Falach, M., Amit, T., Bar-Am, O., Weinstock, M. and Youdim, M. B. H. (2002). The involvement of mitogen-activated protein (MAP) kinase in the regulation of amyloid precursor protein processing by novel cholinesterase inhibitors derived from rasagiline. *FASEB J.* 16(12):1674-1676.
- Yogev-Falach, M., Amit, T., Bar-Am, O. and Youdim, M. B. H. (2003). The importance of propargylamine moiety in the anti- Parkinson drug rasagiline and its derivatives for MAPK- dependent amyloid precursor protein processing. *FASEB J.* 17(15):2325-2327.
- Yogev-Falach, M., Bar-Am, O., Amit, T., Weinreb, O., Youdim, M. B. H., et al. (2006). A multifunctional, neuroprotective drug, ladostigil (TV3326), regulates holo-APP translation and processing. *FASEB J.* 20(12):2177-2179.
- Youdim, M. B. H. and Bakhle, Y. S. (2006). Monoamine oxidase: isoforms and inhibitors in Parkinson's disease and depressive illness. *Br. J. Pharmacol.* 147(S1):S287-S296.
- Zhou, F.-W., Xu, J.-J., Zhao, Y., LeDoux, M. S. and Zhou, F.-M. (2006). Opposite Functions of Histamine H₁ and H₂ Receptors and H₃ Receptor in Substantia Nigra Pars Reticulata. *J. Neurophysiol.* 96(3):1581-1591.
- Zlomuzica, A., Dere, D., Binder, S., De Souza Silva, M. A., Huston, J. P., et al. (2016). Neuronal histamine and cognitive symptoms in Alzheimer's disease. *Neuropharmacol.* 106:135-145.
- Zoete, V., Daina, A., Bovigny, C. and Michielin, O. (2016). SwissSimilarity: a web tool for low to ultra high throughput ligand-based virtual screening. *J. Chem. Inf. Model.* 56:1399 - 1404.

7. List of abbreviations and synonyms

AAS	ascending arousal system
A β 1-i	β -amyloid fragment 1-i
(B/F)RET	(bioluminescence/förster) resonance energy transfer
5-HT	5-hydroxytryptamine, serotonin
5-HT _{2C} R	serotonin 5-HT _{2C} receptor
5-HT ₃ R	serotonin 5-HT ₃ receptor
5-MH	5-methylhistamine
A _{2A} R	adenosine A _{2A} receptor
A _{2A} R	adenosine A _{2A} receptor
aa	amino acid
AAS	ascending arousal system
AChE	acetylcholinesterase
AChE	acetylcholine esterase
ACS	American Chemical Society
AD	Alzheimer's disease
AD	Alzheimer's disease
ADHD	attention-deficit / hyperactivity disorder
ADME	absorption, distribution, metabolism and excretion
ADMET	ADME and toxicology
APP	amyloid precursor protein
ArA	arachidonic acid
ArcN	arcuate nucleus
AS	Alzheimer Syndrom
ASD	autism-spectrum disorder
ASS	Autismus-Spektrum-Störung
AUC _{c-plasma} (t)	area under the plasma-concentration-time curve
BBB	blood-brain barrier
BDNF	brain-derived neurotrophic factor
BTBR	Black and Tan Brachyury, T+ tf/J
BuChE	butyrylcholine esterase
cAMP	cyclic adenosine monophosphate
cDNA	copy DNA
CFP	cyan fluorescent protein
ChE	cholinesterase
CNS	central nervous system
CRE	cAMP response element
CRH	corticotropin-releasing hormone
CYP	cytochrome P450
DA	dopamine
DAO	diamine oxidase
DBB	diagonal band of Broca
DNA	deoxyribose nucleic acid

DSM-5	diagnostic and statistic manual of mental disorders, edition-5
ECL	extracellular loop
EDS	excessive daytime sleepiness
EPM	elevated plus maze
ERK-1/2	extracellular signal-regulated kinase 1/2
ERNEST	European Research Network on Signal Transduction
EST	expressed sequence tag
F-BODIPY	boron-dipyrromethene-4,4-difluoro-4-bora-3a,4a-diaza-s-indacene
FDA	Food and Drug Administration of the United States of America
FP	fluorescence polarisation
G protein	guanosine triphosphate-binding protein
GABA	γ -amino butyric acid
GABAA/BR	GABAA/B receptor
GBD	global burden of diseases
GDP	guanosine diphosphate
GIRK	G protein-coupled inwardly rectifying potassium channels
GPCR	G protein-coupled receptor
GRAFS	glutamate, rhodopsin, adhesion, frizzled/Taste2 and secretin families
GSH	glutathione
GSK3 β	glycogen synthase kinase 3 β
GTP	guanosine triphosphate
GTP γ S	guanosine 5'-O-[gamma-thio]triphosphate)
GTS	Gilles de la Tourette syndrome
GWAS	genome-wide association study
H1R/H2R/H4R	histamine H1/H2/H4 receptor
H3R	histamine H3 receptor
HA	histamine
HDC	L-histidine decarboxylase
hH3R	human (Homo sapiens) isoform of H3R, GPCR-97,
HLA	human leukocyte antigen
HNMT	histamine-N-methyl transferase
i.c.v.	intra-cerebroventricular
ICL	intracellular loop
iodoproxyfan	FUB 249
IUPHAR	International Union of Basic and Clinical Pharmacology
LC	locus caeruleus
LHA	lateral hypothalamic area
LTR	lifetime risk
M1R/M2R/M3R	muscarinic acetylcholine M1/M2/M3 receptor
MAO A/B	monoamine oxidase A/B
MAP	mitogen-activated protein
MAPK	MAP kinase

MBB	marble-burying behaviour
MCH	melanin-concentrating hormone
MDA	malondialdehyde
mean _{geom}	geometric mean
Mepyramine	pyrilamine
mH3R	mouse (<i>Mus musculus</i>) isoform of H3R, [UniProtKB identifier: P58406]
MPT	mesopontine tegmentum
mRNA	messenger RNA
MTDL	multitarget-directed ligand
MTL	Multi-Targeting-Ligand
NAMH	<i>N</i> ^α -methylhistamine
NET	norepinephrine transporter
NMDAR	N-methyl-d-aspartate receptor
ORL1	Opioid receptor-like 1 receptor
ORX	orexin
ORX1R/ORX2R	orexin-1/-2 receptors
ORX-A/ORX-B	orexin-A (hypocretin-1)/orexin B (hypocretin-2)
PAG	periaqueductal grey
PCR	polymerase chain reaction
PD	Parkinson's disease
pD2	negative logarithm of EC50
PFA	perifornix / perifornical area
PI3K	phosphoinositide 3 kinase
PKA	protein kinase A
PKB	protein kinase B
PPI	prepulse inhibition
PS	Parkinson Syndrom
PWS	Prader–Willi syndrome/Prader-Willi-Syndrom (de.)
RAMH	(<i>R</i>)- α -methylhistamine
REM	rapid eye movement
rH3R	rat (<i>Rattus norvegicus</i>) isoform of H3R, [UniProtKB identifier: Q9QYN8]
RNA	ribose nucleic acid
SCN	suprachiasmatic nucleus
SERT	serotonin transporter
SN	substantia nigra
SNc	SN, pars compacta
SNCA	α -synuclein
SNORD	snoRNA cluster
snoRNA	small nucleolar RNA
SNP	single-nucleotide polymorphism
SNr	SN, pars reticulata
SNRPN	small nucleolar riboprotein-N

SNURF	SNRPN upstream reading frame
SOD	superoxide dismutase
SWS	slow-wave sleep
TCB	three-chamber behaviour
teMH	tele-methylhistamine, N ^T -methylhistamine
TM	transmembrane
TMD/H	transmembrane domain/helix
TMN	tuberomammillary nucleus
U.S.A.	United States of America
VLPO	ventrolateral preoptic nucleus
VPA	valproate
YFP	yellow fluorescent protein
ZINC	ZINC is not commercial
μOR	μ-opioid receptor
α ₂ AR	α ₂ adrenoceptor
α-FMH	α-fluoromethylhistidine
β ₂ AR	β ₂ adrenoceptor
κOR	κ opioid receptor
σ ₁ R	σ ₁ receptor

Presentation of aminoacids: Throughout this thesis, amino acids within peptide sequences are depicted by one-letter code followed by the numeric index of consecutive position in the peptide chain as recommended by the Commission on Biochemical Nomenclature of International Union of Pure and Applied Chemistry (IUPAC-IUB) (Nomenclature, 1984). Within this scheme, the numbering of histamine follows the recommendations for histidine. Numeric indices of amino acids in transmembrane regions of GPCRs are followed by superscript indices according to Ballesteros & Weinstein while following the recommendations for most conserved aminoacids in TMHs by Baldwin (Baldwin, 1993; Ballesteros et al., 1995).

Appendix

Acknowledgements

Within the following few lines, I gratefully thank to all who have contributed to my successful work at the Heinrich Heine University Duesseldorf, which was the basis for this submitted thesis. I would like to emphasise that my statements below represent a very short summary of all the commitments that I have received.

Professor Dr Dr h.c. Holger Stark has been a very supportive supervisor for my work, my research and for my personal development in academia. In particular, I would like to thank you for the opportunity to join your team and to grow within my first years as a young scientist. There, I appreciate your teaching on how to achieve a more optimistic view on my results, always keeping the limits of reality in mind, allowing time for reflecting experimentation, its pitfalls and solutions, but always to remain interested in my progress. It was a pleasure that you shared your profound experience in medicinal chemistry research and in pharmacy and to learn about your steady integration of results into the holistic process of drug development. Furthermore, I have always noticed your openness to explore some personal questions on my own, and that you kept financial concerns low in such projects, e.g., in preparing my short-term scientific mission. As a former undergraduate student in your courses, I would like to thank you for the plethora of basic skills that I could benefit from later, during the time as a PhD student. As a prospective junior scientist, I appreciate that your support never ended after the routine work was done, but that you never ran out of some words of advice when it comes to planning my future and for your endless support of my plans.

Further thanks are dedicated to my mentor Prof. Dr Holger Gohlke, for his common interest in proceedings of my work and for his evaluation of this thesis.

Special thanks go to Dr Aleksandra Živković, who probably was the trigger of considering research in the group of Prof. Stark. This acknowledgement is for you, as my former teacher in organic chemistry, my supervisor in the students' course, our radiation protection commissioner, a careful proof-editor of this thesis, and the always-open-door for support and to reflect organisational and technical processes. I admire your continuous pragmatic and rational approach to problems, which I will surely miss in all of my future decisions. Also, it was a pleasure to collaborate with you in one of my research projects, where I could benefit from your experience as a highly talented researcher and analyst.

Within our small subgroup of pharmacological screening & molecular pharmacology, which forms part of the working-group Stark, I always loved the productive and constructive atmosphere. In detail, I would like to thank Mrs Kathrin Grau for her huge commitment in supporting my routine work, which was

essential to stay focussed on several projects and helped to pass many deadlines. Also, your general open mind for problems and your specific observation skills for things that do appear right has to be emphasised. I would like to thank Dr Stefanie Hagenow and Dr Annika Frank for their expert advice, the various scientific discussions and such about unusual German idioms, and for the great social framework programme which I enjoyed a lot and which made our small team unique. Thank you, Annika, for your comprehensive and constructive feedback to this thesis. Furthermore, I recognise Mrs Mariam Dubiel and Mrs Luisa Leitzbach for your openness during the introduction into our screening group. And last but not least, I have been happy for the acquaintances to our short-term interns Mrs Erika Plazas and our B Sc intern Mrs Frauke Stölting.

Regarding the whole working group, I have enjoyed the initial warm welcome, and the consistent kind cooperation in scientific and social matters, with Mr Cristian di Biase, Dr Hjördis Brückmann, Mrs Milica Elek, Mr Markus Falkenstein, Mr Jens Hagenow, Mr Kiril Lutsenko, Mr Markus Schultes, Mr Lars Seiffert, Mrs Sofia Slimi, Dr Lars Stank, and Mr Sicheng 'Stephen' Zhong. You were reliable colleagues not only, but provided an open atmosphere during our working days and within breaks. For the good collaboration during the students' course, I would like to thank Prof. Dr Thomas Kurz, Mrs Milica Elek, Mr Bastian Hahn, Dr Julia Harting, Mrs Hanna Lou Keizer, Dr Tanja Knaab, Mrs Dina Kottke, Dr Vincent Lenhart, Mr Sebastian Pohl, Dr Svenja Schneider and Mrs Petra Stahlke. Among further members of the Institute of Pharmaceutical and Medicinal Chemistry, I acknowledge the help from Dr Alexandra Hamacher, Dr Christopher Pflieger, Mrs Anita Hübsch and Mr Peter Sippel and for their general approachability in daily issues. A PhD time does not consist of work only, but is as well a part of the student's time. I was happy for the compensatory leisure time programme with people mentioned previously, but as well with Dr Yoditha Asfaha, Mr Daniel Becker, Mrs Maira Anna Deters, Dr Barbara Gioffreda, Mrs Susanne Hermans, Mr Oliver Michel and Dr Marc Pflieger.

Numerous projects which form parts of this thesis would not have succeeded without fluent and productive collaborations with external partners. Therefore, I acknowledge the labs of Prof. Dr Maryam Hamzeh-Mivehroud and Dr Nakisa Ghamari (Iran), Prof. Dr Manfred Jung and Mr Ludwig Seifert (Germany), Prof. Dr Katarzyna Kieć-Kononowicz and Dr Dorothea Łażewska (Poland), Prof. Dr Bassem Sadek (United Arab Emirates), Prof. Dr João Paulo dos Santos Fernandes and Dr Michelle Fidelis Corrêa (Brazil).

To the publishers of the research articles that form parts of this thesis, I dedicate thanks for the great language editing services.

Furthermore, I express my gratitude to Prof. Dr Steve J. Hill and Dr Leigh A. Stoddart who were warm hosts during my research stay at the University of Nottingham (England) and excellently introduced me into the practice of NanoBRET assays. In addition to them, I recognise the advice, help and provision of essential resources by Prof. Dr Jillian J. Baker, Dr Marc Soave and Mrs Lydia Simmet-Smith. I have to excuse for every other member of the Institute of Cell Signalling that I have not disclosed by name, but I am grateful for your kind welcome and the good conversations with you. From the organisational part of the short-term scientific mission and for the great care during the pandemic-related cancellation, I would like to thank the grant-holder and STSM-chairperson of the European Research Network on Signal Transduction (ERNEST), Dr Marta Sommer and Prof. Dr Peter Kolb. Finally, I appreciate the kind donation of the Bursary Award by the European Histamine Research Society during the Online Symposium of their 49th Annual Meeting.

Most thanks are dedicated to my family, who was the greatest motivator during highs and especially lows of my PhD time. I would like to thank my parents Evelyn Reiner, Michael Reiner and as well Stefanie Reiner for their good education, for raising me to the person I am today, for keeping the family running, and for your willingness to let me leave my home and make the best out of my career.

In particular, I would like to thank my husband, Steven, for his strong support. You are a fast friend and selflessly decided to accompany me on this journey without any hesitation. I thank you for your steady lovely comprehension for stressful situations without ever demanding. You have taught me the periodic necessity of tranquillity, not to take things too seriously and you are retrieving me from the labyrinth of research, always just before I get lost in it.

Finally, I would like to thank Maximilian and Niclas, to whom this thesis is devoted. From the bottom of my heart, I apologise for the many times that you had to request to spend (more) time with you, and that I always just answered 'I have to go back to work'. I am convinced that you grow to great people, without ever forgetting your roots. I wish that you will make the most out of your lives, and we will try to be the best possible support on any stage where you are!

Scientific CV

Private

David Reiner-Link (né Reiner)
Rudolfstraße 60
42285 Wuppertal
Germany

Current affiliation

Heinrich Heine University
Institute of Pharmaceutical and Medicinal Chemistry
40225 Duesseldorf
Germany

Date of Birth: 18th February 1991
Place of Birth: Frankfurt am Main, Germany
Email: reiner@hhu.de, david.reiner.frankfurt@gmail.com

SCIENTIFIC EDUCATION

2017, February	Legal registration as Apotheker (Pharmacist), Germany
2010 – 2015	Course of studies in Pharmacy, Goethe-University, Frankfurt, Germany (Grade: 2,6) 2017, January: 3 rd federal examination (Grade: 3,0) 2015, December: 2 nd federal examination (Grade: 2,4) 2012, August: 1 st federal examination (Grade: 2,5)
2007 – 2010	Grammar school Pestalozzischule, Idstein, Germany

PROFESSIONAL EXPERIENCE

2017, April – 2020, August	Practicing pharmacist in a public pharmacy Huetten-Apotheke, Heiligenhaus, Germany
2016, June – 2020, September	Doctoral researcher & PhD candidate with Prof. Dr Dr h.c. Holger Stark, Institute of Pharmaceutical and Medicinal Chemistry, Heinrich Heine University Duesseldorf, Germany
2015, December - 2016, June	Pre-registration year in a public pharmacy Adler Apotheke, Velbert, Germany
2011, August	Internship as a student employee R&D LGCR Pharmaceutical Sciences FF, Sanofi-Aventis Pharma Deutschland GmbH, Frankfurt, Germany

SCIENTIFIC CONFERENCES & EXCHANGE

2020, March	Short-Term Scientific Mission of EU-COST action CA18133 (European Research Network on Signal Transduction) with Dr. Leigh Stoddart and Prof. Dr. Stephen J. Hill Institute of Cell Signalling, University of Nottingham, United Kingdom
2019, March	International PhD student/Postdocs meeting of the German Pharmaceutical Society (DPhG e.V.) Darmstadt, Germany

AWARDS

2020, 2 nd July	49 th Annual Meeting, Online Symposium of the European Histamine Research Society 1 st prize, Bursary Award
----------------------------	-----------------------------------------------------------------------------------------------------------------------------------------

INVOLVEMENT IN ASSOCIATIONS

2019 – 2020	Board-Member of the Organisation Committee XLIX th Annual Meeting of the European Histamine Research Society, Muelheim a.d.R., Germany
since 2019	Member ERNEST - European Research Network on Signal Transduction EU-COST Action CA18133
2013, May - 2014, November	President German Pharmaceutical Students' Association (BPhD e.V.)
2012, May - 2013, May	Liaison Secretary European Pharmaceutical Students' Association (EPSA)
since 2012	Member German Pharmaceutical Society (DPhG e.V.)

LANGUAGE PROFILE

English (C1), French (B1), Spanish (A2)

METHODOLOGICAL SKILLS

GPCR binding assays	radiometric, fluorescence polarisation, BRET, <i>advanced skills</i>
Cell signalling	cAMP response element-driven reportergene assays, <i>advanced skills</i>
Tissue-culture	E.coli, mammalian and insect cell lines, <i>advanced skills</i>
Molecular biology	PCR, cloning, electrophoresis, transformation, <i>mediocre skills</i>
Pharmaceutical analytics	qualitative, quantitative and instrumental analytics, <i>mediocre skills</i>

RESEARCH INTERESTS

GPCR pharmacology	allostery, target binding kinetics, receptor structure, receptor oligomerisation, biased signalling, non-rhodopsin-like GPCRs
Screening techniques	fluorescent & radiometric approaches, label-free techniques

Düsseldorf, den 01. September 2020

David Reiner-Link

List of publications & presentations

RESEARCH ARTICLES WITHIN THIS THESIS

- REINER D, SEIFERT L, DECK C, SCHÜLE R, JUNG M and STARK H. Epigenetics meets GPCR – Inhibition of histone H3 methyltransferase (G9a) and histamine H3 receptor for Prader-Willi Syndrome. *Sci. Rep.* **2020**, 10:13558. (IF: 3.998, 2019)
- EISSA N, AZIMULLAH S, JAYAPRAKASH P, JAYARAJ RL, REINER D, OJHA SK, BEIRAM R, STARK H, ŁAŻEWSKA D, KIEĆ-KONONOWICZ K and SADEK B. The Dual-Active Histamine H3 Receptor Antagonist and Acetylcholine Esterase Inhibitor E100 Alleviates Autistic-Like Behaviors and Oxidative Stress in Valproic Acid Induced Autism in Mice. *Int. J. Mol. Sci.* **2020**, 21:3996. (IF: 4.556, 2019)
- ŁAŻEWSKA D, OLEJARZ-MACIEJ A, REINER D, KALETA M, LATA CZ G, ZYGMUNT M, DOROZ-PŁONKA A, KARCZ T, FRANK A, STARK H and KIEĆ-KONONOWICZ K. Dual Target Ligands with 4-tert-Butylphenoxy Scaffold as Histamine H3 Receptor Antagonists and Monoamine Oxidase B Inhibitors. *Int. J. Mol. Sci.* **2020**, 21:3411. (IF: 4.556, 2019)
- REINER D, ZIVKOVIC A, LABEEUW O, KRIEF S, CAPET M and STARK H. Novel pyrrolidinone derivative lacks claimed histamine H3 receptor stimulation in receptor binding and functional studies. *Eur. J. Med. Chem.* **2020**, 191:112150. (IF: 5.572, 2019)
- CORRÊA MF, REINER D, FERNANDES GAB, VARELA MT, ARANHA CMSQ, STARK H and DOS SANTOS FERNANDES JP. Profiling of LINS01 compounds at human dopamine D2 and D3 receptors. *J. Chem. Sci.* **2020**, 132. (IF: 1.406, 2019)
- GHAMARI N, DASTMALCHI S, ZAREI O, ARIAS-MONTAÑO JA, REINER D, USTUN-ALKAN F, STARK H and HAMZEH-MIVEHROUD M. In Silico and In Vitro Studies of Two Non-Imidazole Multiple Targeting Agents at Histamine H3 Receptors and Cholinesterase Enzymes. *Chem. Biol. Drug Des.* **2020**, 95:279-290. (IF: 2.548, 2019)
- EISSA N, AZIMULLAH S, JAYAPRAKASH P, JAYARAJ RL, REINER D, OJHA SK, BEIRAM R, STARK H, ŁAŻEWSKA D, KIEĆ-KONONOWICZ K and SADEK B. The dual-active histamine H3 receptor antagonist and acetylcholine esterase inhibitor E100 ameliorates stereotyped repetitive behavior and neuroinflammation in sodium valproate induced autism in mice. *Chem.-Biol. Interact.* **2019**, 312:108775. (IF: 3.723, 2019)
- LUTSENKO K, HAGENOW S, AFFINI A, REINER D and STARK H. Rasagiline derivatives combined with histamine H3 receptor properties. *Bioorg. Med. Chem. Lett.* **2019**, 29:126612. (IF: 2.572, 2019)
- REINER D and STARK H. Ligand binding kinetics at histamine H3 receptors by fluorescence-polarization with real-time monitoring. *Eur. J. Pharmacol.* **2019**, 848:112-120. (IF: 3.263, 2019)
- GHAMARI N, ZAREI O, REINER D, DASTMALCHI S, STARK H and HAMZEH-MIVEHROUD M. Histamine H3 receptor ligands by hybrid virtual screening, docking, molecular dynamics simulations, and investigation of their biological effects. *Chem. Biol. Drug Des.* **2019**, 93:832-843. (IF: 2.548, 2019)
- KHANFAR MA, REINER D, HAGENOW S and STARK H. Design, synthesis, and biological evaluation of novel oxadiazole- and thiazole-based histamine H3R ligands. *Bioorg. Med. Chem.* **2018**, 26:4034-4046. (IF: 3.073, 2019)

FURTHER RESEARCH ARTICLES

DOMÍNGUEZ-ÁLVAREZ E, ŁAŻEWSKA D, SZABÓ Z, HAGENOW S, REINER D, GAJDÁCS M, SPENGLER G, STARK H, HANDZLIK J and KIEĆ-KONONOWICZ K. The Search for Histamine H4 Receptor Ligands with Anticancer Activity among Novel (Thio)urea Derivatives. *ChemistrySelect* **2019**, 4:10943-10952. (IF: 1.811, 2019)

ŁAŻEWSKA D, KALETA M, HAGENOW S, MOGILSKI S, LATACZ G, KARCZ T, LUBELSKA A, HONKISZ E, HANDZLIK J, REINER D, SATAŁA G, FILIPEK B, STARK H and KIEĆ-KONONOWICZ K. Novel naphthyloxy derivatives – Potent histamine H3 receptor ligands. Synthesis and pharmacological evaluation. *Bioorg. Med. Chem.* **2018**, 26:2573-2585. (IF: 3.073, 2019)

PREPARED RESEARCH ARTICLES

KUDER KJ, KOTAŃSKA M, SZCZEPAŃSKA K, MIKA K, REINER D, STARK H and KIEĆ-KONONOWICZ K. H-bond acceptor-substituted piperazine derivatives as potential histamine H3 receptor ligands with antioxidant properties. [Submitted, 2020]

SERGEeva OA, MAZUR K, LUTSENKO K, REINER D, HAAS HL and STARK H. OLHA (*N*^α-oleoylhistamine) modulates activity of mouse brain histaminergic neurons. [Prepared, 2020]

GROSICKI M, ADAMI M, MICHELONI C, GŁUCH-LUTWIN M, SIWEK A, LATACZ G, ŁAŻEWSKA D, WIĘCEK M, HAGENOW S, REINER D, STARK H, and KIEĆ-KONONOWICZ K. The pharmacology of 1,3,5-triazine and 1*H*-indole like derivatives against the human H₄ receptor – the lessons from the human eosinophils adhesion assay. [Prepared, 2020]

REVIEWS

REINER D and STARK H. PPI – Wie war das noch? Praxiswissen zu Wirkungen, Nebenwirkungen und Interaktionen. *Deutsche Apotheker Zeitung* **2019**, 159:2780-2784.

GHAMARI N, ZAREI O, ARIAS-MONTAÑO J-A, REINER D, DASTMALCHI S, STARK H and HAMZEH-MIVEHROUD M. Histamine H3 receptor antagonists/inverse agonists: Where do they go? *Pharmacol. Ther.* **2019**, 200:69-84. (IF 10.577, 2019)

BRÜCKMANN H, FRANK A, REINER D and STARK H. Pharmakotherapie des Restless-Legs-Syndroms – eine detaillierte Betrachtung. Pharmacotherapy of RLS - a detailed view. *Pharmakon* **2018**, 6:35-47.

CONFERENCE CONTRIBUTIONS

REINER D, SEIFERT L, DECK C, SCHÜLE R, JUNG M and STARK H. Histone H3 methyltransferases & Histamine H3 receptors as targets for Prader-Willi syndrome. *presenting author* Online Symposium, European Histamine Research Society, July 2020.

ARANHA CMSQ, REINER D, STARK H and DOS SANTOS FERNANDES. LINS05 compounds as potential multitarget agents: screening assessment of H3R, D3R and AChE Online Symposium, European Histamine Research Society, July 2020.

FOGEL WA, STASIAK A, FALKENSTEIN M, REINER D and STARK H. Histamine H₃ receptor antagonism as valuable component for multitarget directed ligands (MTDL). MuTaLig COST-action CA15135, Meeting, Izmir/Turkey, March 2020.

- ŁAŻEWSKA D, OLEJARZ-MACIEJ A, REINER D, DOROZ-PŁONKA A, FRANK A, STARK H and KIEĆ-KONONOWICZ K. The search for monoamine oxidase B among analogues of the potent histamine H₃ receptor ligand DL76.
MuTaLig COST-action CA15135, Meeting, Izmir/Turkey, March 2020.
- FOGEL WA, KHANFAR MA, REINER D, HAGENOW S, STASIAK A and STARK H. Addressing GPCRs and Metabolic Enzymes Simultaneously to Fight Neurodegenerative Diseases - Histamine H₃ Receptor Affinity Combined with Monoamine Oxidase Inhibition.
GPCR Pharmacology: Activation, Signalling and Drug Design, ERNEST COST CA18133 Meeting, Belfast/UK, October 2019, abstract book (p. 59).
- CORREA MF, REINER D, FERNANDES GAB, VARELA MT, STARK H and DOS SANTOS FERNANDEZ JP. Evaluation of the Antihistamines LINS01 as Ligands of Dopamine D_{2/3} Receptors.
9th BrazMedChem, Pirenopolis/Brazil, September 2019.
- LAZEWSKA D, ZAREBA P, HAGENOW S, KALETA M, WIECEK M, REINER D, FRANK A, MALAWSKA B, STARK H and KIEC-KONONOWICZ K. Azepanylhexoyl Derivatives – Histamine H₃ Receptor Affinity, Cholinesterase Inhibitory Activity and ADME/TOX Prediction.
EFMC/ACSMEDI Medicinal Chemistry Frontiers 2019, Krakow/Poland, June 2019, abstract book (p. 144), poster (P052).
- SADEK B, VENKATACHALAM K, ZHONG S, FRANK A, HAGENOW S, REINER D and STARK H. The Multi-targeting Ligand ST713 Incorporating Histamine H₃R and Dopamine D_{2R/D3R} Antagonist Pharmacophores Palliates Autism-Like Behavioural Phenotypes in BTBR T+*tjfl*/J Mice.
48th Annual Meeting of the EHRS, Krakow/Poland, May 2019.
- REINER D and STARK H. Kinetics of Drug-Target Interaction at Histamine H₃ Receptors by Fluorescence Polarization. *presenting author*
DPHG-Doktorandentagung, Darmstadt/Germany, March 2019.
- REINER D, FRANK A, KISS DJ, KESERÜ GM and STARK H. Binding Kinetics at Histamine and Dopamine Receptor Subtypes.
XVII Conference of the Polish Histamine Research Society "Biogenic Amines and Related Biologically Active Compounds", Lodz/Poland, October 2018, abstract book (p. 16).
- SZCZEPANSKA K, KARZCZ T, MOGLINSKI S, KUDER KJ, REINER D, KOTANSA M, STARK H, SADEK B and KIEC-KONONOWICZ. Step Forward for Novel Histamine H₃ Receptor Ligands: 4-Pyridyl-piperazine Derivatives with Promising Multidirectional Pharmacological Properties.
9th Polish Meeting on Medicinal Chemistry, Lublin/Poland, September 2018.
- ZAREBA P, BAJDA M, LAZEWSKA D, REINER D, FRANK A, STARK H, KIEC-KONONOWICZ and MALAWSKA B. Cholinesterases Inhibition of Novel Histamine H₃ Receptor Ligands as Multifunctional Ligands on Alzheimer's Disease.
9th Polish Meeting on Medicinal Chemistry, Lublin/Poland, September 2018.
- ARANHA CMSQ, FERNANDES GAB, CORREA MF, VARELA MT, REINER D, STARK H and DOS SANTOS FERNANDES JP. Dihydrobenzofuranyl-piperazines as Procognitive Agents: Preliminary Dopamine D_{2R/D3R} Profiling.
MedChem Brasilia, Brasilia/Brazil, July 2018.
- STARK H, KHANFAR MA, REINER D and HAGENOW S. Design, Synthesis, and Biological Evaluation of Novel Oxadiazole- and Thiazole-based Histamine H₃R Ligands.
World Histamine Symposium 2018, Kobe/Japan, July 2018, abstract book (p. O17).

Eidesstattliche Erklärung

Ich versichere an Eides Statt, dass die Dissertation von mir selbständig und ohne unzulässige fremde Hilfe unter Beachtung der „Grundsätze zur Sicherung guter wissenschaftlicher Praxis an der Heinrich-Heine-Universität Düsseldorf“ erstellt worden ist. Weiterhin versichere ich, dass diese Dissertation nicht bereits einer anderen Fakultät vorgelegt worden ist und bisher keine erfolglosen und auch keine erfolgreichen Promotionsverfahren für mich eröffnet wurden.

Düsseldorf, den 01. September 2020

David Reiner-Link

Erklärungen zum Promotionsgesuch

Im Rahmen des Antrags auf Zulassung zum Promotionsverfahren erkläre ich entsprechend §5, Abs.1 der Promotionsordnung der Mathematisch-Naturwissenschaftlichen Fakultät der Heinrich-Heine-Universität Düsseldorf vom 15.06.2018, dass das Promotionsgesuch für die Erlangung des Grades „Doktor der Naturwissenschaften“ (*doctor rerum naturalium*, Dr. rer. nat.) gestellt wird, dass die Disputation in englischer Sprache abgelegt wird und dass auf den Ausschluss der Öffentlichkeit vom Vortrag und von der Befragung im Rahmen der Disputation verzichtet wird.

Düsseldorf, den 01. September 2020

David Reiner-Link